A variety of materials, such as biological soft tissues, exhibit large inter- and intra-subject microstructural variations that cannot be captured with individual material tests on the macroscopic observation scale. In such scenarios, multiscale modelling approaches are used instead, which explicitly incorporate the microstructure and provide macroscopic quantities through suitable homogenisation methods. This enables the description of biological soft tissue behaviour arising from microstructural changes, for example, those caused by disease. This thesis, therefore, deals with the multiscale continuum-mechanical modelling of materials and the particular application of such methods to the description of skeletal muscle tissue. Besides a general introduction to the subject, novel analytical estimates for the effective macroscopic potential of two-phase, hyperelastic, incompressible solids are presented. These are based on the so-called tangent second-order homogenisation method and are applicable for highly nonlinear, anisotropic material behaviour at large strains. Subsequently, a novel multiscale model for skeletal muscle is presented, which describes the macroscopic behaviour of soft tissue as a direct consequence of properties at smaller scales, such as the stiffness and arrangement of individual collagen fibres. The methods and models presented in this thesis are discussed by means of representative examples, thus demonstrating their merits in comparison to alternative approaches.

ISBN 978-3-946412-06-9

CBM-07 (2021)

C. Bleiler

Homogenisation Methods Applied to Skeletal Muscle Modelling

Continuum-Mechanical Modelling Across Scales: Homogenisation Methods and Their Application to Microstructurally-Based Skeletal Muscle Modelling

Christian Bleiler

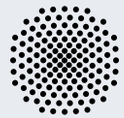

vorgelegt an der
Universität Stuttgart

Continuum-Mechanical Modelling Across Scales: Homogenisation Methods and Their Application to Microstructurally-Based Skeletal Muscle Modelling

Von der Fakultät Bau- und Umweltingenieurwissenschaften der Universität Stuttgart
und dem Stuttgart Center for Simulation Science
zur Erlangung der Würde eines Doktor-Ingenieurs (Dr.-Ing.)
genehmigte Abhandlung

Vorgelegt von

Dipl.-Ing. Christian Bleiler

aus Ulm

Hauptberichter:	Prof. Oliver Röhrle, PhD
1. Mitberichter:	Prof. Dr.-Ing. Jörg Schröder
2. Mitberichter:	Prof. Pedro Ponte Castañeda, PhD

Tag der mündlichen Prüfung: 6. April 2021

Institut für Modellierung und Simulation Biomechanischer Systeme
der Universität Stuttgart

2021

Report No.: CBM-07 (2021)
Institute for Modelling and Simulation of Biomechanical Systems
Chair for Continuum Biomechanics and Mechanobiology
University of Stuttgart, Germany, 2021

Editor:
Prof. O. Röhrle, PhD

ISBN 978-3-946412-06-9
(D 93 – Dissertation, Universität Stuttgart)

Zusammenfassung

Diese Arbeit beschäftigt sich mit der mehrskaligen Modellierung von Materialien im Rahmen der Kontinuumsmechanik und der Anwendung solcher Methoden zur mechanischen Beschreibung von Skelettmuskelgewebe. Zur Motivation seien die folgenden Bemerkungen gemacht: Das makroskopisch beobachtete Verhalten von Materialien ist die Folge eines komplexen Zusammenspiels verschiedenster Phänomene und Strukturen auf mehreren Längenskalen. Im Grunde ist demnach jedes Material ein Kompositmaterial mit hochgradig heterogener Mikrostruktur und erscheint nur in einer idealisierten makroskopischen Betrachtung als homogen. Die kontinuumsmechanische Beschreibung von Materialien erfolgt meist über einen Einskalenansatz unter der Nutzung dieser makroskopischen Homogenität. Es gibt jedoch Szenarien, in welchen die Anwendung eines solchen Einskalenansatzes problematisch und nicht zielführend ist. Üblicherweise sind hierfür unzureichende experimentelle Daten auf der Makroskala verantwortlich, welche jedoch bei der Kalibrierung von kontinuumsmechanischen Modellen essentiell notwendig sind. Dieser Mangel an validen experimentellen Daten tritt vor allem bei der Modellierung von biologischem Gewebe, und insbesondere bei Weichgewebe, auf. Dies liegt daran, dass das Gewebe in vielen unterschiedlichen Zuständen auftreten kann und etwa gesundes und krankhaftes Material große Unterschiede im mechanischen Verhalten aufweist. Bei Skelettmuskelgewebe kommt hinzu, dass im Körper sehr viele verschiedene Muskeln zu finden sind. Dies führt darüber hinaus zu einer großen Variabilität verschiedener Muskeln ein und derselben Person, jedoch ebenso desselben Muskeltyps unterschiedlicher Personen. Diese Variabilitäten können durch makroskopische Modellansätze kaum oder nur schwer erfasst werden und erfordern daher die Anwendung mehrskaliger Modellansätze, welche die Variabilitäten der Mikrostruktur direkt miteinbeziehen. Die konsistente Formulierung mehrskaliger Modellansätze im Allgemeinen und die Anwendung dieser auf Skelettmuskelgewebe im Speziellen sind daher die Ziele der vorliegenden Arbeit.

Die Arbeit beginnt im ersten Teil mit der Einführung der kinematischen Beschreibung deformierbarer Körper im Rahmen der Kontinuumsmechanik für große Deformationen und Verzerrungen sowie dem Spannungsprinzip und den materialunabhängigen physikalischen Bilanzgleichungen. Anschließend werden die grundlegenden Konzepte der Materialtheorie erläutert, was vor allem die konstitutiven Prinzipien und die Formulierung hyperelastischer Potentiale miteinbezieht. Diese Betrachtungen sind – im Rahmen der Anwendbarkeit von Kontinuumstheorien – skalenunabhängig und allgemein anwendbar. Bei der Mehrskalenmodellierung werden diese Prinzipien auf mehrere Skalen angewandt, dies wird im zweiten Teil der Arbeit erläutert. Weiterhin werden hierbei statistische Betrachtungen der Mikrostruktur diskutiert und die grundlegenden Prinzipien des Skalenübergangs mechanischer Größen eingeführt. Basierend auf diesen Ausführungen erfolgt die Formulierung analytischer Methoden zur näherungsweisen Berechnung der makroskopischen Verzerrungsenergie von hyperelastischen Kompositmaterialien auf Basis der „tangent second-order“-Homogenisierungsmethode. Ein Hauptfokus ist hierbei die Bereitstellung von makrosko-

pischen Größen für faserbasierte Zweiphasenmaterialien, bei welchen die Phasen inkompressibles und anisotropes Materialverhalten aufweisen. Solche Mikrostrukturen sind vor allem bei biologischen Materialien anzutreffen. Es sei zudem angemerkt, dass die in dieser Arbeit diskutierten analytischen Homogenisierungsmethoden auf statistischen Parametern der Mikrostruktur beruhen und somit, im Gegensatz zu numerischen Ansätzen, keine vollständige Auflösung der üblicherweise unbekannten Mikrostruktur benötigen. Hierdurch sind diese Ansätze besonders für die Beschreibung von biologischen Materialien geeignet. Der zweite Teil dieser Arbeit wird durch einige Erläuterungen zu Homogenisierungsansätzen von Fasernetzwerkmaterialien abgeschlossen. Die Methoden sind insbesondere bei der Beschreibung von Kollagenfasernetzwerken hilfreich, eignen sich in ihrer Methodik jedoch auch für die allgemeine Beschreibung von gummiartigen Materialien.

Aufbauend auf die allgemeinen methodischen Erläuterungen in den ersten beiden Teilen, erfolgt im dritten Teil der vorliegenden Arbeit die Einführung eines kontinuumsmechanischen Mehrskalenmodellierungsansatzes zur Beschreibung von Skelettmuskelgewebe. Der große Vorteil des neuen Modells liegt darin, dass es vollständig auf der Beschreibung mechanischer Eigenschaften sowie der Zusammensetzung des Materials auf kleineren Längenskalen beruht. Im Speziellen wird ein Zweiphasenmaterial vorgestellt. Die beiden Phasen repräsentieren darin die Muskelfasern sowie die extrazelluläre Matrix, welche die Kollagenfasern beinhaltet. Die Unterscheidung zwischen Muskelfaser und der extrazellulären Matrix hat den Vorteil, dass die mechanischen (oder andere) Eigenschaften dieser beiden Phasen individuell beschrieben werden können. Dies ist der grundlegende Unterschied zu makroskopischen Einskalenansätzen und insbesondere von Vorteil, da für die kleineren Längenskalen oftmals mehr und hochwertigere experimentelle Daten vorliegen. Die vorgenommene mechanische Beschreibung der beiden Phasen und die verwendeten analytischen Homogenisierungsansätze resultieren in einem makroskopischen Materialmodell für Skelettmuskelgewebe mit acht Modellparametern. Der Vorteil dieser Parameter ist hierbei ihre direkte mikromechanische Bedeutung. Darüber hinaus verzichtet der Mehrskalenmodellansatz auf jegliche Notwendigkeit der makroskopischen Modellkalibrierung, was vor allem im Hinblick auf die oft unzureichende Datenlage auf der Makroskala von großem Wert ist. Dies ist ein entscheidender Unterschied zu einskaligen Modellansätzen, deren Anwendbarkeit durch die notwendige Kalibrierung an makroskopische Daten oftmals eingeschränkt ist. Der in dieser Arbeit vorgestellte Modellansatz eröffnet viele Möglichkeiten, wobei ein Hauptaugenmerk auf der Modellierung von stark verändertem Gewebe liegt. Derartige Veränderungen in der mikroskopischen Struktur gehen oft mit einem krankhaften und pathologischen Zustand des Gewebes einher. Das präsentierte Mehrskalenmodell erlaubt es, solche morphologischen Veränderungen direkt über die mikrostrukturbasierten Modellparameter zu beschreiben.

Abstract

This work deals with the multiscale modelling of materials in the context of continuum mechanics and the application of such methods for the mechanical description of skeletal muscle tissue. The following comments should be made as a short motivation: The macroscopically observed behaviour of materials is the result of a complex interplay of different phenomena and structures on several length scales. Each material is therefore a composite material with a highly heterogeneous microstructure and only appears homogeneous in an idealised macroscopic view. The continuum-mechanical description of materials is usually done by means of a single-scale approach using the macroscopic homogeneity. However, there are cases in which the use of such a single-scale approach is no longer appropriate. Insufficient macroscopic experimental data are usually responsible for this. However, these are essential for the calibration of continuum-mechanical models. This lack of valid experimental data especially occurs when modelling biological tissues, in particular soft biological tissues. This is due to the fact that the tissue can appear in many different states and that, for example, healthy and diseased material exhibits great differences in material behaviour. When treating skeletal muscle tissue, it additionally has to be considered that there are many different muscles in the body. This further leads to a large variability between different muscles of the same person, but also between the same muscle type of different persons. These variabilities can hardly be captured by macroscopic single-scale modelling approaches and therefore require the use of multiscale modelling approaches that directly include the variability of the microstructure. The consistent formulation of multiscale model approaches in general and the application of these to skeletal muscle tissue in particular are therefore the goals of the this thesis.

The thesis begins in the first part with the introduction of the kinematical description of deformable bodies in the context of large-strain continuum mechanics as well as the stress principle and the material-independent physical balance relations. After that, the basic concepts of material theory are explained, which especially includes the constitutive principles and the formulation of hyperelastic potentials. These considerations are independent of the scale (as far as continuum theories are considered) and generally applicable. In multiscale modelling, these principles are applied to several scales, which is explained in the second part of this thesis. Furthermore, statistical considerations of the microstructure are discussed and the basic principles of the scale transition of mechanical quantities are introduced. Based on these explanations, analytical estimates for the macroscopic strain energy of hyperelastic composite materials are formulated. The estimates are based on the so-called tangent second-order homogenisation method. A main focus here is to provide estimates for two-phase fibre composites in which the phases have incompressible and anisotropic material behaviour. The investigation of such microstructures is of particular importance when modelling soft biological tissues. It should also be noted that the analytical homogenisation methods discussed in this work are based on statistical parameters of the microstructure and therefore, in contrast to numerical approaches, do not require a

complete resolution of the usually unknown microstructure. This makes these approaches particularly suitable for the description of biological tissue. The second part of this thesis is completed by some explanations on homogenisation techniques for materials made of fibrous or chain-like networks. The methods are very suitable for the description of collagen fibre networks, but their methodology is also applicable for the general description of rubber-like materials.

Based on the general explanations of the first two parts, the third part of this thesis is concerned with the detailed introduction and discussion of a multiscale continuum-mechanical modelling framework for the description of skeletal muscle tissue. The key feature of this model is that the macroscopic material response is entirely based on the mechanical description of the material characteristics and composition on smaller scales. In detail, a two-phase model is proposed and the two phases were identified as the muscle fibres and the extracellular matrix (the collageneous tissues). Differentiating between muscle fibre and extracellular matrix has the advantage that the mechanical (or other) properties of the two phases can be described individually, as opposed to a macroscopic single-scale modelling approach. This is beneficial as there often exist more comprehensive and higher quality experimental data for microscopic constituents than on the macroscale. The descriptions of the phases and the application of analytical homogenisation schemes entails a constitutive muscle model for the macroscopic behaviour of skeletal muscle tissue with eight model parameters. The key advantage of this approach is that the parameters have direct microstructural meanings. Moreover, this novel modelling approach does not require any calibration on the macroscale, on which data obtained from experiments are rather uncertain. This clearly differentiates the proposed model from single-scale material models, in which the material parameters are obtained (and limited) through extensive macroscopic calibration to experimental data. The new modelling framework offers great potential for a variety of applications, in particular for scenarios where the microstructure of the muscle tissue undergoes morphological changes. Such structural changes are often associated with diseases and pathological conditions and can be directly included in the model through the adaption of the respective microstructurally-based model parameters.

Vorwort

Diese Arbeit entstand im Rahmen meiner Tätigkeit als wissenschaftlicher Mitarbeiter in der Forschungsgruppe für Kontinuumsbiomechanik und Mechanobiologie am Institut für Modellierung und Simulation biomechanischer Systeme (vormals am Institut für Mechanik). Viele Menschen haben auf verschiedenste Art und Weise zu dieser Arbeit beigetragen und ich möchte mich an dieser Stelle stellvertretend bei einigen bedanken.

Meinem Hauptberichter, Herrn Professor Oliver Röhrle, danke ich sehr herzlich für seine stetige Unterstützung und für sein Vertrauen, auch Forschungsrichtungen abseits von ursprünglich vorgesehenen Wegen einzuschlagen. Die gewährte Freiheit und seine Offenheit gegenüber neuen Themenfeldern habe ich immer sehr geschätzt. Seit dem Besuch von Professor Röhrles Vorlesungen hat mich die Biomechanik fasziniert und ich bin sehr froh, dass ich dieses spannende Gebiet über die Jahre vertieft kennenlernen (auch durch die Möglichkeit zahlreicher Konferenzbesuche) und mit ihm gemeinsam viele neue Aspekte ergründen durfte.

Herrn Professor Jörg Schröder danke ich für die Übernahme des Berichts, die investierte Zeit und die hilfreichen Kommentare. Sein Interesse an der Arbeit hat mich sehr gefreut.

Key ideas of this work emerged in initial discussions with Professor Pedro Ponte Castañeda. I am deeply grateful for his continuous guidance and support, for his patient explanations when I had no idea about homogenisation theories, and of course for his acceptance to do the report. His vast knowledge and scientific rigour were and are both inspiration and motivation. Sincere thanks also for the opportunity of doing a research stay with him in Philadelphia.

An dieser Stelle danke ich auch Herrn Professor Wolfgang Ehlers und Herrn Professor Manfred Bischoff, zwei meiner akademischen Lehrer, sehr herzlich für ihre gut organisierten Vorlesungen und für ihr Engagement in der universitären Lehre. Mein Interesse an der Kontinuumsmechanik wurde maßgeblich durch ihre Vorlesungen und ihre hilf- und lehrreichen Ausführungen und Erklärungen geprägt – die dadurch erlangten Grundkenntnisse waren essentiell für die Erstellung dieser Arbeit.

Zahlreichen (aktuellen und ehemaligen) Kolleginnen und Kollegen sei für die gute gemeinsame Zeit am Institut für Modellierung und Simulation biomechanischer Systeme sowie am Institut für Mechanik gedankt – unter anderen Sami Bidier, Davina Fink, Andreas Hessenthaler, Sergio Morales, Mylena Mordhorst, Harnoor Saini, Laura Schmid und Michael Sprenger. Meinen langjährigen Bürokollegen, Thomas Heidlauf und Thomas Klotz, sei Danke gesagt für eine Vielzahl lehrreicher Diskussionen über die Biomechanik, Skelettmuskelphysiologie und prinzipielle Fragen der Modellierung, welche mich den Antworten auf neue (und manchmal die immer gleichen) Forschungsfragen jedesmal ein Stück näher brachten. An Arndt Wagner geht ein besonderer Dank für die jahr(zehnt)elange Begleitung als Dozent, Diplomarbeitsbetreuer, Kollege und Ratgeber.

Meiner Familie, insbesondere meinen Eltern und meiner Ehefrau Carina, danke ich für das fortwährende Vertrauen in mich und das Gelingen der Arbeit. Bei Carina bedanke ich mich zudem für alle Unterstützung, für die orthographische Beratung, für ihre Geduld – auch und besonders in Momenten, wenn die Langsamkeit meiner Person mal wieder raumgreifend zu sein schien – und vor allem für den immer wieder benötigten und sehr hilfreichen Druck, ohne welchen die Fertigstellung dieser Arbeit vermutlich im Unbestimmten verblieben wäre.

Stuttgart, im Juni 2021 Christian Bleiler

Contents

Appendix

1 Introduction

Mechanics is an important area of physics and represents a valuable tool for the description of most diverse phenomena in materials across various scales. From an engineering perspective, by mechanics one means the field of *classical mechanics* and leaves behind the physical theory of quantum mechanics. Thereby, it is the aim to describe and mathematically capture physical phenomena, which are in the field of classical mechanics especially the motion of and the forces upon a physical object. The historical development and foundation of the field is closely related to the names of Isaac Newton (1643-1727), Leonhard Euler (1707-1783), and Joseph-Louis Lagrange (1736-1813), of course next to many others. The extension of the concepts of classical mechanics to the three-dimensional field theory of *continuum mechanics* as it is known nowadays relies on the remarkable contributions of, for example, Augustin-Louis Cauchy (1789-1857) and Augustus Edward Hough Love (1863-1940) on the mathematical description of elasticity as well as on the foundation of rational thermodynamics, especially by Clifford Ambrose Truesdell (1919-2000). The subsequent developments in the 20th century brought a unified nonlinear theory for the description of deformable bodies at large strains and combined the material phenomena of elasticity, viscosity, and plasticity. Thereby, the key assumption of continuum mechanics is that an object is continuous and one disregards the real composition of materials made of discrete atoms. Hence, continuum theories, which are grouped under the general term *continuum physics*, are usually applicable at length scales larger than interatomic distances, which is in the magnitude of ångstroms ($1\,\text{Å} = 10^{-10}\,\text{m}$). Furthermore, since it is rigorously based on field equations, modern continuum mechanics is not limited to purely mechanical problems, but can be connected to other classical field theories, like electrodynamics, in order to describe multiphysics problems. If mechanical principles and methods are employed to investigate biological materials and tissues, one arrives at the subdiscipline of *biomechanics*. This field is probably as old as mechanics itself and, for instance, already Leonardo Da Vinci (1452-1519) shaped the idea of *bionics* or *biologically inspired engineering*, which aims in understanding biological principles and subsequently transferring them to engineering systems. In the modern era, the combination of the achievements of continuum mechanics and the biomechanical ideas established the term *continuum biomechanics*. Undoubtedly one of the pioneers of this field was Yuang-Chen Fung (1919-2019). In the second part [143, p. vii] of this seminal book series on biomechanics, he gave a very vivid statement on what this field is and has as its object:

> *"Biomechanics aims to explain the mechanics of life and living. From molecules to organisms, everything must obey the laws of mechanics. Clarification of mechanics clarifies many things. Biomechanics helps us to appreciate life. It sensitizes us to observe nature. It is a tool for design and invention of devices to improve the quality of life. It is a useful tool, a simple tool, a valuable tool, an unavoidable tool. It is a necessary part of biology and engineering."*

This directly points out that biomechanical problems affect phenomena across the scales—*from molecules to organisms*—and that it depicts a classical interdisciplinary field at the intersection of *biology and engineering*. The applications of modern continuum biomechan-

ics are numerous and cover areas such as bionics and its development to *tissue engineering* as well as the modelling of prosthetic devices. The core, however, is the modelling and simulation of biological tissues, which are usually categorised into *hard (mineralised) tissues*, like bones, and *soft tissues*, such as skins, arteries, blood vessels, muscles, tendons, and ligaments. From a practical point of view, the general procedures and steps for the continuum-mechanical description of a biological material do not differ from the ones for a non-biological material and one can employ the same concepts and methods. A meaningful continuum-mechanical description of a physical object, be it biological or non-biological, always requires the awareness of what kind of phenomena shall be investigated and described, and, in turn, the identification of the scale on which the desired results appear. This scale is referred to as the *observation scale*. In brief, one has to know what one wants to achieve with the modelling process. With this at hand, the modelling process consists of (i) the formulation of the required governing equations of the problem and, as a necessary subsequent step, (ii) the formulation of appropriate constitutive equations and the collection of reliable experimental data in order to be able to close the mechanical problem and to (iii) solve the resulting initial-boundary-value problems. Especially the second step including the formulation of constitutive relations is not always straightforward and leads to the motivation of this thesis.

1.1 Motivation

Continuum-mechanical principles can be employed for the modelling of phenomena in materials at various length scales. In engineering applications with man-made materials, like steel and rubber-like materials, as well as in many biomechanical studies one aims to investigate phenomena which appear on the scale of millimetres or larger. This is frequently referred to as the continuum-mechanical *macroscale*. Phenomena and quantities on this scale are called *macroscopic*. As outlined above, the formulation of continuum-mechanical models is not completed by having the governing equations in terms of physical balance principles. Rather, the crucial subsequent step is the formulation of constitutive relations and the calibration of those to experimental data. During the last decades, the increasing number of continuum-mechanical applications for various material types led to a countless number of most diverse analytical constitutive relations. If those constitutive equations are appropriately calibrated to reliable experimental data on the macroscopic scale, which is in this case the observation scale, one ends up with a *single-scale model*. Such models are well-founded and usually result in fast, efficient, and easy-to-implement formulations in a numerical setup. However, there exist cases in which such approaches are no longer suitable. There are a number of reasons for this. For instance, they can be categorised as experimental issues (e i) if no reliable multi-axial experimental data exists to properly calibrate the (possibly anisotropic) constitutive model, (e ii) if the experimental data only describes one specimen or subject and is not representative for the whole material type, or (e iii) if the conditions of the experimental setup do not represent the conditions under which the model shall be investigated. If any (or even several) of those reasons holds true, the use of a single-scale modelling approach and the meaningfulness of the thereon based results become limited and questionable. A possible remedy to this problem is to apply a *multiscale* modelling approach. Thus, instead of making use of experimental data only on the observation scale, a multiscale approach also takes into account data from

smaller scales. Ideally, this shifts the constitutive modelling and the calibration step from the data-poor macroscale to data-rich(er) smaller scales. Of course, such an approach only makes sense if the data on the smaller scales is of better quality. Consequently, a multiscale approach in this context always has to be accompanied with appropriate *upscaling* and *homogenisation* steps, such that the results become available on the macroscopic observation scale. Multiscale models which are a consequence of the experimental issues (e i)-(e iii) are rather "implicitly" motivated and the multiscale aspect is in this case an auxiliary tool to overcome the issues at hand. Besides that, there might be a more "explicit" motivation for applying multiscale models. Reasons for that stem from an application point of view and exist, for example, (a i) if more understanding of the small-scale effects is desired, (a ii) if localisation effects require small-scale considerations, (a iii) if one aims to construct an optimal macroscopic behaviour by specifically manipulating small-scale components, (a iv) if one wants to predict the macroscopic response due to structural variations on smaller scales. Under these circumstances, the observation scale is no longer clearly defined, because phenomena on at least two scales are then of interest and the interconnections between the scales move into focus.

Hence, multiscale modelling approaches serve as powerful tools, either as pragmatic auxiliary tools or as sophisticated tool for a deeper investigation of phenomena across scales. However, we emphasise that multiscale models are not better than single-scale approaches by definition. They demand for considerable effort in the modelling process, such as the need for reliable upscaling and homogenisation methods, and usually increase the complexity of the resulting models. In turn, the higher complexity eventually entails higher computational costs when solving actual problems. Further, it always has to be reminded that modelling on more than one scale plus capturing interscale effects directly results in the need of more modelling assumptions. While a single-scale approach smears all small-scale effects and we might thus say that it accounts for them in an intrinsic manner, a multiscale approach actually has to resolve small-scale effects and requires more information and more knowledge about a system. In conclusion, there has to be a clear justification, such as the exemplary reasons above, to use multiscale models instead of a single-scale approach.

In this work, the previously outlined principles and findings are elucidated with the example of the continuum-mechanical modelling and investigation of *skeletal muscle tissue*. This soft biological tissue is part of the musculoskeletal system and depicts the decisive organic system for the establishment and control of voluntary movement of the body. Skeletal muscle tissue is a complex material in which characteristic structures across various scales give rise to the macroscopic behaviour. Thereby, the most prominent feature of muscles is their ability to convert chemical energy into elastic energy and mechanical deformations due to neural stimulations, which is referred to as the *active behaviour of muscles*. Those mechanisms take place in the *sarcomeres*, which are also called the contractile units and are the smallest functional unit inside the *muscle fibres*. In turn, the muscle fibres are the characteristic structural component of muscle tissue. They run through the muscle in an aligned manner and are surrounded by the second characteristic structure: the extracellular matrix. Very important components of the extracellular matrix are the collagen fibres, which typically provide stiffness and stability in biological tissues. The multiscale aspect of skeletal muscle tissue becomes obvious when noting that sarcomeres appear on length scales in the magnitude of about $2\,\mu\text{m} = 2 \times 10^{-6}\,\text{m}$ and collagen fibres in the magnitude

of about 100 nm $= 10^{-7}$ m, while the material response on the macroscopic scale is in the range of millimetres or centimetres. A deep understanding and the reliable prediction of the occurring deformations and inner forces in the muscle material is fundamental for a variety of applications, such as, for example, the design of prosthetic devices, the analysis of human movement, the investigation of tissue behaviour under diseased conditions, and many more. However, capturing the mechanical behaviour and the interplay of the complex small-scale structures in skeletal muscles within a single-scale continuum-mechanical modelling framework is a challenging and yet mainly unresolved task. This is due to several reasons, in particular because obtaining comprehensive (ideally in-vivo) experimental data for the proper calibration of macroscopic constitutive material relations is extremely difficult or even impossible. For instance, referring to issue (e i), there are experimental studies which observed that muscle tissue shows its stiffest tensile response in the muscle fibre direction [344], transverse to the muscle fibre direction [471], or in a 45° angle to the muscle fibre direction [338]. Thus, it is impossible to capture the macroscopic material symmetry conditions in a reliable manner, since different experiments predicted different such properties. Of course, this is related to the issue (e ii) and the strong inter- and intra-subject variations in skeletal muscle tissues. This means that the mechanical properties of skeletal muscle tissue can be very different between different muscles of one person (subject), hence, between different muscles in the different body regions. Moreover, muscle properties may be very different for one muscle type in different persons. Hence, one experimental sample is usually not representative for the whole material class of skeletal muscles. It would require many different experimental tests to capture these tissue-inherent variations. However, since this is not available, capturing the inter- and intra-tissue variability of biological tissue within a single-scale continuum-mechanical modelling framework is hardly possible. In addition to the issues (e i) and (e ii), also point (e iii) holds true for skeletal muscle tissue and for soft biological tissues in general. Since in-vivo material testing of biological tissues is not (at least not non-destructive) possible, experiments have to be performed ex-vivo. Yet, as soon as a biological tissue is extracted from its natural environment it may undergo severe structural changes. For instance, dehydration is a frequent problem during tissue extraction and sample preparation. Thus, material tests on such samples eventually show a very distinct mechanical behaviour compared to the biological tissue in the living body. Summarising, all of the previously outlined experimental issues are present for skeletal muscle tissue and clearly justify and even require the application of a multiscale modelling approach and the direct incorporation of small-scale effects. Apart from overcoming the issues related to the insufficiency of macroscopic experimental data, a multiscale modelling approach for skeletal muscle tissue at the same time offers a lot of novel and powerful possibilities. While (a iii) obviously does not apply for biological tissues, all the other application-based points hold true. For instance, related to (a i), a multiscale approach can offer a direct connection between macroscopic deformation states and the associated deformation of structures at smaller scales, such as the stretch in collagen fibres. In skeletal muscles and soft biological tissues in general, the recruitment of collagen fibres due to macroscopic deformations is a critical aspect. Such considerations directly lead to point (a ii), because the information of localised stresses and strains on smaller scales allow to model for example failure of the respective structural elements. However, maybe the most interesting aspect is related to (a iv) and the possibility of predicting the macroscopic material response due to variations

of the small-scale structures. This is a crucial aspect when dealing with the modelling of living tissues, as they are eventually subject to significant morphological changes across the scales. Reasons for such changes are manifold and can be, for example, growth of the biological tissue due to exercise or loading as well as atrophy due to numerous diseases or post-operative immobilisation. Single-scale macroscopic modelling approaches cannot be used to describe the macroscopic behaviour subject to such structural variations in a natural way, which means without the calibration of the model to macroscopic experimental data. Such data, however, cannot be acquired in an in-vivo, subject-specific way for every specific variation of the muscle tissue. In contrast, there exists an impressive amount of experimental data reporting on small-scale changes of skeletal muscles, which in a multiscale approach can be directly included.

1.2 Objectives and contextualisation of this thesis

Encouraged by the preceding explanations, this thesis mainly focuses on two aspects, namely, the investigation and appropriate extension of *analytical nonlinear homogenisation methods* and, based on that, the introduction of a novel *multiscale model of skeletal muscle tissue*. These objectives shall be clarified in this section. Since this thesis relies on a broad fundament of previous scientific works and studies in the fields of, in particular, continuum mechanics, biomechanics, and experimental biology, the novel aspects of the work are embedded in the context of historical and recent works. Further relevant references are of course provided directly in the text throughout this thesis.

1.2.1 Micromechanics and homogenisation

The consideration of multiscale models gives rise to the need of appropriate *scale-bridging methods*. For the way from smaller to larger scales, this leads to the concept of upscaling and homogenisation methods. This work is rigorously based on the principles of continuum mechanics, such that even the smallest scales are still significantly larger than interatomic distances. There are methods that bridge the atomistic to continuum scales, such as the so-called quasi-continuum methods, see Tadmor et al. [469] as well as Tadmor & Miller [468] and Podio-Guidugli [372], but this is not the purpose in this work. Scale-bridging in multiscale continuum mechanics is closely linked to the term *(continuum) micromechanics*, which is often referred to Hill [211], see also Zaoui [524]. This term can be given the general meaning of describing methods which predict the large-scale material response on the basis of a direct modelling and incorporation of small-scale structures. The focus of this thesis is on the treatment of elasticity problems, which is reflected in the following literature review. However, most of these methods can be straightforwardly extended for the treatment of viscosity, plasticity, or general multiphysics problems.

Analytical homogenisation of linear-elastic materials The fundamental contributions of Voigt [495] and Reuss [398] can be considered as a starting point for the contemporary continuum-mechanical treatment of multiscale problems. They assumed equal deformations and equal stresses, respectively, in the heterogeneous small-scale structures and thereby provided rigorous upper and lower *bounds* for the effective macroscopic properties for certain material classes. In the context of polycrystals, the Voigt–Reuss-bounds

are also referred to as Taylor–Sachs bounds due to Taylor [475] and Sachs [412]. The formulation of optimal bounds and envelopes for the effective large-scale behaviour for classes of materials with specific small-scale characteristics is a fundamental auxiliary tool for the appraisal and validity check of homogenisation methods. Important contributions to this topic were provided by, for example, Francfort & Murat [132]. The fundamental basis of almost any sophisticated homogenisation method are the so-called *inclusion problems*, which aim to provide solutions for the effective behaviour to the problem of isolated inclusions embedded in an infinite matrix medium. First works by Einstein [114] considered rigid inclusions, whereas the outstanding work of Eshelby [122] generalised the problem to elastic ellipsoidal inclusions and represents an important ingredient of a lot of subsequent methods. Hashin & Shtrikman [185] provided a further milestone in the field by introducing a *variational procedure* for the estimation of effective properties and the concept of suitably chosen *polarisation fields* relative to a *homogeneous comparison material*. The thereon based *Hashin–Shtrikman upper and lower bounds* formulated by Hashin & Shtrikman [186, 187] significantly improve the Voigt–Reuss bounds. Further, the key concept of scale-bridging, be it in terms of the inclusion problem, the variational procedure or following nonlinear methods, is the existence of a suitable *representative volume element* and the consistent formulation of boundary conditions and admissible small-scale fields which satisfy the Hill macro-homogeneity condition due to Hill [214]. A further important class of analytical estimates is obtained by applying self-consistent schemes, formulated by, for example, Hershey [202], Kröner [264], Budiansky [62], and Hill [211]. While classical inclusion problems consider that the inclusions are surrounded by a matrix with prominent morphological role, the self-consistent schemes assume that the inclusions are embedded in the a priori unknown effective material itself and negate the occurrence of a distinct matrix. Closely related to this idea are the estimates by Hashin & Rosen [184] for composites with composite sphere assemblage microstructure and, in analogy to that, by Hashin [181] for composites with composite cylinder assemblage microstructure. Further, Mori & Tanaka [342] and Benveniste [31] provided estimates which approximate the self-consistent scheme well for specific scenarios but may deliver unphysical results in other cases.

Homogenisation of nonlinear materials The field of scale-bridging and homogenisation for materials with nonlinear material behaviour can be separated into the numerical methods and analytical methods. The former rely on the resolution and discretisation of the geometries and the solution of proper boundary-value problems on each considered length scale. This can be achieved by multiscale-finite-element-methods such as the ones proposed by Ghosh et al. [161], Smit et al. [447], Miehe et al. [330], Geers et al. [154], or Schröder [422]. Two-scale versions of these models are usually referred to as the FE^2-method. Besides that, Fourier-based methods, making use of fast Fourier transforms, were proposed by Moulinec & Suquet [345] and Michel et al. [327]. The formulation of appropriate boundary conditions for the small-scale problems satisfying the Hill macrohomogeneity condition is fundamental for all those numerical approaches. In the field of analytical homogenisation, a basic step was made by Ogden [360] in providing nonlinear versions of the Voigt–Reuss upper and lower bounds, which are applicable to finite elasticity. In the same spirit, the pioneering work of Willis [518] generalised the variational principles of Hashin & Shtrikman [185] to nonlinear elasticity. Doing so, a nonlinear heterogeneous material can be related to a homogeneous reference ma-

terial by utilising appropriate polarisation fields. This idea was further developed in the works of Talbot & Willis [472] and Willis [519]. Further, based on the introduction of new variational principles, Ponte Castañeda [374, 375] suggested the concept of a *linear heterogeneous comparison material* or *linear comparison composite*, see also Suquet [465] and Olson [365]. With this fundamental concept, the effective properties of a nonlinear heterogeneous material can be obtained from the homogenisation problem of a suitably chosen linear heterogeneous material. Thus, the above mentioned linear techniques keep their elementary importance and the ideas from there remain the core of a large number of nonlinear homogenisation methods. Moreover, Talbot & Willis [473] proposed a hybrid variational principle combining the polarisation fields of Willis [518] with the concept of the linear comparison composite of Ponte Castañeda [374], which in the elasticity case introduces the idea of a *linear thermoelastic comparison composite*. In view of some inherent restrictions and shortcomings of these variational principles, Ponte Castañeda [376] proposed a new variational homogenisation method which gave rise to a whole class of so-called *second-order methods*. The original version relied on the second-order Taylor expansion of the underlying nonlinear potentials and naturally resulted in the formulation of a linear thermoelastic comparison composite. This method was given a rigorous variational interpretation in the subsequent works of Ponte Castañeda & Willis [384] and Ponte Castañeda & Tiberio [382], which demonstrated that the principles represent a further generalisation of the hybrid method of Talbot & Willis [473]. The fact that the comparison composites are based on the tangent moduli of the nonlinear behaviour suggested their designation as *tangent second-order (TSO) methods*. An improved version for incompressible materials was presented by Avazmohammadi & Ponte Castañeda [19]. However, the tangent choice is only an approximation and the second-order methods were subsequently developed with the goal of finding optimal choices for the linear comparison composites. This led to the *generalised second-order (GSO) method* by Ponte Castañeda [377] and Lopez-Pamies & Ponte Castañeda [298, 299] as well as the most recent version, the *fully-optimised second-order (FO-SO) method* by Ponte Castañeda [379, 380] and Furer & Ponte Castañeda [147]. Second-order methods were successfully applied for the description of many different materials and microstructures. For fibre composites, Lahellec et al. [272] formulated second-order estimates for periodic microstructures with cylindrical fibres and incompressible phases, while Brun et al. [61] provided estimates for the same type of microstructures but considering compressible phases. For composites with *randomly* distributed cylindrical fibres and incompressible phases like the ones that are at the focus of this contribution, Agoras et al. [4] formulated accurate and easy-to-use second-order estimates for isotropic phases with generalised Neo-Hookean (I_1-based) strain-energy functions. Moreover, for composites with Neo-Hookean phases, deBotton et al. [92] provided an elegant estimate that is based on the sequentially laminated (SL) homogenisation procedure. Further, Lopez-Pamies & Idiart [297] generalised the results of deBotton et al. [92] and included an additional J_4-based anisotropic fibre energy contribution. However, none of these homogenisation methods is applicable if the phases exhibit *generally anisotropic* behaviour. In particular, we are not aware of any estimates for the effective response of hyperelastic composites with anisotropic matrix phase. Yet, such a scenario would be of great interest for biological materials, in which, for instance, aligned collageneous structures cause highly direction-dependent behaviour

in the matrix phase. By further noting that biological materials are usually assumed to be incompressible, we arrive at the following objectives and aspects:

- Formulation of analytical estimates for two-phase hyperelastic fibre composites with *random microstructures* and *anisotropic* phase behaviour
- Performing asymptotic analyses to obtain the consistent expressions of the estimate in the limits as fibre and matrix become *incompressible*
- Formulating a *constrained variational principle* for the description of incompressible inclusions by introducing an appropriate *Lagrange functional*
- Usage of *generic deformation gradients* for the case of transversely isotropic phases and a thereon based reduction of the homogenisation to solving for *four scalar unknowns*
- Demonstrating the consistent linearisation of the estimates by recovering corresponding linear-elastic estimates
- Providing closed-form analytical expressions for phases where the isotropic part is Neo-Hookean

Homogenisation of fibrous or chain-like networks Special scale-bridging and homogenisation methods are employed if the small-scale of a material can be modelled as a network of chains or fibres with a certain orientation in space. This is especially the case for two material classes: Rubber-like materials with their underlying structure of *polymer chain networks* and (soft) biological tissues which consist of certain collageneous network structures and different types of *collagen fibres*. For the case of rubber-like materials, this problem was discussed in the fundamental works of Treloar [481] and Treloar & Riding [483] and led to the formulation of the *full network model*, see also Wu & van der Giessen [522]. The essence of this multiscale modelling approach is the parametrisation of single chains in terms of spherical coordinates and the subsequent assignment of an energy potential for each space orientation. The homogenisation step represents an averaging procedure in terms of an integration over all space orientations. Conceptually the same method was proposed by Lanir [275, 276] for the modelling of collageneous fibre networks, however without referring to the earlier network models for rubber-like materials. A modelling approach which basically led to the same structure of equations is referred to as *microplane model*. It was formulated by Bažant & Oh [25] for concrete and was later generalised by Carol et al. [73]. Further terms for the network models used in the literature are the very natural designation *microsphere model*, formulated in the seminal work of Miehe et al. [329], as well as the pragmatic term *angular integration model*. The continuous distribution of chains (or fibres) over the space orientations is usually accounted for in a stochastical manner by means of a *orientation density function*. Rubber-like materials commonly have a uniform chain distribution, while the consideration of the nonuniform case is essential in collageneous tissues, which often show preferred alignments of fibres. If the continuous distributions degenerate to some discrete orientations, the network models simplify to formulations like the earlier published three-chain model of James & Guth [247] and Wang & Guth [505]. Moreover, the classical network models contain an affinity assumption for the deformation of the space orientations. In contrast, there also exist non-affine formulations, such as the variational-based non-affine microsphere model

by Miehe et al. [329], the homogenisation scheme based on a maximal advance path constraint by Tkachuk & Linder [477] as well as the models based on a variational energy relaxation by Chen et al. [76] and Govindjee et al. [170]. Moreover, certain discrete versions of network models have a non-affine character as well, such as the four-chain models of Flory & Rehner [131] and Treloar [480] and the eight-chain models of Arruda & Boyce [13] and Kroon [266]. In the field of biomechanics, full network have been successfully employed for the modelling of, for instance, tendons and ligaments by Hurschler et al. [234], articular cartilage by Federico & Herzog [127] and Ateshian et al. [15] as well as blood vessels by Alastrué et al. [7]. In a similar fashion, microplane models have been suggested by Caner & Carol [69] for blood vessels and Caner et al. [70] for the intervertebral disc. In this thesis, the use of a network model for the collageneous tissue in skeletal muscles encourages the investigation of *transversely isotropic distributions* of the collagen fibres. A theoretical investigation of this scenario consequently leads to the following investigations and extensions to the existing network models:

- Formulation of analytical expressions for the *macroscopically-driven fibre stretches* in affine network models
- Introduction of a fully *invariant-based formulation for affine network models* with transversely isotropic fibre distributions
- Implementation of high-order *Lebedev-* and *Sloan–Womersley*-type numerical quadrature schemes for the integration over the orientation space of the network model

Stochastical modelling of single chains/fibres and fibre bundles An elementary aspect in network models is the modelling of single chains and fibres. In line with the historical origin of the network models, the first elementary contributions treated the entropic-elastic nature of polymer chain molecules in rubber-like materials and lead to the formulations based on *Gaussian statistics* in the works of Kuhn [268, 269] and based on non-Gaussian *Langevin statistics* in the works of Kuhn & Grün [270] and James & Guth [247]. Those concepts rely on the composition of the single polymer chains out of highly uncorrelated rigid bonds, which serves well for the description of rubbers. For the characterisation of collagen fibres, the occurrence of higher correlated bonds in the underlying collagen molecules suggested the use of concepts like the *worm-like chain model* by Kratky & Porod [261] and its development by Marko & Siggia [315]. Network models for soft biological tissue based on a worm-like chain description of collagen fibres were for example proposed by Garikipati et al. [149], Kuhl et al. [267], Alastrué et al. [7], and Menzel & Waffenschmidt [321]. However, it was pointed out by Buehler & Wong [64] and Garikipati et al. [150], amongst others, that the purely entropic elasticity description of the worm-like chain model is not able to capture the energy-elastic behaviour of collagen fibres at higher stretches, where the initially highly crimped collagen fibres become straight and the stretch-based energetic elasticity becomes dominant in comparison to the bending-based entropic elasticity. Hence, alternative models for collagen fibres were proposed, such as the elastica-based model of Garikipati et al. [150], a microstructurally-based approach by Grytz & Meschke [172] as well as the comprehensive multiscale approach by Maceri et al. [306] which couples the nano-, micro-, and macroscale. Further, studies linking the atomistic and continuum scales were

performed by Buehler [63] and Gautieri et al. [152]. Those studies consider the whole deformation process of collagen fibres including bending stiffness at lower, stretching stiffness at higher stretches and the transition in between. However, a reasonable assumption is to neglect the bending contributions and to solely account for the stretching stiffness in terms of a spring-like quadratic energy potential which comes into play when the fibre deformation exceeds a certain threshold stretch at which the fibres become fully uncurled. Such formulations were proposed by, for example, Lake & Armeniades [273], Decraemer et al. [93] as well as Lanir [275, 276]. These energetic energy formulations are usually accompanied with stochastical descriptions for the threshold stretch distribution in terms of a *undulation (or waviness) distribution function*. This concept can be interpreted either as a description of an actual aggregate of several fibres, a fibre bundle, with different threshold stretches or as the appropriate ensemble average of a space orientation in network models in line with the concept of a representative volume element. A variety of well-known probability functions has been suggested for the definition of undulation distributions, such as, for instance, the beta distribution by Avazmohammadi et al. [18], Chen et al. [76], Gindre et al. [163], Lokshin & Lanir [294], Sverdlik & Lanir [467], Weisbecker et al. [510], the gamma distribution by Sacks [413] and Bischoff [36], or the Weibull distribution by Hurschler et al. [234]. The incorporation of such probability functions naturally leads to an integral formulation, which eventually leads to some cumbersome expressions in combination with network models, since this leads to triple integrals. In order to overcome this aspect, this thesis has the following aims:

- Reformulation of the integral expressions for the stochastical modelling of space orientations with undulation distribution functions into *convolution-based expressions*
- Derivation of *novel stochastical-based fibre energies* based on closed-form solutions of the convolution expressions for *beta- and triangularly distributed fibre undulations*

1.2.2 Continuum biomechanics and muscle modelling

The field of continuum biomechanics covers a huge variety of subdisciplines and applications, of which this thesis treats the special field of soft tissue mechanics and particularly skeletal muscle modelling. Pioneering contributions in this field are the early works of Fung [142, 146], in which he showed the characteristic *J-shaped* relationship between tensile strain and the associated stress in soft biological tissues and gave first overviews on possible applications and possibilities of biomechanical investigations, respectively. Thereby, the J-shaped strain-stress relationship with its flat toe region at lower strains and the stiffening effect at higher strains is typical for a majority of soft tissues and loading scenarios and shows up across different possible observations scales. Presumably, Fung's magnum opus [145] on the mechanics of living tissues and the follow-up textbook [143] represent the most comprehensive overviews on the various biomechanical applications. However, as discussed in the very interesting review article of Humphrey [232], the developments in modern continuum biomechanics go hand in hand with the general concurrent progress in finite (in)elasticity theory.

Muscle modelling In the field of skeletal muscle modelling, much credit should be given to the pioneering work of Hill [207] which established the field of the so-called

Hill-type muscle models. As also outlined in the comprehensive review paper of Zajac [523], such models have a one-dimensional character. The extension of those models to three-dimensional formulations is strongly connected to the developments in the theory of fibre-reinforced materials, as presented in the seminal works of Spencer [455, 457] and further works by, for instance, Weiss et al. [511] and Qiu & Pence [393]. Subsequently, three-dimensional, transversely-isotropic models, which assume that the muscle fibres exhibit a reinforcing characteristic, were proposed by, for instance, Martins et al. [319], Johansson et al. [249], Oomens et al. [367], Blemker et al. [47], Röhrle et al. [407], Röhrle & Pullan [408], Böl et al. [54], Ehret et al. [112], Heidlauf & Röhrle [193], and Sharifimajd & Stålhand [435]. Moreover, the very special feature of skeletal muscles is their ability to convert chemical into mechanical energy due to neural stimulations. This is commonly referred to as active behaviour and various ways have been suggested for the incorporation of this behaviour into continuum-mechanical models. A pragmatic approach is the introduction of an additional stress contribution which represents the active behaviour. This is commonly referred to as *active stress approach*. An alternative method is based on a multiplicative decomposition of the deformation gradient into elastic and inelastic parts, which was originally proposed by Lee & Liu [281] in the field of elastoplasticity. By considering the inelastic part as the active muscle contribution, so-called *active strain models* were proposed by, for example, Kondaurov & Nikitin [257], Martins et al. [318], Nardinocchi & Teresi [349], Stålhand et al. [462], Hernández-Gascón et al. [201], Göktepe et al. [164], and Pezzuto et al. [370]. In both approaches, the active contributions can either have a macroscopic constitutive character or can incorporate detailed multiscale activation dynamics. The latter models are usually based on the pioneering works of Hodgkin & Huxley [216] on the modelling of the electrical behaviour of the membrane of excitable cells and Huxley [235] on the cross-bridge theory, which explains the mechanism in the sarcomeres during activation. Comprehensive models which incorporate such multiscale activation dynamics and coupled chemo-electro-mechanical effects were formulated by, for instance, Röhrle et al. [407] and Heidlauf & Röhrle [193]. Much more references and details on the microscopic activation dynamics and muscle modelling in general can be found in the review papers of Smith et al. [453] and Röhrle et al. [409].

Multiscale approaches in biomechanics Multiscale continuum-mechanical approaches, which link small-scale structures with the macroscopic material response, have been proposed for numerous biological tissues and applications. For example, Hurschler et al. [234] proposed a multiscale model for tendons and ligaments, Marino & Wriggers [314] for tendons, Maceri et al. [306], Chen et al. [76], Marino & Vairo [312] for general collageneous and fibrous tissues, Maceri et al. [307] for arterial walls, Ricken et al. [400] for the liver, and Ehlers & Wagner [110] for the brain. Furthermore, the microstructural effects of osteoarthritis in cartilage were studied by Mabuma et al. [305], multiphase bone-cement injection processes by Bleiler et al. [46], and the incorporation of the mechanical behaviour of the giant protein titin into the overall behaviour of skeletal muscle tissue was investigated by Heidlauf et al. [192]. The majority of multiscale investigations on the mechanical behaviour of biological tissues is based on the description of the underlying protein structures. It is due to protein, in particular collagen networks and structures, that biological tissues often show a highly hierarchical structure with clear construction across the scales, as outlined by Fratzl &

Weinkamer [135]. Such hierarchical structures can be detected in soft as well as in hard biological tissues, such that multiscale studies have also been frequently suggested, for example, for bone tissue, see Hellmich et al. [199] or Reisinger et al. [397]. In the field of skeletal muscle modelling, multiscale approaches for the description of the mechanical behaviour have been rarely used. However, such models have a high potential to significantly improve this field of research. For example, it would be beneficial to have multiscale models which predict the macroscopic material symmetry properties in a *bottom-up* characteristic solely based on the responsible small-scale structures, since recent material tests by Takaza et al. [471], Böl et al. [53] as well as Mohammadkhah et al. [338] provided experimental evidence that the theory of fibre-reinforced materials is an inappropriate framework for the macroscopic modelling of skeletal muscles. Basically all of the few multiscale muscle models at hand follow the basic idea of describing the muscle as a two-phase material consisting of muscle fibres and collageneous tissue. This is essentially what Fung [145, ch. 9] proposed in his fundamental book on biomechanics. Based on this, a continuum-mechanical multiscale muscle model was proposed by Spyrou et al. [459] and further developed by Spyrou et al. [460]. However, a major drawback of these studies is the very simple description of the collageneous network which does not account for general loading conditions. This is also the case for the structural model of Gindre et al. [163], which is in addition to that not consistently formulated within the framework of continuum mechanics. Furthermore, purely microscale-based studies without multiscale characteristic were proposed by Sharafi & Blemker [434] and Virgilio et al. [494]. Hence, in order to improve the field of muscle modelling and to overcome limitations of existing approaches, first versions for a comprehensive multiscale muscle model based on analytical homogenisation methods were given in a series of proceedings by Bleiler et al. [40, 41, 42, 43]. These studies were followed by Bleiler et al. [44], in which a first complete version of a novel microstructurally-based muscle model was presented. The detailed derivation of this model based on the previous general explanations about multiscale modelling is one main goal of this work. This includes:

- Introduction of a *novel multiscale continuum-mechanical modelling framework* for the description of skeletal muscle tissue
- Usage of this framework to formulate a *novel microstructurally-based two-phase model* of the passive behaviour of skeletal muscle tissue
- Introduction of a detailed *fibre network model for the extracellular matrix* based on the parametrisation of the helical fibre arrangement of the collageneous tissues in muscles
- Deriving effective macroscopic energies and stresses based on an affine Voigt-type and a non-affine TSO-based approach
- Providing a comprehensive literature review on the microstructurally-based model parameters
- Showing the capabilities of the model to predict the anisotropic characteristics of skeletal muscle tissue observed in experiments *without applying constitutive assumptions on the macroscale*

1.3 Outline of this thesis

Following this introductory chapter, this thesis is structured as follows.

Part I introduces the basic concepts and fundamentals of *continuum mechanics and material theory*.
Chapter 2 provides the basic knowledge on the large-strain kinematical description of a continuous, deformable body and appropriate deformation and strain measures. This is followed by the introduction of the concept of stress and the material-independent physical balance relations.
These explanations are continued in **Chapter 3**, where we present the basics of material theory and outline the process of constitutive modelling in continuum mechanics. The chapter starts with the formulation of the basic boundary-value problem of continuum mechanics and introduces the constitutive framework as well as the resulting restrictions upon the constitutive equations obtained from basic thermodynamical principles. This is followed by further topics, such as the discussion of variational principles in continuum mechanics, the invariant theory, linearisation conditions and some examples for analytical strain-energy functions.

Part II is concerned with the field of *continuum micromechanics* and the concepts of *multiscale modelling and homogenisation*.
The basic concepts of multiscale modelling and, in particular, the formulation of different scales, are introduced in **Chapter 4**. It directly builds up on Part I and transfers the kinematical and constitutive concepts to the multiscale framework, which means that separate boundary-value problems are formulated on the micro- and the macroscale. This is followed by explanations on the statistical description of the microstructure of a material. Further, the scales are connected by means of an appropriate *scale transition* of the deformation and stress measures and an *extremum principle* for the effective energy on the macroscopic scale is introduced.
In **Chapter 5**, we present *estimates for the effective strain energy of a hyperelastic composite* in the pre-bifurcation state by means of the tangent second-order homogenisation method. After a general formulation of the method, the estimate is specialised to the description of two-phase fibre composites with random microstructures and incompressible, anisotropic phase behaviour. In this context, asymptotic analyses are carried out to obtain the consistent expressions of the estimate in the incompressible limits of the two phases. Further estimates for some specific composite types are presented in **Appendix C**.
In **Chapter 6**, basic concepts and associated homogenisation techniques for *fibrous or chain-like networks* are discussed. This is essential for the treatment of collageneous tissues.

Part III introduces a novel *multiscale framework for the microstructurally-based modelling of skeletal muscle tissue*. Subsequently, the muscle fibres and the extracellular matrix are identified as the two most important structural components of the muscle and a two-phase model is formulated.
A detailed discussion of the relevant scales and the microstructural characterisation of skeletal muscle tissue is provided in **Chapter 7**. This is followed by the *constitutive modelling of the two phases*. In particular, a detailed fibre network model for the extracellular matrix based on the parametrisation of the helical fibre arrangement of the collageneous tissues is introduced. This is followed by the derivation of effective macroscopic energies

and stresses based on an affine Voigt-type and a non-affine TSO-based approach.
In **Chapter 8**, we provide a *comprehensive literature review on the microstructurally-based model parameters* and *show the capabilities of the model* to predict the anisotropic characteristics of skeletal muscle tissue observed in experiments without applying constitutive assumptions on the macroscale.

Chapter 9 concludes this thesis and presents an outlook on possible applications and future extensions of the discussed methods.

Moreover, basics on the herein applied mathematical notation, basic rules of tensor calculus and further mathematical topics and details that complement the explanations in this thesis are provided in **Appendix A** and **Appendix B**. Further remarks and results on the tangent second-order homogenisation estimates presented in Chapter 5 are given in **Appendix C**.

Part I

Continuum Mechanics

2 Fundamentals of Continuum Mechanics

This chapter introduces the basic concepts of continuum mechanics, in particular the material-independent kinematical relations and balance principles. In this regard, continuum mechanics represents a three-dimensional field theory for the description of deformable bodies. A complete review of the field is not the scope of this chapter, it rather provides the fundamentals to the extent required for the remainder of this work. More comprehensive overviews can be found, for example, in the textbooks of Truesdell [488], Truesdell & Noll [490], Ogden [362], Smith [448], Marsden & Hughes [316], Holzapfel [221], and the references therein.

2.1 Kinematics

Starting point is the description of the kinematical relations and geometric mappings of a material body $\mathscr{B}$ that is subject to finite deformations and strains. Thereby, the material body represents a physical object and is mathematically described as a coherent manifold of an infinite number of particles (or material points) $\mathscr{P} \in \mathscr{B}$.

2.1.1 Motion of a body

At a certain time $t \in \mathscr{T} = [t_\mathrm{A}, t_\Omega] \subseteq \mathcal{R}_+$, the material body $\mathscr{B}$ occupies a Euclidian space $\mathcal{B}_t \subset \mathcal{R}^3$, which is called a *configuration* of the body. The bijective placement

$$\boldsymbol{\mathscr{X}}_t : \left\{ \begin{array}{l} \mathscr{B} \times \mathscr{T} \;\rightarrow\; \mathcal{B}_t \subset \mathcal{R}^3 \\ \mathscr{P} \;\mapsto\; \boldsymbol{x} \,=\, \boldsymbol{\mathscr{X}}_t(\mathscr{P}) \end{array} \right. \tag{2.1}$$

maps each particle $\mathscr{P} \in \mathscr{B}$ of the material body to a Euclidian point $\boldsymbol{x} \in \mathcal{B}_t$. A sequence of configurations, parametrised by the time t, describes the *motion* of the material body. It proves useful to define an arbitrary *reference configuration* $\mathcal{B}_0$ at time t_0 and the according reference placement

$$\boldsymbol{\mathscr{X}}_0 : \left\{ \begin{array}{l} \mathscr{B} \;\rightarrow\; \mathcal{B}_0 \subset \mathcal{R}^3 \\ \mathscr{P} \;\mapsto\; \boldsymbol{X} \,=\, \boldsymbol{\mathscr{X}}_0(\mathscr{P}) \,, \end{array} \right. \tag{2.2}$$

which allows to identify each particle $\mathscr{P}$ by its reference position vector $\boldsymbol{X}$. Since $\boldsymbol{\mathscr{X}}_0$ inherits from $\boldsymbol{\mathscr{X}}_t$ the property of being a bijective map, we are able to identify the material point $\mathscr{P} = \boldsymbol{\mathscr{X}}_0^{-1}(\boldsymbol{X})$ by its referential position using the inverse map $\boldsymbol{\mathscr{X}}_0^{-1}$. In addition to the reference configuration, one designates a *current or actual configuration* $\mathcal{B}$ at time t and introduces the placement

$$\boldsymbol{\chi} : \left\{ \begin{array}{l} \mathcal{B}_0 \times \mathscr{T} \;\rightarrow\; \mathcal{B} \subset \mathcal{R}^3 \\ (\boldsymbol{X}, t) \;\mapsto\; \boldsymbol{x} \,=\, \boldsymbol{\chi}(\boldsymbol{X}, t) \,, \end{array} \right. \tag{2.3}$$

as the *deformation map* from the reference to the current configuration. The placement $\boldsymbol{\chi}$ has the essential feature of mapping material points $\mathscr{P}$ from their referential position $\boldsymbol{X}$ in $\mathcal{B}_0$ to their respective current position $\boldsymbol{x}$ in $\mathcal{B}$ and is thus referred to as *point map*. The inverse deformation $\boldsymbol{\chi}^{-1}$ allows to identify the referential position $\boldsymbol{X} = \boldsymbol{\chi}^{-1}(\boldsymbol{x}, t)$ of a particle by means of its current position $\boldsymbol{x}$. Moreover, quantities living in the reference

configuration are often labelled as *material* or *Lagrangean* whereas quantities in the current configuration are labelled as *spatial* or *Eulerian*. We further want to introduce the difference between current position $\boldsymbol{x}$ and the referential position $\boldsymbol{X}$ as the *displacement vector* $\boldsymbol{u} = \boldsymbol{x} - \boldsymbol{X}$.

2.1.2 The deformation gradient

The placement $\boldsymbol{\chi}(\boldsymbol{X}, t)$ provides the map of material points $\mathscr{P}$ and, thus, of the material body $\mathscr{B}$ between the reference and the current configuration. In addition to that, knowledge about further geometric mapping mechanisms beyond the point map are of interest. Therefore, the gradient of the placement $\boldsymbol{\chi}(\boldsymbol{X}, t)$ with respect to the reference position $\boldsymbol{X}$ is introduced as the second-order tensor

$$\boldsymbol{F}(\boldsymbol{X}, t) := \frac{\partial \boldsymbol{\chi}(\boldsymbol{X}, t)}{\partial \boldsymbol{X}} = \nabla_{\boldsymbol{X}} \boldsymbol{\chi}(\boldsymbol{X}, t) = \mathrm{Grad}[\boldsymbol{\chi}(\boldsymbol{X}, t)] \,. \tag{2.4}$$

It is referred to as the *deformation gradient*. In (2.4), the notations $\nabla_{\boldsymbol{X}}(\cdot)$ and $\mathrm{Grad}[(\cdot)]$ denote the gradient of a quantity $(\cdot)$ with respect to reference positions $\boldsymbol{X}$. The deformation gradient is the key quantity for the description of local deformations in finite-strain kinematics and will further play an essential role in scale-transition approaches of mechanical quantities in Part II. Since the deformation map[1] $\boldsymbol{\chi}$ is bijective, the deformation gradient $\boldsymbol{F}$ has to be invertible and entails the condition $J := \det[\boldsymbol{F}] \neq 0$. Therein, the common notation J for $\det[\boldsymbol{F}]$ refers to its designation as the *Jacobian*. For the initial state at time $t = t_0$, the current and reference configurations coincide, which means that

$$\boldsymbol{F}\big|_{t=t_0} = \mathrm{Grad}[\boldsymbol{X}] = \boldsymbol{I} \quad \text{and} \quad \det[\boldsymbol{F}]\big|_{t=t_0} = \det[\boldsymbol{I}] = 1 \,. \tag{2.5}$$

Thus, the non-zero requirement for the (continuous) Jacobian is strengthened to the condition

$$J = \det[\boldsymbol{F}] > 0 \,. \tag{2.6}$$

It is further remarked that the deformation gradient $\boldsymbol{F}$ excludes information on rigid-body translations, which becomes obvious when formulating a general deformation map $\boldsymbol{\chi}(\boldsymbol{X}, t) = \boldsymbol{f}(\boldsymbol{X}, t) + \boldsymbol{c}(t)$. Then, it can be seen that only the $\boldsymbol{X}$-dependent part $\boldsymbol{f}$ contributes to the deformation gradient, while for the constant translation $\mathrm{Grad}[\boldsymbol{c}] = \boldsymbol{0}$.

Tangent and line map The natural feature of the deformation gradient is to transform material tangent or line elements to their spatial counterparts. To demonstrate this, a material curve $\hat{\boldsymbol{C}}(\vartheta) \subset \mathcal{B}_0$ and the according spatial curve $\hat{\boldsymbol{c}}(\vartheta, t) \subset \mathcal{B}$ are defined, both parametrised by and being differentiable with respect to a parameter $\vartheta \in \mathcal{R}$. It is then straightforward to introduce a material tangent vector $\hat{\boldsymbol{T}} = \mathrm{d}\hat{\boldsymbol{C}}(\vartheta)/\mathrm{d}\vartheta$ to the material curve $\hat{\boldsymbol{C}}(\vartheta)$ as well as the spatial tangent vector $\hat{\boldsymbol{t}} = \mathrm{d}\hat{\boldsymbol{c}}(\vartheta, t)/\mathrm{d}\vartheta$ to the spatial curve $\hat{\boldsymbol{c}}(\vartheta, t)$. If material and spatial curves refer for identical ϑ to the same particle $\mathscr{P}$, they are linked by $\hat{\boldsymbol{c}}(\vartheta, t) = \boldsymbol{\chi}(\hat{\boldsymbol{C}}(\vartheta), t)$. By consulting the chain rule and recalling that $\boldsymbol{X} = \hat{\boldsymbol{C}}(\vartheta)$ at a fixed ϑ, the spatial tangent vector can be formulated as

$$\hat{\boldsymbol{t}}(\boldsymbol{X}, t) = \frac{\mathrm{d}\hat{\boldsymbol{c}}(\vartheta, t)}{\mathrm{d}\vartheta} = \frac{\mathrm{d}\boldsymbol{\chi}(\hat{\boldsymbol{C}}(\vartheta), t)}{\mathrm{d}\vartheta} = \mathrm{Grad}[\boldsymbol{\chi}(\boldsymbol{X}, t)] \, \frac{\mathrm{d}\hat{\boldsymbol{C}}(\vartheta)}{\mathrm{d}\vartheta} = \boldsymbol{F}(\boldsymbol{X}, t) \, \hat{\boldsymbol{T}}(\boldsymbol{X}) \,. \tag{2.7}$$

[1] It shall be remarked that the deformation map $\boldsymbol{\chi}(\boldsymbol{X}, t)$ and quantities based on the map, like the deformation gradient $\boldsymbol{F}(\boldsymbol{X}, t)$, are generally dependent on the reference position $\boldsymbol{X}$ and the time t. However, the arguments are omitted for the sake of a compact notation when there is no danger of uncertainty.

Thus, the deformation gradient acts as a *tangent map*:

$$\boldsymbol{F} : \begin{cases} T_{\boldsymbol{X}}\mathcal{B}_0 \rightarrow T_{\boldsymbol{x}}\mathcal{B} \\ \hat{\boldsymbol{T}} \mapsto \hat{\boldsymbol{t}} = \boldsymbol{F}\,\hat{\boldsymbol{T}}\,, \end{cases} \tag{2.8}$$

where $T_{\boldsymbol{X}}\mathcal{B}_0$ and $T_{\boldsymbol{x}}\mathcal{B}$ denote tangent spaces of the material and the spatial domain, respectively. Considering a slightly different notation, the tangent vectors $\hat{\boldsymbol{T}}$ and $\hat{\boldsymbol{t}}$ can be related to infinitesimal line elements $\mathrm{d}\boldsymbol{X}$ and $\mathrm{d}\boldsymbol{x}$ in the reference and the current configuration, respectively. With this, together with the invertibility of $\boldsymbol{F}$, the tangent map can be formulated as the classical covariant *push-forward* and *pull-back* transformations of line elements:

$$\mathrm{d}\boldsymbol{x} = \boldsymbol{F}\,\mathrm{d}\boldsymbol{X} \quad \text{and} \quad \mathrm{d}\boldsymbol{X} = \boldsymbol{F}^{-1}\,\mathrm{d}\boldsymbol{x}\,. \tag{2.9}$$

Normal map The material surface $\hat{S}(\boldsymbol{X}) = c \subset \mathcal{B}_0$ is introduced as a level set with c being a constant scalar value. An according spatial surface $\hat{s}(\boldsymbol{x}) = c \subset \mathcal{B}$ shall refer to the same level set and is obtained via the deformation map $\boldsymbol{\chi}$, hence, $\hat{s}(\boldsymbol{x}) = \hat{s}(\boldsymbol{\chi}(\boldsymbol{X}, t))$. Through use of standard vector calculus, surface normal vectors are given by the gradient of a level set and we can define the material normal vector $\hat{\boldsymbol{N}} = \mathrm{Grad}[\hat{S}(\boldsymbol{X})]$ and the spatial normal vector $\hat{\boldsymbol{n}} = \mathrm{grad}[\hat{s}(\boldsymbol{x})]$, where $\mathrm{grad}[(\cdot)] = \partial(\cdot)/\partial\boldsymbol{x}$ is the derivative of $(\cdot)$ with respect to the current position $\boldsymbol{x}$. Using the chain rule, one obtains

$$\begin{aligned} \hat{\boldsymbol{n}}(\boldsymbol{X}, t) &= \mathrm{grad}[\hat{s}(\boldsymbol{x})] = \mathrm{grad}[\hat{s}(\boldsymbol{\chi}(\boldsymbol{X}, t))] = \mathrm{grad}[\hat{S}(\boldsymbol{X})] \\ &= \mathrm{grad}^{\,T}[\boldsymbol{X}]\,\mathrm{Grad}[\hat{S}(\boldsymbol{X})] = \boldsymbol{F}^{-T}(\boldsymbol{X}, t)\,\hat{\boldsymbol{N}}(\boldsymbol{X})\,, \end{aligned} \tag{2.10}$$

where $\mathrm{grad}[\boldsymbol{X}] = \nabla_{\boldsymbol{x}}\boldsymbol{X} = (\partial\boldsymbol{x}/\partial\boldsymbol{X})^{-1}$ is identified as the inverse deformation gradient $\boldsymbol{F}^{-1}$. With this, the *normal map* is given by

$$\boldsymbol{F}^{-T} : \begin{cases} T^*_{\boldsymbol{X}}\mathcal{B}_0 \rightarrow T^*_{\boldsymbol{x}}\mathcal{B} \\ \hat{\boldsymbol{N}} \mapsto \hat{\boldsymbol{n}} = \boldsymbol{F}^{-T}\,\hat{\boldsymbol{N}}\,, \end{cases} \tag{2.11}$$

where $T^*_{\boldsymbol{X}}\mathcal{B}_0$ and $T^*_{\boldsymbol{x}}\mathcal{B}$ denote cotangent (dual) spaces of the material and the spatial domain, respectively. The map (2.11) represents a contravariant push-forward transformation, whereas the associated contravariant pull-back transport is given by $\hat{\boldsymbol{N}} = \boldsymbol{F}^T\hat{\boldsymbol{n}}$.

Area map At the intersection of two material curves, $\hat{\boldsymbol{C}}_{(1)}(\vartheta) \subset \mathcal{B}_0$ and $\hat{\boldsymbol{C}}_{(2)}(\vartheta) \subset \mathcal{B}_0$, the cross product of their respective tangent vectors $\hat{\boldsymbol{T}}_{(1)}$ and $\hat{\boldsymbol{T}}_{(2)}$ defines a material vector $\mathrm{d}\boldsymbol{A} = \hat{\boldsymbol{T}}_{(1)} \times \hat{\boldsymbol{T}}_{(2)}$ of an infinitesimal area element. Subsequently, a spatial area vector is given by $\mathrm{d}\boldsymbol{a} = \hat{\boldsymbol{t}}_{(1)} \times \hat{\boldsymbol{t}}_{(2)}$ as the cross product of the spatial tangent vectors $\hat{\boldsymbol{t}}_{(1)}$ and $\hat{\boldsymbol{t}}_{(2)}$. By use of the tangent map (2.8) and the very elegant notation of the double (tensor) cross product, see Appendix A.4, one obtains

$$\mathrm{d}\boldsymbol{a} = \hat{\boldsymbol{t}}_{(1)} \times \hat{\boldsymbol{t}}_{(2)} = \boldsymbol{F}\hat{\boldsymbol{T}}_{(1)} \times \boldsymbol{F}\hat{\boldsymbol{T}}_{(2)} = \tfrac{1}{2}\,(\boldsymbol{F} \gg\!\ll \boldsymbol{F})\,(\hat{\boldsymbol{T}}_{(1)} \times \hat{\boldsymbol{T}}_{(2)}) = \mathrm{cof}[\boldsymbol{F}]\,\mathrm{d}\boldsymbol{A}\,, \tag{2.12}$$

and the cofactor $\mathrm{cof}[\boldsymbol{F}] = (\boldsymbol{F} \gg\!\ll \boldsymbol{F})/2$ of the deformation gradient is identified as the *area map*. The push-forward and pull-back transformations of area elements are thus given by

$$\mathrm{d}\boldsymbol{a} = \mathrm{cof}[\boldsymbol{F}]\,\mathrm{d}\boldsymbol{A} \quad \text{and} \quad \mathrm{d}\boldsymbol{A} = \mathrm{cof}[\boldsymbol{F}]^{-1}\,\mathrm{d}\boldsymbol{a}\,. \tag{2.13}$$

Volume map Considering now the intersection of three material curves, $\hat{\boldsymbol{C}}_{(i)}(\vartheta) \subset \mathcal{B}_0$ with $i = 1, 2, 3$, an infinitesimal material volume element $\mathrm{d}V = (\hat{\boldsymbol{T}}_{(1)} \times \hat{\boldsymbol{T}}_{(2)}) \cdot \hat{\boldsymbol{T}}_{(3)}$ is defined as the scalar triple product of the three associated material tangent vectors $\hat{\boldsymbol{T}}_{(i)}$. In analogy, a spatial volume element $\mathrm{d}v = (\hat{\boldsymbol{t}}_{(1)} \times \hat{\boldsymbol{t}}_{(2)}) \cdot \hat{\boldsymbol{t}}_{(3)}$ is formulated in terms of the scalar triple product of spatial tangent vectors $\hat{\boldsymbol{t}}_{(i)}$. Using once more the tangent map (2.8) and the double cross product notation yields the relation

$$\begin{aligned} \mathrm{d}v &= (\hat{\boldsymbol{t}}_{(1)} \times \hat{\boldsymbol{t}}_{(2)}) \cdot \hat{\boldsymbol{t}}_{(3)} = (\boldsymbol{F}\hat{\boldsymbol{T}}_{(1)} \times \boldsymbol{F}\hat{\boldsymbol{T}}_{(2)}) \cdot \boldsymbol{F}\hat{\boldsymbol{T}}_{(3)} \\ &= \tfrac{1}{6}\,[(\boldsymbol{F} \gg\!\ll \boldsymbol{F}) \cdot \boldsymbol{F}]\,(\hat{\boldsymbol{T}}_{(1)} \times \hat{\boldsymbol{T}}_{(2)}) \cdot \hat{\boldsymbol{T}}_{(3)} = \det[\boldsymbol{F}]\,\mathrm{d}V \end{aligned} \tag{2.14}$$

and the determinant $\det[\boldsymbol{F}] = [(\boldsymbol{F} \gg\!\ll \boldsymbol{F}) \cdot \boldsymbol{F}]/6$ of the deformation gradient is identified as the *volume map*. Thus, the push-forward and pull-back transformations for infinitesimal volume elements are given by

$$\mathrm{d}v = \det[\boldsymbol{F}]\,\mathrm{d}V \quad \text{and} \quad \mathrm{d}V = \det[\boldsymbol{F}]^{-1}\,\mathrm{d}v\,, \tag{2.15}$$

respectively. Material interpenetration and unphysical deformations are excluded through restriction (2.6).

2.1.3 The Cauchy–Green tensors, stretch, and shear

After having introduced the tangent and line map, it is of interest to formulate measures which quantify the deformation. To do so, we first consider the scalar product of two spatial line elements $\mathrm{d}\boldsymbol{x}$ and make use of the line map (2.9):

$$\mathrm{d}\boldsymbol{x} \cdot \mathrm{d}\boldsymbol{x} = \boldsymbol{F}\,\mathrm{d}\boldsymbol{X} \cdot \boldsymbol{F}\,\mathrm{d}\boldsymbol{X} = \mathrm{d}\boldsymbol{X} \cdot \boldsymbol{F}^T\boldsymbol{F}\,\mathrm{d}\boldsymbol{X} =: \mathrm{d}\boldsymbol{X} \cdot \boldsymbol{C}\,\mathrm{d}\boldsymbol{X} \quad \rightarrow \quad \boldsymbol{C} = \boldsymbol{F}^T\boldsymbol{F}\,. \tag{2.16}$$

Therein, the second-order tensor $\boldsymbol{C} \in \mathcal{SYM}(3)$ is introduced as the *right Cauchy–Green deformation tensor*, where $\mathcal{SYM}$ is the class of symmetric tensors. In a similar fashion, starting with the square $\mathrm{d}\boldsymbol{X} \cdot \mathrm{d}\boldsymbol{X}$ of material line elements, the *left* Cauchy–Green tensor $\boldsymbol{B} = \boldsymbol{F}\boldsymbol{F}^T \in \mathcal{SYM}(3)$ is presented. For physical reasons, the Cauchy–Green tensors are positive definite. In addition to rigid-body translations, which are already disregarded by the deformation gradient, the Cauchy–Green tensors exclude contributions from rigid-body rotations as well. This is easy to show by considering the deformation gradient $\boldsymbol{F}$ to be a pure rotation tensor $\boldsymbol{R} \in \mathcal{SO}(3)$, where $\mathcal{SO}(3)$ is the special orthogonal group and implies that $\boldsymbol{R}^{-1} = \boldsymbol{R}^T$ and $\det[\boldsymbol{R}] = 1$. Then, $\boldsymbol{C} = \boldsymbol{F}^T\boldsymbol{F} = \boldsymbol{R}^T\boldsymbol{R} = \boldsymbol{R}^{-1}\boldsymbol{R} = \boldsymbol{I}$ and, equivalently, $\boldsymbol{B} = \boldsymbol{R}\,\boldsymbol{R}^T = \boldsymbol{R}\,\boldsymbol{R}^{-1} = \boldsymbol{I}$. This shows that the Cauchy–Green tensors have for pure rotations at any time t the same value than for the reference state at t_0. This feature makes these deformation measures well-suited as a basis for stress calculations.

Stretch To quantify the local deformation in a certain direction of the material body $\mathscr{B}$, the length $|\hat{\boldsymbol{t}}| = |\boldsymbol{F}\hat{\boldsymbol{T}}|$ of a spatial tangent vector $\hat{\boldsymbol{t}}$ is related to the reference length $|\hat{\boldsymbol{T}}|$ of the associated material vector $\hat{\boldsymbol{T}}$. If $\hat{\boldsymbol{T}}$ is assumed to be a unit vector with $|\hat{\boldsymbol{T}}| = 1$, we can introduce the *stretch*

$$\begin{aligned} \lambda(\boldsymbol{X}, t; \hat{\boldsymbol{T}}) = \lambda_{\hat{\boldsymbol{T}}}(\boldsymbol{X}, t) &:= |\hat{\boldsymbol{t}}(\boldsymbol{X}, t)| = \|\hat{\boldsymbol{t}}(\boldsymbol{X}, t)\|_2 \\ &= \sqrt{\hat{\boldsymbol{t}}(\boldsymbol{X}, t) \cdot \hat{\boldsymbol{t}}(\boldsymbol{X}, t)} = \sqrt{\hat{\boldsymbol{T}}(\boldsymbol{X}) \cdot \boldsymbol{C}(\boldsymbol{X}, t)\,\hat{\boldsymbol{T}}(\boldsymbol{X})} \end{aligned} \tag{2.17}$$

in direction $\hat{\boldsymbol{T}}$ at the reference position $\boldsymbol{X}$ and time t as Euclidian norm of the spatial vector $\hat{\boldsymbol{t}}$. Note that no difference will be made between the notations $\lambda_{\hat{\boldsymbol{T}}}$ and $\lambda_{\hat{\boldsymbol{t}}}$. It is visible from (2.17) that the right Cauchy–Green tensor $\boldsymbol{C}$ is involved in the calculation of the stretch λ. This is not surprising when recalling that $\boldsymbol{C}$ was introduced in (2.16) by means of the square of line elements, which resembles a squared stretch. Consequently, the stretch inherits from $\boldsymbol{C}$ the independence on rigid-body deformations (translations *and* rotations). It is common to differentiate three different states of stretch and a material is called *extended* if $\lambda > 1$, *unstretched* if $\lambda = 1$, and *compressed* if $0 < \lambda < 1$, whereas zero and negative stretches are not possible due to the positive definiteness of $\boldsymbol{C}$.

Shear and reorientation To measure the motion of two material directions relative to each other, the material angle $\hat{\Theta}(\boldsymbol{X}; \hat{\boldsymbol{T}}_{(1)}, \hat{\boldsymbol{T}}_{(2)})$ and spatial angle $\hat{\theta}(\boldsymbol{X}, t; \hat{\boldsymbol{T}}_{(1)}, \hat{\boldsymbol{T}}_{(2)})$ between two material tangent (unit) vectors $\hat{\boldsymbol{T}}_{(1)}$ and $\hat{\boldsymbol{T}}_{(2)}$ and their according spatial counterparts $\hat{\boldsymbol{t}}_{(1)}$ and $\hat{\boldsymbol{t}}_{(2)}$, respectively, are introduced through the relations

$$\cos[\hat{\Theta}] = \hat{\boldsymbol{T}}_{(1)} \cdot \hat{\boldsymbol{T}}_{(2)} \quad \text{and} \quad \cos[\hat{\theta}] = \frac{\hat{\boldsymbol{t}}_{(1)} \cdot \hat{\boldsymbol{t}}_{(2)}}{|\hat{\boldsymbol{t}}_{(1)}||\hat{\boldsymbol{t}}_{(2)}|} = \frac{\hat{\boldsymbol{T}}_{(1)} \cdot \boldsymbol{C}\, \hat{\boldsymbol{T}}_{(2)}}{\lambda_{\hat{\boldsymbol{T}}_{(1)}} \lambda_{\hat{\boldsymbol{T}}_{(2)}}} \,. \tag{2.18}$$

The decrease of the difference $\Delta_{\hat{\Theta}\hat{\theta}} = \hat{\Theta} - \hat{\theta}$ is called the *angle of shear* in the plane spanned by the two vectors $\hat{\boldsymbol{T}}_{(1)}$ and $\hat{\boldsymbol{T}}_{(2)}$. Further, we call $\hat{\gamma} = \tan[|\Delta_{\hat{\Theta}\hat{\theta}}|] \geq 0$ the *amount of shear*. Like the stretch λ, the shear measures depend on the Cauchy–Green tensor $\boldsymbol{C}$ and thus exclude rigid-body deformations. If one of the two material directions, say $\hat{\boldsymbol{T}}_{(1)}$, is regarded as some direction of reference, the shear angle $\Delta_{\hat{\Theta}\hat{\theta}}$ serves as a measure for the *reorientation or realignment* of the direction $\hat{\boldsymbol{T}}_{(2)}$ with respect to $\hat{\boldsymbol{T}}_{(1)}$.

2.1.4 Deformation decomposition

For later use, it proves useful to introduce certain multiplicative decompositions of the deformation gradient $\boldsymbol{F}$.

Polar decomposition Any proper deformation gradient $\boldsymbol{F}$ can be subjected to a unique polar decomposition such that

$$\boldsymbol{F} = \boldsymbol{R}\boldsymbol{U} = \boldsymbol{V}\boldsymbol{R}\,, \tag{2.19}$$

where $\boldsymbol{U}, \boldsymbol{V} \in \mathcal{SYM}(3)$ are referred to as symmetric *right (material) and left (spatial) stretch tensors* and $\boldsymbol{R} \in \mathcal{SO}(3)$ is a proper orthogonal rotation tensor. Recalling (2.16) and using $\boldsymbol{U}^T = \boldsymbol{U}$ and $\boldsymbol{R}^{-1} = \boldsymbol{R}^T$, it is easy to show that $\boldsymbol{C} = (\boldsymbol{R}\boldsymbol{U})^T (\boldsymbol{R}\boldsymbol{U}) = \boldsymbol{U}^T\boldsymbol{R}^T\boldsymbol{R}\boldsymbol{U} = \boldsymbol{U}\boldsymbol{U} = \boldsymbol{U}^2$. Equivalently, for the spatial counterparts we find $\boldsymbol{B} = \boldsymbol{V}^2$. Thus, the pairs $\{\boldsymbol{U}, \boldsymbol{C}\}$ and $\{\boldsymbol{V}, \boldsymbol{B}\}$ each share the same sets of eigenvectors, while their eigenvalues are connected through $\lambda^2_{\boldsymbol{U}(i)} = \lambda^2_{\boldsymbol{V}(i)} = \lambda_{\boldsymbol{C}(i)} = \lambda_{\boldsymbol{B}(i)}$ $(i = 1, 2, 3)$, where $\lambda_{(\cdot)(i)}$ are the eigenvalues of $(\cdot)$. The eigenvalues $\lambda_{\boldsymbol{U}(i)} \in \mathcal{R}_+$ of $\boldsymbol{U}$ and $\boldsymbol{V}$ are called the *principal stretches*. They are identical to the *singular values* (not necessarily to the eigenvalues) of the deformation gradient $\boldsymbol{F}$. Obviously, the stretch tensors $\boldsymbol{U}$ and $\boldsymbol{V}$ exclude rigid-body rotations and the stretch of a material direction $\hat{\boldsymbol{T}}$, as defined in (2.17), can be expressed as $\lambda_{\hat{\boldsymbol{T}}} = |\boldsymbol{U}\hat{\boldsymbol{T}}|$.

Triangular decomposition In a variety of mathematical applications, it is helpful to perform a unique so-called *QR decomposition* of a matrix into an orthogonal matrix and

an upper triangular part. In the field of continuum mechanics, such a decomposition was proposed for the deformation gradient by Srinivasa [461] and further discussed by Freed & Srinivasa [138]. It reads

$$\boldsymbol{F} = \mathfrak{Q}\mathfrak{R}\,, \tag{2.20}$$

such that $\mathfrak{Q} \in \mathcal{SO}(3)$ is a proper orthogonal rotation tensor and $\mathfrak{R}$ depicts a tensor with an upper triangular coefficient matrix, hence, at least three zero-coefficients $\mathfrak{R}_{21} = \mathfrak{R}_{31} = \mathfrak{R}_{32} = 0$. The here so-called triangular decomposition has the benefit that the coefficients of $\mathfrak{R}$ have direct physical meaning and can be correlated to specific stretches and shears. Further, since $\mathfrak{Q}$ is a pure rotation, the stretch in material direction $\hat{\boldsymbol{T}}$, defined in (2.17), can be formulated as $\lambda_{\hat{\boldsymbol{T}}} = |\mathfrak{R}\hat{\boldsymbol{T}}|$, in which the expression $\mathfrak{R}\hat{\boldsymbol{T}}$ profits from the three zero entries of $\mathfrak{R}$ and usually leads to more compact notations than stretch calculations via $\lambda_{\hat{\boldsymbol{T}}} = |\boldsymbol{F}\hat{\boldsymbol{T}}|$ or $\lambda_{\hat{\boldsymbol{T}}} = |\boldsymbol{U}\hat{\boldsymbol{T}}|$. Such simplified expressions will be very useful in Part II of this work. It is remarked that $\mathfrak{Q} \neq \boldsymbol{R}$, which means that polar and triangular decomposition obey different rotation tensors.

Volumetric-deviatoric decomposition In addition to the previous decompositions, which focus on the exclusion of rigid-body rotations, the decomposition

$$\boldsymbol{F} = \boldsymbol{F}_{\mathrm{v}}\,\breve{\boldsymbol{F}} \quad \text{with} \quad \boldsymbol{F}_{\mathrm{v}} := J^{1/3}\boldsymbol{I} \tag{2.21}$$

divides the deformation gradient into a volumetric deformation $\boldsymbol{F}_{\mathrm{v}}$ and a purely deviatoric, volume-preserving part $\breve{\boldsymbol{F}} \in \mathcal{SL}(3)$, where $\mathcal{SL}$ is group of the special linear tensors, hence, $\det[\breve{\boldsymbol{F}}] = 1$. This decomposition was originally proposed by Flory [129]. The corresponding decomposition of the stretch tensor $\boldsymbol{U} = \boldsymbol{U}_{\mathrm{v}}\breve{\boldsymbol{U}}$ (with $\boldsymbol{U}_{\mathrm{v}} = \boldsymbol{F}_{\mathrm{v}}$) goes back to Richter [399]. Based on (2.21), the right Cauchy–Green tensor can be decomposed to $\boldsymbol{C} = \boldsymbol{C}_{\mathrm{v}}\breve{\boldsymbol{C}}$, where $\boldsymbol{C}_{\mathrm{v}} := J^{2/3}\boldsymbol{I}$ and $\breve{\boldsymbol{C}} = \breve{\boldsymbol{F}}^T\breve{\boldsymbol{F}} \in \mathcal{SL}(3)$ so that $\det[\breve{\boldsymbol{C}}] = 1$.

2.1.5 Measures of strain

Strain measures are defined such that they exclude rigid-body deformations and, additionally, vanish for the unstretched state. A general class of strain tensors was for example proposed by Seth [429] and Hill [213]. The material formulations of the *Seth-Hill family* are based on the right stretch tensor $\boldsymbol{U}$ and read

$$\boldsymbol{E}_m = \begin{cases} \frac{1}{m}(\boldsymbol{U}^m - \boldsymbol{I}) & m \neq 0\,, \\ \ln[\boldsymbol{U}] & m = 0\,, \end{cases} \tag{2.22}$$

where $m \in \mathcal{R}$ and $\boldsymbol{E}_m \in \mathcal{SYM}(3)$. Obviously, it holds that $\boldsymbol{E}_m = \boldsymbol{0}$ whenever $\boldsymbol{U} = \boldsymbol{I}$ for arbitrary choices of m, while in this case $\boldsymbol{F}$ can still be an arbitrary rotation tensor $\boldsymbol{R} \in \mathcal{SO}(3)$. The general formulation (2.22) includes common strain measures for special choices of m, for example, the Green–Lagrange strain $\boldsymbol{E}_2 = (\boldsymbol{C} - \boldsymbol{I})/2$ for $m = 2$, the Biot strain $\boldsymbol{E}_1 = \boldsymbol{U} - \boldsymbol{I}$ for $m = 1$, and the logarithmic Hencky strain tensor $\boldsymbol{E}_0 = \ln[\boldsymbol{U}]$ for $m = 0$. The strain tensors $\boldsymbol{E}_m$ share the set of eigenvectors with the right stretch tensor $\boldsymbol{U}$, while the associated eigenvalues are distinct for each choice of m. For instance, the eigenvalues of the Hencky strain tensor $\boldsymbol{E}_0$ are given by the logarithm of the principal stretches, viz: $\lambda_{\boldsymbol{E}_0(i)} = \ln[\lambda_{\boldsymbol{U}(i)}]$ $(i = 1, 2, 3)$. The Hencky strain is a very convenient measure for finite strains, especially because it resembles some features from small-strain considerations. A comprehensive discussion on the geometric properties of logarithmic strains can be found in Neff et al. [350].

2.2 The concept of stress

The previous section introduced the basic kinematical relations for a material body $\mathscr{B}$ subject to finite deformations and strains. If in a body occur strains and motions of material particles $\mathscr{P}$ relative to each other, it is consequent to postulate that this gives rise to internal forces in the body. This is described by the concept of *stress*, which characterises a force related to a certain area. As a standard procedure, *Euler's cut principle* is considered and a material subdomain $\mathcal{B}_S \subset \mathcal{B}_0$ is imaginary cut out of the material body $\mathcal{B}_0$. The associated particle positions $\boldsymbol{x} = \boldsymbol{\chi}(\boldsymbol{X} \in \mathcal{B}_S) \in \mathcal{B}_{S_t} \subset \mathcal{B}$ in the spatial subdomain $\mathcal{B}_{S_t}$ are obtained by the deformation map $\boldsymbol{\chi}$. The forces arising at the cut surface $\partial\mathcal{B}_{S_t}$ are quantified by the *Cauchy (spatial) traction vector* $\boldsymbol{t}(\boldsymbol{x}, t; \boldsymbol{n})$, which depends on the outward-oriented *unit* surface normal vector $\boldsymbol{n}(\boldsymbol{x}, t) \in T^*_{\boldsymbol{x}}\mathcal{B}_{S_t}$. The traction vector $\boldsymbol{t} = \mathrm{d}\boldsymbol{\mathfrak{f}}/\mathrm{d}a$ relates a current force element $\mathrm{d}\boldsymbol{\mathfrak{f}}$ to a spatial area element $\mathrm{d}a$ and thus measures the current force per current area. Of course, it is known from *Newton's third law of motion*[2] that the stress vector $\boldsymbol{t}$ is in balance with a counterpart on the surface of the body $\mathcal{B} \setminus \mathcal{B}_{S_t}$ with opposed oriented normal vector $-\boldsymbol{n}$, such that

$$\boldsymbol{t}(\boldsymbol{x}, t; \boldsymbol{n}) = -\boldsymbol{t}(\boldsymbol{x}, t; -\boldsymbol{n})\,. \tag{2.23}$$

This is referred to as *Cauchy's lemma*. As it is of interest to have a stress measure which is independent of the surface normal vector $\boldsymbol{n}$, the *Cauchy theorem* states a linear relation between the stress vector $\boldsymbol{t}$ and the according surface normal vector $\boldsymbol{n}$ via

$$\boldsymbol{t}(\boldsymbol{x}, t; \boldsymbol{n}) =: \boldsymbol{\sigma}(\boldsymbol{x}, t)\, \boldsymbol{n}(\boldsymbol{x}, t) \tag{2.24}$$

and introduces $\boldsymbol{\sigma}$ as the *Cauchy (true) stress tensor*. Further, with the oriented area elements $\mathrm{d}\boldsymbol{a} = \boldsymbol{n}\,\mathrm{d}a$ and $\mathrm{d}\boldsymbol{A} = \boldsymbol{N}\,\mathrm{d}A$, and recalling the area map (2.13), the current force element $\mathrm{d}\boldsymbol{\mathfrak{f}} = \boldsymbol{t}\,\mathrm{d}a$ can be reformulated as

$$\mathrm{d}\boldsymbol{\mathfrak{f}} = \boldsymbol{t}\,\mathrm{d}a = \boldsymbol{\sigma}\,\mathrm{d}\boldsymbol{a} = \boldsymbol{\sigma}\,\mathrm{cof}[\boldsymbol{F}]\,\mathrm{d}\boldsymbol{A} =: \boldsymbol{P}\,\mathrm{d}\boldsymbol{A} = \boldsymbol{P}\boldsymbol{N}\,\mathrm{d}A\,. \tag{2.25}$$

This allows to identify

$$\boldsymbol{T}(\boldsymbol{X}, t; \boldsymbol{N}) := \boldsymbol{P}(\boldsymbol{X}, t)\, \boldsymbol{N}(\boldsymbol{X}) \tag{2.26}$$

as the *nominal traction vector* that measures the current force per referential area element $\mathrm{d}A$. Further, $\boldsymbol{P} = \boldsymbol{\sigma}\,\mathrm{cof}[\boldsymbol{F}]$ is referred to as the *first Piola–Kirchhoff (nominal) stress tensor* and is of substantial importance for continuum-mechanical formulations that account for current forces but the geometry of the referential body $\mathcal{B}_0$.

2.3 Physical balance relations

The preceding considerations have to be complemented by the introduction of physical balance relations in order to obtain governing equations for continuum-mechanical problems. Hence, in this section a general balance structure is formulated and subsequently used to

[2] Published 1686 in Newton's famous work *Philosophiæ Naturalis Principia Mathematica* and known as *actio est reactio*. In its original Latin version it reads: *"Lex III: Actioni contrariam semper et æqualem esse reactionem: sive corporum duorum actiones in se mutuo semper esse æquales et in partes contrarias dirigi."*

axiomatically introduce individual balances for the physical quantities mass, momentum, moment of momentum, energy, and entropy. Further balance relations for quantities related to electromagnetic phenomena are not presented here, but can be found, for example, in the book of ERINGEN & MAUGIN [120].

2.3.1 General balance structure

A general balance structure for a continuous, volume-specific quantity $\Psi \in \mathcal{R}$ in a subset $\mathcal{B}_S \subseteq \mathcal{B}_0$ of the material domain $\mathcal{B}_0$ is obtained by investigating the temporal change of the associated integrated quantity $\int_{\mathcal{B}_S} \Psi \, \mathrm{d}V$. It is postulated that the *rate of the volume integral* is then given by

$$\frac{\mathrm{d}}{\mathrm{d}t} \int_{\mathcal{B}_S} \Psi \, \mathrm{d}V = \int_{\partial\mathcal{B}_S} (\boldsymbol{\phi} \cdot \boldsymbol{N}) \, \mathrm{d}A + \int_{\mathcal{B}_S} \zeta \, \mathrm{d}V + \int_{\mathcal{B}_S} \hat{\Psi} \, \mathrm{d}V \tag{2.27}$$

and constitutes a general balance for the scalar-valued quantity $\Psi \in \mathcal{R}$. By the same arguments, a general balance for vector-valued, volume-specific quantity $\boldsymbol{\Psi} \in \mathcal{R}^3$ is introduced as

$$\frac{\mathrm{d}}{\mathrm{d}t} \int_{\mathcal{B}_S} \boldsymbol{\Psi} \, \mathrm{d}V = \int_{\partial\mathcal{B}_S} (\boldsymbol{\Phi} \, \boldsymbol{N}) \, \mathrm{d}A + \int_{\mathcal{B}_S} \boldsymbol{\zeta} \, \mathrm{d}V + \int_{\mathcal{B}_S} \hat{\boldsymbol{\Psi}} \, \mathrm{d}V \, . \tag{2.28}$$

The balances (2.27) and (2.28) state that the rates of the volume integrals on the left hand sides are in equilibrium with the *fluxes* $\boldsymbol{\phi} \in \mathcal{R}^3$, $\boldsymbol{\Phi} \in \mathcal{R}^{3\otimes 3}$ over the surface $\partial\mathcal{B}_S$, the *supply* terms $\zeta \in \mathcal{R}$, $\boldsymbol{\zeta} \in \mathcal{R}^3$ in $\mathcal{B}_S$, and the *production* terms $\hat{\Psi} \in \mathcal{R}$, $\hat{\boldsymbol{\Psi}} \in \mathcal{R}^3$ in $\mathcal{B}_S$, respectively. Subsequently, integration and differentiation on the left hand sides of (2.27) and (2.28) can be interchanged since the boundaries of the integration refer to the time-invariant material subdomain $\mathcal{B}_S$. By further applying the respective scalar- and vector-valued *Gaussian integral (divergence) theorems*, see Eqs (A.25) and (A.26), on the surface flux terms, one obtains the *global* balance forms

$$\int_{\mathcal{B}_S} \dot{\Psi} \, \mathrm{d}V = \int_{\mathcal{B}_S} [\mathrm{Div}[\boldsymbol{\phi}] + \zeta + \hat{\Psi}] \, \mathrm{d}V \quad \text{and} \quad \int_{\mathcal{B}_S} \dot{\boldsymbol{\Psi}} \, \mathrm{d}V = \int_{\mathcal{B}_S} [\mathrm{Div}[\boldsymbol{\Phi}] + \boldsymbol{\zeta} + \hat{\boldsymbol{\Psi}}] \, \mathrm{d}V \, , \tag{2.29}$$

where a dot over $(\cdot)$ denotes the (total) time derivative $\mathrm{d}(\cdot)/\mathrm{d}t$ and $\mathrm{Div}[(\cdot)]$ is a material divergence operator. Finally, since the balances (2.29) shall be fulfilled for any subdomain $\mathcal{B}_S \subseteq \mathcal{B}_0$, we can apply the *localisation theorem*

$$\int_{\mathcal{B}_S} (\cdot) \, \mathrm{d}V = 0 \quad \forall \, \mathcal{B}_S \subseteq \mathcal{B}_0 \quad \rightarrow \quad (\cdot) = 0 \quad \forall \, \boldsymbol{X} \in \mathcal{B}_0 \tag{2.30}$$

on the global forms in order to obtain the *local* balance forms

$$\dot{\Psi} = \mathrm{Div}[\boldsymbol{\phi}] + \zeta + \hat{\Psi} \quad \text{and} \quad \dot{\boldsymbol{\Psi}} = \mathrm{Div}[\boldsymbol{\Phi}] + \boldsymbol{\zeta} + \hat{\boldsymbol{\Psi}} \, , \tag{2.31}$$

which have to be fulfilled at each material particle position $\boldsymbol{X}$.

2.3.2 Balance of mass

The scalar-valued mass of the subdomain $\mathcal{B}_S \subseteq \mathcal{B}_0$ is given by $\mathcal{M} = \int_{\mathcal{B}_S} \rho_0(\boldsymbol{X}) \, \mathrm{d}V$ in terms of the referential mass density $\rho_0(\boldsymbol{X})$. In this work, we only consider closed systems where

the mass is a conserved quantity and it can therefore be easily concluded that the rate of the referential mass is zero, hence

$$\dot{\mathcal{M}} = \frac{\mathrm{d}}{\mathrm{d}t} \int_{\mathcal{B}_S} \rho_0 \, \mathrm{d}V = 0 \,. \tag{2.32}$$

Comparing (2.32) to the general balance (2.27), the mass density $\Psi^{\mathcal{M}}$, the mass flux $\boldsymbol{\phi}^{\mathcal{M}}$, the mass supply $\zeta^{\mathcal{M}}$ as well as the mass production $\hat{\Psi}^{\mathcal{M}}$ can be identified as

$$\Psi^{\mathcal{M}} = \rho_0 \,, \quad \boldsymbol{\phi}^{\mathcal{M}} = \mathbf{0} \,, \quad \zeta^{\mathcal{M}} = 0 \,, \quad \hat{\Psi}^{\mathcal{M}} = 0 \,. \tag{2.33}$$

Using these findings in the local form $(2.31)_1$ results in the intuitive expression

$$\dot{\rho}_0 = 0 \tag{2.34}$$

for the local mass balance stating that the initial mass density ρ_0 of the material is constant over time.

2.3.3 Balance of linear momentum

The vector-valued linear momentum of the subdomain $\mathcal{B}_S \subseteq \mathcal{B}_0$ is given by $\boldsymbol{\mathcal{I}} = \int_{\mathcal{B}_S} \rho_0 \, \dot{\boldsymbol{x}} \, \mathrm{d}V$ in terms of the velocity $\dot{\boldsymbol{x}} = \mathrm{d}\boldsymbol{x}/\mathrm{d}t$. It is stated that the temporal change of the momentum in $\mathcal{B}_S$ is equal to the sum of contact forces $\mathfrak{f}$ acting on the surface $\partial\mathcal{B}_S$ and volume forces $\mathfrak{b}$ in $\mathcal{B}_S$, which means that $\dot{\boldsymbol{\mathcal{I}}} = \mathfrak{f} + \mathfrak{b}$. The contact forces $\mathfrak{f} = \int_{\partial\mathcal{B}_S} \boldsymbol{P}\boldsymbol{N} \, \mathrm{d}A$ are obtained by an integration of (2.25), while the volume forces are introduced as $\mathfrak{b} = \int_{\mathcal{B}_S} \rho_0 \, \boldsymbol{b} \, \mathrm{d}V$ in terms of the mass-specific external body force $\boldsymbol{b}$. Thus, we can write

$$\frac{\mathrm{d}}{\mathrm{d}t} \int_{\mathcal{B}_S} \rho_0 \, \dot{\boldsymbol{x}} \, \mathrm{d}V = \int_{\partial\mathcal{B}_S} \boldsymbol{P}\boldsymbol{N} \, \mathrm{d}A + \int_{\mathcal{B}_S} \rho_0 \, \boldsymbol{b} \, \mathrm{d}V \,. \tag{2.35}$$

By comparing with (2.28), we can identify the momentum density $\boldsymbol{\Psi}^{\boldsymbol{\mathcal{I}}}$, the momentum flux $\boldsymbol{\Phi}^{\boldsymbol{\mathcal{I}}}$, the momentum supply $\boldsymbol{\zeta}^{\boldsymbol{\mathcal{I}}}$, and the momentum production $\hat{\boldsymbol{\Psi}}^{\boldsymbol{\mathcal{I}}}$ as

$$\boldsymbol{\Psi}^{\boldsymbol{\mathcal{I}}} = \rho_0 \, \dot{\boldsymbol{x}} \,, \quad \boldsymbol{\Phi}^{\boldsymbol{\mathcal{I}}} = \boldsymbol{P} \,, \quad \boldsymbol{\zeta}^{\boldsymbol{\mathcal{I}}} = \rho_0 \, \boldsymbol{b} \,, \quad \hat{\boldsymbol{\Psi}}^{\boldsymbol{\mathcal{I}}} = \mathbf{0} \,. \tag{2.36}$$

Then, substituting these terms into the general form $(2.31)_2$, applying the product rule for the time derivation of $\boldsymbol{\Psi}^{\boldsymbol{\mathcal{I}}}$, and making use of (2.34), we can identify

$$\rho_0 \, \ddot{\boldsymbol{x}} = \mathrm{Div}[\boldsymbol{P}] + \rho_0 \, \boldsymbol{b} \tag{2.37}$$

as the local momentum balance. Note that (2.37) can be regarded as a continuum version of *Newton's second law of motion*.

A commonly applied simplification of the momentum balance is to neglect the body forces, $\boldsymbol{b} = \mathbf{0}$, which means that effects like gravitation are disregarded. If we further assume *quasi-static* conditions, the inertia-related left hand side term in (2.37) drops out, since $\ddot{\boldsymbol{x}} \approx \mathbf{0}$, and the momentum balance can under these assumptions be reduced to

$$\mathrm{Div}[\boldsymbol{P}] = \mathbf{0} \,. \tag{2.38}$$

2.3.4 Balance of moment of momentum

The vector-valued moment of momentum of the subdomain $\mathcal{B}_S \subseteq \mathcal{B}_0$ with respect to the origin $\mathcal{O}$ of the inertial basis system is given by $\boldsymbol{\mathcal{L}} = \int_{\mathcal{B}_S} \boldsymbol{x} \times \rho_0 \, \dot{\boldsymbol{x}} \, \mathrm{d}V$. In analogy to the linear momentum balance, it is postulated that the temporal change of $\boldsymbol{\mathcal{L}}$ is equal to the sum of the torques $\mathfrak{f}^{\boldsymbol{\mathcal{L}}} = \int_{\partial\mathcal{B}_S} \boldsymbol{x} \times \boldsymbol{P}\boldsymbol{N} \, \mathrm{d}A$ due to the surface force $\mathfrak{f}$ and $\mathfrak{b}^{\boldsymbol{\mathcal{L}}} = \int_{\mathcal{B}_S} \boldsymbol{x} \times \rho_0 \, \boldsymbol{b} \, \mathrm{d}V$ due to the volume force $\mathfrak{b}$, hence $\dot{\boldsymbol{\mathcal{L}}} = \mathfrak{f}^{\boldsymbol{\mathcal{L}}} + \mathfrak{b}^{\boldsymbol{\mathcal{L}}}$. Then, we can directly formulate

$$\frac{\mathrm{d}}{\mathrm{d}t} \int_{\mathcal{B}_S} \boldsymbol{x} \times \rho_0 \, \dot{\boldsymbol{x}} \, \mathrm{d}V = \int_{\partial\mathcal{B}_S} \boldsymbol{x} \times \boldsymbol{P}\boldsymbol{N} \, \mathrm{d}A + \int_{\mathcal{B}_S} \boldsymbol{x} \times \rho_0 \, \boldsymbol{b} \, \mathrm{d}V \tag{2.39}$$

and, by comparing with (2.28), we can identify the density $\boldsymbol{\Psi}^{\boldsymbol{\mathcal{L}}}$, the flux $\boldsymbol{\Phi}^{\boldsymbol{\mathcal{L}}}$, the supply $\boldsymbol{\zeta}^{\boldsymbol{\mathcal{L}}}$, and the production $\hat{\boldsymbol{\Psi}}^{\boldsymbol{\mathcal{L}}}$ of the moment of momentum as

$$\boldsymbol{\Psi}^{\boldsymbol{\mathcal{L}}} = \boldsymbol{x} \times \rho_0 \, \dot{\boldsymbol{x}} \,, \quad \boldsymbol{\Phi}^{\boldsymbol{\mathcal{L}}} = \boldsymbol{x} \times \boldsymbol{P} \,, \quad \boldsymbol{\zeta}^{\boldsymbol{\mathcal{L}}} = \boldsymbol{x} \times \rho_0 \, \boldsymbol{b} \,, \quad \hat{\boldsymbol{\Psi}}^{\boldsymbol{\mathcal{L}}} = \boldsymbol{0} \,. \tag{2.40}$$

Inserting these relation in the local form $(2.31)_2$, applying the product rule (A.57) on $\dot{\boldsymbol{\Psi}}^{\boldsymbol{\mathcal{L}}}$, reformulating the divergence term to $\mathrm{Div}[\boldsymbol{x} \times \boldsymbol{P}] = \boldsymbol{x} \times \mathrm{Div}[\boldsymbol{P}] + \boldsymbol{F} \times \boldsymbol{P}$, and subsequently simplifying by means of the preceding balances (2.34) and (2.37) leads to

$$\boldsymbol{F} \times \boldsymbol{P} = \boldsymbol{\mathcal{E}}(\boldsymbol{F}\boldsymbol{P}^T) = \boldsymbol{0} \quad \leftrightarrow \quad \boldsymbol{F}\boldsymbol{P}^T = \boldsymbol{P}\boldsymbol{F}^T \,. \tag{2.41}$$

Therein, expression $(2.41)_1$ reformulates the tensor cross product by means of the third-order fundamental tensor $\boldsymbol{\mathcal{E}}$, see (A.6), and $(2.41)_2$ is obtained since $(2.41)_1$ states that the skew-symmetric part $\mathrm{skw}[\boldsymbol{F}\boldsymbol{P}^T]$ has to be zero. Note that reformulating $(2.41)_2$ by means of $\boldsymbol{P} = \boldsymbol{\sigma} \, \mathrm{cof}[\boldsymbol{F}] = \boldsymbol{\sigma} \, \det[\boldsymbol{F}] \boldsymbol{F}^{-T}$ yields the well-known symmetry condition $\boldsymbol{\sigma}^T = \boldsymbol{\sigma}$ for the Cauchy stress tensor.

2.3.5 Balance of energy

The scalar-valued *internal energy* of the subdomain $\mathcal{B}_S \subseteq \mathcal{B}_0$ is given by $\mathcal{E}^{\varepsilon} = \int_{\mathcal{B}_S} \rho_0 \, \varepsilon \, \mathrm{d}V$ in terms of the *mass-specific internal energy* ε. In turn, the total energy $\mathcal{E} = \mathcal{E}^{\varepsilon} + \mathcal{E}^{\mathcal{K}}$ of the subdomain $\mathcal{B}_S \subseteq \mathcal{B}_0$ is given by the sum of the internal energy and the kinetic energy $\mathcal{E}^{\mathcal{K}} = \int_{\mathcal{B}_S} (\rho_0 \, \dot{\boldsymbol{x}} \cdot \dot{\boldsymbol{x}})/2 \, \mathrm{d}V$. The *first law of thermodynamics* now postulates that the temporal change of $\mathcal{E}$ equals the sum $\mathcal{P} = \mathcal{P}^{\mathcal{M}} + \mathcal{P}^{\mathcal{Q}}$ of external mechanical power $\mathcal{P}^{\mathcal{M}} = \int_{\partial\mathcal{B}_S} \dot{\boldsymbol{x}} \cdot \boldsymbol{P}\boldsymbol{N} \, \mathrm{d}A + \int_{\mathcal{B}_S} \dot{\boldsymbol{x}} \cdot \rho_0 \, \boldsymbol{b} \, \mathrm{d}V$ and thermal (non-mechanical) power $\mathcal{P}^{\mathcal{Q}} = -\int_{\partial\mathcal{B}_S} \boldsymbol{q} \cdot \boldsymbol{N} \, \mathrm{d}A + \int_{\mathcal{B}_S} \rho_0 \, r \, \mathrm{d}V$. Therein, $\boldsymbol{q}$ denotes the inwards-oriented heat flux (convection) vector and r is the external heat supply (radiation). Then, the resulting balance equation $\dot{\mathcal{E}} = \mathcal{P}$ is given by

$$\frac{\mathrm{d}}{\mathrm{d}t} \int_{\mathcal{B}_S} \rho_0 \, (\varepsilon + \tfrac{1}{2} \, \dot{\boldsymbol{x}} \cdot \dot{\boldsymbol{x}}) \, \mathrm{d}V = \int_{\partial\mathcal{B}_S} \dot{\boldsymbol{x}} \cdot \boldsymbol{P}\boldsymbol{N} - \boldsymbol{q} \cdot \boldsymbol{N} \, \mathrm{d}A + \int_{\mathcal{B}_S} \rho_0 \, (\dot{\boldsymbol{x}} \cdot \boldsymbol{b} + r) \, \mathrm{d}V \,. \tag{2.42}$$

By a comparison with (2.27), the energy density $\Psi^{\mathcal{E}}$, the energy flux $\boldsymbol{\phi}^{\mathcal{E}}$, the energy supply $\zeta^{\mathcal{E}}$, and the energy production $\hat{\Psi}^{\mathcal{E}}$ are identified as

$$\Psi^{\mathcal{E}} = \rho_0 \, (\varepsilon + \tfrac{1}{2} \, \dot{\boldsymbol{x}} \cdot \dot{\boldsymbol{x}}) \,, \quad \boldsymbol{\phi}^{\mathcal{E}} = \boldsymbol{P}^T \dot{\boldsymbol{x}} - \boldsymbol{q} \,, \quad \zeta^{\mathcal{E}} = \rho_0 \, (\dot{\boldsymbol{x}} \cdot \boldsymbol{b} + r) \,, \quad \hat{\Psi}^{\mathcal{E}} = 0 \,. \tag{2.43}$$

Inserting these relations in the local form $(2.31)_1$, making repeated use of the product rule, inter alia (A.56), for $\dot{\Psi}^{\mathcal{E}}$, reformulating the divergence term to $\mathrm{Div}[\boldsymbol{P}^T \dot{\boldsymbol{x}}] = \mathrm{Div}[\boldsymbol{P}] \cdot \dot{\boldsymbol{x}} + \boldsymbol{P} \cdot \mathrm{Grad}[\dot{\boldsymbol{x}}]$, introducing the velocity gradient $\dot{\boldsymbol{F}} = \mathrm{Grad}[\dot{\boldsymbol{x}}]$, and subsequently simplifying by means of the preceding balances (2.34) and (2.37) leads to the local energy balance

$$\rho_0 \, \dot{\varepsilon} = \boldsymbol{P} \cdot \dot{\boldsymbol{F}} - \mathrm{Div}[\boldsymbol{q}] + \rho_0 \, r \,. \tag{2.44}$$

2.3.6 Balance of entropy

The scalar-valued *entropy* of the subdomain $\mathcal{B}_S \subseteq \mathcal{B}_0$ is given by $\mathcal{H} = \int_{\mathcal{B}_S} \rho_0\, \eta \, \mathrm{d}V$ in terms of the *mass-specific entropy* η. Before introducing a balance relation for the entropy $\mathcal{H}$, it shall be remarked that understanding this thermodynamical property is not as intuitive as for the previously considered quantities, like momentum or energy, and a more illustrative access to the topic may be provided, for example, in the textbook of Müller & Weiss [347]. The usual continuum-mechanical approach to the concept of entropy is an axiomatical introduction of the balance equation for the temporal change of $\mathcal{H}$, reading

$$\dot{\mathcal{H}} = \frac{\mathrm{d}}{\mathrm{d}t} \int_{\mathcal{B}_S} \rho_0\, \eta \, \mathrm{d}V = \int_{\partial\mathcal{B}_S} (\boldsymbol{\phi}^{\mathcal{H}} \cdot \boldsymbol{N}) \, \mathrm{d}A + \int_{\mathcal{B}_S} \zeta^{\mathcal{H}} \, \mathrm{d}V + \int_{\mathcal{B}_S} \rho_0\, \hat{\eta} \, \mathrm{d}V \,, \tag{2.45}$$

and subsequently introducing constitutive expressions for the entropy flux $\boldsymbol{\phi}^{\mathcal{H}}$ and for the entropy supply $\zeta^{\mathcal{H}}$, see, for example, Eckart [104] and Müller [346]. This leads to

$$\Psi^{\mathcal{H}} = \rho_0\, \eta \,, \quad \boldsymbol{\phi}^{\mathcal{H}} := -\frac{\boldsymbol{q}}{\theta} \,, \quad \zeta^{\mathcal{H}} := \frac{\rho_0\, r}{\theta} \,, \quad \hat{\Psi}^{\mathcal{H}} = \rho_0\, \hat{\eta} \,, \tag{2.46}$$

where θ is the *thermodynamic (absolute) temperature* and where we identified the entropy density $\Psi^{\mathcal{H}}$ and the entropy production $\hat{\Psi}^{\mathcal{H}}$ by comparing (2.45) with the general balance (2.27). Inserting relations (2.46) into $(2.31)_1$ and simplifying by means of (2.34) yields the local entropy balance

$$\rho_0\, \dot{\eta} = -\operatorname{Div}\left[\frac{\boldsymbol{q}}{\theta}\right] + \frac{\rho_0\, r}{\theta} + \rho_0\, \hat{\eta} \,. \tag{2.47}$$

Dissipation inequality In contrast to the other four balances, the equation for the entropy contains a production term, which implies that the entropy is not a conserved quantity. The *second law of thermodynamics* or *dissipation postulate* states that the production of entropy must never be negative, which means that

$$\hat{\Psi}^{\mathcal{H}} = \rho_0\, \hat{\eta} \geq 0 \tag{2.48}$$

and, applied to (2.47), $\rho_0\, \dot{\eta} + \operatorname{Div}[\boldsymbol{q}/\theta] - \rho_0\, r/\theta \geq 0$. Reformulation of this expression by means of $\operatorname{Div}[\boldsymbol{q}/\theta] = -\boldsymbol{q} \cdot \operatorname{Grad}[\theta]/\theta^2 + \operatorname{Div}[\boldsymbol{q}]/\theta$, the energy balance (2.44), a multiplication with $\theta > 0$, and the introduction of the mass-specific *Helmholtz free energy*

$$\psi := \varepsilon - \theta\eta \tag{2.49}$$

leads to the *Clausius-Duhem inequality*

$$\mathcal{D} := \boldsymbol{P} \cdot \dot{\boldsymbol{F}} - \rho_0\, \dot{\psi} - \rho_0\, \dot{\theta}\eta - \frac{1}{\theta}\, \boldsymbol{q} \cdot \operatorname{Grad}[\theta] \geq 0 \,. \tag{2.50}$$

Therein, $\mathcal{D} = \rho_0\, \theta\hat{\eta}$ is introduced as the local *dissipation* and the term $\boldsymbol{P} \cdot \dot{\boldsymbol{F}}$, originated in the energy balance, is the *stress power*. A positive dissipation $\mathcal{D} > 0$ characterises *irreversible* processes, whereas a vanishing dissipation $\mathcal{D} = 0$ means that a process is *reversible*. Finally, when restricting to isothermal processes, it follows that $\dot{\theta} = 0$ as well as $\operatorname{Grad}[\theta] = \boldsymbol{0}$ and (2.50) reduces to the *Clausius-Planck inequality*

$$\mathcal{D} = \boldsymbol{P} \cdot \dot{\boldsymbol{F}} - \rho_0\, \dot{\psi} \geq 0 \,. \tag{2.51}$$

3 Fundamentals of Material Theory

This chapter presents some fundamental knowledge of *material theory*, which is the consequent continuation of the considerations from the previous chapter in order to treat continuum-mechanical problems. In this sense, this chapter starts with the formulation of the basic boundary-value problem of continuum mechanics and introduces the constitutive framework as well as the resulting restrictions upon the constitutive equations obtained from basic thermodynamical principles. This is followed by further topics, such as the discussion of variational principles in continuum mechanics, invariant theory and some examples for analytical strain-energy functions. The choice of the discussed topics is motivated by the applications in the following chapters and the explanations and principles may serve as a toolbox for the following chapters. The presented approach to the topic of material theory is by no means complete and it is referred to the classical textbooks of, for example, Truesdell [488], Truesdell & Noll [490], Ogden [362], and Šilhavý [438] for comprehensive overviews on material theory and constitutive modelling.

3.1 The mechanical boundary-value problem

The basic kinematical principles and the evaluation of the physical balance relations in the preceding chapter laid the foundation for the formulation of the *mechanical boundary-value problem*, which is the basic starting point for the treatment of continuum-mechanical problems. Up to now, the presented framework is capable of describing general thermodynamical processes, which generally results in the *primary variables* $\{\boldsymbol{\chi}, \theta\}$ and a *response function* set $\mathcal{R} = \{\psi, \boldsymbol{P}, \eta, \boldsymbol{q}\}$. However, in this work continuum-mechanical problems will be treated under the following assumptions:

i. neglection of body forces: $\boldsymbol{b} = \boldsymbol{0}$,

ii. quasi-static conditions and the neglection of inertia effects: $\ddot{\boldsymbol{x}} \approx \boldsymbol{0}$ as well as

iii. isothermal conditions: $\dot{\theta} = 0$ and $\mathrm{Grad}[\theta] = \boldsymbol{0}$.

The first two assumptions entail that we can proceed with the balance of momentum in the reduced form (2.38), whereas the third assumption entails a constant temperature θ in $\mathscr{B}$ and makes the evaluation of the energy balance superfluous. This will reduce the set of response functions to $\mathcal{R} = \{\psi, \boldsymbol{P}\}$ by withdrawing the entropy η and the heat flux $\boldsymbol{q}$.

3.1.1 Problem formulation

Let the body $\mathscr{B}$ undergo some deformation from its referential configuration $\mathcal{B}_0$ to a current configuration $\mathcal{B}$. The deformation is described by the map of the associated particles $\mathscr{P} \in \mathscr{B}$ from their reference position $\boldsymbol{X} \in \mathcal{B}_0$ to a current position $\boldsymbol{x} \in \mathcal{B}$. This is formulated in terms of the deformation map $\boldsymbol{\chi}$ as introduced in Eq. (2.3). From a physical point of view, it is only consequent to postulate that the body $\mathscr{B}$ interacts with its surrounding in space and to formulate these interactions in the form of conditions which act on the referential boundary points $\boldsymbol{X} \in \partial\mathcal{B}_0$. When the nature of the interaction is such that

it constraints the motion $\boldsymbol{\chi}$ of the body on the whole or a part of its boundary $\partial\mathcal{B}_0$ to a prescribed value $\overline{\boldsymbol{\chi}}$, the body is subject to *Dirichlet boundary conditions*

$$\boldsymbol{\chi} = \overline{\boldsymbol{\chi}} \quad \text{on} \quad \partial\mathcal{B}_{\boldsymbol{\chi}} \subseteq \partial\mathcal{B}_0 \,. \tag{3.1}$$

Consequently, $\partial\mathcal{B}_{\boldsymbol{\chi}}$ is referred to as the Dirichlet surface. A second type of conditions is given when the tractions $\boldsymbol{T} = \boldsymbol{P}\boldsymbol{N}$ on the Neumann surface $\partial\mathcal{B}_{\boldsymbol{T}} \subseteq \partial\mathcal{B}_0$ are prescribed by a traction vector $\overline{\boldsymbol{T}}$, thus giving the *Neumann boundary conditions*

$$\boldsymbol{P}\boldsymbol{N} = \overline{\boldsymbol{T}} \quad \text{on} \quad \partial\mathcal{B}_{\boldsymbol{T}} \subseteq \partial\mathcal{B}_0 \,. \tag{3.2}$$

Further, one specific material position $\boldsymbol{X} \in \partial\mathcal{B}_0$ on the boundary must be subject to exactly one type of boundary condition, hence relating Dirichlet and Neumann surface through

$$\partial\mathcal{B}_{\boldsymbol{\chi}} \cup \partial\mathcal{B}_{\boldsymbol{T}} = \partial\mathcal{B}_0 \quad \text{and} \quad \partial\mathcal{B}_{\boldsymbol{\chi}} \cap \partial\mathcal{B}_{\boldsymbol{T}} = \emptyset \,. \tag{3.3}$$

Summarising, the mechanical boundary-value problem is defined by finding the *kinematically admissible* deformation map[1]

$$\boldsymbol{\chi} = \{\boldsymbol{\chi} \mid \boldsymbol{\chi} = \overline{\boldsymbol{\chi}} \text{ on } \partial\mathcal{B}_{\boldsymbol{\chi}}\} \,, \tag{3.4}$$

satisfying the Dirichlet boundary conditions, subject to the Neumann boundary conditions (3.2). From the previous chapter, we know that the balance of momentum has to be fulfilled, hence

$$\mathrm{Div}[\boldsymbol{P}] = \boldsymbol{0} \text{ in } \mathcal{B}_0 \,, \tag{3.5}$$

and that the first Piola–Kirchhoff stress $\boldsymbol{P}$ has to satisfy the balance of moment of momentum as given in Eq. (2.41).

3.1.2 The need for constitutive relations

The preceding considerations treated the formulation of the mechanical boundary-value problem. However, it was not investigated whether the problem is solvable with the equations at hand. Therefore, we now want to confront the unknowns and the equations of the problem presented in Section 3.1.1. On the side of the unknowns, we directly identify the deformation map $\boldsymbol{\chi}$ and the first Piola–Kirchhoff stress tensor $\boldsymbol{P}$, hence, the deformation and the occurring stresses in the body $\mathscr{B}$ have to determined. Furthermore, it is strongly suggested to aim for a thermodynamically consistent formulation, which additionally demands for the evaluation of the entropy inequality. This entails that the Helmholtz free energy ψ has to be specified. In summary, we have

$$\left.\begin{array}{ll} \text{deformation map } \boldsymbol{\chi} & 3 \text{ unknowns} \\ \text{stress tensor } \boldsymbol{P} & 9 \text{ unknowns} \\ \text{free Helmholtz energy } \psi & 1 \text{ unknown} \end{array}\right\} \quad \rightarrow \quad 13 \text{ unknowns} \,. \tag{3.6}$$

[1] Note that it might be useful to pose some further mathematical requirements on the function space of the deformation map $\boldsymbol{\chi}$. In this sense, Eq. (3.4) might be strengthened to $\boldsymbol{\chi} = \{\boldsymbol{\chi} \in W^{1,p} \mid \boldsymbol{\chi} = \overline{\boldsymbol{\chi}} \text{ on } \partial\mathcal{B}_{\boldsymbol{\chi}}\}$, where $W^{1,p}$ is the *Sobolev space* of weakly differentiable functions, see, for example, Ciarlet [80] or Šilhavý [438]. Such clarifications are important in numerical treatments of the mechanical problem when dealing with the formulation of appropriate ansatz spaces for trial and test functions, such as in the finite-element-method.

On the equation side, we find

$$\left.\begin{array}{ll} \text{balance of momentum } \operatorname{Div}[\boldsymbol{P}] = \boldsymbol{0} & 3 \text{ equations} \\ \text{balance of moment of momentum } \boldsymbol{F}\boldsymbol{P}^T = \boldsymbol{P}\boldsymbol{F}^T & 3 \text{ equations} \end{array}\right\} \quad \rightarrow \quad 6 \text{ equations}\,. \tag{3.7}$$

It is easy to recognize that there is a gap between the number of unknowns and the number of equations and that there are $13 - 6 = 7$ equations missing for the solution of the boundary-value problem. However, this observation is very welcome when recalling the nature of the equations formulated so far and realising that they are fully independent of any specific material behaviour. Consequently, the kinematical considerations and physical balance equations investigated so far are referred to as *material-independent* relations. In order to solve the mechanical boundary-value problem, further *constitutive, material-dependent* relations have to be formulated. These allow for the incorporation of individual characteristics of materials and to account for specific mechanical properties like stiffness or direction-dependence. For the purely mechanical problem at hand, it can be concluded that the deformation map $\boldsymbol{\chi}$ is a *primary variable* and determined by using the balance of momentum, whereas one additional constitutive relation for the free energy ψ and six constitutive relations for the first Piola–Kirchhoff stress have to be added. The number of constitutive relations for the first Piola–Kirchhoff stress is hereby reduced from 9 to 6 by making use of the balance of moment of momentum.

In order to formulate physically meaningful theories, the constitutive relations should be investigated on the basis of some basic *thermodynamical principles*, which will be presented in the next section.

3.2 Constitutive framework

As outlined in the preceding section, the solution of the mechanical problem demands for the formulation of constitutive relations in addition to the physical balance equations. In the here considered mechanical problem, the Helmholtz free energy ψ and the first Piola–Kirchhoff stress tensor $\boldsymbol{P}$. Those two quantities are therefore identified as the *response functions* $\mathcal{R} = \{\psi, \boldsymbol{P}\}$ of the mechanical process. This section presents the basic thermodynamical principles of material modelling, which provide the basis for the meaningful formulation specific material laws.

3.2.1 Principle of determinism

A fundamental idea of constitutive modelling is the *principle of determinism*, which states that the present response of a system is completely determined by its past and present state. In this sense, the present response must not be dependent on any future events and determinism therefore implies *causality*. Applied to the mechanical problem at hand, the principle states that $\psi(\boldsymbol{X}, t)$ and $\boldsymbol{P}(\boldsymbol{X}, t)$ at point $\boldsymbol{X} \in \mathcal{B}_0$ and time $t \in \mathcal{R}_+$ are entirely determined by the full history $\boldsymbol{\chi}_{\mathscr{T}_t}(\boldsymbol{Y} \in \mathcal{B}_0)$ of the deformation map $\boldsymbol{\chi}$ at *all* points $\boldsymbol{Y} \in \mathcal{B}_0$ and at *all* times $\mathscr{T}_t = \{t_\mathrm{A}, t\}$. Following the seminal work of Noll [356] by introducing the *energy functional* $\mathfrak{G}_\psi$ and the *stress functional* $\mathfrak{G}_{\boldsymbol{P}}$, the above ideas result in the notation

$$\psi(\boldsymbol{X}, t) = \mathfrak{G}_\psi(\boldsymbol{\chi}_{\mathscr{T}_t}(\boldsymbol{Y})) \quad \text{and} \quad \boldsymbol{P}(\boldsymbol{X}, t) = \mathfrak{G}_{\boldsymbol{P}}(\boldsymbol{\chi}_{\mathscr{T}_t}(\boldsymbol{Y}))\,. \tag{3.8}$$

By choosing the same argument $\boldsymbol{\chi}_{\mathscr{T}_t}(\boldsymbol{Y})$ for both (all) functionals $\mathfrak{G}_\psi$ and $\mathfrak{G}_{\boldsymbol{P}}$, this formulation also meets the *principle of equipresence* as proposed by Truesdell [487].

For a variety of history- and path-dependent material behaviours, such as viscosity or plasticity, it is convenient to replace the dependence on the full motion history $\boldsymbol{\chi}_{\mathscr{T}_t}(\boldsymbol{Y})$ by a dependence on the present motion $\boldsymbol{\chi}(\boldsymbol{Y},t)$ at time t and an adaptable number of *internal variables*, see Coleman & Gurtin [81]. Any required knowledge on the motion history is then imprinted in the internal variables. Here, we will proceed with the investigation of purely elastic problems and the neglection of any history-dependent effects. The statements in (3.8) then simplify to

$$\psi(\boldsymbol{X},t) = \mathfrak{G}_\psi(\boldsymbol{\chi}(\boldsymbol{Y},t)) \quad \text{and} \quad \boldsymbol{P}(\boldsymbol{X},t) = \mathfrak{G}_{\boldsymbol{P}}(\boldsymbol{\chi}(\boldsymbol{Y},t)) \tag{3.9}$$

and express that the present responses $\psi(\boldsymbol{X})$ and $\boldsymbol{P}(\boldsymbol{X})$ at point $\boldsymbol{X} \in \mathcal{B}_0$ and time t are determined by the present deformation $\boldsymbol{\chi}(\boldsymbol{Y})$ at all points $\boldsymbol{Y} \in \mathcal{B}_0$ at time t. For the sake of a compact notation, the argument t is dropped in the following, but the time-dependence should be kept in mind.

3.2.2 Principle of local action

The dependence of the present response of $\psi(\boldsymbol{X})$ and $\boldsymbol{P}(\boldsymbol{X})$ at a specific point $\boldsymbol{X}$ in $\mathcal{B}_0$ on the deformation of the entire points $\boldsymbol{Y}$ in $\mathcal{B}_0$ is a very general statement and might not prove useful for the construction of constitutive theories. For instance, coupling of forces at a point position $\boldsymbol{X}$ with forces at distant points is already included in the continuum-mechanical theory by the concept of stress and the accompanied formulation of traction vectors $\boldsymbol{T}(\boldsymbol{X})$ at each position $\boldsymbol{X}$. In this sense, the *principle of local action*, proposed by Noll [356], states that the material response at point $\boldsymbol{X}$ is only influenced by the motion $\boldsymbol{\chi}(\boldsymbol{Y})$ of points $\boldsymbol{Y} \in \mathcal{N}_{\boldsymbol{X}}$ in a *small and smooth neighbourhood* $\mathcal{N}_{\boldsymbol{X}}$ of $\boldsymbol{X}$. Consequently, the motion $\boldsymbol{\chi}(\boldsymbol{Y})$ can be approximated by the first-order Taylor expansion

$$\boldsymbol{\chi}(\boldsymbol{Y}) \approx \boldsymbol{\chi}(\boldsymbol{X}) + \mathrm{Grad}[\boldsymbol{\chi}(\boldsymbol{X})](\boldsymbol{Y}-\boldsymbol{X})\,, \tag{3.10}$$

where it is easy to identify the deformation gradient $\boldsymbol{F}(\boldsymbol{X}) = \mathrm{Grad}[\boldsymbol{\chi}(\boldsymbol{X})]$. With this, the constitutive relations are reformulated to

$$\psi(\boldsymbol{X}) = \mathfrak{G}_\psi(\boldsymbol{\chi}(\boldsymbol{X}),\boldsymbol{F}(\boldsymbol{X})) \quad \text{and} \quad \boldsymbol{P}(\boldsymbol{X}) = \mathfrak{G}_{\boldsymbol{P}}(\boldsymbol{\chi}(\boldsymbol{X}),\boldsymbol{F}(\boldsymbol{X}))\,, \tag{3.11}$$

and the constitutive functionals $\mathfrak{G}_\psi$ and $\mathfrak{G}_{\boldsymbol{P}}$ get the meaning of constitutive functions. Consequently, the principle of local action infers that the arguments of these two functions are the motion $\boldsymbol{\chi}(\boldsymbol{X})$ and the deformation gradient $\boldsymbol{F}(\boldsymbol{X})$ at point $\boldsymbol{X}$. If the constitutive relation of a material satisfies (3.11), hence, if the set of arguments only includes first and no higher gradients of the motion, it is called *material of order one*. Higher order material theories are obtained by considering further terms in the Taylor expansion (3.10) and lead to gradient-extended material formulations. Further note that if the smoothness of the neighbourhood $\mathcal{N}_{\boldsymbol{X}}$ is not satisfied and one has to deal with discontinuities and long-range forces, like for cracked materials, one might have to take into account nonlocal effects, such as it is done by the peridynamic theory, introduced by Silling [439]. Comprehensive explanations on nonlocal theories can also be found in the book of Eringen [119].

3.2.3 Principle of material frame-indifference

Let the body $\mathscr{B}$ undergo some arbitrary deformation map $\boldsymbol{\chi}$ into some spatial configuration $\mathcal{B}$. A particle $\mathscr{P} \in \mathscr{B}$ of the body obeys specific properties and material responses, such as, for example, the free energy ψ and the stress tensor $\boldsymbol{P}$ in the configuration $\mathcal{B}$. To have a physically meaningful theory, it is absolutely indispensable that the material response of a particle $\mathscr{P}$ in the configuration $\mathcal{B}$ is invariant with respect to the frame of reference in which the material response is observed. Thus, any constitutive theory *must* satisfy the *principle of material frame-indifference*[2], formulated by Noll [355, 356]. To investigate this principle, it proves useful to notice that the change of a frame of reference can be equivalently regarded as a certain rigid-body transformation superimposed on the spatial configuration[3] $\mathcal{B}$, see Holzapfel [221]. Then, it is consequent to formulate the transformation $\boldsymbol{x}^*(\boldsymbol{X}) = \boldsymbol{\chi}^*(\boldsymbol{X}) = \boldsymbol{Q}\,\boldsymbol{\chi}(\boldsymbol{X}) + \boldsymbol{c} = \boldsymbol{Q}\,\boldsymbol{x}(\boldsymbol{X}) + \boldsymbol{c}$, which applies a rigid-body rotation $\boldsymbol{Q} \in \mathcal{SO}(3)$ and a rigid-body translation $\boldsymbol{c} \in \mathcal{R}^3$ on the spatial configuration $\boldsymbol{x}$. We require that $\boldsymbol{\chi}^*|_{t=t_0} = \boldsymbol{X}^* = \boldsymbol{X}$ such that $\partial(\cdot)/\partial\boldsymbol{X}^* = \partial(\cdot)/\partial\boldsymbol{X}$. Hence, the transformed deformation gradient is obtained by $\boldsymbol{F}^* = \mathrm{Grad}[\boldsymbol{\chi}^*] = \boldsymbol{Q}\boldsymbol{F}$, where it is recalled that the deformation gradient disregards rigid-body translations, see Section 2.1.2. The scalar free energy transforms simply as $\psi^* = \psi$, whereas the transformed stress $\boldsymbol{P}^* = \boldsymbol{Q}\boldsymbol{P}$ is obtained by using the relation $\boldsymbol{P}^*\boldsymbol{N}^* = \boldsymbol{T}^* = \boldsymbol{Q}\boldsymbol{T} = \boldsymbol{Q}\boldsymbol{P}\boldsymbol{N}$, the invariance of the referential normal vector $\boldsymbol{N}^* = \boldsymbol{N}$, and the transformation of the traction vector $\boldsymbol{T}^* = \boldsymbol{Q}\boldsymbol{T}$. The important transformations can thus be summarised as

$$\boldsymbol{\chi} \Rightarrow \boldsymbol{\chi}^* = \boldsymbol{Q}\boldsymbol{\chi} + \boldsymbol{c}\,, \quad \boldsymbol{F} \Rightarrow \boldsymbol{F}^* = \boldsymbol{Q}\boldsymbol{F}\,, \quad \psi \Rightarrow \psi^* = \psi\,, \quad \boldsymbol{P} \Rightarrow \boldsymbol{P}^* = \boldsymbol{Q}\boldsymbol{P}\,. \tag{3.12}$$

The principle of material frame indifference then demands that

$$\begin{aligned} \psi^*(\boldsymbol{X}) &= \mathfrak{G}_\psi(\boldsymbol{\chi}^*(\boldsymbol{X}), \boldsymbol{F}^*(\boldsymbol{X})) = \psi(\boldsymbol{X}) = \mathfrak{G}_\psi(\boldsymbol{\chi}(\boldsymbol{X}), \boldsymbol{F}(\boldsymbol{X}))\,, \\ \boldsymbol{P}^*(\boldsymbol{X}) &= \mathfrak{G}_{\boldsymbol{P}}(\boldsymbol{\chi}^*(\boldsymbol{X}), \boldsymbol{F}^*(\boldsymbol{X})) = \boldsymbol{Q}\boldsymbol{P}(\boldsymbol{X}) = \boldsymbol{Q}\mathfrak{G}_{\boldsymbol{P}}(\boldsymbol{\chi}(\boldsymbol{X}), \boldsymbol{F}(\boldsymbol{X}))\,. \end{aligned} \tag{3.13}$$

However, since (3.13) has to be valid for arbitrary values of $\boldsymbol{Q} \in \mathcal{SO}(3)$ and $\boldsymbol{c} \in \mathcal{R}^3$ (as long as $\boldsymbol{X}^* = \boldsymbol{X}$), it must equally hold for the specific choices $\boldsymbol{Q} = \boldsymbol{I}$ and $\boldsymbol{c} = -\boldsymbol{u}$. Then, since we obtain $\boldsymbol{\chi}^* = \boldsymbol{X}$ and $\boldsymbol{F}^* = \boldsymbol{F}$, relations (3.13) become $\psi = \mathfrak{G}^*_\psi(\boldsymbol{X}, \boldsymbol{F}) = \mathfrak{G}_\psi(\boldsymbol{\chi}, \boldsymbol{F})$ and $\boldsymbol{P} = \mathfrak{G}^*_{\boldsymbol{P}}(\boldsymbol{X}, \boldsymbol{F}) = \mathfrak{G}_{\boldsymbol{P}}(\boldsymbol{\chi}, \boldsymbol{F})$, and it is concluded that the deformation map $\boldsymbol{\chi}$ is no appropriate argument for the construction of constitutive relations. This is a further implication of the principle of local action accompanied with the principle of frame indifference and essentially states that the constitutive relations at point $\boldsymbol{X}$ must only depend on the *localisation* of the motion in the small neighbourhood $\mathcal{N}_{\boldsymbol{X}}$. Summarising, the conditions for the constitutive relations read

$$\mathfrak{G}_\psi(\boldsymbol{Q}\boldsymbol{F}) = \mathfrak{G}_\psi(\boldsymbol{F}) \quad \text{and} \quad \mathfrak{G}_{\boldsymbol{P}}(\boldsymbol{Q}\boldsymbol{F}) = \boldsymbol{Q}\mathfrak{G}_{\boldsymbol{P}}(\boldsymbol{F}) \quad \forall \boldsymbol{Q} \in \mathcal{SO}(3)\,. \tag{3.14}$$

[2] Alternative terms are principle of observer-invariance or principle of material objectivity. However, Noll [357] suggests to avoid the terms observer and objectivity in this context.

[3] In principle, invariance with respect to an arbitrary change of observer is referred to as the *Zaremba–Jaumann form*, whereas invariance with respect to a rigid-body motion of the spatial configuration is referred to as the *Hooke–Poisson–Cauchy form*, see Truesdell & Noll [490]. The equivalence of those two approaches is by no means general and has been subject to lively discussions, see, for example, the article of Frewer [139], which provides an exhaustive overview on the historical development of the concept of frame-indifference, as well as the article of Liu & Sampaio [292]. For the concerns here, the two forms can be used equivalently in the sense of satisfying Euclidian frame-indifference, see Svendsen & Bertram [466].

If the constitutive relations of a material satisfy (3.14), it is called *simple material*. Further note that the principle of frame indifference is not only demanded for the response functions ψ and $\boldsymbol{P}$, but it is also an intuitive requirement for any kind of material properties.

3.2.4 Principle of material symmetry

Next, let the body $\mathscr{B}$ undergo some deformation into a spatial configuration $\mathcal{B}$, now governed by the deformation gradient $\boldsymbol{F}$. A material of the most general type is expected to show distinct responses of the free energy ψ and the stress $\boldsymbol{P}$ to the same deformation, dependent on how the body is oriented in space before the deformation is applied. This means that the material response relies on the information of the initial orientation of the body $\mathscr{B}$ in its reference configuration $\mathcal{B}_0$. The material is then called *direction-dependent* or *anisotropic*. However, a large number of materials shows certain invariance characteristics of the response functions upon specific rotations $\boldsymbol{Q} \in \mathcal{MG}$ of the reference configuration $\mathcal{B}_0$, where $\mathcal{MG}$ is referred to as the *symmetry group* of the material. From a physical point of view, it would be logical that the symmetry group $\mathcal{MG} \subseteq \mathcal{SO}(3)$ has to be a subset of the proper orthogonal rotation group, thus providing shape- and volume-preserving transformations. However, from a more general mathematical and geometrical point of view, the symmetry group $\mathcal{MG}$ must be allowed to be a subset of the full orthogonal group $\mathcal{O}(3)$, which additionally includes reflections (so-called rotoinversions) with $\det[\boldsymbol{Q}] = -1$. For instance, $\boldsymbol{Q} = -\boldsymbol{I} \in \mathcal{O}(3)$ represents a so-called central inversion. Such transformations are of course unachievable for real physical objects and rather have an imaginary character. They are necessary to be consistent with the classical works on crystallography and the characterisation of the complete (also point) symmetries in materials. For completeness, note that according to Gurtin & Williams [178] the symmetry group $\mathcal{MG} \subseteq \mathcal{O}(3) \subset \mathcal{SL}(3)$ has to be at least a subset of the special linear group $\mathcal{SL}(3)$ of general volume-preserving transformations, which allows for a generalisation of the theory to fluids.

The *principle of material symmetry* now demands for the invariance of the material response functions with respect to proper orthogonal rotations $\boldsymbol{Q} \in \mathcal{MG}$ of the reference configuration. A mathematical investigation of a rotated reference configuration gives the notation $\boldsymbol{X}^+ = \boldsymbol{Q}\boldsymbol{X}$ for the rotated reference position and the associated deformation gradient $\boldsymbol{F}^+ = \partial\boldsymbol{\chi}/\partial\boldsymbol{X}^+ = \partial\boldsymbol{\chi}/\partial\boldsymbol{X}\,\partial\boldsymbol{X}/\partial\boldsymbol{X}^+ = \boldsymbol{F}\boldsymbol{Q}^T$, by using $\partial\boldsymbol{X}/\partial\boldsymbol{X}^+ = \boldsymbol{Q}^{-1}$ and recalling $\boldsymbol{Q}^{-1} = \boldsymbol{Q}^T$. Again, the scalar free energy transforms as $\psi^+ = \psi$, whereas the rotated first Piola–Kirchhoff stress tensor $\boldsymbol{P}^+ = \boldsymbol{P}\boldsymbol{Q}^T$ is obtained by using the relation $\boldsymbol{P}^+\boldsymbol{N}^+ = \boldsymbol{P}^+\boldsymbol{Q}\boldsymbol{N} = \boldsymbol{T}^+ = \boldsymbol{T} = \boldsymbol{P}\boldsymbol{N}$ with the invariance $\boldsymbol{T}^+ = \boldsymbol{T}$ of the nominal traction vector and the contravariant transport $\boldsymbol{N}^+ = \boldsymbol{Q}^{-T}\boldsymbol{N} = \boldsymbol{Q}\boldsymbol{N}$ of the referential normal vector. We can thus summarise the referential transformations as

$$\boldsymbol{X} \Rightarrow \boldsymbol{X}^+ = \boldsymbol{Q}\boldsymbol{X}\,, \quad \boldsymbol{F} \Rightarrow \boldsymbol{F}^+ = \boldsymbol{F}\boldsymbol{Q}^T\,, \quad \psi \Rightarrow \psi^+ = \psi\,, \quad \boldsymbol{P} \Rightarrow \boldsymbol{P}^+ = \boldsymbol{P}\boldsymbol{Q}^T\,. \tag{3.15}$$

The invariance condition associated with the principle of material symmetry then demands that

$$\begin{aligned} \psi^+(\boldsymbol{X}^+) &= \mathfrak{G}_\psi(\boldsymbol{F}^+) = \psi(\boldsymbol{X}) = \mathfrak{G}_\psi(\boldsymbol{F})\,, \\ \boldsymbol{P}^+(\boldsymbol{X}^+) &= \mathfrak{G}_{\boldsymbol{P}}(\boldsymbol{F}^+) = \boldsymbol{P}(\boldsymbol{X})\boldsymbol{Q}^T = \mathfrak{G}_{\boldsymbol{P}}(\boldsymbol{F})\boldsymbol{Q}^T \qquad \forall \boldsymbol{Q} \in \mathcal{MG}\,. \end{aligned} \tag{3.16}$$

This results in the relations

$$\mathfrak{G}_\psi(\boldsymbol{F}\boldsymbol{Q}^T) = \mathfrak{G}_\psi(\boldsymbol{F}) \quad \text{and} \quad \mathfrak{G}_{\boldsymbol{P}}(\boldsymbol{F}\boldsymbol{Q}^T) = \mathfrak{G}_{\boldsymbol{P}}(\boldsymbol{F})\boldsymbol{Q}^T \quad \forall \boldsymbol{Q} \in \mathcal{MG} \tag{3.17}$$

for the constitutive functions. Note that a specific symmetry group can be formulated as

$$\mathcal{MG} = \{\boldsymbol{Q} \in \mathcal{O}(3) \mid \mathfrak{G}_\psi(\boldsymbol{F}) = \mathfrak{G}_\psi(\boldsymbol{F}\boldsymbol{Q}^T)\}\,. \tag{3.18}$$

Due to the obvious similarity to the principle of material frame-indifference, which formulates an invariance condition on the actual configuration, the principle of material symmetry is referred to as invariance of referential rotations. The structure of both principles suggest the formulation of material response functions in terms of *scalar invariants* of the Cauchy–Green strain tensors and an adaptable number of *structural tensors*, which account for the symmetry group $\mathcal{MG}$ of the material. Explanations on the theory of invariants and further investigations for the special cases of isotropy and transverse isotropy follow in Section 3.5.

3.2.5 Principle of dissipation

In order to guarantee the *thermodynamical consistency* of constitutive material relations, the dissipation inequality as introduced in Section 2.3.6 has to be fulfilled for all admissible deformations. Since we restrict attention to isothermal processes, it suffices to investigate the dissipation inequality in the reduced form (2.51). Further, only reversible, fully elastic processes are subject of this work such that the inequality can be transformed into an equality, giving

$$\mathcal{D} = \boldsymbol{P} \cdot \dot{\boldsymbol{F}} - \rho_0\, \dot{\psi} = 0 \tag{3.19}$$

for the local dissipation of the material. To proceed, we consider the chain rule and reformulate the temporal rate of the free energy to $\dot{\psi} = \partial_{\boldsymbol{F}}\psi \cdot \dot{\boldsymbol{F}}$, which transforms the dissipation to $\mathcal{D} = (\boldsymbol{P} - \rho_0\, \partial_{\boldsymbol{F}}\psi) \cdot \dot{\boldsymbol{F}} = 0$. Note that $\partial_{\boldsymbol{F}}\psi$ depicts the tensor-valued derivative of the free energy ψ with respect to the deformation gradient $\boldsymbol{F}$. The *Coleman–Noll procedure*, see Coleman & Noll [83], now states that the dissipation equation has to be fulfilled for all admissible deformation rates $\dot{\boldsymbol{F}}$. It is easy to show that this results in the well-known relation $\boldsymbol{P}(\boldsymbol{X}) = \rho_0\, \partial_{\boldsymbol{F}}\psi(\boldsymbol{X})$, defining the first Piola–Kirchhoff stress tensor $\boldsymbol{P}$ as tensor-valued derivative of the free energy ψ with respect to the deformation gradient $\boldsymbol{F}$, weighted by the initial density ρ_0. For the following consideration, it proves useful to proceed with the *volume-specific* Helmholtz energy $\mathscr{W} := \rho_0\, \psi$, which is referred to as *strain- or stored-energy*. This allows to summarise the *principle of dissipation* by

$$\mathcal{D} = 0 \quad \rightarrow \quad \boldsymbol{P}(\boldsymbol{X}) = \partial_{\boldsymbol{F}}\mathscr{W}(\boldsymbol{X})\,. \tag{3.20}$$

In conclusion, the stress tensor $\boldsymbol{P}$ at $\boldsymbol{X}$ and hence the stresses in the whole body $\mathscr{B}$ are fully specified by the definition of a scalar-valued *hyperelastic potential* in terms of the strain-energy function $\mathscr{W}$ and the deformation quantified by $\boldsymbol{F}$. Further, it is easy to observe that (3.20) is consistent with the material frame indifference condition $(3.14)_2$ for the Piola–Kirchhoff stress $\boldsymbol{P}$, since $\boldsymbol{P}(\boldsymbol{Q}\boldsymbol{F}) = \partial_{\boldsymbol{F}}\mathscr{W}(\boldsymbol{Q}\boldsymbol{F}) = \boldsymbol{Q}\partial_{\boldsymbol{F}}\mathscr{W}(\boldsymbol{F}) = \boldsymbol{Q}\boldsymbol{P}(\boldsymbol{F})$. Note that from here on, the difference between the function $\mathfrak{G}_\psi$ and the value ψ (or the volume-specific form $\mathscr{W}$) is not explicitly stated and ψ and $\mathscr{W}$ can have both meanings, which shall become clear from the context. The evaluation of the dissipation inequality is the essential tool for the construction of constitutive theories, not only for the here investigated case of elasticity, but especially when dealing with irreversible and rate-dependent effects. These aspects are frequently treated by the connection of the internal variable approach and the dissipation principle in order to obtain thermodynamically consistent evolution equations for the description of internal processes, see, for example, Coleman & Gurtin [81].

3.3 Internal constraints

The preceding considerations were based on the maxim that the motion of the body $\mathscr{B}$ is not subject to any kinematical restrictions on the *inside* of the body and that the deformation map $\boldsymbol{\chi}(\boldsymbol{X})$ and the according deformation gradient $\boldsymbol{F}(\boldsymbol{X})$ are only limited by arguments of physical meaningfulness, such as the exclusion of material interpenetration, and the boundary conditions on the surface. However, there are scenarios for which we may constitutively assume that a material is subject to *internal constraints* that additionally restrict the possible motion of a material particle $\mathscr{P}$ at each time t. This is treated by introducing a scalar-valued constraint function $\mathscr{R}$ such that

$$\mathscr{R}(\boldsymbol{F}) = \mathscr{R}(\boldsymbol{Q}\boldsymbol{F}) = 0 \quad \forall \boldsymbol{Q} \in \mathcal{SO}(3)\,. \tag{3.21}$$

If more than one, say N, constraints are imposed on the motion, a constraint function $\mathscr{R}_i$ $(i = 1, 2, ..., N)$ for each of them has to be formulated. Further, since imposing an internal constraint is a constitutive assumption, $\mathscr{R}$ has to satisfy the principle of frame-indifference. This is guaranteed through (3.21) by means of the frame-indifference condition for scalar functions, reminiscent to $(3.14)_1$. It shall be remarked that the assumption of a constrained motion may not only depend on the considered material alone, but also on the conditions under which the material shall be investigated. For instance, certain assumptions may be useful for specific loading regimes, but not for the material in general. It is also clear that assuming such constraints is always an idealisation of the real behaviour.

Note that Antman & Marlow [11] refer to constraints of form (3.21) as *local constraints* and additionally introduce the concept of so-called global constraints as a generalisation of the local form. Moreover, consice explanations on internal constraints are also given in Carlson & Tortorelli [72], whereas a thermodynamical perspective on the topic is provided by Gurtin & Podio-Guidugli [176].

3.3.1 Principle of determinism for constrained materials

The principle of determinism as formulated in Section 3.2.1 is not compatible with the concept of internal constraints. While the free energy ψ (and, thus, the strain energy $\mathscr{W}$) is still fully determined by the deformation history $\boldsymbol{\chi}_{\mathscr{T}_t}$, as stated in $(3.8)_1$, the stress tensor $\boldsymbol{P}$ is now determined by the deformation history $\boldsymbol{\chi}_{\mathscr{T}_t}$ only up to a *reaction stress* tensor $\boldsymbol{\mathcal{C}} \in \mathcal{R}^{3\otimes 3}$, which does no work in any motion satisfying the constraint $\mathscr{R}$. This leads to the *principle of determinism for constrained materials*, see, for example, Truesdell & Noll [490] or Smith [448]. For elastic materials, the stress tensor is then given by

$$\boldsymbol{P} = \mathfrak{G}_{\boldsymbol{P}}(\boldsymbol{F}) + \boldsymbol{\mathcal{C}} \tag{3.22}$$

and the stress contribution from the functional $\mathfrak{G}_{\boldsymbol{P}}(\boldsymbol{F})$, determined by the present deformation gradient $\boldsymbol{F}$, becomes the *extra (or determinate) stress*. In order to specify the reaction stress $\boldsymbol{\mathcal{C}}$, it is useful to recognise that if the constraint function $\mathscr{R}$ is zero, also its temporal rate $\dot{\mathscr{R}}$ has to be zero. Connecting this to the requirement that $\boldsymbol{\mathcal{C}}$ must not contribute to the work, and hence to the stress power $\boldsymbol{P} \cdot \dot{\boldsymbol{F}}$, during any motion satisfying the constraint $\mathscr{R}$ leads to

$$\left.\begin{aligned} \mathscr{R} = 0 \quad \rightarrow \quad \dot{\mathscr{R}} = \partial_{\boldsymbol{F}}\mathscr{R} \cdot \dot{\boldsymbol{F}} = 0 \\ \boldsymbol{\mathcal{C}} \cdot \dot{\boldsymbol{F}} = 0 \end{aligned}\right\} \quad \rightarrow \quad \boldsymbol{\mathcal{C}} = \alpha_{\mathscr{R}}\, \partial_{\boldsymbol{F}}\mathscr{R} \quad \text{with} \quad \alpha_{\mathscr{R}} \in \mathcal{R}\,. \tag{3.23}$$

Thus, the stress contribution $\boldsymbol{\mathcal{C}}$ associated with the constraint $\mathscr{R}$ is given by the tensor-valued derivative $\partial_{\boldsymbol{F}}\mathscr{R}$ of the constraint with respect to the deformation gradient and a scalar multiplier $\alpha_{\mathscr{R}} \in \mathcal{R}$. The scalar $\alpha_{\mathscr{R}}$ thereby has the role of a *Lagrange multiplier*, which becomes clear in Section 3.4.3 where we look at the problem of internal constraints from a variational perspective. In actual problems, the scalar $\alpha_{\mathscr{R}}$ has to be determined from the motion $\boldsymbol{\chi}$ and the boundary conditions on the surface of the body $\mathscr{B}$. Connecting the finding of this section with the outcome of the principle of dissipation in Section 3.2.5, we can write the first Piola–Kirchhoff stress tensor for constrained materials in the form

$$\boldsymbol{P} = \partial_{\boldsymbol{F}}\mathscr{W} + \alpha_{\mathscr{R}}\,\partial_{\boldsymbol{F}}\mathscr{R}\,. \tag{3.24}$$

3.3.2 The assumption of material incompressibility

Many materials are characterised through a resistance to volumetric deformations which is several orders of magnitude higher than their resistance to deviatoric (non-volumetric) deformations. From an idealised point of view, such materials can then be considered to belong to the class of *incompressible materials* and, thus, obey an infinite volumetric stiffness. As pointed out before, such idealising assumptions have to be justified by, for example, experimental observations and have to stay valid for the range of motions that shall be investigated. In order to express the incompressibility assumption in terms of a constraint function of the form (3.21), we recall the volume map (2.15) and demand for the equality of current volume elements $\mathrm{d}v$ and referential volume element $\mathrm{d}V$. This leads to the incompressibility constraint function

$$\mathscr{R}(\boldsymbol{F}) = \det[\boldsymbol{F}] - 1 = 0\,. \tag{3.25}$$

By considering the invariant characteristic of the determinant, $\det[\boldsymbol{Q}\boldsymbol{F}] = \det[\boldsymbol{Q}]\det[\boldsymbol{F}] = \det[\boldsymbol{F}]$, we observe that (3.25) directly satisfies the frame-indifference condition $\mathscr{R}(\boldsymbol{Q}\boldsymbol{F}) = \mathscr{R}(\boldsymbol{F})$. The derivative of the constraint function $\mathscr{R}$ with respect to the deformation gradient is identified as

$$\partial_{\boldsymbol{F}}\mathscr{R} = \det[\boldsymbol{F}]\boldsymbol{F}^{-T}\,, \tag{3.26}$$

see (A.55). Consequently, inserting (3.26) into (3.24) gives the first Piola–Kirchhoff stress tensor for incompressible materials as

$$\boldsymbol{P} = \partial_{\boldsymbol{F}}\mathscr{W} + \wp\det[\boldsymbol{F}]\boldsymbol{F}^{-T}\,, \tag{3.27}$$

where $\wp$ denotes the scalar multiplier $\alpha_{\mathscr{R}}$ for this specific type of constraint. At this point, it makes sense to note that the *hydrostatic pressure* in a material is given by

$$p = -\tfrac{1}{3}\operatorname{tr}[\boldsymbol{\sigma}] = -\tfrac{1}{3}\,\boldsymbol{\sigma}\cdot\boldsymbol{I} \tag{3.28}$$

in terms of the trace of the Cauchy true stress tensor $\boldsymbol{\sigma}$. In order to obtain the pressure in terms of the here used first Piola–Kirchhoff stress $\boldsymbol{P}$, we recall the relation $\boldsymbol{P} = \boldsymbol{\sigma}\operatorname{cof}[\boldsymbol{F}]$ from Section 2.2, reformulate it to $\boldsymbol{\sigma} = J^{-1}\boldsymbol{P}\boldsymbol{F}^{T}$, and make use of the rule $\boldsymbol{P}\boldsymbol{F}^{T}\cdot\boldsymbol{I} = \boldsymbol{P}\cdot\boldsymbol{F}$, yielding

$$p = -\tfrac{1}{3}J^{-1}\boldsymbol{P}\cdot\boldsymbol{F}\,. \tag{3.29}$$

With this formulation at hand, the hydrostatic pressure in an incompressible material is derived from the stress tensor (3.27) as

$$p = -\tfrac{1}{3}J^{-1}\,\partial_{\boldsymbol{F}}\mathscr{W}\cdot\boldsymbol{F} - \wp\,, \tag{3.30}$$

where we used the relation $\boldsymbol{F}^{-T} \cdot \boldsymbol{F} = 3$. Eq. (3.30) clearly shows that the scalar multiplier $\wp$ associated with the incompressibility constraint represents an *additional* hydrostatic pressure contribution. However, $\wp$ is not the overall pressure in the material, since there is still a hydrostatic contribution from the extra stress $\partial_{\boldsymbol{F}} \mathscr{W}$.

The assumption of material incompressibility will be frequently employed throughout this work. However, we will not explicitly enforce the frequently used notation $\boldsymbol{P}_{\mathrm{E}}$ for the extra stresses $\partial_{\boldsymbol{F}} \mathscr{W}$, as used by, for example, Truesdell & Noll [490]. Instead, we emphasise that the derivative $\partial_{\boldsymbol{F}} \mathscr{W}$ of the strain-energy function necessarily has to be supplemented by the contribution of the Lagrange multiplier in order to obtain the complete stress formulation when the material is subject to internal constraints. Hence, incompressibility always leads to stress formulations as given in Eq. (3.27).

3.4 Variational principles in mechanics

In the previous sections, the basic thermodynamical principles of constitutive material modelling were presented. Especially the result of the evaluation of the dissipation principle in Section 3.2.5 pointed out the importance of the strain-energy $\mathscr{W}$ (the volume-specific version of the Helmholtz free energy ψ) when considering mechanical problems. In the purely elastic case, as considered here, the strain-energy function $\mathscr{W}$ acts as an elastic potential and fully describes the material behaviour. The occurrence of a potential suggests to approach the mechanical problem from a *variational* perspective and appropriate *extremum principles* for the energy. These considerations proof useful in a variety of continuum-mechanical investigations and will be used later in this work. Here, we present a compact summary of some fundamental variational principles to introduce the basic ideas and notation. For far more comprehensive approaches to the topic, we especially refer to the highly recommendable textbook of Lanczos [274] as well as to the works of Oden & Reddy [358] and Sewell [430]. Further valuable explanations on the variational approach in finite elasticity are provided in Ogden [362].

3.4.1 Basics on variational calculus

Consider a scalar-valued function $F : \mathcal{R}^n \to \mathcal{R}$ of n scalar variables $\mathfrak{q}_n$. The elementary problem of variational calculus is to find a specific configuration of variables $\mathfrak{q}_n$ under which the function value F becomes *stationary*:

$$F(\mathfrak{q}) \quad \to \quad \text{stat} \tag{3.31}$$

Therein, the generalised vector $\mathfrak{q} = [\mathfrak{q}_1, \mathfrak{q}_2, \dots, \mathfrak{q}_n]$ contains the n scalar variables. The solution of this problem is achieved by finding the set of variables $\mathfrak{q}$ under which the *variation* δF of the function F vanishes. Doing so, the variation δF is obtained by performing the *Gateaux derivative* of F with respect to $\mathfrak{q}$, giving

$$\delta F(\mathfrak{q}, \delta\mathfrak{q}) = \frac{\mathrm{d}}{\mathrm{d}\varepsilon} F(\mathfrak{q} + \varepsilon\delta\mathfrak{q})\big|_{\varepsilon=0} = \sum_{i=1}^{n} \frac{\partial F}{\partial \mathfrak{q}_i}\, \delta\mathfrak{q}_i \overset{!}{=} 0\,, \tag{3.32}$$

where the third expression is obtained by a consequent elimination of the parameter ε. In Eq. (3.32), the variations $\delta\mathfrak{q} = [\delta\mathfrak{q}_1, \delta\mathfrak{q}_2, \dots, \delta\mathfrak{q}_n]$ have the character of *infinitesimal*

virtual changes or test functions of the variables $\mathfrak{q}$. Considering the virtual nature of the variations $\delta\mathfrak{q}$, it is consequent to demand that the variation δF has to vanish for arbitrary values $\delta\mathfrak{q}$. This subsequently leads to the well-known statement

$$\delta F = 0 \quad \rightarrow \quad \frac{\partial F}{\partial \mathfrak{q}_i} = 0 \quad \text{for } i = 1, \dots, n\,. \tag{3.33}$$

Hence, stationarity of F requires that the n first derivatives of function F with respect to the variables $\mathfrak{q}_i$ are zero. With this, we can write that the variational problem

$$F(\mathfrak{q}) = \operatorname*{stat}_{\mathfrak{q}^* \in \mathcal{R}^n} F(\mathfrak{q}^*) \tag{3.34}$$

is solved by finding the specific set

$$\mathfrak{q} = \{\mathfrak{q}_1, \mathfrak{q}_2, \dots, \mathfrak{q}_n\} = \arg\left\{ \operatorname*{stat}_{\mathfrak{q}^*} F(\mathfrak{q}^*) \right\} \tag{3.35}$$

of variables such that the variation δF vanishes. In (3.34), the generalised vector $\mathfrak{q}^* = [\mathfrak{q}_1^*, \mathfrak{q}_2^*, \dots, \mathfrak{q}_n^*]$ contains the so-called *trial functions*. Moreover, it is well-known from basic analysis that a stationary value can have the character of an *extremal value*, hence, it might depict a minimum or maximal value of the function F. This is explored by considering the second variation $\delta^2 F$ of the function F, which consequently involves the second derivatives of F with respect to the variables $\mathfrak{q}_i$. An extremum exists if $\delta^2 F \neq 0$ and its type is then determined by the positiveness or negativeness of the second variation. Hence, finding the stationary value of a function is the basic step also when searching for an extremal value. It shall be further remarked that finding the stationary value can be sufficient for the estimation of an extremal value, if adequate properties of the underlying problem are a priori known. For example, strict convexity of the function F will always entail that a stationary value minimises the function and makes a further investigation of the second variation superfluous.

In continuum mechanics, variational problems usually arise in an integral form, meaning that one aims to find a stationary solution of some scalar-valued functional $I : \mathcal{R}^n \rightarrow \mathcal{R}$, such that

$$I(\mathfrak{q}) = \int_a^b F(\mathfrak{q}(p), \mathfrak{q}'(p), p)\, \mathrm{d}x \quad \rightarrow \quad \text{stat}\,, \tag{3.36}$$

containing the scalar-valued function $F : \mathcal{R}^n \rightarrow \mathcal{R}$, a generalised vector $\mathfrak{q}(x) \in \mathcal{R}^n$ with n scalar functions $\mathfrak{q}_i(x)$, and a vector $\mathfrak{q}' = \partial_p \mathfrak{q}(x)$ containing the derivatives of $\mathfrak{q}(x)$ with respect to the coordinate x. Further, the definite integral is defined over the closed interval $x \in (a, b)$ and some values $\mathfrak{q}(a) = \mathfrak{q}_a$ and $\mathfrak{q}(b) = \mathfrak{q}_b$ are prescribed at the boundaries. With that, the problem stated in (3.36) can be summarised by

$$I(\mathfrak{q}) = \operatorname*{stat}_{\mathfrak{q}^* \in \mathcal{K}(\mathfrak{q})} I(\mathfrak{q}^*)\,, \tag{3.37}$$

where we formulated the set

$$\mathcal{K}(\mathfrak{q}) = \{\mathfrak{q} \in \mathcal{R}^n \mid \mathfrak{q}(a) = \mathfrak{q}_a \text{ and } \mathfrak{q}(b) = \mathfrak{q}_b\} \tag{3.38}$$

of admissible solutions compatible with the boundary conditions. Now, by demanding that the variation of the functional I vanishes, we arrive at

$$\delta I(\mathfrak{q}, \delta\mathfrak{q}) = \delta \int_a^b F(\mathfrak{q}, \mathfrak{q}', x)\, \mathrm{d}x = \int_a^b \delta F(\mathfrak{q}, \delta\mathfrak{q}, \mathfrak{q}', x)\, \mathrm{d}x = 0\,, \tag{3.39}$$

where use was made of the elementary feature that the operations of variation and integration are interchangeable. Hence, the variation of a definite integral is equal to the definite integral of the variation, see LANCZOS [274, ch. 9]. Further, it is an essential requirement that the test functions $\delta\mathbf{q} = [\delta\mathbf{q}_1, \delta\mathbf{q}_2, \dots, \delta\mathbf{q}_n]$ *vanish on the boundary*, meaning that $\delta\mathbf{q}_i(a) = \delta\mathbf{q}_i(b) = 0$ for $i = 1, \dots, n$. The solution of (3.39), which equally solves the original problem (3.36), is found by solving the associated system

$$\frac{\mathrm{d}}{\mathrm{d}x}\frac{\partial F}{\partial \mathbf{q}_i'} - \frac{\partial F}{\partial \mathbf{q}_i} = 0 \quad \text{for } i = 1, \dots, n \tag{3.40}$$

of n differential equations under the consideration of the admissible solution set $\mathcal{K}(\mathbf{q})$. Eqs (3.40) are a one-dimensional version of the *Euler–Lagrange* equations, since the integral is performed on the line domain $x \in (a, b)$. The generalisation of these principles to three-dimensional domains will be done in the next section.

3.4.2 The principle of minimum potential energy in elastostatics

Starting point for a variational treatment of the mechanical problem is the formulation of the *elastostatic potential*

$$\Pi(\boldsymbol{\chi}) = \Pi_{\mathrm{int}}(\boldsymbol{\chi}) + \Pi_{\mathrm{ext}}(\boldsymbol{\chi}) \tag{3.41}$$

of the body $\mathscr{B}$, where $\Pi(\boldsymbol{\chi})$ is the sum of the stored elastic (internal) energy $\Pi_{\mathrm{int}}(\boldsymbol{\chi})$ in the body $\mathscr{B}$ and the work $\Pi_{\mathrm{ext}}(\boldsymbol{\chi})$ from external loads. The first term is described by a referential volume integral, reading

$$\Pi_{\mathrm{int}}(\boldsymbol{\chi}) = \int_{\mathcal{B}_0} \mathscr{W}(\boldsymbol{F})\,\mathrm{d}V \tag{3.42}$$

in terms of the hyperelastic energy potential $\mathscr{W}$. Thus, it denotes the hyperelastic energy storage in the body $\mathscr{B}$. Under the neglection of body forces, the work from external loads is given by

$$\Pi_{\mathrm{ext}}(\boldsymbol{\chi}) = -\int_{\partial\mathcal{B}_{\boldsymbol{T}}} \overline{\boldsymbol{T}} \cdot \boldsymbol{\chi}\,\mathrm{d}A \tag{3.43}$$

as a Neumann surface integral in terms of the surface tractions $\overline{\boldsymbol{T}}$. The *principle of minimum potential energy* in elastostatics now describes that an equilibrium state is given when the elastostatic potential Π reaches a minimum value for a motion $\boldsymbol{\chi}$, hence,

$$\Pi(\boldsymbol{\chi}) \quad \to \quad \min\,. \tag{3.44}$$

We directly observe that Π denotes an energy functional, since it is defined in terms of integrals of functions of $\boldsymbol{\chi}$, and we see the similarity to the problem described in (3.36). Thus, use can be made of the notations presented in the previous section and the present minimisation problem can be summarised by

$$\Pi(\boldsymbol{\chi}) = \min_{\boldsymbol{\chi}^* \in \mathcal{K}} \Pi(\boldsymbol{\chi}^*) \quad \text{such that} \quad \boldsymbol{\chi} = \arg\Big\{ \min_{\boldsymbol{\chi}^* \in \mathcal{K}} \Pi(\boldsymbol{\chi}^*) \Big\}\,. \tag{3.45}$$

In accordance to the observations before, see Eq. (3.38), the trial functions $\boldsymbol{\chi}^*$ have to meet certain constraints. This is considered by the introduction of the set[4]

$$\mathcal{K} = \{\boldsymbol{\chi}^* \mid \boldsymbol{\chi}^* = \overline{\boldsymbol{\chi}} \text{ on } \partial\mathcal{B}_{\boldsymbol{\chi}}\} \tag{3.46}$$

[4] See the footnote on page 30.

of kinematically admissible deformation fields, which essentially accounts for the Dirichlet boundary conditions prescribed on the Dirichlet surface $\partial\mathcal{B}_{\boldsymbol{\chi}} \subset \partial\mathcal{B}_0$ of the body. Now, we recall from Section 3.4.1 that the first step for finding an extremal value of a functional is always to search for a stationary solution and that the type of the value can be determined by considering either the second variation or appropriate a priori knowledge on the underlying problem. Hence, the problem given in (3.45) can be reformulated to

$$\Pi(\boldsymbol{\chi}) = \operatorname*{stat}_{\boldsymbol{\chi}^* \in \mathcal{K}} \Pi(\boldsymbol{\chi}^*) \quad \text{such that} \quad \boldsymbol{\chi} = \arg\left\{ \operatorname*{stat}_{\boldsymbol{\chi}^* \in \mathcal{K}} \Pi(\boldsymbol{\chi}^*) \right\} \tag{3.47}$$

and the postulation that the problem is such that the stationary value depicts a minimum value. Discussions on appropriate requirements for the existence of minimisers will follow in Section 3.6.3. We further note that a variational principle as formulated in (3.47) is called *principle of stationary potential energy*. Finally, a stationary solution of the energy functional Π requires that the variation $\delta\Pi$ vanishes:

$$\delta\Pi(\boldsymbol{\chi}, \delta\boldsymbol{\chi}) = \delta\Pi_{\text{int}}(\boldsymbol{\chi}, \delta\boldsymbol{\chi}) + \delta\Pi_{\text{ext}}(\delta\boldsymbol{\chi}) \overset{!}{=} 0\,. \tag{3.48}$$

By recalling that the operations of variation and integration can be interchanged, we can write the variation of the elastic energy storage as

$$\delta\Pi_{\text{int}}(\boldsymbol{\chi}, \delta\boldsymbol{\chi}) = \delta \int_{\mathcal{B}_0} \mathscr{W}(\boldsymbol{F})\,\mathrm{d}V = \int_{\mathcal{B}_0} \partial_{\boldsymbol{F}} \mathscr{W}(\boldsymbol{F}) \cdot \delta\boldsymbol{F}\,\mathrm{d}V = \int_{\mathcal{B}_0} \boldsymbol{P}(\boldsymbol{F}) \cdot \mathrm{Grad}[\delta\boldsymbol{\chi}]\,\mathrm{d}V\,. \tag{3.49}$$

Therein, use was made of $\delta\boldsymbol{F} = \delta\mathrm{Grad}[\boldsymbol{\chi}] = \mathrm{Grad}[\delta\boldsymbol{\chi}]$, since the gradient operator and the variation are interchangeable as well. Moreover, applying the divergence theorem $\boldsymbol{P} \cdot \mathrm{Grad}[\delta\boldsymbol{\chi}] = \mathrm{Div}[\boldsymbol{P}^T\delta\boldsymbol{\chi}] - \mathrm{Div}[\boldsymbol{P}] \cdot \delta\boldsymbol{\chi}$, the Gaussian integral theorem on the resulting first divergence term, and using $\boldsymbol{P}^T\delta\boldsymbol{\chi} \cdot \boldsymbol{N}\mathrm{d}A = \boldsymbol{P}\boldsymbol{N} \cdot \delta\boldsymbol{\chi}\mathrm{d}A$, the variation $\delta\Pi_{\text{int}}$ can be reformulated to

$$\delta\Pi_{\text{int}}(\boldsymbol{\chi}, \delta\boldsymbol{\chi}) = \int_{\mathcal{B}_0} -\mathrm{Div}[\boldsymbol{P}(\boldsymbol{F})] \cdot \delta\boldsymbol{\chi}\,\mathrm{d}V + \int_{\partial\mathcal{B}_{\boldsymbol{T}}} \boldsymbol{P}(\boldsymbol{F})\boldsymbol{N} \cdot \delta\boldsymbol{\chi}\,\mathrm{d}A\,. \tag{3.50}$$

In a similar fashion, the variation of the work of external loads is derived as

$$\delta\Pi_{\text{ext}}(\delta\boldsymbol{\chi}) = -\delta \int_{\partial\mathcal{B}_{\boldsymbol{T}}} \overline{\boldsymbol{T}} \cdot \boldsymbol{\chi}\,\mathrm{d}A = -\int_{\partial\mathcal{B}_{\boldsymbol{T}}} \overline{\boldsymbol{T}} \cdot \delta\boldsymbol{\chi}\,\mathrm{d}A\,. \tag{3.51}$$

Having the formulations (3.50) and (3.51), Eq. (3.48) is rewritten to

$$\delta\Pi(\boldsymbol{\chi}, \delta\boldsymbol{\chi}) = \int_{\mathcal{B}_0} -\mathrm{Div}[\boldsymbol{P}(\boldsymbol{F})] \cdot \delta\boldsymbol{\chi}\,\mathrm{d}V + \int_{\partial\mathcal{B}_{\boldsymbol{T}}} (\boldsymbol{P}(\boldsymbol{F})\boldsymbol{N} - \overline{\boldsymbol{T}}) \cdot \delta\boldsymbol{\chi}\,\mathrm{d}A = 0\,. \tag{3.52}$$

Recalling that the variation $\delta\Pi$ has to vanish for arbitrary values of the virtual test functions $\delta\boldsymbol{\chi} = \{\delta\boldsymbol{\chi} \mid \delta\boldsymbol{\chi} = \boldsymbol{0} \text{ on } \partial\mathcal{B}_{\boldsymbol{\chi}}\}$, we find stationarity when the following set of equations is fulfilled:

$$\left.\begin{aligned} \text{Euler–Lagrange equations} \quad & \mathrm{Div}[\boldsymbol{P}] = \boldsymbol{0} \quad \text{in } \mathcal{B}_0 \\ \text{kinematically admissible field} \quad & \boldsymbol{\chi} = \overline{\boldsymbol{\chi}} \quad \text{on } \partial\mathcal{B}_{\boldsymbol{\chi}} \\ \text{equilibrium on Neumann boundary} \quad & \boldsymbol{P}\boldsymbol{N} = \overline{\boldsymbol{T}} \quad \text{on } \partial\mathcal{B}_{\boldsymbol{T}}\,. \end{aligned}\right\} \tag{3.53}$$

Therein, the Euler–Lagrange equations $(3.53)_1$ can be considered as a generalisation of (3.40) to the three-dimensional space and depict a system of nine scalar differential equations. Of course, we directly identify them as the momentum balance, $(3.53)_2$ as the Dirichlet boundary conditions, and $(3.53)_3$ as the Neumann boundary conditions from Section 3.1.1 and observe that Eqs (3.53) exactly describe the mechanical boundary-value problem. However, Eqs (3.53) are obtained by a rigorous variational treatment of the problem and the stationarity of elastic potentials.

3.4.3 The principle of stationary potential energy under constraints

It was shown in Section 3.3 that the motion of a body $\mathscr{B}$ might be subject to internal constraints, each of those being represented by a scalar constraint function $\mathscr{R} = 0$. The variational formulation of the mechanical problem offers a very elegant way of taking into account such additional constraints. This shall be briefly discussed in this section. From Section 3.4.2, we inherit the problem of finding a motion $\boldsymbol{\chi}$ under which the elastostatic potential Π becomes stationary. Explanations on the connection of stationary and extremal values were provided before. Now, we say that the motion of the body $\mathscr{B}$ is restricted by one internal constraint and the problem is to find the motion $\boldsymbol{\chi}$ under which the elastostatic functional Π becomes stationary *and* the constraint function $\mathscr{R} = 0$ is fulfilled. This constitutes a *variational problem under constraints* and is treated by the *Lagrange multiplier method*. The key idea of this approach is to replace the original functional, here Π, by a *Lagrange functional* $\mathscr{L}$. The latter is composed of the original functional and an additional term, which contains the constraint function $\mathscr{R}$ multiplied by a scalar *Lagrange multiplier* $\alpha_{\mathscr{R}}$. For the elastostatic problem, we can subsequently formulate

$$\mathscr{L}(\boldsymbol{\chi}, \alpha_{\mathscr{R}}) := \Pi(\boldsymbol{\chi}) + \Pi^{\mathscr{R}}(\boldsymbol{\chi}, \alpha_{\mathscr{R}}) \quad \text{where} \quad \Pi^{\mathscr{R}}(\boldsymbol{\chi}, \alpha_{\mathscr{R}}) = \int_{\mathcal{B}_0} \alpha_{\mathscr{R}}\, \mathscr{R}(\boldsymbol{F})\, \mathrm{d}V\,. \tag{3.54}$$

It is then searched for the stationary solution of the Lagrange functional $\mathscr{L}$ such that

$$\mathscr{L}(\boldsymbol{\chi}, \alpha_{\mathscr{R}}) \quad \rightarrow \quad \text{stat}\,. \tag{3.55}$$

Doing so, stationarity has to be fulfilled with respect to the motion $\boldsymbol{\chi}$ and with respect to the Lagrange multiplier $\alpha_{\mathscr{R}}$. This results in the formulations

$$\Pi(\boldsymbol{\chi}) = \underset{\boldsymbol{\chi}^* \in \mathcal{K}}{\text{stat}}\, \underset{\alpha^*_{\mathscr{R}}}{\text{stat}}\, \mathscr{L}(\boldsymbol{\chi}^*, \alpha^*_{\mathscr{R}}) \quad \text{such that} \quad \boldsymbol{\chi} = \arg\Big\{ \underset{\boldsymbol{\chi}^* \in \mathcal{K}}{\text{stat}}\, \underset{\alpha^*_{\mathscr{R}}}{\text{stat}}\, \mathscr{L}(\boldsymbol{\chi}^*, \alpha^*_{\mathscr{R}}) \Big\} \tag{3.56}$$

with the additional trial function $\alpha^*_{\mathscr{R}}$ for the Lagrange multiplier. In order to obtain stationarity, the variation of the Lagrange functional has to vanish:

$$\delta\mathscr{L}(\boldsymbol{\chi}, \alpha_{\mathscr{R}}, \delta\boldsymbol{\chi}, \delta\alpha_{\mathscr{R}}) = \delta\Pi(\boldsymbol{\chi}, \delta\boldsymbol{\chi}) + \delta\Pi^{\mathscr{R}}(\boldsymbol{\chi}, \alpha_{\mathscr{R}}, \delta\boldsymbol{\chi}, \delta\alpha_{\mathscr{R}}) \overset{!}{=} 0 \tag{3.57}$$

with the additional virtual test function $\delta\alpha_{\mathscr{R}}$. Since the original functional Π is independent of $\alpha_{\mathscr{R}}$, its variation $\delta\Pi$ is identical to the formulation in (3.52). In contrast, the term $\Pi^{\mathscr{R}}$ is dependent on $\boldsymbol{\chi}$ and $\alpha_{\mathscr{R}}$, such that its variation becomes

$$\delta\Pi^{\mathscr{R}}(\boldsymbol{\chi}, \alpha_{\mathscr{R}}, \delta\boldsymbol{\chi}, \delta\alpha_{\mathscr{R}}) = \int_{\mathcal{B}_0} \alpha_{\mathscr{R}}\, \partial_{\boldsymbol{F}}\mathscr{R} \cdot \mathrm{Grad}[\delta\boldsymbol{\chi}]\, \mathrm{d}V + \int_{\mathcal{B}_0} \partial_{\alpha_{\mathscr{R}}} \alpha_{\mathscr{R}}\, \mathscr{R} \cdot \delta\alpha_{\mathscr{R}}\, \mathrm{d}V\,. \tag{3.58}$$

Reformulating the first integral on the right hand side in the same fashion than $\delta\Pi_{\text{int}}$ in the previous section, we arrive at

$$\begin{aligned}\delta\Pi^{\mathscr{R}}(\boldsymbol{\chi},\alpha_{\mathscr{R}},\delta\boldsymbol{\chi},\delta\alpha_{\mathscr{R}}) = \int_{\mathcal{B}_0} -\operatorname{Div}[\alpha_{\mathscr{R}}\,\partial_{\boldsymbol{F}}\mathscr{R}]\cdot\delta\boldsymbol{\chi}\,\mathrm{d}V + \int_{\partial\mathcal{B}_{\boldsymbol{T}}}[\alpha_{\mathscr{R}}\,\partial_{\boldsymbol{F}}\mathscr{R}]\boldsymbol{N}\cdot\delta\boldsymbol{\chi}\,\mathrm{d}A \\ + \int_{\mathcal{B}_0}\mathscr{R}\cdot\delta\alpha_{\mathscr{R}}\,\mathrm{d}V\,.\end{aligned} \tag{3.59}$$

From the last integral, we directly observe that stationarity of $\mathscr{L}$ with respect to the Lagrange multiplier $\alpha_{\mathscr{R}}$ gives nothing else than the constraint function $\mathscr{R}$ itself. The remaining two integrals in $\delta\Pi^{\mathscr{R}}$ can be directly combined with the integrals in $\delta\Pi$, such that a stationary solution of $\mathscr{L}$ is obtained by fulfilling the following set of equations:

$$\left.\begin{aligned} \text{Euler–Lagrange equations} \quad & \operatorname{Div}[\partial_{\boldsymbol{F}}\mathscr{W} + \alpha_{\mathscr{R}}\,\partial_{\boldsymbol{F}}\mathscr{R}] = \boldsymbol{0} \quad \text{in } \mathcal{B}_0 \\ \text{internal constraint} \quad & \mathscr{R} = 0 \quad \text{in } \mathcal{B}_0 \\ \text{kinematically admissible field} \quad & \boldsymbol{\chi} = \overline{\boldsymbol{\chi}} \quad \text{on } \partial\mathcal{B}_{\boldsymbol{\chi}} \\ \text{equilibrium on Neumann boundary} \quad & [\partial_{\boldsymbol{F}}\mathscr{W} + \alpha_{\mathscr{R}}\,\partial_{\boldsymbol{F}}\mathscr{R}]\boldsymbol{N} = \overline{\boldsymbol{T}} \quad \text{on } \partial\mathcal{B}_{\boldsymbol{T}}\,. \end{aligned}\right\} \tag{3.60}$$

By comparing those results with Section 3.3, it is easy to conclude that the expression $\partial_{\boldsymbol{F}}\mathscr{W} + \alpha_{\mathscr{R}}\,\partial_{\boldsymbol{F}}\mathscr{R}$ constitutes the first Piola–Kirchhoff stress $\boldsymbol{P}$ for the case of constrained problems. Moreover, the statement in Section 3.3.1 of $\alpha_{\mathscr{R}}$ being a Lagrange multiplier is clearly justified by the variational approach. We note that although the Lagrange multiplier method starts with a trivial operation of adding a zero-valued integral function, here $\Pi^{\mathscr{R}}$, the outcome is the introduction of the additional *non-zero* stress contribution $\alpha_{\mathscr{R}}\,\partial_{\boldsymbol{F}}\mathscr{R}$. This additional term can be interpreted as the stress which is required to satisfy the constraint $\mathscr{R}$. It is thus indispensable for a consistent treatment of constrained problems.

3.5 Theory of invariants and material symmetry groups

So far, the considerations from Sections 3.2.3 and 3.2.4 left us with invariance conditions for the energy $\mathscr{W}$ and the stress tensor $\boldsymbol{P}$ with respect to proper transformations of the actual configuration, given by Eqs (3.14), and with respect to proper orthogonal rotations of the reference configuration, where the rotations belong to the material symmetry group $\mathcal{MG}$, given by Eqs (3.17). Of course, it is desirable to have formulations which *a priori* satisfy these two requirements and we thus recapitulate the invariance conditions and consequently discuss the *theory of invariants*, which will subsequently provide the desired formulations.

3.5.1 Implications of frame-indifference

First, the frame-indifference condition for the free energy response function $\mathfrak{G}_\psi$ from $(3.14)_1$ is formulated in terms of the strain-energy function $\mathscr{W}$, reading

$$\mathscr{W}(\boldsymbol{F}) = \mathscr{W}(\boldsymbol{Q}\boldsymbol{F}) \quad \forall\boldsymbol{Q}\in\mathcal{SO}(3)\,, \tag{3.61}$$

where the argument $\boldsymbol{Q}\boldsymbol{F} = \boldsymbol{F}^*$ represents the deformation gradient associated with a transformed actual configuration. Frame-indifference is easily achieved by making use of

deformation measures that are invariant to such rotations. This motivates the use of the right Cauchy–Green strain tensor $\boldsymbol{C}$, which is a Lagrangean quantity and is therefore unaffected by changes of the actual frame. The invariance is directly visible from $\boldsymbol{C}^* = (\boldsymbol{F}^T)^*\boldsymbol{F}^* = (\boldsymbol{Q}\boldsymbol{F})^T(\boldsymbol{Q}\boldsymbol{F}) = \boldsymbol{F}^T\boldsymbol{Q}^{-1}\boldsymbol{Q}\boldsymbol{F} = \boldsymbol{F}^T\boldsymbol{F} = \boldsymbol{C}$. By further recalling the connection $\boldsymbol{C} = \boldsymbol{U}^2$ and the fact that $\{\boldsymbol{U}, \boldsymbol{C}\}$ share the same set of eigenvectors, see Section 2.1.4, we observe that the right stretch tensor $\boldsymbol{U}$ is a Lagrangean quantity and provides frame-indifferent formulations as well. Hence, an energy

$$\mathscr{W}(\boldsymbol{F}) := \mathscr{W}(\boldsymbol{F}^T\boldsymbol{F}) = \mathscr{W}(\boldsymbol{C}) = \mathscr{W}(\boldsymbol{U}) \tag{3.62}$$

will always satisfy (3.61). As explained in Section 3.2.5, the consistent frame-indifference of the Piola–Kirchhoff stress tensor,

$$\boldsymbol{P}(\boldsymbol{Q}\boldsymbol{F}) = \boldsymbol{Q}\boldsymbol{P}(\boldsymbol{F}) \quad \forall \boldsymbol{Q} \in \mathcal{SO}(3)\,, \tag{3.63}$$

directly follows from the frame-indifference of the strain-energy, hence, from (3.62).

3.5.2 Invariant formulations for isotropic tensor functions

In the previous section, we observed that a priori frame-indifferent formulations are provided by utilising Lagrangean (material) deformation measures as arguments for the strain energy $\mathscr{W}$. From the considerations in Section 3.2.4, we know that the constitutive functions additionally have to satisfy certain invariance conditions with respect to referential rotations $\boldsymbol{Q} \in \mathcal{MG}$, which belong to the symmetry group $\mathcal{MG}$ of the material. It is clear that the frame-indifferent Lagrangean quantities $\boldsymbol{C}$ and $\boldsymbol{U}$ are affected by such referential transformations, which is easy to observe when investigating the transformed right Cauchy–Green tensor $\boldsymbol{C}^+ = (\boldsymbol{F}^T)^+\boldsymbol{F}^+ = (\boldsymbol{F}\boldsymbol{Q}^T)^T(\boldsymbol{F}\boldsymbol{Q}^T) = \boldsymbol{Q}\boldsymbol{F}^T\boldsymbol{F}\boldsymbol{Q}^T = \boldsymbol{Q}\boldsymbol{C}\boldsymbol{Q}^T$. Further, since we have formulations based on the Lagrangean strain tensor $\boldsymbol{C}$, it is consequent to consider the associated second Piola–Kirchhoff stress tensor $\boldsymbol{S} = \boldsymbol{F}^{-1}\boldsymbol{P}$ for the following investigations. While $\boldsymbol{P}$ is a two-field tensor and has one Eulerian and one Langrangean basis, the second Piola–Kirchhoff stress is fully Langrangean. This explains its computation, which is essentially the covariant pull-back operation of the first (Eulerian) basis of $\boldsymbol{P}$. The second Piola–Kirchhoff stress is symmetric. This becomes clear from its definition $\boldsymbol{S} = \boldsymbol{F}^{-1}\boldsymbol{P}$ and inserting from the balance of moment of momentum, given by Eq. $(2.41)_2$, the relation $\boldsymbol{P} = \boldsymbol{F}\boldsymbol{P}^T\boldsymbol{F}^{-T}$, which results in $\boldsymbol{S} = \boldsymbol{F}^{-1}\boldsymbol{F}\boldsymbol{P}^T\boldsymbol{F}^{-T} = (\boldsymbol{F}^{-1}\boldsymbol{P})^T = \boldsymbol{S}^T$. A rotated reference configuration with $\boldsymbol{F}^+ = \boldsymbol{F}\boldsymbol{Q}^T$ affects the Lagrangean stress as $\boldsymbol{S}^+ = (\boldsymbol{F}^{-1}\boldsymbol{P})^+ = (\boldsymbol{F}\boldsymbol{Q}^T)^{-1}\boldsymbol{P}\boldsymbol{Q}^T = \boldsymbol{Q}\boldsymbol{S}\boldsymbol{Q}^T$. Relations (3.15) can then be rewritten in terms of $\boldsymbol{C}, \boldsymbol{S}$ and $\mathscr{W}$ to

$$\boldsymbol{X} \Rightarrow \boldsymbol{X}^+ = \boldsymbol{Q}\boldsymbol{X}\,,\ \boldsymbol{C} \Rightarrow \boldsymbol{C}^+ = \boldsymbol{Q}\boldsymbol{C}\boldsymbol{Q}^T\,,\ \mathscr{W} \Rightarrow \mathscr{W}^+ = \mathscr{W}\,,\ \boldsymbol{S} \Rightarrow \boldsymbol{S}^+ = \boldsymbol{Q}\boldsymbol{S}\boldsymbol{Q}^T\,. \tag{3.64}$$

With this, we subsequently reformulate the invariance conditions (3.18) to

$$\left.\begin{aligned} \mathscr{W}(\boldsymbol{C}) &= \mathscr{W}(\boldsymbol{Q}\boldsymbol{C}\boldsymbol{Q}^T) \\ \boldsymbol{Q}\boldsymbol{S}(\boldsymbol{C})\boldsymbol{Q}^T &= \boldsymbol{S}(\boldsymbol{Q}\boldsymbol{C}\boldsymbol{Q}^T) \end{aligned}\right\} \quad \forall \boldsymbol{Q} \in \mathcal{MG}\,. \tag{3.65}$$

Now, the aim is to find an irreducible set of scalar arguments, which replaces the argument tensor $\boldsymbol{C}$ in the scalar-valued tensor function for $\mathscr{W}$ and the tensor-valued tensor function

for $\boldsymbol{S}$. Those scalar arguments shall be invariant upon referential rotations $\boldsymbol{Q} \in \mathcal{MG}$. This requirement leads to the *theory of invariants* and the field of representation theorems for isotropic tensor functions. Comprehensive explanations on this topic are provided in the classical mathematical works by, for example, Weyl [514] and Schur [427]. However, we have to observe that relations (3.65) represent anisotropic tensor functions in the argument $\boldsymbol{C}$, since $\boldsymbol{Q} \in \mathcal{MG}$ has to be a member of the symmetry group. In contrast, isotropic tensor functions are characterised through formulations where $\boldsymbol{Q} \in \mathcal{O}(3)$ can be a member of the whole group of orthogonal transformations. Hence, we have to appropriately modify the formulations in order to make use of the representation theorems for isotropic tensor functions. This is done by enriching the set of argument tensors, which is in (3.65) only $\boldsymbol{C}$, by means of a set $\boldsymbol{\Xi}$ of so-called structural tensors. This approach is referred to as the *concept of structural tensors* and was introduced by Boehler [50]. In general, the set $\boldsymbol{\Xi}$ can contain an adaptable number of first-, second-, and higher-order tensors. A set with i first-order, j second-order, and k fourth-order structural tensors might then be given by

$$\boldsymbol{\Xi} = \{\boldsymbol{\Xi}_{\boldsymbol{m}}, \boldsymbol{\Xi}_{\boldsymbol{M}}, \boldsymbol{\Xi}_{\mathbb{M}}\} \quad \text{where} \quad \begin{cases} \boldsymbol{\Xi}_{\boldsymbol{m}} = \{\boldsymbol{m}_1, \dots, \boldsymbol{m}_i\} \\ \boldsymbol{\Xi}_{\boldsymbol{M}} = \{\boldsymbol{M}_1, \dots, \boldsymbol{M}_j\} \\ \boldsymbol{\Xi}_{\mathbb{M}} = \{\mathbb{M}_1, \dots, \mathbb{M}_k\} \end{cases} \tag{3.66}$$

and $i, j, k \in \mathcal{N}$. It is consequent to introduce the associated transformations

$$\boldsymbol{Q} \star \boldsymbol{\Xi} = \{\boldsymbol{Q} \star \boldsymbol{\Xi}_{\boldsymbol{m}}, \boldsymbol{Q} \star \boldsymbol{\Xi}_{\boldsymbol{M}}, \boldsymbol{Q} \star \boldsymbol{\Xi}_{\mathbb{M}}\} \tag{3.67}$$

of the structural tensors, where the "$\star$" depicts a generalised transformation which is distinct for the different subsets $\boldsymbol{\Xi}_{\boldsymbol{m}}$, $\boldsymbol{\Xi}_{\boldsymbol{M}}$, and $\boldsymbol{\Xi}_{\mathbb{M}}$:

$$\begin{aligned} \boldsymbol{Q} \star \boldsymbol{\Xi}_{\boldsymbol{m}} &= \{\boldsymbol{Q}\boldsymbol{m}_1, \dots, \boldsymbol{Q}\boldsymbol{m}_i\} \\ \boldsymbol{Q} \star \boldsymbol{\Xi}_{\boldsymbol{M}} &= \{\boldsymbol{Q}\boldsymbol{M}_1\boldsymbol{Q}^T, \dots, \boldsymbol{Q}\boldsymbol{M}_j\boldsymbol{Q}^T\} \\ \boldsymbol{Q} \star \boldsymbol{\Xi}_{\mathbb{M}} &= \{(\boldsymbol{Q} \otimes \boldsymbol{Q})^{T_{23}}\, \mathbb{M}_1\, (\boldsymbol{Q}^T \otimes \boldsymbol{Q}^T)^{T_{23}}, \dots, (\boldsymbol{Q} \otimes \boldsymbol{Q})^{T_{23}}\, \mathbb{M}_k\, (\boldsymbol{Q}^T \otimes \boldsymbol{Q}^T)^{T_{23}}\}\,. \end{aligned} \tag{3.68}$$

The key property of the set of structural tensors is that it reflects the material symmetry in the sense of being invariant under rotations of the symmetry group $\mathcal{MG}$, hence,

$$\boldsymbol{\Xi} = \boldsymbol{Q} \star \boldsymbol{\Xi} \quad \forall \boldsymbol{Q} \in \mathcal{MG}\,. \tag{3.69}$$

Now, the decisive step is to reformulate Eqs (3.65) by means of an extended list $(\boldsymbol{C}, \boldsymbol{\Xi})$ of arguments instead of $\boldsymbol{C}$ alone. This leads to the representation

$$\left.\begin{aligned} \mathscr{W}(\boldsymbol{C}, \boldsymbol{\Xi}) &= \mathscr{W}(\boldsymbol{Q}\boldsymbol{C}\boldsymbol{Q}^T, \boldsymbol{Q} \star \boldsymbol{\Xi}) \\ \boldsymbol{Q}\boldsymbol{S}(\boldsymbol{C}, \boldsymbol{\Xi})\boldsymbol{Q}^T &= \boldsymbol{S}(\boldsymbol{Q}\boldsymbol{C}\boldsymbol{Q}^T, \boldsymbol{Q} \star \boldsymbol{\Xi}) \end{aligned}\right\} \quad \forall \boldsymbol{Q} \in \mathcal{O}(3)\,. \tag{3.70}$$

The valuable outcome of this formulation is that $\boldsymbol{Q}$ is no longer restricted to be a member of the material symmetry group $\mathcal{MG}$. Thus, Eqs (3.70) represent isotropic tensor functions in the extended list $(\boldsymbol{C}, \boldsymbol{\Xi})$ of arguments. In this sense, Zheng [526] refers to this procedure as *isotropicisation* of anisotropic tensor functions. The form given in (3.70) allows to apply the classical representation theorems for isotropic tensor functions, which aim for a replacement of the tensorial arguments $(\boldsymbol{C}, \boldsymbol{\Xi})$ by an *integrity basis* $\mathscr{I}$ consisting of

arguments	**invariants**
$\boldsymbol{v}$	$\boldsymbol{v}\cdot\boldsymbol{v}$
$\boldsymbol{A}$	$\mathrm{tr}[\boldsymbol{A}], \mathrm{tr}[\boldsymbol{A}^2], \mathrm{tr}[\boldsymbol{A}^3]$
$\boldsymbol{A}, \boldsymbol{v}$	$\boldsymbol{v}\cdot\boldsymbol{A}\boldsymbol{v}, \boldsymbol{v}\cdot\boldsymbol{A}^2\boldsymbol{v}$
$\boldsymbol{A}_1, \boldsymbol{A}_2$	$\mathrm{tr}[\boldsymbol{A}_1\boldsymbol{A}_2], \mathrm{tr}[\boldsymbol{A}_1\boldsymbol{A}_2^2], \mathrm{tr}[\boldsymbol{A}_1^2\boldsymbol{A}_2], \mathrm{tr}[\boldsymbol{A}_1^2\boldsymbol{A}_2^2]$
$\boldsymbol{A}_1, \boldsymbol{A}_2, \boldsymbol{A}_3$	$\mathrm{tr}[\boldsymbol{A}_1\boldsymbol{A}_2\boldsymbol{A}_3]$

Table 3.1: Integrity bases for isotropic tensor functions for $\boldsymbol{v} \in \mathcal{R}^3$ and $\boldsymbol{A}, \boldsymbol{A}_1, \boldsymbol{A}_2, \boldsymbol{A}_3 \in \mathcal{SYM}(3)$.

scalar invariants. The existence of a finite number of invariants for a given set of tensorial arguments is commonly referred to as Hilbert's theorem [205]. There exists an extensive amount of literature on integrity bases for specific sets of argument tensors, ranging from the early works of Wang [502, 503, 504] and Smith [449, 450] (who had some controversy), to the works of Boehler [50], Spencer [455, 458], and Zheng [526]. Extensions to irreducible bases for fourth-order argument tensors were provided by Betten [33, 34] and Betten & Helisch [35]. A compact overview of integrity bases for first- and second-order arguments and some combinations thereof is given in Table 3.1. Finally, the definition of the structural tensors allows to define the material symmetry group

$$\mathcal{MG} = \{\boldsymbol{Q} \in \mathcal{O}(3) \mid \boldsymbol{\Xi} = \boldsymbol{Q} \star \boldsymbol{\Xi}\} \tag{3.71}$$

as the invariance group of the set $\boldsymbol{\Xi}$ of structural tensors. In turn, of course, the set of structural tensors has to be defined such that it satisfies (3.69) and subsequently specifies the symmetry group $\mathcal{MG}$. A comprehensive list of structural tensors for different classes of symmetries is provided by, for example, Zheng & Spencer [527]. Remark that much deeper insights into the topic of invariant theory, representation theorems, and material symmetry classes are given in the monographs by Schröder [420] and Apel [12].

3.5.3 The isotropic symmetry group

The simplest symmetry class is given when a material does not show a preferred behaviour in any specific direction. The behaviour of the material is then direction-independent and commonly referred to as *isotropic* or *spherically symmetric*. In this context, it is interesting to note that there exist two types of isotropy, one with a centre of symmetry and one without a centre of symmetry, see, for example, Voigt [496]. The former is obtained when the material symmetry group is identical to the full orthogonal group, hence, $\mathcal{MG} = \mathcal{O}(3)$, whereas the latter is given when the symmetry group is restricted to the proper orthogonal group, hence, $\mathcal{MG} = \mathcal{SO}(3)$, also known as *hemitropy*. Proceeding with $\mathcal{MG} = \mathcal{O}(3)$, we notice that Eqs (3.65) become isotropic tensor functions and that the definition of structural tensors becomes superfluous. The resulting irreducible integrity basis $\mathscr{I}^J_{\mathrm{iso}} = \{J_1, J_2, J_3\}$ for the single tensor argument $\boldsymbol{C}$ is directly received from Table 3.1 as

$$J_1 = \mathrm{tr}[\boldsymbol{C}]\,, \quad J_2 = \mathrm{tr}[\boldsymbol{C}^2]\,, \quad J_3 = \mathrm{tr}[\boldsymbol{C}^3] \tag{3.72}$$

with the three *basic invariants* J_1, J_2, and J_3. Thus, we see that the response functions of an isotropic material are specified by three scalar arguments. However, the choice of the invariants is by no means unique. For example, in continuum-mechanical applications use is frequently made of the set $\mathscr{I}^I_{\text{iso}} = \{I_1, I_2, I_3\}$ of *principal invariants* I_1, I_2, and I_3, defined by

$$I_1 = \text{tr}[\boldsymbol{C}]\,, \quad I_2 = \text{tr}\big[\text{cof}[\boldsymbol{C}]\big]\,, \quad I_3 = \det[\boldsymbol{C}]\,. \tag{3.73}$$

They can be found, for example, in the early work of Rivlin & Ericksen [403]. The principal invariant set $\mathscr{I}^I_{\text{iso}}$ is connected to the basic invariant set $\mathscr{I}^J_{\text{iso}}$ through

$$J_1 = I_1\,, \quad J_2 = I_1^2 - 2I_2\,, \quad J_3 = I_1^3 - 3I_1I_2 + 3I_3\,. \tag{3.74}$$

An interesting alternative notation of the set $\mathscr{I}^I_{\text{iso}}$ is derived from (3.73) by making use of the rules (A.12), (A.17), (A.13), and (A.15), thus yielding

$$I_1 = \boldsymbol{F} \cdot \boldsymbol{F}\,, \quad I_2 = \text{cof}[\boldsymbol{F}] \cdot \text{cof}[\boldsymbol{F}]\,, \quad I_3 = \det[\boldsymbol{F}]^2 = J^2\,. \tag{3.75}$$

Comparing these relations to Eqs (2.9), (2.13), and (2.15), one finds that the three principal invariants are defined by the squared operators of the transport of line, area, and volume elements, respectively. Furthermore, relation $(3.75)_3$ makes clear that any occurrence of I_3 can be replaced in terms of the Jacobian J. The probably most intuitive set of invariants for one tensor argument is given in terms of its three eigenvalues, since they hold a natural invariance as well. The proof for that is straightforward and provided in Appendix A.5. We observed in Section 2.1.4 that the eigenvalues $\lambda_{\boldsymbol{C}(i)} = \lambda^2_{\boldsymbol{U}(i)}$ of $\boldsymbol{C}$ are directly connected to the principal stretches $\lambda_{\boldsymbol{U}(i)}$, entailing that the use of either of these values is appropriate. If the set $\mathscr{I}^\lambda_{\text{iso}} = \{\lambda_{\boldsymbol{U}(1)}, \lambda_{\boldsymbol{U}(2)}, \lambda_{\boldsymbol{U}(3)}\}$ of principal stretches is used, we can observe the connection to the principal invariants as

$$\begin{aligned} &I_1 = \lambda^2_{\boldsymbol{U}(1)} + \lambda^2_{\boldsymbol{U}(2)} + \lambda^2_{\boldsymbol{U}(3)}, \quad I_2 = \lambda^2_{\boldsymbol{U}(1)}\lambda^2_{\boldsymbol{U}(2)} + \lambda^2_{\boldsymbol{U}(2)}\lambda^2_{\boldsymbol{U}(3)} + \lambda^2_{\boldsymbol{U}(1)}\lambda^2_{\boldsymbol{U}(3)}\,, \\ &I_3 = \lambda^2_{\boldsymbol{U}(1)}\lambda^2_{\boldsymbol{U}(2)}\lambda^2_{\boldsymbol{U}(3)}. \end{aligned} \tag{3.76}$$

Concluding, a variety of integrity bases is suitable for the description of isotropic material behaviour and we can summarise that

$$\mathcal{MG} = \mathcal{O}(3) \quad \rightarrow \quad \mathscr{W}(\boldsymbol{F}) := \mathscr{W}(\mathscr{I}^J_{\text{iso}}) = \mathscr{W}(\mathscr{I}^I_{\text{iso}}) = \mathscr{W}(\mathscr{I}^\lambda_{\text{iso}})\,. \tag{3.77}$$

Hence, formulating the strain-energy in terms of either of the three presented invariant sets guarantees a proper invariant formulation for materials of the isotropic symmetry group.

3.5.4 The transversely isotropic symmetry group

A material belongs to the symmetry group of *transverse isotropy* or cylindrical symmetry if it exhibits one preferred (or privileged) direction with a distinct behaviour. This direction is described by a referential unit vector $\boldsymbol{a}_0$, such that $|\boldsymbol{a}_0| = 1$. The vectors $\boldsymbol{a}_0^\perp$ perpendicular to $\boldsymbol{a}_0$, characterised by $\boldsymbol{a}_0 \cdot \boldsymbol{a}_0^\perp = 0$, form the *transverse plane* with isotropic material behaviour. It is thus referred to as the isotropy plane. The most intuitive symmetry property of the transversely isotropic group is the invariance of the material behaviour with respect to rotations around the preferred direction $\boldsymbol{a}_0$. To describe this, it proofs useful to introduce the *Euler–Rodrigues formula*

$$\boldsymbol{Q}^{\varpi}_{\boldsymbol{n}} = \boldsymbol{n} \otimes \boldsymbol{n} + \cos[\varpi](\boldsymbol{I} - \boldsymbol{n} \otimes \boldsymbol{n}) - \sin[\varpi]\boldsymbol{\mathcal{E}}\boldsymbol{n}\,, \tag{3.78}$$

which defines the rotation tensor for arbitrary rotations with angle ϖ around a unit vector $\boldsymbol{n}$. The rotational symmetry around $\boldsymbol{a}_0$ can then be described by rotation tensors

$$\boldsymbol{Q}^{\varpi}_{\boldsymbol{a}_0} = \boldsymbol{a}_0 \otimes \boldsymbol{a}_0 + \cos[\varpi](\boldsymbol{I} - \boldsymbol{a}_0 \otimes \boldsymbol{a}_0) - \sin[\varpi]\boldsymbol{\mathcal{E}}\boldsymbol{a}_0 \quad \text{for} \quad 0 \leq \varpi < 2\pi\,. \tag{3.79}$$

It is obvious that the vector $\boldsymbol{a}_0$ is unaffected by such rotations, since $\boldsymbol{Q}^{\varpi}_{\boldsymbol{a}_0}\boldsymbol{a}_0 = \boldsymbol{a}_0$. Now, we have to note that there exist five types of transverse isotropy and the rotational symmetry forms one of them. A further type is defined in terms of a so-called two-fold axis transverse to $\boldsymbol{a}_0$. Using the above defined perpendicular vector $\boldsymbol{a}_0^{\perp}$, this symmetry is described by a rotation tensor

$$\boldsymbol{Q}^{\pi}_{\boldsymbol{a}_0^{\perp}} = 2\,\boldsymbol{a}_0^{\perp} \otimes \boldsymbol{a}_0^{\perp} - \boldsymbol{I}\,. \tag{3.80}$$

This rotation transforms the preferred direction to $\boldsymbol{Q}^{\pi}_{\boldsymbol{a}_0^{\perp}}\boldsymbol{a}_0 = -\boldsymbol{a}_0$ and indicates that choosing $\boldsymbol{a}_0$ or its opposite $-\boldsymbol{a}_0$ to describe the preferred direction must not influence the material response. The rotations $\boldsymbol{Q}^{\varpi}_{\boldsymbol{a}_0}$ and $\boldsymbol{Q}^{\pi}_{\boldsymbol{a}_0^{\perp}}$, completed by the central inversion $-\boldsymbol{I}$, are the group generators for the complete cylindrical symmetry group. Materials belonging to this symmetry group have to be invariant with respect to these three transformations *and* combinations of them. With this, the group can be described by

$$\mathcal{MG}_{\text{ti}} = \{\boldsymbol{Q}^{\varpi}_{\boldsymbol{a}_0}, \boldsymbol{Q}^{\pi}_{\boldsymbol{a}_0^{\perp}}, -\boldsymbol{I} \mid 0 \leq \varpi < 2\pi\} \subset \mathcal{O}(3)\,. \tag{3.81}$$

Now, an appropriate structural tensor for this material group can be defined by

$$\boldsymbol{M} = \boldsymbol{a}_0 \otimes \boldsymbol{a}_0 \quad \text{with} \quad \boldsymbol{M}^T = \boldsymbol{M}\,, \quad \boldsymbol{M}\boldsymbol{M} = \boldsymbol{M}\,, \quad \text{tr}[\boldsymbol{M}] = 1\,, \tag{3.82}$$

see, for example, Spencer [456, 457], or Zheng & Spencer [527]. We see that $\boldsymbol{M} \in \mathcal{SYM}(3)$ is symmetric and idempotent. It can easily be shown that $\boldsymbol{M} = \boldsymbol{Q}\boldsymbol{M}\boldsymbol{Q}^T$ for all $\boldsymbol{Q} \in \mathcal{MG}_{\text{ti}}$. From Section 3.5.2, we know that the subsequent step is to find an integrity basis for the two argument tensors $\{\boldsymbol{C}, \boldsymbol{M}\}$. With Table (3.1), we see that an integrity basis for two tensor arguments generally consists of ten scalar invariants. Three invariants are associated with the argument $\boldsymbol{C}$ alone and given in terms of either of the sets $\mathscr{I}^J_{\text{iso}}$, $\mathscr{I}^I_{\text{iso}}$, or $\mathscr{I}^{\lambda}_{\text{iso}}$ from the previous section. Three additional invariants are associated with the argument $\boldsymbol{M}$ alone, given by

$$\text{tr}[\boldsymbol{M}]\,, \quad \text{tr}[\boldsymbol{M}^2]\,, \quad \text{tr}[\boldsymbol{M}^3]\,, \tag{3.83}$$

whereas the four mixed invariants are given by

$$\text{tr}[\boldsymbol{C}\boldsymbol{M}]\,, \quad \text{tr}[\boldsymbol{C}\boldsymbol{M}^2]\,, \quad \text{tr}[\boldsymbol{C}^2\boldsymbol{M}]\,, \quad \text{tr}[\boldsymbol{C}^2\boldsymbol{M}^2]\,. \tag{3.84}$$

However, the properties of $\boldsymbol{M}$, given in Eq. (3.82), directly reveal that the three invariants in (3.83) are constant and equal to one. Thus, they are of no further use. Moreover, it is deduced that the first two and the last two invariants given in (3.84) are equal. The two only relevant invariants associated with the structural tensor $\boldsymbol{M}$ are therefore

$$J_4 = \text{tr}[\boldsymbol{C}\boldsymbol{M}]\,, \quad J_5 = \text{tr}[\boldsymbol{C}^2\boldsymbol{M}]\,. \tag{3.85}$$

Reformulating the first of these invariants by means of

$$J_4 = \boldsymbol{a}_0 \cdot \boldsymbol{C}\boldsymbol{a}_0 = \boldsymbol{F}\boldsymbol{a}_0 \cdot \boldsymbol{F}\boldsymbol{a}_0 = \boldsymbol{a} \cdot \boldsymbol{a} = \lambda_{\boldsymbol{a}}^2 \tag{3.86}$$

and recalling relation (2.17) shows that J_4 has a direct physical interpretation and represents the squared stretch $\lambda_{\boldsymbol{a}}^2$ of the material in the direction initially aligned with $\boldsymbol{a}_0$. In contrast, a comparable physical meaning for J_5 can only be found in combinations with other invariants, which will be shown later. An integrity basis for transversely isotropic material behaviour can now be formulated by augmenting an integrity basis for the strain tensor $\boldsymbol{C}$, say the principal invariants $\mathscr{I}_{\text{iso}}^I$, with the two additional mixed invariants J_4 and J_5, resulting in the set $\mathscr{I}_{\text{ti}}^I = \{I_1, I_2, I_3, J_4, J_5\}$. This set was already introduced by Ericksen & Rivlin [118]. However, as discussed for the isotropic integrity bases, the set of invariants for the material group $\mathcal{MG}_{\text{ti}}$ is not unique and there exist a variety of sets of five invariants for transverse isotropy. For instance, Schröder & Neff [425] suggest to formulate an invariant

$$K_1 = \text{tr}[\text{cof}[\boldsymbol{C}]\boldsymbol{M}] = \text{cof}[\boldsymbol{F}]\boldsymbol{a}_0 \cdot \text{cof}[\boldsymbol{F}]\boldsymbol{a}_0 = J_5 - I_1 J_4 + I_2 \,, \tag{3.87}$$

which can be used to replace J_5 in the set $\mathscr{I}_{\text{ti}}^I$, leading to a set $\mathscr{I}_{\text{ti}}^{I'} = \{I_1, I_2, I_3, J_4, K_1\}$. Such an integrity basis was also proposed by Steigmann [463]. Unlike J_5, K_1 has a direct physical meaning and describes the deformation of an area element in the plane normal to the preferred direction $\boldsymbol{a}_0$. This becomes clear when we recall the area map in Eq. (2.13). Yet, not only the choice of a specific integrity basis is not unique, as there are multiple options for the structural tensor as well. For instance, one can formulate a tensor

$$\boldsymbol{D} = \boldsymbol{I} - \boldsymbol{M} \quad \text{with} \quad \boldsymbol{D}^T = \boldsymbol{D} \,, \quad \boldsymbol{D}\boldsymbol{D} = \boldsymbol{D} \,, \quad \text{tr}[\boldsymbol{D}] = 2 \,, \tag{3.88}$$

which also satisfies the invariance condition $\boldsymbol{Q}\boldsymbol{D}\boldsymbol{Q}^T = \boldsymbol{D}$ for $\boldsymbol{Q} \in \mathcal{MG}_{\text{ti}}$. The two relevant mixed invariants for the tensor arguments $\{\boldsymbol{C}, \boldsymbol{D}\}$ can then be formulated by

$$K_2 = \text{tr}[\boldsymbol{C}\boldsymbol{D}] = I_1 - J_4 \,, \quad K_3 = \text{tr}[\text{cof}[\boldsymbol{C}]\boldsymbol{D}] = I_1 J_4 - J_5 = I_2 - K_1 \,, \tag{3.89}$$

see Schröder & Neff [425]. This will lead to an integrity basis $\mathscr{I}_{\text{ti}}^{I''} = \{I_1, I_2, I_3, K_2, K_3\}$ While the J_4-invariant controls the deformation of line elements aligned with the preferred direction $\boldsymbol{a}_0$, K_2 serves as a measure for the stretch in the transverse plane. Such a formulation is beneficial if the transverse isotropy in a material is not caused by the occurrence of aligned fibres in the preferred direction, but has its origin in a laminated microstructure. Ultimately, the different invariant sets can of course be converted into each other and none of them is better by definition. Yet, the choice of a set can be very beneficial in specific situations and can possibly simplify subsequent formulations. In this sense, especially physically motivated invariant sets can be useful, such as the ones proposed by, for example, Bischoff-Beiermann & Bruhns [39], Criscione et al. [84], Lu & Zhang [302], deBotton et al. [92], and Furer & Ponte Castañeda [148]. Thereby, deBotton et al. [92] made use of an invariant set introduced in the seminal work of Ericksen & Rivlin [118]. Further, the formulation of invariants is not restricted to the usage of the right Cauchy–Green tensor $\boldsymbol{C}$. Hence, Steigmann [463] discussed an integrity basis based on the stretch tensor $\boldsymbol{U}$, whereas Schröder et al. [424] formulated a set on the basis of the logarithmic Hencky strain tensor $\boldsymbol{E}_0$. By making use of the triangular decomposition of the deformation gradient, as discussed in Section 2.1.4, Srinivasa [461] found an invariant set based on the coefficients of the upper triangular tensor $\mathfrak{R}$. In this work, we will make particular use of the formulations of Criscione et al. [84] and deBotton et al. [92], which have the convenient property that they allow to introduce generic, invariant-based deformation gradients. This is discussed in the following.

Invariant-based representations of deformation gradients An interesting set of invariants for the transversely isotropic symmetry group was introduced by Ericksen & Rivlin [118] and is denoted by $\mathscr{I}_{\mathrm{ti}}^{\mathfrak{er}} = \{\Gamma_{33}, \mathfrak{er}_1, \mathfrak{er}_2, \mathfrak{er}_4, \cos[\mathfrak{er}_3 - 2\mathfrak{er}_5]\}$. In terms of the set $\mathscr{I}_{\mathrm{ti}}^{I}$, the first four invariants of the set $\mathscr{I}_{\mathrm{ti}}^{\mathfrak{er}}$ are given by

$$\Gamma_{33} = J_4\,, \quad \mathfrak{er}_1 = \tfrac{1}{2}\,(I_1 - J_4)\,, \quad \mathfrak{er}_2 = \tfrac{1}{2}\,\sqrt{(I_1 + J_4)^2 - 4I_2 - 4J_5}\,, \quad \mathfrak{er}_4 = \sqrt{J_5 - J_4^2}\,, \tag{3.90}$$

whereas the fifth invariant is defined by

$$\cos[\mathfrak{er}_3 - 2\mathfrak{er}_5] = \frac{I_1 J_5 + 2I_3 + J_4(I_1 J_4 + J_4^2 - 2I_2 - 3J_5)}{(J_5 - J_4^2)\sqrt{(I_1 + J_4)^2 - 4I_2 - 4J_5}}\,. \tag{3.91}$$

We directly observe that the denominator of the fifth invariant contains the invariants $\mathfrak{er}_2$ and $\mathfrak{er}_4$ and $\cos[\mathfrak{er}_3 - 2\mathfrak{er}_5]$ is thus undefined if either one or both of these two invariants is zero. Of course, one could as well formulate relations between the set $\mathscr{I}_{\mathrm{ti}}^{\mathfrak{er}}$ and, for example, $\mathscr{I}_{\mathrm{ti}}^{I''}$. In this case, one would directly identify that, for instance, $\mathfrak{er}_1 = K_2/2$ and that K_3 occurs in $\mathfrak{er}_2$ and $\cos[\mathfrak{er}_3 - 2\mathfrak{er}_5]$. Further, relations (3.90) and (3.91) can easily be inverted in order to give equations for set $\mathscr{I}_{\mathrm{ti}}^{I}$ in terms of $\mathscr{I}_{\mathrm{ti}}^{\mathfrak{er}}$, reading

$$\begin{aligned} &I_1 = \Gamma_{33} + 2\mathfrak{er}_1\,, \quad I_2 = 2\Gamma_{33}\mathfrak{er}_1 + \mathfrak{er}_1^2 - \mathfrak{er}_2^2 - \mathfrak{er}_4^2\,, \\ &I_3 = \Gamma_{33}\,(\mathfrak{er}_1^2 - \mathfrak{er}_2^2) + \mathfrak{er}_4^2\,(\mathfrak{er}_2\cos[\mathfrak{er}_3 - 2\mathfrak{er}_5] - \mathfrak{er}_1)\,, \quad J_4 = \Gamma_{33}\,, \quad J_5 = \Gamma_{33}^2 + \mathfrak{er}_4^2\,. \end{aligned} \tag{3.92}$$

The benefit of using the set $\mathscr{I}_{\mathrm{ti}}^{\mathfrak{er}}$ may not manifest through the original representations given in Eqs (3.90) and (3.91), but through an invariant set $\mathscr{I}_{\mathrm{ti}}^{i} = \{\lambda_\ell, \lambda_{\mathrm{t}}, \gamma_\ell, \gamma_{\mathrm{t}}, \psi_\gamma\}$ introduced by deBotton et al. [92]. On the basis of the work of Ericksen & Rivlin [118], deBotton et al. [92] reformulated and renamed the original invariants. Further, they made the choice $\mathfrak{er}_3 = \pi/2$. Finally, their invariants are defined in terms of set $\mathscr{I}_{\mathrm{ti}}^{I}$ by

$$\begin{aligned} \lambda_\ell = \sqrt{J_4}\,, \quad \lambda_{\mathrm{t}} = \sqrt[4]{\frac{I_3}{J_4}}\,, \quad \gamma_\ell = \sqrt{\frac{J_5}{J_4} - J_4}\,, \quad \gamma_{\mathrm{t}} = \sqrt{I_1 - \frac{J_5}{J_4} - 2\sqrt{\frac{I_3}{J_4}}}\,, \\ \tan[2\psi_\gamma] = \frac{2\,\lambda_{\mathrm{t}}\,H \mp \gamma_{\mathrm{t}}\,\sqrt{\gamma_\ell^4\,\gamma_{\mathrm{t}}^2\,(4\,\lambda_{\mathrm{t}}^2 + \gamma_{\mathrm{t}}^2) - H^2}}{\gamma_{\mathrm{t}}\,H \pm 2\,\lambda_{\mathrm{t}}\,\sqrt{\gamma_\ell^4\,\gamma_{\mathrm{t}}^2\,(4\,\lambda_{\mathrm{t}}^2 + \gamma_{\mathrm{t}}^2) - H^2}}\,, \end{aligned} \tag{3.93}$$

where H in the fifth invariant is given by

$$H = (2\,\lambda_{\mathrm{l}}^2 + \gamma_{\mathrm{l}}^2)(2\lambda_{\mathrm{t}}^2 + \gamma_{\mathrm{t}}^2) + 2\,\lambda_{\mathrm{t}}^4 - 2I_2\,. \tag{3.94}$$

The advantage of this set is the direct link between the invariants and their physical meaning with respect to a transversely isotropic material, namely, $\lambda_\ell > 0$ is a measure for the stretch along the preferred direction, $\lambda_{\mathrm{t}} > 0$ is a stretch transverse to the preferred axis, $\gamma_\ell \geq 0$ is the longitudinal shear along the axis, and $\gamma_{\mathrm{t}} \geq 0$ is the transverse shear. By referring to the transverse plane, longitudinal and transverse shear are also called out-of-plane and in-plane shear, respectively. If the transverse isotropy is caused by aligned fibres in the microstructure, these two shear modes may also be denoted as along-fibre and cross-fibre shear, respectively. The fifth invariant $\psi_\gamma \in [0, \pi)$ is π-periodic and can be interpreted as a coupling measure between the different shear deformations. This coupling measure can be chosen arbitrarily whenever $\gamma_\ell\,\gamma_{\mathrm{t}} = 0$, hence, when longitudinal

and transverse shear do not occur simultaneously. This characteristic reminds of the invariant $\cos[\mathfrak{e}\mathfrak{r}_3 - 2\mathfrak{e}\mathfrak{r}_5]$ in the original set $\mathscr{I}_{\mathrm{ti}}^{\mathfrak{er}}$. As a result, we make the choice $\psi_\gamma = 0$ when $\gamma_\ell\,\gamma_\mathrm{t} = 0$. We further remark that relations $(3.93)_{1-4}$ for λ_ℓ, λ_t, γ_ℓ and γ_t do not contain the I_2-invariant, which implies that a transversely isotropic material may only have a dependency on I_2 for coupled shear deformations. Besides the direct physical interpretation of its invariants, the remarkable benefit of using set $\mathscr{I}_{\mathrm{ti}}^{\imath}$ is that it allows to introduce a generic, invariant-based representation of any deformation gradient. In detail, deBOTTON ET AL. [92] showed that an arbitrary deformation gradient $\boldsymbol{F}$ can be written as a product of a proper orthogonal rotation, say $\boldsymbol{R}^{\imath} \in \mathcal{SO}(3)$, and a generic deformation gradient given by

$$\boldsymbol{F}^{\imath} = \begin{bmatrix} \lambda_\mathrm{t} & 0 & 0 \\ \gamma_\mathrm{t} & \lambda_\mathrm{t} & 0 \\ \gamma_\ell\,\cos[\psi_\gamma] & \gamma_\ell\,\sin[\psi_\gamma] & \lambda_\ell \end{bmatrix} \boldsymbol{e}_i^{\imath} \otimes \boldsymbol{e}_j^{\imath} \tag{3.95}$$

with $i = 1, 2, 3$. Therein, the $\boldsymbol{e}_i^{\imath}$-basis is defined such that $\boldsymbol{e}_3^{\imath}$ is collinear with the preferred direction $\boldsymbol{a}_0$. Recalling the principle of frame-indifference, outlined in Sections 3.2.3 and 3.5.1, we observe that the connection $\boldsymbol{F} = \boldsymbol{R}^{\imath}\boldsymbol{F}^{\imath}$ describes a change of the frame of reference, indicated by the rotation $\boldsymbol{R}^{\imath}$. Besides that, however, $\boldsymbol{F}$ and $\boldsymbol{F}^{\imath}$ are equivalent deformations with the difference that the $\boldsymbol{e}_i^{\imath}$-system is always aligned with the preferred direction $\boldsymbol{a}_0$. Moreover, the tensor $\boldsymbol{F}^{\imath}$ has a lower triangular coefficient matrix and always contains at least three coefficients which are zero. These features are especially helpful for multiscale analysis and will prove useful in the investigations in Parts II and III. In brief, the benefit of using a deformation gradient of form (3.95) when dealing with transverse isotropy is that setting up $\boldsymbol{F}^{\imath}$ only requires the knowledge on the deformation through a set of transversely isotropic invariants (which can be any of the so far introduced), but no explicit knowledge on the original deformation gradient $\boldsymbol{F}$. In multiscale analysis, for instance, it suffices to have the information about a deformation on a larger scale in terms of invariants and to pass the deformation to a smaller scale in the form of a tensor $\boldsymbol{F}^{\imath}$. Doing this, a further advantage is that the (at least) three zero coefficients of $\boldsymbol{F}^{\imath}$ eventually lead to a significant simplification of subsequent expressions. We remark that although $\boldsymbol{F}^{\imath}$ with its lower triangular form seems to be similar to the upper triangular tensor $\mathfrak{R}$ from the triangular decomposition introduced in Eq. (2.20), it is very different in nature. While $\mathfrak{R}$ has to be computed from the decomposition $\boldsymbol{F} = \mathfrak{Q}\mathfrak{R}$ and requires to have an explicit expression for $\boldsymbol{F}$ (or at least $\boldsymbol{C}$), the tensor $\boldsymbol{F}^{\imath}$ is invariant-based and does not require the knowledge of the actual deformation. From a mathematical point of view, however, $\boldsymbol{F}^{\imath}$ could of course as well be computed from $\boldsymbol{F}$ by employing a *QL decomposition*. Proceeding, relations for the set $\mathscr{I}_{\mathrm{ti}}^{I}$ in terms of set $\mathscr{I}_{\mathrm{ti}}^{\imath}$ are obtained by either inverting Eqs (3.93) or by directly computing $\{I_1, I_2, I_3, J_4, J_5\}$ from $\boldsymbol{C}^{\imath} = \boldsymbol{F}^{\imath T}\boldsymbol{F}^{\imath}$ by making use of Eqs (3.73), (3.85), and $\boldsymbol{M} = \boldsymbol{e}_3^{\imath} \otimes \boldsymbol{e}_3^{\imath}$. We obtain

$$\begin{aligned} I_1 &= \lambda_\ell^2 + 2\lambda_\mathrm{t}^2 + \gamma_\ell^2 + \gamma_\mathrm{t}^2\,, \\ I_2 &= \tfrac{1}{2}\big((2\lambda_\ell^2 + \gamma_\ell^2)(2\lambda_\mathrm{t}^2 + \gamma_\mathrm{t}^2) + 2\lambda_\mathrm{t}^4 - \gamma_\ell^2\gamma_\mathrm{t}(\gamma_\mathrm{t}\cos[2\psi_\gamma] + 2\lambda_\mathrm{t}\sin[2\psi_\gamma])\big)\,, \\ I_3 &= \lambda_\ell^2\lambda_\mathrm{t}^4\,, \quad J_4 = \lambda_\ell^2\,, \quad J_5 = \lambda_\ell^2(\lambda_\ell^2 + \gamma_\ell^2)\,. \end{aligned} \tag{3.96}$$

At this point, it is beneficial for later use to introduce the *axisymmetric shear* $\gamma_\mathrm{a}^2 = \lambda_\ell^2 + 2\lambda_\mathrm{t}^2 - 3$. This additional shear value allows to compare deformations with uniaxial stretch along and/or transverse to the preferred direction with longitudinal and transverse

shear deformations. The three (squared) shear values add up as $\gamma_{\mathrm{a}}^2 + \gamma_\ell^2 + \gamma_{\mathrm{t}}^2 = I_1 - 3$. Furthermore, we note again that the invariant ψ_γ only occurs in connection with the I_2-invariant, but not in the expressions of the other ones.

Besides the invariant set $\mathscr{I}_{\mathrm{ti}}^{\imath}$ and its associated invariant-based deformation gradient $\boldsymbol{F}^{\imath}$, an alternative set with similar benefits was introduced by Criscione et al. [84] and is denoted by $\mathscr{I}_{\mathrm{ti}}^{\jmath\prime} = \{J, \lambda_M, \xi^{\jmath}, \gamma_\ell^{\jmath}, \cos[2\phi_\gamma]\}$. It is connected to the set $\mathscr{I}_{\mathrm{ti}}^{I}$ by

$$\begin{aligned} \lambda_M = J^{-1/3}\sqrt{J_4}\,, \quad \xi^{\jmath} = \sqrt{\frac{I_1 J_4 - J_5}{2J\sqrt{J_4}} + \sqrt{\left(\frac{I_1 J_4 - J_5}{2J\sqrt{J_4}}\right)^2 - 1}}\,, \quad \gamma_\ell^{\jmath} = \sqrt{\frac{J_5}{J_4^2} - 1}\,, \\ \cos[2\phi_\gamma] = \frac{I_1 J_4 J_5 + I_1 J_4^3 + 2J^2 J_4 - J_5^2 - 2I_2 J_4^2 - J_4^2 J_5}{(J_5 - J_4^2)\sqrt{I_1^2 J_4^2 + J_5^2 - 2I_1 J_4 J_5 - 4J^2 J_4}}\,, \end{aligned} \tag{3.97}$$

and J is the well-known Jacobian $J = I_3^{1/2}$. This set of invariants is reminiscent to the original set $\mathscr{I}_{\mathrm{ti}}^{\mathfrak{er}}$ of Ericksen & Rivlin [118] with the choice $\mathfrak{er}_3 = 0$, as can be seen through the fifth invariant $\cos[2\phi_\gamma]$. Like the invariant $\psi_\gamma \in \mathscr{I}_{\mathrm{ti}}^{\imath}$, the fifth invariant $\cos[2\phi_\gamma]$ may become indeterminate, here if $\xi^{\jmath} = 1$ or $\gamma_\ell^{\jmath} = 0$. The inverse relationships to Eqs (3.97) read

$$\begin{aligned} I_1 &= J^{2/3}\left(\lambda_M^2(1+\gamma_\ell^{\jmath 2}) + \lambda_M^{-1}(\xi^{\jmath 2} + \xi^{\jmath -2})\right), \\ I_2 &= J^{4/3}\left(\lambda_M^{-2} + \lambda_M(\xi^{\jmath 2} + \xi^{\jmath -2}) + \lambda_M\gamma_\ell^{\jmath 2}(\xi^{\jmath 2}\sin[\phi_\gamma]^2 + \xi^{\jmath -2}\cos[\phi_\gamma]^2)\right), \\ I_3 &= J^2\,, \quad J_4 = J^{2/3}\lambda_M^2\,, \quad J_5 = J^{4/3}\lambda_M^4(1+\gamma_\ell^{\jmath 2})\,. \end{aligned} \tag{3.98}$$

In order to compute I_2, one has to employ Eq. $(3.97)_5$ and solve it for the angle ϕ_γ. The usefulness of set $\mathscr{I}_{\mathrm{ti}}^{\jmath\prime}$ shows up in a slightly different notation, which results in the set $\mathscr{I}_{\mathrm{ti}}^{\jmath} = \{\lambda_\ell, \lambda_1, \lambda_2, \gamma_\ell, \phi_\gamma\}$. In terms of set $\mathscr{I}_{\mathrm{ti}}^{\jmath\prime}$, the set $\mathscr{I}_{\mathrm{ti}}^{\jmath}$ reads

$$\lambda_\ell = J^{1/3}\lambda_M\,, \quad \lambda_1 = J^{1/3}\lambda_M^{-1/2}\xi^{\jmath}\,, \quad \lambda_2 = J^{1/3}\lambda_M^{-1/2}\xi^{\jmath-1}\,, \quad \gamma_\ell = J^{1/3}\lambda_M\gamma_\ell^{\jmath}\,, \tag{3.99}$$

whereas ϕ_γ has to be computed from Eq. $(3.97)_5$. Similar to what deBotton et al. [92] noted for the deformation gradient $\boldsymbol{F}^{\imath}$, Criscione et al. [84] earlier showed that there is a deformation gradient $\boldsymbol{F}^{\jmath}$ which is connected to any general deformation gradient $\boldsymbol{F}$ by $\boldsymbol{F} = \boldsymbol{R}^{\jmath}\boldsymbol{F}^{\jmath}$ where $\boldsymbol{R}^{\jmath} \in \mathcal{SO}(3)$. Thus, the set $\mathscr{I}_{\mathrm{ti}}^{\jmath}$ also allows to introduce a generic, invariant-based deformation gradient

$$\boldsymbol{F}^{\jmath} = \begin{bmatrix} \lambda_1 & 0 & 0 \\ 0 & \lambda_2 & 0 \\ \gamma_\ell\cos[\phi_\gamma] & \gamma_\ell\sin[\phi_\gamma] & \lambda_\ell \end{bmatrix} \boldsymbol{e}_i^{\jmath} \otimes \boldsymbol{e}_j^{\jmath}\,, \tag{3.100}$$

where the $\boldsymbol{e}_3^{\jmath}$-axis is collinear with the preferred direction $\boldsymbol{a}_0$. Consequently, $\boldsymbol{e}_3^{\jmath}$ is collinear with $\boldsymbol{e}_3^{\imath}$ as well. The invariant-based deformation gradient $\boldsymbol{F}^{\jmath}$ has all the above mentioned benefits of the tensor $\boldsymbol{F}^{\jmath}$, however, it even exhibits at least four zero coefficients. Further, the invariants of set $\mathscr{I}_{\mathrm{ti}}^{I}$ in terms of set $\mathscr{I}_{\mathrm{ti}}^{\jmath}$ read

$$\begin{aligned} I_1 &= \lambda_\ell^2 + \lambda_1^2 + \lambda_2^2 + \gamma_\ell^2\,, \\ I_2 &= \lambda_1^{-2}\left(1 + \lambda_\ell^{-2}\gamma_\ell^2\cos[\phi_\gamma]^2\right) + \lambda_2^{-2}\left(1 + \lambda_\ell^{-2}\gamma_\ell^2\sin[\phi_\gamma]^2\right), \\ I_3 &= \lambda_\ell^2\lambda_1^2\lambda_2^2\,, \quad J_4 = \lambda_\ell^2\,, \quad J_5 = \lambda_\ell^2(\lambda_\ell^2 + \gamma_\ell^2) \end{aligned} \tag{3.101}$$

These relations are obtained by making use of $\boldsymbol{C}^{\jmath} = \boldsymbol{F}^{\jmath T}\boldsymbol{F}^{\jmath}$, $\boldsymbol{M} = \boldsymbol{e}_3^{\jmath} \otimes \boldsymbol{e}_3^{\jmath}$ and Eqs (3.73) and (3.85). By comparing Eqs (3.96) and (3.101), we note that the invariants λ_ℓ and γ_ℓ are the same for the sets $\mathscr{I}_{\mathrm{ti}}^{\imath}$ and $\mathscr{I}_{\mathrm{ti}}^{\jmath}$. Furthermore, it is possible to relate the invariants λ_1, λ_2 and ϕ_γ of set $\mathscr{I}_{\mathrm{ti}}^{\jmath}$ to set $\mathscr{I}_{\mathrm{ti}}^{\imath}$ in terms of

$$\lambda_1 = \frac{\sqrt{\gamma_{\mathrm{t}}^2 + 4\,\lambda_{\mathrm{t}}^2} + \gamma_{\mathrm{t}}}{2}\,, \quad \lambda_2 = \frac{\sqrt{\gamma_{\mathrm{t}}^2 + 4\,\lambda_{\mathrm{t}}^2} - \gamma_{\mathrm{t}}}{2}\,, \quad \cos[2\phi_\gamma] = \frac{H}{\gamma_\ell^2 \gamma_{\mathrm{t}} \sqrt{\gamma_{\mathrm{t}}^2 + 4\lambda_{\mathrm{t}}^2}}\,, \tag{3.102}$$

where H is given in Eq. (3.94). This points out that the sets $\mathscr{I}_{\mathrm{ti}}^{\imath}$ and $\mathscr{I}_{\mathrm{ti}}^{\jmath}$ are closely related to each other. Further, it allows to use a generic deformation gradient $\boldsymbol{F}^{\jmath}$, as given in Eq. (3.100), but prescribing λ_1 and λ_2 in terms of λ_{t} and γ_{t}. This combines the advantage of the simplicity of $\boldsymbol{F}^{\jmath}$ with its at least four zero coefficients with the more intuitive physical meanings of λ_{t} and γ_{t}. For completeness, note that λ_1, λ_2 and λ_ℓ depict the principal stretches of a generalised plane-strain deformation (in the transverse plane), represented by $\boldsymbol{F}^{\imath}|_{\gamma_\ell=0}$. This means that $\boldsymbol{F}^{\jmath}|_{\gamma_\ell=0} = \mathrm{diag}[\lambda_1, \lambda_2, \lambda_\ell]$ is the diagonalisation of $\boldsymbol{F}^{\imath}|_{\gamma_\ell=0}$. The representations of $\boldsymbol{F}^{\imath}$ and $\boldsymbol{F}^{\jmath}$ in Eqs (3.95) and (3.100), respectively, can formally be regarded as plane-strain deformations superimposed with out-of-plane shear, see, for example, Horgan & Saccomandi [230].

Finally, the outcomes of this section shall be combined with some considerations concerning incompressible materials. As discussed in Section 3.3.2, the motion of incompressible materials is subject to a constraint function $\det[\boldsymbol{F}] = 1$, as defined in (3.25). Relating this constraint to the invariant set $\mathscr{I}^I$, we obtain that $I_3 = J = 1$ holds in the case of incompressibility, see Eq. $(3.75)_3$. This means that the third invariant I_3 is of no further use and isotropic, incompressible material behaviour is subsequently only dependent on two remaining invariants. For transverse isotropy, the I_3-invariant appears explicitly in the sets $\mathscr{I}_{\mathrm{ti}}^{I}$, $\mathscr{I}_{\mathrm{ti}}^{I'}$ as well as in $\mathscr{I}_{\mathrm{ti}}^{I''}$, which means that incompressibility causes a *reduction to four invariants*. For instance, $\mathscr{I}_{\mathrm{ti}}^{I}$ reduces to $\{I_1, I_2, J_4, J_5\}$. For the set $\mathscr{I}_{\mathrm{ti}}^{\imath}$, the incompressibility condition is considered by exploiting Eq. $(3.96)_3$, which yields $\lambda_\ell^2\lambda_{\mathrm{t}}^4 = \lambda_\ell\lambda_{\mathrm{t}}^2 = 1$ and results in $\lambda_{\mathrm{t}} = \lambda_\ell^{-1/2}$. Subsequently, the invariant λ_{t} can be dropped from invariant set $\mathscr{I}_{\mathrm{ti}}^{\imath}$, which reduces to $\{\lambda_\ell, \gamma_\ell, \gamma_{\mathrm{t}}, \phi_\gamma\}$. This has an implication for the generic deformation gradient representation $\boldsymbol{F}^{\imath}$, as this then reads

$$\boldsymbol{F}^{\imath} = \begin{bmatrix} \lambda_\ell^{-1/2} & 0 & 0 \\ \gamma_{\mathrm{t}} & \lambda_\ell^{-1/2} & 0 \\ \gamma_\ell\,\cos[\psi_\gamma] & \gamma_\ell\,\sin[\psi_\gamma] & \lambda_\ell \end{bmatrix} \boldsymbol{e}_i^{\imath} \otimes \boldsymbol{e}_j^{\imath}\,. \tag{3.103}$$

In analogy, exploiting Eq. $(3.101)_3$ yields $\lambda_\ell^2\lambda_1^2\lambda_2^2 = \lambda_\ell\lambda_1\lambda_2 = 1$ as incompressibility constraint for the invariant set $\mathscr{I}_{\mathrm{ti}}^{\jmath}$. Hence, the invariant λ_2 can be dropped from $\mathscr{I}_{\mathrm{ti}}^{\jmath}$ as it can be expressed as $\lambda_2 = (\lambda_\ell\lambda_1)^{-1}$. This reduces $\mathscr{I}_{\mathrm{ti}}^{\jmath}$ to $\{\lambda_\ell, \lambda_1, \gamma_\ell, \phi_\gamma\}$. The generic tensor $\boldsymbol{F}^{\jmath}$ can then be rewritten to

$$\boldsymbol{F}^{\jmath} = \begin{bmatrix} \lambda_1 & 0 & 0 \\ 0 & (\lambda_1\lambda_\ell)^{-1} & 0 \\ \gamma_\ell\,\cos[\phi_\gamma] & \gamma_\ell\,\sin[\phi_\gamma] & \lambda_\ell \end{bmatrix} \boldsymbol{e}_i^{\jmath} \otimes \boldsymbol{e}_j^{\jmath}\,. \tag{3.104}$$

The implications of incompressibility on the invariant sets $\mathscr{I}_{\mathrm{ti}}^{I}$, $\mathscr{I}_{\mathrm{ti}}^{I}$, and $\mathscr{I}_{\mathrm{ti}}^{I}$ are summarised in Table 3.2. Finally, note that the axisymmetric shear in the incompressible case

integrity basis	**incompressibility reduction**
$\mathscr{I}_{\mathrm{ti}}^{I} = \{I_1, I_2, I_3, J_4, J_5\}$	$I_3 = 1 \;\rightarrow\; \{I_1, I_2, J_4, J_5\}$
$\mathscr{I}_{\mathrm{ti}}^{\imath} = \{\lambda_\ell, \lambda_{\mathrm{t}}, \gamma_\ell, \gamma_{\mathrm{t}}, \psi_\gamma\}$	$\lambda_\ell \lambda_{\mathrm{t}}^2 = 1 \;\rightarrow\; \lambda_{\mathrm{t}} = \lambda_\ell^{-1/2} \;\rightarrow\; \{\lambda_\ell, \gamma_\ell, \gamma_{\mathrm{t}}, \psi_\gamma\}$
$\mathscr{I}_{\mathrm{ti}}^{\jmath} = \{\lambda_\ell, \lambda_1, \lambda_2, \gamma_\ell, \phi_\gamma\}$	$\lambda_\ell \lambda_1 \lambda_2 = 1 \;\rightarrow\; \lambda_2 = (\lambda_\ell \lambda_1)^{-1} \;\rightarrow\; \{\lambda_\ell, \lambda_1, \gamma_\ell, \phi_\gamma\}$

Table 3.2: The three integrity bases $\mathscr{I}_{\mathrm{ti}}^{I}$, $\mathscr{I}_{\mathrm{ti}}^{\imath}$, and $\mathscr{I}_{\mathrm{ti}}^{\jmath}$ as well as the associated reductions to four invariants in the case of incompressibility.

reads

$$\gamma_{\mathrm{a}} = \begin{cases} +\sqrt{\lambda_\ell^2 + 2\lambda_\ell^{-1} - 3} & \text{if } \lambda_\ell \geq 1 \\ -\sqrt{\lambda_\ell^2 + 2\lambda_\ell^{-1} - 3} & \text{if } \lambda_\ell < 1\,. \end{cases} \tag{3.105}$$

Hence, the plus and the minus sign correspond to tension and to compression along the preferred direction, respectively, whereas $\gamma_{\mathrm{a}} = 0$ if the preferred axis is unstretched ($\lambda_\ell = 1$).

3.6 Further physical and mathematical requirements

This section presents some further physical and mathematical considerations when dealing with potential-based elastostatic problems. The preceding investigations in this chapter showed that the elastic energy is the decisive quantity in the case of hyperelastictity. Thus, this section especially contains investigations and remarks on further requirements upon the formulation of hyperelastic strain-energy potentials.

3.6.1 Normalisation

The reference configuration $\mathcal{B}_0$ of the body $\mathscr{B}$ was introduced in Section 2.1.1 in a rather arbitrary manner as the configuration which is defined by the reference placement $\mathscr{X}_0$ at time t_0. However, the previous investigations showed that the deformation gradient $\boldsymbol{F}$, which relates the actual configuration $\mathcal{B}$ to the reference configuration $\mathcal{B}_0$, is the key kinematical quantity and serves as argument for the response functions of the mechanical process. This means that the stored energy $\mathscr{W}$ and the stress $\boldsymbol{P}$ crucially depend on the definition of the reference configuration $\mathcal{B}_0$. In continuum mechanics, it is common practice that one proceeds from an *energy-free* and *stress-free* reference configuration, which means that

$$\mathscr{W}(\boldsymbol{F})\big|_{\boldsymbol{F}=\boldsymbol{I}} = 0 \qquad \text{and} \qquad \boldsymbol{P}(\boldsymbol{F})\big|_{\boldsymbol{F}=\boldsymbol{I}} = \boldsymbol{0}\,. \tag{3.106}$$

Note that although the evaluation of the dissipation principle revealed that the stress tensor is connected to the energy in the sense of being the derivative, see Eq. (3.20), an energy-free reference configuration does not imply that it is stress-free as well. Rather, the two conditions in (3.106) have to be satisfied separately. Moreover, if we consider a material which is subject to internal constraints, as outlined in Section 3.3, we have to recall that the stress tensor is then defined by Eq. (3.24). In the process of constitutive modelling, it only makes sense to demand that the extra stress, given by $\partial_{\boldsymbol{F}}\mathscr{W}$, vanishes

in the reference configuration. Hence, in order to account for both, unconstrained and constrained materials, Eqs (3.106) have to be formulated as

$$\mathscr{W}(\boldsymbol{F})\big|_{\boldsymbol{F}=\boldsymbol{I}} = 0 \qquad \text{and} \qquad \partial_{\boldsymbol{F}}\mathscr{W}(\boldsymbol{F})\big|_{\boldsymbol{F}=\boldsymbol{I}} = \boldsymbol{0}\,. \tag{3.107}$$

Finding a configuration which fulfils Eqs (3.107) is not always straightforward and is especially difficult or even impossible when biological tissues are considered. If the identification of an energy- and stress-free reference configuration in the absence of external forces on the body is not achievable and one has to proceed with a reference placement which does not satisfy Eqs (3.107), one arrives at the theory of prestressed or *residually stressed materials*. Doing so, a symmetric residual stress tensor $\boldsymbol{\tau} \in \mathcal{SYM}(3)$ is identified, such that

$$\mathrm{Div}[\boldsymbol{\tau}] = \boldsymbol{0} \quad \text{in } \mathcal{B}_0 \qquad \text{and} \qquad \boldsymbol{\tau}\boldsymbol{N} = \boldsymbol{0} \quad \text{on } \partial\mathcal{B}_0\,. \tag{3.108}$$

The first relation states that the residual stress $\boldsymbol{\tau}$ has to fulfil the equilibrium equation, whereas the second equation accounts for the fact that the unloaded reference configuration must not have any surface tractions. In summary, the treatment of mechanical problems either demands for the identification (or at least definition) of an unloaded reference configuration that is energy- and stress-free in the sense of Eqs (3.107) or an unloaded reference configuration with a residual stress $\boldsymbol{\tau}$ that satisfies Eqs (3.108). In any case, the state of stress in the reference configuration has to be specified in order to have meaningful statements for the stress in any actual configuration at time $t > t_0$. For more detailed explanations on residually stressed materials, we refer to Hoger [219, 220], Ogden [363], Shams et al. [433], or Ahamed et al. [6]. The identification of the reference configuration and the connection to residual stresses are very decisive aspects for the modelling of biological tissues and were discussed, for example, by Chuong & Fung [79], Fung [144], Holzapfel et al. [222], Balzani [24], or Gee et al. [153]. Particular phenomena like residual stresses related to tissue growth are discussed by Rodriguez et al. [406], whereas residual stresses due to osmotic effects are treated by Lanir [277].

3.6.2 Growth conditions

From a physical point of view, it is very reasonable that extreme values of deformations must accompany extreme values of the associated stored elastic energy and associated stresses in a material. As a consequence, physically meaningful strain-energy functions have to meet appropriate *growth conditions*, which can be formulated as follows:

$$\mathscr{W} \to +\infty \quad \text{as} \quad \begin{cases} \det[\boldsymbol{F}] \to 0^+ \\ (\|\boldsymbol{F}\| + \|\operatorname{cof}[\boldsymbol{F}]\| + \det[\boldsymbol{F}]) \to +\infty\,. \end{cases} \tag{3.109}$$

Therein, $\|\boldsymbol{A}\| = \sqrt{\boldsymbol{A}\cdot\boldsymbol{A}}$ denotes the norm of a tensor $\boldsymbol{A}$. It is an easy matter to see that the three terms $\boldsymbol{F}$, $\operatorname{cof}[\boldsymbol{F}]$, and $\det[\boldsymbol{F}]$, which occur in (3.109), are connected to the transport of line, area, and volume elements, respectively. In this sense, the terms are also directly connected to the invariant set $\mathscr{I}^I = \{I_1, I_2, I_3\}$, see Eqs (3.75). Thus, the conditions in (3.109) are very intuitive and self explanatory, as they simply state that the strain-energy $\mathscr{W}$ has to tend to infinity when the sum of line, area, and volume element stretches goes to infinity or when the volume is compressed towards $\det[\boldsymbol{F}] \to 0^+$. Note for

completeness that the second condition in (3.109) can be formulated in a sharper version in terms of the *coerciveness inequality*

$$\mathscr{W} \geq \alpha \left[\|\boldsymbol{F}\|^p + \|\operatorname{cof}[\boldsymbol{F}]\|^q + \det[\boldsymbol{F}]^r \right] + \beta \quad \exists \{\alpha, p, q, r > 0, \beta\} \in \mathcal{R} \tag{3.110}$$

see CIARLET [80]. Strain-energies $\mathscr{W}$ satisfying Eq. (3.110) are then referred to as *coercive*.

3.6.3 Existence of minimisers

In Section 3.4, the basic mechanical boundary-value problem has been approached from a rigorous variational perspective and the governing equations in (3.53) were derived by exploiting the principle of minimum potential energy. In this context, it was highlighted that the fundamental step for obtaining equilibrium solutions of the mechanical problem is to find a motion function $\boldsymbol{\chi}$ such that the elastostatic potential $\Pi(\boldsymbol{\chi})$ becomes stationary. The details on the associated boundary conditions and the incorporation of further kinematical constraints were discussed in Sections 3.4.2 and 3.4.3 and are not repeated at this point. In order to guarantee that a stationary solution of the variational problem represents a minimum value, the functional Π has to satisfy further requirements. This means that one seeks to ensure the *existence of minimisers*, which are deformation states $\boldsymbol{\chi}$ that minimise the functional Π. Sufficient conditions for this requirement are reviewed here in a rather compact manner. For complete overviews and further insights to the topic, we refer to the comprehensive works of KRAWIETZ [262], ŠILHAVÝ [438], SCHRÖDER [421], and DACOROGNA [87]. According to these works, the existence of minimisers is guaranteed if the functional

$$\Pi(\boldsymbol{\chi}) = \int_{\mathcal{B}_0} \mathscr{W}(\boldsymbol{F}) \, \mathrm{d}V + \Pi_{\text{ext}}(\boldsymbol{\chi}) \,, \tag{3.111}$$

is *coercive* and satisfies the *sequentially weakly lower semicontinuity* condition.

Convexity An intuitive first approach for the sequentially weakly lower semicontinuity condition is to demand for the convexity of the functional Π. However, instead of investigating a global convexity statement for the functional Π on the whole domain $\mathcal{B}_0$, it proves useful to formulate a *local* convexity statement for the strain-energy function $\mathscr{W}(\boldsymbol{F})$ at $\boldsymbol{X} \in \mathcal{B}_0$. Such a local statement is very convenient as associated mathematical conditions can then directly be posed as further requirements during the process of the constitutive formulation of strain-energy functions. Convexity conditions for the scalar-valued tensor function $\mathscr{W}$ are given by the three equivalent statements

$$\left.\begin{aligned} & \mathscr{W}(\boldsymbol{F} + \lambda \Delta\boldsymbol{F}) \leq \lambda \mathscr{W}(\boldsymbol{F} + \Delta\boldsymbol{F}) + (1-\lambda)\mathscr{W}(\boldsymbol{F}) \quad \forall\, 0 \leq \lambda \leq 1 \\ \Leftrightarrow\ & \mathscr{W}(\boldsymbol{F}) + \partial_{\boldsymbol{F}}\mathscr{W}(\boldsymbol{F}) \cdot \Delta\boldsymbol{F} \leq \mathscr{W}(\boldsymbol{F} + \Delta\boldsymbol{F}) \\ \Leftrightarrow\ & \Delta\boldsymbol{F} \cdot \partial^2_{\boldsymbol{F}\boldsymbol{F}}\mathscr{W}(\boldsymbol{F})\, \Delta\boldsymbol{F} \geq 0 \,. \end{aligned}\right\} \tag{3.112}$$

Therein, $\Delta\boldsymbol{F}$ depicts a perturbation of the deformation state $\boldsymbol{F}$. The first condition in (3.112) is the basic mathematical convexity statement and essentially states that each line between the points $(\boldsymbol{F}, \mathscr{W}(\boldsymbol{F}))$ and $(\boldsymbol{F}+\Delta\boldsymbol{F}, \mathscr{W}(\boldsymbol{F}+\Delta\boldsymbol{F}))$ must not be below the curve $\mathscr{W}$ itself. The second condition is obtained from the first one by a limit case investigation as $\lambda \to 0$ and the appropriate directional Gateaux derivative. It involves the first derivative $\partial_{\boldsymbol{F}}\mathscr{W}$ which is easily identified as the first Piola–Kirchhoff stress $\boldsymbol{P}$, see Eq. (3.20). This second convexity form states that the tangent line to the curve $\mathscr{W}$ at $(\boldsymbol{F}, \mathscr{W}(\boldsymbol{F}))$ must not

be above the curve $\mathscr{W}$ at $\boldsymbol{F}+\Delta\boldsymbol{F}$. Finally, the third statement is obtained from the second one by another application of a directional Gateaux derivative and yields an infinitesimal statement. It is probably the most useful convexity notation in continuum mechanics and demands that the second derivative $\partial^2_{\boldsymbol{F}\boldsymbol{F}}\mathscr{W}$ of $\mathscr{W}$ with respect to $\boldsymbol{F}$ is positive semidefinite. This second derivative is a fundamental quantity in continuum mechanics and is introduced as the fourth-order (nominal) *elasticity tensor*

$$\mathbb{L}(\boldsymbol{F}) := \partial^2_{\boldsymbol{F}\boldsymbol{F}}\mathscr{W}(\boldsymbol{F})\,. \tag{3.113}$$

It is also called tangent modulus or incremental stiffness. Simo & Marsden [440] and Marsden & Hughes [316] refer to $\mathbb{L}$ as the first elasticity tensor, motivated by the direct connection to the first Piola–Kirchhoff stress $\boldsymbol{P}$ through $\mathbb{L} = \partial_{\boldsymbol{F}}\boldsymbol{P}$. The elasticity tensor $\mathbb{L}$ is major but in general not minor symmetric, such that $\mathbb{L}^T = \mathbb{L}$. However, we remark that the nominal elasticity tensor has material as well as spatial counterparts, which are major and minor symmetric. For instance, the material elasticity tensor is defined as $\mathbb{C} = 4\,\partial^2_{\boldsymbol{C}\boldsymbol{C}}\mathscr{W}$. It is associated with the already introduced second Piola–Kirchhoff stress $\boldsymbol{S} = 2\,\partial_{\boldsymbol{C}}\mathscr{W}$, which is symmetric and thus causes the minor symmetry of $\mathbb{C}$. The two material quantities are connected to the here used nominal ones by $\boldsymbol{P} = \boldsymbol{F}\boldsymbol{S}$ (a push-forward operation of the first basis of $\boldsymbol{S}$, as explained in Section 3.5.2) and

$$\mathbb{L} = (\boldsymbol{F}\otimes\boldsymbol{I})^{T_{23}}\,\mathbb{C}\,(\boldsymbol{F}^T\otimes\boldsymbol{I})^{T_{23}} + (\boldsymbol{I}\otimes\boldsymbol{S})^{T_{23}} \tag{3.114}$$

see Simo & Marsden [440], Marsden & Hughes [316] or Curnier [85]. Some implications and further explanations on symmetry properties of fourth-order tensors are provided in Appendix A.7.2. Proceeding with the convexity considerations, we note that in order to formulate the convexity statement in the infinitesimal form $(3.112)_3$, the strain-energy function $\mathscr{W}$ has to be twice differentiable, which is generally the case. Note that the convexity statements (3.112) can be strengthened to strict convexity if they are changed to strict inequalities, hence, by replacing $\leq$ by $<$ and $\geq$ by $>$. Reformulating Eq. $(3.112)_3$ in terms of strict convexity then demands that the elasticity tensor $\mathbb{L}$ is positive definite. A convex strain-energy in the sense of Eqs (3.112) or in the strictly convex form ensures the sequentially weakly lower semicontinuity of the elastostatic functional Π. However, it is a too restrictive demand, as, for instance, strict convexity entails that any solution is unique and stable. Therefore, it excludes structural instabilities, such as buckling phenomena, which have to be included in a reasonable large-strain theory, see Hill [209]. Moreover, convexity (both, strict and non-strict) is incompatible with the principle of material frame-indifference, see Coleman & Noll [82], and it violates the growth condition $(3.109)_1$ in the limit $\det[\boldsymbol{F}] \to 0^+$. In summary, convexity of the strain-energy $\mathscr{W}$ is not reasonable and alternative concepts have to be consulted. This motivates the introduction of so-called *weak convexity* statements.

Quasiconvexity A fundamental weak convexity statement is the concept of *quasiconvexity*, introduced by Morrey [343]. The quasiconvexity condition reads

$$\mathscr{W}(\boldsymbol{F}) \leq \frac{1}{\mathrm{vol}[\mathcal{B}_S]}\int_{\mathcal{B}_S}\mathscr{W}(\boldsymbol{F}+\mathrm{Grad}[\tilde{\boldsymbol{\chi}}])\,\mathrm{d}V\,. \tag{3.115}$$

Therein, the integral is defined over the subdomain $\mathcal{B}_S \subset \mathcal{B}_0$ and $\tilde{\boldsymbol{\chi}}$ are fluctuations of the placement function $\boldsymbol{\chi}$ in $\mathcal{B}_S$. The fluctuations have to vanish on the boundary of

the subdomain, thus, $\tilde{\boldsymbol{\chi}} = \boldsymbol{0}$ on $\partial\mathcal{B}_S$. Eq. (3.115) states that the energy level caused by a homogeneous deformation $\boldsymbol{F}$ in $\mathcal{B}_S$ is always lower (or equal) than the energy level caused by any perturbed state $\boldsymbol{F} + \mathrm{Grad}[\tilde{\boldsymbol{\chi}}]$. The homogeneous deformation thus depicts a minimiser to the functional $\mathscr{W}$. Morrey [343] showed that quasiconvexity in the sense of Eq. (3.115), together with appropriate growth conditions, is a necessary and sufficient condition for weakly lower semicontinuity. However, the quasiconvexity condition involves an integral statement and is not as practical to check as a local statement. Furthermore, quasiconvexity only makes sense if a material is homogeneous in the subdomain $\mathcal{B}_S$. Microscopically *heterogeneous* materials in $\mathcal{B}_S$ generally depict a minimum energy for heterogeneous deformations, which conflicts with the statement in Eq. (3.115). This will become clear in Part II of this work. Condition (3.115) also excludes the possibility of stability problems in the subdomain $\mathcal{B}_S$, which is not acceptable when considering materials which are heterogeneous in $\mathcal{B}_S$. Moreover, quasiconvexity conflicts with the growth condition $(3.109)_1$ in the limit $\det[\boldsymbol{F}] \to 0^+$.

Polyconvexity A very useful weak convexity statement was formulated in the seminal work of Ball [23] and is referred to as *polyconvexity*. It is less restrictive than convexity, but a stronger statement than quasiconvexity. Thus, polyconvexity implies quasiconvexity and is therefore a sufficient condition for weakly lower semicontinuity. Yet, it is a local statement and it thus easier to handle than the integral condition of quasiconvexity. Moreover, polyconvexity does not share any of the above mentioned drawbacks of quasiconvexity, which makes it the most valuable tool to check the existence of minimiser. The key idea behind the concept of polyconvexity is to introduce an extended list of arguments, reading $\boldsymbol{\mathcal{F}} = \{\boldsymbol{F}, \mathrm{cof}[\boldsymbol{F}], \det[\boldsymbol{F}]\}$. Subsequently, the strain-energy function $\mathscr{W}$ is (strictly) polyconvex if it can be written as a function $\mathscr{W}(\boldsymbol{\mathcal{F}}) : \mathcal{R}^{3\otimes3} \times \mathcal{R}^{3\otimes3} \times \mathcal{R} \to \mathcal{R}$ that is (strictly) convex with respect to the 19-dimensional argument $\boldsymbol{\mathcal{F}}$. In terms of the second (Gateaux) derivative of $\mathscr{W}(\boldsymbol{\mathcal{F}})$ with respect to $\boldsymbol{\mathcal{F}}$, polyconvexity can be expressed in form of the statement

$$\delta\boldsymbol{\mathcal{F}} \cdot \partial^2_{\boldsymbol{\mathcal{F}}\boldsymbol{\mathcal{F}}}\mathscr{W}(\boldsymbol{\mathcal{F}})\,\delta\boldsymbol{\mathcal{F}} \geq 0 \tag{3.116}$$

and demands for the positive semidefiniteness of the $\mathcal{R}^{19\times19}$-matrix $\partial^2_{\boldsymbol{\mathcal{F}}\boldsymbol{\mathcal{F}}}\mathscr{W}$. If the strain energy is given as an additive function $\mathscr{W}(\boldsymbol{\mathcal{F}}) = \mathscr{W}_1(\boldsymbol{F}) + \mathscr{W}_2(\mathrm{cof}[\boldsymbol{F}]) + \mathscr{W}_3(\det[\boldsymbol{F}])$, polyconvexity is ensured if each function $\mathscr{W}_i$ $(i = 1, 2, 3)$ is convex in its associated argument. In turn, this can be proven by the positive semidefiniteness of the fourth-order tensors $\partial^2_{\boldsymbol{F}\boldsymbol{F}}\mathscr{W}$ (the elasticity tensor $\mathbb{L}$) and $\partial^2_{\mathrm{cof}[\boldsymbol{F}]\,\mathrm{cof}[\boldsymbol{F}]}\mathscr{W}$ as well as the non-negativity of the scalar derivative $\partial^2_{J^2}\mathscr{W}$. This makes it easy to give polyconvexity an intuitive physical interpretation by noting that the extended list $\boldsymbol{\mathcal{F}} = \{\boldsymbol{F}, \mathrm{cof}[\boldsymbol{F}], \det[\boldsymbol{F}]\}$ contains the operators of the line, area and volume transport, which we already identified in the growth conditions (3.109). Thus, polyconvexity can be understood as convexity with respect to changes of line, area, and volume elements. Further, Eqs (3.75) recalls a direct connection between invariant set $\mathscr{I}^I = \{I_1, I_2, I_3\}$ and the argument list $\boldsymbol{\mathcal{F}}$. Hence, it can be concluded that a strain-energy function $\mathscr{W}(\mathscr{I}^I) = \mathscr{W}_1(I_1) + \mathscr{W}_2(I_2) + \mathscr{W}_3(I_3)$ is polyconvex if it can be formulated as the sum of functions $\mathscr{W}_i$ $(i = 1, 2, 3)$ that are each convex in their argument I_i. Furthermore, an extension of such investigations to the polyconvexity of transversely isotropic invariants can be found in Schröder & Neff [425].

Rank-one convexity A further weak convexity statement is the *rank-one convexity*. It is the weakest among the ones discussed so far and describes the convexity of a function

along a straight line, where the difference between the start and end point of the line is expressed by a rank-one, second-order tensor. Applied to the present problem, rank-one convexity of the strain-energy function $\mathscr{W}$ is described by the same form than in Eqs (3.112) with the difference that the perturbation $\Delta\boldsymbol{F} = \boldsymbol{\eta} \otimes \boldsymbol{\zeta}$ is now given by the rank-one tensor $\boldsymbol{\eta}\otimes\boldsymbol{\zeta}$ with $\boldsymbol{\eta}, \boldsymbol{\zeta} \in \mathcal{R}^3 \setminus \{\boldsymbol{0}\}$. The infinitesimal rank-one convexity condition then reads

$$(\boldsymbol{\eta} \otimes \boldsymbol{\zeta}) \cdot \partial^2_{\boldsymbol{F}\boldsymbol{F}} \mathscr{W}(\boldsymbol{F})(\boldsymbol{\eta} \otimes \boldsymbol{\zeta}) \geq 0 \tag{3.117}$$

with the elasticity tensor $\mathbb{L}(\boldsymbol{F}) = \partial^2_{\boldsymbol{F}\boldsymbol{F}} \mathscr{W}(\boldsymbol{F})$. Eq. (3.117) is also known as the *Legendre-Hadamard strong ellipticity* condition. This analogy entails that a rank-one convex strain-energy function $\mathscr{W}$ leads to strongly elliptic problems. The interesting physical implication of this is that strong ellipticity ensures wave propagations with real wave speeds through the material. With this physical connection, the vector $\boldsymbol{\zeta}$ is given the meaning of the direction of wave propagation and $\boldsymbol{\eta}$ represents a polarisation vector. Subsequently, it is useful to reformulate Eq. (3.117) to

$$\boldsymbol{\eta} \cdot \mathscr{A}(\boldsymbol{\zeta})\, \boldsymbol{\eta} \geq 0 \tag{3.118}$$

and to introduce the symmetric second-order *acoustic tensor*

$$\mathscr{A} = (\mathbb{L}^{T_{23}}\boldsymbol{\zeta})\boldsymbol{\zeta} = \mathrm{L}_{ikjl}\, \zeta_k\, \zeta_l\, \boldsymbol{e}_i \otimes \boldsymbol{e}_j\,. \tag{3.119}$$

The symmetry of the acoustic tensor $\mathscr{A} \in \mathcal{SYM}(3)$ is directly visible through its index notation $\mathscr{A}_{ij} = \mathrm{L}_{ikjl}\, \zeta_k\, \zeta_l$ $(i, j, k, l = 1, 2, 3)$ and the major symmetry of the elasticity tensor $\mathbb{L}$. Further, the rank-one convexity conditions in Eqs (3.117) and (3.118) can be strengthened to strict rank-one convexity by replacing $\geq$ with $>$. With this, we can formulate the equivalence of the following statements: (i) strict rank-one convexity of $\mathscr{W}$, (ii) strong ellipticity of the problem, (iii) wave propagations with real positive wave speeds, and (iv) positive definiteness of the acoustic tensor $\mathscr{A}$. The last statement requires that the acoustic tensor only has real and positive eigenvalues, as they are directly connected to the wave speeds. However, instead of solving an eigenvalue problem, the positive definiteness of the symmetric acoustic tensor can be exploited by investigating the positiveness of its leading principal minors, leading to the three simple conditions

$$\mathscr{A}_{11} > 0\,, \quad \mathscr{A}_{11}\mathscr{A}_{22} - \mathscr{A}_{12}\mathscr{A}_{21} > 0\,, \quad \det[\mathscr{A}] > 0\,. \tag{3.120}$$

This is referred to as *Sylvester's criterion*. In practical application, the conditions in (3.120) have to be checked for every space orientation vector $\boldsymbol{\zeta}$. Failure of Sylvester's criterion, and hence, the loss of strong ellipticity, does not necessarily lead to instability problems in the sense of buckling or bifurcation phenomena. Rather, it indicates equilibrium states with continuous displacement fields but discontinuous deformation gradient along a singular surface with normal direction $\boldsymbol{\zeta}$. Further investigations on material behaviour under the loss of strong ellipticity can be found in Knowles & Sternberg [253, 254]. Finally, we remark that although it seems reasonable to demand for the positiveness of wave speeds through a material and, hence, strict rank-one convexity, there are scenarios where rank-one convexity and the allowance of a possible zero eigenvalue of the acoustic tensor is appropriate. For instance, it was shown in the works of Ericksen [117], Truesdell & Noll [490, Sec. 78] and Scott & Hayes [428] that the incompressibility

condition, given in Eq. (3.25), implies that the acoustic tensor has a zero eigenvalue and waves do not propagate in the direction of the associated eigenvector. Hence, the consideration of internally constrained materials may require appropriate modifications of the ellipticity conditions, see, for instance, Zee & Sternberg [525].

Concluding remarks The convexity statements presented in this section are connected in a hierarchical manner, which means that stronger convexity conditions imply the weaker conditions, while the opposite does not hold in general. For continuous functions, such as the strain-energy function $\mathscr{W}$, the hierarchy is given by

$$\textit{convexity} \;\Rightarrow\; \textit{polyconvexity} \;\Rightarrow\; \textit{quasiconvexity} \;\Rightarrow\; \textit{rank-one convexity}\,.$$

Thus, polyconvexity of the strain-energy function induces the weaker statements of quasiconvexity and rank-one convexity. It is therefore not only a sufficient condition for weakly lower semicontinuity, which comes with the quasiconvexity, but also ensures the physical meaningful demand for wave propagations with real wave speed through the material. Moreover, polyconvexity is a local condition and by that serves as a valuable and easy check if the strain-energy function $\mathscr{W}$ is specified in terms of closed-form analytical expressions. It is also a meaningful tool to ensure the physical meaningfulness of constitutive theories during the construction of strain-energy functions. On the other hand, rank-one convexity is the weakest of the above statements, but it has the convenient feature that it is equivalent to the Legendre-Hadamard strong ellipticity condition and has the physical implication of real wave speeds. Therefore, the check for rank-one convexity is very useful in situations where the polyconvexity condition is not suitable, such as for multiscale analysis, where the strain-energy at higher scales is not given in a closed-form expression, but is determined by a homogenisation of energies from smaller scales. This becomes clearer in Part II.

3.7 Further remarks on constitutive modelling

To conclude the explanations on material theory, this section presents some further aspects with respect to the formulation of strain-energy functions. The section briefly introduces the concept of Legendre transforms and complementary energies as well as a constitutive deviatoric-volumetric split of the energy $\mathscr{W}$. After that, we introduce some constitutive strain-energy functions and conclude with explanations on the connection between the finite theory and the infinitesimal small-strain theory. The results and outcomes of the here discussed topics are picked up again later in this work.

3.7.1 Legendre transforms and the idea of complementary energies

For a variety of applications in continuum mechanics, the concept of *Legendre transformations* serves as very useful mathematical tool. It is a so-called contact transformation and can be used to change dependencies of functions. An overview on the basic principles, in particular the difference between the classical Legendre, the Legendre-Fenchel, and a here used generalised Legendre transform, is provided in Appendix B.1. The reader is referred to, for example, Rockafellar [405] or Sewell [430] for deeper insights in the topic.

The transforms of thermodynamical potentials: Complementary energies Legendre transformations are an essential mathematical tool in continuum mechanics and general thermodynamics. They allow to change the dependencies of thermodynamic potentials and the classical idea behind the transformations is that the energy of a thermodynamic system shall be expressible in terms of arguments which are observable and measurable. We already applied this idea in Section 2.3.6 without explicitly stating it. There, we introduced the Helmholtz free energy $\psi = \varepsilon - \theta\eta$ in terms of the internal energy ε, which is essentially a Legendre transform with respect to the conjugate pair $\{\theta, \eta\}$. Using the Helmholtz energy ψ (or the volume-specific version $\mathscr{W} = \rho_0\psi$) instead of ε is justified because the internal energy is a function of the deformation (expressed, for example, in terms of $\boldsymbol{F}$) and the entropy η. Clearly, the entropy is a cumbersome quantity and not measurable. However, the partial derivative $\partial_\eta \varepsilon = \theta$ of the internal energy $\varepsilon(\boldsymbol{F}, \eta)$ with respect to the entropy yields the (absolute) temperature, which is a well manageable quantity. Hence, it makes sense to perform a partial Legendre transform of the internal energy with respect to the conjugate pair $\{\theta, \eta\}$. In terms of the generalised Legendre transform, as defined in Eq. (B.6), we obtain $\varepsilon^*(\boldsymbol{F}, \theta) = \operatorname{stat}_\eta\{\theta\eta - \varepsilon(\boldsymbol{F}, \eta)\}$ with $\theta = \partial_\eta \varepsilon$. If one now assumes that η represents a value where $\theta\eta - \varepsilon$ becomes stationary, it becomes clear that the Helmholtz free energy is nothing else than the negative Legendre transform of the internal energy, hence, $\psi = -\varepsilon^*$. We thus call the Helmholtz energy $\psi(\boldsymbol{F}, \theta)$ the negative *caloric complementary energy* compared to $\varepsilon(\boldsymbol{F}, \eta)$. This means that the volume-specific Helmholtz energy $\mathscr{W}$ can be written as $\mathscr{W}(\boldsymbol{F}, \theta) = -\rho_0 \operatorname{stat}_\eta\{\theta\eta - \varepsilon(\boldsymbol{F}, \eta)\}$ with the partial derivatives $\partial_{\boldsymbol{F}}\mathscr{W} = \boldsymbol{P}$, see Eq. (3.20), and $\partial_\theta \mathscr{W} = -\rho_0\eta$. We see that the formulation of a strain-energy $\mathscr{W}$ relies on the stationarity of the entropy, which is a key requirement for the application of minimum energy principles as introduced in Section 3.4.2. Furthermore, with our knowledge about the derivative $\partial_{\boldsymbol{F}}\mathscr{W} = \boldsymbol{P}$, we identify $\{\boldsymbol{F}, \boldsymbol{P}\}$ as a conjugate pair and may perform the associated Legendre transformation

$$\mathscr{U}(\boldsymbol{P}, \theta) := \operatorname*{stat}_{\boldsymbol{F}}\{\boldsymbol{F} \cdot \boldsymbol{P} - \mathscr{W}(\boldsymbol{F}, \theta)\}\,, \tag{3.121}$$

where $\mathscr{U}$ is introduced as the volume-specific *Gibbs energy* or *free enthalpy* (which is *multi-valued for non-convex* $\mathscr{W}$, see in this context also the remarks in Section 4.3.5). The derivative of $\mathscr{U}$ with respect to $\boldsymbol{P}$ reads $\partial_{\boldsymbol{P}}\mathscr{U} = \boldsymbol{F}$. Thus, the Gibbs energy is the *mechanical complementary energy* compared to the strain energy $\mathscr{W}$. The description of mechanical problems in terms of the Gibbs energy $\mathscr{U}$ instead of $\mathscr{W}$ can be beneficial in a variety of applications. For instance, Rajagopal & Srinivasa [394, 395] explained that a Gibbs-formulation is very suitable for problems that are subject to internal constraints, which we discussed in Section 3.3, since kinematical constraints for $\boldsymbol{F}$ then turn into simple constitutive assumptions. We will not follow such procedures in this work, however, formulations reminiscent to Eq. (3.121) will arise as a mathematical consequence in Section 5.1. For completeness, the last of the four important thermodynamical potentials is the *enthalpy* $\mathscr{H}(\boldsymbol{P}, \eta) := -\operatorname{stat}_\theta\{\theta\eta - \mathscr{U}(\boldsymbol{P}, \theta)\}$, which is the negative caloric complementary energy compared to the Gibbs energy $\mathscr{U}$ and, likewise, the volume-specific mechanical complementary energy compared to the internal energy $\varepsilon(\boldsymbol{F}, \eta)$.

3.7.2 Deviatoric-volumetric split of the energy

In Section 2.1.4 and Eq. (2.21), we showed that the deformation gradient $\boldsymbol{F} = \boldsymbol{F}_{\mathrm{v}}\,\breve{\boldsymbol{F}}$ might be decomposed into a purely volumetric deformation $\boldsymbol{F}_{\mathrm{v}}$ and a purely deviatoric deform-

ation $\breve{\boldsymbol{F}}$. Based on this kinematical decomposition, one may constitutively introduce an additive split of the strain-energy, reading

$$\mathscr{W}(\boldsymbol{F}) = \mathscr{W}_{\text{dev}}(\breve{\boldsymbol{F}}) + \mathscr{W}_{\text{vol}}(J) \tag{3.122}$$

where $\mathscr{W}_{\text{dev}}$ is the energy contribution due to the isochoric deformation and $\mathscr{W}_{\text{vol}}$ is energy associated with the volumetric deformation, see, for example, Ogden [359], Simo et al. [442] and Miehe [328]. On the basis of the energy decoupling in Eq. (3.122), also the first Piola–Kirchhoff stress gets a decoupled representation, reading

$$\boldsymbol{P} = \partial_{\boldsymbol{F}}\mathscr{W} = \partial_{\boldsymbol{F}}\mathscr{W}_{\text{dev}} + \partial_{\boldsymbol{F}}\mathscr{W}_{\text{vol}} =: \boldsymbol{P}_{\text{dev}} + \boldsymbol{P}_{\text{vol}}\,. \tag{3.123}$$

Therein, the deviatoric stress $\boldsymbol{P}_{\text{dev}}$ and the volumetric stress $\boldsymbol{P}_{\text{vol}}$ are given by

$$\boldsymbol{P}_{\text{dev}} = J^{-1/3}\mathbb{D}\breve{\boldsymbol{P}}\,, \quad \text{with} \quad \breve{\boldsymbol{P}} = \partial_{\breve{\boldsymbol{F}}}\mathscr{W}_{\text{dev}}\,, \quad \text{and} \quad \boldsymbol{P}_{\text{vol}} = J\partial_J\mathscr{W}_{\text{vol}}\boldsymbol{F}^{-T}\,, \tag{3.124}$$

respectively, by a consequent use of the chain rule and the derivation rules provided in Appendix A.6. The deviatoric stress $\boldsymbol{P}_{\text{dev}}$ in Eq. $(3.124)_1$ contains the fourth-order projection tensor $\mathbb{D}$, which is associated with the derivative of the deviatoric deformation $\breve{\boldsymbol{F}} = J^{-1/3}\boldsymbol{F}$ with respect to $\boldsymbol{F}$ and is defined as

$$\mathbb{D} = \mathbb{I} - \tfrac{1}{3}\boldsymbol{F}^{-T} \otimes \boldsymbol{F} \quad \text{such that} \quad \partial_{\boldsymbol{F}}\breve{\boldsymbol{F}} = J^{-1/3}\mathbb{D}^T\,. \tag{3.125}$$

Therein, $\mathbb{I}$ is the fourth-order identical map. It is easy to show that the projection tensor $\mathbb{D}$ is symmetric, $\mathbb{D} = \mathbb{D}^T$, and idempotent, $\mathbb{D}\mathbb{D} = \mathbb{D}$. We note that from a mathematical point of view a deviatoric tensor should be traceless and the non-deviatoric remainder should be a spherical tensor. However, these characteristics are not exhibited through the first Piola–Kirchhoff stress contributions $\boldsymbol{P}_{\text{dev}}$ and $\boldsymbol{P}_{\text{vol}}$, but through the associated Cauchy stress representation

$$\boldsymbol{\sigma} = J^{-1}\boldsymbol{P}\boldsymbol{F}^T = J^{-1}\boldsymbol{P}_{\text{dev}}\boldsymbol{F}^T + J^{-1}\boldsymbol{P}_{\text{vol}}\boldsymbol{F}^T =: \boldsymbol{\sigma}_{\text{dev}} + \boldsymbol{\sigma}_{\text{vol}} \tag{3.126}$$

in the actual configuration. After some algebra and using already introduced tensor calculation rules, we obtain the two stress contributions

$$\boldsymbol{\sigma}_{\text{dev}} = J^{-1/3}(\breve{\boldsymbol{\sigma}} - \tfrac{1}{3}\,\text{tr}[\breve{\boldsymbol{\sigma}}]\boldsymbol{I})\,, \quad \text{with} \quad \breve{\boldsymbol{\sigma}} = J^{-1}\breve{\boldsymbol{P}}\boldsymbol{F}^T\,, \quad \text{and} \quad \boldsymbol{\sigma}_{\text{vol}} = \partial_J\mathscr{W}_{\text{vol}}\boldsymbol{I}\,. \tag{3.127}$$

It is an easy matter to show that $\boldsymbol{\sigma}_{\text{dev}}$ is traceless, $\text{tr}[\boldsymbol{\sigma}_{\text{dev}}] = 0$, and we clearly see that $\boldsymbol{\sigma}_{\text{vol}}$ is a spherical tensor. Moreover, in Eq. (3.28) we showed that the trace of the Cauchy stress is connected to the hydrostatic pressure and formulated the associated equation for the first Piola–Kirchhoff stress in (3.29). Thus, $\boldsymbol{P}_{\text{dev}}$, although not traceless, shows its deviatoric nature through a vanishing hydrostatic pressure, hence

$$-\tfrac{1}{3}J^{-1}\boldsymbol{P}_{\text{dev}} \cdot \boldsymbol{F} = J^{-4/3}(\breve{\boldsymbol{P}} - \tfrac{1}{3}(\breve{\boldsymbol{P}} \cdot \boldsymbol{F})\boldsymbol{F}^{-T}) \cdot \boldsymbol{F} = 0\,. \tag{3.128}$$

In this sense, the fourth-order tensor $\mathbb{D}$ can be referred to as a nominal version of the classical deviatoric projection tensor $\mathbb{I} - (\boldsymbol{I} \otimes \boldsymbol{I})/3$.

For completeness, the nominal elasticity tensor associated with the deviatoric-volumetric energy decoupling reads

$$\mathbb{L} = \partial^2_{\boldsymbol{F}\boldsymbol{F}}\mathscr{W} = \partial^2_{\boldsymbol{F}\boldsymbol{F}}\mathscr{W}_{\text{dev}} + \partial^2_{\boldsymbol{F}\boldsymbol{F}}\mathscr{W}_{\text{vol}} = \mathbb{L}_{\text{dev}} + \mathbb{L}_{\text{vol}}\,, \tag{3.129}$$

where the deviatoric part $\mathbb{L}_{\text{dev}}$ and the volumetric part $\mathbb{L}_{\text{vol}}$ are given by

$$\begin{aligned}\mathbb{L}_{\text{dev}} &= \tfrac{1}{3}J^{-1/3}\big[(\check{\boldsymbol{P}}\cdot\boldsymbol{F})(\boldsymbol{F}^{-T}\otimes\boldsymbol{F}^{-T})^{T_{24}} - \mathbb{D}\check{\boldsymbol{P}}\otimes\boldsymbol{F}^{-T} + \boldsymbol{F}^{-T}\otimes\check{\boldsymbol{P}}\big] + J^{-2/3}\mathbb{D}\check{\mathbb{L}}\,,\\ \mathbb{L}_{\text{vol}} &= (J\partial_J\mathscr{W}_{\text{vol}} + J^2\partial^2_{J^2}\mathscr{W}_{\text{vol}})\boldsymbol{F}^{-T}\otimes\boldsymbol{F}^{-T} - J\partial_J\mathscr{W}_{\text{vol}}(\boldsymbol{F}^{-T}\otimes\boldsymbol{F}^{-T})^{T_{24}}\,,\end{aligned} \tag{3.130}$$

respectively, where $\check{\mathbb{L}} = \partial^2_{\check{\boldsymbol{F}}\check{\boldsymbol{F}}}\mathscr{W}_{\text{dev}} = \partial_{\check{\boldsymbol{F}}}\boldsymbol{P}_{\text{dev}}$.

At this point, we emphasise that the decoupled energy representation in Eq. (3.122) is not a mathematical consequence from the deformation decomposition, but rather is a constitutive *assumption*. It can be useful when dealing with moderate volumetric deformations or incompressible materials, however, Penn [369] and Ehlers & Eipper [108] remarked that the additive energy decoupling is inappropriate and may deliver unphysical results when large volumetric deformations occur. A further weakness of the energy decoupling can be shown by taking a deformation gradient $\boldsymbol{F} = \lambda\boldsymbol{I}$, which depicts a pure volume dilatation. The non-volumetric deformation gradient then reads $\check{\boldsymbol{F}} = J^{-1/3}\lambda\boldsymbol{I} = \boldsymbol{I}$, since $J = \lambda^3$. Consequently, the associated deviatoric energy and stress parts vanish if they properly fulfil the normalisation conditions from Section 3.6.1, hence, $\mathscr{W}_{\text{dev}} = 0$ and $\boldsymbol{P}_{\text{dev}} = \boldsymbol{0}$. The remaining volumetric stress $\boldsymbol{P}_{\text{vol}}$ (or $\boldsymbol{\sigma}_{\text{vol}}$), however, represents a hydrostatic stress state and is thus isotropic, regardless of the symmetry conditions of the material. This means that pure volume dilatations induce an isotropic state of stress even in anisotropic materials, which appears to be a very restrictive consequence of the deviatoric-volumetric energy decoupling. In this connection, it is interesting to look at the implications of the energy decoupling (3.122) for transversely isotropic materials based on the invariant set $\mathscr{I}^I_{\text{ti}}$. The dependence of the deviatoric energy $\mathscr{W}_{\text{dev}}$ on the deviatoric deformation $\check{\boldsymbol{F}}$ then suggests to formulate isochoric versions of the invariants I_1, I_2, J_4, and J_5, which are based on the isochoric right Cauchy–Green tensor $\check{\boldsymbol{C}} = J^{-2/3}\boldsymbol{C}$:

$$\check{I}_1 = J^{-2/3}I_1\,,\quad \check{I}_2 = J^{-4/3}I_2\,,\quad \check{J}_4 = J^{-2/3}J_4\,,\quad \check{J}_5 = J^{-4/3}J_5\,. \tag{3.131}$$

For the above mentioned purely volumetric deformation $\boldsymbol{F} = \lambda\boldsymbol{I}$ all of these isochoric invariants remain constant, see, for example, $\check{J}_4 = J^{-2/3}J_4 = J^{-2/3}\,\text{tr}[\lambda^2\boldsymbol{I}\boldsymbol{M}] = 1$. Since the anisotropic invariants $\check{J}_4$ and $\check{J}_5$ do not get activated by the volumetric deformation, the resulting material behaviour becomes isotropic. Based on these observations and some other arguments, Sansour [417] and Helfenstein et al. [197] suggested that the energy function of transversely isotropic materials subject to some deviatoric-volumetric energy should not be dependent on the isochoric versions $\check{J}_4$ and $\check{J}_5$, but on J_4 and J_5 based on the complete deformation $\boldsymbol{F}$.

3.7.3 Connection to the infinitesimal theory

So far, the considerations in this work dealt with the general continuum-mechanical theory and hyperelastic framework for large deformations and large strains. Now, in addition to the already outlined constitutive principles and physical requirements in this chapter, a meaningful large-strain material description has to fulfil some linearisation conditions, which means that it has to recover results from the well-founded small-strain theory of linear elasticity. Thus, this sections aims to bring the large-strain theory into context with the infinitesimal theory of small-strain continuum mechanics. A comprehensive review on geometrical linearisation is not the scope of this section and we refer to the textbooks of Ogden [362] and Haupt [189], amongst others, for further explanations.

Small-strain continuum mechanics The starting point for the investigation of small-strain continuum mechanics is the assumption that the deformation gradient describing an actual configuration at time $t > t_0$ does not differ much from the initial deformation gradient in the reference configuration at t_0, which means that $\boldsymbol{F} \approx \boldsymbol{F}|_{t=t_0} = \boldsymbol{I}$. In order to obtain a *linearised strain-energy* $\mathscr{W}_{\text{lin}}$, it is straightforward to perform a *Taylor expansion* of the strain-energy $\mathscr{W}(\boldsymbol{F})$ around $\boldsymbol{F} = \boldsymbol{I}$. Since we aim to obtain a quadratic elastic potential, a second-order Taylor expansion is applied and we define the linearised energy as $\mathscr{W}_{\text{lin}} := \mathcal{T}_2\{\mathscr{W}(\boldsymbol{F}), \boldsymbol{I}\}$, where $\mathcal{T}_n\{f(x), x_0\}$ denotes the n-th-order Taylor expansion of $f(x)$ around x_0. We obtain the expression

$$\mathscr{W}_{\text{lin}}(\boldsymbol{F}) = \mathscr{W}(\boldsymbol{F})\big|_{\boldsymbol{F}=\boldsymbol{I}} + \partial_{\boldsymbol{F}}\mathscr{W}(\boldsymbol{F})\big|_{\boldsymbol{F}=\boldsymbol{I}} \cdot (\boldsymbol{F}-\boldsymbol{I}) + \tfrac{1}{2}(\boldsymbol{F}-\boldsymbol{I}) \cdot \partial^2_{\boldsymbol{F}\boldsymbol{F}}\mathscr{W}(\boldsymbol{F})\big|_{\boldsymbol{F}=\boldsymbol{I}}(\boldsymbol{F}-\boldsymbol{I})\,. \tag{3.132}$$

Of course, we identify the first Piola–Kirchhoff stress tensor $\boldsymbol{P} = \partial_{\boldsymbol{F}}\mathscr{W}$ and the nominal elasticity tensor $\mathbb{L} = \partial^2_{\boldsymbol{F}\boldsymbol{F}}\mathscr{W}$ for unconstrained materials, whereas these tensors become the respective extra quantities for constrained materials. In either case, the first two terms in Eq. (3.132) vanish in the reference configuration for properly normalised materials, such that (3.132) directly simplifies by means of $\mathscr{W}(\boldsymbol{F})|_{\boldsymbol{F}=\boldsymbol{I}} = 0$ and $\partial_{\boldsymbol{F}}\mathscr{W}(\boldsymbol{F})|_{\boldsymbol{F}=\boldsymbol{I}} = \boldsymbol{0}$. Further, we identify $\mathbb{L}(\boldsymbol{F})|_{\boldsymbol{F}=\boldsymbol{I}} =: \mathbb{L}_{\text{lin}}$ as the linearised elasticity tensor. Obviously, $\mathbb{L}_{\text{lin}}$ is independent of the deformation and thus depicts a constant fourth-order tensor. Moreover, the linearised elasticity tensor is major- and minor symmetric, like the material elasticity tensor $\mathbb{C}$. This means that $\mathbb{L}_{\text{lin}}$ has at most 21 independent coefficients, see also Appendix A.7.2. In order to specify the term $\boldsymbol{F}-\boldsymbol{I}$, we recall the definition of the displacement vector $\boldsymbol{u} = \boldsymbol{x} - \boldsymbol{X}$ and compute its gradient with respect to the reference configuration, giving $\text{Grad}[\boldsymbol{u}] = \text{Grad}[\boldsymbol{x}] - \text{Grad}[\boldsymbol{X}] = \boldsymbol{F} - \boldsymbol{I}$. Hence, we see that Eq. (3.132) contains the *displacement gradient* $\boldsymbol{H} := \text{Grad}[\boldsymbol{u}] = \boldsymbol{F} - \boldsymbol{I}$. This second-order tensor is the key quantity in the process of geometrical linearisation, since the assumption $\boldsymbol{F} \approx \boldsymbol{I}$ can subsequently be formulated as $\|\boldsymbol{H}\| = \delta \ll 1$. Doing so, other quantities may be expressed in terms of $\boldsymbol{H}$ and δ which allows for an asymptotic analysis by omitting all terms of order δ^2 and higher. In this spirit, a further prominent characteristic of the displacement gradient appears when we split it into a symmetric part $\text{sym}[\boldsymbol{H}] = (\boldsymbol{H} + \boldsymbol{H}^T)/2$ and a skew-symmetric part $\text{skw}[\boldsymbol{H}] = (\boldsymbol{H} - \boldsymbol{H}^T)/2$, such that $\boldsymbol{H} = \text{sym}[\boldsymbol{H}] + \text{skw}[\boldsymbol{H}]$. When $\|\boldsymbol{H}\| \ll 1$, those two parts can be identified as the *linearised strain tensor* $\boldsymbol{\varepsilon} := \text{sym}[\boldsymbol{H}]$ and the *linearised rotation tensor* $\boldsymbol{\omega} := \text{skw}[\boldsymbol{H}]$, see, for example, Haupt [189], and we obtain,

$$\boldsymbol{H} = \boldsymbol{\varepsilon} + \boldsymbol{\omega} \quad \text{with} \quad \boldsymbol{\varepsilon} = \boldsymbol{\varepsilon}^T \quad \text{and} \quad \boldsymbol{\omega} = -\boldsymbol{\omega}^T\,. \tag{3.133}$$

Substituting these findings into the linearised energy in Eq. (3.132) and investigating the resulting expression $(\boldsymbol{\varepsilon} + \boldsymbol{\omega}) \cdot \mathbb{L}_{\text{lin}}(\boldsymbol{\varepsilon} + \boldsymbol{\omega})$, we observe that the rotation tensor $\boldsymbol{\omega}$ does not contribute to the energy because of the symmetry properties of $\mathbb{L}_{\text{lin}}$ and the skew-symmetry of $\boldsymbol{\omega}$. Finally, we obtain the well-known expressions

$$\mathscr{W}_{\text{lin}}(\boldsymbol{\varepsilon}, \boldsymbol{\Xi}) = \tfrac{1}{2}\boldsymbol{\varepsilon} \cdot \mathbb{L}_{\text{lin}}(\boldsymbol{\Xi})\boldsymbol{\varepsilon} \quad \text{and} \quad \boldsymbol{\sigma}_{\text{lin}}(\boldsymbol{\varepsilon}, \boldsymbol{\Xi}) = \partial_{\boldsymbol{\varepsilon}}\mathscr{W}_{\text{lin}} = \mathbb{L}_{\text{lin}}(\boldsymbol{\Xi})\boldsymbol{\varepsilon} \tag{3.134}$$

for the linearised energy $\mathscr{W}_{\text{lin}}$ and the linearised stress $\boldsymbol{\sigma}_{\text{lin}}$ by using the derivation rules (A.64) and (A.68). Moreover, as we consider anisotropic materials, the linear energy is a function of the strain tensor $\boldsymbol{\varepsilon}$ and possibly a set of structural tensors, denoted by $\boldsymbol{\Xi}$ from Eq. (3.66), which is a consequence of the general anisotropy of the elasticity tensor $\mathbb{L}_{\text{lin}}(\boldsymbol{\Xi})$. Before proceeding, we want to recapitulate the implications of the previous results. The linearised strain-energy in Eq. (3.134) was derived by considering the general

nonlinear energy $\mathscr{W}$ at small strains around $\boldsymbol{F} \approx \boldsymbol{I}$ and $\mathscr{W}_{\text{lin}}$ was found to be identical to the formulations of classical linear elasticity. Therefore, one can take a general nonlinear strain-energy function, compute its elasticity tensor $\mathbb{L} = \partial^2_{\boldsymbol{F}\boldsymbol{F}}\mathscr{W}$, evaluate it for the undeformed state and compare the resulting linearised elasticity tensor $\mathbb{L}_{\text{lin}}$ with elasticity tensors from the theory of small-strain continuum mechanics. Doing so, one obtains a direct connection between the nonlinear large-strain formulation and the small-strain theory. Subsequently, one can formulate conditions for the nonlinear strain-energy, such that it linearises properly in the small-strain regime. In this sense, this procedure guarantees the *compatibility* between large-strain and small-strain formulations.

Representation of linear elasticity tensors Here, we want to provide representations of the linear elasticity tensor $\mathbb{L}_{\text{lin}}$ for the two special cases of isotropy and transverse isotropy. For the isotropic case, it is well known that two material parameters are sufficient to fully characterise a linear-elastic materials. We choose the first Lamé constant Λ and the second Lamé constant (the shear modulus) μ, which results in the following representation of the elasticity tensor $\mathbb{L}^{\text{iso}}_{\text{lin}}$ and the associated strain-energy:

$$\mathbb{L}^{\text{iso}}_{\text{lin}} = 2\mu\,\mathbb{I}_{\text{sym}} + \Lambda\,\boldsymbol{I}\otimes\boldsymbol{I} \quad \text{and} \quad \mathscr{W}_{\text{lin}}(\boldsymbol{\varepsilon}) = \mu\,\text{tr}[\boldsymbol{\varepsilon}^2] + \tfrac{1}{2}\Lambda\,\text{tr}[\boldsymbol{\varepsilon}]^2\,. \tag{3.135}$$

Therein, the energy is obtained by inserting the tensor $\mathbb{L}^{\text{iso}}_{\text{lin}}$ into Eq. $(3.134)_1$. The relations in Eqs (3.135) describe an isotropic linear-elastic *Hooke material*, which hints that it is the three-dimensional extension of a linear-elastic Hookean spring. The two scalars $\text{tr}[\boldsymbol{\varepsilon}]$ and $\text{tr}[\boldsymbol{\varepsilon}^2]$ in $\mathscr{W}_{\text{lin}}$ denote isotropic small-strain invariants and follow directly from the two tensor bases $\boldsymbol{I}\otimes\boldsymbol{I}$ and $\mathbb{I}_{\text{sym}}$ of $\mathbb{L}^{\text{iso}}_{\text{lin}}$ by the operations $\boldsymbol{\varepsilon}\cdot(\boldsymbol{I}\otimes\boldsymbol{I})\boldsymbol{\varepsilon} = \boldsymbol{\varepsilon}\cdot\mathbb{I}_{\text{tr}}\boldsymbol{\varepsilon} = \boldsymbol{\varepsilon}\cdot\text{tr}[\boldsymbol{\varepsilon}]\boldsymbol{I} = \text{tr}[\boldsymbol{\varepsilon}]^2$ and $\boldsymbol{\varepsilon}\cdot\mathbb{I}_{\text{sym}}\boldsymbol{\varepsilon} = \boldsymbol{\varepsilon}\cdot\boldsymbol{\varepsilon} = \text{tr}[\boldsymbol{\varepsilon}^2]$. Note that it makes no difference for the small-strain invariant $\text{tr}[\boldsymbol{\varepsilon}^2]$ and the energy $\mathscr{W}_{\text{lin}}$ when the symmetrising map $\mathbb{I}_{\text{sym}}$ is replaced by the identical map $\mathbb{I}$, because of the symmetry of $\boldsymbol{\varepsilon}$. However, it is necessary to keep the more general notation with $\mathbb{I}_{\text{sym}} = (\mathbb{I}+\mathbb{I}_T)/2$ in order to be able to compare it to the linearised results from large-strain formulations. Further, as expected, the isotropic small-strain elasticity tensor $\mathbb{L}^{\text{iso}}_{\text{lin}}$ is not dependent on any structural tensor and can be written as a linear combination of the fundamental fourth-order tensors $\mathbb{I}_{\text{sym}}$ and $\mathbb{I}_{\text{tr}}$. In contrast, the formulation of anisotropic linear-elastic elasticity tensors demands for an enriched tensor basis, as the elasticity tensor $\mathbb{L}_{\text{lin}}(\boldsymbol{\Xi})$ then becomes a function of a certain set $\boldsymbol{\Xi}$ of structural tensors, see Eq. (3.134). For the special case of transverse isotropy, Walpole [499, 500] outlined that the elasticity tensor can be represented as a linear combination of a set of six elementary fourth-order tensors $\mathbb{E}^{[\alpha]}$, $\alpha = 1,2,3,4,5,6$. The six elementary tensors contain different combinations of the transversely isotropic structural tensors $\boldsymbol{M}$ and $\boldsymbol{D}$, which were introduced in Eqs (3.82) and (3.88), respectively. The definitions and some alternative representations of the six elementary tensors are provided in Appendix A.7.3. Subsequently, the transversely isotropic small-strain elasticity tensor $\mathbb{L}^{\text{ti}}_{\text{lin}}(\boldsymbol{M})$ becomes a function of the structural tensor $\boldsymbol{M}$, since $\boldsymbol{D} = \boldsymbol{I} - \boldsymbol{M}$ is itself dependent on $\boldsymbol{M}$. Following Walpole [500], we obtain the formulation

$$\mathbb{L}^{\text{ti}}_{\text{lin}}(\boldsymbol{M}) = 2\kappa_{\text{t}}\,\mathbb{E}^{[1]} + n\,\mathbb{E}^{[2]} + 2\mu_{\text{t}}\,\mathbb{E}^{[3]} + 2\mu_{\ell}\,\mathbb{E}^{[4]} + l\,(\mathbb{E}^{[5]} + \mathbb{E}^{[6]})\,. \tag{3.136}$$

Hence, a linear-elastic transversely isotropic material is in general described by five material parameters. In Eq. (3.136), those parameters are the transverse (or plane-strain) bulk modulus κ_{t}, the transverse (in-plane) shear modulus μ_{t}, and the longitudinal (out-of-plane)

shear modulus μ_ℓ. Moreover, l is related to the longitudinal Poisson's ratio $\nu_\ell = l/(2\kappa_\mathrm{t})$ whereas n is connected to the longitudinal Young's modulus $E_\ell = n - l^2/\kappa_\mathrm{t}$. A compact notation for expression (3.136) can be given by $\mathbb{L}^{\mathrm{ti}}_{\mathrm{lin}} = (2\kappa_\mathrm{t}, n, 2\mu_\mathrm{t}, 2\mu_\ell, l, l)$, which simply lists the scalar pre-factors of the six elementary tensors, see WALPOLE [500]. This representation can be referred to as *Walpole's notation*. However, note that a slightly different notation $\mathbb{L}^{\mathrm{ti}}_{\mathrm{lin}} = (2\kappa_\mathrm{t}, l, l, n, 2\mu_\mathrm{t}, 2\mu_\ell)$ was used in an earlier work, see WALPOLE [499], and one may find both forms in the literature. Furthermore, we remark that the choice of the five material parameters is by no means unique and one may choose a different set, accompanied with a different notation for the elasticity tensor. For instance, SPENCER [457] proposed a parameter set $\{\Lambda, \mu_\ell, \mu_\mathrm{t}, \alpha, \beta\}$, which results in the elasticity tensor

$$\mathbb{L}^{\mathrm{ti}}_{\mathrm{lin}}(\boldsymbol{M}) = 2\mu_\mathrm{t}\,\mathbb{E}^{[1]} + n'\,\mathbb{E}^{[2]} + 2\mu_\mathrm{t}\,\mathbb{E}^{[3]} + 2\mu_\ell\,\mathbb{E}^{[4]} + \alpha\,(\mathbb{E}^{[5]} + \mathbb{E}^{[6]}) + \Lambda\,\boldsymbol{I}\otimes\boldsymbol{I}\,, \tag{3.137}$$

where $n' = 4\mu_\ell - 2\mu_\mathrm{t} + 2\alpha + \beta$, see also SCHRÖDER [420]. The nice feature of this representation is that the parameters α and β are directly linked to the anisotropic behaviour and become zero for isotropy. Then, it is straightforward to observe that $\mathbb{L}^{\mathrm{ti}}_{\mathrm{lin}}$ from Eq. (3.137) simplifies to the isotropic form given in Eq. $(3.135)_1$ by employing Eq. (A.89). If we further confine the attention to incompressible, transversely isotropic materials, a spectral decomposition of the elasticity tensor leads to the representation

$$\mathbb{L}^{\mathrm{ti}}_{\mathrm{lin}}(\boldsymbol{M}) = 2\mu_\mathrm{a}\,\mathbb{E}^{[\mathrm{a}]} + 2\mu_\mathrm{t}\,\mathbb{E}^{[3]} + 2\mu_\ell\,\mathbb{E}^{[4]} + 3\kappa_\infty\mathbb{J}\,, \tag{3.138}$$

as shown by PONTE CASTAÑEDA [378] and FEDERICO ET AL. [126]. Therein, $\mathbb{E}^{[\mathrm{a}]}$ is an axisymmetric shear projection tensor and $\mathbb{J}$ is a projection tensor, which are both defined as combinations of $\mathbb{E}^{[1]}$, $\mathbb{E}^{[2]}$, $\mathbb{E}^{[5]}$, and $\mathbb{E}^{[6]}$, see Eqs (A.91) and $(A.92)_1$, respectively. Further, μ_a is an axisymmetric shear modulus and the bulk modulus κ_∞ tends to infinity because of the incompressibility. Thus, the elasticity tensor $\mathbb{L}^{\mathrm{ti}}_{\mathrm{lin}}$ in the case of incompressibility becomes a function of three material parameters. For later use, it proves useful to rearrange Eq. (3.138) and to replace the bulk modulus by the first Lamé constant $\Lambda_\infty = \kappa_\infty - 2\mu_\mathrm{a}/3$, giving

$$\mathbb{L}^{\mathrm{ti}}_{\mathrm{lin}}(\boldsymbol{M}) = 2\mu_\mathrm{a}\,(\mathbb{E}^{[1]} + \mathbb{E}^{[2]}) + 2\mu_\mathrm{t}\,\mathbb{E}^{[3]} + 2\mu_\ell\,\mathbb{E}^{[4]} + \Lambda_\infty\,\boldsymbol{I}\otimes\boldsymbol{I}\,, \tag{3.139}$$

where now the Lamé constant Λ_∞ tends to infinity. Finally, note that the linearised energy $\mathscr{W}_{\mathrm{lin}}(\boldsymbol{\varepsilon}, \boldsymbol{M})$ for transversely isotropic materials is derived by inserting one of the above formulations for $\mathbb{L}^{\mathrm{ti}}_{\mathrm{lin}}(\boldsymbol{M})$ into Eq. $(3.134)_1$. This will not be spelled out here in detail, but we remark that exploiting the respective scalar products $\boldsymbol{\varepsilon}\cdot\mathbb{E}^{[\alpha]}\boldsymbol{\varepsilon}$ results in a formulation of the energy in terms of the four transversely isotropic small-strain invariants $\mathrm{tr}[\boldsymbol{\varepsilon}]$, $\mathrm{tr}[\boldsymbol{\varepsilon}^2]$, $\mathrm{tr}[\boldsymbol{\varepsilon}\boldsymbol{M}]$, and $\mathrm{tr}[\boldsymbol{\varepsilon}^2\boldsymbol{M}]$, see SCHRÖDER [420].

3.8 Analytical formulations for strain-energy functions

In this section, we bring together the investigations on material theory made so far and present explicit formulations for strain-energy functions in line with the formulated constitutive requirements. Doing so, we recall that frame-indifference requirements and the principles of material symmetry are satisfied if the strain energy $\mathscr{W}$ is formulated in terms of appropriate scalar invariants, as explained in Section 3.5. Further important requirements were outlined in Section 3.6, such as a proper normalisation in the reference state,

physically meaningful growth conditions, and the fulfilment of certain weak convexity conditions. Moreover, the large-strain formulations should be consistent with the well-founded small-strain theory. Here, we will focus on a few analytical strain-energy functions, since the countless number of available constitutive models in the literature makes it impossible to give a complete overview. For more examples and a broader overview, the interested reader is referred to, for example, the book of Holzapfel et al. [222] as well as to the articles of Ogden [361], Beatty [27] and Boyce & Arruda [58], which are concerned with rubber-like materials, and the impressive review of Chagnon et al. [74] that deals with constitutive models for soft biological tissues. Here, it proves useful to start with the introduction of an additive energy split in the following.

3.8.1 A distortional-dilatational energy split

The strain energy $\mathscr{W}(\boldsymbol{F})$ of a hyperelastic material may be additively split as

$$\mathscr{W}(\boldsymbol{F}) = \mathscr{W}_{\mu}(\boldsymbol{F}) + \mathscr{W}_{\Lambda}(J)\,. \tag{3.140}$$

We refer to this as *distortional-dilatational energy split*. The key idea of such a formulation is the division of the total energy $\mathscr{W}$ into a contribution $\mathscr{W}_{\mu}$ which is mostly dependent on the stiffness of the material against distortional deformations and a contribution $\mathscr{W}_{\Lambda}$ which is solely dependent on the stiffness of the material against dilatational (volumetric) deformations. Doing so, it makes sense that the dilatational part $\mathscr{W}_{\Lambda}$ is a function of the Jacobian J. The designation of the subscripts μ and Λ is inspired of the two Lamé parameters from linear elasticity, where Λ quantifies the stiffness against dilatational deformations. This becomes clearer in a few moments. We highlight that the split in Eq. (3.140) is very different to the one proposed in Section 3.7.2. While for the latter formulation, the deviatoric energy part $\mathscr{W}_{\text{dev}}$ is only dependent on the isochoric deformation $\breve{\boldsymbol{F}}$, the distortional part $\mathscr{W}_{\mu}(\boldsymbol{F})$ still depends on the full deformation $\boldsymbol{F}$. Of course, the nomenclature of these two additive splits is in some sense arbitrary, since the usage of the terms deviatoric-volumetric and distortional-dilatational could be motivated for both splits. In this work, we stick to the introduced naming in order to distinguish between the two decompositions. We further specify the two energy contributions $\mathscr{W}_{\mu}$ and $\mathscr{W}_{\Lambda}$ by demanding that both of them satisfy the normalisation and linearisation conditions *separately*. For the distortional part, the normalisation conditions become

$$\mathscr{W}_{\mu[\boldsymbol{I}]} = 0 \quad \text{and} \quad \partial_{\boldsymbol{F}}\mathscr{W}_{\mu[\boldsymbol{I}]} = \boldsymbol{0}\,. \tag{3.141}$$

Therein and henceforth, the subscript $[\boldsymbol{I}]$ is an abbreviation for $(\cdot)|_{\boldsymbol{F}=\boldsymbol{I}}$ and indicates the evaluation of the quantity $(\cdot)$ in the reference state ($\boldsymbol{F} = \boldsymbol{I}$). For the dilatational part, we can specify the derivative

$$\partial_{\boldsymbol{F}}\mathscr{W}_{\Lambda}(J) = J\partial_J\mathscr{W}_{\Lambda}\boldsymbol{F}^{-T}\,, \tag{3.142}$$

which is similar to Eq. $(3.124)_2$. Evaluating formulation (3.142) for the reference state, with $\boldsymbol{F}_{[\boldsymbol{I}]}^{-T} = \boldsymbol{I}$ and $J_{[\boldsymbol{I}]} = \det[\boldsymbol{I}] = 1$, leads us to the normalisation conditions

$$\mathscr{W}_{\Lambda[\boldsymbol{I}]} = 0 \quad \text{and} \quad \partial_J\mathscr{W}_{\Lambda[\boldsymbol{I}]} = 0\,. \tag{3.143}$$

In order to exploit the linearisation of the dilatational energy part, we compute the second derivative with respect to $\boldsymbol{F}$, reading

$$\partial^2_{\boldsymbol{F}\boldsymbol{F}}\mathscr{W}_{\Lambda} = (J\partial_J\mathscr{W}_{\Lambda} + J^2\partial^2_{J^2}\mathscr{W}_{\Lambda})\boldsymbol{F}^{-T}\otimes\boldsymbol{F}^{-T} - J\partial_J\mathscr{W}_{\Lambda}(\boldsymbol{F}^{-T}\otimes\boldsymbol{F}^{-T})^{T_{24}}\,. \tag{3.144}$$

Subsequently, this fourth-order tensor is evaluated in the reference state and use is made of the normalisation condition $(3.143)_2$, which leads to

$$\partial^2_{\boldsymbol{F}\boldsymbol{F}} \mathscr{W}_{\Lambda[\boldsymbol{I}]} = \partial^2_{J^2} \mathscr{W}_{\Lambda[\boldsymbol{I}]} \boldsymbol{I} \otimes \boldsymbol{I} \quad \rightarrow \quad \partial^2_{J^2} \mathscr{W}_{\Lambda[\boldsymbol{I}]} = \Lambda \,. \tag{3.145}$$

Therein, the formulation of the normalisation condition $(3.145)_2$ is motivated by a comparison of $\partial^2_{\boldsymbol{F}\boldsymbol{F}} \mathscr{W}_{\Lambda[\boldsymbol{I}]}$ with the small-strain elasticity tensors from Eqs (3.135) and (3.137), where the first Lamé constant Λ is the pre-factor associated with the tensor base $\boldsymbol{I} \otimes \boldsymbol{I}$. Note that choosing $\Lambda > 0$ would directly guarantee the strict convexity of the dilatational energy part $\mathscr{W}_\Lambda$ in the sense of condition $(3.116)_3$. However, demanding for the (poly)convexity with respect to the Jacobian J for each of the two energy terms, $\mathscr{W}_\mu$ and $\mathscr{W}_\Lambda$, is a stronger condition than Eq. $(3.116)_3$ and there is no need to do that here.

3.8.2 Linearisation conditions for $\mathscr{I}^I_{\mathrm{ti}}$-dependent strain energies

Based on the preceding explanations on the small-strain theory in Section 3.7.3 and the energy split in Section 3.8.1, we will now formulate the *linearisation conditions* for the distortional part of transversely-isotropic strain energies that are defined in terms of the invariant set $\mathscr{I}^I_{\mathrm{ti}}$. The resulting formulations will be especially relevant in the process of showing the consistent linearisation of the nonlinear homogenisation methods in Chapter 5. Further explanations and explicit examples for $\mathscr{I}^I_{\mathrm{ti}}$-dependent energies follow in the next section, whereas the considerations here are made in a generic sense in order to provide the necessary basics. The values of invariant set $\mathscr{I}^I_{\mathrm{ti}}$ for the referential state, described by $\boldsymbol{F} = \boldsymbol{C} = \boldsymbol{I}$, are obtained from the definitions in Eqs (3.73), (3.85) and $\mathrm{tr}[\boldsymbol{I}] = 3$, $\det[\boldsymbol{I}] = 1$, and $\mathrm{tr}[\boldsymbol{M}] = 1$, giving

$$\boldsymbol{F} = \boldsymbol{I} \quad \rightarrow \quad I_1 = I_2 = 3 \,, \quad J = J_4 = J_5 = 1 \,. \tag{3.146}$$

For a transversely isotropic material with a distortional energy of the form $\mathscr{W}_\mu(I_1, I_2, J, J_4, J_5)$, the associated distortional part of the first Piola–Kirchhoff (extra) stress tensor $\boldsymbol{P}_\mu = \partial_{\boldsymbol{F}} \mathscr{W}_\mu$ and the distortional part of the (extra) elasticity tensor $\mathbb{L}_\mu = \partial^2_{\boldsymbol{F}\boldsymbol{F}} \mathscr{W}_\mu$ are obtained by straightforward derivations and a consequent use of the chain rule. In particular, carrying out the derivations for invariant-based strain energies leads to a typical structure consisting of scalar derivatives of the energy with respect to the invariants and the associated *tensor generators*, which are derivatives of the invariants with respect to $\boldsymbol{F}$. The tensor generators are provided in Eq. (A.75). Subsequently, the first derivative of $\mathscr{W}_\mu(I_1, I_2, J, J_4, J_5)$ with respect to $\boldsymbol{F}$ is given by

$$\begin{aligned} \boldsymbol{P}_\mu = \partial_{\boldsymbol{F}} \mathscr{W}_\mu = {} & 2\, \partial_{I_1} \mathscr{W}_\mu \, \boldsymbol{F} + 2\, \partial_{I_2} \mathscr{W}_\mu \, \boldsymbol{F}(I_1 \boldsymbol{I} - \boldsymbol{C}) + J \partial_J \mathscr{W}_\mu \, \boldsymbol{F}^{-T} \\ & + 2\, \partial_{J_4} \mathscr{W}_\mu \, \boldsymbol{F}\boldsymbol{M} + 2\, \partial_{J_5} \mathscr{W}_\mu \, (\boldsymbol{F}\boldsymbol{C}\boldsymbol{M} + \boldsymbol{F}\boldsymbol{M}\boldsymbol{C}) \,. \end{aligned} \tag{3.147}$$

For the sake of brevity, the details on this derivation as well as the computation of the elasticity tensor are moved to Appendix A.7.1. Since the linearised results in Eq. (3.134) rely on a properly normalised material behaviour, the first step is to provide appropriate *normalisation conditions* which guarantee an energy- and stress-free reference state. The normalisation condition for the energy reads

$$\mathscr{W}_{\mu[\boldsymbol{I}]} = 0 \,. \tag{3.148}$$

Further, exploiting $\partial_{\boldsymbol{F}} \mathscr{W}_{\mu[\boldsymbol{I}]}$ yields an expression with two tensor bases $\boldsymbol{I}$ and $\boldsymbol{M}$. Their respective scalar pre-factors have to be zero in order to guarantee $\partial_{\boldsymbol{F}} \mathscr{W}_{\mu[\boldsymbol{I}]} = \boldsymbol{0}$. This leads to the additional normalisation conditions

$$2\,\partial_{I_1} \mathscr{W}_{\mu[\boldsymbol{I}]} + 4\,\partial_{I_2} \mathscr{W}_{\mu[\boldsymbol{I}]} + \partial_J \mathscr{W}_{\mu[\boldsymbol{I}]} = 0 \quad \text{and} \quad \partial_{J_4} \mathscr{W}_{\mu[\boldsymbol{I}]} + 2\,\partial_{J_5} \mathscr{W}_{\mu[\boldsymbol{I}]} = 0\,. \tag{3.149}$$

In order to obtain the linearisation conditions, the second derivative $\partial^2_{\boldsymbol{F}\boldsymbol{F}} \mathscr{W}_{\mu}$ has to be evaluated in the reference configuration and subsequently compared with the small-strain counterpart $\mathbb{L}^{\text{ti}}_{\text{lin}}$. It proves useful to employ for the comparison the formulation for $\mathbb{L}^{\text{ti}}_{\text{lin}}$ given in Eq. (3.137), because it directly separates the Λ-term from the other terms, which is in line with the distortional-dilatational energy split. Exploiting the general elasticity tensor in Eq. (A.78) for $\boldsymbol{F} = \boldsymbol{I}$ leads to a formulation that contains ten tensor bases. These are $\boldsymbol{I} \otimes \boldsymbol{I}$, $\boldsymbol{I} \otimes \boldsymbol{M}$, $\boldsymbol{M} \otimes \boldsymbol{I}$ and their respective transpositions T_{23} and T_{24} as well as the totally symmetric tensor $\boldsymbol{M} \otimes \boldsymbol{M}$. A comparison of the scalar pre-factors (consisting of first and second derivatives of $\mathscr{W}_{\mu}$ with respect to the invariants) associated with the ten tensor bases with the respective pre-factors in Eq. (3.137) leads to the linearisation conditions

$$\begin{aligned}
-\mu_{\text{t}} &= 2\,\partial_{I_2} \mathscr{W}_{\mu[\boldsymbol{I}]} + \partial_J \mathscr{W}_{\mu[\boldsymbol{I}]}\,, \\
\mu_{\ell} &= 2\,\partial_{I_1} \mathscr{W}_{\mu[\boldsymbol{I}]} + 2\,\partial_{I_2} \mathscr{W}_{\mu[\boldsymbol{I}]} + 2\,\partial_{J_5} \mathscr{W}_{\mu[\boldsymbol{I}]}\,, \\
2\mu_{\text{t}} &= 4\,\partial^2_{I_1^2} \mathscr{W}_{\mu[\boldsymbol{I}]} + 16\,\partial^2_{I_1 I_2} \mathscr{W}_{\mu[\boldsymbol{I}]} + 16\,\partial^2_{I_2^2} \mathscr{W}_{\mu[\boldsymbol{I}]} + 4\,\partial^2_{I_1 J} \mathscr{W}_{\mu[\boldsymbol{I}]} \\
&\quad + 8\,\partial^2_{I_2 J} \mathscr{W}_{\mu[\boldsymbol{I}]} + \partial^2_{J^2} \mathscr{W}_{\mu[\boldsymbol{I}]} - \partial_J \mathscr{W}_{\mu[\boldsymbol{I}]}\,, \\
\alpha &= 4\,\partial^2_{I_1 J_4} \mathscr{W}_{\mu[\boldsymbol{I}]} + 8\,\partial^2_{I_2 J_4} \mathscr{W}_{\mu[\boldsymbol{I}]} + 8\,\partial^2_{I_1 J_5} \mathscr{W}_{\mu[\boldsymbol{I}]} + 16\,\partial^2_{I_2 J_5} \mathscr{W}_{\mu[\boldsymbol{I}]} \\
&\quad + 2\,\partial^2_{J J_4} \mathscr{W}_{\mu[\boldsymbol{I}]} + 4\,\partial^2_{J J_5} \mathscr{W}_{\mu[\boldsymbol{I}]}\,, \\
\beta + 4\mu_{\ell} - 4\mu_{\text{t}} &= 4\,\partial^2_{J_4^2} \mathscr{W}_{\mu[\boldsymbol{I}]} + 16\,\partial^2_{J_4 J_5} \mathscr{W}_{\mu[\boldsymbol{I}]} + 16\,\partial^2_{J_5^2} \mathscr{W}_{\mu[\boldsymbol{I}]} + 8\,\partial_{J_5} \mathscr{W}_{\mu[\boldsymbol{I}]}\,.
\end{aligned} \tag{3.150}$$

A slightly different notation for these conditions was given by Merodio & Ogden [322]. If we confine the attention to incompressible materials, the corresponding linearisation conditions are obtained by a comparison of $\partial^2_{\boldsymbol{F}\boldsymbol{F}} \mathscr{W}_{\mu[\boldsymbol{I}]}$ with the incompressible small-strain elasticity tensor that is given in Eq. (3.139). This leads to

$$\begin{aligned}
-\mu_{\text{t}} &= 2\,\partial_{I_2} \mathscr{W}_{\mu[\boldsymbol{I}]} + \partial_J \mathscr{W}_{\mu[\boldsymbol{I}]}\,, \\
\mu_{\ell} &= 2\,\partial_{I_1} \mathscr{W}_{\mu[\boldsymbol{I}]} + 2\,\partial_{I_2} \mathscr{W}_{\mu[\boldsymbol{I}]} + 2\,\partial_{J_5} \mathscr{W}_{\mu[\boldsymbol{I}]}\,, \\
\mu_{\text{a}} + \mu_{\text{t}} &= 4\,\partial^2_{I_1^2} \mathscr{W}_{\mu[\boldsymbol{I}]} + 16\,\partial^2_{I_1 I_2} \mathscr{W}_{\mu[\boldsymbol{I}]} + 16\,\partial^2_{I_2^2} \mathscr{W}_{\mu[\boldsymbol{I}]} + 4\,\partial^2_{I_1 J} \mathscr{W}_{\mu[\boldsymbol{I}]} \\
&\quad + 8\,\partial^2_{I_2 J} \mathscr{W}_{\mu[\boldsymbol{I}]} + \partial^2_{J^2} \mathscr{W}_{\mu[\boldsymbol{I}]} - \partial_J \mathscr{W}_{\mu[\boldsymbol{I}]}\,, \\
\mu_{\text{t}} - \mu_{\text{a}} &= 4\,\partial^2_{I_1 J_4} \mathscr{W}_{\mu[\boldsymbol{I}]} + 8\,\partial^2_{I_2 J_4} \mathscr{W}_{\mu[\boldsymbol{I}]} + 8\,\partial^2_{I_1 J_5} \mathscr{W}_{\mu[\boldsymbol{I}]} + 16\,\partial^2_{I_2 J_5} \mathscr{W}_{\mu[\boldsymbol{I}]} \\
&\quad + 2\,\partial^2_{J J_4} \mathscr{W}_{\mu[\boldsymbol{I}]} + 4\,\partial^2_{J J_5} \mathscr{W}_{\mu[\boldsymbol{I}]}\,, \\
3\mu_{\text{a}} - 3\mu_{\text{t}} &= 4\,\partial^2_{J_4^2} \mathscr{W}_{\mu[\boldsymbol{I}]} + 16\,\partial^2_{J_4 J_5} \mathscr{W}_{\mu[\boldsymbol{I}]} + 16\,\partial^2_{J_5^2} \mathscr{W}_{\mu[\boldsymbol{I}]} + 8\,\partial_{J_5} \mathscr{W}_{\mu[\boldsymbol{I}]}\,.
\end{aligned} \tag{3.151}$$

At this point, we note that the distortional energy part is usually formulated such that the J-dependent contributions are decoupled from the rest. Hence, such energy functions follow a further additive split and can be written as

$$\mathscr{W}_{\mu}(I_1, I_2, J, J_4, J_5) = \mathscr{W}^{I}_{\mu}(I_1, I_2, J_4, J_5) + \mathscr{W}^{J}_{\mu}(J)\,. \tag{3.152}$$

Based on that, the normalisation conditions from Eq. (3.149) transform to

$$2\,\partial_{I_1} \mathscr{W}^{I}_{\mu[\boldsymbol{I}]} + 4\,\partial_{I_2} \mathscr{W}^{I}_{\mu[\boldsymbol{I}]} + \partial_J \mathscr{W}^{J}_{\mu[\boldsymbol{I}]} = 0 \quad \text{and} \quad \partial_{J_4} \mathscr{W}^{I}_{\mu[\boldsymbol{I}]} + 2\,\partial_{J_5} \mathscr{W}^{I}_{\mu[\boldsymbol{I}]} = 0\,. \tag{3.153}$$

Further, the decoupled form in Eq. (3.152) implies that the mixed second derivatives which involve J vanish, hence

$$\partial^2_{I_1 J}\mathscr{W}_\mu = \partial^2_{I_2 J}\mathscr{W}_\mu = \partial^2_{J J_4}\mathscr{W}_\mu = \partial^2_{J J_5}\mathscr{W}_\mu = 0\,. \tag{3.154}$$

These relations can be subsequently used to simplify the linearisation conditions in Eqs (3.150) and (3.151). Hence, the linearisation conditions (3.151) for incompressible materials transform to

$$\begin{aligned}
2\,\partial_{I_2}\mathscr{W}^I_{\mu[\boldsymbol{I}]} + \partial_J \mathscr{W}^J_{\mu[\boldsymbol{I}]} &= -\mu_{\mathrm{t}}\,,\\
2\,\partial_{I_1}\mathscr{W}^I_{\mu[\boldsymbol{I}]} + 2\,\partial_{I_2}\mathscr{W}^I_{\mu[\boldsymbol{I}]} + 2\,\partial_{J_5}\mathscr{W}^I_{\mu[\boldsymbol{I}]} &= \mu_\ell\,,\\
4\,\partial^2_{I_1^2}\mathscr{W}^I_{\mu[\boldsymbol{I}]} + 16\,\partial^2_{I_1 I_2}\mathscr{W}^I_{\mu[\boldsymbol{I}]} + 16\,\partial^2_{I_2^2}\mathscr{W}^I_{\mu[\boldsymbol{I}]} + \partial^2_{J^2}\mathscr{W}^J_{\mu[\boldsymbol{I}]} - \partial_J \mathscr{W}^J_{\mu[\boldsymbol{I}]} &= \mu_{\mathrm{a}} + \mu_{\mathrm{t}}\,,\\
4\,\partial^2_{I_1 J_4}\mathscr{W}^I_{\mu[\boldsymbol{I}]} + 8\,\partial^2_{I_2 J_4}\mathscr{W}^I_{\mu[\boldsymbol{I}]} + 8\,\partial^2_{I_1 J_5}\mathscr{W}^I_{\mu[\boldsymbol{I}]} + 16\,\partial^2_{I_2 J_5}\mathscr{W}^I_{\mu[\boldsymbol{I}]} &= \mu_{\mathrm{t}} - \mu_{\mathrm{a}}\,,\\
4\,\partial^2_{J_4^2}\mathscr{W}^I_{\mu[\boldsymbol{I}]} + 16\,\partial^2_{J_4 J_5}\mathscr{W}^I_{\mu[\boldsymbol{I}]} + 16\,\partial^2_{J_5^2}\mathscr{W}^I_{\mu[\boldsymbol{I}]} + 8\,\partial_{J_5}\mathscr{W}^I_{\mu[\boldsymbol{I}]} &= 3\mu_{\mathrm{a}} - 3\mu_{\mathrm{t}}\,.
\end{aligned} \tag{3.155}$$

3.8.3 Examples of strain-energy functions

Now, some examples for analytical strain-energy functions are presented. These functions are introduced here in a fully generic way and have to be able to describe the elastic energy at the material point in a phenomenological sense. Thus, the mathematical structure of the strain-energy function has to be such that it allows a proper *calibration* to experimental data. In contrast, the energy at a material point can also be described by considering effects and structures from smaller scales, which anticipates the ideas of Part II. Here, as a continuation of the preceding considerations, we focus on $\mathscr{I}^I_{\mathrm{ti}}$-based energies. However, it shall be remarked that there is a variety of alternative formulations, for instance, based on the invariant sets $\mathscr{I}^J_{\mathrm{ti}}$, see Criscione et al. [84], or the set of principal stretches $\mathscr{I}^\lambda_{\mathrm{iso}}$. The latter formulations for isotropic behaviour, given by $\mathscr{W}(\boldsymbol{F}) = \mathscr{W}(\lambda_{\boldsymbol{U}(1)}, \lambda_{\boldsymbol{U}(2)}, \lambda_{\boldsymbol{U}(3)})$, involve the important class of *Ogden-type materials*, see, for example, Ogden [361, 362], as well as formulations based on the *Valanis–Landel hypothesis* $\mathscr{W}(\boldsymbol{F}) = w(\lambda_{\boldsymbol{U}(1)}) + w(\lambda_{\boldsymbol{U}(2)}) + w(\lambda_{\boldsymbol{U}(3)})$ proposed by Valanis & Landel [491].

Expressions for the dilatational energy $\mathscr{W}_\Lambda$ The dilatational energy part $\mathscr{W}_\Lambda$ has to satisfy the normalisation conditions (3.143) and the linearisation condition $(3.145)_2$. A simple and useful formulation in line with those conditions is given by

$$\mathscr{W}_\Lambda(J) = \tfrac{1}{2}\Lambda(J-1)^2 \quad \text{with} \quad \partial_J \mathscr{W}_\Lambda = \Lambda(J-1) \quad \text{and} \quad \partial^2_{J^2}\mathscr{W}_\Lambda = \Lambda\,. \tag{3.156}$$

This formulation assumes a deformation-independent constant volumetric stiffness, which results in a classical quadratic potential. Exploiting the limit values $\lim_{J\to 0^+}\mathscr{W}_\Lambda = \Lambda/2$ and $\lim_{J\to\infty}\mathscr{W}_\Lambda = \infty$, we observe that this energy generally fulfils the growth conditions (3.109) for $J \to \infty$. However, for $J \to 0^+$, an infinite limit value of $\mathscr{W}_\Lambda$ is only obtained for $\Lambda \to \infty$, which essentially describes the case of incompressibility. Consequently, using a dilatational energy as given in (3.156) implies that the growth condition in the limit as $J \to 0^+$ for compressible materials has to be treated by the J-dependence of the distortional part. An alternative formulation which directly satisfies the growth conditions was for example proposed by Miehe [328] and is given by

$$\mathscr{W}_\Lambda(J) = \Lambda(J - \ln[J] - 1) \quad \text{with} \quad \partial_J \mathscr{W}_\Lambda = \Lambda\Big(1 - \frac{1}{J}\Big) \quad \text{and} \quad \partial^2_{J^2}\mathscr{W}_\Lambda = \frac{\Lambda}{J^2}\,. \tag{3.157}$$

Therein, the logarithmic term is a typical ingredient of energies with infinite growth as the compression tends to zero. More formulations for volumetric/dilatational energy contributions and their characteristics can be found in the very comprehensive work of Hartmann & Neff [180]. Herein, we will proceed with the dilatational energy as defined in Eq. (3.156).

Expressions for the distortional energy $\mathscr{W}_\mu$ For $\mathscr{I}^I_{\mathrm{ti}}$-dependent distortional energies, the associated normalisation and linearisation conditions are formulated in Section 3.8.2. If $\mathscr{W}_\mu$ can be represented according to the decoupled form given in Eq. (3.152), the usual procedure is to employ an energy $\mathscr{W}_\mu^I$ and to formulate the J-dependent part $\mathscr{W}_\mu^J$ according to $\mathscr{W}_\mu^I$ such that the normalisation and linearisation conditions are satisfied. Here, we want to show this procedure for the special case of isotropic I_1-J-dependent energy functions, $\mathscr{W}_\mu(I_1, J) = \mathscr{W}_\mu^I(I_1) + \mathscr{W}_\mu^J(J)$, and only briefly comment on some J_4-dependent energy forms. Further strain-energy functions will be introduced where they are required. For isotropic I_1-J-dependent energies, proper normalisation is fulfilled by satisfying Eqs (3.148) and (3.149), where the latter simplifies to $2\,\partial_{I_1}\mathscr{W}_{\mu[\boldsymbol{I}]} + \partial_J\mathscr{W}_{\mu[\boldsymbol{I}]} = 0$. The elasticity tensor for the considered energy type reduces to the form given in Eq. (A.81) and the associated linearisation conditions degenerate from the general notation in Section 3.8.2 to the very compact expressions

$$2\,\partial_{I_1}\mathscr{W}^I_{[\boldsymbol{I}]} = \mu\,, \quad \partial_J\mathscr{W}^J_{[\boldsymbol{I}]} = -\mu\,, \quad 4\,\partial^2_{I_1^2}\mathscr{W}^I_{[\boldsymbol{I}]} + \partial^2_{J^2}\mathscr{W}^J_{[\boldsymbol{I}]} = \mu\,. \tag{3.158}$$

These relations can also be obtained directly by exploiting Eq. (A.81) for the reference state and comparing the result to the distortional part $2\mu\,\mathbb{I}_{\mathrm{sym}}$ of the isotropic linear-elastic elasticity tensor $\mathbb{L}^{\mathrm{iso}}_{\mathrm{lin}}$, which is given in Eq. (3.135). We note that satisfying the conditions $(3.158)_1$ and $(3.158)_2$ immediately entails the fulfilment of the normalisation condition for the stress. A very simple, yet powerful and widely used strain-energy function is known as the *Neo-Hooke model* and reads

$$\mathscr{W}_\mu^I(I_1) = \tfrac{1}{2}\mu\,(I_1 - 3) \quad \text{with} \quad \partial_{I_1}\mathscr{W}_\mu^I = \tfrac{1}{2}\mu \quad \text{and} \quad \partial^2_{I_1^2}\mathscr{W}_\mu^I = 0\,. \tag{3.159}$$

This model relies on one material parameter, which can be identified as the small-strain shear modulus (or second Lamé constant) μ. The idea behind the designation of the Neo-Hooke model is that it is an extension of the linear-elastic Hooke model to large-strain hyperelasticity, see Rivlin [402]. This is also indicated when we recall Eq. $(3.75)_1$ and formulate the Neo-Hooke model as $\mathscr{W}_\mu^I(\boldsymbol{F}) = \mu\,(\boldsymbol{F}\cdot\boldsymbol{F} - 3)/2$, which shows its character as a classical quadratic potential. However, despite the simplicity of the Neo-Hooke model, it is interesting that approaching it from a different perspective shows some remarkable characteristics. With Eq. $(3.76)_1$, we can reformulate the model to $\mathscr{W}_\mu^I(\mathscr{I}^\lambda_{\mathrm{iso}}) = \mu\,(\lambda^2_{\boldsymbol{U}(1)} + \lambda^2_{\boldsymbol{U}(2)} + \lambda^2_{\boldsymbol{U}(3)} - 3)/2$ in terms of the principal stretches $\mathscr{I}^\lambda_{\mathrm{iso}}$. This allows to identify the Neo-Hooke model as a special case of the Ogden-type model, see Ogden [361, 362]. Moreover, the considerations in Section 6.2.2 will show that the Neo-Hooke model can be given a micromechanical meaning. Proceeding, an appropriate extension term $\mathscr{W}_\mu^J$ for the Neo-Hookean model which guarantees proper normalisation and linearisation can be given by

$$\mathscr{W}_\mu^J(J) = -\mu\ln[J] \quad \text{with} \quad \partial_J\mathscr{W}_\mu^J = -\frac{\mu}{J} \quad \text{and} \quad \partial^2_{J^2}\mathscr{W}_\mu^J = \frac{\mu}{J^2}\,. \tag{3.160}$$

We note that this logarithmic term satisfies the growth condition as $J \to 0^+$ and it is thus a suitable partner for the quadratic volumetric energy given in Eq. (3.156), which lacks

this property for finite values of Λ. An overall energy formulation of the form

$$\mathscr{W}(I_1, J) = \tfrac{1}{2}\mu\,(I_1 - 3) - \mu \ln[J] + \mathscr{W}_\Lambda(J) \tag{3.161}$$

can be referred to as *Simo-Pister* model, see Simo & Pister [441]. This formulation has an own name because it depicts a generalisation of the originally incompressible Neo-Hookean model to the compressible regime. At this point, we note that the Neo-Hooke model is only capable of describing mildly nonlinear material behaviour. This becomes obvious through the vanishing second derivative in Eq. $(3.159)_2$. Material models for $\mathscr{W}_\mu^I(I_1)$ which extend this formulation to more general nonlinear behaviour are often called *generalised Neo-Hooke* models, making the Neo-Hooke model an eponym for a whole class of material models. One such generalisation was proposed by Delfino et al. [94] and reads

$$\mathscr{W}_\mu^I(I_1) = \frac{\mu}{b}\left\{\exp\left[\frac{b}{2}\,(I_1 - 3)\right] - 1\right\}. \tag{3.162}$$

It is called *Delfino model* or simply I_1-based exponential model[5]. In addition to the material parameter μ, it contains a second parameter, b, which governs the nonlinearity. Taking the limit of Eq. (3.162) for $b \to 0$ shows that the Demiray model contains the Neo-Hooke model as special case. Further, the derivatives of Eq. (3.162) are

$$\partial_{I_1}\mathscr{W}_\mu^I = \frac{\mu}{2}\exp\left[\frac{b}{2}\,(I_1 - 3)\right] \quad \text{and} \quad \partial^2_{I_1^2}\mathscr{W}_\mu^I = \frac{\mu b}{4}\exp\left[\frac{b}{2}\,(I_1 - 3)\right], \tag{3.163}$$

giving the referential values $\partial_{I_1}\mathscr{W}^I_{\mu[\boldsymbol{I}]} = \mu/2$ and $\partial^2_{I_1^2}\mathscr{W}^I_{\mu[\boldsymbol{I}]} = \mu b/4$. The latter value suggests that the Demiray model requires a modified formulation of the energy part $\mathscr{W}_\mu^J$ in order to satisfy the linearisation condition $(3.158)_3$. The logarithmic term from Eq. (3.160) thus has to be enriched appropriately, giving the formulation

$$\mathscr{W}_\mu^J(J) = -\mu \ln[J] - \frac{\mu\, b}{8}\,(J-1)^2 \tag{3.164}$$

with the associated first and second derivative

$$\partial_J\mathscr{W}_\mu^J = -\frac{\mu}{J} - \frac{\mu b}{4}\,(J-1) \quad \text{and} \quad \partial^2_{J^2}\mathscr{W}_\mu^J = \frac{\mu}{J^2} - \frac{\mu b}{4}. \tag{3.165}$$

It is easy to observe that the energy $\mathscr{W}_\mu^J$ and its derivatives degenerate to the Neo-Hookean formulations given in Eqs (3.160) for $b = 0$. A further widely used generalised Neo-Hookean material model is the *Gent model*, proposed by Gent [158]. It reads

$$\mathscr{W}_\mu^I(I_1) = -\frac{J_\mathrm{m}\,\mu}{2}\,\ln\left[1 - \frac{I_1 - 3}{J_\mathrm{m}}\right] \tag{3.166}$$

[5] A slightly different formulation has been proposed earlier by Demiray [95] and reads

$$\mathscr{W}_\mu^I(I_1) = \frac{\mu}{2b}\left\{\exp[b\,(I_1 - 3)] - 1\right\}.$$

Similar exponential functions were also formulated by Gou [169] and Fung [141]. In general, such exponential-based strain-energy functions are sometimes referred to as Fung-type models, because they represent generalisations of Fung's studies on the exponential form of stress-strain-relations in biological tissues, see, for example, Fung [146].

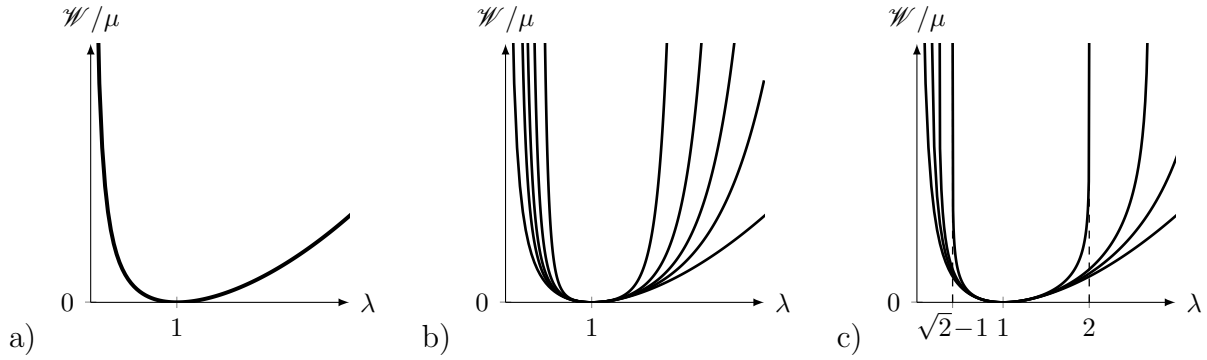

Figure 3.1: Comparison of the strain energy $\mathscr{W}$ due to an incompressible uniaxial deformation with $\boldsymbol{F} = \mathrm{diag}[\lambda, 1/\sqrt{\lambda}, 1/\sqrt{\lambda}]$ in terms of the stretch λ. The associated first principal invariant of $\boldsymbol{C}$ is $I_1 = \lambda^2 + 2/\lambda$. The results are normalised with respect to the shear parameter μ and given as $\mathscr{W}/\mu$. a) The Neo-Hooke energy. b) The Demiray energy for $b \to 0$ (identical to the Neo-Hooke model) as well as $b = 0.5, 1, 2, 5$. Increasing values of b increase the energy. c) The Gent energy for $J_\mathrm{m} \to \infty$ (identical to the Neo-Hooke model) as well as $J_\mathrm{m} = 10, 5, 2$. Decreasing values of J_m increase the energy. The Gent model has an asymptotic behaviour when $\lambda^2 + 2/\lambda - 3 = J_\mathrm{m}$. For $J_\mathrm{m} = 2$, this lock-up occurs for a compressive stretch $\lambda = \sqrt{2} - 1$ and a tensile stretch $\lambda = 2$.

and contains the shear parameter μ and a so-called lock-up parameter J_m. The key feature of this model is its asymptotic behaviour when $I_1 - 3$ reaches the value J_m, which emulates a lock-up and infinite elastic energy beyond a certain deformation. The Gent model simplifies to the Neo-Hooke model when the lock-up parameter tends to infinity. Further, the derivatives of Eq. (3.166) are

$$\partial_{I_1} \mathscr{W}_\mu^I = \frac{\mu J_\mathrm{m}}{2\,(J_\mathrm{m} - I_1 + 3)} \quad \text{and} \quad \partial^2_{I_1^2} \mathscr{W}_\mu^I = \frac{\mu J_\mathrm{m}}{2\,(J_\mathrm{m} - I_1 + 3)^2}\,, \tag{3.167}$$

An appropriate J-dependent energy term for a proper linearisation is given by

$$\mathscr{W}_\mu^J(J) = -\mu \ln[J] - \frac{\mu}{J_\mathrm{m}}\,(J-1)^2 \tag{3.168}$$

with the derivatives

$$\partial_J \mathscr{W}_\mu^J = -\frac{\mu}{J} - \frac{2\mu}{J_\mathrm{m}}\,(J-1) \quad \text{and} \quad \partial^2_{J^2} \mathscr{W}_\mu^J = \frac{\mu}{J^2} - \frac{2\mu}{J_\mathrm{m}}\,. \tag{3.169}$$

A brief comparison between the three introduced energy functions is provided in Figure 3.1. Note that further generalised Neo-Hookean models can be found in the literature, such as, for example, the formulation proposed by Lopez-Pamies [296].

At this point, we want to remark that the logarithmic supplementary energy term, which is given in Eq. (3.160) and occurs in Eqs (3.164) and (3.168), can be replaced by an alternative formulation. The energy term was introduced such that the first and second derivatives satisfy certain conditions. Hence, we might consider the second-order Taylor expansion of the logarithmic term around $J = 1$, reading

$$\mathcal{T}_2\{-\ln[J], 1\} = \tfrac{1}{2}\,(J-1)(J-3)\,, \tag{3.170}$$

and construct an alternative energy term

$$\mathscr{W}_\mu^J(J) = \tfrac{1}{2}\mu\,(J-1)(J-3) \quad \text{with} \quad \partial_J \mathscr{W}_\mu^J = \mu\,(J-2) \quad \text{and} \quad \partial^2_{J^2} \mathscr{W}_\mu^J = \mu\,. \tag{3.171}$$

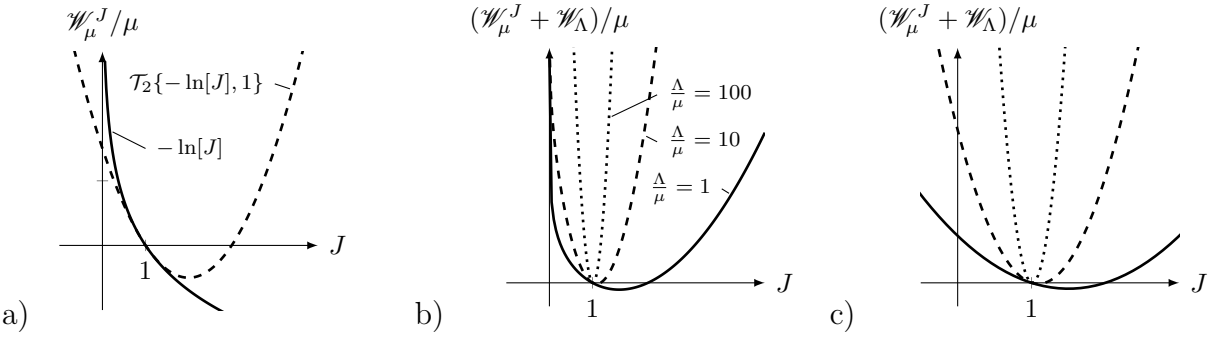

Figure 3.2: a) Visualisation of the logarithmic energy term $\mathscr{W}_\mu^J$, normalised with respect to μ, and the associated second-order Taylor expansion $\mathcal{T}_2$. b) The sum of the J-dependent energy terms $\mathscr{W}_\mu^J + \mathscr{W}_\Lambda$ with the logarithm-based $\mathscr{W}_\mu^J$ from Eq. (3.160) for different ratios Λ/μ, normalised with respect to μ. c) The same scenario as in b), but with the non-logarithmic formulation of $\mathscr{W}_\mu^J$ from Eq. (3.171). The solid, dashed and dotted lines in c) refer to the same ratios of Λ/μ than in b).

Consequently, this form for $\mathscr{W}_\mu^J$ and its first and second derivative deliver the same values in the reference state and can be used as an alternative to the logarithmic terms in Eqs (3.160), (3.164), and (3.168). A visualisation is given in Figure 3.2a. Obviously, the non-logarithmic energy term has no asymptotic behaviour for $J \to 0$, since $\mathscr{W}_\mu^J|_{J=0} = 3\mu/2$. This means that it does not satisfy the growth conditions for finite values of Λ when accompanied with the dilatational term given in Eq. (3.156). However, while the sum $\mathscr{W}_\mu^J + \mathscr{W}_\Lambda$ with logarithmic term guarantees the consistent growth condition independent of the value Λ, see Figure 3.2b, the non-logarithmic term appropriately emulates this behaviour for large ratios of Λ/μ, see Figure 3.2c.

Finally, we want to give a very brief overview on the different possibilities of the incorporation of anisotropic (transversely isotropic) material behaviour during the process of constitutive formulation of energy functions. A very simple method is to supplement a purely isotropic energy with a purely anisotropic contribution, which results in

$$\mathscr{W}_\mu^I(I_1, I_2, J_4, J_5) = \mathscr{W}_{\text{iso}}(I_1, I_2) + \mathscr{W}_{\text{aniso}}(J_4, J_5) \tag{3.172}$$

Such formulations are widely used, however, we emphasise that such simplifying decouplings always have to be justified by experimental observations. Further, energy formulations in line with the split in Eq. (3.172) are often employed with purely J_4-dependent anisotropic contributions. Recalling Eq. (3.86) and the consequent meaning of the J_4-invariant as the stretch of the material in preferred direction $\boldsymbol{a}_0$, it becomes clear that J_4-dependent contributions only influence the material behaviour in the axis of the preferred direction. A very common class of materials which can be characterised by such energy formulations are so-called fibre-reinforced materials, which show a stiffer behaviour for stretches in the direction $\boldsymbol{a}_0$ than in the other ones. Consequently, decoupled energies of the form in Eq. (3.172) with $\mathscr{W}_{\text{aniso}}(J_4)$ describe so-called *augmented isotropic materials with unidirectional reinforcement*. The most simple purely J_4-based energy is the quadratic function

$$\mathscr{W}_{\text{aniso}}(J_4) = \tfrac{1}{2}\mu\,(J_4 - 1)^2\,, \tag{3.173}$$

which is called *standard reinforcing model*, see, for example, Triantafyllidis & Abeyaratne [484] or Qiu & Pence [392, 393]. A similar energy can be formulated

in terms of $\sqrt{J_4} = \lambda_{\boldsymbol{a}}$, reading

$$\mathscr{W}_{\text{aniso}}(\lambda_{\boldsymbol{a}}) = \tfrac{1}{2}\mu\,(\lambda_{\boldsymbol{a}} - 1)^2 \quad \text{with} \quad \partial_{\lambda_{\boldsymbol{a}}}\mathscr{W}_{\text{aniso}} = \mu\,(\lambda_{\boldsymbol{a}} - 1) \quad \text{and} \quad \partial^2_{\lambda^2_{\boldsymbol{a}}}\mathscr{W}_{\text{aniso}} = \mu\,, \tag{3.174}$$

see, for instance, Humphrey et al. [233] or Alastrué et al. [8]. The constant second derivative of this energy reminds of a classical linear-elastic spring. We further note that the strain measure $J_4 - 1$ in Eq. (3.173) represents a one-dimensional version of the Green–Lagrange strain $\boldsymbol{E}_2$, whereas the strain measure $\lambda_{\boldsymbol{a}} - 1$ in Eq. (3.174) depicts a one-dimensional version of the Biot strain $\boldsymbol{E}_1$, compare Section 2.1.5. Further, as for the previously discussed I_1-based energy functions, there are alternative formulations to the simple quadratic potentials in Eqs (3.173) and (3.174) that are capable of describing more general nonlinear material behaviour. One such model was proposed by Holzapfel et al. [222] and reads

$$\mathscr{W}_{\text{aniso}}(J_4) = \frac{\mu}{2b}\left(\exp[b\,(J_4 - 1)^2] - 1\right). \tag{3.175}$$

It is easy to deduce that this formulation simplifies to expression (3.173) if $b \to 0$. Hence, $\mu > 0$ is a stiffness parameter and $b > 0$ serves as a dimensionless material parameter which governs the nonlinearity. Note that all of the here discussed J_4-based energy contributions are usually restricted to positive values of J_4, which means that the reinforcements only act if the material direction $\boldsymbol{a}_0$ is extended. Of course, this highlights that these formulations are only meaningful for the description of very special materials. For the characterisation of general transversely isotropic material behaviour, the decoupling that is proposed in Eq. (3.172) is not appropriate and more general strain-energy functions have to be considered. Therefore, we might generalise it to

$$\mathscr{W}^I_{\mu}(I_1, I_2, J_4, J_5) = \mathscr{W}_{\text{iso}}(I_1, I_2) + \mathscr{W}_{\text{aniso}}(J_4, J_5) + \mathscr{W}_{\text{coupl}}(I_1, I_2, J_4, J_5)\,, \tag{3.176}$$

where the coupling term $\mathscr{W}_{\text{coupl}}$ addresses possible interconnections between the isotropic and the anisotropic invariants. Models which are in line with such a general structure were proposed by, for example, Itskov & Aksel [244] and Schröder et al. [426]. The latter model is split into a purely isotropic energy contribution, $\mathscr{W}_{\mu,\text{i}}$, and an anisotropic contribution, $\mathscr{W}_{\mu,\text{a}}$, such that $\mathscr{W}_{\mu} = \mathscr{W}_{\mu,\text{i}} + \mathscr{W}_{\mu,\text{a}}$. The anisotropic contribution relies on the full set of invariants and reads

$$\begin{aligned}\mathscr{W}_{\mu,\text{a}}(I_1, I_2, J, J_4, J_5) &= \alpha_1\,(J_5 - I_1 J_4 + I_2) + \alpha_2\,J_4^{\alpha_3} J^{-2/3} + \alpha_4\,(I_1 J_4 - J_5) + \alpha_5\,J_4^{\alpha_6} \\ &= \alpha_1\,K_1 + \alpha_2\,J_4^{\alpha_3} J^{-2/3} + \alpha_4\,K_3 + \alpha_5\,J_4^{\alpha_6}\,.\end{aligned} \tag{3.177}$$

Therein, α_i for $i = 1, 2, 3, 4, 5, 6$ are material parameters which underlie some restrictions, see Schröder et al. [426]. However, the interesting aspect is the occurrence of coupled invariant terms and how two of the invariant bases can be connected to the physically meaningful invariant set $\mathscr{I}''_{\text{ti}}$, which was discussed in Section 3.5.4.

Part II

Micromechanics and Homogenisation

4 Continuum Micromechanics

This chapter discusses the basic concepts and relations in the field of *continuum micromechanics* and multiscale modelling. Doing so, the multiscale considerations build up on the previous part, which dealt with the kinematical description of a physical body in terms of configurations and set a framework for the thermodynamically consistent and physically meaningful description of elastic material behaviour in terms of hyperelastic strain-energy potentials. If continuum-mechanical investigations are not done on a single-scale, but on a multiscale basis, the previously outlined kinematical and constitutive concepts apply across each of the considered scales. Hence, this gives rise to the formulation of separate boundary-value problems on each scales. This has to be accompanied with appropriate *scale bridging* methods, in particular *upscaling* and *homogenisation* methods in order to provide effective quantities on the largest scale, which is usually the observation scale. The basic fundamentals of these concepts are provided in this chapter, but the intention is far from giving a complete overview. We instead refer to the comprehensive overviews on the broad field of micromechanics and homogenisation that were given by Suquet [464], Ponte Castañeda & Suquet [381], Nemat-Nasser & Hori [352], Milton [335], Buryachenko [65], Zohdi & Wriggers [528], and the references therein. It is further remarked that this study is only concerned with the treatment of solid materials or at least such which can suitably be described by the framework of solid mechanics. The modelling of materials which include phases with different states of matter, such as fluid-saturated porous materials, leads to alternative methods like the theory of mixtures or the theory of porous media. The reader is referred to Atkin & Craine [16], Bowen [57], de Boer [52], and Ehlers [106] for elaborate overviews on such approaches.

4.1 The multiscale problem

The starting point of continuum-mechanical multiscale investigations is the kinematical description and general setting of the mechanical problem on each of the considered length scales. In this context, the typical scheme for a modelling approach across several length scales is depicted in Figure 4.1. It establishes the identification of three important length scales: The overall mechanical problem lives on the *macroscale* and is specified by the characteristic macroscopic length l_{macro}. This length scale characterises the size of the overall specimen, which appears on this scale as a homogeneous material. However, every material is heterogeneous at closer examinations if looking at smaller scales. In this connection, a lot of materials show typical inhomogeneities, such as inclusions, fibres or pores. The size of these inhomogeneities constitutes the *microstructure* of a material and defines the *microscale* and microscopic length l_{micro}. In between the micro- and the macroscale, it is essential to define an intermediate length scale which is referred to as the *mesoscale*. A proper definition of the mesoscale designates it as a *representative volume element* ($\mathscr{RVE}$). According to Hill [210], the $\mathscr{RVE}$ has to contain a sufficient number of inhomogeneities such that it captures the microstructure properly in a statistical sense. This property is strongly related to the principle of *statistical uniformity*, which demands that the statistical properties of the $\mathscr{RVE}$ are invariant under translations. In addition to that, Drugan & Willis [99] suggested another definition of the $\mathscr{RVE}$, requiring that it is the smallest

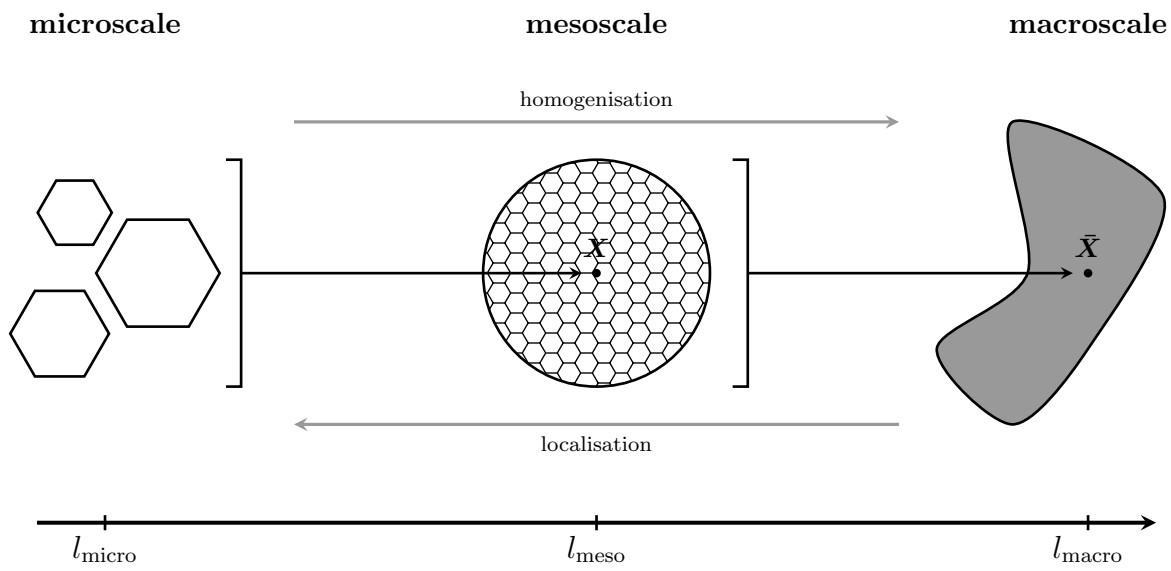

Figure 4.1: The modelling approach across several scales.

possible volume sample of the microstructure which represents the macroscopic material behaviour with sufficient accuracy. Thus, we recognise that the proper formulation of the $\mathscr{RVE}$ bounds the mesoscopic length scale from below and from above. This is expressed by the hypothesis of *separation of length scales*, which reads

$$l_{\text{micro}} < l_{\text{meso}} \ll l_{\text{macro}} \tag{4.1}$$

This is also referred to as Hashin's *MMM principle* [183]. Satisfaction of the inequality relations (4.1) has the key consequence that macroscopic quantities appear *uniform* on the microscopic length scale, in particular on the boundary of the microstructure. In addition, it is assumed that the macroscopic length scale not only characterises the size of the overall structure, but also the scale of variation of the body force and macroscopic external boundary conditions. This means that those quantities fluctuate on scales much larger than l_{micro} and can therefore be neglected on the microscale. It is further remarked that the separation of length scales does not pose any requirement on the absolute size of the scales. Although the characteristic length scale of inhomogeneities in a lot of applications is in the order of micrometres (μm), the prefixes micro, meso, and macro do not imply a direct connection to absolute sizes, but rather stand for small, middle and large by referring to their Greek roots *mikrós*, *mésos*, and *makrós*, respectively. This means that the size of a $\mathscr{RVE}$ that is actually required cannot be determined generally. Investigations for certain microstructures in numerical applications were carried out by Drugan & Willis [99], Moulinec & Suquet [345], and Kanit et al. [250].

Next, after having defined the critical length scales for continuum-mechanical multiscale approaches, we proceed with describing the kinematical relations and the general mechanical problem separately on the macro- and the microscale.

4.1.1 The macroscale problem

In analogy to the scale-independent considerations in Section 2.1, we start with the description of the motion of a macroscopic body $\bar{\mathscr{B}}$, which is composed of an infinite number

of macroscopic particles (or material points) $\bar{\mathscr{P}} \in \bar{\mathscr{P}}$. Subsequently, the *macro-motion* is defined in terms of the macroscopic reference placement $\bar{\boldsymbol{\mathscr{X}}}_0$ and the deformation map $\bar{\boldsymbol{\chi}}$, which are given by

$$\bar{\boldsymbol{\mathscr{X}}}_0 : \left\{ \begin{array}{l} \bar{\mathscr{B}} \to \bar{\mathcal{B}}_0 \subset \mathcal{R}^3 \\ \bar{\mathscr{P}} \mapsto \bar{\boldsymbol{X}} = \bar{\boldsymbol{\mathscr{X}}}_0(\bar{\mathscr{P}}) \end{array} \right. \quad \text{and} \quad \bar{\boldsymbol{\chi}} : \left\{ \begin{array}{l} \bar{\mathcal{B}}_0 \times \mathscr{T} \to \bar{\mathcal{B}} \subset \mathcal{R}^3 \\ (\bar{\boldsymbol{X}}, t) \mapsto \bar{\boldsymbol{x}} = \bar{\boldsymbol{\chi}}(\bar{\boldsymbol{X}}, t) \,. \end{array} \right. \tag{4.2}$$

These maps provide the referential position vector $\bar{\boldsymbol{X}} \in \bar{\mathcal{B}}_0$ of the macroscopic particle $\bar{\mathscr{P}}$ in the reference configuration $\bar{\mathcal{B}}_0$ as well as the actual position vector $\bar{\boldsymbol{x}} \in \bar{\mathcal{B}}$ in the actual configuration $\bar{\mathcal{B}}$, respectively. Henceforth, macroscopic quantities will be labelled by an overbar. Having defined the deformation map $\bar{\boldsymbol{\chi}}$, it is straightforward to formulate the associated macrocopic deformation gradient

$$\bar{\boldsymbol{F}}(\bar{\boldsymbol{X}}) = \mathrm{Grad}[\bar{\boldsymbol{\chi}}(\bar{\boldsymbol{X}})] \,. \tag{4.3}$$

In line with the general explanations in Section 2.1.2, $\bar{\boldsymbol{F}}$ and the thereon based cofactor $\mathrm{cof}[\bar{\boldsymbol{F}}]$ and the macroscopic Jacobian $\bar{J} := \det[\bar{\boldsymbol{F}}] > 0$ serve as maps for macroscopic line, area, and volume elements, respectively. Accordingly, the macroscopic right Cauchy–Green strain tensor is given by

$$\bar{\boldsymbol{C}} = \bar{\boldsymbol{F}}^T \bar{\boldsymbol{F}} \,. \tag{4.4}$$

Furthermore, in a hyperelastic framework the strain-energy at the macroscopic material point $\bar{\mathscr{P}}$, parametrised by $\bar{\boldsymbol{X}}$, is described by the macroscopic potential $\bar{\mathscr{W}}(\bar{\boldsymbol{F}})$. In accordance to Section 3.2.5, the Coleman–Noll procedure and a vanishing macroscopic dissipation, $\bar{\mathcal{D}} = 0$, entail the connection to the macroscopic first Piola–Kirchhoff stress tensor

$$\bar{\boldsymbol{P}}(\bar{\boldsymbol{F}}) = \partial_{\bar{\boldsymbol{F}}} \bar{\mathscr{W}}(\bar{\boldsymbol{F}}) \,. \tag{4.5}$$

With this, the general macroscopic boundary-value problem is defined in direct analogy to the explanations in Sections 3.1.1, 3.4.2, and 3.4.3, and reads

$$\mathrm{Div}[\bar{\boldsymbol{P}}] = \boldsymbol{0} \text{ in } \bar{\mathcal{B}}_0 \,, \quad \bar{\boldsymbol{\chi}} = \overline{\boldsymbol{\chi}} \text{ on } \partial\bar{\mathcal{B}}_{\boldsymbol{\chi}} \subseteq \partial\bar{\mathcal{B}}_0 \,, \quad \bar{\boldsymbol{P}}\bar{\boldsymbol{N}} = \overline{\boldsymbol{T}} \text{ on } \partial\bar{\mathcal{B}}_{\boldsymbol{T}} \subseteq \partial\bar{\mathcal{B}}_0 \,, \tag{4.6}$$

where $\overline{\boldsymbol{\chi}}$ are prescribed displacements on the macroscopic Dirichlet boundary $\bar{\mathcal{B}}_{\boldsymbol{\chi}}$ and $\overline{\boldsymbol{T}}$ are prescribed tractions on the macroscopic Neumann boundary $\partial\bar{\mathcal{B}}_{\boldsymbol{T}}$. At this point, we note that a direct description of the strain-energy $\bar{\mathscr{W}}$ in terms of analytical functions, such as the ones proposed in Section 3.8, leads to classical single-scale formulations. In contrast, the key idea of a multiscale approach is that the macroscopic energy $\bar{\mathscr{W}}$ and, accordingly, the macroscopic stress $\bar{\boldsymbol{P}}$ are derived by the explicit incorporation of microstructural effects.

4.1.2 The microscale problem

On the microscale, an infinite number of microscopic material points $\mathscr{P} \in \mathscr{B}$ constitutes the microstructure $\mathscr{B}$. The *micro-motion* is described by the microscopic reference placement $\boldsymbol{\mathscr{X}}_0$ and the deformation map $\boldsymbol{\chi}$, which are given by

$$\boldsymbol{\mathscr{X}}_0 : \left\{ \begin{array}{l} \mathscr{B} \to \mathcal{B}_0 \subset \mathcal{R}^3 \\ \mathscr{P} \mapsto \boldsymbol{X} = \boldsymbol{\mathscr{X}}_0(\mathscr{P}) \end{array} \right. \quad \text{and} \quad \boldsymbol{\chi} : \left\{ \begin{array}{l} \mathcal{B}_0 \times \mathscr{T} \to \mathcal{B} \subset \mathcal{R}^3 \\ (\boldsymbol{X}, t) \mapsto \boldsymbol{x} = \boldsymbol{\chi}(\boldsymbol{X}, t) \,. \end{array} \right. \tag{4.7}$$

They define the referential position $\boldsymbol{X} \in \mathcal{B}_0$ of the microscopic material point $\mathscr{P}$ in the microscopic reference configuration $\mathcal{B}_0$ and the actual position $\boldsymbol{x} \in \mathcal{B}$ in the microscopic actual configuration $\mathcal{B}$, respectively. The microscopic deformation gradient is given by

$$\boldsymbol{F}(\boldsymbol{X}) = \mathrm{Grad}[\boldsymbol{\chi}(\boldsymbol{X})] \,. \tag{4.8}$$

Now, a key assumption is that the microstructure $\mathscr{B}$ might consist of N distinct *phases* $\mathcal{B}_0^\alpha$, where α indicates the phases. Therein, a phase is a spatial region with uniform physical properties and does not have the sometimes used meaning of a state of matter. Furthermore, in this work the terms *phase*, *constituent*, and *component* can be used interchangeably. In the context of purely mechanical considerations, the proper definition of a phase of course only demands for uniformity with respect to mechanical properties, like stiffness. For hyperelastic phases, the mechanical constitutive behaviour is described by individual strain-energy functions $\mathscr{W}^\alpha(\boldsymbol{F})$ for each phase. We proceed with the introduction of the *characteristic functions*

$$\mathscr{X}^\alpha(\boldsymbol{X}) = \begin{cases} 1 & \text{if } \boldsymbol{X} \in \mathcal{B}_0^\alpha \,, \\ 0 & \text{else} \,. \end{cases} \tag{4.9}$$

They are also referred to as *phase distribution functions* or *phase indicator functions* and describe the distribution of the phases in the reference configuration $\mathcal{B}_0$. Thus, they require (or contain, depending on the point of view) *complete knowledge* about the microstructure of a material. However, the characteristic functions are also the basis for the statistical description of microstructures, which follows in Section 4.2.1, and serve as fundamental basis for analytical homogenisation methods. We further presume the *saturation condition*

$$\sum_\alpha \mathscr{X}^\alpha(\boldsymbol{X}) = 1 \quad \text{such that} \quad \mathcal{B}_0 = \bigcup_\alpha \mathcal{B}_0^\alpha \,. \tag{4.10}$$

It is remarked that this does not exclude the occurrence of voids or pore spaces in the microstructure, since such regions represent distinct phases. Consequently, the *local strain-energy function* of the heterogeneous microstructure at each material point $\boldsymbol{X}$ is given by

$$\mathscr{W}(\boldsymbol{X}, \boldsymbol{F}) = \sum_\alpha \mathscr{X}^\alpha(\boldsymbol{X})\, \mathscr{W}^\alpha(\boldsymbol{F}) \,. \tag{4.11}$$

Based on that, we can specify the local first Piola–Kirchhoff stress tensor

$$\boldsymbol{P}(\boldsymbol{X}, \boldsymbol{F}) = \partial_{\boldsymbol{F}} \mathscr{W}(\boldsymbol{X}, \boldsymbol{F}) = \sum_\alpha \mathscr{X}^\alpha(\boldsymbol{X})\, \boldsymbol{P}^\alpha(\boldsymbol{F}) \quad \text{where} \quad \boldsymbol{P}^\alpha(\boldsymbol{F}) = \partial_{\boldsymbol{F}} \mathscr{W}^\alpha(\boldsymbol{F}) \tag{4.12}$$

by making use of the Coleman–Noll procedure and the assumption of non-dissipative behaviour, $\mathcal{D} = 0$, on the microscale. We refer to $\boldsymbol{P}^\alpha$ as the *partial stress tensors*. Furthermore, the local momentum balance in the microstructure reads

$$\mathrm{Div}[\boldsymbol{P}] = \boldsymbol{0} \quad \text{in} \quad \mathcal{B}_0 \,. \tag{4.13}$$

The complete specification of the microscopic boundary-value problem would further demand the formulation of boundary conditions on the surface $\partial\mathcal{B}_0$. However, this is left open at this point and follows in the process of micro-macro transition in Section 4.3.

4.1.3 Microstructural interface conditions

A heterogeneous microstructure $\mathscr{B}$ consists of distinct phases $\mathcal{B}_0^\alpha$ with a certain spatial arrangement, which is described by the characteristic functions $\mathscr{X}^\alpha$. The union of the boundaries of two different phases, say $\mathcal{B}_0^{\alpha_{(i)}}$ and $\mathcal{B}_0^{\alpha_{(j)}}$, depicts a *phase interface* or *interphase*[1] $\Gamma_{\mathcal{B}^{\alpha_{(ij)}}} = \partial\mathcal{B}_0^{\alpha_{(i)}} \cup \partial\mathcal{B}_0^{\alpha_{(j)}}$. Consequently, the material properties across these mathematically idealised sharp interfaces become discontinuous and appropriate *jump conditions* have to be formulated for the microscopic deformations and stress fields. To do so, we introduce the *interface jump* of an arbitrary scalar field $f(\boldsymbol{X})$ across a general interface $\Gamma_\mathcal{B} \subset \mathcal{B}_0$ as

$$[\![f(\boldsymbol{X})]\!] = \lim_{\epsilon\to 0} \big[f(\boldsymbol{X} + \epsilon\boldsymbol{N}_\Gamma) - f(\boldsymbol{X} - \epsilon\boldsymbol{N}_\Gamma)\big] = f^+(\boldsymbol{X}) - f^-(\boldsymbol{X}) \quad \forall \boldsymbol{X} \in \Gamma_\mathcal{B}\,. \tag{4.14}$$

Therein, $\boldsymbol{N}_\Gamma \in T^*_{\boldsymbol{X}}\mathcal{B}_0$ denotes a unit vector normal to the interface $\Gamma_\mathcal{B}$. For a scalar field $f(\boldsymbol{X})$ which is continuous in $\mathcal{B}_0$ and continuously differentiable in $\mathcal{B}_0 \setminus \Gamma_\mathcal{B}$, the *Hadamard lemma* states that a continuous scalar field $c(\boldsymbol{X})$ relates the gradient $\mathrm{Grad}[f(\boldsymbol{X})]$ across the interface $\Gamma_\mathcal{B}$ via

$$[\![\mathrm{Grad}[f(\boldsymbol{X})]]\!] = c(\boldsymbol{X})\boldsymbol{N}_\Gamma(\boldsymbol{X}) \quad \forall \boldsymbol{X} \in \Gamma_\mathcal{B}\,, \tag{4.15}$$

see, for example, Truesdell [488] or Šilhavý [438]. In Eq. (4.15), the scalar field $c(\boldsymbol{X})$ represents the *jump amplitude* across the interface. Consequently, an interface represents a *singular surface* with respect to a scalar field $f(\boldsymbol{X})$ whenever the jump in Eq. (4.14), the amplitude c in Eq. (4.15), or both are not equal to zero. For vector- and tensor-valued field quantities, the scalar relations in Eqs (4.14) and (4.15) hold for each of the respective scalar coefficients. In this work, we only consider material interfaces, which are characterised by discontinuous material properties. Hence, they are fixed to certain material points $\boldsymbol{X}$ and do not move in the reference configuration $\mathcal{B}_0$. By doing so, we exclude phenomena such as phase transformations, which are described by so-called non-material, moving referential interfaces and associated interface driving forces, see, for example, Abeyaratne & Knowles [2]. Moreover, we will not assign interfacial energies $\mathscr{W}^{\Gamma_\mathcal{B}}$ on $\Gamma_\mathcal{B}$, but refer to Gurtin & Murdoch [175] and Gurtin et al. [177] for details on the theory of so-called elastic material surfaces and surface stresses.

Geometrical compatibility Under the assumption that the different phases $\mathcal{B}_0^\alpha$ in the microstructure $\mathscr{B}$ are perfectly bonded to each other at their respective interfaces, it follows that the deformation map $\boldsymbol{\chi}(\boldsymbol{X} \in \mathcal{B}_0)$ has to be continuous in $\mathcal{B}_0$ and continuously differentiable in $\mathcal{B}_0 \setminus \Gamma_\mathcal{B}$, which is accompanied with the jump condition

$$[\![\boldsymbol{\chi}(\boldsymbol{X})]\!] = \boldsymbol{0} \quad \forall \boldsymbol{X} \in \Gamma_\mathcal{B}\,. \tag{4.16}$$

This expression prevents the description of processes such as fracture in the microstructure, which are not the focus of this work. Yet, it shall be remarked that when dealing with such, it proves useful to formulate the *opening or stretch gap* $[\![\boldsymbol{\chi}]\!]^\perp = (\boldsymbol{N}_\Gamma \otimes \boldsymbol{N}_\Gamma)\,[\![\boldsymbol{\chi}]\!] \geq \boldsymbol{0}$ and the *sliding or slip gap* $[\![\boldsymbol{\chi}]\!]^\parallel = (\boldsymbol{I} - \boldsymbol{N}_\Gamma \otimes \boldsymbol{N}_\Gamma)\,[\![\boldsymbol{\chi}]\!]$, such that $[\![\boldsymbol{\chi}]\!]^\perp + [\![\boldsymbol{\chi}]\!]^\parallel = [\![\boldsymbol{\chi}]\!]$. This

[1] For the objectives of this work, it is sufficient to proceed with the notation of two-dimensional interfaces between two phases. The formulation of a one-dimensional union $\Gamma_{\mathcal{B}^{\alpha_{(ijk)}}} = \partial\mathcal{B}_0^{\alpha_{(i)}} \cup \partial\mathcal{B}_0^{\alpha_{(j)}} \cup \partial\mathcal{B}_0^{\alpha_{(k)}}$ of the boundaries of three phases $\mathcal{B}_0^{\alpha_{(i)}}$, $\mathcal{B}_0^{\alpha_{(j)}}$, and $\mathcal{B}_0^{\alpha_{(k)}}$, which Gray & Hassanizadeh [171] referred to as *common lines*, is not necessary.

allows to distinguish between geometrical discontinuities normal and tangential to the interface $\Gamma_{\mathcal{B}}$. Here, however, the condition (4.16) allows the application of the Hadamard lemma (4.15) to formulate a jump condition for the deformation gradient $\boldsymbol{F}$ across the interface $\Gamma_{\mathcal{B}}$, hence,

$$[\![\mathrm{Grad}[\boldsymbol{\chi}]]\!] = [\![\boldsymbol{F}]\!] = \boldsymbol{c} \otimes \boldsymbol{N}_\Gamma \quad \text{such that} \quad [\![\boldsymbol{F}]\!]\boldsymbol{N}_\Gamma = \boldsymbol{c} \quad \text{and} \quad [\![\boldsymbol{F}]\!]\boldsymbol{N}_\Gamma^\perp = \boldsymbol{0}\,. \tag{4.17}$$

Therein, $\boldsymbol{c} \in \mathcal{R}^3$ is the vector-valued jump amplitude and $\boldsymbol{N}_\Gamma^\perp$ is a unit vector tangential to the interface $\Gamma_{\mathcal{B}}$ so that $\boldsymbol{N}_\Gamma \cdot \boldsymbol{N}_\Gamma^\perp = 0$. The jump condition in Eq. (4.17) is usually referred to as the *kinematical compatibility condition*. It states that the deformation gradients on both sides of the interface are rank-one connected, since $\boldsymbol{c} \otimes \boldsymbol{N}_\Gamma$ is a simple tensor with $\mathrm{rank}[\boldsymbol{c} \otimes \boldsymbol{N}_\Gamma] = 1$. Further, the deformation gradient jump has no tangential components, as stated in Eq. $(4.17)_3$, which is in line with physical intuition because the deformation continuity in Eq. (4.16) does not allow any gradually jumps along the interface.

Statical compatibility In general, the occurrence of singular surfaces and non-differentiable regions $\Gamma_{\mathcal{B}}$ in the referential domain $\mathcal{B}_0$ demands for the formulation of appropriate jump conditions for the physical balance relations from Section 2.3. While the local balances are valid at material points $\boldsymbol{X} \in \mathcal{B}_0 \setminus \Gamma_{\mathcal{B}}$ inside the continuously differentiable phase domains, this is not the case for points $\boldsymbol{X} \in \Gamma_{\mathcal{B}}$ at the singular surfaces due to possible jumps of the associated physical quantities. Hence, a general treatment requires to formulate additional *balance relations at the interface*, as explained in detail by, for instance, Truesdell [488, 489] and Šilhavý [438]. In this work, however, this is not necessary as we restrict to isothermal, purely hyperelastic problems without interfacial energies as well as to the consideration of material interfaces which are fixed in the reference configuration. We remain with a simple version of the balance of momentum at the interface $\Gamma_{\mathcal{B}} \subset \mathcal{B}_0$ that reads

$$[\![\boldsymbol{T}(\boldsymbol{X})]\!] = [\![\boldsymbol{P}(\boldsymbol{X})]\!]\boldsymbol{N}_\Gamma(\boldsymbol{X}) = \boldsymbol{0} \quad \forall \boldsymbol{X} \in \Gamma_{\mathcal{B}}\,, \tag{4.18}$$

for which we recalled Eq. (2.26). Eq. (4.18) demands for the *traction continuity* across the interface and is referred to as *statical compatibility condition*. It is a very intuitive requirement for material interfaces which are in equilibrium and describes the absence of any driving forces that would move the interface in the reference configuration $\mathcal{B}_0$.

4.2 Microscale statistics

4.2.1 Microstructural statistics

It has been pointed out in the beginning of Section 4.1 that the mesoscale has to constitute an $\mathscr{RVE}$ and that it has to satisfy the principle of statistical uniformity. In this context, it is important to distinguish between two types of materials, that is, such with periodic microstructures and such with random microstructures. In materials of the first kind, the microstructure consists of a periodic arrangement of *unit cells*, which contain the typical heterogeneities and phase geometries. This means that for these materials a unit cell completely specifies the microstructure and serves as a proper definition of the $\mathscr{RVE}$. Such periodic microstructures can usually be found in man-made materials. On the other side, in particular biological tissues can be classified as materials with random microstructures, for

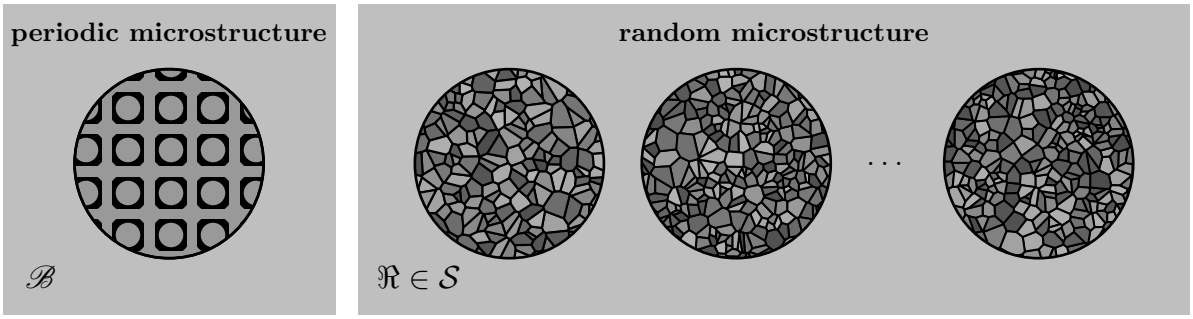

Figure 4.2: Periodic versus random microstructures. A representative microstructure $\mathscr{B}$ serves as a unit cell and fully specifies the material in the periodic case, whereas a sample space $\mathcal{S}$ consisting of an ensemble of different realisations $\Re \in \mathcal{S}$ describes the material in the case of random microstructures.

which the definition of an $\mathscr{RVE}$ requires some further considerations. For such materials, it is not possible to identify one specific microstructure as a representative unit cell a priori. In contrast, there are various *realisations* $\Re \in \mathcal{S}$ of the microstructure which together constitute a *sample space* $\mathcal{S}$. This is visualised in Figure 4.2. This means that for materials with random microstructures, the considerations on the microscale problem in Section 4.1.2 have to be formulated for a whole ensemble of different realisations. Doing so, the characteristic functions $\mathscr{X}^\alpha$ then become a function of the material point $\boldsymbol{X}$ and the realisation $\Re$, which transforms Eq. (4.9) into

$$\mathscr{X}^\alpha(\boldsymbol{X}, \Re) = \begin{cases} 1 & \text{if } \boldsymbol{X} \in \mathcal{B}_0^\alpha(\Re)\,, \\ 0 & \text{else}\,. \end{cases} \tag{4.19}$$

Thus, the characteristic functions carry the full information about the microstructural composition of all realisations across the sample space. However, it is very unlikely that one has such a complete knowledge about an entire sample space of microstructures and, hence, a complete definition of $\mathscr{X}^\alpha(\boldsymbol{X}, \Re)$. Rather, it proves useful to capture the characteristics of the microscopic geometry and the sample space in a statistical sense. This gives rise to a broad field of research which is often referred to as *statistical continuum mechanics*. Fundamental contributions to this field were provided by Beran [32] and Kröner [265] as well as in the classical works on probability theory, such as the one by Kolmogorov [256]. Proceeding, in the context of random microstructures, it is consequent to describe the different realisations in terms of *ensemble averages* over the sample space $\mathcal{S}$. This consequently leads to the formulation of statistical moments of the characteristic function $\mathscr{X}(\boldsymbol{X}, \Re)$, such as the *one-point probability function*

$$\mathfrak{p}^\alpha(\boldsymbol{X}) = \frac{1}{\dim[\mathcal{S}]} \int_{\mathcal{S}} \mathscr{X}^\alpha(\boldsymbol{X}, \Re)\, \mathrm{d}\Re\,. \tag{4.20}$$

The value $\mathfrak{p}^\alpha(\boldsymbol{X})$ describes the probability of finding phase α at point $\boldsymbol{X}$ across all realisations $\Re$. Likewise, the two-point probability function

$$\mathfrak{p}^{\alpha_{(ij)}}(\boldsymbol{X}_{(1)}, \boldsymbol{X}_{(2)}) = \frac{1}{\dim[\mathcal{S}]} \int_{\mathcal{S}} \mathscr{X}^{\alpha_{(i)}}(\boldsymbol{X}_{(1)}, \Re)\, \mathscr{X}^{\alpha_{(j)}}(\boldsymbol{X}_{(2)}, \Re)\, \mathrm{d}\Re \tag{4.21}$$

describes the probability of finding simultaneously phase $\alpha_{(i)}$ at point $\boldsymbol{X}_{(1)}$ and phase $\alpha_{(j)}$ at point $\boldsymbol{X}_{(2)}$. In Eqs (4.20) and (4.21), $\dim[\mathcal{S}]$ denotes the dimension of the sample space

and provides, together with the saturation condition (4.10), that the probability functions satisfy the conditions

$$\sum_{\alpha} \mathfrak{p}^{\alpha}(\boldsymbol{X}) = 1\,, \quad \sum_{\alpha_{(i)}} \mathfrak{p}^{\alpha_{(ij)}}(\boldsymbol{X}_{(1)}, \boldsymbol{X}_{(2)}) = \mathfrak{p}^{\alpha_{(j)}}(\boldsymbol{X}_{(2)})\,, \quad \sum_{\alpha_{(j)}} \mathfrak{p}^{\alpha_{(ij)}}(\boldsymbol{X}_{(1)}, \boldsymbol{X}_{(2)}) = \mathfrak{p}^{\alpha_{(i)}}(\boldsymbol{X}_{(1)}) \tag{4.22}$$

Further, the principle of Eqs (4.20) and (4.21) can be generalised to the notation of n-point probability functions, which correlate the probabilities at n different points and theoretically allow for an exact description of the microstructure in the limit case as n tends to infinity. However, such higher-order formulations are not employed in this work. We note that the one- and two-point probabilities, $\mathfrak{p}^{\alpha}(\boldsymbol{X})$ and $\mathfrak{p}^{\alpha_{(ij)}}(\boldsymbol{X}_{(1)}, \boldsymbol{X}_{(2)})$, depend on the absolute positions $\boldsymbol{X}$, $\boldsymbol{X}_{(1)}$ and $\boldsymbol{X}_{(2)}$. This conflicts with the principle of statistical uniformity, which demands that well-defined statistical descriptors should be invariant to translations of the microstructure. A natural way to achieve this is to make use of the assumption of *ergodicity*. In an ergodic system, the ensemble average over the sample space $\mathcal{S}$ at one point is identical to the volume average over all points in a single realisation $\Re \in \mathcal{S}$. It follows that the ensemble averages in Eqs (4.20) and (4.21) can be replaced by a volume average over one microstructure, say $\mathscr{B}$ with its reference configuration $\mathcal{B}_0$. Then, the one-point probability from Eq. (4.20) can be formulated as

$$\mathfrak{p}^{\alpha} = \frac{1}{\mathrm{vol}[\mathcal{B}_0]} \int_{\mathcal{B}_0} \mathscr{X}^{\alpha}(\boldsymbol{X})\, \mathrm{d}V = \frac{\mathrm{vol}[\mathcal{B}_0^{\alpha}]}{\mathrm{vol}[\mathcal{B}_0]} =: n^{\alpha} \quad \text{with} \quad \sum_{\alpha} n^{\alpha} = 1\,. \tag{4.23}$$

Hence, the volume integral of the characteristic functions $\mathscr{X}^{\alpha}$ over $\mathcal{B}_0$ denotes the volume $\mathrm{vol}[\mathcal{B}_0^{\alpha}]$ of phase $\mathcal{B}_0^{\alpha}$, whereas its volume average, or first moment, represents the *volume fraction* of phase α. $\mathfrak{p}^{\alpha}$ can also be referred to as the *expectation value* of $\mathscr{X}^{\alpha}$ in $\mathcal{B}_0$. The saturation condition $(4.23)_2$ for n^{α} directly follows from the equivalent condition for $\mathscr{X}^{\alpha}$, see Eq. (4.10). In the following, it proves useful to define an operator $\langle(\cdot)\rangle$ for the volume average of a quantity $(\cdot)$ over $\mathcal{B}_0$ as well as an operator $\langle(\cdot)\rangle^{\alpha}$ for the volume average of a quantity $(\cdot)$ over phase $\mathcal{B}_0^{\alpha}$, reading

$$\big\langle(\cdot)\big\rangle := \frac{1}{\mathrm{vol}[\mathcal{B}_0]} \int_{\mathcal{B}_0} (\cdot)\, \mathrm{d}V \quad \text{and} \quad \big\langle(\cdot)\big\rangle^{\alpha} := \frac{1}{\mathrm{vol}[\mathcal{B}_0^{\alpha}]} \int_{\mathcal{B}_0^{\alpha}} (\cdot)\, \mathrm{d}V^{\alpha} \tag{4.24}$$

The volume fraction is then simply written as $n^{\alpha} = \langle \mathscr{X}^{\alpha} \rangle$, whereas we obtain $\langle \mathscr{X}^{\alpha} \rangle^{\alpha} = 1$ for the phase average. In this connection, the two averaging operators can be linked by recalling the saturation condition (4.10), which allows to write the volume integral over $\mathcal{B}_0$ as the sum of volume integrals over the phases (subdomains) $\mathcal{B}_0^{\alpha}$, such that $\int_{\mathcal{B}_0} (\cdot)\, \mathrm{d}V = \sum_{\alpha} \int_{\mathcal{B}_0^{\alpha}} (\cdot)\, \mathrm{d}V^{\alpha}$. Then, with Eqs (4.24) and (4.23), we obtain

$$\big\langle(\cdot)\big\rangle = \frac{1}{\mathrm{vol}[\mathcal{B}_0]} \sum_{\alpha} \mathrm{vol}[\mathcal{B}_0^{\alpha}] \big\langle(\cdot)\big\rangle^{\alpha} = \sum_{\alpha} n^{\alpha} \big\langle(\cdot)\big\rangle^{\alpha}\,. \tag{4.25}$$

Moreover, the two-point probability function is obtained as

$$\mathfrak{p}^{\alpha_{(ij)}}(\boldsymbol{X}_{(1)} - \boldsymbol{X}_{(2)}) = \big\langle \mathscr{X}^{\alpha_{(i)}}(\boldsymbol{X}_{(1)} - \boldsymbol{X}_{(3)})\, \mathscr{X}^{\alpha_{(j)}}(\boldsymbol{X}_{(2)} - \boldsymbol{X}_{(3)}) \big\rangle \tag{4.26}$$

While the definition in terms of the ensemble average in Eq. (4.21) depends on the absolute positions of $\boldsymbol{X}_{(1)}$ and $\boldsymbol{X}_{(2)}$, the volume average only depends on the relative difference

$\boldsymbol{X}_{(1)} - \boldsymbol{X}_{(2)}$. This means, though, that the volume average still depends on the orientation of the configuration $\mathcal{B}_0$, which reflects the general anisotropy of the microstructure. In turn, the microstructure is *statistically isotropic* if the two-point probability is only sensitive to the distance $|\boldsymbol{X}_{(1)} - \boldsymbol{X}_{(2)}|$. This can be regarded as a spherical symmetry of the microstructural arrangement. However, it is emphasised that this does not imply isotropy with respect to the mechanical response of the microstructure, since the isotropically arranged phases can still have anisotropic material behaviour. A generalisation of the spherical symmetry (of the microstructural arrangement, not the mechanical behaviour) to an *ellipsoidal symmetry* was formulated by Willis [516] and leads to the formulation

$$\mathfrak{p}^{\alpha_{(ij)}}(\boldsymbol{X}_{(1)} - \boldsymbol{X}_{(2)}) = \mathfrak{p}^{\alpha_{(ij)}}(|(\boldsymbol{Z}_{\mathrm{d}}^{\alpha_{(ij)}})^{-T}(\boldsymbol{X}_{(1)} - \boldsymbol{X}_{(2)})|)\,. \tag{4.27}$$

Therein, the second-order shape tensor $\boldsymbol{Z}_{\mathrm{d}}^{\alpha_{(ij)}}$ serves as a descriptor for the preferred distribution of the microstructure. The notation of ellipsoidal symmetry in Eq. (4.27) recovers statistical isotropy for $\boldsymbol{Z}_{\mathrm{d}}^{\alpha_{(ij)}} = \boldsymbol{I}$.

In addition to (or instead of) the so far introduced n-point probability functions, many other methods can be employed to describe the statistical features of microstructures. For instance, a useful statistical measure is the lineal-path function by Lu & Torquato [301]. It quantifies the probability that a complete line segment between two points $\boldsymbol{X}_{(1)}$ and $\boldsymbol{X}_{(2)}$ is located in the same phase. Moreover, measures exist which incorporate the area and/or the curvature of phase boundaries, see, for example, Hassanizadeh & Gray [188]. Further measures and elaborate overviews about the statistical description of microscopic morphologies can be found in Torquato [478] and Buryachenko [65]. Finally, we remark that for the prescription of scalar statistical quantities, in particular one-point probabilities, one frequently employs *probability density functions*. They are used, for example, to describe the distribution of the alignment of fibres in network models or single crystals in polycrystals. Some basic remarks on probability theory and examples for univariate probability density functions, such as the Beta and the trianglar distribution, are presented in Appendix B.2. Such formulations are of fundamental importance for the homogenisation methods for fibrous networks in Chapter 6.

Summarising, the morphology of random microstructures can be well described by means of statistical descriptors. Though, instead of calculating the statistical measures from actual microstructures, it is also possible to define *material classes* which are characterised by certain statistical characteristics. Hence, if a multiscale method relies on statistical descriptors instead of the characteristic functions $\mathscr{X}$, it directly accounts for the complete sample space of all statistically possible realisations. Likewise, it is possible to construct a geometry (hence, the characteristic function $\mathscr{X}$) according to statistical descriptors. Together with the ergodicity assumption, this leads to the formulation of so-called statistically similar $\mathscr{RVE}$, see Schröder et al. [423], or statistically representative unit cells, see Geers et al. [155], which aim to be statistically equivalent to a whole sample space.

4.2.2 Field statistics

Besides the statistical description of the microscopic morphology, it proves useful to formulate similar statistical measures for the deformation and stress fields, here $\boldsymbol{F}$ and $\boldsymbol{P}$, in the phases. This is done in terms of statistical moments of the fields in the phases, such that the first moment is defined in terms of the averaging operator $\langle(\cdot)\rangle^{\alpha}$ as defined in

Eq. $(4.24)_2$. With this, we introduce the field averages (first moments) of the deformation gradient and first Piola–Kirchhoff stress as

$$\bar{\boldsymbol{F}}_\alpha := \big\langle \boldsymbol{F} \big\rangle^\alpha \quad \text{and} \quad \bar{\boldsymbol{P}}^\alpha := \big\langle \boldsymbol{P} \big\rangle^\alpha . \tag{4.28}$$

In the same spirit, higher moments of the fields can be formulated, such as the second moment $\langle \boldsymbol{F} \otimes \boldsymbol{F} \rangle^\alpha$ of the deformation gradient field. This can be used to introduce in the expression of a fourth-order *phase fluctuation covariance tensor*

$$\mathbb{C}_{\boldsymbol{F}}^\alpha = \big\langle (\boldsymbol{F} - \bar{\boldsymbol{F}}_\alpha) \otimes (\boldsymbol{F} - \bar{\boldsymbol{F}}_\alpha) \big\rangle^\alpha = \big\langle \boldsymbol{F} \otimes \boldsymbol{F} \big\rangle^\alpha - \bar{\boldsymbol{F}}_\alpha \otimes \bar{\boldsymbol{F}}_\alpha . \tag{4.29}$$

Further details on field statistics were outlined by, for example, Bobeth & Diener [48], Kreher [263] or Idiart & Ponte Castañeda [239].

4.3 Scale transition and effective quantities

So far, separate mechanical problems have been defined on the micro- and the macroscale. The only connection between the micro- and the macroscopic problem was made in terms of the hypothesis of separation of length scales. However, the process of scale transition is the fundamental step of multiscale modelling. Thus, this section is concerned with the introduction of the important relations and principles for a proper scale transition between micro- and macroscopic quantities, which in particular affects the relevant deformation and stress measures. Subsequently, an extremum principle is introduced which gives the effective strain-energy on the macroscale in terms of the local strain-energies in the microstructure. Further note that in the process of scale transition, the upscaling of microscopic quantities to their macroscopic counterparts is called *homogenisation*, whereas going from larger to smaller scales is referred to as *localisation*, as depicted in Figure 4.1.

4.3.1 Micro-macro transition: Connecting the scales

The important step of scale transition is to connect the microscopic deformation and stress measures with their macroscopic counterparts. This means that the deformation and stress states at a macroscopic position $\bar{\boldsymbol{X}} \in \bar{\mathcal{B}}_0$ have to be linked to the associated deformation and stress fields in the underlying microstructure $\mathcal{B}_0$. In this context, it seems as an intuitive attempt to define a macroscopic quantity as the volume average of its microscopic counterpart over the $\mathscr{RVE}$. However, it has been pointed out in the seminal contribution of Hill [214] that this connection is not necessarily true and a macroscopic quantity rather has to be defined in terms of *surface* values on the boundary $\partial\mathcal{B}_0$ of the $\mathscr{RVE}$. It can be shown that the conjugate pair $\{\boldsymbol{F}, \boldsymbol{P}\}$ satisfies this requirement and, thus, that the deformation gradient and the first Piola–Kirchhoff stress represent the suitable deformation and stress measures in the context of scale transition. To see this more explicitly, we consider the volume average of the microscopic deformation gradient field $\boldsymbol{F} = \mathrm{Grad}[\boldsymbol{\chi}]$ and obtain

$$\big\langle \boldsymbol{F} \big\rangle = \frac{1}{\mathrm{vol}[\mathcal{B}_0]} \int_{\mathcal{B}_0} \mathrm{Grad}[\boldsymbol{\chi}] \, \mathrm{d}V = \frac{1}{\mathrm{vol}[\mathcal{B}_0]} \int_{\partial\mathcal{B}_0} \boldsymbol{\chi} \otimes \boldsymbol{N} \, \mathrm{d}A . \tag{4.30}$$

In the derivation of this result, we employed the integral theorem (A.24) to convert the volume into a surface integral, for which it is essential to require the continuity of $\boldsymbol{\chi}$ in

$\mathcal{B}_0$, as formulated in Eq. (4.16). We observe that the volume average of $\boldsymbol{F}$ over $\mathcal{B}_0$ is expressible in terms of the microscopic deformation field $\boldsymbol{\chi}$ on the boundary $\partial\mathcal{B}_0$. This allows to connect the macroscopic deformation gradient $\bar{\boldsymbol{F}}$ to the microscopic fields via[2]

$$\bar{\boldsymbol{F}} := \big\langle \boldsymbol{F} \big\rangle \,. \tag{4.31}$$

We emphasise that this is a special property of the deformation gradient and cannot be generalised to other deformation measures. For instance, we may recall the definition of the macroscopic right Cauchy strain from Eq. (4.4) and connect it with (4.31), which results in $\bar{\boldsymbol{C}} = (\langle \boldsymbol{F} \rangle)^T \langle \boldsymbol{F} \rangle \neq \langle \boldsymbol{F}^T \boldsymbol{F} \rangle = \langle \boldsymbol{C} \rangle$. Moreover, with Eqs (4.25), $(4.28)_1$ and (4.31), the macroscopic deformation gradient can be linked to the phase averages $\bar{\boldsymbol{F}}_\alpha$ via

$$\bar{\boldsymbol{F}} = \sum_\alpha n^\alpha \bar{\boldsymbol{F}}_\alpha \,, \tag{4.32}$$

which is referred to as the *overall average deformation condition*.

Subsequently, we formulate the micro-macro transition of the first Piola–Kirchhoff stress in the same spirit as for the deformation gradient. To do so, it makes sense to formulate the identity

$$\boldsymbol{P} = \boldsymbol{P}\,\mathrm{Grad}^T[\boldsymbol{X}] = \mathrm{Div}[(\boldsymbol{P} \otimes \boldsymbol{X})^{T_{23}}] - \mathrm{Div}[\boldsymbol{P}] \otimes \boldsymbol{X} \,, \tag{4.33}$$

for which we used $\boldsymbol{I} = \boldsymbol{I}^T = \mathrm{Grad}^T[\boldsymbol{X}]$ and the divergence theorem given in Eq. (A.23). By recalling the microscopic momentum balance (4.13), we observe that the last term in (4.33) vanishes in $\mathcal{B}_0$ and we obtain $\boldsymbol{P} = \mathrm{Div}[(\boldsymbol{P} \otimes \boldsymbol{X})^{T_{23}}]$ in $\mathcal{B}_0$. Based on this, we formulate the volume average of $\boldsymbol{P}$ over $\mathcal{B}_0$ and subsequently transform the volume into a surface integral by employing the integral theorem given in Eq. (A.27), hence

$$\begin{aligned} \big\langle \boldsymbol{P} \big\rangle &= \frac{1}{\mathrm{vol}[\mathcal{B}_0]} \int_{\mathcal{B}_0} \mathrm{Div}[(\boldsymbol{P} \otimes \boldsymbol{X})^{T_{23}}]\,\mathrm{d}V = \frac{1}{\mathrm{vol}[\mathcal{B}_0]} \int_{\partial\mathcal{B}_0} (\boldsymbol{P} \otimes \boldsymbol{X})^{T_{23}} \boldsymbol{N}\,\mathrm{d}A \\ &= \frac{1}{\mathrm{vol}[\mathcal{B}_0]} \int_{\partial\mathcal{B}_0} \boldsymbol{P}\boldsymbol{N} \otimes \boldsymbol{X}\,\mathrm{d}A = \frac{1}{\mathrm{vol}[\mathcal{B}_0]} \int_{\partial\mathcal{B}_0} \boldsymbol{T} \otimes \boldsymbol{X}\,\mathrm{d}A \,. \end{aligned} \tag{4.34}$$

In the derivation of this result, we further utilised the traction continuity condition (4.18). From (4.34), we observe that the volume average of $\boldsymbol{P}$ is expressible in terms of the averaged microscopic tractions $\boldsymbol{T}$ over the boundary $\partial\mathcal{B}_0$, which allows to define

$$\bar{\boldsymbol{P}} := \big\langle \boldsymbol{P} \big\rangle \tag{4.35}$$

as the consistent scale transition of the first Piola–Kirchhoff stress. For completeness, it is remarked that in the absence of traction continuity at interfaces $\Gamma_\mathcal{B}$ in $\mathcal{B}_0$ (that is, if Eq. (4.18) is not valid), the macroscopic stress $\bar{\boldsymbol{P}}$ is defined in terms of the surface integrals in (4.34), which for such a case will not be identical to the volume average.

[2]Note that the fundamental relationship (4.31) is only valid in the case of a continuous microscopic deformation field, as described by Eq. (4.16). In the presence of discontinuities in $\mathcal{B}_0$, the macroscopic deformation gradient $\bar{\boldsymbol{F}}$ is defined in terms of the surface integral from expression (4.30), which gives

$$\begin{aligned} \bar{\boldsymbol{F}} := \frac{1}{\mathrm{vol}[\mathcal{B}_0]} \int_{\partial\mathcal{B}_0} \boldsymbol{\chi} \otimes \boldsymbol{N}\,\mathrm{d}A &= \frac{1}{\mathrm{vol}[\mathcal{B}_0]} \int_{\mathcal{B}_0} \mathrm{Grad}[\boldsymbol{\chi}]\,\mathrm{d}V + \frac{1}{\mathrm{vol}[\mathcal{B}_0]} \int_{\Gamma_\mathcal{B}} [\![\boldsymbol{\chi}]\!] \otimes \boldsymbol{N}_\Gamma\,\mathrm{d}A \\ &= \big\langle \boldsymbol{F} \big\rangle + \frac{1}{\mathrm{vol}[\mathcal{B}_0]} \int_{\Gamma_\mathcal{B}} [\![\boldsymbol{\chi}]\!] \otimes \boldsymbol{N}_\Gamma\,\mathrm{d}A \,, \end{aligned}$$

see Schröder [421]. Hence, one has to proceed from an extended integral theorem and the volume average alone is then no longer suited as definition of the macroscopic deformation gradient.

4.3.2 The Hill macrohomogeneity condition

An essential requirement for the micro-macro scale transition is the fulfilment of the so-called *Hill macrohomogeneity condition*, which was formulated by Hill [214]. It states that the averaged microscopic incremental work in the $\mathscr{RVE}$ has to be equal to the local work increment at the macroscale. By utilising the work conjugate pair $\{\boldsymbol{F}, \boldsymbol{P}\}$, the Hill condition reads

$$\big\langle \boldsymbol{P} \cdot \delta \boldsymbol{F} \big\rangle = \bar{\boldsymbol{P}} \cdot \delta \bar{\boldsymbol{F}} \,, \tag{4.36}$$

where $\delta \boldsymbol{F}$ and $\delta \bar{\boldsymbol{F}}$ refer to deformation increments (or variations) on the micro- and the macroscale, respectively. Note, the Hill condition can alternatively be formulated in terms of micro- and macroscopic deformation rates, $\dot{\boldsymbol{F}}$ and $\dot{\bar{\boldsymbol{F}}}$, which entails a condition for the equivalence of micro- and macroscopic stress powers. Regardless of whether the Hill condition is formulated in terms of deformation increments or deformation rates, it can be utilised to derive boundary conditions on $\partial\mathcal{B}_0$ which close the microscopic boundary-value problem. To do so, the Hill condition, here given in the form (4.36), has to be formulated in terms of surface integrals over $\partial\mathcal{B}_0$. This is achieved by employing the integral theorems and thereon based reformulations from Section 4.3.1. Doing so, an identity for the term on the left hand side of Eq. (4.36) is found as

$$\big\langle \boldsymbol{P} \cdot \delta \boldsymbol{F} \big\rangle = \frac{1}{\mathrm{vol}[\mathcal{B}_0]} \int_{\partial\mathcal{B}_0} \boldsymbol{T} \cdot \delta \boldsymbol{\chi} \, \mathrm{d}A \,. \tag{4.37}$$

Further, three different identities are found for the right-hand side term:

$$\bar{\boldsymbol{P}} \cdot \delta \bar{\boldsymbol{F}} = \begin{cases} \bar{\boldsymbol{P}} \cdot \frac{1}{\mathrm{vol}[\mathcal{B}_0]} \int_{\partial\mathcal{B}_0} \delta \boldsymbol{\chi} \otimes \boldsymbol{N} \, \mathrm{d}A & = \frac{1}{\mathrm{vol}[\mathcal{B}_0]} \int_{\partial\mathcal{B}_0} \bar{\boldsymbol{P}} \boldsymbol{N} \cdot \delta \boldsymbol{\chi} \, \mathrm{d}A \\ \frac{1}{\mathrm{vol}[\mathcal{B}_0]} \int_{\partial\mathcal{B}_0} \boldsymbol{T} \otimes \boldsymbol{X} \, \mathrm{d}A \cdot \delta \bar{\boldsymbol{F}} & = \frac{1}{\mathrm{vol}[\mathcal{B}_0]} \int_{\partial\mathcal{B}_0} \boldsymbol{T} \cdot \delta \bar{\boldsymbol{F}} \boldsymbol{X} \, \mathrm{d}A \\ \bar{\boldsymbol{P}} \langle \mathrm{Grad}^T[\boldsymbol{X}] \rangle \cdot \delta \bar{\boldsymbol{F}} & = \frac{1}{\mathrm{vol}[\mathcal{B}_0]} \int_{\partial\mathcal{B}_0} \bar{\boldsymbol{P}} \boldsymbol{N} \cdot \delta \bar{\boldsymbol{F}} \boldsymbol{X} \, \mathrm{d}A \,. \end{cases} \tag{4.38}$$

The first identity makes use of Eqs (4.30) and (4.31), whereas the second identity employs Eqs (4.34) and (4.35). The third identity relies on $\boldsymbol{I} = \langle \mathrm{Grad}^T[\boldsymbol{X}] \rangle$ and $\mathrm{Div}[\bar{\boldsymbol{P}}] = \boldsymbol{0}$ in $\mathcal{B}_0$. Reformulating Eq. (4.36) by means of $\langle \boldsymbol{P} \cdot \delta \boldsymbol{F} \rangle - \bar{\boldsymbol{P}} \cdot \delta \bar{\boldsymbol{F}} - \bar{\boldsymbol{P}} \cdot \delta \bar{\boldsymbol{F}} + \bar{\boldsymbol{P}} \cdot \delta \bar{\boldsymbol{F}} = 0$ and inserting Eqs (4.37) and (4.38) yields, after some algebra,

$$\int_{\partial\mathcal{B}_0} (\boldsymbol{T} - \bar{\boldsymbol{P}} \boldsymbol{N}) \cdot (\delta \boldsymbol{\chi} - \delta \bar{\boldsymbol{F}} \boldsymbol{X}) \, \mathrm{d}A = 0 \tag{4.39}$$

see also Hill [215], Nemat-Nasser [351] or Schröder [421]. By setting either the first or the second bracket in (4.39) to zero, one directly derives Dirichlet- and Neumann-type boundary conditions:

$$\left.\begin{array}{rl} \text{affine boundary displacements:} & \boldsymbol{\chi} = \bar{\boldsymbol{F}} \boldsymbol{X} \\ \text{uniform boundary tractions:} & \boldsymbol{T} = \bar{\boldsymbol{P}} \boldsymbol{N} \end{array}\right\} \quad \forall \boldsymbol{X} \in \partial\mathcal{B}_0 \,. \tag{4.40}$$

The application of either of these two conditions on the boundary of the $\mathscr{RVE}$ satisfies the Hill condition (4.36) and completes the microscopic boundary-value problem. Further, note that from Eq. (4.39) a third type of so-called periodic boundary conditions can be derived. These are based on the decomposition of the boundary $\partial\mathcal{B}_0 = \partial\mathcal{B}_0^+ \cup \partial\mathcal{B}_0^-$ into

opposite faces, $\partial\mathcal{B}_0^+$ and $\partial\mathcal{B}_0^-$, and the application of periodic displacement fluctuations, $\tilde{\boldsymbol{\chi}}^+ = \tilde{\boldsymbol{\chi}}^-$, as well as anti-periodic tractions, $\boldsymbol{T}^+ = -\boldsymbol{T}^-$. In this context, the fluctuations $\tilde{\boldsymbol{\chi}}$ arise from an additive decomposition of microscopic quantities into a term that is uniform in the $\mathscr{RVE}$ and a fluctuation term, reading $(\cdot) = \langle(\cdot)\rangle + (\tilde{\cdot})$. Consequently,

$$\boldsymbol{\chi} = \langle\boldsymbol{\chi}\rangle + \tilde{\boldsymbol{\chi}} \quad \text{such that} \quad \boldsymbol{F} = \mathrm{Grad}[\boldsymbol{\chi}] = \bar{\boldsymbol{F}} + \tilde{\boldsymbol{F}} \quad \text{with} \quad \tilde{\boldsymbol{F}} = \mathrm{Grad}[\tilde{\boldsymbol{\chi}}]\,. \tag{4.41}$$

It is clear that the volume average of the fluctuation terms has to vanish, hence, $\langle\tilde{\boldsymbol{F}}\rangle = \boldsymbol{0}$.

4.3.3 Extremum principles for the effective energy

In the previous section, the evaluation of the Hill condition and the thereon based formulation of energetically consistent boundary conditions on $\partial\mathcal{B}_0$ complemented the equilibrium condition (4.13) in $\mathcal{B}_0$ and thus closed the microscopic boundary-value problem. With this, together with the explanations in Section 3.4, suitable extremum principles can be employed to obtain the microscopic deformation field in the $\mathscr{RVE}$ driven by the macroscopic deformation gradient $\bar{\boldsymbol{F}}$ and, in turn, the *effective energy* $\bar{\mathscr{W}}$ at a macroscopic point $\bar{\boldsymbol{X}} \in \bar{\mathcal{B}}_0$ as the volume average of the local energy field over the $\mathscr{RVE}$. To do so, we identify the elastic potential in the $\mathscr{RVE}$ as the volume average

$$\Pi(\boldsymbol{F}) = \big\langle \mathscr{W}(\boldsymbol{X}, \boldsymbol{F}) \big\rangle \quad \rightarrow \quad \min\,, \tag{4.42}$$

where, according to the principle of minimum potential energy introduced in Section 3.4.2, the local deformation gradient field in the $\mathscr{RVE}$ has to be such that Π in minimised. As a consequence, we define the effective energy $\bar{\mathscr{W}}$ by means of the variational functional

$$\bar{\mathscr{W}}(\bar{\boldsymbol{F}}) := \min_{\boldsymbol{F}\in\mathcal{K}(\bar{\boldsymbol{F}})} \Pi(\boldsymbol{F}) = \min_{\boldsymbol{F}\in\mathcal{K}(\bar{\boldsymbol{F}})} \Big\{ \big\langle \mathscr{W}(\boldsymbol{X}, \boldsymbol{F}) \big\rangle \Big\} = \min_{\boldsymbol{F}\in\mathcal{K}(\bar{\boldsymbol{F}})} \Big\{ \sum_\alpha n^\alpha \big\langle \mathscr{W}^\alpha(\boldsymbol{F}) \big\rangle^\alpha \Big\}\,. \tag{4.43}$$

Hence, the microscopic deformation gradient $\boldsymbol{F}$ becomes a trial field for the variational problem. It is subject to differential constraints by means of the set $\mathcal{K}(\bar{\boldsymbol{F}})$ of kinematically admissible deformation gradients, which is given by

$$\mathcal{K}(\bar{\boldsymbol{F}}) = \{\boldsymbol{F} \,|\, \exists\, \boldsymbol{\chi}(\boldsymbol{X}) \text{ with } \boldsymbol{F} = \mathrm{Grad}[\boldsymbol{\chi}(\boldsymbol{X})] \text{ in } \mathcal{B}_0 \text{ such that } \boldsymbol{\chi} = \bar{\boldsymbol{F}}\boldsymbol{X} \text{ on } \partial\mathcal{B}_0\} \tag{4.44}$$

and accounts for the affine displacement boundary conditions. Further, the last expression in Eq. (4.43) is obtained by employing Eq. (4.25) and noting from Eqs (4.11) and (4.9) that $\langle\mathscr{W}\rangle^\alpha = \langle\sum_\alpha \mathscr{X}^\alpha \mathscr{W}^\alpha\rangle^\alpha = \langle\mathscr{W}^\alpha\rangle^\alpha$. By looking at Eq. (4.43), we recognise that the computation of the effective energy $\bar{\mathscr{W}}(\bar{\boldsymbol{F}})$ contains two important steps: Firstly, the *localisation* of the deformation to obtain the microscopic deformation gradient field $\boldsymbol{F}(\boldsymbol{X})$ in $\mathcal{B}_0$, driven by the macroscopic deformation $\bar{\boldsymbol{F}}$ at $\bar{\mathcal{P}} \in \bar{\mathcal{B}}_0$, and secondly, the *homogenisation* of the microscopic local energy field $\mathscr{W}(\boldsymbol{X}, \boldsymbol{F})$ towards its counterpart $\bar{\mathscr{W}}$ on the macroscale. This highlights the two-way coupling of scale effects in multiscale problems. Moreover, it is remarked that alternatively to the deformation-driven scenario as it is described by the principle of minimum potential energy in Eq. (4.43), one can likewise formulate a *principle of minimum complementary energy* for the effective macroscopic Gibbs energy, which reads $\bar{\mathscr{U}}(\bar{\boldsymbol{P}}) = \min_{\boldsymbol{P}\in\mathcal{S}(\bar{\boldsymbol{P}})}\{\langle\mathscr{U}(\boldsymbol{X}, \boldsymbol{P})\rangle\}$. This constitutes a stress-driven scenario, as the set $\mathcal{S}(\bar{\boldsymbol{P}})$ of statically admissible stress fields essentially accounts

for the uniform traction boundary conditions, $\boldsymbol{T} = \bar{\boldsymbol{P}}\boldsymbol{N}$ on $\partial\mathcal{B}_0$. We note that the computation of an effective Gibbs energy $\bar{\mathscr{U}}(\bar{\boldsymbol{P}})$ makes most sense if the phases' behaviour is defined in terms of the respective microscopic Gibbs energy $\mathscr{U}(\boldsymbol{X}, \boldsymbol{P})$. In contrast, it is generally rather difficult to formulate a suitable homogenisation problem for $\bar{\mathscr{U}}$ if the microscale is described by means of $\mathscr{W}(\boldsymbol{X}, \boldsymbol{F})$. This is because, as elaborated in Section 3.6.3, the strain energy $\mathscr{W}$ is for finite deformations non-convex—and, for instance, polyconvex instead—and so there is no one-to-one relation between $\mathscr{W}$ and $\mathscr{U}$ in the sense of Eq. (3.121). Yet, in presence of convex $\mathscr{W}$ and under the separation of length scales hypothesis, described by Eq. (4.1), both the microscopic as well as the macroscopic Gibbs energy, $\mathscr{U}(\boldsymbol{X}, \boldsymbol{P})$ and $\bar{\mathscr{U}}(\bar{\boldsymbol{P}})$, are the complementary energies to $\mathscr{W}(\boldsymbol{X}, \boldsymbol{F})$ and $\bar{\mathscr{W}}(\bar{\boldsymbol{F}})$, respectively, and the connection is given through the Legendre transformation that provided in Eq. (3.121).

This section is concluded by two remarks. Firstly, the here presented variational principles for $\bar{\mathscr{W}}$ and $\bar{\mathscr{U}}$ equally hold for materials with random as well as periodic microstructures. However, in the latter case the sets $\mathcal{K}(\bar{\boldsymbol{F}})$ and $\mathcal{S}(\bar{\boldsymbol{P}})$ have to be formulated such that they account for the previously discussed periodic boundary conditions. This work focuses on materials with random microstructures and we refer to, for example, Bensoussan et al. [30], Moulinec & Suquet [345] and Miehe et al. [330] for further details about the periodic case. Secondly, it is noted that Eq. (4.43) applies to materials which are on the macroscale in line with the principle of local action, as discussed in Section 3.2.2. This means that it is sufficient to consider the deformation gradient $\bar{\boldsymbol{F}}$ in a deformation-driven scenario. The treatment of higher-order, gradient-extended materials requires further attention, as explained by, for example, Kouznetsova et al. [258].

4.3.4 Convergence and uniqueness of energy functionals

From a physical point of view, it is reasonable to postulate the existence of solutions for the variational problem given in Eq. (4.43) and, thus, that the heterogeneous material behaviour in the microstructure can be described by a homogenised energy functional $\bar{\mathscr{W}}$ on the macroscale. However, the associated mathematical problem of homogenisation is not trivial and requires careful treatment to show that the averages of the possibly highly fluctuating microscopic fields converge to the homogeneous macroscopic fields. The mathematics of this problem are far beyond the scope of this work and we a priori assume the existence of solutions for the variational problem in this work. Yet, we want to mention that a particularly useful concept for a rigorous mathematical treatment is the notation of Γ-convergence as proposed by De Giorgi [89], see also Dal Maso [88]. For further explanations, it is referred to the comprehensive overviews by Müller [348], Allaire [10], Braides & Defranceschi [59], and Schröder [421].

Next, we recall from Sections 3.4.1 and 3.4.2 that a first attempt in finding minimum solutions of a variational problem, such as the one for $\bar{\mathscr{W}}$ in (4.43), is to find a value for which the variational statement becomes stationary. Hence, it makes sense to define the effective energy

$$\widetilde{\bar{\mathscr{W}}}(\bar{\boldsymbol{F}}) := \underset{\boldsymbol{F}\in\mathcal{K}(\bar{\boldsymbol{F}})}{\operatorname{stat}} \Pi(\boldsymbol{F}) = \underset{\boldsymbol{F}\in\mathcal{K}(\bar{\boldsymbol{F}})}{\operatorname{stat}} \Big\{ \big\langle \mathscr{W}(\boldsymbol{X}, \boldsymbol{F}) \big\rangle \Big\} = \underset{\boldsymbol{F}\in\mathcal{K}(\bar{\boldsymbol{F}})}{\operatorname{stat}} \Big\{ \sum_{\alpha} n^{\alpha} \big\langle \mathscr{W}^{\alpha}(\boldsymbol{F}) \big\rangle^{\alpha} \Big\} \tag{4.45}$$

by means of a stationary variational principle. Yet, it was pointed out in Section 3.6.3 that problems in nonlinear elasticity are non-convex in nature which means that the solution

of the stationary problem for $\widetilde{\mathscr{W}}$ is generally non-unique for finite deformations. More specifically, for small deformations $\bar{\boldsymbol{F}} \approx \boldsymbol{I}$ around the reference configuration, the energy $\widetilde{\mathscr{W}}$ is unique and depicts a minimiser, such that $\widetilde{\mathscr{W}} = \bar{\mathscr{W}}$. However, as the deformation increases, the material may reach points at which the solution bifurcates into different branches associated with different energy levels. Beyond such *bifurcation points*, an equilibrium solution of the stationary problem (4.45) is not necessarily a minimiser. This means that the energy $\bar{\mathscr{W}}$ based on Eq. (4.45) is generally lower or equal to the energy $\widetilde{\mathscr{W}}$, such that $\bar{\mathscr{W}} \leq \widetilde{\mathscr{W}}$. The bifurcation points can be understood as the *onset of instabilities*, which may be associated with phenomena such as buckling or failure of the material. Those instabilities can develop at various wavelengths of the material, as explained in the seminal works of Triantafyllidis & Maker [485] and Geymonat et al. [160]. In particular, one distinguishes between short-wavelength and long-wavelength instabilities, which may appear on the microscopic and macroscopic length scale, respectively. In the context of periodic microstructures, the onset of both of these instability types and how they possibly interact was studied by, for example, Miehe et al. [331], Michel et al. [325, 326] and Slesarenko & Rudykh [445]. For materials with random microstructures, which are the focus of this work, the detection of short-wavelength (microscopic) instabilities is a much harder task than for periodic microstructures. Yet, it is not even clear whether random microstructures can accommodate microscopic instabilities at all, because the missing periodicity in the microstructure may prevent the formation of such, as explained by Lopez-Pamies & Ponte Castañeda [299] and Michel et al. [325, 326]. Furthermore, Geymonat et al. [160] pointed out that the first bifurcation point is usually associated with a long-wavelength instability. This is very convenient as the detection of the onset of such macroscopic instabilities is an easier task because they can be determined by appropriate investigations of the effective potential $\widetilde{\mathscr{W}}$, following the explanations made in Section 3.6.3. In particular, the onset of the first bifurcation point is indicated by the loss of strong ellipticity of the macroscopic material response and can thus be traced by checking the positive semidefiniteness of the macroscopic acoustic tensor

$$\widetilde{\mathscr{A}} = (\widetilde{\mathbb{L}}^{T_{23}}\boldsymbol{\zeta})\boldsymbol{\zeta}\,, \quad \text{where} \quad \widetilde{\mathbb{L}} = \partial^2_{\bar{\boldsymbol{F}}\bar{\boldsymbol{F}}}\widetilde{\mathscr{W}} \tag{4.46}$$

is the fourth-order elasticity tensor associated with the effective macroscopic potential $\widetilde{\mathscr{W}}$. Expression $(4.46)_1$ directly follows from the definition of the acoustic tensor in Eq. (3.119). In conclusion, it suffices for *pre-bifurcation* investigations to consider the effective energy $\widetilde{\mathscr{W}}$ obtained from the stationary principle (4.45), since $\widetilde{\mathscr{W}}$ depicts a minimiser in the sense of the minimum principle (4.43), such that $\widetilde{\mathscr{W}} = \bar{\mathscr{W}}$, until the onset of the first bifurcation point. In turn, this can still be detected by the loss of rank-one convexity (strong ellipticity) of $\widetilde{\mathscr{W}}$. This was studied, for example, by Agoras et al. [5] for materials with fibrous microstructure. The pre-bifurcation behaviour of fibre composites will be the focus in Chapter 5. For completeness, we refer to Miehe et al. [331], Avazmohammadi & Ponte Castañeda [21] and Furer & Ponte Castañeda [148] for detailed studies on the respective post-bifurcation behaviour of such materials.

4.3.5 Uniform microscopic fields: Voigt- and Reuss-type bounds

The deformation and stress fields in the microstructure (the $\mathscr{RVE}$) are generally non-uniform and highly dependent on the microscopic location $\boldsymbol{X}$, which is a direct consequence

of the heterogeneous distribution of the phases (as defined by the characteristic functions $\mathscr{X}^\alpha$) and the associated non-uniform distribution of material properties. More specifically, as the microscopic deformation gradient field $\boldsymbol{F}(\boldsymbol{X})$ was identified in Section 4.3.3 as the deformation which minimises the averaged energy $\Pi(\boldsymbol{F})$ in the $\mathscr{RVE}$, as stated by Eq. (4.43), we have

$$\boldsymbol{F}(\boldsymbol{X}) = \arg \min_{\boldsymbol{F} \in \mathcal{K}(\bar{\boldsymbol{F}})} \left\{ \left\langle \mathscr{W}(\boldsymbol{X}, \boldsymbol{F}) \right\rangle \right\} . \tag{4.47}$$

Of course, with the explanations from the previous section, $\boldsymbol{F}(\boldsymbol{X})$ can in the pre-bifurcation regime be equivalently obtained from the stationary principle (4.45). Now, we note that while it is undoubtedly meaningful from a physical point of view to expect an energy relaxation by means of the variational principles (4.43) or (4.45) and associated heterogeneous deformations in the microstructure, the Hill macrohomogeneity condition given in Eq. (4.36) can also be satisfied by making certain *affinity assumptions* for the microscopic fields. This is easy to see by utilising the Hill condition in its surface integral form (4.39) and the boundary conditions (4.40) derived from it. Then, the assumption of uniform deformations in the $\mathscr{RVE}$ results in

$$\boldsymbol{F}(\boldsymbol{X}) = \bar{\boldsymbol{F}} \quad \rightarrow \quad \bar{\mathscr{W}}_{\mathrm{V}}(\bar{\boldsymbol{F}}) = \sum_{\alpha} n^\alpha \, \mathscr{W}^\alpha(\bar{\boldsymbol{F}}) \, , \tag{4.48}$$

where the *Voigt estimate* $\bar{\mathscr{W}}_{\mathrm{V}}$ is identified as a simple weighted averaging of the phase energies $\mathscr{W}^\alpha$ evaluated at the macroscopic deformation $\bar{\boldsymbol{F}}$. Hence, the Voigt estimate accounts for the microstructural morphology only through the volume fractions n^α, which depict the first moments of the characteristic functions $\mathscr{X}^\alpha$, see Eq. (4.23). The assumption of a uniform deformation field, which is also called *affine deformation assumption* or *Voigt assumption*, is usually referred to the seminal work of Voigt [495]. It is interesting to note that the Voigt assumption, as stated in Eq. $(4.48)_1$, is not only consistent with the affine boundary displacements formulated in (4.40), and thus with the Hill condition (4.36), but also with the geometrical compatibility conditions (4.16) and (4.17) (with jump amplitude $\boldsymbol{c} = \boldsymbol{0}$). However, the Voigt assumption is generally not consistent with the statical compatibility condition (4.18) and is thus unable to satisfy traction continuity across interface boundaries. The missing ability to guarantee equilibrium in $\mathcal{B}_0$ has the consequence that $\bar{\mathscr{W}}_{\mathrm{V}}$ generally overestimates the real occurring elastic energy in the $\mathscr{RVE}$. In fact, Ogden [360] showed that the Voigt estimate depicts a rigorous *upper bound* for the effective macroscopic behaviour of materials whose characteristic functions $\mathscr{X}^\alpha$ have first moments (volume fractions) n^α. This means that despite its simplicity, the Voigt *bound* serves as a valuable tool, be it as first guess or validity check for more sophisticated homogenisation approaches. Moreover, the Voigt bound may predict the energy in the $\mathscr{RVE}$ exactly if the uniformity of the deformation field holds true. This is the case for some specific loading conditions and materials classes, as shown by Dvorak [103] and He et al. [191]. Further, it may be useful to proceed with the Voigt estimate if reasonable physical arguments suggest that the deformation in a microstructure behaves nearly uniform. Such an assumption is applied in Chapter 6 for the modelling of fibrous networks and in Chapter 7 for the presented multiscale muscle model.

Instead of assuming an affine microscopic deformation field, it is also possible to apply a respective affinity assumption for the microscopic stress fields so that $\boldsymbol{P}(\boldsymbol{X}) = \bar{\boldsymbol{P}}$. This is commonly referred to as *Reuss assumption*, in reference to the work of Reuss [398]. The

assumption of uniform stresses in the $\mathscr{RVE}$ is consistent with the uniform stress boundary conditions in (4.40) and thus with the Hill condition (4.36). Further, opposed to the Voigt assumption, stress affinity is consistent with the statical compatibility condition (4.18), but generally not with the geometrical compatibility conditions (4.16) and (4.17). If the phase's behaviour is described in terms of Gibbs energies $\mathscr{U}^\alpha(\boldsymbol{P})$, stress affinity directly leads to an expression for the effective Gibbs energy $\bar{\mathscr{U}}_\mathrm{R}$ that reads

$$\boldsymbol{P}(\boldsymbol{X}) = \bar{\boldsymbol{P}} \quad \rightarrow \quad \bar{\mathscr{U}}_\mathrm{R}(\bar{\boldsymbol{P}}) = \sum_\alpha n^\alpha \, \mathscr{U}^\alpha(\bar{\boldsymbol{P}}) \,. \tag{4.49}$$

Ogden [360] showed that a rigorous *lower bound* $\bar{\mathscr{W}}_\mathrm{R}$ for the effective strain energy is obtained by means of a Legendre transform of $\bar{\mathscr{U}}_\mathrm{R}$ if the microscale is described in terms of a convex strain energy $\mathscr{W}$—such that $\mathscr{U}^\alpha$ in Eq. (4.49) can be uniquely determined from $\mathscr{W}^\alpha$ by means of Eq. (3.121). However, we have noted before that convexity of the strain energy $\mathscr{W}$ in the context of hyperelastic large-strains problems is unphysical, see Section 3.6.3. Thus, there is not necessarily a one-to-one connection between $\boldsymbol{F}$ and $\boldsymbol{P}$ and, consequently, no unique relation between $\mathscr{W}$ and $\mathscr{U}$ in the sense of the Legendre transformation formulated in Eq. (3.121). Yet, it is possible to enforce uniqueness by employing instead a Legendre-Fenchel transformation, as defined in Eq. (B.2), which consequently replaces the stationary operator in Eq. (3.121) by the supremum. See also Section B.1 for further details on the different transformations. A Reuss-type lower bound is then derived in terms of the *convex envelope*

$$\bar{\mathscr{W}}_\mathrm{R}(\bar{\boldsymbol{F}}) = \sup_{\bar{\boldsymbol{P}}} \{ \bar{\boldsymbol{F}} \cdot \bar{\boldsymbol{P}} - \bar{\mathscr{U}}_\mathrm{R}(\bar{\boldsymbol{P}}) \} \quad \text{with} \quad \bar{\mathscr{U}}_\mathrm{R} = \sum_\alpha \left[n^\alpha \sup_{\boldsymbol{F}} \{ \boldsymbol{F} \cdot \boldsymbol{P} - \mathscr{W}^\alpha(\boldsymbol{F}) \} \right] . \tag{4.50}$$

Unfortunately, for non-convex (such as polyconvex) energy functions $\mathscr{W}$, this bound is not always useful and can lead to trivial results, since, for example, $\mathrm{cof}[\boldsymbol{F}]$ and $\mathrm{def}[\boldsymbol{F}]$ are non-convex in $\boldsymbol{F}$ and corresponding energy terms lead to trivial Legendre-Fenchel transforms with respect to $\boldsymbol{F}$. As a remedy, Ponte Castañeda [373] proposed to employ a *polyconvex envelope*, which results in a sensible lower Reuss-type bound that is generally tighter than the bound based on the convex envelope in (4.50). More detailed explanations are omitted here, as Reuss-type bounds are not used in this work. Yet, for more details on polyconvex (as well as convex, quasiconvex, and rank-one convex) envelopes, we refer to the works of, for example, Dacorogna [86, 87] and Kohn & Strang [255].

By summarising the findings in this and the previous section, we can formulate the inequality

$$\bar{\mathscr{W}}_\mathrm{R} \leq \bar{\mathscr{W}} \leq \widetilde{\mathscr{W}} \leq \bar{\mathscr{W}}_\mathrm{V} \,, \tag{4.51}$$

where $\bar{\mathscr{W}}_\mathrm{R}$ refers to a lower Reuss-type bound that is suitably selected depending on the problem at hand. We recall that in the present work, the focus on the pre-bifurcation regime leads to the equality of $\bar{\mathscr{W}}$ and $\widetilde{\mathscr{W}}$. Further, we remark that the Voigt and Reuss bounds are also well-known as Taylor and Sachs bounds, by referring to the works of Taylor [475] and Sachs [412].

5 Variational Homogenisation of Nonlinear Composites

In this chapter, we present *estimates* for the effective strain energy $\widetilde{\mathscr{W}}$ of a hyperelastic composite in the pre-bifurcation state. The proposed homogenisation is based on the *tangent second-order* method, which utilises variational principles and a suitably chosen "linear comparison material". This enables to employ well-known homogenisation methods for linear materials, like Hashin–Shrikhman-methods, to provide estimates for effective strain energies of nonlinear materials. The homogenisation principles in this chapter are generally applicable to n-phase materials, but we put a particularly emphasis on two-phase composites in which a matrix phase contains aligned circular fibres, which are randomly distributed within the transverse plane. Further, as the estimate shall be applicable for biological tissues, appropriate derivations are made to obtain consistent estimates in the limit as the two phases become incompressible.

Note that parts of this chapter have been published in Bleiler et al. [45].

5.1 The Tangent Second-Order Method

This section introduces the *tangent second-order* (TSO) homogenisation method, which was proposed by Ponte Castañeda & Tiberio [382] and enables to generate estimates for the variational homogenisation problem as defined in Eq. (4.45). The main idea of the TSO method is to appropriately linearise the actual nonlinear composite in order to obtain expressions for which the well-established homogenisation methods for linear material behaviour can be used. To do so, the TSO method is based on the construction of a fictitious *linear comparison composite* ($\mathcal{LCC}$) with the same microstructure (hence, the same characteristic functions $\mathscr{X}^\alpha$) as the actual nonlinear composite (in the undeformed configuration). The linear behaviour of the phases of the $\mathcal{LCC}$ is determined from suitable variational principles such that it represents the appropriate linearisation of the actual nonlinear phases. Further details on the TSO method can also be found in Ponte Castañeda [376], Ponte Castañeda & Willis [384], Ponte Castañeda & Tiberio [382], and Avazmohammadi & Ponte Castañeda [19].

The $\mathcal{LCC}$ is characterised by its local strain-energy function

$$\mathscr{W}_{\text{lin}}(\boldsymbol{X},\boldsymbol{F}) = \sum_\alpha \mathscr{X}^\alpha(\boldsymbol{X})\,\mathscr{W}^\alpha_{\text{lin}}(\boldsymbol{F})\,, \quad \text{with} \quad \mathscr{W}^\alpha_{\text{lin}}(\boldsymbol{F}) = \tfrac{1}{2}\,\boldsymbol{F}\cdot\mathbb{L}^\alpha_{\text{lin}}\boldsymbol{F} \tag{5.1}$$

and the phasewise constant fourth-order modulus tensors $\mathbb{L}^\alpha_{\text{lin}}$, as opposed to the nonlinear local energy $\mathscr{W}(\boldsymbol{X},\boldsymbol{F})$ defined in Eq. (4.11). The aim is now to find an $\mathcal{LCC}$ that optimally represents the actual nonlinear composite. For this purpose, it is useful to define the difference energy function $(\mathscr{W}-\mathscr{W}_{\text{lin}})(\boldsymbol{X},\boldsymbol{F})$ and its respective generalised Legendre transform

$$(\mathscr{W}-\mathscr{W}_{\text{lin}})^*(\boldsymbol{X},\boldsymbol{\mathfrak{P}}) = \operatorname*{stat}_{\boldsymbol{F}}\big\{\boldsymbol{\mathfrak{P}}\cdot\boldsymbol{F} - \mathscr{W}(\boldsymbol{X},\boldsymbol{F}) + \mathscr{W}_{\text{lin}}(\boldsymbol{X},\boldsymbol{F})\big\}\,, \tag{5.2}$$

where $\boldsymbol{\mathfrak{P}}\in\mathcal{R}^{3\otimes3}$ is a generally non-symmetric polarisation tensor and the energy function $\mathscr{W}$ is assumed to be sufficiently smooth in $\boldsymbol{F}$. More details on the Legendre transform and

especially the employed generalised form can be found in Appendix B.1. From there, we further know that the generalised Legendre transform $(\cdot)^{**}$ of the complementary function $(\cdot)^{*}$ is always the original function $(\cdot)$, which allows us to write the local energy of the actual nonlinear composite as

$$\mathscr{W}(\boldsymbol{X},\boldsymbol{F}) = \mathscr{W}_{\text{lin}}(\boldsymbol{X},\boldsymbol{F}) + \operatorname*{stat}_{\boldsymbol{\mathfrak{P}}}\big\{\boldsymbol{\mathfrak{P}}\cdot\boldsymbol{F} - (\mathscr{W}-\mathscr{W}_{\text{lin}})^{*}(\boldsymbol{X},\boldsymbol{\mathfrak{P}})\big\}\,. \tag{5.3}$$

The stationarity conditions of the Legendre transformations in Eqs (5.2) and (5.3) are given by

$$\boldsymbol{\mathfrak{P}} = \partial_{\boldsymbol{F}}(\mathscr{W}-\mathscr{W}_{\text{lin}})(\boldsymbol{X},\boldsymbol{F}) \quad\text{and}\quad \boldsymbol{F} = \partial_{\boldsymbol{\mathfrak{P}}}(\mathscr{W}-\mathscr{W}_{\text{lin}})^{*}(\boldsymbol{X},\boldsymbol{\mathfrak{P}})\,, \tag{5.4}$$

respectively. The local energy function (5.3) in connection with Eq. (4.45) can now be used to generate an expression for the overall energy $\widetilde{\mathscr{W}}$, which—after interchanging the stationarity operations—reads

$$\widetilde{\mathscr{W}}(\bar{\boldsymbol{F}}) = \operatorname*{stat}_{\boldsymbol{\mathfrak{P}}}\Big\{\operatorname*{stat}_{\boldsymbol{F}\in\mathcal{K}(\bar{\boldsymbol{F}})}\big\{\big\langle\mathscr{W}_{\text{lin}}(\boldsymbol{X},\boldsymbol{F}) + \boldsymbol{\mathfrak{P}}\cdot\boldsymbol{F}\big\rangle\big\} - \big\langle(\mathscr{W}-\mathscr{W}_{\text{lin}})^{*}(\boldsymbol{X},\boldsymbol{\mathfrak{P}})\big\rangle\Big\}\,. \tag{5.5}$$

This formulation is an *exact* variational statement for the effective strain energy $\widetilde{\mathscr{W}}$ of a nonlinear composite. However, different to the nonlinear expression given in Eq. (4.45), the stationary problem for $\boldsymbol{F}$ in Eq. (5.5) is linear. Further, the polarisation tensor $\boldsymbol{\mathfrak{P}}$ has the character of a trial field for the variational problem. This is advantageous since $\boldsymbol{\mathfrak{P}}$ is not subject to any differential constraints, as opposed to $\boldsymbol{F}$ in the original formulation (4.45).

To generate *estimates* for the variational problem given by (5.5), an appropriate non-trivial choice is to assume that the polarisation tensor is phasewise constant:

$$\boldsymbol{\mathfrak{P}}(\boldsymbol{X}) = \sum_{\alpha}\mathscr{X}^{\alpha}(\boldsymbol{X})\,\boldsymbol{\mathfrak{P}}^{\alpha}\,. \tag{5.6}$$

Inserting Eq. (5.6) into Eq. (5.5) yields the *variational estimate*

$$\widetilde{\mathscr{W}}(\bar{\boldsymbol{F}}) \approx \operatorname*{stat}_{\boldsymbol{\mathfrak{P}}^{\alpha}}\Big\{\widetilde{\mathscr{W}_{\text{T}}}(\bar{\boldsymbol{F}},\boldsymbol{\mathfrak{P}}) - \sum_{\alpha} n^{\alpha}\,(\mathscr{W}-\mathscr{W}_{\text{lin}})^{*}(\boldsymbol{\mathfrak{P}}^{\alpha})\Big\}\,, \tag{5.7}$$

which is an *approximation* of the variational expression given in (5.5). Although the following relations for $\widetilde{\mathscr{W}}$ are formulated as standard equalities, we need to keep in mind the approximate character. In Eq. (5.7), the term $\widetilde{\mathscr{W}_{\text{T}}}$ is defined as

$$\widetilde{\mathscr{W}_{\text{T}}}(\bar{\boldsymbol{F}},\boldsymbol{\mathfrak{P}}) = \operatorname*{stat}_{\boldsymbol{F}\in\mathcal{K}(\bar{\boldsymbol{F}})}\Big\{\big\langle\mathscr{W}_{\text{lin}}(\boldsymbol{X},\boldsymbol{F}) + \boldsymbol{\mathfrak{P}}\cdot\boldsymbol{F}\big\rangle\Big\}\,, \tag{5.8}$$

which depicts the effective energy associated with a *fictitious linear thermoelastic* (or *prestressed*) material. Now, it proves useful to introduce the (phasewise) constant second-order tensors $\boldsymbol{\mathfrak{F}}_{\alpha}$ dual to $\boldsymbol{\mathfrak{P}}^{\alpha}$, and to reformulate the polarisation tensors $\boldsymbol{\mathfrak{P}}^{\alpha}$ by using the stationarity condition $(5.4)_1$ in terms of phase $\mathcal{B}_0^{\alpha}$, giving

$$\boldsymbol{\mathfrak{P}}^{\alpha} = \boldsymbol{P}^{\alpha} - \mathbb{L}^{\alpha}_{\text{lin}}\boldsymbol{\mathfrak{F}}_{\alpha} \quad\text{with}\quad \boldsymbol{P}^{\alpha} = \partial_{\boldsymbol{F}}\mathscr{W}^{\alpha}(\boldsymbol{\mathfrak{F}}_{\alpha})\,. \tag{5.9}$$

Further, by making use of Eq. (5.2) in terms of phase $\mathcal{B}_0^{\alpha}$ and assuming the stationary solution

$$\boldsymbol{\mathfrak{F}}_{\alpha} = \arg\operatorname*{stat}_{\boldsymbol{F}}\big\{\boldsymbol{\mathfrak{P}}^{\alpha}\cdot\boldsymbol{F} - \mathscr{W}^{\alpha}(\boldsymbol{F}) + \mathscr{W}^{\alpha}_{\text{lin}}(\boldsymbol{F})\big\}\,, \tag{5.10}$$

one obtains

$$(\mathscr{W}^\alpha - \mathscr{W}^\alpha_{\text{lin}})^* (\mathfrak{P}^\alpha) = \boldsymbol{P}^\alpha \cdot \mathfrak{F}_\alpha - \mathscr{W}^\alpha(\mathfrak{F}_\alpha) - \tfrac{1}{2}\mathfrak{F}_\alpha \cdot \mathbb{L}^\alpha_{\text{lin}} \mathfrak{F}_\alpha \,. \tag{5.11}$$

Inserting relations $(5.9)_1$, and (5.11) into the variational expression (5.7) leads to the expression

$$\widetilde{\mathscr{W}}(\bar{\boldsymbol{F}}) = \operatorname*{stat}_{\mathfrak{F}_\alpha} \Big\{ \sum_\alpha n^\alpha \big[\mathscr{W}^\alpha(\mathfrak{F}_\alpha) + \boldsymbol{P}^\alpha \cdot \big\langle \boldsymbol{F} - \mathfrak{F}_\alpha \big\rangle^\alpha + \tfrac{1}{2} \big\langle (\boldsymbol{F} - \mathfrak{F}_\alpha) \cdot \mathbb{L}^\alpha_{\text{lin}} (\boldsymbol{F} - \mathfrak{F}_\alpha) \big\rangle^\alpha \big] \Big\} \,. \tag{5.12}$$

Following Ponte Castañeda & Willis [384] and Ponte Castañeda & Tiberio [382], the evaluation of the stationarity condition in this expression finally leads to the relation

$$\mathfrak{F}_\alpha = \big\langle \boldsymbol{F} \big\rangle^\alpha = \bar{\boldsymbol{F}}_\alpha \,. \tag{5.13}$$

Hence, the variables $\mathfrak{F}_\alpha$ have to be set equal to the phase averages $\bar{\boldsymbol{F}}_\alpha$ of the deformation gradient field associated with the linear problem in Eq. (5.8). Furthermore, evaluating a second-order stationarity condition for Eq. (5.12) by considering the second derivative with respect to $\mathfrak{F}_\alpha$, we can deduce the relation

$$\mathbb{L}^\alpha_{\text{lin}} = \mathbb{L}^\alpha_{\text{t}} \quad \text{with} \quad \mathbb{L}^\alpha_{\text{t}} := \mathbb{L}^\alpha = \partial^2_{\boldsymbol{F}\boldsymbol{F}} \mathscr{W}^\alpha(\bar{\boldsymbol{F}}_\alpha) \,, \tag{5.14}$$

stating that the constant tensors $\mathbb{L}^\alpha_{\text{lin}}$ are chosen equal to the *tangent elasticity tensors* $\mathbb{L}^\alpha_{\text{t}}$ of the hyperelastic phases. Using prescription (5.13) in (5.12) and after some algebra, it can be shown that the *estimate* for the effective nonlinear energy can be reformulated to

$$\widetilde{\mathscr{W}}(\bar{\boldsymbol{F}}) = \sum_\alpha n^\alpha \big[\mathscr{W}^\alpha(\bar{\boldsymbol{F}}_\alpha) + \tfrac{1}{2} (\bar{\boldsymbol{F}} - \bar{\boldsymbol{F}}_\alpha) \cdot \boldsymbol{P}^\alpha(\bar{\boldsymbol{F}}_\alpha) \big] \,, \tag{5.15}$$

see Ponte Castañeda & Tiberio [382] for details. Thus, the estimate for the effective behaviour of the nonlinear composite is fully specified in terms of the tensors $\bar{\boldsymbol{F}}_\alpha$, which represent the phase averages in the $\mathcal{LCC}$ associated with the linear thermoelastic problem given in Eq. (5.8). In turn, the phase averages can be obtained from appropriate *linear homogenisation methods*. To do so, given the linearity of the problem, the superposition principle can be utilised in order to express the phase averages in the form

$$\bar{\boldsymbol{F}}_\alpha = \mathbb{A}^\alpha \bar{\boldsymbol{F}} + \boldsymbol{A}^\alpha \,, \tag{5.16}$$

in accordance to the expressions given by Laws [278]. Therein, the fourth-order tensors $\mathbb{A}^\alpha$ are the *strain concentration tensors* of the phases, introduced by Hill [210, 212], and the second-order tensors $\boldsymbol{A}^\alpha$ account for the thermoelastic nature of problem (5.8). The tensors have to satisfy the summation rules

$$\sum_\alpha n^\alpha \mathbb{A}^\alpha = \mathbb{I} \quad \text{and} \quad \sum_\alpha n^\alpha \boldsymbol{A}^\alpha = \boldsymbol{0} \,. \tag{5.17}$$

Subsequently, the tensors $\mathbb{A}^\alpha$ and $\boldsymbol{A}^\alpha$ are determined by applying suitable linear homogenisation approaches. Appropriate formulations and more details can be found, for example, in the works of Laws [278] and Willis [517]. In particular, generalised Hashin–Shtrikman estimates lead to prescriptions for $\mathbb{A}^\alpha$ and $\boldsymbol{A}^\alpha$ as given by Eqs *(29)-(33)* in Ponte Castañeda & Tiberio [382], whereas self-consistent estimates are obtained from Eqs *(3.13)-(3.15)* given in Bornert & Ponte Castañeda [56]. In this work, the focus on two-phase materials allows to employ simplified equations for the estimation of the phase averages, which is shown in the following. Moreover, we remark for completeness that the effective first Piola–Kirchhoff stress $\widetilde{\boldsymbol{P}} = \partial_{\bar{\boldsymbol{F}}} \widetilde{\mathscr{W}}$ associated with the macroscopic energy (5.15) is given in Eq. (C.1) in Appendix C.1, along with some further comments.

5.1.1 Specialisation to two-phase materials

We now restrict our attention to two-phase materials containing a matrix phase, $\mathcal{B}_0^{\mathrm{M}}$, and a fibre (inclusion) phase, $\mathcal{B}_0^{\mathrm{F}}$, such that $\alpha = \{\mathrm{F}, \mathrm{M}\}$. It follows that we require an appropriate set of equations for the estimation of the 18 unknown scalar coefficients of the two phase averages $\bar{\boldsymbol{F}}_{\mathrm{F}}$ and $\bar{\boldsymbol{F}}_{\mathrm{M}}$ to compute the effective energy in Eq. (5.15). In this regard, we first note that the overall average condition for the deformation gradient, given in Eq. (4.32), simplifies for the given two-phase material to

$$\bar{\boldsymbol{F}} = n^{\mathrm{F}}\, \bar{\boldsymbol{F}}_{\mathrm{F}} + n^{\mathrm{M}}\, \bar{\boldsymbol{F}}_{\mathrm{M}}\,. \tag{5.18}$$

Hence, as the overall deformation gradient $\bar{\boldsymbol{F}}$ is prescribed, one of the phase average tensors can be written in terms of the other one and the two-phase homogenisation problem reduces to finding the remaining nine scalar coefficients of either $\bar{\boldsymbol{F}}_{\mathrm{F}}$ or $\bar{\boldsymbol{F}}_{\mathrm{M}}$. Further, the focus on two-phase materials allows to utilise an appropriate extension of the work of Levin [283] and to formulate the phase averages from Eq. (5.16) as

$$\bar{\boldsymbol{F}}_\alpha = \mathbb{A}^\alpha \bar{\boldsymbol{F}} + (\mathbb{A}^\alpha - \mathbb{I})(\mathbb{L}^{\mathrm{M}} - \mathbb{L}^{\mathrm{F}})^{-1}(\mathfrak{P}^{\mathrm{M}} - \mathfrak{P}^{\mathrm{F}}) \tag{5.19}$$

for $\alpha = \{\mathrm{F}, \mathrm{M}\}$. Therein, the polarisation tensors $\mathfrak{P}^{\mathrm{F}}$ and $\mathfrak{P}^{\mathrm{M}}$ are defined by Eq. (5.9), along with prescriptions (5.13) and (5.14). Further, the two strain concentration tensors $\mathbb{A}^{\mathrm{F}}$ and $\mathbb{A}^{\mathrm{M}}$ are connected through the relations

$$n^{\mathrm{F}}\, \mathbb{A}^{\mathrm{F}} + n^{\mathrm{M}}\, \mathbb{A}^{\mathrm{M}} = \mathbb{I} \quad \text{and} \quad \bar{\mathbb{L}}_{\mathrm{lin}} = n^{\mathrm{F}}\, \mathbb{L}^{\mathrm{F}} \mathbb{A}^{\mathrm{F}} + n^{\mathrm{M}}\, \mathbb{L}^{\mathrm{M}} \mathbb{A}^{\mathrm{M}}\,, \tag{5.20}$$

where the first equation is the respective two-phase version of Eq. $(5.17)_1$. The benefit of relations (5.19) and (5.20) is that they reduce the thermoelastic homogenisation problem for the $\mathcal{LCC}$, given in Eq. (5.8), to finding the effective elasticity tensor $\bar{\mathbb{L}}_{\mathrm{lin}}$ of a two-phase linear-elastic composite with phase stiffness tensors $\mathbb{L}^{\mathrm{F}}$ and $\mathbb{L}^{\mathrm{M}}$. This becomes more clear by formulating Eq. (5.19) for the phase average of the fibre phase, $\bar{\boldsymbol{F}}_{\mathrm{F}}$, and replacing therein the strain concentration $\mathbb{A}^{\mathrm{F}}$ by making use of Eqs (5.20). This leads to the formulation

$$\bar{\boldsymbol{F}} - \bar{\boldsymbol{F}}_{\mathrm{F}} = \left[n^{\mathrm{F}}(\bar{\mathbb{L}}_{\mathrm{lin}} - \mathbb{L}^{\mathrm{M}})^{-1} + (\mathbb{L}^{\mathrm{M}} - \mathbb{L}^{\mathrm{F}})^{-1}\right]\left[\mathbb{L}^{\mathrm{M}}(\bar{\boldsymbol{F}}_{\mathrm{M}} - \bar{\boldsymbol{F}}_{\mathrm{F}}) - \Delta\boldsymbol{P}\right], \tag{5.21}$$

where $\Delta\boldsymbol{P} = \boldsymbol{P}^{\mathrm{M}}(\bar{\boldsymbol{F}}_{\mathrm{M}}) - \boldsymbol{P}^{\mathrm{F}}(\bar{\boldsymbol{F}}_{\mathrm{F}})$. Hence, the two tensorial equations (5.18) and (5.21) provide the required 18 scalar equations for the estimation of the two phase averages $\bar{\boldsymbol{F}}_{\mathrm{F}}$ and $\bar{\boldsymbol{F}}_{\mathrm{M}}$. Now, linear estimates of any type can be chosen for $\bar{\mathbb{L}}_{\mathrm{lin}}$. For instance, Voigt and Reuss estimates are obtained with the prescriptions

$$\bar{\mathbb{L}}_{\mathrm{V}} = \big\langle \mathbb{L} \big\rangle = n^{\mathrm{F}}\, \mathbb{L}^{\mathrm{F}} + n^{\mathrm{M}}\, \mathbb{L}^{\mathrm{M}} \quad \text{and} \quad \bar{\mathbb{L}}_{\mathrm{R}} = \big\langle \mathbb{L}^{-1} \big\rangle^{-1} = \big(n^{\mathrm{F}}\, (\mathbb{L}^{\mathrm{F}})^{-1} + n^{\mathrm{M}}\, (\mathbb{L}^{\mathrm{M}})^{-1}\big)^{-1}. \tag{5.22}$$

It is easy to see that substituting $\bar{\mathbb{L}}_{\mathrm{V}}$ for $\bar{\mathbb{L}}_{\mathrm{lin}}$ in (5.21) leads to uniform deformation fields $\bar{\boldsymbol{F}}_\alpha = \bar{\boldsymbol{F}}$, in agreement with the explanations made in Section 4.3.5. Consequently, the Voigt estimate is associated with strain concentration tensors $\mathbb{A}^\alpha = \mathbb{I}$. However, while the Voigt and Reuss estimates account for the microstructure only through the volume fractions n^α, a more sophisticated estimate of Hashin–Shtrikman type for composites with particulate microstructures was formulated by Willis [516] and reads

$$\bar{\mathbb{L}}_{\mathrm{HS}} = \mathbb{L}^{\mathrm{M}} + n^{\mathrm{F}}\left[n^{\mathrm{M}}\, \mathbb{P} - (\mathbb{L}^{\mathrm{M}} - \mathbb{L}^{\mathrm{F}})^{-1}\right]^{-1}, \tag{5.23}$$

Therein, $\mathbb{P}$ is a fourth-order microstructural tensor which accounts for the two-point statistics of the composite. It is defined as

$$\mathbb{P} = \frac{1}{4\pi \det[\boldsymbol{Z}]} \int_{|\boldsymbol{\xi}|=1} \mathbb{H}(\boldsymbol{\xi}) [\boldsymbol{Z}^{-1}\boldsymbol{\xi} \cdot \boldsymbol{Z}^{-1}\boldsymbol{\xi}]^{-3/2} \, \mathrm{d}A \,, \tag{5.24}$$

wherein the fourth-order tensor $\mathbb{H}$ is given by

$$\mathbb{H} = (\mathscr{B} \otimes \boldsymbol{\xi} \otimes \boldsymbol{\xi})^{T_{23}} \quad \text{with} \quad \mathscr{B} = \mathscr{A}^{-1} \quad \text{and} \quad \mathscr{A} = \left((\mathbb{L}^{\mathrm{M}})^{T_{23}} \, \boldsymbol{\xi}\right) \boldsymbol{\xi} \,. \tag{5.25}$$

Hence, the second-order tensor $\mathscr{B} \in \mathcal{SYM}(3)$ is the inverse of the acoustic tensor $\mathscr{A}$, which was introduced in Eq. (3.119) and is henceforth defined in terms of the elasticity tensor of the matrix phase, $\mathbb{L}^{\mathrm{M}}$. Further, $\mathbb{P}$ contains the second-order tensor $\boldsymbol{Z} = \boldsymbol{Z}_{\mathrm{i}} = \boldsymbol{Z}_{\mathrm{d}}$, where $\boldsymbol{Z}_{\mathrm{i}}$ serves as an descriptor for the shape and the orientation of the fibre (inclusion) phase and $\boldsymbol{Z}_{\mathrm{d}}$ for its spatial distribution in the microstructure. By recalling Eq. (4.27), we see that $\boldsymbol{Z}$ therefore accounts for the two-point probability of the characteristic functions $\mathscr{X}^{\alpha}$ (describing the microstructure) by making use of the notation of ellipsoidal symmetry. Remark that it is also possible to prescribe $\boldsymbol{Z}_{\mathrm{i}}$ and $\boldsymbol{Z}_{\mathrm{d}}$ separately, which leads to the formulation of two different $\mathbb{P}$-tensors and according changes of the subsequent formulations, see Ponte Castañeda & Willis [383] for details. Furthermore, we note that the microstructural $\mathbb{P}$-tensor is closely linked to another fourth-order microstructural tensor, which is commonly referred to as *Eshelby tensor*[1] and denoted by $\mathbb{S}$. The two tensors are connected through $\mathbb{S} = \mathbb{P}\mathbb{L}^{\mathrm{M}}$. Now, as we make use in the following of the Hashin–Shtrikman estimate (5.23), we can substitute $\bar{\mathbb{L}}_{\mathrm{HS}}$ into Eq. (5.21), which yields, after some algebra,

$$\bar{\boldsymbol{F}} - \bar{\boldsymbol{F}}_{\mathrm{F}} = \mathbb{P} \left[\mathbb{L}^{\mathrm{M}}(\bar{\boldsymbol{F}} - \bar{\boldsymbol{F}}_{\mathrm{F}}) - n^{\mathrm{M}} \, \Delta \boldsymbol{P}\right] . \tag{5.26}$$

Together with the overall average condition, given in Eq. (5.18), this tensorial equation represents the required set of equations for the estimation of the two phase averages $\bar{\boldsymbol{F}}_{\mathrm{F}}$ and $\bar{\boldsymbol{F}}_{\mathrm{M}}$. Finally, instead of using the tangent elasticity tensor $\mathbb{L}^{\mathrm{M}}$ evaluated at the phase average $\bar{\boldsymbol{F}}_{\mathrm{M}}$, as described in Eq. (5.14), we follow Avazmohammadi & Ponte Castañeda [19] and make use in Eq. (5.26) of the simpler prescription

$$\mathbb{L}^{\mathrm{M}} := \partial^2_{\boldsymbol{F}\boldsymbol{F}} \mathscr{W}^{\alpha}(\bar{\boldsymbol{F}}) \,. \tag{5.27}$$

5.1.2 Two-phase composites with aligned fibrous microstructures

The preceding section accounted for two-phase materials in which the shape, the orientation and the distribution (of the centre) of the inclusions (the fibre phase) are of ellipsoidal symmetry, characterised by the shape tensor $\boldsymbol{Z}$. A special class of materials is derived from this notation if the inclusions are taken to be of spheroidal shape, whose axis of symmetry shall be denoted by the referential unit vector $\bar{\boldsymbol{a}}_0$. A general shape tensor for such spheroidal inclusions is given by $\boldsymbol{Z} = (\boldsymbol{I} - \bar{\boldsymbol{a}}_0 \otimes \bar{\boldsymbol{a}}_0) + \omega \, \bar{\boldsymbol{a}}_0 \otimes \bar{\boldsymbol{a}}_0$, where ω is the aspect ratio. This allows to describe very different kinds of inclusion shapes, such as spherical ones

[1] The microstructural Eshelby tensor $\mathbb{S}$ must not be confused with the *energy-momentum tensor* or so-called Eshelby stress tensor, formulated by Eshelby [121, 123]. The latter is usually defined as $\boldsymbol{\Sigma} = \mathscr{W}\boldsymbol{I} - \boldsymbol{F}^T\boldsymbol{P}$ and is of particular importance in the field of configurational forces, see, for instance, Gurtin [174]. Despite their same origin in the seminal works of Eshelby, these two equally named tensors have only been related to each other in the recent work of Alhasadi & Federico [9].

($\omega = 1$) as well as prolate ($\omega > 1$) or oblate ($\omega < 1$) inclusions including the limit cases as the inclusions become long-fibres ($\omega \to \infty$) or pancake-shaped layers ($\omega \to 0$). In the following, we focus on the long-fibre case and assume that the composite is composed of a matrix phase which contains inclusions of circular cylindrical shape that are aligned along the preferred axis $\bar{\boldsymbol{a}}_0$ and distributed randomly and isotropically in the plane transverse to it. Materials of this kind are referred to as fibre composites or composites with fibrous microstructure. Subsequently, Lopez-Pamies [295] showed that in the limit as the aspect ratio of the shape tensor $\boldsymbol{Z}$ goes to infinity, $\omega \to \infty$, Eq. (5.24) for the microstructural $\mathbb{P}$-tensor simplifies to

$$\mathbb{P} = \frac{1}{2\pi} \int_0^{2\pi} \mathbb{H}(\boldsymbol{\xi}) \, \mathrm{d}\varsigma \quad \text{with} \quad \boldsymbol{\xi} = \cos[\varsigma] \, \boldsymbol{e}_1 + \sin[\varsigma] \, \boldsymbol{e}_2 + 0 \, \boldsymbol{e}_3 \, . \tag{5.28}$$

Therein, ς is an angle ranging from 0 to 2π and the Cartesian $\boldsymbol{e}_i$-coordinate system ($i = 1, 2, 3$) represents a laboratory frame of reference. The $\boldsymbol{e}_3$-direction thereby coincides with the alignment of the cylindrical inclusions, hence, $\boldsymbol{e}_3 = \bar{\boldsymbol{a}}_0$. Now, considering Eq. (5.28), together with relation $(5.25)_1$, in index notation form, reading

$$\mathrm{P}_{ijkl} = \frac{1}{2\pi} \int_0^{2\pi} \mathscr{B}_{ik} \, \xi_j \, \xi_l \, \mathrm{d}\varsigma \, , \tag{5.29}$$

makes it easy to deduce that $\mathbb{P}$ is major symmetric and that

$$\mathrm{P}_{i3kl} = \mathrm{P}_{ijk3} = 0 \tag{5.30}$$

($i, j, k, l = 1, 2, 3$) due to $\xi_3 = 0$. These zero-coefficients imply that $\mathbb{P}$ is not of full rank and it can be shown that $\mathrm{nullity}[\mathbb{P}] = 3$, where $\mathrm{nullity}[\mathbb{P}]$ is the dimension of the null space (or kernel) $\ker[\mathbb{P}] = \{\boldsymbol{\mathfrak{N}} \in \mathcal{R}^{3\otimes 3} \mid \mathbb{P}\,\boldsymbol{\mathfrak{N}} = \boldsymbol{0}\}$. Further details and explanations on null spaces of tensors are provided in Appendix A.5. Employing the findings from Eq. (5.30) in Eqs (5.26) and (5.18) directly points out that

$$(\bar{\boldsymbol{F}}_{\mathrm{F}})_{i3} = (\bar{\boldsymbol{F}}_{\mathrm{M}})_{i3} = \bar{F}_{i3} \tag{5.31}$$

for $i = 1, 2, 3$. Thus, the homogenisation problem for two-phase composites with fibrous microstructure reduces to finding the *six remaining unknowns* of either $\bar{\boldsymbol{F}}_{\mathrm{F}}$ or $\bar{\boldsymbol{F}}_{\mathrm{M}}$ by extracting the required set of equations from Eqs (5.26) and (5.18). In this work, we regard the six unknown coefficients of $\bar{\boldsymbol{F}}_{\mathrm{F}}$ as primary unknowns. The set of unknowns will later be further reduced by utilising incompressibility assumptions and an appropriate generic form of the overall deformation gradient $\bar{\boldsymbol{F}}$, see Section 5.3.2.

In the following, it proves useful to proceed with a modified version of Eq. (5.26), which requires some remarks beforehand. From relation (5.30) and $\mathrm{nullity}[\mathbb{P}] \neq 0$, it becomes obvious that there exists no inverse tensor $\mathbb{P}^{-1}$ satisfying the relation $\mathbb{P}^{-1}\mathbb{P} = \mathbb{I}$. Thus, it is generally not possible to bring $\mathbb{P}$ from the right to the left hand side of Eq. (5.26). However, it is possible to find a tensor $\{\mathbb{P}^{-1}\}^{\flat}$ such that $\{\mathbb{P}^{-1}\mathbb{P} = \mathbb{I}\}^{\flat}$, where $\{\cdot\}^{\flat}$ denotes a subspace of the full tensor space. Fourth- and second-order tensors of this subspace are defined as $\{\mathbb{A} = \mathrm{A}_{ijkl} \, \boldsymbol{e}_i \otimes \boldsymbol{e}_j \otimes \boldsymbol{e}_k \otimes \boldsymbol{e}_l\}^{\flat}$ and $\{\boldsymbol{B} = B_{ij} \, \boldsymbol{e}_i \otimes \boldsymbol{e}_j\}^{\flat}$, respectively, with $i, k = 1, 2, 3$ and $j, l = 1, 2$. The associated matrix representations of the coefficients are provided in Eq. (A.85) in Appendix A.7.2. Hence, by making use of this subspace notation, we are able to provide a modified version of Eq. (5.26), which reads

$$\left\{[\mathbb{P}^{-1} - \mathbb{L}^{\mathrm{M}}](\bar{\boldsymbol{F}} - \bar{\boldsymbol{F}}_{\mathrm{F}}) + n^{\mathrm{M}} \, \Delta\boldsymbol{P} = \boldsymbol{0}\right\}^{\flat} . \tag{5.32}$$

This tensorial equation provides the six required scalar equations for the six unknown coefficients $(\bar{\boldsymbol{F}}_{\mathrm{F}})_{ij}$ with $i = 1, 2, 3$ and $j = 1, 2$.

5.2 Fibre composites with incompressible phases

In Section 5.1.2, we formulated general estimates for two-phase hyperelastic composites consisting of aligned circular cylindrical inclusions that are embedded in a matrix phase. Therein, the two phases, $\mathcal{B}_0^{\mathrm{F}}$ and $\mathcal{B}_0^{\mathrm{M}}$, were considered as compressible and anisotropic, since their strain-energy functions were not specified or restricted otherwise. To apply the estimate to the special case in which the materials exhibit incompressible phases, appropriate investigations in the limit as the volumetric stiffnesses of the phases tend to infinity have to be carried out. This is done in this section by means of asymptotic expansions of the relevant terms and equations, first in the incompressibility limit of the fibre and subsequently for the matrix phase. To do so, it proves useful to express the strain-energy functions of the two phases in terms of the distortional-dilatational energy split which was introduced in Section 3.8.1. Hence, the additive split given in Eq. (3.140) leads to

$$\mathscr{W}^{\alpha}(\boldsymbol{F}) = \mathscr{W}_{\mu}^{\alpha}(\boldsymbol{F}) + \mathscr{W}_{\Lambda}^{\alpha}(\boldsymbol{F}) \quad \text{where} \quad \mathscr{W}_{\Lambda}^{\alpha}(\boldsymbol{F}) = \tfrac{1}{2}\Lambda^{\alpha}\,(J-1)^2 \tag{5.33}$$

such that the dilatational part is taken to be of the form introduced in (3.156) and Λ^{α} are the first Lamé constants of the two phases. The special case of incompressible behaviour of phase $\mathcal{B}_0^{\alpha}$ is recovered when Λ^{α} tends to infinity and

$$\lim_{\Lambda^{\alpha}\to\infty} \mathscr{W}_{\Lambda}^{\alpha}(\boldsymbol{F}) = \begin{cases} 0 & \text{for } J = 1\,, \\ \infty & \text{else}\,. \end{cases} \tag{5.34}$$

Further, we note that (5.33) entails a corresponding split of the first Piola–Kirchhoff stress tensor of the phases:

$$\boldsymbol{P}^{\alpha}(\boldsymbol{F}) = \boldsymbol{P}_{\mu}^{\alpha}(\boldsymbol{F}) + \boldsymbol{P}_{\Lambda}^{\alpha}(\boldsymbol{F}) \quad \text{where} \quad \boldsymbol{P}_{\Lambda}^{\alpha}(\boldsymbol{F}) = \partial_{\boldsymbol{F}}\mathscr{W}_{\Lambda}^{\alpha}(\boldsymbol{F}) = \Lambda^{\alpha} J(J-1)\boldsymbol{F}^{-T} \tag{5.35}$$

is the dilatational stress and the distortional stress is given by $\boldsymbol{P}_{\mu}^{\alpha}(\boldsymbol{F}) = \partial_{\boldsymbol{F}}\mathscr{W}_{\mu}^{\alpha}(\boldsymbol{F})$.

5.2.1 Asymptotic analysis for incompressible fibres

If the fibre phase is characterised by an energy of form (5.33), the Lamé constant Λ^{F} tends to infinity in the case of incompressibility. As a consequence, an appropriate asymptotic analysis has to be carried out to obtain the consistent versions of Eqs (5.15) and (5.32) in the incompressible limit of the fibres. This is done by introducing a small parameter $\iota = 1/\Lambda^{\mathrm{F}}$ and the following expansion for the phase average of the fibre deformation field:

$$\bar{\boldsymbol{F}}_{\mathrm{F}} = \bar{\boldsymbol{F}}_{\mathrm{F}0} + \iota\,\bar{\boldsymbol{F}}_{\mathrm{F}1} + \mathcal{O}(\iota^2)\,. \tag{5.36}$$

Based on this, it proves useful to formulate the associated expansions for the Jacobian

$$\bar{J}_{\mathrm{F}} = \det[\bar{\boldsymbol{F}}_{\mathrm{F}}] = \det[\bar{\boldsymbol{F}}_{\mathrm{F}0} + \iota\,\bar{\boldsymbol{F}}_{\mathrm{F}1} + \mathcal{O}(\iota^2)] = \bar{J}_{\mathrm{F}0} + \iota\,\bar{J}_{\mathrm{F}1} + \mathcal{O}(\iota^2) \tag{5.37}$$

as well as for the inverse

$$\bar{\boldsymbol{F}}_{\mathrm{F}}^{-1} = (\bar{\boldsymbol{F}}_{\mathrm{F}}^{-1})_0 + \iota(\bar{\boldsymbol{F}}_{\mathrm{F}}^{-1})_1 + \mathcal{O}(\iota^2)\,. \tag{5.38}$$

Therein, the expansion terms read

$$\bar{J}_{\mathrm{F}0} = \det[\bar{\boldsymbol{F}}_{\mathrm{F}0}] \quad \text{and} \quad \bar{J}_{\mathrm{F}1} = \operatorname{cof}[\bar{\boldsymbol{F}}_{\mathrm{F}0}] \cdot \bar{\boldsymbol{F}}_{\mathrm{F}1} \tag{5.39}$$

as well as

$$(\bar{\boldsymbol{F}}_{\mathrm{F}}^{-1})_0 = \bar{\boldsymbol{F}}_{\mathrm{F}0}^{-1} \quad \text{and} \quad (\bar{\boldsymbol{F}}_{\mathrm{F}}^{-1})_1 = -\bar{\boldsymbol{F}}_{\mathrm{F}0}^{-1}\bar{\boldsymbol{F}}_{\mathrm{F}1}\bar{\boldsymbol{F}}_{\mathrm{F}0}^{-1}\,. \tag{5.40}$$

Making use of expansions (5.36)-(5.40), together with Eq. (5.35), we continue with the resulting expansion for the nominal fibre stress, that is,

$$\boldsymbol{P}^{\mathrm{F}} = \iota^{-1}\,\boldsymbol{P}_{-1}^{\mathrm{F}} + \boldsymbol{P}_{0}^{\mathrm{F}} + \mathcal{O}(\iota)\,, \tag{5.41}$$

where, after some algebra, we find

$$\begin{aligned} \boldsymbol{P}_{-1}^{\mathrm{F}} &= \bar{J}_{\mathrm{F}0}\,(\bar{J}_{\mathrm{F}0}-1)\,\bar{\boldsymbol{F}}_{\mathrm{F}0}^{-T} \quad \text{and} \\ \boldsymbol{P}_{0}^{\mathrm{F}} &= \boldsymbol{P}_{\mu}^{\mathrm{F}} + \bar{J}_{\mathrm{F}1}\,(2\bar{J}_{\mathrm{F}0}-1)\,\bar{\boldsymbol{F}}_{\mathrm{F}0}^{-T} + \bar{J}_{\mathrm{F}0}\,(\bar{J}_{\mathrm{F}0}-1)\,(\bar{\boldsymbol{F}}_{\mathrm{F}}^{-1})_1^{T}\,. \end{aligned} \tag{5.42}$$

Now, the expansions for $\bar{\boldsymbol{F}}_{\mathrm{F}}$ and $\boldsymbol{P}^{\mathrm{F}}$, given in Eqs (5.36) and (5.42), are substituted into Eq. (5.32), which gives

$$\left\{[\mathbb{P}^{-1}-\mathbb{L}^{\mathrm{M}}](\bar{\boldsymbol{F}}-\bar{\boldsymbol{F}}_{\mathrm{F}0}-\iota\bar{\boldsymbol{F}}_{\mathrm{F}1}-\mathcal{O}(\iota^2)) + n^{\mathrm{M}}\,(\boldsymbol{P}^{\mathrm{M}}-\iota^{-1}\boldsymbol{P}_{-1}^{\mathrm{F}}-\boldsymbol{P}_{0}^{\mathrm{F}}-\mathcal{O}(\iota)) = \boldsymbol{0}\right\}^{\flat}. \tag{5.43}$$

In the incompressible limit of the fibre, parameter ι tends to zero and terms associated with $\mathcal{O}(\iota)$ drop out. Subsequently, we are left with the collection of terms associated with ι^{-1} and ι^{0}, which gives

$$\begin{aligned} \iota^{-1}:&\quad \left\{n^{\mathrm{M}}\,\boldsymbol{P}_{-1}^{\mathrm{F}} = \boldsymbol{0}\right\}^{\flat}, \\ \iota^{0}:&\quad \left\{[\mathbb{P}^{-1}-\mathbb{L}^{\mathrm{M}}](\bar{\boldsymbol{F}}-\bar{\boldsymbol{F}}_{\mathrm{F}0}) + n^{\mathrm{M}}\,(\boldsymbol{P}^{\mathrm{M}}-\boldsymbol{P}_{0}^{\mathrm{F}}) = \boldsymbol{0}\right\}^{\flat}. \end{aligned} \tag{5.44}$$

With Eq. $(5.42)_1$, it is easy to see that the only meaningful (and non-trivial) solution for the first equation in (5.44) is provided by $\bar{J}_{\mathrm{F}0}=1$, which entails, with Eq. $(5.39)_1$, that $\bar{\boldsymbol{F}}_{\mathrm{F}0} \in \mathcal{SL}(3)$ has to be a unimodular tensor so that $\det[\bar{\boldsymbol{F}}_{\mathrm{F}0}]=1$. In turn, this means that the phase average $\bar{\boldsymbol{F}}_{\mathrm{F}}$ in the incompressible limit has to be unimodular as well, such that

$$\det[\bar{\boldsymbol{F}}_{\mathrm{F}}] = 1 \quad \text{if} \quad \Lambda^{\mathrm{F}} \to \infty\,. \tag{5.45}$$

This is a very meaningful condition for the phase average $\bar{\boldsymbol{F}}_{\mathrm{F}}$, because the phase averages $\bar{\boldsymbol{F}}_{\alpha}$ actually describe the deformation in the $\mathcal{LCC}$. In turn, the homogenisation of the $\mathcal{LCC}$ is based on the estimate of Hashin–Shtrikman type given in Eq. (5.23), which considers uniform strain and stress fields inside the inclusion (fibre phase). Further, from Section 3.3.2 we know that material incompressibility is associated with a local constraint equation as given in Eq. (3.25), which leads for incompressible fibres to the local condition $\det[\boldsymbol{F}(\boldsymbol{X}\in\mathcal{B}_0^{\mathrm{F}})]=1$. Hence, the uniformity of the fields in the fibre phase entails that condition (5.45) for $\bar{\boldsymbol{F}}_{\mathrm{F}}$ is identical to the phase average of the local (exact) incompressibility condition, $\langle\det[\boldsymbol{F}(\boldsymbol{X}\in\mathcal{B}_0^{\mathrm{F}})]=1\rangle^{\mathrm{F}}$, because $\det[\langle\boldsymbol{F}\rangle^{\mathrm{F}}] = \langle\det[\boldsymbol{F}]\rangle^{\mathrm{F}}$. However, a similar relation cannot be formulated for the matrix phase, because of the generally non-uniform fields inside the matrix. Further, we note that condition (5.45) allows to express one of the six unknown coefficients of $\bar{\boldsymbol{F}}_{\mathrm{F}}$ in terms of the other ones, which means that one remains with the determination of five unknown coefficients of $\bar{\boldsymbol{F}}_{\mathrm{F}}$. This will be useful below. Now,

we continue with the evaluation of expression $(5.44)_2$. Therein, the stress tensor $\boldsymbol{P}_0^{\mathrm{F}}$, which is defined in $(5.42)_2$, is simplified by making use of $\bar{J}_{\mathrm{F}0} = 1$ and we obtain

$$\boldsymbol{P}_0^{\mathrm{F}} = \boldsymbol{P}_\mu^{\mathrm{F}} + \bar{J}_{\mathrm{F}1}\, \bar{\boldsymbol{F}}_{\mathrm{F}0}^{-T} \,. \tag{5.46}$$

From this, we see that $(\bar{\boldsymbol{F}}_{\mathrm{F}}^{-1})_1^T$ drops out of expression $(5.44)_2$. However, this is not the case for the scalar term $\bar{J}_{\mathrm{F}1}$, which is reasonable since it replaces an indeterminate form "$\infty \times 0$" arising in $\boldsymbol{P}_\Lambda^{\mathrm{F}}$ as $\Lambda^{\mathrm{F}} \to \infty$ and $(\bar{J}_{\mathrm{F}} - 1) \to 0$, cf. Eq. $(5.35)_2$. In fact, by again recalling Section 3.3.2, we see that the stress expression in Eq. (5.46) is reminiscent of Eq. (3.27). This means that the term $\bar{J}_{\mathrm{F}1}\, \bar{\boldsymbol{F}}_{\mathrm{F}0}^{-T}$ can be interpreted as an additional hydrostatic stress contribution, which is required to enforce the incompressibility constraint (5.45) in the fibre phase. Further, the rigorous variational interpretation in Section 3.4.3 showed that the scalar multiplier in the additional stress contribution from Section 3.3.2 is indeed a Lagrange multiplier. Hence, as $\bar{J}_{\mathrm{F}1}$ represents such a scalar factor in Eq. (5.46), we can clearly identify $\bar{J}_{\mathrm{F}1}$ as a Lagrange multiplier. To show this more explicitly, we will formulate the associated constrained variational principle for incompressible fibres in Section 5.2.2. This will point out that the Lagrange multiplier arises from the fact that the variational expression (4.45) has to be solved subject to the local incompressibility constraint in the fibre phase. Based on these considerations, we rename $\bar{J}_{\mathrm{F}1} =: \wp^{\mathrm{F}}$ and proceed with the symbol $\wp^{\mathrm{F}}$ to emphasise its characteristic as an additional *constraint pressure*. By further renaming $\boldsymbol{P}_0^{\mathrm{F}} =: \boldsymbol{P}_{\mu\wp}^{\mathrm{F}}$ and noting from Eq. (5.36) that $\bar{\boldsymbol{F}}_{\mathrm{F}} = \bar{\boldsymbol{F}}_{\mathrm{F}0}$ if $\iota \to 0$, we obtain in the incompressible fibre limit

$$\boldsymbol{P}_{\mu\wp}^{\mathrm{F}} = \boldsymbol{P}_\mu^{\mathrm{F}} + \wp^{\mathrm{F}}\, \bar{\boldsymbol{F}}_{\mathrm{F}}^{-T} \,. \tag{5.47}$$

and

$$\left\{ [\mathbb{P}^{-1} - \mathbb{L}^{\mathrm{M}}](\bar{\boldsymbol{F}} - \bar{\boldsymbol{F}}_{\mathrm{F}}) + n^{\mathrm{M}}\, \Delta \boldsymbol{P}_\wp = \boldsymbol{0} \right\}^\flat , \tag{5.48}$$

where $\Delta \boldsymbol{P}_\wp = \boldsymbol{P}^{\mathrm{M}}(\bar{\boldsymbol{F}}_{\mathrm{M}}) - \boldsymbol{P}_{\mu\wp}^{\mathrm{F}}(\bar{\boldsymbol{F}}_{\mathrm{F}}, \wp^{\mathrm{F}})$. At this point, we note that Eq. (5.48) provides the six required equations required for the determination of the *five* remaining unknowns of $\bar{\boldsymbol{F}}_{\mathrm{F}}$ *plus* the additional constraint pressure $\wp^{\mathrm{F}}$. Furthermore, we have to investigate the fibre energy $\mathscr{W}^{\mathrm{F}}$ in order to provide the consistent formulation for the effective energy $\widetilde{\mathscr{W}}$, given by expression (5.15), in the incompressible fibre limit. Yet, it is easy to see, with Eqs (5.37) and (5.33) as well as with $\bar{J}_{\mathrm{F}0} = 1$, that in this case $\mathscr{W}_\Lambda^{\mathrm{F}} = 0$ such that $\mathscr{W}^{\mathrm{F}} = \mathscr{W}_\mu^{\mathrm{F}}$. Hence, the effective energy is given by

$$\widetilde{\mathscr{W}}(\bar{\boldsymbol{F}}) = n^{\mathrm{F}} \left[\mathscr{W}_\mu^{\mathrm{F}}(\bar{\boldsymbol{F}}_{\mathrm{F}}) + \tfrac{1}{2}(\bar{\boldsymbol{F}} - \bar{\boldsymbol{F}}_{\mathrm{F}}) \cdot \boldsymbol{P}_{\mu\wp}^{\mathrm{F}}(\bar{\boldsymbol{F}}_{\mathrm{F}}, \wp^{\mathrm{F}}) \right] + n^{\mathrm{M}} \left[\mathscr{W}^{\mathrm{M}}(\bar{\boldsymbol{F}}_{\mathrm{M}}) + \tfrac{1}{2}(\bar{\boldsymbol{F}} - \bar{\boldsymbol{F}}_{\mathrm{M}}) \cdot \boldsymbol{P}^{\mathrm{M}}(\bar{\boldsymbol{F}}_{\mathrm{M}}) \right] , \tag{5.49}$$

where $\bar{\boldsymbol{F}}_{\mathrm{F}}$, $\bar{\boldsymbol{F}}_{\mathrm{M}}$ and $\wp^{\mathrm{F}}$ are obtained from Eqs (5.48) and (5.18) subject to condition (5.45).

To show that the new constrained formulation is consistent with the original formulation in the limit case as the fibre phase becomes incompressible, we compare the effective strain energies based on Eqs (5.15) and (5.32) with the newly introduced formulation, which is based on Eqs (5.49) and (5.48). To do so, we consider isotropic Neo-Hookean energies for both of the phases. Hence, the distortional parts are given by $\mathscr{W}_\mu^\alpha(I_1, J) = \mu^\alpha\, (I_1 - 3 + (J-1)(J-3))/2$ and the dilatational parts $\mathscr{W}_\Lambda^\alpha = \Lambda^\alpha\, (J-1)^2/2$ (see above). To provide some evidence for the consistency of the new formulation, we choose for the above described composite a fibre volume fraction of $n^{\mathrm{F}} = 0.3$, apply a macroscopic transverse shear $\bar{\gamma}_{\mathrm{t}} = 2$ and investigate for different stiffness ratios $\Lambda^\alpha/\mu^\alpha$ the effective strain energy. Figure 5.1 shows for four selected and genuine different stiffness combinations the results

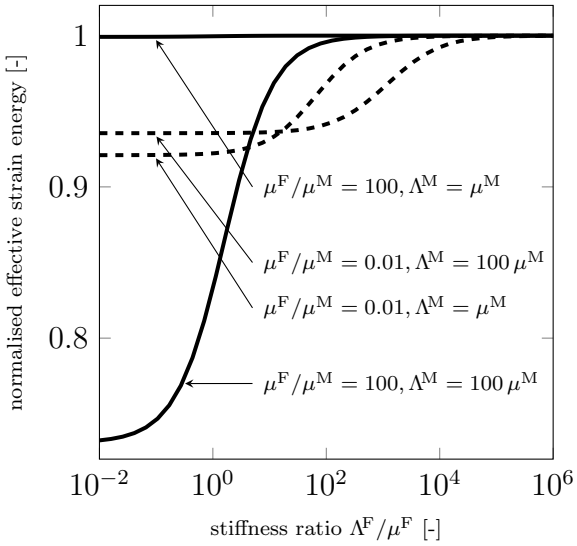

Figure 5.1: Effective strain energy $\widetilde{\mathscr{W}}$ computed from Eq. (5.15) normalised to the effective strain energy computed from Eq. (5.49) for composites with a matrix and fibre phase that exhibit Neo-Hookean behaviour under a macroscopic transverse shear $\bar{\gamma}_{\mathrm{t}} = 2.0$. The volume fraction is $n^{\mathrm{F}} = 0.3$. Estimate (5.15) tends to (5.49) as the volumetric stiffness of the fibre phase increases and tends to infinity.

of the original energy formulation (5.15) normalised to the new formulation (5.49). The results clearly demonstrate that the formulations coincide when the Lamé constant of the fibre phase, Λ^{F}, tends to infinity.

5.2.2 *Interlude:* A constrained variational principle for incompressible fibres

This section gives a rigorous variational interpretation to the results obtained in the previous section by means of the asymptotic analysis for incompressible fibres. Further, we show why a direct application of constrained variational principles causes problems in the context of the herein used TSO homogenisation method.

We recall from Section 3.3 that internal material constraints are described by a local constraint function $\mathscr{R}(\boldsymbol{F}) = 0$, see Eq. (3.21). Correspondingly, an internal material constraint in a specific phase $\mathcal{B}_0^\alpha$ of a multi-phase material is associated with a local constraint function $\mathscr{R}^\alpha(\boldsymbol{F}(\boldsymbol{X})) = 0$ for $\boldsymbol{X} \in \mathcal{B}_0^\alpha$. Further, it was shown in Section 3.4.3 that the consideration of internal constraints in variational formulations leads to the formulation of a Lagrange functional, see Eq. (3.54). Applied to the multiscale variational problem (4.45), the incorporation of an internal constraint function $\mathscr{R}^\alpha$ would lead to a Lagrange function $\mathscr{L}(\boldsymbol{F}, \alpha_{\mathscr{R}^\alpha}) = \Pi(\boldsymbol{F}) + \Pi^{\mathscr{R}^\alpha}(\boldsymbol{F}, \alpha_{\mathscr{R}^\alpha})$ where

$$\Pi^{\mathscr{R}^\alpha}(\boldsymbol{F}, \alpha_{\mathscr{R}^\alpha}) = \frac{1}{\mathrm{vol}[\mathcal{B}_0]} \int_{\mathcal{B}_0} \mathscr{X}^\alpha(\boldsymbol{X}) \alpha_{\mathscr{R}^\alpha}(\boldsymbol{X})\, \mathscr{R}^\alpha(\boldsymbol{F})\, \mathrm{d}V = n^\alpha \big\langle \alpha_{\mathscr{R}^\alpha}(\boldsymbol{X})\, \mathscr{R}^\alpha(\boldsymbol{F}) \big\rangle^\alpha . \quad (5.50)$$

Then, stationarity of $\mathscr{L}$ with respect to the Lagrange multiplier $\alpha_{\mathscr{R}^\alpha}$ requires that the local constraint function $\mathscr{R}^\alpha(\boldsymbol{F}(\boldsymbol{X})) = 0$ has to be satisfied *at any local point* $\boldsymbol{X} \in \mathcal{B}_0^\alpha$ on the microscale. However, this cannot be achieved by the present TSO estimate, as given by Eq. (5.15), because the local deformation field enters the estimate for $\widetilde{\mathscr{W}}$ only by means of the first moments (phase averages) $\boldsymbol{F}_\alpha$ and the exact microscopic resolution of the deformation remains unknown. In general, the incorporation of local Lagrange

multipliers within the TSO method would require in addition to the approximation of the microscopic deformation field also an appropriate approximation of the local Lagrange multiplier fields. Such an approach was presented by LAHELLEC ET AL. [272] to enforce material incompressibility of both phases, however, this may lead to some unclear physical interpretations of the approximated constraint functions. An alternative approach to satisfy the material constraint $\mathscr{R}^\alpha(\boldsymbol{F})$ locally at $\boldsymbol{X} \in \mathcal{B}_0^\alpha$ would be to approximate the constraint function by means of $\mathscr{R}^\alpha(\bar{\boldsymbol{F}}_\alpha)$, hence, to evaluate the constraint functions at the phase averages $\bar{\boldsymbol{F}}_\alpha$. Yet, this does not lead to physically meaningful results, because $\mathscr{R}^\alpha$ is generally nonlinear in its argument $\boldsymbol{F}$ such that the phase average of the constraint function, $\langle \mathscr{R}^\alpha(\boldsymbol{F})\rangle^\alpha$, is generally not equal to the constraint function evaluated at the phase average, $\mathscr{R}^\alpha(\langle \boldsymbol{F}\rangle^\alpha) = \mathscr{R}^\alpha(\bar{\boldsymbol{F}}_\alpha)$. Concluding, it is not useful in general to employ a constrained variational principle based on the formulation of a Lagrange functional $\mathscr{L}$ in the context of the present TSO formulation. However, we remarked in the previous section that the herein employed estimate of Hashin–Shtrikman type for the $\mathcal{LCC}$, given by expression (5.23), assumes uniform fields in the fibre phase $\mathcal{B}_0^{\mathrm{F}}$. This means that for a fibre phase which is subject to an internal constraint function $\mathscr{R}^{\mathrm{F}}$, the phase average of $\mathscr{R}^{\mathrm{F}}$ is *equal* to the constraint function evaluated at the phase average $\bar{\boldsymbol{F}}_{\mathrm{F}}$, hence $\langle \mathscr{R}^{\mathrm{F}}(\boldsymbol{F})\rangle^{\mathrm{F}} = \mathscr{R}^{\mathrm{F}}(\bar{\boldsymbol{F}}_{\mathrm{F}})$. Thus, it can be shown that stationarity of the respective Lagrange functional can be achieved by satisfying the constraint evaluated at the phase average $\bar{\boldsymbol{F}}_{\mathrm{F}}$, which is an available quantity in the TSO formulation. We show this in the following for the case of an incompressible fibre phase, which is associated with the constraint function

$$\mathscr{R}^{\mathrm{F}} = \det[\boldsymbol{F}(\boldsymbol{X})] - 1 = 0 \quad \text{if} \quad \boldsymbol{X} \in \mathcal{B}_0^{\mathrm{F}}\,, \tag{5.51}$$

compare Eq. (3.25). Hence, the local deformation gradient in the fibre phase has to be unimodular, such that $\boldsymbol{F}(\boldsymbol{X}) \in \mathcal{SL}_3$ if $\boldsymbol{X} \in \mathcal{B}_0^{\mathrm{F}}$. Subsequently, this constraint is included into the original variational problem (4.45) by formulating the associated Lagrange functional

$$\mathscr{L}(\boldsymbol{F}, \wp^{\mathrm{F}}) := \Pi(\boldsymbol{F}) + \Pi^{\mathscr{R}^{\mathrm{F}}}(\boldsymbol{F}, \wp^{\mathrm{F}}) \quad \text{with} \quad \Pi(\boldsymbol{F}) = n^{\mathrm{F}}\big\langle \mathscr{W}_\mu^{\mathrm{F}}(\boldsymbol{F})\big\rangle^{\mathrm{F}} + n^{\mathrm{M}}\big\langle \mathscr{W}^{\mathrm{M}}(\boldsymbol{F})\big\rangle^{\mathrm{M}}. \tag{5.52}$$

Therein, only the distortional energy part, $\mathscr{W}_\mu^{\mathrm{F}}$, of the fibre phase is considered, since the dilatational part has to be zero in case of incompressibility. Further the constraint functional $\Pi^{\mathscr{R}^{\mathrm{F}}}$ is given by

$$\Pi^{\mathscr{R}^{\mathrm{F}}}(\boldsymbol{F}, \wp^{\mathrm{F}}) = \frac{1}{\mathrm{vol}[\mathcal{B}_0]} \int_{\mathcal{B}_0} \mathscr{X}^{\mathrm{F}} \wp^{\mathrm{F}} \left(\det[\boldsymbol{F}] - 1\right) \mathrm{d}V = n^{\mathrm{F}} \big\langle \wp^{\mathrm{F}} \left(\det[\boldsymbol{F}] - 1\right)\big\rangle^{\mathrm{F}}\,, \tag{5.53}$$

where $\wp^{\mathrm{F}}$ denotes the Lagrange multiplier associated with the incompressibility constraint (5.51). Subsequently, we follow the explanations made in Section 3.4.3 and demand for stationarity of the Lagrange functional $\mathscr{L}$ with respect to the deformation field and the Lagrange multiplier. This leads to the effective overall energy

$$\widetilde{\mathscr{W}}(\bar{\boldsymbol{F}}) = \underset{\boldsymbol{F}\in\mathcal{K}(\bar{\boldsymbol{F}})}{\mathrm{stat}} \underset{\wp^{\mathrm{F}}}{\mathrm{stat}}\, \mathscr{L}(\boldsymbol{F}, \wp^{\mathrm{F}}) = \underset{\boldsymbol{F}\in\mathcal{K}(\bar{\boldsymbol{F}})}{\mathrm{stat}} \underset{\wp^{\mathrm{F}}}{\mathrm{stat}} \left\{ n^{\mathrm{F}}\big\langle \mathscr{W}_{\mu\wp}^{\mathrm{F}}(\boldsymbol{F}, \wp^{\mathrm{F}})\big\rangle^{\mathrm{F}} + n^{\mathrm{M}}\big\langle \mathscr{W}^{\mathrm{M}}(\boldsymbol{F})\big\rangle^{\mathrm{M}} \right\}, \tag{5.54}$$

where summing up Π and $\Pi^{\mathscr{R}^{\mathrm{F}}}$ leads to the fibre energy

$$\mathscr{W}_{\mu\wp}^{\mathrm{F}}(\boldsymbol{F}, \wp^{\mathrm{F}}) := \mathscr{W}_\mu^{\mathrm{F}}(\boldsymbol{F}) + \wp^{\mathrm{F}} \left(\det[\boldsymbol{F}] - 1\right). \tag{5.55}$$

Then, stationarity of expression (5.54) with respect to the Lagrange multiplier $\wp^{\mathrm{F}}$ is obtained by satisfying

$$\partial_{\wp^{\mathrm{F}}} \mathscr{L}(\boldsymbol{F}, \wp^{\mathrm{F}}) = n^{\mathrm{F}} \left\langle \det[\boldsymbol{F}] - 1 \right\rangle^{\mathrm{F}} = 0 \quad \rightarrow \quad \left\langle \det[\boldsymbol{F}] \right\rangle^{\mathrm{F}} - 1 = 0 \,. \tag{5.56}$$

The uniformity of the fields, in particular the deformation field, in the fibre phase can now be used to reformulate the last expression to $\langle \det[\boldsymbol{F}] \rangle^{\mathrm{F}} - 1 = \det[\langle \boldsymbol{F} \rangle^{\mathrm{F}}] - 1 = \det[\bar{\boldsymbol{F}}_{\mathrm{F}}] - 1 = 0$. Hence, it is shown that the formulation of a unimodular phase average $\bar{\boldsymbol{F}}_{\mathrm{F}} \in \mathcal{SL}(3)$, meaning that

$$\det[\bar{\boldsymbol{F}}_{\mathrm{F}}] - 1 = 0 \,, \tag{5.57}$$

satisfies the stationarity condition of the Lagrange functional with respect to the Lagrange multiplier and thus serves as an equivalent condition for the local (exact) incompressibility condition (5.51). Furthermore, the remaining problem of fulfilling stationarity of $\mathscr{L}$ with respect to $\boldsymbol{F} \in \mathcal{K}(\bar{\boldsymbol{F}})$ can be treated in direct analogy to the derivations performed in Section 5.1 for the original variational problem (4.45). It is easy to see that this leads to an estimate for the overall energy as provided in (5.15) by replacing the fibre energy $\mathscr{W}^{\mathrm{F}}$ with $\mathscr{W}^{\mathrm{F}}_{\mu\wp}$ from Eq. (5.55). Further, the associated equation for the estimation of the phase average $\bar{\boldsymbol{F}}_{\mathrm{F}}$ is obtained by replacing in Eqs (5.26) and (5.32) the fibre stress $\boldsymbol{P}^{\mathrm{F}}$ by

$$\boldsymbol{P}^{\mathrm{F}}_{\mu\wp}(\bar{\boldsymbol{F}}_{\mathrm{F}}, \wp^{\mathrm{F}}) = \partial_{\boldsymbol{F}} \mathscr{W}^{\mathrm{F}}_{\mu\wp}(\bar{\boldsymbol{F}}_{\mathrm{F}}, \wp^{\mathrm{F}}) = \boldsymbol{P}^{\mathrm{F}}_{\mu}(\bar{\boldsymbol{F}}_{\mathrm{F}}) + \wp^{\mathrm{F}} \det[\bar{\boldsymbol{F}}_{\mathrm{F}}] \, \bar{\boldsymbol{F}}_{\mathrm{F}}^{-T} \,, \tag{5.58}$$

where $\boldsymbol{P}^{\mathrm{F}}_{\mu} = \partial_{\boldsymbol{F}} \mathscr{W}^{\mathrm{F}}_{\mu}$ denotes the distortional fibre stress contribution. At this point, it is a simple matter to observe, with (5.57), that the outcome of the herein presented constrained variational principle *exactly* corresponds to the results obtained in the previous section by means of the asymptotic analysis. Hence, the constrained variational principle leads to the energy estimate (5.49) and the tensorial equation (5.48). In turn, this clearly justifies the meaning of $\bar{J}_{F1}$, arising in the stress expression (5.46), as the Lagrange multiplier $\wp^{\mathrm{F}}$, which is associated with the local incompressibility constraint (5.51) in the fibre phase.

5.2.3 Asymptotic analysis for incompressible matrix behaviour

Sections 5.2.1 and 5.2.2 focused on the derivation of the TSO estimate for incompressible fibres and a generally compressible matrix phase. In this section, we investigate the limit case as the matrix becomes incompressible as well. We say that the energy of the matrix phase, $\mathscr{W}^{\mathrm{M}}$, is formulated in terms of the additive split given in (5.33). Then, incompressibility of the matrix is described by a Lamé constant Λ^{M} that tends to infinity. Now, for the estimate given in (5.49), it becomes clear that finite values for $\widetilde{\mathscr{W}}$ can only be obtained if $\bar{J}_{\mathrm{M}} = \det[\bar{\boldsymbol{F}}_{\mathrm{M}}] = 1$. However, while condition (5.45) for the phase average of the fibre phase is justified by the uniformity of the fields in the fibre phase of the $\mathcal{LCC}$, this is not the case for the condition $\det[\bar{\boldsymbol{F}}_{\mathrm{M}}] = 1$, because the fields in the matrix are generally non-uniform. Furthermore, it can be shown that the simultaneous prescription of condition (5.45) and $\det[\bar{\boldsymbol{F}}_{\mathrm{M}}] = 1$ in estimate (5.49) is inconsistent with the overall incompressibility constraint, $\bar{J} = \det[\bar{\boldsymbol{F}}] = 1$, which was already discussed by Ponte Castañeda & Tiberio [382] and Avazmohammadi & Ponte Castañeda [19]. Yet, if both phases are incompressible, the overall incompressibility constraint has to be satisfied and its violation is unacceptable. To resolve this issue, we introduce an approximation inspired by the work of Avazmohammadi & Ponte Castañeda [19] and

consisting in a split of the distortional and dilatational parts of the matrix strain-energy function $\mathscr{W}^{\mathrm{M}}$, as given by (5.33), in expression (5.49) for the homogenised strain-energy function of the fibre composite. This leads to the approximation

$$\widetilde{\mathscr{W}}(\bar{\boldsymbol{F}}) \approx \widetilde{\mathscr{W}_{\mu}}(\bar{\boldsymbol{F}}) + \widetilde{\mathscr{W}_{\Lambda}}(\bar{\boldsymbol{F}})\,, \tag{5.59}$$

where

$$\widetilde{\mathscr{W}_{\Lambda}}(\bar{\boldsymbol{F}}) = \frac{1}{2} \operatorname*{stat}_{\boldsymbol{F}\in\mathcal{K}(\bar{\boldsymbol{F}})} \big\{\ \Lambda^{\mathrm{M}} \big\langle \mathscr{X}^{\mathrm{M}}(\boldsymbol{X})\,(J-1)^2 \big\rangle \big\} \tag{5.60}$$

is the effective energy of an elastic fluid with incompressible fibrous inclusions, satisfying the condition $\det[\boldsymbol{F}] = 1$ in the fibre phase, compare Ponte Castañeda [373]. It is easy to see that, in the limit as $\Lambda^{\mathrm{M}} \to \infty$, the expression (5.60) for $\widetilde{\mathscr{W}_{\Lambda}}$ is infinite unless $\det[\boldsymbol{F}] = 1$ in the matrix phase, thus implying the overall incompressibility constraint

$$\det[\bar{\boldsymbol{F}}] = 1\,. \tag{5.61}$$

On the other hand, the term $\widetilde{\mathscr{W}_{\mu}}$ in expression (5.59) corresponds to the homogenised strain-energy function of the fibre composite, as given by expression (5.49), but with the matrix strain-energy function $\mathscr{W}^{\mathrm{M}}$ replaced by its distortional component $\mathscr{W}_{\mu}^{\mathrm{M}}$, such that

$$\widetilde{\mathscr{W}_{\mu}}(\bar{\boldsymbol{F}}) = n^{\mathrm{F}}\big[\mathscr{W}_{\mu}^{\mathrm{F}}(\bar{\boldsymbol{F}}_{\mathrm{F}}) + \tfrac{1}{2}(\bar{\boldsymbol{F}}-\bar{\boldsymbol{F}}_{\mathrm{F}})\cdot\boldsymbol{P}_{\mu\wp}^{\mathrm{F}}(\bar{\boldsymbol{F}}_{\mathrm{F}},\wp^{\mathrm{F}})\big] + n^{\mathrm{M}}\big[\mathscr{W}_{\mu}^{\mathrm{M}}(\bar{\boldsymbol{F}}_{\mathrm{M}}) + \tfrac{1}{2}(\bar{\boldsymbol{F}}-\bar{\boldsymbol{F}}_{\mathrm{M}})\cdot\boldsymbol{P}_{\mu}^{\mathrm{M}}(\bar{\boldsymbol{F}}_{\mathrm{M}})\big]\,, \tag{5.62}$$

where the stress tensor $\boldsymbol{P}^{\mathrm{M}}$ has correspondingly been replaced by its distortional part $\boldsymbol{P}_{\mu}^{\mathrm{M}}$. In turn, the five unknown coefficients of $\bar{\boldsymbol{F}}_{\mathrm{F}}$ and the constraint pressure $\wp^{\mathrm{F}}$ are obtained from Eq. (5.48) by also replacing $\boldsymbol{P}^{\mathrm{M}}$ with $\boldsymbol{P}_{\mu}^{\mathrm{M}}$, such that

$$\big\{[\mathbb{P}^{-1} - \mathbb{L}^{\mathrm{M}}](\bar{\boldsymbol{F}} - \bar{\boldsymbol{F}}_{\mathrm{F}}) + n^{\mathrm{M}}\,\Delta\boldsymbol{P}_{\mu\wp} = \boldsymbol{0}\big\}^{\flat}\,, \tag{5.63}$$

with $\Delta\boldsymbol{P}_{\mu\wp} = \boldsymbol{P}_{\mu}^{\mathrm{M}}(\bar{\boldsymbol{F}}_{\mathrm{M}}) - \boldsymbol{P}_{\mu\wp}^{\mathrm{F}}(\bar{\boldsymbol{F}}_{\mathrm{F}},\wp^{\mathrm{F}})$. It follows that the effective strain-energy function of the fibre composite is given by $\widetilde{\mathscr{W}}(\bar{\boldsymbol{F}}) \approx \widetilde{\mathscr{W}_{\mu}}(\bar{\boldsymbol{F}})$, which leads to the expression

$$\widetilde{\mathscr{W}}(\bar{\boldsymbol{F}}) \approx n^{\mathrm{F}}\,\big[\mathscr{W}_{\mu}^{\mathrm{F}}(\bar{\boldsymbol{F}}_{\mathrm{F}}) + \tfrac{1}{2}(\bar{\boldsymbol{F}}-\bar{\boldsymbol{F}}_{\mathrm{F}})\cdot\boldsymbol{P}_{\mu\wp}^{\mathrm{F}}(\bar{\boldsymbol{F}}_{\mathrm{F}},\wp^{\mathrm{F}})\big] + n^{\mathrm{M}}\,\big[\mathscr{W}_{\mu}^{\mathrm{M}}(\bar{\boldsymbol{F}}_{\mathrm{M}}) + \tfrac{1}{2}(\bar{\boldsymbol{F}}-\bar{\boldsymbol{F}}_{\mathrm{M}})\cdot\boldsymbol{P}_{\mu}^{\mathrm{M}}(\bar{\boldsymbol{F}}_{\mathrm{M}})\big]\,, \tag{5.64}$$

subject to the overall incompressibility constraint (5.61). However, because of the energy split (5.59), it is also necessary to take the limit as $\Lambda^{\mathrm{M}} \to \infty$ in expression (5.63) for $\bar{\boldsymbol{F}}_{\mathrm{F}}$ and $\wp^{\mathrm{F}}$. For this purpose, it is recalled that the elasticity tensor $\mathbb{L}^{\mathrm{M}}$ in Eq. (5.63) is described by

$$\mathbb{L}^{\mathrm{M}}(\bar{\boldsymbol{F}}) = \mathbb{L}_{\mu}^{\mathrm{M}}(\bar{\boldsymbol{F}}) + \Lambda^{\mathrm{M}}\,\mathbb{L}_{\Lambda}^{\mathrm{M}}(\bar{\boldsymbol{F}}) \quad \text{with} \quad \mathbb{L}_{\Lambda}^{\mathrm{M}} = \tfrac{1}{2}\,\partial_{\boldsymbol{F}\boldsymbol{F}}^2[(J-1)^2]\,. \tag{5.65}$$

Therein, according to Avazmohammadi & Ponte Castañeda [19], the term $\Lambda^{\mathrm{M}}\,\mathbb{L}_{\Lambda}^{\mathrm{M}}$ is required to enforce the incompressibility constraint. The first term is obtained by evaluating $\mathbb{L}_{\mu}^{\mathrm{M}} = \partial_{\boldsymbol{F}\boldsymbol{F}}^2\mathscr{W}_{\mu}^{\mathrm{M}}$ at $\bar{\boldsymbol{F}}$. Now, we note from expression (5.65) that in the incompressible limit of the matrix ($\Lambda^{\mathrm{M}} \to \infty$) some terms of the elasticity tensor $\mathbb{L}^{\mathrm{M}}$ become unbounded. However, the unbounded terms of $\mathbb{L}^{\mathrm{M}}$ enter Eq. (5.63) not only explicitly but also implicitly through the inverse of the microstructural tensor $\mathbb{P}$. In this way, it is possible to perform an asymptotic analysis for the expressions depending on Λ^{M} and to obtain in the

incompressible limit of the matrix regular expressions for the coefficients of $\{\mathbb{P}^{-1} - \mathbb{L}^{\mathrm{M}}\}^{\flat}$ by ruling out the unbounded terms. To do so, we utilise Eq. (5.65) and write the elasticity tensor as

$$\mathbb{L}^{\mathrm{M}} = \mathbb{L}^{\mathrm{M}}_{\mu} + \epsilon^{-1}\,\mathbb{L}^{\mathrm{M}}_{\Lambda}\,, \tag{5.66}$$

where $\epsilon = 1/\Lambda^{\mathrm{M}}$ is introduced as a small parameter tending to zero in the limit case as the matrix becomes incompressible. Then, recalling Eq. (5.25) and making use of the distributive law, the acoustic tensor is accordingly written as

$$\mathscr{A} = \mathscr{A}_{\mu} + \epsilon^{-1}\mathscr{A}_{\Lambda} \quad \text{with} \quad \mathscr{A}_{\mu} = \big((\mathbb{L}^{\mathrm{M}}_{\mu})^{T_{23}}\boldsymbol{\xi}\big)\boldsymbol{\xi} \quad \text{and} \quad \mathscr{A}_{\Lambda} = \big((\mathbb{L}^{\mathrm{M}}_{\Lambda})^{T_{23}}\boldsymbol{\xi}\big)\boldsymbol{\xi}\,. \tag{5.67}$$

Further, we recall from Eq. (5.25) that the tensor $\mathscr{B} = \mathscr{A}^{-1}$ is the inverse of the acoustic tensor. Making use of the notation of the outer tensor (double cross) product, see Appendix A.4, and the symmetry of $\mathscr{A}$, we can write $\mathscr{B}$ as

$$\mathscr{B} = \det[\mathscr{A}]^{-1}\,\mathrm{cof}[\mathscr{A}] = \frac{3\,\mathscr{A} \gg\!\ll \mathscr{A}}{(\mathscr{A} \gg\!\ll \mathscr{A}) \cdot \mathscr{A}}\,, \tag{5.68}$$

By inserting the relations (5.67) into (5.68) and simplifying by means of $\det[\mathscr{A}_{\Lambda}] = 0$ and $\mathrm{cof}[\mathscr{A}_{\Lambda}] = \mathbf{0}$, we arrive at

$$\mathscr{B} = \frac{\epsilon\,\mathrm{cof}[\mathscr{A}_{\mu}] + \mathscr{A}_{\mu} \gg\!\ll \mathscr{A}_{\Lambda}}{\epsilon\,\det[\mathscr{A}_{\mu}] + \mathrm{cof}[\mathscr{A}_{\mu}] \cdot \mathscr{A}_{\Lambda}}\,. \tag{5.69}$$

Consequently, $\mathscr{B}$ is expanded to second order in ϵ as follows:

$$\mathscr{B} = \mathscr{B}_0 + \epsilon\,\mathscr{B}_1 + \epsilon^2\,\mathscr{B}_2 + \mathcal{O}(\epsilon^3)\,, \tag{5.70}$$

where the tensors $\mathscr{B}_0$, $\mathscr{B}_1$, and $\mathscr{B}_2$ are identified as

$$\begin{aligned} \mathscr{B}_0 &= \frac{\mathscr{A}_{\mu} \gg\!\ll \mathscr{A}_{\Lambda}}{\mathrm{cof}[\mathscr{A}_{\mu}] \cdot \mathscr{A}_{\Lambda}}\,, \quad \mathscr{B}_1 = \frac{\mathrm{cof}[\mathscr{A}_{\mu}]}{\mathrm{cof}[\mathscr{A}_{\mu}] \cdot \mathscr{A}_{\Lambda}} - \frac{\det[\mathscr{A}_{\mu}]\;\mathscr{A}_{\mu} \gg\!\ll \mathscr{A}_{\Lambda}}{(\mathrm{cof}[\mathscr{A}_{\mu}] \cdot \mathscr{A}_{\Lambda})^2}\,, \quad \text{and} \\ \mathscr{B}_2 &= \frac{(\det[\mathscr{A}_{\mu}])^2\;\mathscr{A}_{\mu} \gg\!\ll \mathscr{A}_{\Lambda}}{(\mathrm{cof}[\mathscr{A}_{\mu}] \cdot \mathscr{A}_{\Lambda})^3} - \frac{\det[\mathscr{A}_{\mu}]\;\mathrm{cof}[\mathscr{A}_{\mu}]}{(\mathrm{cof}[\mathscr{A}_{\mu}] \cdot \mathscr{A}_{\Lambda})^2} \end{aligned} \tag{5.71}$$

Thus, $\mathscr{B}_0$ can be easily identified as the limiting value $\lim_{\Lambda^{\mathrm{M}} \to \infty} \mathscr{B}$. Then, based on Eqs (5.28) and (5.25), it is straightforward to introduce the associated expansion

$$\mathbb{P} = \mathbb{P}_0 + \epsilon\,\mathbb{P}_1 + \epsilon^2\,\mathbb{P}_2 + \mathcal{O}(\epsilon^3) \quad \text{where} \quad \mathbb{P}_i = \frac{1}{2\pi}\int_0^{2\pi} (\mathscr{B}_i \otimes \boldsymbol{\xi} \otimes \boldsymbol{\xi})^{T_{23}}\,\mathrm{d}\varsigma \tag{5.72}$$

and $i = 0, 1, 2$. Obviously, the property presented in (5.30) for $\mathbb{P}$ is equally observed for $\mathbb{P}_0$, $\mathbb{P}_1$, and $\mathbb{P}_2$, hence,

$$(\mathbb{P}_0)_{i3kl} = (\mathbb{P}_0)_{ijk3} = (\mathbb{P}_1)_{i3kl} = (\mathbb{P}_1)_{ijk3} = (\mathbb{P}_2)_{i3kl} = (\mathbb{P}_2)_{ijk3} = 0\,. \tag{5.73}$$

Having obtained the expansion for $\mathbb{P}$ for an incompressible matrix phase, given in $(5.72)_1$, we can formulate the consistent expression for the inverse $\{\mathbb{P}^{-1}\}^{\flat}$. Before doing this, we first notice that the leading-order term $\{\mathbb{P}_0\}^{\flat}$ does not have full rank, which implies that $\{\mathbb{P}\}^{\flat}$ becomes in the limit of a fully incompressible matrix singular. In detail, we can find

that $\lim_{\epsilon\to 0}\operatorname{nullity}[\{\mathbb{P}\}^\flat] = \operatorname{nullity}[\{\mathbb{P}_0\}^\flat] = 1$. Thus, the required inverse tensor $\{\mathbb{P}^{-1}\}^\flat$ cannot be computed from a simple inversion of the leading-order term $\{\mathbb{P}_0\}^\flat$. However, since the singularity of $\{\mathbb{P}\}^\flat$ is originated in the asymptotic expansion $(5.72)_1$, it is possible to formulate an appropriate asymptotic series expansion for the inverse in the limit case as $\epsilon \to 0$, reading

$$\left\{\mathbb{P}^{-1} = \epsilon^{-1}\,\mathbb{X}_{-1} + \mathbb{X}_0 + \mathcal{O}(\epsilon)\right\}^\flat , \tag{5.74}$$

see, for example, Avrachenkov et al. [22] or Franchi & Paruolo [133]. To compute the tensors $\{\mathbb{X}_{-1}\}^\flat$ and $\{\mathbb{X}_0\}^\flat$ in (5.74), we employ the so-called *basic generalised inverse method* as presented by Avrachenkov et al. [22] and therefore first introduce the following two matrices

$$\mathbf{P}^{(0)} = \left[\left\{\mathrm{P}_0\right\}^\flat\right] \in \mathcal{R}^{6\times 6} \qquad \text{and} \qquad \mathbf{P}^{(1)} = \mathbf{P} = \begin{bmatrix}\left\{\mathrm{P}_0\right\}^\flat & 0^{6\times 6}\\ \left\{\mathrm{P}_1\right\}^\flat & \left\{\mathrm{P}_0\right\}^\flat\end{bmatrix} \in \mathcal{R}^{12\times 12} . \tag{5.75}$$

Therein, $\mathbf{P}^{(0)}$ depicts the 2D matrix representation of $\{\mathbb{P}_0\}^\flat$, whereas $\mathbf{P}^{(1)}$ is an augmented block matrix and contains the 2D matrix representations of $\{\mathbb{P}_0\}^\flat$ and $\{\mathbb{P}_1\}^\flat$. At this point, it shall be remarked that the sufficiency of the expansion in (5.74) can be shown by utilising the rank test of Sain & Massey [414], which is performed by finding the minimum value $n \in \mathcal{N}_+$ for which $\operatorname{rank}[\mathbf{P}^{(n)}] = \operatorname{rank}[\mathbf{P}^{(n-1)}] + \dim[\mathbf{P}^{(0)}]$. Here, we can show that $\operatorname{rank}[\mathbf{P}^{(1)}] = \operatorname{rank}[\mathbf{P}^{(0)}] + \dim[\mathbf{P}^{(0)}]$, since $\operatorname{rank}[\mathbf{P}^{(1)}] = 11$, $\operatorname{rank}[\mathbf{P}^{(0)}] = 5$, and $\dim[\mathbf{P}^{(0)}] = 6$, and thus identify n as 1. Thereby n serves as a measure for the order of the singularity as ϵ tends to zero and indicates that (5.74) is sufficient. Further, it makes clear that $\mathbf{P}^{(n)}|_{n=1} = \mathbf{P}$ is the augmented matrix with which we have to proceed. The key step is now the computation of

$$\mathbf{G} = \mathbf{P}^\dagger = \begin{bmatrix}\mathrm{G}_{00} & \mathrm{G}_{01}\\ \mathrm{G}_{10} & \mathrm{G}_{11}\end{bmatrix} \in \mathcal{R}^{12\times 12} , \tag{5.76}$$

where $\mathbf{P}^\dagger$ denotes the *Moore–Penrose generalised inverse* of $\mathbf{P}$. It is highlighted that as $\mathbf{P}$ is a simple, two-dimensional matrix, the computation of the generalised inverse can be directly and easily performed with numerical standard tools. Further details about the valuable notation of generalised inverses, which are also referred to as pseudoinverses, are provided by Shinozaki et al. [437] and Ben-Israel & Greville [29]. Subsequently, we extract the two submatrices $\mathrm{G}_{00} \in \mathcal{R}^{6\times 6}$ and $\mathrm{G}_{01} \in \mathcal{R}^{6\times 6}$ from the block matrix, $\mathbf{G}$, and identify them as the 2D matrix representations of the fourth-order tensors $\{\mathbb{G}_{00}\}^\flat$ and $\{\mathbb{G}_{01}\}^\flat$, respectively. With those two tensors at hand, we specify the two unknown tensors in expansion (5.74) as

$$\left\{\mathbb{X}_{-1} = \mathbb{G}_{01}\right\}^\flat \qquad \text{and} \qquad \left\{\mathbb{X}_0 = \mathbb{G}_{00}\,(\mathbb{I} - \mathbb{P}_1\,\mathbb{X}_{-1}) - \mathbb{X}_{-1}\,\mathbb{P}_2\,\mathbb{X}_{-1}\right\}^\flat , \tag{5.77}$$

see Avrachenkov et al. [22]. Now, we can use the expansions given in (5.66) and (5.74) and formulate $\{\mathbb{P}^{-1} - \mathbb{L}^{\mathrm{M}} = \epsilon^{-1}\,(\mathbb{X}_{-1} - \mathbb{L}^{\mathrm{M}}_\Lambda) + \mathbb{X}_0 - \mathbb{L}^{\mathrm{M}}_\mu + \mathcal{O}(\epsilon)\}^\flat$. In the incompressible matrix limit, we have $\epsilon \to 0$ so that first- and higher-order terms in ϵ drop out. Further, in the case that the overall deformation is isochoric, as stated in Eq. (5.61), it can be shown that $\{\mathbb{X}_{-1} = \mathbb{L}^{\mathrm{M}}_\Lambda\}^\flat$. This cancels out the terms associated with ϵ^{-1} and leads to the result

$$\lim_{\Lambda^{\mathrm{M}}\to\infty} \left\{\mathbb{P}^{-1} - \mathbb{L}^{\mathrm{M}}\right\}^\flat = \left\{\mathbb{X}_0 - \mathbb{L}^{\mathrm{M}}_\mu\right\}^\flat . \tag{5.78}$$

Subsequently, utilising (5.78) in expression (5.63) leads to

$$\left\{[\mathbb{X}_0 - \mathbb{L}_\mu^{\mathrm{M}}](\bar{\boldsymbol{F}} - \bar{\boldsymbol{F}}_{\mathrm{F}}) + n^{\mathrm{M}}\,\Delta\boldsymbol{P}_{\mu\wp} = \boldsymbol{0}\right\}^{\flat}. \tag{5.79}$$

In conclusion, the asymptotic expansion provides for the incompressible matrix limit a closed-form expression of Eq. (5.63). From the tensorial equation (5.79), together with condition (5.45), one obtains the six scalar equations necessary to solve for the six unknowns, that is, the five unknown coefficients $(\bar{\boldsymbol{F}}_{\mathrm{F}})_{ij}$ $(i = 1,2,3$ and $j = 1,2)$ and the constraint pressure $\wp^{\mathrm{F}}$. Further, the overall energy is given by Eq. (5.64), while the associated macroscopic stress is given in Eq. (C.7).

5.3 Fibre composites with incompressible, transversely isotropic phases

In the previous section, the TSO estimate was specialised to incompressible behaviour of both phases $\mathcal{B}_0^\alpha$. Since no restrictions were made on the direction-dependence of the distortional phase energy parts $\mathscr{W}_\mu^\alpha$, the phases and, consequently, the overall composite behaviour were considered until now as generally anisotropic. In this section, we focus on transversely isotropic phases, where the preferred direction coincides with the alignment of the fibrous inclusions. This will consequently lead to an overall transversely isotropic behaviour. These considerations lead to simplifications of the underlying equations, in particular, by making use of appropriate generic representations of the deformation gradients.

5.3.1 Transversely isotropic phase behaviour

If the mechanical behaviour of the two phases $\mathcal{B}_0^\alpha$ belongs to the symmetry group of transverse isotropy, the distortional part of the local strain energies, $\mathscr{W}_\mu^\alpha(\boldsymbol{C}, \boldsymbol{M}^\alpha)$, becomes a function of the Cauchy–Green tensor $\boldsymbol{C}$ and a structural tensor $\boldsymbol{M}^\alpha$. Therein, the structural tensor accounts for the preferred direction of phase $\mathcal{B}_0^\alpha$ by means of a referential unit vector $\boldsymbol{a}_0^\alpha$, such that $\boldsymbol{M}^\alpha = \boldsymbol{a}_0^\alpha \otimes \boldsymbol{a}_0^\alpha$. This was explained in detail in Section 3.5.4. From there, we further know that a sufficient integrity basis for the two argument tensors $\{\boldsymbol{C}, \boldsymbol{M}^\alpha\}$ is given in terms of five scalar invariants. A variety of applicable invariant sets was introduced, such as $\mathscr{I}_{\mathrm{ti}}^{I}$, $\mathscr{I}_{\mathrm{ti}}^{I'}$, $\mathscr{I}_{\mathrm{ti}}^{I''}$, $\mathscr{I}_{\mathrm{ti}}^{\mathfrak{er}}$, $\mathscr{I}_{\mathrm{ti}}^{\mathfrak{i}}$, and $\mathscr{I}_{\mathrm{ti}}^{\mathfrak{j}}$. Any of those sets can be used for the definition of the phase strain-energy functions $\mathscr{W}_\mu^\alpha$ in the present context. Yet, for the following considerations in this chapter we employ the invariant set $\mathscr{I}_{\mathrm{ti}}^{I}$, which has already been subject to some further investigations in Sections 3.8.2 and 3.8.3. Further, we assume that the phase energies follow the additive split introduced in Eq. (3.152), such that

$$\mathscr{W}_\mu^\alpha(I_1, I_2, J, J_4, J_5) = \mathscr{W}_\mu^{\alpha I}(I_1, I_2, J_4, J_5) + \mathscr{W}_\mu^{\alpha J}(J)\,. \tag{5.80}$$

Hence, the J-dependent (or I_3-dependent) energy contribution is separated from the other terms. A general representation of the energy contribution $\mathscr{W}_\mu^{\alpha I}$ was provided in Eq. (3.176) and reads

$$\mathscr{W}_\mu^{\alpha I} = \mathscr{W}_{\mathrm{iso}}^\alpha(I_1, I_2) + \mathscr{W}_{\mathrm{aniso}}^\alpha(J_4, J_5) + \mathscr{W}_{\mathrm{coupl}}^\alpha(I_1, I_2, J_4, J_5)\,. \tag{5.81}$$

Since the phase energies have to normalise properly, the normalisation conditions (3.148) and (3.149) have to be fulfilled. It is further required that $\mathscr{W}_\mu^{\alpha I}$ and $\mathscr{W}_\mu^{\alpha J}$ fulfil the linearisation conditions, here for incompressible material behaviour, given in Eq. (3.155). We recall that to fulfil those conditions, the J-dependent term $\mathscr{W}_\mu^{\alpha J}$ has to be chosen dependent on the other energy contribution $\mathscr{W}_\mu^{\alpha I}$. In this process, it was shown in Section 3.8.3 that the energy term $\mathscr{W}_\mu^{\alpha J}$ usually contains a logarithmic term in J, as in Eq. (3.160). However, in agreement with the observations in Avazmohammadi & Ponte Castañeda [20], we found that replacing the logarithmic term with the polynomial-type term from the Taylor expansion (3.170) leads to better-behaved TSO estimates. In the context of compressible phases, it was further explained that the polynomial term, in connection with the here chosen dilatational energy $(5.33)_2$, suffers from correctly addressing the growth conditions as $J \to 0$. However, as the phases are considered as incompressible and $\Lambda^\alpha \to \infty$, this deficiency does not apply here.

5.3.2 Overall transversely isotropic behaviour

In the following, we assume that the preferred directions $\boldsymbol{a}_0^\alpha$ of the two phases are collinear with the alignment of the cylindrical inclusions, such that $\boldsymbol{a}_0^\alpha = \bar{\boldsymbol{a}}_0$. Hence, by recalling Eq. $(5.28)_2$, we set within the given laboratory frame of reference $\boldsymbol{a}_0^\alpha = \boldsymbol{e}_3$. If we further recall that the shape tensor $\boldsymbol{Z}$ was chosen in Section 5.1.2 such that the inclusions are distributed isotropically in the plane transverse to their alignment, together with the explanations from Section 3.5.4, it can be seen that the overall material behaviour becomes invariant to all transformations which belong to the symmetry group of transverse isotropy, $\mathcal{MG}_{\mathrm{ti}}$. As a consequence, the overall behaviour on the macroscopic scale becomes transversely isotropic and the vector $\bar{\boldsymbol{a}}_0$ thus describes the axis of the preferred material behaviour. Further, the effective energy $\widetilde{\mathscr{W}}$ becomes a function of the macroscopic Cauchy–Green tensor $\bar{\boldsymbol{C}}$, defined in (4.4), and a structural tensor $\bar{\boldsymbol{M}} = \bar{\boldsymbol{a}}_0 \otimes \bar{\boldsymbol{a}}_0$. In turn, all of the transversely isotropic invariant sets from Section 3.5.4 can be employed as a proper integrity basis of the two argument tensors $\{\bar{\boldsymbol{C}}, \bar{\boldsymbol{M}}\}$. We note that as the overall behaviour is incompressible, required by the constraint (5.57), the macroscopic energy becomes a function of four invariants and we can make use of the reductions provided in Table 3.2. Hence, the overall energy can be written, for instance, in terms of the invariant sets $\mathscr{I}_{\mathrm{ti}}^I$ and $\mathscr{I}_{\mathrm{ti}}^\imath$ as

$$\widetilde{\mathscr{W}}(\bar{\boldsymbol{C}}, \bar{\boldsymbol{M}}) = \widetilde{\mathscr{W}}(\bar{I}_1, \bar{I}_2, \bar{J}_4, \bar{J}_5) = \widetilde{\mathscr{W}}(\bar{\lambda}_\ell, \bar{\gamma}_\ell, \bar{\gamma}_{\mathrm{t}}, \bar{\psi}_\gamma)\,. \tag{5.82}$$

At this point, we recall from Section 3.5.4 that the two invariant sets $\mathscr{I}_{\mathrm{ti}}^\imath$ and $\mathscr{I}_{\mathrm{ti}}^\jmath$ can be used to formulate equivalent invariant-based deformation gradients, such as $\boldsymbol{F}^\imath$ and $\boldsymbol{F}^\jmath$ in Eqs (3.95) and (3.100), respectively. This is a very convenient property in the context of multiscale analysis, as it can be employed to connect the real occurring macroscopic deformation, quantified by frame-indifferent strain invariants, with a given laboratory frame of reference on the microscale. Hence, we can formulate a *generic macroscopic deformation gradient*, which is based on macroscopic strain invariants and is always properly aligned with respect to the orientation of the microstructure. Here, we employ a deformation gradient of the form $\boldsymbol{F}^\jmath$, since it contains one more zero-coefficient compared to $\boldsymbol{F}^\imath$, but

formulate it in dependence of the set $\mathscr{I}^{\,i}_{\mathrm{ti}}$. This leads to

$$\bar{\boldsymbol{F}} = \begin{bmatrix} \bar{\lambda}_1 & 0 & 0 \\ 0 & \bar{\lambda}_2 & 0 \\ \bar{\gamma}_\ell \cos[\bar{\phi}_\gamma] & \bar{\gamma}_\ell \sin[\bar{\phi}_\gamma] & \bar{\lambda}_\ell \end{bmatrix} \boldsymbol{e}_i \otimes \boldsymbol{e}_j \,, \tag{5.83}$$

where the two stretches

$$\bar{\lambda}_1 = \frac{\sqrt{\bar{\gamma}_{\mathrm{t}}^2 + 4\,\bar{\lambda}_\ell^{-1}} + \bar{\gamma}_{\mathrm{t}}}{2} \quad \text{and} \quad \bar{\lambda}_2 = \frac{\sqrt{\bar{\gamma}_{\mathrm{t}}^2 + 4\,\bar{\lambda}_\ell^{-1}} - \bar{\gamma}_{\mathrm{t}}}{2} \tag{5.84}$$

are obtained from Eqs $(3.102)_{1,2}$, together with $\bar{\lambda}_{\mathrm{t}} = 1/\bar{\lambda}^{-1/2}$ because of the overall incompressibility. The coupling invariant $\bar{\phi}_\gamma$ is defined by Eq. $(3.102)_3$ Further, we formulate for the two phases the associated deformation gradients

$$\bar{\boldsymbol{F}}_\alpha = \begin{bmatrix} \bar{\lambda}_{\alpha 1} & 0 & 0 \\ 0 & \bar{\lambda}_{\alpha 2} & 0 \\ \bar{\gamma}_{\alpha\ell} \cos[\bar{\phi}_{\alpha\gamma}] & \bar{\gamma}_{\alpha\ell} \sin[\bar{\phi}_{\alpha\gamma}] & \bar{\lambda}_\ell \end{bmatrix} \boldsymbol{e}_i \otimes \boldsymbol{e}_j \,, \tag{5.85}$$

where the matrix stretches are given by

$$\bar{\lambda}_{\mathrm{M1}} = \frac{\sqrt{\bar{\gamma}_{\mathrm{Mt}}^2 + 4\,\bar{\lambda}_{\mathrm{Mt}}^2} + \bar{\gamma}_{\mathrm{Mt}}}{2} \quad \text{and} \quad \bar{\lambda}_{\mathrm{M2}} = \frac{\sqrt{\bar{\gamma}_{\mathrm{Mt}}^2 + 4\,\bar{\lambda}_{\mathrm{Mt}}^2} - \bar{\gamma}_{\mathrm{Mt}}}{2} \,, \tag{5.86}$$

whereas the incompressibility constraint (5.45) for the phase average of the fibre phase leads to

$$\bar{\lambda}_{\mathrm{F1}} = \frac{\sqrt{\bar{\gamma}_{\mathrm{Ft}}^2 + 4\,\bar{\lambda}_\ell^{-1}} + \bar{\gamma}_{\mathrm{Ft}}}{2} \quad \text{and} \quad \bar{\lambda}_{\mathrm{F2}} = \frac{\sqrt{\bar{\gamma}_{\mathrm{Ft}}^2 + 4\,\bar{\lambda}_\ell^{-1}} - \bar{\gamma}_{\mathrm{Ft}}}{2} \,, \tag{5.87}$$

because of $\bar{\lambda}_{\mathrm{Ft}} = 1/\sqrt{\bar{\lambda}_\ell}$. From this, it is now easy to observe that the above-made considerations reduce the scalar unknowns within the average fibre deformation tensor $\bar{\boldsymbol{F}}_{\mathrm{F}}$ to three, namely, the longitudinal fibre shear $\bar{\gamma}_\ell$, the transverse fibre shear $\bar{\gamma}_{\mathrm{t}}$ (or, equivalently, the stretch $\bar{\lambda}_{\mathrm{F1}}$), and the coupling invariant $\bar{\phi}_{\mathrm{F}\gamma}$. Thus, the homogenisation is equivalent to solve instead of six only for *four unknowns*, that is, for $\{\bar{\gamma}_{\mathrm{F}\ell}, \bar{\gamma}_{\mathrm{Ft}}, \bar{\phi}_{\mathrm{F}\gamma}, \wp^{\mathrm{F}}\}$ or, equivalently, $\{\bar{\gamma}_{\mathrm{F}\ell}, \bar{\lambda}_{\mathrm{F1}}, \bar{\phi}_{\mathrm{F}\gamma}, \wp^{\mathrm{F}}\}$. The necessary four equations can be extracted from Eq. (5.79). In general, those equations have to be solved numerically. However, there are scenarios for which closed-form solutions of the required equations can be formulated. This is exemplary shown in Appendix C.3 for composites with isotropic Neo-Hookean phases augmented by transversely isotropic energy contributions.

5.3.3 Linearised behaviour of the TSO estimate

An indispensable requirement of the presented estimate for nonlinear composites is that it linearises properly in the limit of small strains ($\bar{\boldsymbol{F}} \approx \boldsymbol{I}$) by recovering the corresponding linear-elastic estimates, here, for incompressible composites with aligned cylindrical inclusions. Hence, as explained in detail in Section 3.7.3, the linearised energy $\widetilde{\mathscr{W}}_{\mathrm{lin}} := \mathcal{T}_2\{\widetilde{\mathscr{W}}(\bar{\boldsymbol{F}}), \boldsymbol{I}\}$ is obtained from the second-order Taylor expansion, which reads

$$\widetilde{\mathscr{W}}_{\mathrm{lin}}(\bar{\boldsymbol{F}}) = \widetilde{\mathscr{W}}(\bar{\boldsymbol{F}})\,\big|_{\bar{\boldsymbol{F}}=\boldsymbol{I}} + \widetilde{\boldsymbol{P}}(\bar{\boldsymbol{F}})\,\big|_{\bar{\boldsymbol{F}}=\boldsymbol{I}} \cdot (\bar{\boldsymbol{F}} - \boldsymbol{I}) + \tfrac{1}{2}\,(\bar{\boldsymbol{F}} - \boldsymbol{I}) \cdot \widetilde{\mathbb{L}}(\bar{\boldsymbol{F}})\,\big|_{\bar{\boldsymbol{F}}=\boldsymbol{I}} (\bar{\boldsymbol{F}} - \boldsymbol{I}) \,, \tag{5.88}$$

compare Eq. (3.132). As the phase energies are required to normalise and linearise properly, formulated in Section (5.3.1), it makes sense that the macroscopic behaviour has an energy- and stress-free reference state as well. Hence, the first two terms in Eq. (5.88) do not contribute to the linearised energy, since $\widetilde{\mathscr{W}_{[\boldsymbol{I}]}} = 0$ and $\widetilde{\boldsymbol{P}}_{[\boldsymbol{I}]} = \boldsymbol{0}$. This can be observed from the respective expressions (5.62) and (C.7) by noting that $\bar{\boldsymbol{F}}_{\alpha[\boldsymbol{I}]} = \bar{\boldsymbol{F}}_{[\boldsymbol{I}]} = \boldsymbol{I}$ and $\wp^{\mathrm{F}}_{[\boldsymbol{I}]} = 0$. Consequently, $\widetilde{\mathbb{L}}_{[\boldsymbol{I}]}$ is identified as the resulting linearised elasticity tensor $\widetilde{\mathbb{L}}_{\mathrm{lin}}$. From the overall energy split, given in Eq. (5.59), it follows that $\widetilde{\mathbb{L}}_{\mathrm{lin}}$ is composed of a distortional term $\widetilde{\mathbb{L}}_{\mu\,\mathrm{lin}} = \partial^2_{\bar{\boldsymbol{F}}\bar{\boldsymbol{F}}}\widetilde{\mathscr{W}_{\mu[\boldsymbol{I}]}}$ and a dilatational term $\widetilde{\mathbb{L}}_{\Lambda\,\mathrm{lin}} = \partial^2_{\bar{\boldsymbol{F}}\bar{\boldsymbol{F}}}\widetilde{\mathscr{W}_{\Lambda[\boldsymbol{I}]}}$, such that

$$\widetilde{\mathbb{L}}_{\mathrm{lin}} = \widetilde{\mathbb{L}}_{\mu\,\mathrm{lin}} + \widetilde{\mathbb{L}}_{\Lambda\,\mathrm{lin}}\,. \tag{5.89}$$

Subsequently, the two elasticity tensors are given by

$$\begin{aligned}
\widetilde{\mathbb{L}}_{\mu\,\mathrm{lin}} &= \partial^2_{\bar{\boldsymbol{F}}\bar{\boldsymbol{F}}}\widetilde{\mathscr{W}_{\mu[\boldsymbol{I}]}} = n^{\mathrm{F}}\,\mathrm{sym}\big[\mathbb{L}^{\mathrm{F}}_{\mu[\boldsymbol{I}]}\mathbb{F}_{\mathrm{F}} + (\partial_{\bar{\boldsymbol{F}}}\wp^{\mathrm{F}}_{[\boldsymbol{I}]}\otimes\boldsymbol{I})(\mathbb{I}-\mathbb{F}_{\mathrm{F}})\big] + n^{\mathrm{M}}\,\mathrm{sym}\big[\mathbb{L}^{\mathrm{M}}_{\mu[\boldsymbol{I}]}\mathbb{F}_{\mathrm{M}}\big] \\
\widetilde{\mathbb{L}}_{\Lambda\,\mathrm{lin}} &= \partial^2_{\bar{\boldsymbol{F}}\bar{\boldsymbol{F}}}\widetilde{\mathscr{W}_{\Lambda[\boldsymbol{I}]}} = \tilde{\Lambda}_{\infty}\boldsymbol{I}\otimes\boldsymbol{I}\,,
\end{aligned} \tag{5.90}$$

where $\mathbb{F}_{\alpha} = \partial_{\bar{\boldsymbol{F}}}\bar{\boldsymbol{F}}_{\alpha}$, see also Eq. (C.2). After some algebra and using the linearisation conditions (3.155), the distortional part can be written as

$$\widetilde{\mathbb{L}}_{\mu\,\mathrm{lin}} = 2\tilde{\mu}_{\mathrm{a}}\,(\mathbb{E}^{[1]}+\mathbb{E}^{[2]}) + 2\tilde{\mu}_{\mathrm{t}}\,\mathbb{E}^{[3]} + 2\tilde{\mu}_{\ell}\,\mathbb{E}^{[4]}\,. \tag{5.91}$$

The fourth-order projection tensors $\mathbb{E}^{[\gamma]}$ ($\gamma = 1,2,3,4$) used therein were introduced in Section 3.7.3. Their definitions are provided in Appendix A.7.3. Further, $\tilde{\mu}_{\mathrm{a}}$, $\tilde{\mu}_{\mathrm{t}}$, and $\tilde{\mu}_{\ell}$ are the resulting effective axisymmetric, transverse and longitudinal shear moduli, which are given by

$$\tilde{\mu}_{\mathrm{a}} = n^{\mathrm{F}}\,\mu^{\mathrm{F}}_{\mathrm{a}} + n^{\mathrm{M}}\,\mu^{\mathrm{M}}_{\mathrm{a}} \quad\text{and}\quad \tilde{\mu}_{\beta} = \mu^{\mathrm{M}}_{\beta}\,\frac{(1+n^{\mathrm{F}})\,\mu^{\mathrm{F}}_{\beta} + n^{\mathrm{M}}\mu^{\mathrm{M}}_{\beta}}{n^{\mathrm{M}}\mu^{\mathrm{F}}_{\beta} + (1+n^{\mathrm{F}})\,\mu^{\mathrm{M}}_{\beta}} \quad\text{with}\quad \beta = \{\mathrm{t},\ell\}\,. \tag{5.92}$$

In Eq. $(5.90)_2$, the effective first Lamé constant $\tilde{\Lambda}_{\infty}$ tends to infinity due to the incompressibility of both phases. Further, it becomes clear from Eq. (5.91) that there are distinct effective transverse and longitudinal shear moduli that depend on the respective shear moduli of the two phases. Further, the two effective shear moduli exactly correspond to the *Hashin–Shtrikman lower bounds* for linear-elastic materials with overall transversely isotropic behaviour and transversely isotropic phases as presented in Hashin [182]. Moreover, the effective axisymmetric shear modulus $\tilde{\mu}_{\mathrm{a}}$ is identified as the *Voigt upper bound*. Note, for I_2- and J_5-independent phase energies ($\partial_{I_2}\mathscr{W}^{\alpha}_{\mu} = \partial_{J_5}\mathscr{W}^{\alpha}_{\mu} = 0$), the two effective moduli $\tilde{\mu}_{\mathrm{t}}$ and $\tilde{\mu}_{\ell}$ become identical, because $\mu^{\alpha}_{\mathrm{t}} = \mu^{\alpha}_{\ell}$, see Eqs (3.155). Furthermore, by neglecting the coupling terms $\mathscr{W}^{\alpha}_{\mathrm{coupl}}$, entailing that $\mu^{\alpha}_{\mathrm{a}} = \mu^{\alpha}_{\mathrm{t}} = \mu^{\alpha}_{\ell}$, the linearised results given in Eqs (5.89)-(5.92) reduce to the estimates for linear-elastic materials with overall transversely isotropic behaviour and isotropic phases as given by Hashin [182, 183]. For completeness, we note that expression (5.88) for the linearised effective energy finally reads $\widetilde{\mathscr{W}_{\mathrm{lin}}}(\bar{\boldsymbol{\varepsilon}},\bar{\boldsymbol{M}}) = \bar{\boldsymbol{\varepsilon}}\cdot\widetilde{\mathbb{L}}_{\mathrm{lin}}(\bar{\boldsymbol{M}})\,\bar{\boldsymbol{\varepsilon}}/2$, where the linear strain tensor $\bar{\boldsymbol{\varepsilon}} = \mathrm{sym}[\bar{\boldsymbol{H}}]$ is defined as the symmetric part of the macroscopic displacement gradient $\bar{\boldsymbol{H}} = \bar{\boldsymbol{F}} - \boldsymbol{I}$. This follows in direct analogy to the considerations from Section 3.7.3, in particular Eqs (3.133) and (3.134).

5.3.4 A special result for augmented isotropic phases with unidirectional reinforcement

In many applications, the strain-energy in the phases can be described by a purely isotropic part and a J_4-based anisotropic contribution. Such energies can be derived from the general expression (5.81) by setting $\partial_{J_5}\mathscr{W}^\alpha = \mathscr{W}^\alpha_{\text{coupl}} = 0$ and read

$$\mathscr{W}^\alpha_\mu(I_1, I_2, J, J_4) = \mathscr{W}^\alpha_{\text{iso}}(I_1, I_2) + \mathscr{W}^\alpha_{\text{aniso}}(J_4) + \mathscr{W}^{\alpha J}_\mu(J)\,. \tag{5.93}$$

They describe so-called *augmented isotropic materials with unidirectional reinforcement*, see, for example, Merodio & Ogden [322] and are very common, for instance, in modelling of biological tissues. Restricting oneself to composites with such phase energies leads in the context of this paper to some interesting results. Namely, one can show that the solution of Eq. (5.79), and hence the average microscopic deformations $\bar{\boldsymbol{F}}_\alpha$, becomes independent of the anisotropic phase energy terms $\mathscr{W}^\alpha_{\text{aniso}}$. For the sake of brevity, the detailed explanations on that are moved to C.2. Subsequently, making use of this finding in expression (5.64) for the effective energy, together with (5.31), it is easy to show that $\widetilde{\mathscr{W}}$ can then be additively split as follows:

$$\partial_{J_5}\mathscr{W}^\alpha_\mu = \mathscr{W}^\alpha_{\text{coupl}} = 0 \quad\rightarrow\quad \widetilde{\mathscr{W}}(\bar{I}_1, \bar{I}_2, \bar{J}_4, \bar{J}_5) = \widetilde{\mathscr{W}}_{\text{g}}(\bar{I}_1, \bar{I}_2, \bar{J}_4, \bar{J}_5) + \sum_\alpha n^\alpha\, \mathscr{W}^\alpha_{\text{aniso}}(\bar{J}_4)\,. \tag{5.94}$$

Therein, $\widetilde{\mathscr{W}}_{\text{g}}$ is the effective energy associated with the isotropic phase energy terms $\mathscr{W}^\alpha_{\text{iso}}(I_1, I_2) + \mathscr{W}^{\alpha J}_\mu(J)$, whereas the anisotropic parts $\mathscr{W}^\alpha_{\text{aniso}}(J_4)$ are homogenised by means of a simple arithmetic (Voigt-type) averaging. It is noted that despite the fact that only isotropic phase energies are considered in the derivation of $\widetilde{\mathscr{W}}_{\text{g}}$, the incorporation of the fibrous microstructure still entails that $\widetilde{\mathscr{W}}_{\text{g}}$ is generally *anisotropic*. Therefore, $\widetilde{\mathscr{W}}_{\text{g}}$ depends on all four macroscopic invariants $\{\bar{I}_1, \bar{I}_2, \bar{J}_4, \bar{J}_5\}$ (or $\{\bar{\lambda}_\ell, \bar{\gamma}_\ell, \bar{\gamma}_{\text{t}}, \bar{\psi}_\gamma\}$).

5.4 Alternative estimates and bounds for incompressible two-phase fibre composites

To put the presented estimate into context with previous works, we want to give a short review on alternative estimates and bounds for the here considered class of hyperelastic materials with incompressible cylindrical inclusions in an incompressible matrix.

Voigt upper bound A simple estimate is obtained in terms of the Voigt estimate, which assumes uniform deformations in the material and depicts a rigorous upper bound. For the given class of hyperelastic materials with incompressible cylindrical inclusions in an incompressible matrix, the Voigt bound reads

$$\widetilde{\mathscr{W}}_{\text{V}}(\bar{\lambda}_\ell, \bar{\gamma}_\ell, \bar{\gamma}_{\text{t}}) = n^{\text{F}}\, \mathscr{W}^{\text{F}}_\mu(\bar{\lambda}_\ell, \bar{\gamma}_\ell, \bar{\gamma}_{\text{t}}) + n^{\text{M}}\, \mathscr{W}^{\text{M}}_\mu(\bar{\lambda}_\ell, \bar{\gamma}_\ell, \bar{\gamma}_{\text{t}})\,. \tag{5.95}$$

As discussed in Section 4.3.5, the Voigt bound accounts for the microstructure only through the volume fractions and generally overestimates the actual energy in the composite. Yet, we already mentioned that the Voigt bound provides exact results for some specific scenarios. For the given fibre composites, this is true for axisymmetric loading cases, where the assumption of a uniform deformation field holds true. This was shown, for example,

by He et al. [191] or Agoras et al. [4]. However, we note that the simplicity of the Voigt bound further entails that the effective behaviour becomes isotropic for isotropic phases ($\mathscr{W}^{\alpha}_{\mathrm{aniso}} = 0$) since it fully ignores the microstructural arrangement of the cylindrical inclusions. This is in contrast to more sophisticated estimates.

Alternative second-order estimates for isotropic phases For isotropic, I_1-based generalised Neo-Hooke phase energies of the form $\mathscr{W}^{\alpha}_{\mu}(\boldsymbol{C}) = \mathscr{W}^{\alpha}_{\mathrm{iso}}(I_1) + \mathscr{W}^{\alpha J}_{\mu}(J)$, Agoras et al. [4] proposed a second-order estimate which consists of a TSO estimate for axisymmetric and longitudinal (out-of-plane) shear deformations and a *generalised second-order* (GSO) estimate for the transverse (in-plane) shear deformations. It reads

$$\widetilde{\mathscr{W}}_{\mathrm{ALP}}(\bar{\lambda}_\ell, \bar{\gamma}_\ell, \bar{\gamma}_\mathrm{t}) = n^{\mathrm{F}}\, \mathscr{W}^{\mathrm{F}}_{\mathrm{iso}}(I^{\mathrm{F}}_1) + n^{\mathrm{M}}\, \mathscr{W}^{\mathrm{M}}_{\mathrm{iso}}(\hat{I}^{\mathrm{M}}_1) + \sum_{\alpha} n^{\alpha}\, \partial_{I_1} \mathscr{W}^{\alpha}_{\mathrm{iso}}(I^{\alpha}_1)\, \bar{\gamma}_{\alpha\ell}\, (\bar{\gamma}_\ell - \bar{\gamma}_{\alpha\ell})\,, \quad (5.96)$$

where $\alpha = \{\mathrm{F}, \mathrm{M}\}$ and I^{F}_1, $\hat{I}^{\mathrm{M}}_1$, I^{M}_1, and $\bar{\gamma}_{\alpha\ell}$ are determined by Eqs *(39)-(42)* in Agoras et al. [4]. The GSO method considers second moments of the field fluctuations inside the phases, meaning that it incorporates the covariance data from Eq. (4.29), as opposed to the TSO which makes use of the first moments only. As a consequence, the GSO method is regarded as more accurate than the TSO method for transverse (in-plane) shear deformations, but requires more computational effort, see Ponte Castañeda [377] and Lopez-Pamies & Ponte Castañeda [299]. Thus, Agoras et al. [4] proposed to only compute the GSO estimate for transverse shear and to set up for the other loadings a hybrid model based on the TSO method. This made it possible to formulate the estimate in the compact form (5.96).

Estimates for a Neo-Hookean matrix phase When restricting the considerations to a Neo-Hookean matrix phase with $\mathscr{W}^{\mathrm{M}}_{\mu}(\boldsymbol{C}) = \mathscr{W}^{\mathrm{M}}_{\mathrm{iso}}(I_1) + \mathscr{W}^{\mathrm{M}J}_{\mu}(J)$ and $\mathscr{W}^{\mathrm{M}}_{\mathrm{iso}} = \mu^{\mathrm{M}}(I_1 - 3)/2$, several closed-form estimates for the class of materials of interest can be found in the literature. For composites with isotropic fibres of Neo-Hookean type ($\mathscr{W}^{\mathrm{F}}_{\mathrm{aniso}} = \mathscr{W}^{\mathrm{F}}_{\mathrm{coupl}} = 0$), Building up on earlier works (deBotton [91]), deBotton et al. [92] introduced an elegant estimate that is based on the sequential laminate procedure and reads

$$\widetilde{\mathscr{W}}_{\mathrm{BHS}}(\bar{\lambda}_\ell, \bar{\gamma}_\ell, \bar{\gamma}_\mathrm{t}) = \tfrac{1}{2}\bar{\mu}\,(\bar{\lambda}^2_\ell + 2\,\bar{\lambda}^{-1}_\ell - 3) + \tfrac{1}{2}\tilde{\mu}\,(\bar{\gamma}^2_\ell + \bar{\gamma}^2_\mathrm{t}) \quad (5.97)$$

where

$$\bar{\mu} = n^{\mathrm{F}}\mu^{\mathrm{F}} + n^{\mathrm{M}}\mu^{\mathrm{M}} \quad \text{and} \quad \tilde{\mu} = \mu^{\mathrm{M}}\, \frac{(1 + n^{\mathrm{F}})\, \mu^{\mathrm{F}} + n^{\mathrm{M}}\mu^{\mathrm{M}}}{n^{\mathrm{M}}\mu^{\mathrm{F}} + (1 + n^{\mathrm{F}})\, \mu^{\mathrm{M}}}\,. \quad (5.98)$$

The so-called BHS estimate is exact for combined longitudinal and axisymmetric shear deformations for the class of fibre-reinforced Neo-Hookean materials with the *composite cylinder assemblage* microstructure of Hashin & Rosen [184].

Lopez-Pamies & Idiart [297] generalised the BHS estimate towards anisotropic fibres, characterised by an isotropic Neo-Hookean part $\mathscr{W}^{\mathrm{F}}_{\mathrm{iso}} = \mu^{\mathrm{F}}(I_1 - 3)/2$ and a general J_4-based anisotropic part $\mathscr{W}^{\mathrm{F}}_{\mathrm{aniso}}(J_4) = \mathscr{W}^{\mathrm{F}}_{\mathrm{aniso}}(\lambda_\ell)$ ($\mathscr{W}^{\mathrm{F}}_{\mathrm{coupl}} = 0$), and derived the estimate

$$\widetilde{\mathscr{W}}_{\mathrm{LI}}(\bar{\lambda}_\ell, \bar{\gamma}_\ell, \bar{\gamma}_\mathrm{t}) = \tfrac{1}{2}\bar{\mu}\,(\bar{\lambda}^2_\ell + 2\,\bar{\lambda}^{-1}_\ell - 3) + \tfrac{1}{2}\tilde{\mu}\,(\bar{\gamma}^2_\ell + \bar{\gamma}^2_\mathrm{t}) + n^{\mathrm{F}}\, \mathscr{W}^{\mathrm{F}}_{\mathrm{aniso}}(\bar{\lambda}_\ell)\,. \quad (5.99)$$

According to Lopez-Pamies & Idiart [297], (5.99) expresses for this specific class of materials an exact stored-energy function. Also note that the additive character of the

anisotropic fibre term given in (5.99) agrees with the findings for the new estimate made in Section 5.3.4.

A further estimate for isotropic phases, based on the Halpin-Tsai equations, is obtained by specialising the results of Guo et al. [173] to Neo-Hookean fibres, giving

$$\widetilde{\mathscr{W}}_{\mathrm{GPM}}(\bar{\lambda}_\ell, \bar{\gamma}_\ell, \bar{\gamma}_\mathrm{t}) = \tfrac{1}{2}\bar{\mu}\,(\bar{\lambda}_\ell^2 + 2\,\bar{\lambda}_\ell^{-1} - 3) + \tfrac{1}{2}\tilde{\mu}\,\bar{\gamma}_\ell^2 + \tfrac{1}{2}\check{\mu}_\mathrm{t}\,\bar{\gamma}_\mathrm{t}^2 \tag{5.100}$$

with

$$\check{\mu}_\mathrm{t} = \mu^\mathrm{M}\,\frac{(1+0.4\,n^\mathrm{F})\,\mu^\mathrm{F} + 0.4\,n^\mathrm{M}\mu^\mathrm{M}}{n^\mathrm{M}\mu^\mathrm{F} + (0.4+n^\mathrm{F})\,\mu^\mathrm{M}}\,. \tag{5.101}$$

Obviously, the GPM estimate corresponds for axisymmetric and longitudinal shear deformations to the BHS estimate, but differs whenever transverse shear loading is involved (that is, for $\bar{\gamma}_\mathrm{t} \neq 0$). Thus, it fails to linearise properly in this mode of deformation.

Further, note that the effective shear moduli given in Eqs (5.98) are equal to the linear effective moduli given in (5.92) and that the energy $\widetilde{\mathscr{W}}_{\mathrm{BHS}}$ (and, hence, $\widetilde{\mathscr{W}}_{\mathrm{LI}}$) might thus be interpreted as a generalisation of the linear results to the hyperelastic regime.

5.5 Results and discussion of the new TSO estimate

This section focuses on investigating the performance of the new TSO estimate. For this purpose, we vary the phase energies and the loading scenarios and compare the new TSO estimate with other estimates given in Section 5.4 subject to their applicability for the respective class of materials. Moreover, we compare the new estimate with literature data obtained from full-field numerical simulations. For all results, we assume unit-less material stiffness which results in unit-less energies and stresses. Further, in order to compare uniaxial deformation in fibre direction with the two shear modes along and across the fibres, we recall from Eq. (3.105) the definition of the axisymmetric shear variable $\gamma_\mathrm{a}^2 = \lambda_\ell^2 + 2\,\lambda_\ell^{-1} - 3$.

5.5.1 Performance of the new estimate for composites with an isotropic Neo-Hookean matrix phase

First, we consider composites in which the matrix phase exhibits an isotropic Neo-Hookean behaviour, described by the energy

$$\mathscr{W}_\mu^\mathrm{M}(I_1, J) = \tfrac{1}{2}\mu^\mathrm{M}\,(I_1 - 3) + \tfrac{1}{2}\mu^\mathrm{M}\,(J-1)(J-3)\,. \tag{5.102}$$

As already mentioned in Section 5.3.1, such polynomial-type terms for the J-dependent energy contribution lead to an improved performance of the presented TSO estimate in comparison to the classical logarithmic terms.

Isotropic Neo-Hookean fibre Figure 5.2 depicts the results if the fibre phase is assumed to behave like an isotropic Neo-Hookean material. This means that the fibre energy $\mathscr{W}_\mu^\mathrm{M}$ is described by a strain-energy function as formulated in Eq. (5.102) for the matrix phase. Further note that some explicit results for this scenario are provided in Appendix C.3.4 by setting $\mathscr{W}_{\mathrm{aniso}}^\mathrm{F} = 0$ in Eq. (C.22). The volume fraction of the fibre phase is set to $n^\mathrm{F} = 0.3$ and the stiffnesses are $\mu^\mathrm{F} = 100$ and $\mu^\mathrm{M} = 1.$. From Figure 5.2a, one can

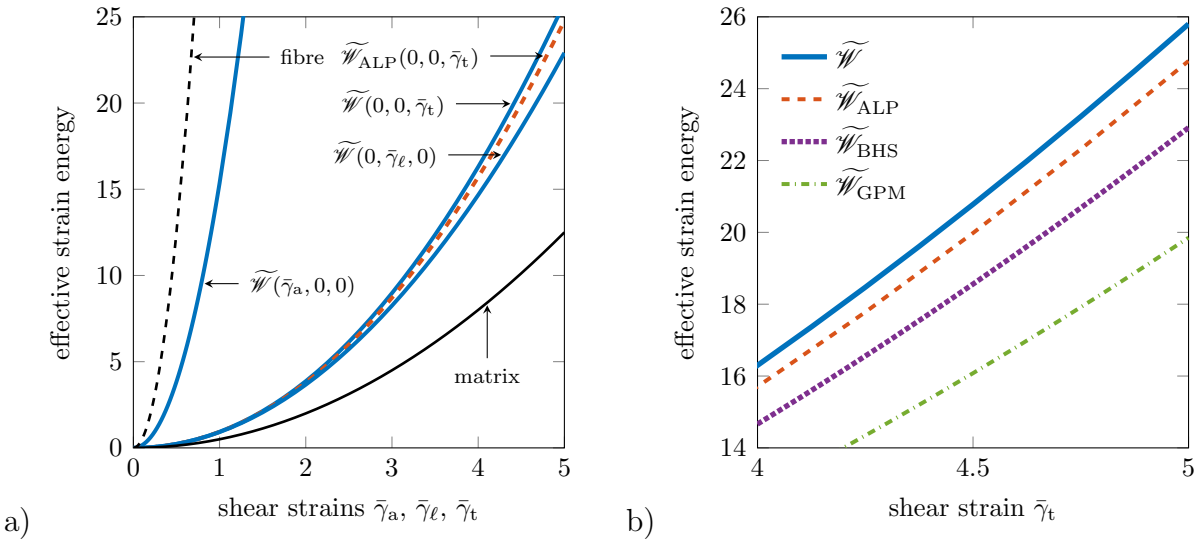

Figure 5.2: Effective energies for composites with Neo-Hookean matrix and Neo-Hookean fibre under the three different shear modes. The material parameters are $\mu^F = 100$, $\mu^M = 1$, and $n^F = 0.3$. a) Results for the second-order estimates $\widetilde{\mathscr{W}}$ and $\widetilde{\mathscr{W}}_{ALP}$. $\widetilde{\mathscr{W}}$ and $\widetilde{\mathscr{W}}_{ALP}$ coincide for axisymmetric and longitudinal shear. b) Comparison of different estimates for transverse shear deformation.

see that the effective energy $\widetilde{\mathscr{W}}(\bar{\gamma}_a,0,0)$ for the axisymmetric shear case is much higher than for the resulting energies due to longitudinal shear, $\widetilde{\mathscr{W}}(0,\bar{\gamma}_\ell,0)$, and transverse shear, $\widetilde{\mathscr{W}}(0,0,\bar{\gamma}_t)$. Further, for this class of composites, the new estimate, the ALP estimate as well as the BHS estimate (and thus the LI estimate) are identical for axisymmetric and for longitudinal shear deformations, that is, $\widetilde{\mathscr{W}}(\bar{\gamma}_a,0,0) = \widetilde{\mathscr{W}}_{ALP}(\bar{\gamma}_a,0,0) = \widetilde{\mathscr{W}}_{BHS}(\bar{\gamma}_a,0,0)$ and $\widetilde{\mathscr{W}}(0,\bar{\gamma}_\ell,0) = \widetilde{\mathscr{W}}_{ALP}(0,\bar{\gamma}_\ell,0) = \widetilde{\mathscr{W}}_{BHS}(0,\bar{\gamma}_\ell,0)$. The Voigt bound predicts for all three shear modes the same energy, which coincides with the axisymmetric mode of the other estimates, that is, $\widetilde{\mathscr{W}}_V = \widetilde{\mathscr{W}}(\bar{\gamma}_a,0,0)$. For transverse shear, the Voigt bound and the BHS estimate predict the same effective energy as for longitudinal shear, whereas the second-order estimates show distinct behaviours for these two shear modes. Figure 5.2b depicts a detailed comparison of the different estimates for the case of transverse shear. From this figure, one can see that the new estimate, $\widetilde{\mathscr{W}}$, is in good agreement with the ALP estimate, which is for this kind of loading equivalent to the GSO estimate and thus regarded as the most accurate one. The GPM estimate predicts a significantly lower effective strain energy than the other estimates.

Next, we compare the new estimates with full-field simulations based on the finite-element method (FEM). Figure 5.3a shows the effective strain energies during longitudinal shear deformation for the new estimate, $\widetilde{\mathscr{W}}$, the Voigt bound, and FEM results by Guo et al. [173]. The new estimate excellently agrees with the FEM solution, while the Voigt bound significantly overestimates the effective strain energy. Note, for this scenario, all other analytical estimates presented in Section 5.4 become identical to $\widetilde{\mathscr{W}}$ and are therefore omitted. Further, for axisymmetric shear loading, all estimates (including the Voigt bound) agree with the FEM solutions performed by Guo et al. [173] (for the mechanically equivalent case of uniaxial tension and compression). Hence, the results are not explicitly shown here. For transverse shear loading, shown in Figure 5.3b, the new estimate, the ALP estimate and the BHS model give virtually identical result

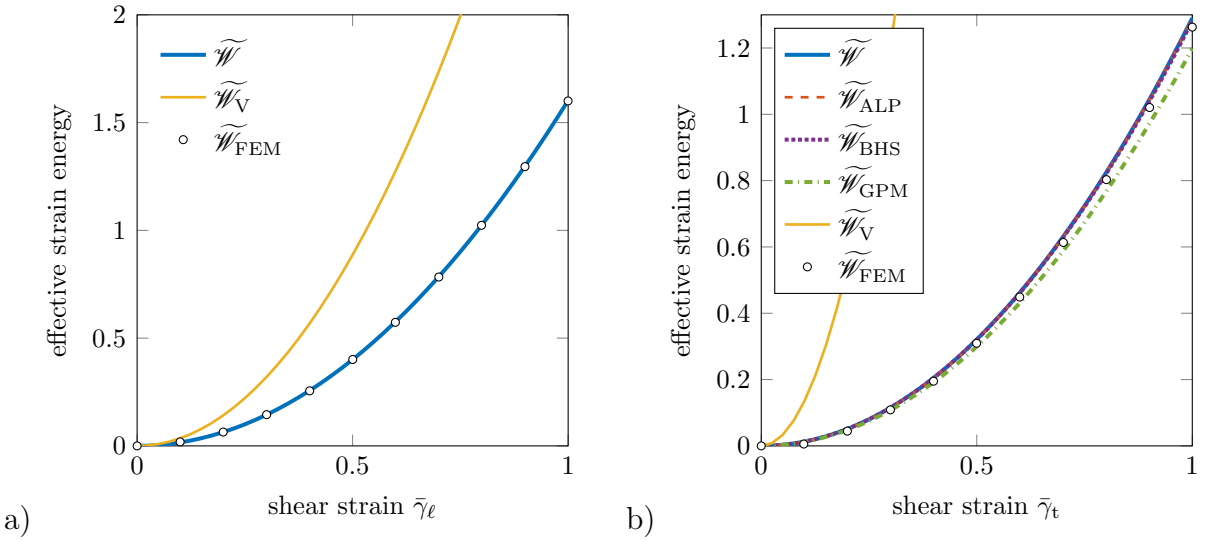

Figure 5.3: Comparison of analytical results and finite-element simulations of Guo et al. [173] for composites with Neo-Hookean matrix and Neo-Hookean fibre. a) Results for longitudinal shear deformation with the material parameters $\mu^\mathrm{F} = 20$, $\mu^\mathrm{M} = 2$, and $n^\mathrm{F} = 0.283$. b) Results for transverse shear deformation with the material parameters $\mu^\mathrm{F} = 200$, $\mu^\mathrm{M} = 2$, $n^\mathrm{F} = 0.126$.

and show very good agreement with the FEM results, while the GPM estimate slightly underestimates the FEM results. As expected for this type of loading, the Voigt bound substantially deviates from the other results. However, as far as the FEM results are concerned, one potentially needs to be careful. Guo et al. [173] considered for the microstructure only a very simple geometry, which means that the microstructure consists of a unit cell with one single cylindrical fibre which is surrounded by matrix material. A more comprehensive numerical study was performed by Moraleda et al. [341], who considered for the microstructure of the representative volume element a random dispersion of several fibres. This arrangement better represents the assumption of random microstructures as assumed within the derivation of the analytical estimates in this work. However, Moraleda et al. [341] considered monodisperse fibre sizes, while the analytical estimates are based on the idea of polydisperse fibre sizes. Hence, care must be taken when comparing and interpreting the analytical and the FEM results against each other. Moreover, Moraleda et al. [341] performed pure shear deformation simulations in the transverse plane, that is, $\bar{\boldsymbol{F}} = \bar{\lambda}\,\boldsymbol{e}_1 \otimes \boldsymbol{e}_1 + 1/\bar{\lambda}\,\boldsymbol{e}_2 \otimes \boldsymbol{e}_2 + 1\,\boldsymbol{e}_3 \otimes \boldsymbol{e}_3$. This is equivalent to a transverse shear deformation with $\bar{\gamma}_\mathrm{t} = \sqrt{\bar{\lambda}^2 + \bar{\lambda}^{-2} - 2}$ and $\bar{\gamma}_\mathrm{a} = \bar{\gamma}_\ell = 0$. Further, they assumed rigid fibres. They did so by assuming in their simulations a shear modulus of the fibres that is 2000 times higher than the one of the matrix, leading to $\mu^\mathrm{F} = 2000$ and $\mu^\mathrm{M} = 1$. Figure 5.4a shows for pure shear deformations in the transverse plane the respective macroscopic stress, $\bar{P} = \partial_{\bar{\lambda}}\widetilde{\mathscr{W}}$, for three different fibre volume fractions. For $n^\mathrm{F} = 0.2$ and $n^\mathrm{F} = 0.3$, the new estimate agrees well with the FEM results up to $\bar{\lambda} \approx 2$. It even maintains smooth behaviour for deformations beyond $\bar{\lambda} \approx 2$. Further, the ALP estimate, $\bar{P}_\mathrm{ALP} = \partial_{\bar{\lambda}}\widetilde{\mathscr{W}}_\mathrm{ALP}$, exhibits a remarkable accuracy for $n^\mathrm{F} = 0.2$ and $n^\mathrm{F} = 0.3$ and almost exactly matches the FEM results. Figure 5.4a also highlights the remarkable accuracy of the ALP estimate for transverse shear deformations. This is not too surprising since the ALP estimate is for transverse shear based on the GSO method proposed

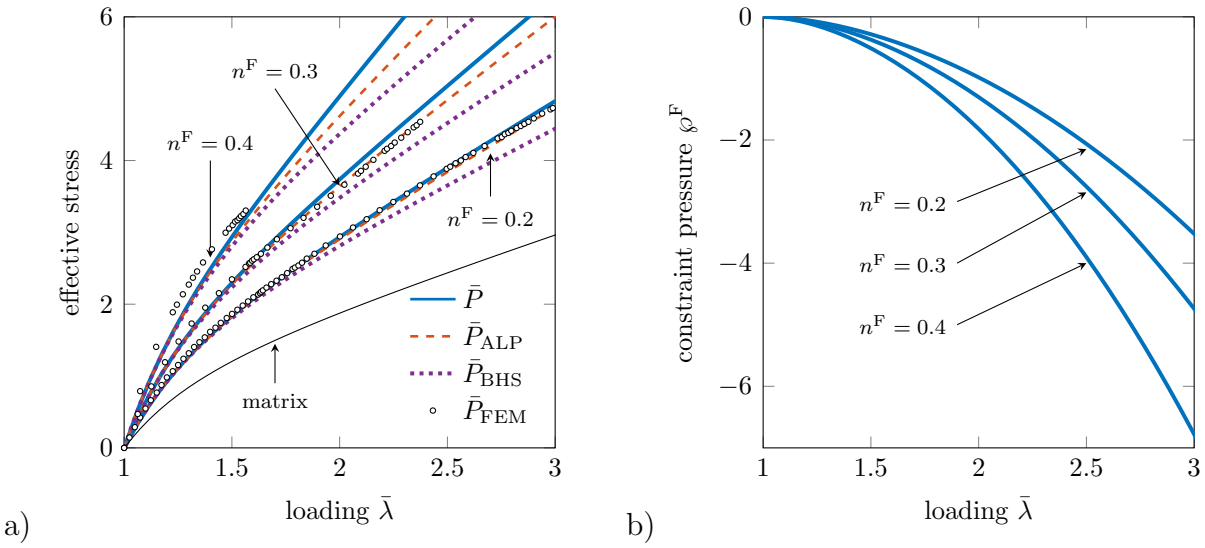

Figure 5.4: Comparison of analytical results and finite-element simulations of Moraleda et al. [341] for composites with Neo-Hookean matrix and Neo-Hookean fibre for pure shear deformations in the transverse plane. The material parameters are $\mu^{\mathrm{F}} = 2000$ and $\mu^{\mathrm{M}} = 1$. a) Effective stresses in loading direction of analytical second-order estimates and FEM results for three different fibre volume fractions. b) Associated values of the Lagrange multiplier $\wp^{\mathrm{F}}$.

by Lopez-Pamies & Ponte Castañeda [299]. In turn, the studies of Moraleda et al. [341] and Avazmohammadi & Ponte Castañeda [19] already revealed that the GSO estimate is very accurate for this scenario. The new estimate presented in this work tends to predict higher stresses than the FEM simulations, which was also observed with the earlier TSO methods by Ponte Castañeda & Tiberio [382] and Avazmohammadi & Ponte Castañeda [19] as well as the earlier GSO method by Lopez-Pamies & Ponte Castañeda [298] (all formulated for rigid fibres), see Avazmohammadi & Ponte Castañeda [19]. It is noteworthy to state that the new estimate maintains a behaviour comparable to the ALP estimate even at higher deformations. This in contrast to earlier TSO methods and the earlier GSO estimate that showed a stiffening behaviour for higher load cases. For a volume fraction $n^{\mathrm{F}} = 0.4$, the new estimate as well as the ALP estimate predict stresses that are lower than the ones predicted by the FEM simulations. However, as already pointed out by Moraleda et al. [341], this discrepancy might be associated with the Hashin–Shtrikman estimates for the $\mathcal{LCC}$ and not with the second-order method. Moreover, the BHS estimate agrees very well with the two second-order estimates for deformations up to $\bar{\lambda} \approx 1.5$ and is below the two second-order estimates at higher deformations. Figure 5.4b shows the associated values of the constraint pressure (Lagrange multiplier) $\wp^{\mathrm{F}}$. For the considered loading and a very stiff fibre, it can be seen that the value of $\wp^{\mathrm{F}}$ becomes negative and thus applies a hydrostatic compressive pressure on the fibre phase in order to maintain its incompressibility. The absolute value $|\wp^{\mathrm{F}}|$ increases with increasing fibre volume fraction n^{F}.

Isotropic exponential-type fibre Next, we investigate the case in which the fibre phase exhibits highly nonlinear behaviour. As discussed in Section 3.8.3, there exists a variety of I_1-based energy functions which generalise the Neo-Hookean energy and are able to describe highly nonlinear material behaviour. One such strain-energy function is the

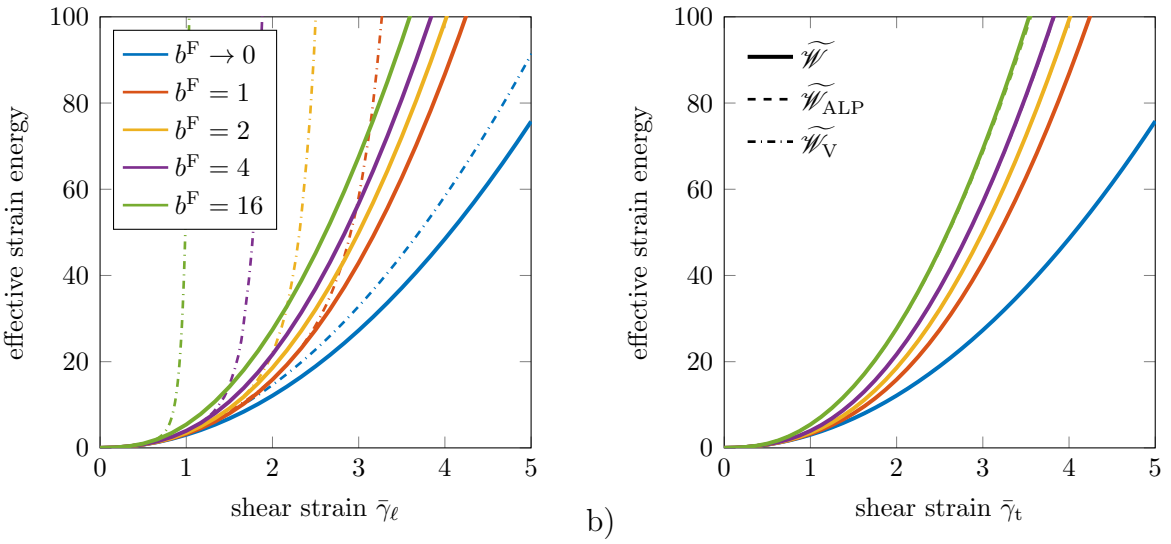

Figure 5.5: Effective energies for composites with Neo-Hookean matrix and exponential-type fibre under longitudinal and transverse shear deformation for different nonlinearities of the fibre. The material parameters are $\mu^\mathrm{F} = 1$, $\mu^\mathrm{M} = 10$, and $n^\mathrm{F} = 0.3$. The legends are for both diagrams. a) Results for longitudinal shear deformation. b) Results for transverse shear deformation. The results for $\widetilde{\mathscr{W}}_\mathrm{V}$ are the same for both loadings.

Delfino model, introduced in Eq. (3.162). Hence, we assume a strain-energy function of the fibre in the following form:

$$\mathscr{W}_\mu^\mathrm{F}(I_1, J) = \frac{\mu^\mathrm{F}}{b^\mathrm{F}} \left\{ \exp\left[\frac{b^\mathrm{F}}{2}(I_1 - 3)\right] - 1 \right\} + \frac{\mu^\mathrm{F}}{2}(J-1)(J-3) - \frac{\mu^\mathrm{F} b^\mathrm{F}}{8}(J-1)^2 . \quad (5.103)$$

Therein, we replaced the logarithmic term in the J-dependent part (3.164) by means of (3.170). We recall that parameter b^F governs the nonlinearity of the energy and that the exponential-type energy includes the Neo-Hookean energy as a special case in the limit as b^F tends to zero. To investigate the new estimate for different fibre nonlinearities, we perform longitudinal and transverse shear simulations for different values of parameter b^F. Figure 5.5a presents for $\mu^\mathrm{F} = 1$, $\mu^\mathrm{M} = 10$, $n^\mathrm{F} = 0.3$, and longitudinal shear deformations, the effective strain energies for the new estimate and the Voigt bound for $b^\mathrm{F} = 1, 2, 4, 16$ and $b^\mathrm{F} \to 0$ (that is, a Neo-Hookean fibre). In this loading case, the new estimate and the ALP essentially show identical behaviour. With increasing stiffness of the fibre, the effective energy of the second-order estimates predicts a moderate increase while the Voigt bound essentially locks up as soon as the nonlinearity of the fibre kicks in. Figure 5.5b depicts the results of the same composites subject to transverse shear loading. Note that the results for the Voigt bound, which are equal to the longitudinal case, are dropped for the sake of visibility. Like in the longitudinal shear case, the results of the new and the ALP estimate are essentially identical (e. g., the relative difference for $b^\mathrm{F} = 16$ and $\bar{\gamma}_\mathrm{t} = 3$ is below 1%).

Anisotropic and highly nonlinear fibre phase behaviour After investigating the behaviour of the new estimate for materials that exhibit a fibre phase with isotropic behaviour, we consider now composites with an anisotropic fibre phase. Assuming purely J_4-dependent energy terms for the fibre phase results in a relatively trivial Voigt-type

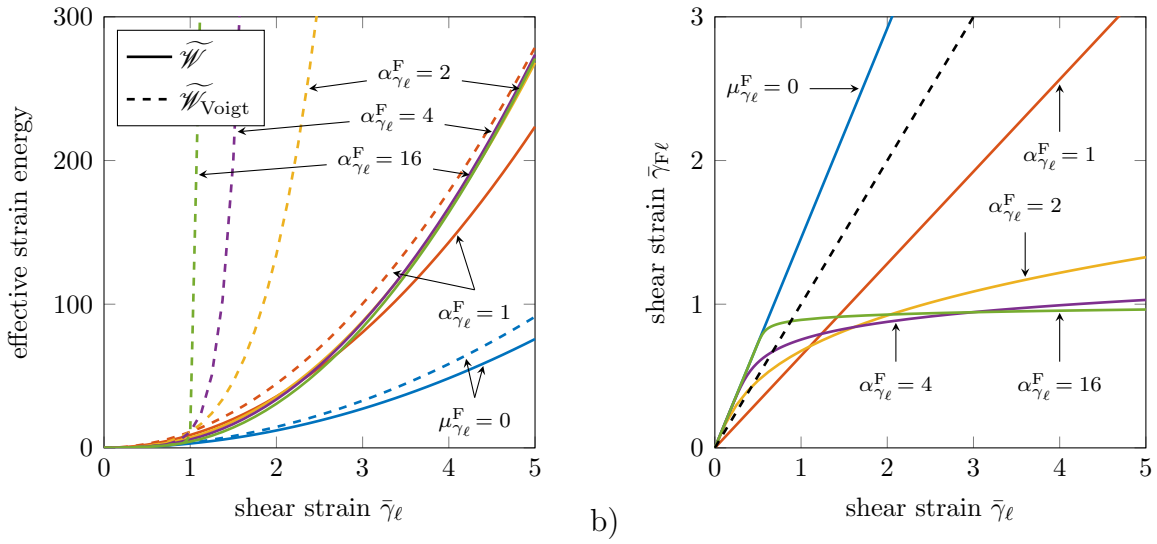

Figure 5.6: Effective energies and microscopic response for composites with Neo-Hookean matrix and anisotropic fibres under longitudinal shear deformation for different nonlinearities of the fibres. The material parameters are $\mu^{\text{F}} = 1$, $\mu^{\text{M}} = 10$, $\mu^{\text{F}}_{\gamma_\ell} = 50$, and $n^{\text{F}} = 0.3$. a) Effective energies for longitudinal shear deformation. b) Longitudinal shear strain of the fibre phase with respect to the overall longitudinal shear strain. The dashed line indicates the uniform field solution, which is assumed by the Voigt bound.

averaging of the J_4-dependent energies, as explained in Section 5.3.4. Hence, we consider fibre phases that contain a more general dependency on J_4 and J_5. For this type of composites, none of the estimates described in Section 5.4, except for the Voigt bound, are applicable. To investigate the estimate, we assume that the fibre energy is given by Eq. (C.22) and its anisotropic part is defined by

$$\mathscr{W}^{\text{F}}_{\text{aniso}}(J_4, J_5) = \frac{\mu^{\text{F}}_{\gamma_\ell}}{2}\left(\frac{J_5}{J_4} - J_4\right)^{\alpha^{\text{F}}_{\gamma_\ell}}, \tag{5.104}$$

which is a modified *standard reinforcing model*, compare Eq. (3.173). Therein, $\mu^{\text{F}}_{\gamma_\ell} \geq 0$ is a longitudinal shear modulus and the exponent, $\alpha^{\text{F}}_{\gamma_\ell} \geq 1$, governs the nonlinearity of the strain-energy function. Taking into account $(3.93)_3$, it becomes apparent that the term in brackets in Eq. (5.104) equals γ_ℓ^2, which points out that the energy term (5.104) acts as a reinforcement solely against longitudinal shear. Figure 5.6a shows the effective strain energies for longitudinal shear deformations with material parameters $\mu^{\text{F}} = 1$, $\mu^{\text{M}} = 10$, $\mu^{\text{F}}_{\gamma_\ell} = 50$, $n^{\text{F}} = 0.3$, and $\alpha_{\gamma_\ell} = \{1, 2, 4, 16\}$. For comparison, we also included the Neo-Hookean fibre case ($\mu^{\text{F}}_{\gamma_\ell} = 0$ such that $\mathscr{W}^{\text{F}}_{\text{aniso}} = 0$), for which the new estimate and the Voigt bound are relatively close to each other. However, for the anisotropic fibre case, the difference between the new estimate and the Voigt bound increases dramatically with increasing nonlinearity (hence, increasing $\alpha^{\text{F}}_{\gamma_\ell}$) of the fibre. Actually, increasing the exponent $\alpha^{\text{F}}_{\gamma_\ell}$ from 2 upwards only causes moderate changes in the effective energy $\widetilde{\mathscr{W}}$ based on the new estimate, whereas this is not the case for the Voigt bound, which tends to blow up at high values of $\alpha^{\text{F}}_{\gamma_\ell}$. Furthermore, it is interesting to look at the associated evolutions of the fibre shear strain $\bar{\gamma}_{\text{F}\ell}$, which are depicted in Figure 5.6b. The Voigt bound assumes uniform deformations, i. e. $\bar{\gamma}_{\text{F}\ell} = \bar{\gamma}_\ell$, regardless of the stiffness of the phases. This entails the extreme high values for the energy $\widetilde{\mathscr{W}}_{\text{Voigt}}$ for high values of $\alpha^{\text{F}}_{\gamma_\ell}$. For the Neo-Hookean

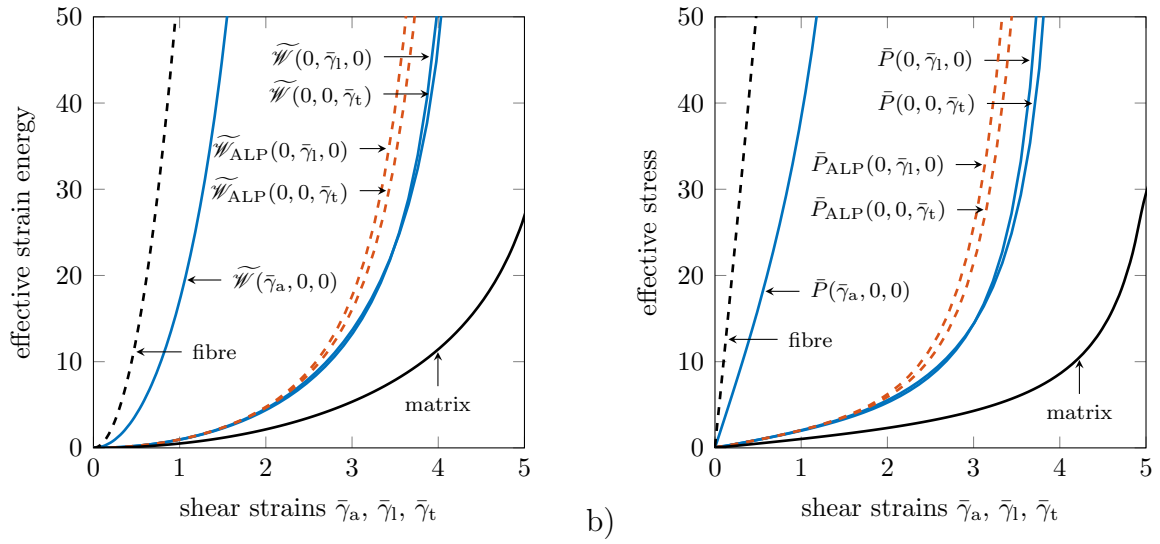

Figure 5.7: Effective responses for composites with Gent-type fibres and matrix under the three different shear modes. The material parameters are $\mu^{\mathrm{F}} = 100$, $J_{\mathrm{m}}^{\mathrm{F}} = 5$, $\mu^{\mathrm{M}} = 1$, $J_{\mathrm{m}}^{\mathrm{M}} = 30$, and $n^{\mathrm{F}} = 0.3$. a) Effective energies for the second-order estimates $\widetilde{\mathscr{W}}$ and $\widetilde{\mathscr{W}}_{\mathrm{ALP}}$. b) The corresponding effective stresses.

case ($\mu_{\gamma_\ell}^{\mathrm{F}} = 0$), the fibre shear $\bar{\gamma}_{\mathrm{F}\ell}$ associated with the new estimate is given by means of the explicit expression (C.24) and shown as blue solid line. For the anisotropic fibre case, the fibre shear can be calculated from Eq. (C.23) by making use of the derivative $\partial_{J_5}\mathscr{W}_{\mathrm{aniso}}^{\mathrm{F}}$ of the considered J_5-dependent energy in (5.104). From the associated curves in Figure 5.6b, it can be observed that higher exponent values α_{γ_ℓ} result in lower values for $\bar{\gamma}_{\mathrm{F}\ell}$ at high overall longitudinal shear strains $\bar{\gamma}_\ell$.

5.5.2 Results for isotropic Gent-type matrix and fibre

In this section, we investigate composites that contain nonlinear phases exhibiting Gent-type behaviour. Hence, by recalling the definition in Eq. (3.166), we assume a strain-energy function

$$\mathscr{W}_{\mu}^{\alpha}(I_1, J) = -\frac{J_{\mathrm{m}}^{\alpha}\,\mu^{\alpha}}{2}\,\ln\left[1 - \frac{I_1 - 3}{J_{\mathrm{m}}^{\alpha}}\right] + \frac{\mu^{\alpha}}{2}\,(J-1)(J-3) - \frac{\mu^{\alpha}}{J_{\mathrm{m}}^{\alpha}}\,(J-1)^2\,, \tag{5.105}$$

As for the Delfino model, the logarithmic term in the J-dependent part Eq. (3.168) is replaced by means of the Taylor expansion (3.170). We recall that the special characteristic of the Gent model is that it locks up when $I_1 - 3$ equals the lock-up parameter J_{m}^{α}. Like for the exponential energy given in (5.103), the Gent energy includes the Neo-Hookean strain-energy function for the special case when $J_{\mathrm{m}}^{\alpha} \to \infty$. Figure 5.7 shows the effective responses for composites consisting of Gent-type fibres and a Gent-type matrix under axisymmetric, longitudinal, and transverse shear deformation. The material parameters are $\mu^{\mathrm{F}} = 100$, $J_{\mathrm{m}}^{\mathrm{F}} = 5$, $\mu^{\mathrm{M}} = 1$, $J_{\mathrm{m}}^{\mathrm{M}} = 30$, and $n^{\mathrm{F}} = 0.3$. This case is very similar to the one shown in Figure 5.2, except for the fact that the material now exhibits, due to the Gent-type behaviour, highly nonlinear phases. The effective strain energies for the second-order estimates $\widetilde{\mathscr{W}}$ and $\widetilde{\mathscr{W}}_{\mathrm{ALP}}$ are presented in Figure 5.7a. The axisymmetric case of the ALP estimate is identical to new estimate and not plotted explicitly. Further, the Voigt bound is identical for all three shear modes and corresponds to the axisymmetric

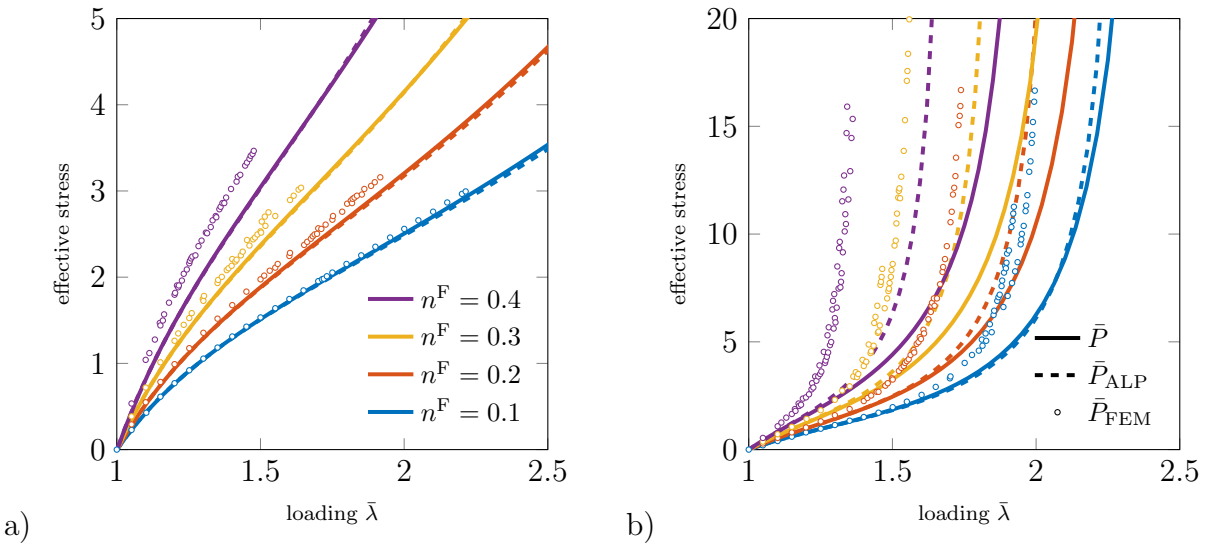

Figure 5.8: Comparison of analytical results and finite-element simulations of Moraleda et al. [341] for composites with Gent-type matrix and Neo-Hookean fibres for pure shear deformations in the transverse plane. The material parameters are $\mu^{\mathrm{F}} = 2000$ and $\mu^{\mathrm{M}} = 1$. Four different fibre volume fractions $n^{\mathrm{F}} = 0.1, 0.2, 0.3, 0.4$ are considered. The legends are valid for both diagrams. a) Effective stresses in loading direction of analytical second-order estimates and FEM results for a matrix lock-up parameter $J_{\mathrm{m}}^{\mathrm{M}} = 50$. b) Effective stresses in loading direction of analytical second-order estimates and FEM results for a matrix lock-up parameter $J_{\mathrm{m}}^{\mathrm{M}} = 5$.

mode, hence $\widetilde{\mathscr{W}}_{\mathrm{V}} = \widetilde{\mathscr{W}}(\bar{\gamma}_{\mathrm{a}}, 0, 0)$. As observed in the previous cases, $\widetilde{\mathscr{W}}$ and $\widetilde{\mathscr{W}}_{\mathrm{ALP}}$ differ for transversal shear, since the ALP estimate is based on the GSO method of Lopez-Pamies & Ponte Castañeda [299]. Moreover, it is interesting to observe that the results for the longitudinal shear loading do no longer coincide. This can be traced to the fact that the ALP estimate is for this deformation based on the earlier TSO method proposed by Ponte Castañeda & Tiberio in 2000, whereas the new estimate is based on the more recent TSO method proposed by Avazmohammadi & Ponte Castañeda in 2013. Figure 5.7b presents the stress measures $\bar{P}$ and $\bar{P}_{\mathrm{ALP}}$ associated to the effective strain energies.

Next, we compare the analytical estimates for a Gent-type matrix with the FEM simulations of Moraleda et al. [341]. We consider pure shear deformations in the transverse plane and different fibre volume fractions. This scenario has already been investigated for a matrix phase exhibiting a Neo-Hookean material behaviour, see Figure 5.3. Like before, the FEM simulations of Moraleda et al. [341] assume monodispersed fibre sizes, such that an exact one-to-one comparison with the analytical estimates is not possible. Further, the fibres are still considered to be nearly rigid by assuming a Neo-Hookean energy that exhibits, in comparison to the matrix, a 2000 times higher shear modulus, compare Moraleda et al. [341]. These assumptions lead to the following material parameters: $\mu^{\mathrm{F}} = 2000$ and $\mu^{\mathrm{M}} = 1$ and the fibre volume fraction, n^{F}, is assumed to vary between 0.1 and 0.4. The comparison between the analytical and FEM approach are depicted in Figure 5.8. Figure 5.8a shows the effective stresses for a matrix phase with lock-up parameter $J_{\mathrm{m}}^{\mathrm{M}} = 50$. Over the investigated range of deformation, the effective stresses of the new estimate are almost identical to those obtained by using the ALP estimate. For smaller fibre volume fractions, the two analytical estimates correspond well to the FEM

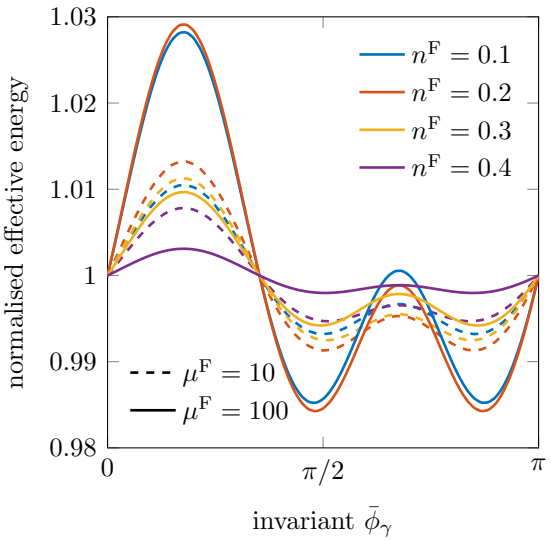

Figure 5.9: Dependence of the new estimate $\widetilde{\mathscr{W}}$ on the invariant $\bar{\phi}_\gamma$ during coupled longitudinal and transverse shear deformation with $\bar{\gamma}_\ell = \bar{\gamma}_\mathrm{t} = 1$ for Gent-type phases and for different fibre volume fractions and fibre shear moduli. The remaining material parameters are $J_\mathrm{m}^\mathrm{F} = 3$, $\mu^\mathrm{M} = 1$, and $J_\mathrm{m}^\mathrm{M} = 3$. The effective energy is normalised to $\widetilde{\mathscr{W}}|_{\bar{\phi}_\gamma = 0}$.

results. The gap between those two estimates increases though with increasing volume fractions. As previously mentioned, this difference may be due to the underlying Hashin–Shtrikman-type estimates for the $\mathcal{LCC}$. Figure 5.8b shows the effective stresses for a stiffer matrix phase and a lock-up parameter $J_\mathrm{m}^\mathrm{M} = 5$. The herein proposed new TSO estimate agrees very well with the ALP estimate for small volume fractions, for instance, for $n^\mathrm{F} = 0.1$, and significantly deviates for higher fibre volume fractions. Like in previous studies, the effective stresses obtained from the analytical estimates and those from the FEM simulations are very different for this scenario. However, the nearly rigid fibres, the highly nonlinear matrix behaviour, and the incompressibility assumption for both phases, pose big challenges not only for the analytical estimates but also for the numerical FEM simulations. Nevertheless, one can observe that the new TSO estimate exhibits smooth behaviour that is similar to the ALP (and, hence, GSO) estimate. It does not show any unphysical behaviour.

5.5.3 The $\bar{I}_2$-$\bar{\phi}_\gamma$-dependence of the overall energy for I_2-independent phase energies

As discussed in Section 5.3.2, the present TSO estimate for fibre-embedded composites generally depends on four of the five macroscopic transversely isotropic invariants, so that $\widetilde{\mathscr{W}} = \widetilde{\mathscr{W}}(\bar{I}_1, \bar{I}_2, \bar{J}_4, \bar{J}_5) = \widetilde{\mathscr{W}}(\bar{\lambda}_\ell, \bar{\gamma}_\ell, \bar{\gamma}_\mathrm{t}, \bar{\phi}_\gamma)$. This means that the effective strain energy $\widetilde{\mathscr{W}}$ depends for coupled longitudinal and transverse shear deformations on the macroscopic $\bar{I}_2$-invariant (and thus on the coupling invariant $\bar{\phi}_\gamma$). This is generally true even for phases whose energies are independent of I_2. In order to investigate this $\bar{I}_2$-$\bar{\phi}_\gamma$-dependence in more detail, we consider a fibre-embedded composite with matrix and fibre phases that exhibit isotropic Gent-type behaviour. We consider four different fibre volume fractions, $n^\mathrm{F} = \{0.1, 0.2, 0.3, 0.4\}$, and two different fibre stiffnesses, $\mu^\mathrm{F} = \{10, 100\}$. The remaining material parameters are $\mu^\mathrm{M} = 1$ and $J_\mathrm{m}^\mathrm{F} = J_\mathrm{m}^\mathrm{M} = 3$. Further, a coupled shear deformation

of $\bar{\gamma}_\ell = \bar{\gamma}_\mathrm{t} = 1.0$ is applied. Figure 5.9 shows the corresponding effective energies $\widetilde{\mathscr{W}}(\bar{\phi}_\gamma)$ as a function of the coupling invariant $\bar{\phi}_\gamma$, normalised with respect to $\widetilde{\mathscr{W}}|_{\bar{\phi}_\gamma=0}$. The results reveal that the influence of the overall energy on the $\bar{\phi}_\gamma$-invariant depends on the phase properties and the volume fractions. However, the $\bar{I}_2$-$\bar{\phi}_\gamma$-dependence of the present TSO estimate for Gent-type phase energies is rather weak. This observations agrees with results by Agoras et al. [4] for estimates that are based on the GSO homogenisation method.

6 Homogenisation of Fibrous Networks

A variety of materials can be modelled at the small-scale as a network of a large number of single chains (or fibres) with a certain orientation in space. This is especially the case for two material classes: Rubber-like materials with their underlying structure of *polymer chain networks* and (soft) biological tissues which consist of certain collageneous network structures and different types of *collagen fibres*. This chapter presents the basic concepts of such network models and the associated homogenisation techniques required to obtain the effective network responses. In this process, an important ingredient of network models is the stochastical description of the orientation of the fibres or chains by means of a probability density function. We will especially focus on scenarios where the orientation leads to an overall behaviour of the network which belongs to the symmetry group of transverse isotropy. Moreover, we recall that the overall goal in this thesis is the application of the presented homogenisation methods to the modelling of collageneous (biological) tissues. However, a lot of concepts for network models were derived in the context of rubber elasticity and there is very little exchange between the research communities. Hence, references for further reading are split between the two fields. In the context of rubber elasticity, we refer to the seminal works of Treloar [482] and Deam & Edwards [90] as well as to the works of Treloar [481], Treloar & Riding [483], and Wu & van der Giessen [522] for details about full network models for polymers and rubber materials. For further reading in the field of network models for collageneous tissues, we refer to the fundamental works of Lanir [275, 276].

6.1 Fundamentals of network models

If a material has on the microscale a characteristic *network-like* structure consisting of a large number of fibres or chains, the effective material behaviour on the macroscale can be obtained from so-called *network models*. The basic idea of a network model is to properly describe the mechanical behaviour and the micro-kinematics of a single fibre and to compute the effective response of the whole network by applying appropriate averaging and homogenisation techniques. In this process, the network model idealises the real microstructure of the material by assuming that the fibres connect the origin of a unit sphere, referred to as *microsphere*, with some point on the associated sphere surface, such that the orientations of the fibres coincide with the ones in the real microstructure. This results in a model as exemplary shown in Figure 6.1a. Subsequently, it proves useful to introduce a unit vector $\mathfrak{r}_0 \in \mathcal{R}^3$ which connects the two end points of a fibre in the undeformed reference configuration. Doing so, it makes sense to describe the vector in spherical coordinates, leading to

$$\mathfrak{r}_0(\Theta, \Phi) = \sin[\Theta]\cos[\Phi]\, \boldsymbol{e}_1^{\mathrm{s}} + \sin[\Theta]\sin[\Phi]\, \boldsymbol{e}_2^{\mathrm{s}} + \cos[\Theta]\, \boldsymbol{e}_3^{\mathrm{s}}\,. \tag{6.1}$$

Therein, $\Theta \in [0, \pi)$ denotes the polar angle, $\Phi \in [0, 2\pi)$ is the azimuthal angle, and the $\boldsymbol{e}_i^{\mathrm{s}}$-coordinate system ($i = 1, 2, 3$) represents a laboratory frame of reference, see Figure 6.1b. It is easy to observe from (6.1) that $|\mathfrak{r}_0| = \sqrt{\mathfrak{r}_0 \cdot \mathfrak{r}_0} = 1$. Now, it is essential to describe the micro-kinematics of the vector $\mathfrak{r}_0$ which is done by means of a general mapping operator

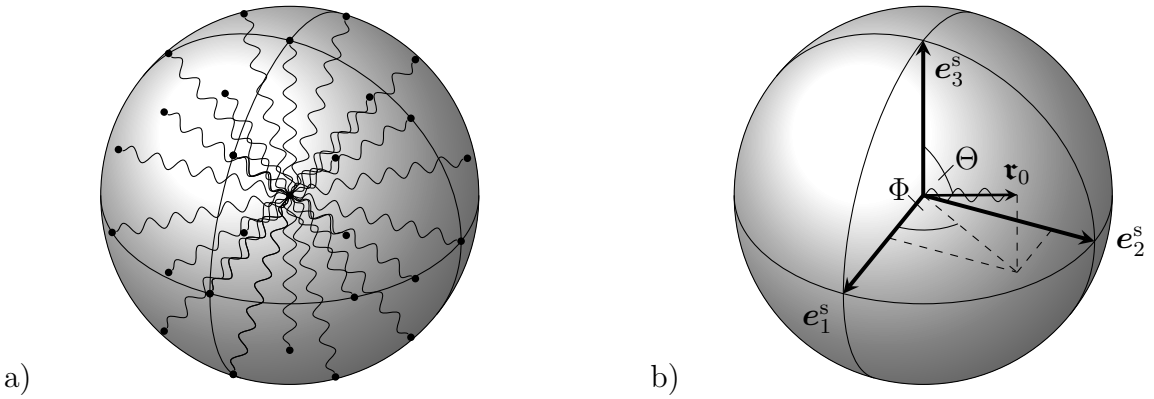

Figure 6.1: a) Visualisation of a microsphere network model consisting of fibres/chains with certain orientations in space. b) The spherical coordinate system and parametrisation of a space orientation, defined by the referential vector $\mathfrak{r}_0$, in the polar angle Θ and the azimuthal angle Φ.

$\mathfrak{F}_\mathfrak{r} : \mathfrak{r}_0 \mapsto \mathfrak{r} = \mathfrak{F}_\mathfrak{r}(\mathfrak{r}_0)$ which yields the vector $\mathfrak{r}$ in the actual configuration. In particular, it is convenient to postulate the existence of a linear map

$$\boldsymbol{F}_\mathfrak{r}(\Theta, \Phi) : \mathfrak{r}_0 \mapsto \mathfrak{r} = \boldsymbol{F}_\mathfrak{r}\, \mathfrak{r}_0 \,, \tag{6.2}$$

where the second-order tensor $\boldsymbol{F}_\mathfrak{r}(\Theta, \Phi)$ describes the micro-deformation of the referential vector $\mathfrak{r}_0$. Next, it is consequent to assign to each vector $\mathfrak{r}_0(\Theta, \Phi)$ a potential $\mathscr{W}_\mathfrak{r}$. As we focus on the purely hyperelastic case, we state that the potential is a function of the micro-deformation $\boldsymbol{F}_\mathfrak{r}$, such that $\mathscr{W}_\mathfrak{r} = \mathscr{W}_\mathfrak{r}(\boldsymbol{F}_\mathfrak{r})$. At this point, it should be emphasised that although the derivations in this section were based on the idea of a network made of actual fibres or chains, the micro-kinematical description in Eq. (6.2) can be regarded in a more general way as the description of the microscopic material behaviour in the direction initially aligned with the vector $\mathfrak{r}_0$. Hence, it serves as a general description of a space orientation and does not necessarily have to be an actual fibre or chain. The space orientation can be regarded as a tube-like segment aligned with the vector $\mathfrak{r}_0$. If we recall some basic kinematical relations from Sections 2.1.2 and 2.1.3, we can formulate the microscopic deformation measures

$$\lambda_\mathfrak{r} = |\mathfrak{r}| = |\boldsymbol{F}_\mathfrak{r}\, \mathfrak{r}_0| \,, \quad \nu_\mathfrak{r} = |\boldsymbol{F}_\mathfrak{r}^{-T} \mathfrak{r}_0| \,, \quad \upsilon_\mathfrak{r} = |\mathrm{cof}[\boldsymbol{F}_\mathfrak{r}] \mathfrak{r}_0| \,, \tag{6.3}$$

where the micro-stretch $\lambda_\mathfrak{r}$, compare also Eq. (2.17), describes the longitudinal stretch of the tube-like segment, whereas $\nu_\mathfrak{r}$ and the area stretch $\upsilon_\mathfrak{r}$ quantify the cross-sectional deformation of the tube. Those micro-kinematical measures are useful for the constitutive formulation of strain-energy functions $\mathscr{W}_\mathfrak{r}$, which is further addressed in Section 6.2.2. However, we also note that if the space orientation shall describe the behaviour of an actual fibre, the real fibre geometry is idealised by the vector $\mathfrak{r}_0$ and the stretch $\lambda_\mathfrak{r}$ describes the end-to-end length and not the contour length of the fibre. This means that any further geometrical information, such as the contour length or waviness of the fibre, has to be accounted for through the constitutive formulation of the strain-energy function $\mathscr{W}_\mathfrak{r}$.

The orientation density function The key idea of the network model is that the orientations of the fibres in the idealised microsphere should be identical to the ones in the real microstructure. Hence, there is a certain probability of finding the end point of a fibre

on a specific point of the microsphere surface. Let this surface be denoted by Ω. Since we further postulate that the number of fibres is large enough to assume a continuous distribution of fibres in the microsphere, the orientation of the fibres can be described in a statistical sense by means of an *orientation density function* (ODF) $\mathfrak{p}(\mathfrak{r}_0) = \mathfrak{p}(\Theta, \Phi)$. The ODF describes the *one-point probability* that the vector $\mathfrak{r}_0$ points to an infinitesimal area element $\mathrm{d}\Omega = \sin[\Theta]\,\mathrm{d}\Theta\,\mathrm{d}\Phi \in \Omega$ of the microsphere surface Ω. Considering the spherical coordinates and the periodicity of the angles Θ and Φ, the ODF has to satisfy the conditions

$$\mathfrak{p}(\mathfrak{r}_0) = \mathfrak{p}(-\mathfrak{r}_0) \quad \text{and} \qquad \mathfrak{p}(\Theta, \Phi) = \mathfrak{p}(\Theta + n\pi, \Phi) = \mathfrak{p}(\Theta, \Phi + 2n\pi) \tag{6.4}$$

with $n \in \mathcal{N}$. These conditions suggest that the field of directional (or spherical) statistics has to be consulted and that the ODF has to be defined in terms of bivariate spherical probability functions, see, for example, Mardia & Jupp [310]. Some basics on directional statistics are also provided in Appendix B.2. Next, it makes sense to introduce a continuous averaging operator over the microsphere surface, reading

$$\big\langle (\cdot) \big\rangle_{\Omega} := \int_{\Omega} \mathfrak{p}(\Theta, \Phi)\,(\cdot)\,\mathrm{d}\Omega \quad \text{with} \quad \int_{\Omega} (\cdot)\,\mathrm{d}\Omega = \int_0^{2\pi} \int_0^{\pi} (\cdot)\,\sin[\Theta]\,\mathrm{d}\Theta\,\mathrm{d}\Phi\,. \tag{6.5}$$

It is consequent to formulate a normalisation condition for the ODF, requiring that

$$\big\langle 1 \big\rangle_{\Omega} = \int_{\Omega} \mathfrak{p}(\Theta, \Phi)\,\mathrm{d}\Omega = 1\,. \tag{6.6}$$

Note that this can be regarded as a continuous version of the saturation condition formulated in Eq. $(4.23)_2$. For completeness, it is further remarked that the ODF can also be chosen as a Dirac Delta function with a certain number of masses, which means that the continuous fibre distribution degenerates to a discrete number of fibres. This procedure would lead to classical discrete chain models that are used in polymer mechanics, such as the three-chain models by James & Guth [247] and Wang & Guth [505], the four-chain model by Flory & Rehner [131] and Treloar [480], or the eight-chain models by Arruda & Boyce [13] and Kroon [266], see also Beatty [28].

Effective network response: Variational energy minimisation Having defined the micro-energy $\mathscr{W}_{\mathfrak{r}}(\boldsymbol{F}_{\mathfrak{r}})$ and the averaging operator (6.5), the averaged stored energy in the microsphere is obtained as $\Pi_{\Omega} = \langle \mathscr{W}_{\mathfrak{r}}(\boldsymbol{F}_{\mathfrak{r}}) \rangle_{\Omega}$. Then, in direct analogy to Section 4.3.3, we demand that the micro-deformations $\boldsymbol{F}_{\mathfrak{r}}$ are such that Π_{Ω} is minimised. Hence, the effective energy $\bar{\mathscr{W}}$ is defined in terms of the variational minimisation problem

$$\bar{\mathscr{W}}(\bar{\boldsymbol{F}}) = \min_{\boldsymbol{F}_{\mathfrak{r}}} \Big\{ \big\langle \mathscr{W}_{\mathfrak{r}}(\boldsymbol{F}_{\mathfrak{r}}) \big\rangle_{\Omega} \Big\}\,. \tag{6.7}$$

Further, the micro-deformations are linked to the macroscopic deformation gradient via

$$\bar{\boldsymbol{F}} = \big\langle \boldsymbol{F}_{\mathfrak{r}} \big\rangle_{\Omega}\,, \tag{6.8}$$

which is a continuous version of the overall average deformation condition (4.32). According to Govindjee et al. [170], it is useful to formulate the variational problem (6.7) in terms of the Lagrange functional

$$\mathscr{L}(\boldsymbol{F}_{\mathfrak{r}}, \boldsymbol{\mathcal{P}}_{\mathfrak{r}}) = \big\langle \mathscr{W}_{\mathfrak{r}}(\boldsymbol{F}_{\mathfrak{r}}) \big\rangle_{\Omega} + \boldsymbol{\mathcal{P}}_{\mathfrak{r}} \cdot \big(\bar{\boldsymbol{F}} - \big\langle \boldsymbol{F}_{\mathfrak{r}} \big\rangle_{\Omega} \big) \tag{6.9}$$

where the second-order tensor $\boldsymbol{\mathcal{P}}_{\mathfrak{r}}$ contains nine scalar Lagrange multipliers that enforce condition (6.8). While the stationarity condition of $\mathscr{L}$ with respect to $\boldsymbol{\mathcal{P}}_{\mathfrak{r}}$ simply results in Eq. (6.8) (as expected), an interesting result appears for the stationarity condition of $\mathscr{L}$ with respect to the micro-deformations $\boldsymbol{F}_{\mathfrak{r}}$, which reads

$$\partial_{\boldsymbol{F}_{\mathfrak{r}}}\mathscr{L} = \left\langle \partial_{\boldsymbol{F}_{\mathfrak{r}}}\mathscr{W}_{\mathfrak{r}}(\boldsymbol{F}_{\mathfrak{r}})\right\rangle_{\Omega} - \boldsymbol{\mathcal{P}}_{\mathfrak{r}} = \boldsymbol{0} \quad \rightarrow \quad \boldsymbol{\mathcal{P}}_{\mathfrak{r}} = \left\langle \partial_{\boldsymbol{F}_{\mathfrak{r}}}\mathscr{W}_{\mathfrak{r}}(\boldsymbol{F}_{\mathfrak{r}})\right\rangle_{\Omega} \tag{6.10}$$

The last expression seems to be a reasonable formulation for the macroscopic first Piola–Kirchhoff stress, as it depicts the average of the microscopic first Piola–Kirchhoff stresses

$$\boldsymbol{P}_{\mathfrak{r}} := \partial_{\boldsymbol{F}_{\mathfrak{r}}}\mathscr{W}_{\mathfrak{r}}(\boldsymbol{F}_{\mathfrak{r}})\,. \tag{6.11}$$

As a matter of fact, it is easy to show that the Lagrange multiplier tensor $\boldsymbol{\mathcal{P}}_{\mathfrak{r}}$ represents the macroscopic stress tensor $\bar{\boldsymbol{P}} = \partial_{\bar{\boldsymbol{F}}}\bar{\mathscr{W}}$ by utilising the derivative of Eq. (6.8) with respect to $\bar{\boldsymbol{F}}$, giving $\mathbb{I} = \langle \partial_{\bar{\boldsymbol{F}}}\boldsymbol{F}_{\mathfrak{r}}\rangle_{\Omega}$, and assuming that $\boldsymbol{F}_{\mathfrak{r}}^{*}$ is a solution for the variational problem. With that, we can formulate

$$\bar{\boldsymbol{P}} = \partial_{\bar{\boldsymbol{F}}}\bar{\mathscr{W}} = \left\langle \partial_{\bar{\boldsymbol{F}}}\mathscr{W}_{\mathfrak{r}}(\boldsymbol{F}_{\mathfrak{r}}^{*})\right\rangle_{\Omega} = \left\langle (\partial_{\bar{\boldsymbol{F}}}\boldsymbol{F}_{\mathfrak{r}}^{*})^{T}\partial_{\boldsymbol{F}_{\mathfrak{r}}^{*}}\mathscr{W}_{\mathfrak{r}}(\boldsymbol{F}_{\mathfrak{r}}^{*})\right\rangle_{\Omega} = \left\langle (\partial_{\bar{\boldsymbol{F}}}\boldsymbol{F}_{\mathfrak{r}}^{*})^{T}\right\rangle_{\Omega}\boldsymbol{\mathcal{P}}_{\mathfrak{r}} = \boldsymbol{\mathcal{P}}_{\mathfrak{r}}\,. \tag{6.12}$$

In addition to the work of Govindjee et al. [170], an attempt to formulate an effective network energy on the basis of a minimisation principle as formulated in (6.7) was made by Chen et al. [76] for the modelling of collageneous tissue. However, instead of a continuous fibre distribution, they proceeded from a discrete number of fibres and formulated an estimate in terms of a TSO homogenisation approach. Moreover, Miehe et al. [329] formulated a variational minimisation principle for the scalar fluctuations of the stretch $\lambda_{\mathfrak{r}}$ and the tube contraction $\nu_{\mathfrak{r}}$ on the surface Ω. This elegant model is known as the non-affine microsphere model. Finally, an energy relaxation based on a so-called maximal advance path constraint was formulated by Tkachuk & Linder [477].

6.2 Affine network model

The variational minimisation problem in Eq. (6.7) generally leads to non-uniform microscopic deformations $\boldsymbol{F}_{\mathfrak{r}}$. Alternatively, one can apply an *affinity assumption*, $\boldsymbol{F}_{\mathfrak{r}} = \bar{\boldsymbol{F}}$, such that each vector $\boldsymbol{\mathfrak{r}}_0$ experiences the macroscopic deformation. This leads to the affine map

$$\bar{\boldsymbol{F}} : \boldsymbol{\mathfrak{r}}_0 \mapsto \boldsymbol{\mathfrak{r}} = \bar{\boldsymbol{F}}\boldsymbol{\mathfrak{r}}_0\,. \tag{6.13}$$

With this, the micro-deformation measures from Eqs (6.3) can be reformulated to

$$\bar{\lambda}_{\mathfrak{r}} = |\boldsymbol{\mathfrak{r}}| = |\bar{\boldsymbol{F}}\boldsymbol{\mathfrak{r}}_0|\,, \quad \bar{\nu}_{\mathfrak{r}} = |\bar{\boldsymbol{F}}^{-T}\boldsymbol{\mathfrak{r}}_0|\,, \quad \bar{\upsilon}_{\mathfrak{r}} = |\mathrm{cof}[\bar{\boldsymbol{F}}]\boldsymbol{\mathfrak{r}}_0|\,. \tag{6.14}$$

Further, the effective network energy is directly given as

$$\bar{\mathscr{W}}_{\mathrm{V}}(\bar{\boldsymbol{F}}) = \left\langle \mathscr{W}_{\mathfrak{r}}(\bar{\boldsymbol{F}})\right\rangle_{\Omega} \tag{6.15}$$

by means of a simple averaging of the fibre energies over the microsphere surface Ω. We recall from Section 4.3.5 that $\bar{\mathscr{W}}_{\mathrm{V}}$ denotes the Voigt estimate, which arises from the assumption of uniform micro-deformations. As stated before, the Voigt estimate is an upper bound for the effective behaviour, but serves as a reasonable prediction if the affinity assumption is justified, for example, by experimental observations.

	$\bar{I}_1$	$\bar{I}_2$	$\bar{I}_3$
$\bar{\lambda}_\mathfrak{r} = \lvert\bar{\boldsymbol{F}}\mathfrak{r}_0\rvert$	$3\langle\bar{\lambda}_\mathfrak{r}^2\rangle_{\Omega_\circ}$	$3\bar{J}^3\langle\bar{\lambda}_\mathfrak{r}^{-5}\rangle_{\Omega_\circ}$	$\langle\bar{\lambda}_\mathfrak{r}^{-3}\rangle_{\Omega_\circ}^{-2}$
$\bar{\nu}_\mathfrak{r} = \lvert\bar{\boldsymbol{F}}^{-T}\mathfrak{r}_0\rvert$	$3\bar{J}^{-1}\langle\bar{\nu}_\mathfrak{r}^{-5}\rangle_{\Omega_\circ}$	$3\bar{J}^2\langle\bar{\nu}_\mathfrak{r}^2\rangle_{\Omega_\circ}$	$\langle\bar{\nu}_\mathfrak{r}^{-3}\rangle_{\Omega_\circ}^{2}$
$\bar{\upsilon}_\mathfrak{r} = \lvert\mathrm{cof}[\bar{\boldsymbol{F}}]\mathfrak{r}_0\rvert$	$3\bar{J}^4\langle\bar{\upsilon}_\mathfrak{r}^{-5}\rangle_{\Omega_\circ}$	$3\langle\bar{\upsilon}_\mathfrak{r}^2\rangle_{\Omega_\circ}$	$\langle\bar{\upsilon}_\mathfrak{r}^{-3}\rangle_{\Omega_\circ}^{-1}$

Table 6.1: Link between the microscopic deformation measures $\bar{\lambda}_\mathfrak{r}$, $\bar{\nu}_\mathfrak{r}$ and $\bar{\upsilon}_\mathfrak{r}$ and the macroscopic principal invariants for isotropic network models.

6.2.1 Closed-form integral forms for isotropic networks

Although we focus in this thesis on non-uniform fibre distributions, we briefly discuss the special case when the fibres are distributed in a uniform manner. For this scenario, the distribution function simplifies to the constant value $\mathfrak{p} = 1/(4\pi)$ and the associated averaging operation, defined in Eq. (6.5), can be formulated as

$$\big\langle(\cdot)\big\rangle_{\Omega_\circ} := \frac{1}{4\pi}\int_\Omega (\cdot)\,\mathrm{d}\Omega = \frac{1}{4\pi}\int_0^{2\pi}\int_0^{\pi}(\cdot)\,\sin[\Theta]\,\mathrm{d}\Theta\,\mathrm{d}\Phi \quad \text{such that} \quad \big\langle 1\big\rangle_{\Omega_\circ} = 1\,. \tag{6.16}$$

With this, together with Eq. (6.1), it is easy to show that

$$\big\langle\mathfrak{r}_0\big\rangle_{\Omega_\circ} = \boldsymbol{0} \quad \text{and} \quad \big\langle\mathfrak{r}_0\otimes\mathfrak{r}_0\big\rangle_{\Omega_\circ} = \tfrac{1}{3}\boldsymbol{I}\,. \tag{6.17}$$

These results further emphasise that a uniform fibre network does not have any preferred orientation and depicts the prime example for spherical symmetry. Consequently, as discussed in Section 3.5.3, the symmetry group of the overall material behaviour is identified as $\mathcal{MG} = \mathcal{O}(3)$ and the effective material response becomes isotropic and invariant with respect to any rotations $\boldsymbol{Q} \in \mathcal{O}(3)$. Any such rotation only leads to a rotated frame of reference, $\boldsymbol{e}_i^{s*} = \boldsymbol{Q}\boldsymbol{e}_i^{s}$, which has no effect on the results of effective quantities computed from the averaging operation in Eq. (6.16). Moreover, it can be shown that the three macroscopic principal invariants of the isotropic set $\mathscr{I}_{\mathrm{iso}}^I$ can be obtained by averaging operations of the micro-deformation measures which are given in (6.14). Such relations were first introduced by Kearsley [251] for $\bar{I}_1$ and $\bar{I}_2$ and later generalised by Carol et al. [73], amongst others. An overview is provided in Table 6.1.

6.2.2 Fibre energies and associated network response

So far, the microscopic energy $\mathscr{W}_\mathfrak{r}$ of a single fibre (or space orientation) was assumed to be a general function of the micro-deformation $\boldsymbol{F}_\mathfrak{r}$. In this section, we provide further results and comment on cases where the energy $\mathscr{W}_\mathfrak{r}$ is a function of the deformation measures formulated in Eq. (6.14).

Formulations based on the stretch $\bar{\lambda}_\mathfrak{r}$ The majority of formulations for $\mathscr{W}_\mathfrak{r}$ is based on the assumption that the energy is a function only of the stretch $\bar{\lambda}_\mathfrak{r}$, such that $\mathscr{W}_\mathfrak{r}(\boldsymbol{F}_\mathfrak{r}) = \mathscr{W}_\mathfrak{r}(\bar{\lambda}_\mathfrak{r})$. This is an appropriate formulation under the assumption that a fibre or a chain shows a one-dimensional spring-like mechanical behaviour. The one-dimensional character becomes clear by formulating the stress tensor $\boldsymbol{P}_\mathfrak{r}$ associated with a single fibre, given by

$$\boldsymbol{P}_\mathfrak{r} = \partial_{\boldsymbol{F}_\mathfrak{r}}\mathscr{W}_\mathfrak{r}(\bar{\lambda}_\mathfrak{r}) = \frac{P_\mathfrak{r}(\bar{\lambda}_\mathfrak{r})}{\bar{\lambda}_\mathfrak{r}}\,\mathfrak{r}\otimes\mathfrak{r}_0 \quad \text{where} \quad P_\mathfrak{r}(\bar{\lambda}_\mathfrak{r}) = \partial_{\bar{\lambda}_\mathfrak{r}}\mathscr{W}_\mathfrak{r}(\bar{\lambda}_\mathfrak{r})\,. \tag{6.18}$$

Therein, use was made of chain rule and the derivative $\partial_{\boldsymbol{F}_\mathfrak{r}}\bar{\lambda}_\mathfrak{r} = \bar{\lambda}_\mathfrak{r}^{-1}\bar{\boldsymbol{F}}\mathfrak{r}_0\otimes\mathfrak{r}_0 = \bar{\lambda}_\mathfrak{r}^{-1}\mathfrak{r}\otimes\mathfrak{r}_0$. Further, $P_\mathfrak{r}$ denotes a scalar nominal stress. With (6.18), we see that $\boldsymbol{P}_\mathfrak{r}$ is associated with a nominal traction vector $\boldsymbol{P}_\mathfrak{r}\,\mathfrak{r}_0 = \bar{\lambda}_\mathfrak{r}^{-1}P_\mathfrak{r}(\bar{\lambda}_\mathfrak{r})\mathfrak{r}$, whereas $\boldsymbol{P}_\mathfrak{r}\,\mathfrak{r}_0^\perp = \boldsymbol{0}$, with $\mathfrak{r}_0\cdot\mathfrak{r}_0^\perp = 0$. This means that a stretch-dependent fibre energy $\mathscr{W}_\mathfrak{r}(\bar{\lambda}_\mathfrak{r})$ does not induce any stress contributions transverse to the vector $\mathfrak{r}_0$. Furthermore, the fourth-order elasticity tensor of a single fibre is obtained as

$$\mathbb{L}_\mathfrak{r} = \partial^2_{\boldsymbol{F}_\mathfrak{r}\boldsymbol{F}_\mathfrak{r}}\mathscr{W}_\mathfrak{r}(\bar{\lambda}_\mathfrak{r}) = \Big(\frac{L_\mathfrak{r}(\bar{\lambda}_\mathfrak{r})}{\bar{\lambda}_\mathfrak{r}^2} - \frac{P_\mathfrak{r}(\bar{\lambda}_\mathfrak{r})}{\bar{\lambda}_\mathfrak{r}^3}\Big)\,\mathfrak{r}\otimes\mathfrak{r}_0\otimes\mathfrak{r}\otimes\mathfrak{r}_0 + \frac{P_\mathfrak{r}(\bar{\lambda}_\mathfrak{r})}{\bar{\lambda}_\mathfrak{r}}\,(\boldsymbol{I}\otimes\mathfrak{r}_0\otimes\mathfrak{r}_0)^{T_{23}} \tag{6.19}$$

where $L_\mathfrak{r}(\bar{\lambda}_\mathfrak{r}) = \partial_{\lambda_\mathfrak{r}}P_\mathfrak{r}(\bar{\lambda}_\mathfrak{r}) = \partial^2_{\lambda_\mathfrak{r}^2}\mathscr{W}_\mathfrak{r}(\bar{\lambda}_\mathfrak{r})$ denotes a scalar nominal stiffness modulus. Note that the results in Eqs (6.18) and (6.19) can be generalised to non-affine deformations by simply replacing $\bar{\lambda}_\mathfrak{r}$ by $\lambda_\mathfrak{r}$ from Eq. $(6.3)_1$ and taking $\mathfrak{r}$ from the general map in Eq. (6.2). Next, we formulate the macroscopic first Piola–Kirchhoff stress tensor $\bar{\boldsymbol{P}}_\mathrm{V}$ associated with the energy $\bar{\mathscr{W}}_\mathrm{V}$ from (6.15), giving

$$\bar{\boldsymbol{P}}_\mathrm{V} = \partial_{\bar{\boldsymbol{F}}}\bar{\mathscr{W}}_\mathrm{V} = \big\langle\boldsymbol{P}_\mathfrak{r}\big\rangle_\Omega = \Big\langle\frac{P_\mathfrak{r}(\bar{\lambda}_\mathfrak{r})}{\bar{\lambda}_\mathfrak{r}}\,\mathfrak{r}\otimes\mathfrak{r}_0\Big\rangle_\Omega = \bar{\boldsymbol{F}}\bar{\boldsymbol{S}}_\mathrm{V} \quad\text{with}\quad \bar{\boldsymbol{S}}_\mathrm{V} = \Big\langle\frac{P_\mathfrak{r}(\bar{\lambda}_\mathfrak{r})}{\bar{\lambda}_\mathfrak{r}}\,\mathfrak{r}_0\otimes\mathfrak{r}_0\Big\rangle_\Omega. \tag{6.20}$$

Therein, the notation in terms of the second Piola–Kirchhoff stress tensor $\bar{\boldsymbol{S}}_\mathrm{V}$ is obtained by noting that, with $\mathfrak{r}\otimes\mathfrak{r}_0 = \bar{\boldsymbol{F}}\,\mathfrak{r}_0\otimes\mathfrak{r}_0$, it is possible to pull the affine deformation $\bar{\boldsymbol{F}}$ in front of the averaging operator $\langle(\cdot)\rangle_\Omega$. This step is very useful, as $\bar{\boldsymbol{S}}_\mathrm{V}$ and the associated tensor base $\mathfrak{r}_0\otimes\mathfrak{r}_0$ are symmetric and only require to carry out a double integral for six coefficients, while the non-symmetric tensor base $\mathfrak{r}\otimes\mathfrak{r}_0$ entails a double integral for each of the nine coefficients. Moreover, note that an averaging operation $\langle\mathfrak{r}_0\otimes\mathfrak{r}_0\rangle_\Omega$ solely applied to the structural-tensor-like dyadic product $\mathfrak{r}_0\otimes\mathfrak{r}_0$ would lead to formulations that are in line with the orientation tensors introduced by Advani & Tucker III [3] and thereon based models by Freed et al. [137] and Gasser et al. [151]. However, it has to be remarked that such a preintegration of the orientations generally does not lead to the same results than the original integration in (6.20) due to the disregarded coupling with the non-constant factor $P_\mathfrak{r}(\bar{\lambda}_\mathfrak{r})/\bar{\lambda}_\mathfrak{r}$. Next, the macroscopic nominal elasticity tensor is obtained as

$$\bar{\mathbb{L}}_\mathrm{V} = \partial_{\bar{\boldsymbol{F}}}\bar{\boldsymbol{P}} = \big\langle\mathbb{L}_\mathfrak{r}\big\rangle_\Omega = \Big\langle\Big(\frac{L_\mathfrak{r}(\bar{\lambda}_\mathfrak{r})}{\bar{\lambda}_\mathfrak{r}^2} - \frac{P_\mathfrak{r}(\bar{\lambda}_\mathfrak{r})}{\lambda_\mathfrak{r}^3}\Big)\,\mathfrak{r}\otimes\mathfrak{r}_0\otimes\mathfrak{r}\otimes\mathfrak{r}_0 + \frac{P_\mathfrak{r}(\lambda_\mathfrak{r})}{\bar{\lambda}_\mathfrak{r}}\,(\boldsymbol{I}\otimes\mathfrak{r}_0\otimes\mathfrak{r}_0)^{T_{23}}\Big\rangle_\Omega, \tag{6.21}$$

We recall that the nominal elasticity tensor is major symmetric and contains 45 independent coefficients, see Table A.2, which means that 45 double integrals have to be carried out in expression (6.21). However, as for the nominal stress, it is possible to reduce this number by employing Eq. (3.114) and computing $\bar{\mathbb{L}}_\mathrm{V}$ from its material counterpart

$$\bar{\mathbb{C}}_\mathrm{V} = \partial_{\bar{\boldsymbol{C}}}\bar{\boldsymbol{S}}_\mathrm{V} = \Big\langle\Big(\frac{L_\mathfrak{r}(\bar{\lambda}_\mathfrak{r})}{\bar{\lambda}_\mathfrak{r}^2} - \frac{P_\mathfrak{r}(\lambda_\mathfrak{r})}{\lambda_\mathfrak{r}^3}\Big)\,\mathfrak{r}_0\otimes\mathfrak{r}_0\otimes\mathfrak{r}_0\otimes\mathfrak{r}_0\Big\rangle_\Omega. \tag{6.22}$$

This fourth-order tensor is *total symmetric* and only contains 15 independent coefficients. Hence, the computation of $\bar{\mathbb{L}}_\mathrm{V}$ by means of Eq. (3.114) only requires to carry out 15 additional double integrals, if we further assume that $\bar{\boldsymbol{S}}_\mathrm{V}$ is already known from the stress computation.

It can be seen that making a specific choice for the energy $\mathscr{W}_\mathfrak{r}(\bar{\lambda}_\mathfrak{r})$ enters the derived stress and stiffness tensors in terms of the scalar derivatives $P_\mathfrak{r}(\bar{\lambda}_\mathfrak{r})$ and $L_\mathfrak{r}(\bar{\lambda}_\mathfrak{r})$. Further, the energy $\mathscr{W}_\mathfrak{r}(\bar{\lambda}_\mathfrak{r})$ can be obtained in very different ways. Of course, it is possible to directly employ well-known constitutive relations, such as the quadratic potential formulated in Eq. (3.174). Yet, also any J_4-based strain-energy function can be applied by noting that we can formulate a respective measure $\bar{J}_{4\mathfrak{r}} = \bar{\lambda}_\mathfrak{r}^2$ for each fibre. Hence, one can also employ the J_4-dependent standard reinforcing model (3.173) or the exponential energy from Eq. (3.175). More such functions can be found in the review paper of Chagnon et al. [74]. Moreover, apart from defining the energy $\mathscr{W}_\mathfrak{r}$ in a constitutive way, it is also possible to derive it from further microstructural considerations and bottom-up approaches. For example, Buehler [63], Grytz & Meschke [172] and Maceri et al. [306] obtained the energy of single collagen fibres by setting up detailed small-scale models and carrying out further homogenisation steps. It this process, it is interesting to note that the elasticity of single fibres (in collageneous tissue) or chains (in polymers) at small scales is often of entropic nature. Hence, if we write the strain energy as

$$\mathscr{W}_\mathfrak{r} = \rho_{\mathfrak{r}0}\psi_\mathfrak{r} = \rho_{\mathfrak{r}0}(\varepsilon_\mathfrak{r} - \theta\eta_\mathfrak{r})\,, \tag{6.23}$$

we see that changes of $\mathscr{W}_\mathfrak{r}$ can be caused by the internal energy $\varepsilon_\mathfrak{r}$, leading to energetic elasticity, or the entropy $\eta_\mathfrak{r}$, leading to entropic elasticity. Models for the latter are usually based on the idea that a single chain consists of multiple segments, the so-called Kuhn segments. Subsequently, conformation changes of the chain are described by means of statistical mechanics and lead to an entropic response. If the segments are rather aligned, one arrives at the *worm-like chain model* by Kratky & Porod [261] and its development by Marko & Siggia [315], which has been used for polymers as well as for proteins and collageneous tissues. If one rather assumes that the chain forms a random coil and the segments are thought to be freely joined with each other, one commonly proceeds from an entropy prescription $\eta_\mathfrak{r} = k\ln[p]$, where k is the Boltzmann constant and p is a probability which is usually described in terms of the Gaussian statistics by Kuhn [268, 269] or the Langevin statistics by Kuhn & Grün [270] and James & Guth [247]. For instance, the Gaussian approach, with $p = p_0\exp[-3\bar{\lambda}_\mathfrak{r}^2/2]$ and $\varepsilon_\mathfrak{r} = 0$, leads to $\mathscr{W}_\mathfrak{r}(\bar{\lambda}_\mathfrak{r}) = 3nk\theta\bar{\lambda}_\mathfrak{r}^2/2 + \mathscr{W}_0$, where p_0 is a normalisation constant, n is the number of chains and $\mathscr{W}_0$ is a constant energy. Interestingly, with Table 6.1, we see that the associated effective energy in a uniform network is found as $\bar{\mathscr{W}}_\mathrm{V}(I_1) = \big\langle\mathscr{W}_\mathfrak{r}\big\rangle_{\Omega_\circ} = nk\theta I_1/2 + \bar{\mathscr{W}}_0$, see also Treloar [479]. Then, with a proper choice for $\bar{\mathscr{W}}_0$ such that $\bar{\mathscr{W}}_\mathrm{V}$ normalises properly and setting $\mu = nk\theta$, we see that the effective network response is identified as the Neo-Hooke energy from Eq. (3.159). However, the single material parameter μ is in this context not just a simple calibration parameter, but has a clear micromechanical meaning and constitutes the product of the number of chains in a unit volume, Boltzmann constant and absolute temperature. Similar relations can also be found for other analytical strain-energy functions from Section 3.8.3. For instance, Horgan & Saccomandi [229] commented on the micromechanical meaning of the Gent function, given in Eq. (3.166), whereas Ehret [111] generalised these considerations to the Ogden-type materials.

Formulations based on the stretch $\bar{\lambda}_\mathfrak{r}$ and the area stretch $\bar{\upsilon}_\mathfrak{r}$ If the fibre energy $\mathscr{W}_\mathfrak{r}$ is in addition to the stretch $\bar{\lambda}_\mathfrak{r}$ also dependent on the area stretch $\bar{\upsilon}_\mathfrak{r}$, we obtain $\mathscr{W}_\mathfrak{r}(\boldsymbol{F}_\mathfrak{r}) = \mathscr{W}_\mathfrak{r}(\bar{\lambda}_\mathfrak{r}, \bar{\upsilon}_\mathfrak{r})$. With this, it is possible to formulate fibre energies in line with

the tube models by Heinrich & Straube [195], Heinrich et al. [196], Heinrich & Kaliske [194], and Edwards & Vilgis [105]. In those approaches, the $\bar{v}_{\mathfrak{r}}$-dependent energy terms account for so-called *tube-like topological constraints*, which are based on the assumption that the deformation of a single fibre may be restricted by the deformation of neighbouring fibres. The tube constraint is a very important ingredient for meaningful network models of rubber elasticity and was applied by, for example, Miehe et al. [329] and Mistry & Govindjee [337]. However, it may also be an interesting approach in modelling collageneous tissue. Further, an interesting observation can be made if the fibre energy based on Gaussian statistics from the previous section is added a similar contribution for the area stretch $\bar{v}_{\mathfrak{r}}$, which subsequently will lead to a quadratic potential in the area stretch $\bar{v}_{\mathfrak{r}}$. With Table 6.1, it can be seen that the associated effective response for a uniform network will contain an additional dependence on the macroscopic $\bar{I}_2$-invariant and leads to formulations reminiscent of the *Mooney-Rivlin strain-energy function* by Mooney [340] and Rivlin & Saunders [404]. Further details can be found in the article of Fried [140].

Formulations based on the stretch $\bar{\lambda}_{\mathfrak{r}}$ and the Jacobian $\bar{J}$ In addition to the deformation measures formulated in Eqs (6.3) and (6.14), one can also define a micro-Jacobian $J_{\mathfrak{r}} = \det[\boldsymbol{F}_{\mathfrak{r}}]$ which describes the volume change of the tube-like segment aligned with the vector $\mathfrak{r}_0$. In an affine network, the micro-Jacobian is equal to the Jacobian associated with the macroscopic deformation gradient and becomes independent of the orientation of $\mathfrak{r}_0$, such that $J_{\mathfrak{r}} = \bar{J}_{\mathfrak{r}} = \bar{J} = \det[\bar{\boldsymbol{F}}]$. In the classical works on rubber elasticity by Wall & Flory [498] and Flory [129, 130], it was explained that a $\bar{J}$-dependent contribution to $\mathscr{W}_{\mathfrak{r}}$ accounts for the energetic elasticity in the network and supplements the entropic description of single chains. In the context of a Gaussian chain description, it was outlined by Boyce & Arruda [58] and Bischoff et al. [38] that such a contribution results at the macroscale in a logarithmic energy term reminiscent of the one given Eq. (3.160). Bischoff et al. [37] explained that this can be interpreted as a *repulsion* term which accounts for interchain repulsive forces. While the $\bar{\lambda}_{\mathfrak{r}}$- and $\bar{J}$-dependent energy contributions have in such a formulation an additive characteristic, such that $\mathscr{W}_{\mathfrak{r}}(\bar{\lambda}_{\mathfrak{r}}, \bar{J}) = \mathscr{W}_{\mathfrak{r}}^{\lambda}(\bar{\lambda}_{\mathfrak{r}}) + \mathscr{W}_{\mathfrak{r}}^{J}(\bar{J})$, it is also possible to formulate an multiplicative coupling by employing the deviatoric energy

$$\mathscr{W}_{\mathfrak{r}}(\breve{\boldsymbol{F}}_{\mathfrak{r}}) = \mathscr{W}_{\mathfrak{r}}(\breve{\lambda}_{\mathfrak{r}}) \quad \text{with} \quad \breve{\lambda}_{\mathfrak{r}} = \bar{J}^{-1/3}\bar{\lambda}_{\mathfrak{r}} \tag{6.24}$$

This form directly follows from the deviatoric-volumetric split explained in Section 3.7.2. The dependence on the isochoric part of the deformation may be motivated through micromechanical considerations, which is often the case in rubber elasticity by referring to the work of Flory [129], or may just represent a constitutive assumption. In any case, it is interesting to formulate the stress tensor of a single fibre resulting from the energy (6.24), reading

$$\boldsymbol{P}_{\mathfrak{r}}(\breve{\lambda}_{\mathfrak{r}}) = \partial_{\boldsymbol{F}_{\mathfrak{r}}}\mathscr{W}_{\mathfrak{r}}(\breve{\lambda}_{\mathfrak{r}}) = \breve{P}_{\mathfrak{r}}(\breve{\lambda}_{\mathfrak{r}})\bar{J}^{-1/3}\big(\bar{\lambda}_{\mathfrak{r}}^{-1}\,\mathfrak{r}\otimes\mathfrak{r}_0 - \tfrac{1}{3}\bar{\lambda}_{\mathfrak{r}}\,\bar{\boldsymbol{F}}^{-T}\big) \quad \text{where} \quad \breve{P}_{\mathfrak{r}}(\breve{\lambda}_{\mathfrak{r}}) = \partial_{\breve{\lambda}_{\mathfrak{r}}}\mathscr{W}_{\mathfrak{r}}(\breve{\lambda}_{\mathfrak{r}})\,. \tag{6.25}$$

It is easy to see that the traction transverse to $\mathfrak{r}_0$ is $\boldsymbol{P}_{\mathfrak{r}}\,\mathfrak{r}_0^{\perp} = -\breve{P}_{\mathfrak{r}}J^{-1/3}\bar{\lambda}_{\mathfrak{r}}\bar{\boldsymbol{F}}^{-T}\mathfrak{r}_0^{\perp}/3 \neq \boldsymbol{0}$, which means that the fibre stress in Eq. (6.25) does not have a one-dimensional characteristic. This is in contrast to the stretch-based formulation in Eq. (6.18). Therefore, Sansour [417] and Helfenstein et al. [197] commented that the energy (6.24) based

on the deviatoric stretch is not appropriate to model a one-dimensional spring-like fibre behaviour. However, the transverse stress contributions could also be thought as (desired) reaction stresses necessary to maintain that the tube-like segment enclosing a fibre (which may represent a surrounding fluid medium) experiences no hydrostatic pressure, since it holds that $p_{\mathfrak{r}} = -\bar{J}^{-1}\boldsymbol{P}_{\mathfrak{r}} \cdot \bar{\boldsymbol{F}}/3 = 0$, compare Eq. (3.29).

6.3 Transversely isotropic networks models

In this section, we investigate the special case of a homogeneous fibre distribution in the azimuthal direction Φ. To do so, we postulate that the ODF is split into two terms, reading

$$\mathfrak{p}(\Theta, \Phi) = \mathfrak{p}_\Theta(\Theta)\, \mathfrak{p}_\Phi(\Phi)\,, \tag{6.26}$$

where $\mathfrak{p}_\Theta(\Theta)$ and $\mathfrak{p}_\Phi(\Phi)$ depict univariate probability functions for the fibre distribution in the polar and the azimuthal direction, respectively. Both the probability functions have to be periodic in their respective argument, hence, $\mathfrak{p}_\Theta(\Theta) = \mathfrak{p}_\Theta(\Theta + n\pi)$ and $\mathfrak{p}_\Phi(\Phi) = \mathfrak{p}_\Phi(\Phi + 2n\pi)$, with $n \in \mathcal{N}$. Such periodic functions can be constructed from any standard univariate probability function by formulating the associated wrapped probability functions, such as exemplary shown for π- and 2π-periodic functions in Eqs (B.33) and (B.30), respectively. However, the special case of a homogeneous distribution in azimuthal direction simplifies $\mathfrak{p}_\Phi$ to the constant value

$$\mathfrak{p}_\Phi = \frac{1}{2\pi}\,. \tag{6.27}$$

For completeness, we note that the averaging operation and the normalisation condition for the remaining polar contribution of the ODF then read

$$\big\langle(\cdot)\big\rangle_\Omega = \frac{1}{2\pi}\int_\Omega \mathfrak{p}_\Theta(\Theta)\,(\cdot)\,\mathrm{d}\Omega \quad \text{and} \quad \int_0^\pi \mathfrak{p}_\Theta(\Theta)\sin[\Theta]\,\mathrm{d}\Theta = 1\,, \tag{6.28}$$

where the last relation directly follows from Eqs (6.6) and (6.26). Obviously, the homogeneous azimuthal fibre distribution entails that the orientation of the $\boldsymbol{e}_1^{\mathrm{s}}$- and $\boldsymbol{e}_2^{\mathrm{s}}$-directions in the laboratory frame of reference becomes completely arbitrary. Hence, we can identify a rotational symmetry around the $\boldsymbol{e}_3^{\mathrm{s}}$-axis and observe that the use of any coordinate system $\boldsymbol{e}_i^{\mathrm{s}*} = \boldsymbol{Q}^{\Phi}_{\boldsymbol{e}_3^{\mathrm{s}}}\boldsymbol{e}_i^{\mathrm{s}}$, with $\Phi \in [0, 2\pi)$, is equivalent and will not change anything in the material behaviour of the network. This suggests that the material response becomes transversely isotropic with $\boldsymbol{e}_3^{\mathrm{s}}$ being a preferred direction. In fact, it is known from Section 3.5.4 that rotational symmetry represents one of the five types of transverse isotropy and it is easy to show that the network with homogeneous azimuthal fibre distribution satisfies the other four types as well. For example, symmetry with respect to a two-fold axis transverse to $\boldsymbol{e}_3^{\mathrm{s}}$ requires that the material behaviour must not change if the preferred direction is rotated by $\boldsymbol{Q}^{\pi}_{\boldsymbol{e}_3^{\mathrm{s}\perp}}\boldsymbol{e}_3^{\mathrm{s}} = -\boldsymbol{e}_3^{\mathrm{s}}$, where the definition of $\boldsymbol{Q}^{\pi}_{\boldsymbol{e}_3^{\mathrm{s}\perp}}$ follows from Eq. (3.80). This symmetry is immediately fulfilled because we demanded $\mathfrak{p}_\Theta(\Theta) = \mathfrak{p}_\Theta(\Theta + n\pi)$ which still implies the symmetry $\mathfrak{p}_\Theta(\mathfrak{r}) = \mathfrak{p}_\Theta(-\mathfrak{r})$, see also Eq. (6.4). Concluding, the network model with homogeneous fibre distribution in azimuthal direction belongs to the transversely isotropic symmetry group

$$\mathcal{MG}_{\mathrm{ti}} = \{\boldsymbol{Q}^{\Phi}_{\boldsymbol{e}_3^{\mathrm{s}}}, \boldsymbol{Q}^{\pi}_{\boldsymbol{e}_3^{\mathrm{s}\perp}}, -\boldsymbol{I} \mid 0 \leq \Phi < 2\pi\} \subset \mathcal{O}(3)\,. \tag{6.29}$$

As a consequence, the effective network behaviour, such as the energy $\bar{\mathscr{W}}_{\mathrm{V}}$, becomes a function of the macroscopic right Cauchy–Green tensor $\bar{\boldsymbol{C}}$ and a structural tensor $\bar{\boldsymbol{M}} = \bar{\boldsymbol{a}}_0 \otimes \bar{\boldsymbol{a}}_0$, where the macroscopic preferred direction $\bar{\boldsymbol{a}}$ has to be collinear with the $\boldsymbol{e}_3^{\mathrm{s}}$-axis of the laboratory frame of reference. Furthermore, any of the invariant sets introduced in Section (3.5.4) can be used as a proper integrity basis for the two macroscopic argument tensors. Yet, as for the TSO estimate in Section 5.3.2, the two invariant sets $\mathscr{I}_{\mathrm{ti}}^{\imath}$ and $\mathscr{I}_{\mathrm{ti}}^{\jmath}$ are particularly useful, because they allow the formulation of generic deformation gradients $\bar{\boldsymbol{F}}^{\imath}$ and $\bar{\boldsymbol{F}}^{\jmath}$ as defined in Eq. (3.95) and (3.100), respectively. The two generic tensors are each defined in coordinate systems $\boldsymbol{e}_i^{\imath}$ and $\boldsymbol{e}_i^{\jmath}$ $(i = 1, 2, 3)$ in which $\boldsymbol{e}_3^{\imath}$ and $\boldsymbol{e}_3^{\jmath}$ are aligned with the preferred direction of the material. Hence, $\bar{\boldsymbol{F}}^{\imath}$ and $\bar{\boldsymbol{F}}^{\jmath}$ are perfectly aligned with the $\boldsymbol{e}_i^{\mathrm{s}}$-coordinate system of the transversely isotropic network and can directly be used for the fibre map in Eq. (6.13). Choosing invariant set $\mathscr{I}_{\mathrm{ti}}^{\imath}$, the vector $\mathfrak{r}$ can then be written as

$$\begin{aligned}\mathfrak{r}(\mathscr{I}_{\mathrm{ti}}^{\imath}; \Theta, \Phi) = \bar{\boldsymbol{F}}^{\imath}(\mathscr{I}_{\mathrm{ti}}^{\imath})\, \mathfrak{r}_0(\Theta, \Phi) = \bar{\lambda}_{\mathrm{t}} \sin[\Theta] \cos[\Phi]\, \boldsymbol{e}_1^{\mathrm{s}} + \sin[\Theta](\bar{\lambda}_{\mathrm{t}} \sin[\Phi] + \bar{\gamma}_{\mathrm{t}} \cos[\Phi])\, \boldsymbol{e}_2^{\mathrm{s}} \\ + \bar{\lambda}_{\ell} \cos[\Theta] + \bar{\gamma}_{\ell} \sin[\Theta] \cos[\Phi - \bar{\psi}_{\gamma}]\, \boldsymbol{e}_3^{\mathrm{s}}\,.\end{aligned} \tag{6.30}$$

Subsequently, it is possible to formulate the deformation measures from Eq. (6.14) in terms of macroscopic invariants. For instance, the stretch of the vector $\mathfrak{r}_0$ reads

$$\begin{aligned}\bar{\lambda}_{\mathfrak{r}}(\mathscr{I}_{\mathrm{ti}}^{\imath}; \Theta, \Phi) &= \bar{\lambda}_{\mathfrak{r}}(\bar{\lambda}_{\ell}, \bar{\lambda}_{\mathrm{t}}, \bar{\gamma}_{\ell}, \bar{\gamma}_{\mathrm{t}}, \bar{\psi}_{\gamma}; \Theta, \Phi) \\ &= \big\{\bar{\lambda}_{\mathrm{t}}^2 \sin^2[\Theta] \cos^2[\Phi] + (\bar{\lambda}_{\mathrm{t}} \sin[\Theta] \sin[\Phi] + \bar{\gamma}_{\mathrm{t}} \sin[\Theta] \cos[\Phi])^2 \\ &+ (\bar{\lambda}_{\ell} \cos[\Theta] + \bar{\gamma}_{\ell} \sin[\Theta] \cos[\Phi - \bar{\psi}_{\gamma}])^2\big\}^{1/2}\,,\end{aligned} \tag{6.31}$$

Hence, the stretch of the vector $\mathfrak{r}_0(\Theta, \Phi)$ can directly be expressed in terms of macroscopic strain invariants. Note, a vector $\mathfrak{r}(\mathscr{I}_{\mathrm{ti}}^{\jmath})$ and the thereon based stretch $\bar{\lambda}_{\mathfrak{r}}(\mathscr{I}_{\mathrm{ti}}^{\jmath})$ can be derived in direct analogy. Further, if the fibre energy $\mathscr{W}_{\mathfrak{r}}(\bar{\lambda}_{\mathfrak{r}})$ is a function of the fibre stretch, the associated stress tensor of a single fibre with respect to a *general deformation* $\bar{\boldsymbol{F}}$ reads

$$\boldsymbol{P}_{\mathfrak{r}}(\mathscr{I}_{\mathrm{ti}}^{\imath}; \Theta, \Phi) = \partial_{\bar{\boldsymbol{F}}} \bar{\mathscr{W}}_{\mathfrak{r}}(\mathscr{I}_{\mathrm{ti}}^{\imath}) = P_{\mathfrak{r}}(\bar{\lambda}_{\mathfrak{r}}) \sum_{\mathfrak{I}^{\imath} \in \mathscr{I}_{\mathrm{ti}}^{\imath}} \{\partial_{\mathfrak{I}^{\imath}} \bar{\lambda}_{\mathfrak{r}}\, \partial_{\bar{\boldsymbol{F}}} \mathfrak{I}^{\imath}\}\,. \tag{6.32}$$

Therein, each of the five summands consists of a scalar-valued derivative $\partial_{\mathfrak{I}^{\imath}} \bar{\lambda}_{\mathfrak{r}}$ and a tensor base $\partial_{\bar{\boldsymbol{F}}} \mathfrak{I}^{\imath}$, where $\mathfrak{I}^{\imath} \in \mathscr{I}_{\mathrm{ti}}^{\imath}$. Explicit relations for the five tensor bases can be found in DE-BOTTON ET AL. [92] and BLEILER ET AL. [44]. They account for the procedure of rotating a general deformation $\bar{\boldsymbol{F}}$, together with the knowledge of the preferred direction $\bar{\boldsymbol{a}}_0$, into the appropriate coordinate system of the generic tensor $\bar{\boldsymbol{F}}^{\imath}$. Further, if the invariant set $\mathscr{I}_{\mathrm{ti}}^{I}$ is used to describe the energy, such that $\bar{\mathscr{W}}_{\mathrm{V}} = \bar{\mathscr{W}}_{\mathrm{V}}(\mathscr{I}_{\mathrm{ti}}^{I})$, one might need to conduct further applications of the chain rule when carrying out the derivatives $\partial_{\mathfrak{I}^{\imath}} \mathfrak{I}^{I}$ for $\mathfrak{I}^{I} \in \mathscr{I}_{\mathrm{ti}}^{I}$ and $\mathfrak{I}^{\imath} \in \mathscr{I}_{\mathrm{ti}}^{\imath}$. Yet, they can be straightforwardly derived from Eqs (3.96). Finally, note that further relations for the invariant-based formulations, such as the effective stress $\bar{\boldsymbol{P}}_{\mathrm{V}}$ or the elasticity tensor $\bar{\mathbb{L}}_{\mathrm{V}}$, defined in Eqs (6.20) and (6.21), can be derived from Eq. (6.32) and further derivations by carefully addressing the required chain rules.

6.4 Numerical quadrature over the sphere

The computation of the effective network response requires to carry out the double integrals associated with the continuous averaging operator $\langle(\cdot)\rangle_{\Omega}$, given in Eq. (6.5). Due

to the possibly highly nonlinear behaviour of single fibres and non-uniform distribution functions $\mathfrak{p}$, it is in general not possible to obtain closed-form solutions of the integrals. Respectively, analytical results may only be found if confining attention to some special cases, such as done by Itskov et al. [245] by restricting to an isotropic network model for which the averaging operator simplifies to $\langle(\cdot)\rangle_{\Omega_\circ}$, see Eq. (6.16). However, in general the integrals have to be carried out by means of numerical quadrature schemes, which means that the continuous averaging operation is approximated by a sum of discrete values evaluated at N_Ω points on the microsphere surface Ω, giving

$$\big\langle f(\mathfrak{r})\big\rangle_\Omega = \int_\Omega f(\mathfrak{r})\,\mathrm{d}\Omega = \int_0^\pi \int_0^{2\pi} f(\mathfrak{r})\,\sin[\Theta]\,\mathrm{d}\Phi\,\mathrm{d}\Theta \approx \sum_{i=1}^{N_\Omega} w_i\, f(\mathfrak{r}^i)\,, \tag{6.33}$$

Therein, w_i $(i = 1,\dots,N_\Omega)$ are N_Ω scalar weighting factors and $\mathfrak{r}^i$ are the associated discrete space orientation vectors. In order to be consistent with the normalisation conditions $(6.16)_2$ and (6.17), they have to satisfy[1]

$$\frac{1}{4\pi}\sum_{i=1}^{N_\Omega} w_i = 1\,, \quad \sum_{i=1}^{N_\Omega} \mathfrak{r}^i = \mathbf{0}\,, \quad \frac{1}{4\pi}\sum_{i=1}^{N_\Omega} w_i\,\mathfrak{r}^i \otimes \mathfrak{r}^i = \tfrac{1}{3}\boldsymbol{I}\,. \tag{6.34}$$

The appropriate choice of weighting factors w_i and space orientations $\mathfrak{r}^i$ is a decisive aspect for meaningful implementations of network models in a numerical setup. An insufficient number of quadrature points or an inappropriate scheme may lead to critical inaccuracies of the results, which was explained in detail in the studies of Verron [493] and Itskov [242]. It can further lead to spurious material anisotropies, see Ehret et al. [113]. In theory, the accuracy of the quadrature can be guaranteed by employing adaptive schemes in connection with an appropriate choice of numerical tolerance values. However, adaptive methods are not optimal when it comes to computational costs and efficiency. Thus, general applications rather demand for reliable and fast non-adaptive quadrature schemes. A variety of different weighting and point sets has been used for microsphere models. For instance, Miehe et al. [329] used an integration scheme by Bažant & Oh [26] with $N_\Omega = 42$ and obtained good results for their isotropic network model (hence, if the averaging operator reduces to $\langle(\cdot)\rangle_{\Omega_\circ}$). Alastrué et al. [7] observed that the scheme of Heo & Xu [200] with $N_\Omega = 368$ is sufficient also for highly anisotropic fibre distributions. In general, it is particularly useful to employ quadrature schemes that offer a variable number of integration points and allow to refine the discretisation if needed. For instance, the very useful family of *Lebedev points* by Lebedev [279] and Lebedev & Laikov [280] offers discretisations from $N_\Omega = 6$ up to $N_\Omega = 5810$. Figure 6.2 exemplary shows the quadrature points for four different discretisations with $N_\Omega = \{6, 50, 230, 770\}$. Therein, the values for $\mathcal{O}_\mathrm{L}$ refer to the degree of spherical harmonics which can be solved exactly with the respective number of points. The finest discretisation, with $N_\Omega = 5810$, is

[1] Note that slightly different formulations may be found in the literature for Eqs $(6.34)_1$ and $(6.34)_3$, which is due to the fact that the ODF $\mathfrak{p}$ is required in this work to normalise according to Eq. (6.6). In contrast, other works may proceed from a normalisation factor $1/(4\pi)$ in front of the integral in Eq. (6.5), such that $\langle(\cdot)\rangle_\Omega := \frac{1}{4\pi}\int_\Omega \mathfrak{p}(\Theta,\Phi)\,(\cdot)\,\mathrm{d}\Omega$. Consequently, with the quadrature $\langle f(\mathfrak{r})\rangle_\Omega \approx \sum_{i=1}^{N_\Omega} w_i f(\mathfrak{r}^i)$ and as Eq. (6.6) becomes $\langle 1\rangle_\Omega = \frac{1}{4\pi}\int_\Omega \mathfrak{p}(\Theta,\Phi)\,\mathrm{d}\Omega = 1$, conditions $(6.34)_1$ and $(6.34)_3$ transform to $\sum_{i=1}^{N_\Omega} w_i = 1$ and $\sum_{i=1}^{N_\Omega} w_i\,\mathfrak{r}^i \otimes \mathfrak{r}^i = \boldsymbol{I}/3$, respectively.

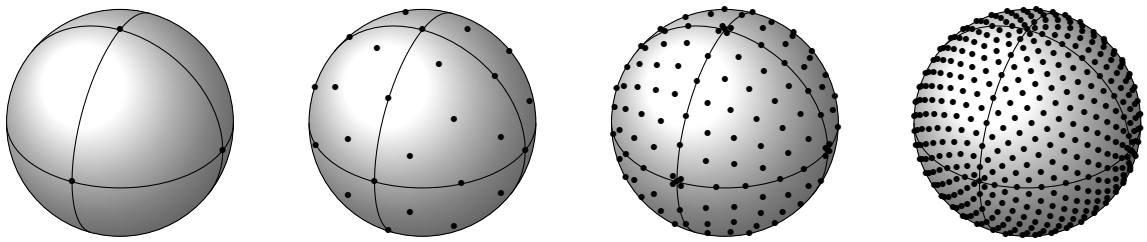

$N_\Omega = 6$, $\mathcal{O}_\mathrm{L} = 3$ $N_\Omega = 50$, $\mathcal{O}_\mathrm{L} = 11$ $N_\Omega = 230$, $\mathcal{O}_\mathrm{L} = 25$ $N_\Omega = 770$, $\mathcal{O}_\mathrm{L} = 47$

Figure 6.2: Lebedev-type quadrature points for different discretisations of the microsphere surface Ω.

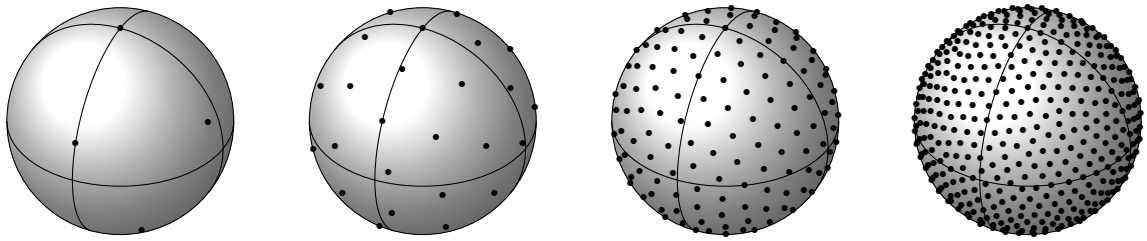

$N_\Omega = 9$, $\mathcal{O}_\mathrm{S} = 2$ $N_\Omega = 49$, $\mathcal{O}_\mathrm{S} = 6$ $N_\Omega = 256$, $\mathcal{O}_\mathrm{S} = 15$ $N_\Omega = 784$, $\mathcal{O}_\mathrm{S} = 27$

Figure 6.3: Sloan–Womersley-type quadrature points for different discretisations of the microsphere surface Ω.

able to exactly solve spherical harmonics up to a degree of $\mathcal{O}_\mathrm{L} = 131$. An additional advantage of the Lebedev points is that they are invariant with respect to octahedral rotations of the microsphere. This is beneficial if certain symmetries of the functions to be integrated shall be exploited. For example, due to the symmetry of the ODF, formulated in Eq. (6.4), it suffices to perform the integration on one half-sphere and double the results. The arrangement of the Lebedev points on the surface of the microsphere easily allows to account for this property. Moreover, an alternative family of quadrature points was proposed by Womersley & Sloan [521] and Sloan & Womersley [446]. The *Sloan–Womersley points* range between $N_\Omega = 4$ in the coarsest version and $N_\Omega = 27556$ in the finest one. Four different discretisations, $N_\Omega = \{9, 49, 256, 784\}$ are visualised in Figure 6.3. Therein, $\mathcal{O}_\mathrm{S}$ refers to the ability of the discretisations to integrate spherical polynomials of degree $\mathcal{O}_\mathrm{S}$ exactly. The finest version with $N_\Omega = 27556$ is associated with $\mathcal{O}_\mathrm{S} = 165$. Unfortunately, the Sloan–Womersley points do not share the convenient symmetry properties with the Lebedev points. In summary, both the Lebedev and the Sloan–Womersley points represent excellent tools for a reliable and efficient numerical integration of the integrals arising in a network model.

Part III

A Microstructurally-based Model for Skeletal Muscle Tissue

7 The Multiscale Muscle Model

This chapter presents a microstructurally-based, two-phase, multiscale model for skeletal muscle tissue. The aim of the model is to provide the macroscopic strain energy on the basis of a detailed description of the mechanically relevant parts of the microstructure. The key feature of the multiscale model is that it does not require any constitutive assumptions or calibration on the macroscale. Many of the topics discussed in the previous chapters are used to derive the model, in particular the explanations on multiscale methods in Part II. Note that this chapter only provides the most necessary basic knowledge of the anatomical and physiological structure of skeletal muscles. For a more general introduction to the topic the interested reader is referred to the comprehensive textbooks of Schmalbruch [419], MacIntosh et al. [308], Lieber [285], or other suitable literature on anatomy.

We remark that parts of this and the following chapter have previously been published in Bleiler et al. [44].

7.1 A two-phase model for skeletal muscle tissue

A human body (and that of others, such as animals) contains three different muscle types, which are the skeletal muscles, the cardiac muscle (the heart) as well as the smooth muscles. We focus on skeletal muscles, which are a very important component of the body and have the primary task of generating force and enabling (voluntary) movement. This is based on their ability to actively contract as a response to neural stimulations. Due to their various tasks in the body, different skeletal muscles show a great diversity in size and shape. One could say that they reflect the architectural principle *form follows function*. However, despite this diversity, different skeletal muscles are basically built the same way. Inside the highly heterogeneous microstructure of skeletal muscle tissue, two structural components are mainly responsible for the mechanical characteristics of the overall material behaviour: (i) the *muscle fibres*, which are the muscle cells and contain the *sarcomeres* (the activatable units), and (ii) the *extracellular matrix* (ECM), which contains the collageneous (connective) tissues with various types of *collagen fibres* and other proteins like elastin. The ECM is in the literature also referred to as *intramuscular connective tis-*

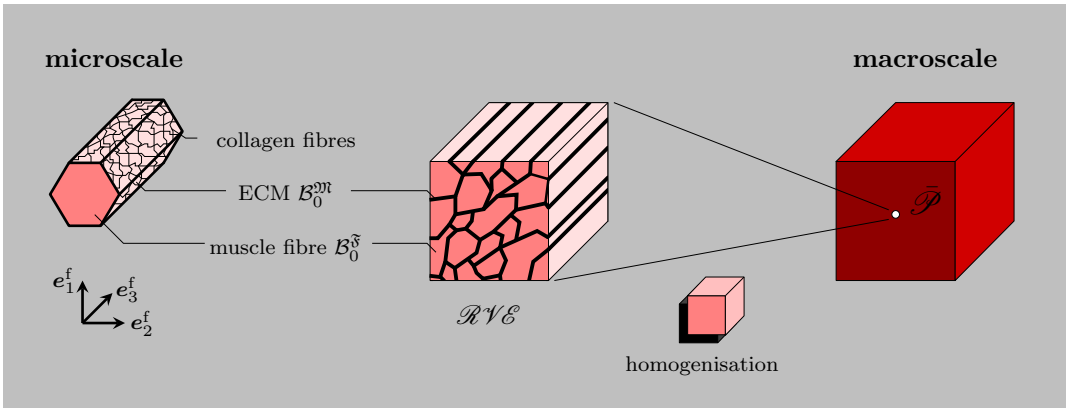

Figure 7.1: Multiscale scheme for the microstructurally-based modelling of skeletal muscle tissue.

sue (IMCT). The muscle fibres are responsible for the excitable (active) behaviour of the muscles, while the extracellular matrix and the collagen fibres contained therein ensure passive stiffness and stability. The extracellular matrix is organised in three different collageneous layers which cover different parts of the muscle tissue. The *endomysium* coats individual muscle fibres, whereas the *perimysium* envelops the muscle fascicles, which are bundles of multiple muscle fibres. Finally, the entire surface of the muscle is covered by the *epimysium*. This constitutes a clear hierarchical structure across the different length scales of skeletal muscle tissue. The aim is now to describe the material at a macroscopic material point $\bar{\mathscr{P}}$ by means of a strain-energy function $\bar{\mathscr{W}}$. As before, the material point is parametrised by the referential position vector $\bar{\boldsymbol{X}}$. We assume that the thick outermost collageneous layer, the epimysium, must be considered as a macroscopic heterogeneity (dependent on the macroscopic position $\bar{\boldsymbol{X}}$) and should not enter the material description for muscle tissue at the point $\bar{\mathscr{P}}$. On the other hand, muscle fibres as well as the endomysial and perimysial layers appear at much smaller length scales and are regarded as microscopic heterogeneities. Thus, we propose a two-phase model for skeletal muscle tissue and postulate that the reference configuration, $\mathcal{B}_0$, of the material consists of a muscle fibre phase $\mathcal{B}_0^{\mathfrak{F}}$ and an extracellular matrix phase $\mathcal{B}_0^{\mathfrak{M}}$. Together with a saturation condition, compare Eq. (4.10), we can formulate[1]

$$\mathcal{B}_0 = \bigcup_{\alpha} \mathcal{B}_0^{\alpha} = \mathcal{B}_0^{\mathfrak{F}} \cup \mathcal{B}_0^{\mathfrak{M}} \quad \text{with} \quad \alpha = \{\mathfrak{F}, \mathfrak{M}\}\,. \tag{7.1}$$

The associated multiscale scheme of the two-phase model is visualised in Figure 7.1. In the following, we provide some further explanations and modelling assumptions regarding this multiscale approach.

7.1.1 The length scales and the representative volume element

The multiscale approach shown in Figure 7.1 requires a meaningful definition of the individual scales. However, this is not easy when dealing with biological tissues and the associated variability in the material structure. This is already evident in the definition of the macroscopic length scale, which describes the size of the entire muscle. Without including other muscle types like smooth and cardiac muscles, the human body contains about 650 skeletal muscles (mostly occurring in pairs). The largest ones are the latissimus dorsi and the gluteus maximus muscle, which have lengths in the range of decimetres ($10^{-1}\,\mathrm{m}$). In contrast to this, the stapedius muscle in the ear, which is the smallest, is less than a millimetre ($10^{-3}\,\mathrm{m}$) in size. This means that the macroscopic length scale already shows variations of two orders of magnitude. However, it is assumed that the macroscopic variability is to some extent associated with according variabilities on the micro- and mesoscale and that the relative proportions remain comparable. For the following considerations, we assume that the macroscale is in the range of centimetres, such that $l_{\mathrm{macro}} \sim 10^{-2}\,\mathrm{m}$, which is true for most muscles responsible for the movement of the human body. Furthermore, we know from Section 4.1 that the microscopic length l_{micro} is

[1] The letters $\mathfrak{F}$ and $\mathfrak{M}$ are used to indicate that associated quantities refer to the muscle fibre and the extracellular matrix. This serves to clearly distinguish such quantities from the considerations in Chapter 5, where the letters F and M were used to describe general two-phase composites with a fibre and a matrix phase.

defined by the size of typical inhomogeneities on the microscale, which is here identified as one muscle fibre with the coating layer of extracellular, collageneous tissue. As the name suggests, muscle fibres are long fibre-like structures, which are aligned with the $\boldsymbol{e}_3^{\mathrm{f}}$-axis. In this connection, the $\boldsymbol{e}_i^{\mathrm{f}}$-coordinate system ($i = 1, 2, 3$) represents a laboratory frame of reference for the description of the microstructure, see Figure 7.1. Their cross-sections have an irregular, polygonal shape in the transverse $\boldsymbol{e}_1^{\mathrm{f}}$-$\boldsymbol{e}_2^{\mathrm{f}}$-plane and "diameters" of about $50 - 80\,\mu$m. This makes it easy to identify the microscopic length scale in the range of around $l_{\mathrm{micro}} \sim 5 \cdot 10^{-5}\,\mathrm{m}$. After having defined l_{micro} and l_{macro}, we still need an appropriate definition of the representative volume element and the associated mesoscopic length scale. We recall from Section 4.1 that the $\mathscr{RVE}$ should be chosen such that it guarantees statistical uniformity and that it should be the smallest possible volume sample of the microstructure which represents the macroscopic material behaviour with sufficient accuracy. As the here employed analytical homogenisation methods do not require an actual geometrical model of the microstructure, one can say that the first requirement is automatically met if the $\mathscr{RVE}$ itself is described by mean of representative statistical parameters of the microstructure. With regard to the second requirement, it has to be examined how many muscle fibres the $\mathscr{RVE}$ must contain. In this context, it is useful to consider existing literature on related micromechanical studies of muscle tissue. For instance, Sharafi & Blemker [434] investigated in their microscopic studies an ensemble of about 15 muscle fibres and a size of about $200\,\mu$m. Martin et al. [317] and Virgilio et al. [494] used for their studies about an agent-based model a similar geometry consisting of 14 fibres and a size of about $200\,\mu$m. Furthermore, Spyrou et al. [459] employed in their multiscale muscle model (based on the FE^2 homogenisation method) a simple $\mathscr{RVE}$ with only two fibres, whereas their follow-up work considered a much larger $\mathscr{RVE}$ with about 50 muscle fibres and a size of $350\,\mu$m, see Spyrou et al. [460]. All in all, $l_{\mathrm{meso}} \sim 10^{-4}\,\mathrm{m}$ seems to be a suitable assumption for the mesoscopic length scale and the magnitude of the $\mathscr{RVE}$. It should also be noted that this size roughly corresponds to that of a muscle fascicle. In conclusion, the multiscale muscle model can be regarded to well satisfy the hypothesis of separation of length scales formulated in Eq. (4.1). In particular, the difference between meso- and macroscopic length scale is two orders in magnitude. However, the large variability of skeletal muscle tissue must be pointed out again. This prevents a clear and generally valid definition of the absolute length of the scales. The principle of scale separation may require individual validation in special cases.

7.1.2 Perfect bonding between the muscle fibres and the extracellular matrix

The muscle model is based on the assumption that the muscle fibres and the extracellular matrix are perfectly bonded at their interface. Hence, we assume that the model satisfies geometrical compatibility according to Eq. (4.16) as well as statical compatibility according to Eq. (4.18), such that $[\![\boldsymbol{\chi}(\boldsymbol{X})]\!] = \boldsymbol{0}$ and $[\![\boldsymbol{T}(\boldsymbol{X})]\!] = [\![\boldsymbol{P}(\boldsymbol{X})]\!]\boldsymbol{N}_\Gamma(\boldsymbol{X}) = \boldsymbol{0}$ for all $\boldsymbol{X} \in \Gamma_{\mathcal{B}} = \partial\mathcal{B}_0^{\mathfrak{F}} \cup \partial\mathcal{B}_0^{\mathfrak{M}}$. The reason for this is the strong interconnection between the endomysium and a part of the muscle fibre's cell membrane, which is called basement membrane. A protein called *dystrophin* plays an important role in this. However, it must be noted that the assumption of perfect bonding at the interface is very suitable for the description of healthy muscle, but might be wrong and inappropriate when dealing with pathological cases and diseased muscles. For example, one such disease is the Duchenne muscular dystrophy, which is associated with a lack of dystrophin and thus leads to a massive

weakening of the muscle structure. Similar consequences can be observed for a number of other forms of muscular dystrophy.

7.1.3 Statistical description of the microstructure

Skeletal muscle tissue is a prime example for a random composite and the presence of a multitude of possible realisations $\Re \in \mathcal{S}$ of the microstructure. However, it is completely clear that a detailed description of characteristic functions $\mathscr{X}^{\alpha}(\boldsymbol{X}, \Re)$ cannot be realised for the entire sample space $\mathcal{S}$ and instead a statistical description of one representative microstructure should be made based on the ergodicity assumption. Then, the one-point probabilities of the two characteristic functions $\mathscr{X}^{\alpha}(\boldsymbol{X})$, $\alpha \in \{\mathfrak{F}, \mathfrak{M}\}$, are described by the respective volume fractions $n^{\mathfrak{F}}$ and $n^{\mathfrak{M}}$, compare Eq. (4.23). Further, we postulate that the two-point probability $\mathfrak{p}^{\mathfrak{FM}}$ can be described by means of a shape tensor $\boldsymbol{Z}_{\mathrm{d}}^{\mathfrak{FM}}$ due to an ellipsoidal symmetry of the microstructure, see Eq. (4.27). Since the $\boldsymbol{e}_3^{\mathrm{f}}$-axis has already been identified as the longitudinal axis of the muscle fibres, we remain with the characterisation of the $\boldsymbol{e}_1^{\mathrm{f}}$-$\boldsymbol{e}_2^{\mathrm{f}}$-plane transverse to it. Once again it must be mentioned that the characterisation of the structure is strongly dependent on whether healthy or pathological tissue is considered. In general, the $\boldsymbol{e}_1^{\mathrm{f}}$-$\boldsymbol{e}_2^{\mathrm{f}}$-plane shows in healthy muscle tissue a quite regular arrangement of the polygonal muscle fibres (muscle cells) and an associated uniform distribution of their midpoints. This can be evaluated from sufficiently high-resolution cross-sectional images and appropriate image processing tools. An alternative and very elegant method for such characterisations is based on the similarity of microscopic muscle cross-sections and artificially generated *Voronoi tessellations*, which were established by Dirichlet [97] (and thus also known as Dirichlet tessellation) and Voronoi [497]. In particular, Sánchez-Gutiérrez et al. [415, 416] showed that the polygonal (cell) pattern in the $\boldsymbol{e}_1^{\mathrm{f}}$-$\boldsymbol{e}_2^{\mathrm{f}}$-plane of skeletal muscles agrees very well with *centroidal* Voronoi tessellations[2]. This similarity enables the generation of representative artificial cell patterns and the determination of further statistical parameters based on the examination of this data. In our case, the isotropic distribution of the midpoints of the muscle fibres can be derived from this. Hence, it can be concluded that the $\mathscr{RVE}$ is statistically isotropic in the $\boldsymbol{e}_1^{\mathrm{f}}$-$\boldsymbol{e}_2^{\mathrm{f}}$-plane and that the shape tensor can be formulated as

$$\boldsymbol{Z}_{\mathrm{d}}^{\mathfrak{FM}} = (\boldsymbol{I} - \boldsymbol{e}_3^{\mathrm{f}} \otimes \boldsymbol{e}_3^{\mathrm{f}}) + \omega\, \boldsymbol{e}_3^{\mathrm{f}} \otimes \boldsymbol{e}_3^{\mathrm{f}} \quad \text{with} \quad \omega \to \infty\,, \tag{7.2}$$

see also Section 5.1.2. Moreover, it is useful to not only describe the two-point probability of the characteristic functions, $\mathscr{X}^{\alpha}$, but also the *average shape* of the muscle fibres in the $\mathscr{RVE}$. A reasonable approach is to assume that this can be described with the same

[2] In brief, the centroidal Voronoi tessellation starts with a Poisson–Voronoi diagram, based on randomly distributed generating points (starting seeds), and proceeds with an iterative process in which the centroid of a current Voronoi cell (also known as Dirichlet region or Thiessen polygon) is chosen as a generating point of the next tessellation, see Lloyd [293] and Du et al. [100]. Doing so, Sánchez-Gutiérrez et al. [416] showed that, for example, the distribution of the number of cell edges in the Voronoi diagram correlates well with the associated frequency in the real muscle tissue after four iteration steps (resulting in a distribution in which about 50% of the cells have hexagonal shape). Similar examples for other biological tissues were also shown by Honda [227, 228] and Bock et al. [49]. Moreover, in contrast to these isotropic distributions, the generation of anisotropic Voronoi tessellations is explained, for example, in Labelle & Shewchuk [271] and Du & Wang [101]. This might be relevant—again—for certain pathological cases. For completeness, basic considerations on the statistics of Voronoi diagrams are provided by Aurenhammer [17].

shape tensor as the distribution, leading to $\boldsymbol{Z}_{\mathrm{i}} = \boldsymbol{Z}_{\mathrm{d}}^{\mathfrak{FM}}$, where $\boldsymbol{Z}_{\mathrm{i}}$ refers to the shape of the fibres. Such a prescription leads to the muscle material being described as a two-phase composite with circular cylindrical fibres that are aligned along the preferred axis $\boldsymbol{e}_3^{\mathrm{f}}$ and distributed randomly and isotropically in the plane transverse to it. This is supported by the quite uniform pattern of the muscle fibres (cells) in cross-sectional images of the muscle or in appropriately generated Voronoi diagrams. In this connection, Takaza et al. [470] evaluated high-resolution images and formulated best-fit ellipses for the polygonal cross-sections of the muscle fibres in the $\boldsymbol{e}_1^{\mathrm{f}}$-$\boldsymbol{e}_2^{\mathrm{f}}$-plane. They observed that the average ratio of long axis to short axis of the ellipses was about 1.65, but they did not identify any preferred orientation of the fibres in an *averaged sense*. This emphasises that Eq. (7.2) also serves as an appropriate description of the shape of a muscle fibre in the $\mathscr{RVE}$ in an averaged sense.

7.2 Constitutive modelling of the phases

One of the key advantages of the presented two-phase framework is that the mechanical behaviour of the two phases can be described separately. Doing so, the constitutive modelling and the application of appropriate assumptions is shifted from the macroscopic to the microscopic scale. In the following, we introduce the constitutive material descriptions for the two phases, first for the muscle fibre phase and then for the extracellular matrix phase. As the extracellular matrix is the key contributor to the passive mechanical material behaviour, we introduce a detailed model based on the parametrisation of single collagen fibres. The computation of the effective response of the whole ensemble of collagen fibres will subsequently lead to equations which are in line with the ones arising in the network models from Chapter 6. Before we specify the constitutive behaviour of the two phases in more detail, model assumptions are discussed that apply to both phases.

Hyperelastic behaviour of both phases Within this work, we assume that both phases exhibit purely hyperelastic material behaviour. We thus ignore any rate- or history-dependent phenomena such as viscoelasticity of the phases. Hence, the mechanical constitutive behaviour of the two phases is fully described by hyperelastic potentials (strain-energy functions) $\mathscr{W}^{\alpha}(\boldsymbol{F})$ for $\alpha = \{\mathfrak{F}, \mathfrak{M}\}$. As already noted in Section 3.2.1, the consideration of history-dependent material behaviour, such as viscosity, would require the addition of internal variables to the list of arguments for the energies $\mathscr{W}^{\alpha}$.

Existence of an energy- and stress-free reference configuration of both phases It was already noted in Section 3.6.1 that the definition of an energy- and stress-free reference configuration can sometimes be challenging when treating biological materials. This can be due to a variety of phenomena in the microstructure of biological tissues. Typical examples are tissue growth or osmotic effects, see the references mentioned in Section 3.6.1. For the investigations in this thesis, we assume that both phases normalise properly in the reference configuration, such that

$$\mathscr{W}^{\alpha}(\boldsymbol{F})\big|_{\boldsymbol{F}=\boldsymbol{I}} = 0 \quad \text{and} \quad \boldsymbol{P}^{\alpha}(\boldsymbol{F})\big|_{\boldsymbol{F}=\boldsymbol{I}} = \boldsymbol{0}\,, \tag{7.3}$$

for $\alpha = \{\mathfrak{F}, \mathfrak{M}\}$. However, we note that the presented multiscale model offers an elegant option for integrating residual stresses if needed. That is because they can be formulated exactly in the phase in which they occur.

Incompressibility of both phases and the overall muscle tissue In the continuum-mechanical treatment of soft biological tissues, it is usually assumed that physiologically realistic deformations are accompanied by negligibly small volumetric strains and that the material can thus be modelled as incompressible. This is attributed to the high water content in the tissue. In skeletal muscles, water makes up about 76–77% of the total mass, as measured by Iseri et al. [240], Hargens et al. [179], and Ward & Lieber [506]. The resulting (nearly) incompressible material behaviour of the whole muscle was shown in experiments by Takaza et al. [471] and Böl et al. [53]. However, high water contents can be found not only in the entire muscle, but also in each of the two phases themselves, see Sjøgaard & Saltin [444]. This suggests that in the considered two-phase model according incompressibility assumptions can be formulated individually for both phases on the microscale, leading to the two separate constraint functions

$$\mathscr{R}^{\mathfrak{F}} = \det[\boldsymbol{F}(\boldsymbol{X})]-1=0 \quad \forall \boldsymbol{X} \in \mathcal{B}_0^{\mathfrak{F}} \quad \text{and} \quad \mathscr{R}^{\mathfrak{M}} = \det[\boldsymbol{F}(\boldsymbol{X})]-1=0 \quad \forall \boldsymbol{X} \in \mathcal{B}_0^{\mathfrak{M}}\,. \tag{7.4}$$

Indeed, it was shown in experiments of Huxley [237], Elliott et al. [115], Elliott & Millman [116] as well as Smith et al. [451] that isolated muscle fibres are practically incompressible upon deformation, thus justifying constraint $\mathscr{R}^{\mathfrak{F}}$ in Eq. $(7.4)_1$. Moreover, incompressibility is also a very common and reasonable assumption when modelling collageneous tissues. This was shown in experiments by Carew et al. [71], Chuong & Fung [78], and Holzapfel et al. [222] for arterial walls, which have a similar structure than the extracellular matrix in skeletal muscles. Hence, it makes sense to apply constraint $\mathscr{R}^{\mathfrak{M}}$ in the present model. The simultaneous demand for incompressibility in both phases inevitably results in the incompressibility of the muscle tissue at the macroscale and the corresponding constraint equation

$$\mathscr{R} = \det[\bar{\boldsymbol{F}}(\bar{\boldsymbol{X}})] - 1 = 0\,. \tag{7.5}$$

Yet, we remark that this is a direct consequence from Eq. (7.4) and does *not* depict an additional modelling assumption on the macroscale.

7.2.1 The muscle fibres

The muscle fibres (the cells of skeletal muscle tissue) are composed of bundles of parallel myofibrils, which in turn contain the serially arranged sarcomeres. Individual sarcomeres are separated from each other by the Z-discs and contain the proteins actin, myosin and titin. The sarcomeres are responsible for the "active" behaviour of muscle tissue through activation-triggered structural changes of the proteins actin and myosin. That is, neural stimulations trigger the conversion of chemical energy, provided by the hydrolysis of adenosine triphosphate (ATP), into mechanical energy (and non-mechanical energy in the form of heat) and lead to a contraction of the sarcomeres. Further, the passive stiffness of the muscle fibres is mainly addressed to titin. There is rich literature which focused on the investigation and mechanical characterisation of individual components inside the muscle fibre. Above all, a lot of studies treated the sarcomere dynamics and the behaviour of the two proteins actin and myosin upon activation, such as the ones by Weber & Portzehl [508], Huxley [235], Huxley & Simmons [236], Lieber & Baskin [286], and many others. Comprehensive studies on the structure of titin and its contribution to the muscle fibre stiffness were presented by, for example, Linke et al. [290], Prado

et al. [386], Li et al. [284], and Herzog [203]. Moreover, Goldstein et al. [165], Luther [304], and Ogneva et al. [364] investigated the stiffness of the Z-disc. Each of these structures contributes to the stored elastic energy in the muscle fibres during passive deformation and/or active contraction. Thus, a comprehensive description for the energy function $\mathscr{W}^{\mathfrak{F}}$ has to account for the energies of the individual structural elements and their spatial arrangement in the fibre. Alternatively, it is also possible to describe the mechanical behaviour of the muscle fibre using a constitutive approach for the strain-energy function and to calibrate the model to experimental data of isolated muscle fibres. Appropriate experiments on skinned muscle fibres (without the surrounding collaganeous tissue) were performed by, for example, Hellam & Podolsky [198], Gollapudi & Lin [166], Meyer & Lieber [324], Smith et al. [452], and Rehorn et al. [396]. Under non-active conditions, Meyer & Lieber [324] as well as Smith et al. [452] exhibited nearly-linear stress-strain behaviour of individual muscle fibres during uniaxial tensile tests. Based on these observations and by focusing herein on the *passive mechanical behaviour* of muscle fibres, we utilise an isotropic I_1-based Neo-Hookean energy formulation

$$\mathscr{W}_{\mu}^{\mathfrak{F}}(\boldsymbol{F}) = \tfrac{1}{2}\mu^{\mathfrak{F}}\,(I_1 - 3) + \tfrac{1}{2}\mu^{\mathfrak{F}}\,(J-1)(J-3)\,. \tag{7.6}$$

Note that this depicts the distortional energy contribution according to the distortional-dilatational split[3] from Eq. (3.140). The associated first Piola–Kirchhoff stress tensor can be computed from the derivative $\boldsymbol{P}_{\mu}^{\mathfrak{F}} = \partial_{\boldsymbol{F}}\mathscr{W}_{\mu}^{\mathfrak{F}}$ or by making use of the generic form provided in Eq. (3.147) and the scalar derivatives of $\mathscr{W}_{\mu}^{\mathfrak{F}}$ with respect to invariants I_1 and J which are given in Eqs $(3.159)_2$ and $(3.171)_2$. The stress tensor reads

$$\boldsymbol{P}_{\mu}^{\mathfrak{F}}(\boldsymbol{F}) = \mu^{\mathfrak{F}}\,\boldsymbol{F} + \mu^{\mathfrak{F}}(J^2 - 2J)\,\boldsymbol{F}^{-T}\,. \tag{7.7}$$

The here proposed Neo-Hookean strain-energy function well describes the behaviour of the muscle fibre that is observed in uniaxial experiments. Beyond that, however, multi-axial test data are necessary to make conclusions about the direction-dependent properties of muscle fibre. It can be assumed that the structure of the individual muscle fibre components can result in pronounced anisotropy, which must be taken into account in further investigations.

7.2.2 The extracellular matrix

The mix of various types of collagen fibres as well as elastin fibres within a ground substance of proteoglycans is characteristic for the extracellular matrix within soft biological tissues. In the following, only a rough overview of the components considered relevant for the mechanical behaviour of the ECM will be given. For detailed insights into the highly complex structure of the ECM, we refer to the comprehensive surveys of Mayne

[3] Note that the phase energies were formulated in Bleiler et al. [44] by means of the deviatoric-volumetric energy split from Section 3.7.2. Thus, the fibre energy was introduced as $\mathscr{W}^{\mathfrak{F}}(\boldsymbol{F}) = \mu^{\mathfrak{F}}\,(\breve{I}_1 - 3)/2$ based on the deviatoric part of the first invariant, $\breve{I}_1$, given in Eq. (3.131). The associated first Piola–Kirchhoff stress reads $\boldsymbol{P}^{\mathfrak{F}}(\boldsymbol{F}) = \mu^{\mathfrak{F}} J^{-2/3}\mathbb{D}\boldsymbol{F} = \mu^{\mathfrak{F}} J^{-2/3}(\boldsymbol{F} - I_1\,\boldsymbol{F}^{-T}/3)$, where the projection tensor $\mathbb{D}$ has been defined in Eq. (3.125). The formulations based on the deviatoric-volumetric energy split are completely equivalent with the here presented formulations based on the distortional-dilatational split for a muscle model that is based on the Voigt assumption, which will be introduced in Section 7.3.2. However, phase energies based on the deviatoric-volumetric split cannot be used for the TSO estimates from Chapter 5, which is why the phase energies used here are based on the distortional-dilatational split.

& Sanderson [320], Purslow & Duance [390], Kjær [252], Purslow [388], Gillies & Lieber [162], and citations therein. For the mechanical characterisation of the ECM by means of a strain-energy function, it is commonly accepted to apply an additive split which reads

$$\mathscr{W}_{\mu}^{\mathfrak{M}}(\boldsymbol{F}) = \mathscr{W}_{\mathrm{g}}^{\mathfrak{M}}(\boldsymbol{F}) + \mathscr{W}_{\mathrm{c}}^{\mathfrak{M}}(\boldsymbol{F})\,. \tag{7.8}$$

Therein, an isotropic groundmatrix part $\mathscr{W}_{\mathrm{g}}^{\mathfrak{M}}$ accounts for the direction-independent behaviour of the ground substance and the elastin fibres, whereas a generally anisotropic part $\mathscr{W}_{\mathrm{c}}^{\mathfrak{M}}$ describes the collagen reinforcement. This additive split was first proposed by Weizsäcker et al. [512] and Holzapfel & Weizsäcker [226].

The groundmatrix The energy $\mathscr{W}_{\mathrm{g}}^{\mathfrak{M}}$ describes the elastic contributions from the amorphous, gel-like ground substance of the ECM and the elastin fibres contained therein. The ground substance is mainly composed of water and trapped molecules like proteoglycan. This arrangement is typical for the ECM of soft biological tissues and is often associated with the presence of osmotic pressures, see, for example, Lu et al. [303]. The presence of osmotically active constituents in skeletal muscle tissue was for example studied by Fenn [128]. Further, measurements on the "osmotically active water fraction" in muscles and further explanations were provided in the works of Hill [206], Hill & Kupalov [208] as well as Millman et al. [334]. The studies suggested that osmotic effects and fluid flow between the ECM and the muscle fibre can particularly occur during and after increased muscle activity, which might lead to phenomena such as swelling of the tissue. However, such effects are not accounted for in the present analysis and we postulate that the contribution of the ground substance is mainly through hydrostatic pressure due to the incompressibility constraint $\mathscr{R}^{\mathfrak{M}}$ in Eq. $(7.4)_2$. Next, in addition to the ground substance, the elastin fibres are the other important component of the groundmatrix. It is interesting to note that the arrangement of elastin fibres in the ECM is very similar to the structure of polymer chains in rubber-like materials. Hence, elastin forms a random (thus uniformly distributed) network of coiled fibres which leads to an entropic nature of the network elasticity. This direct similarity to rubber elasticity[4] has been shown by Hoeve & Flory [217, 218], Dorrington & McCrum [98], Gosline [168], and Aaron & Gosline [1]. At this point, it is interesting to recall some explanations from Chapter 6, especially those made in the context of Eq. (6.23). There it was explained that a purely entropic energy of a single fibre, $\mathscr{W}_{\mathfrak{r}} = -\rho_{\mathfrak{r}0}\theta\eta_{\mathfrak{r}}$, and the assumption of Gaussian statistics for the entropy $\eta_{\mathfrak{r}}$ leads for uniform fibre networks to an effective energy reminiscent of the Neo-Hookean strain-energy function. This is quite remarkable, since Weizsäcker et al. [512] and Holzapfel & Weizsäcker [226] also adopted a Neo-Hookean strain-energy function for the groundmatrix contribution $\mathscr{W}_{\mathrm{g}}^{\mathfrak{M}}$ in connection with the split introduced in Eq. (7.8). Hence, it is reasonable to describe the groundmatrix of the ECM by means of the isotropic, I_1-based strain-energy function

$$\mathscr{W}_{\mathrm{g}}^{\mathfrak{M}}(\boldsymbol{F}) = \tfrac{1}{2}\mu^{\mathfrak{M}}\,(I_1 - 3) + \tfrac{1}{2}\mu^{\mathfrak{M}}\,(J-1)(J-3)\,, \tag{7.9}$$

[4] Weis-Fogh & Andersen [509] made a contradictory statement and argued that there is a significant contribution of energetic elasticity. Thus, they questioned that the theory of rubber elasticity and random network conformation is appropriate for modelling elastin. This entailed some lively discussions and responses by other authors, in particular by Hoeve & Flory [218]. In the end, subsequent studies (mentioned in the text) showed that the results of Weis-Fogh & Andersen [509] have to be adequately taken into account, but that the assumption of the random network conformation of elastin is still correct.

where $\mu^{\mathfrak{M}}$ is the ground-state shear modulus of the groundmatrix. We remark that the derivation of the Neo-Hookean energy from a network model with Gaussian statistics would lead to a micromechanical meaning of the stiffness parameter $\mu^{\mathfrak{M}}$, because it would be the product of the number of elastin chains in a unit volume, the Boltzmann constant and the absolute temperature. However, we assume that the Neo-Hookean part of the energy $\mathscr{W}_{\mathrm{g}}^{\mathfrak{M}}$ does not only describe the elastin network, but may also include contributions from other groundmatrix components and thus proceed with a more general meaning of parameter $\mu^{\mathfrak{M}}$. Further, the first Piola–Kirchhoff stress associated with Eq. (7.9) is given by

$$\boldsymbol{P}_{\mathrm{g}}^{\mathfrak{M}}(\boldsymbol{F}) = \mu^{\mathfrak{M}}\,\boldsymbol{F} + \mu^{\mathfrak{M}}(J^2 - 2J)\,\boldsymbol{F}^{-T}\,. \tag{7.10}$$

An experimental confirmation and some further comments on the applicability of the Neo-Hooke energy for modelling networks of elastin fibres (and hence the groundmatrix of the ECM) can also be found in Watton et al. [507].

The collagen reinforcement The collageneous structures in the ECM of the muscle are described by means of the elastic energy $\mathscr{W}_{\mathrm{c}}^{\mathfrak{M}}$. The collageneous structures themselves are compounds of a large number of different collagen fibre types. In skeletal muscles, one can identify (at least) fibres of type I, III, IV, V, VI, VIII, XII, XIII, XIV, XV, XVIII, and XIX, see Kovanen [259]. The various types can vary greatly in their mechanical properties and their structural arrangement in the tissue. The amount and the influence on the mechanical material behaviour of the different collagen fibre types usually depends on the examined tissue, but the most dominant one is typically the collagen of type I. It exhibits among the different collagen types the largest contribution to the stiffness of biological tissues, see Gelse et al. [156]. One reason for that is its very aligned characteristic. While there are collagen fibre types which form a loose random network similar to the previously considered elastin fibres, collagen of type I is usually arranged in a very structured, helical manner. In skeletal muscles, the type I fibres in the endomysium form a helical wrapping around individual muscle fibres, see Figure 7.2a, whereas a similar wrapping around muscle fascicles is provided by the perimysium, see Purslow & Trotter [391] and Purslow [389]. The whole muscle is accordingly coated by type I fibres in the epimysium, which is not taken into account here.

In the following we present a modelling framework that allows the consideration of different collagen fibre types and their individual properties, such as orientation and distribution. After these more general introductions, we will focus on the contribution of the collagen fibres of type I. Starting point is a geometrical model of an idealised muscle fibre that represents the shape of the polygonal fibres in the $\mathscr{RVE}$ in an averaged sense. A suitable formulation was presented in Section 7.1.3 by defining the average muscle fibre by means of the shape tensor $\boldsymbol{Z}_{\mathrm{i}} = \boldsymbol{Z}_{\mathrm{d}}^{\mathfrak{F}\mathfrak{M}}$, given in Eq. (7.2). Hence, the geometrical model for an average (idealised) muscle fibre in the $\mathscr{RVE}$ is defined as a cylinder of which the longitudinal axis is aligned with the $\boldsymbol{e}_3^{\mathrm{f}}$-axis and the cross section in the $\boldsymbol{e}_1^{\mathrm{f}}$-$\boldsymbol{e}_2^{\mathrm{f}}$-plane is circular. This is exemplary shown in Figure 7.2b. Further, as the energy $\mathscr{W}_{\mathrm{c}}^{\mathfrak{M}}$ has to account for the collagen fibres in the endo- as well as in the perimysial layer, we postulate that an idealised muscle fascicle can accordingly be described by such a cylindrical geometry. We assume that the different collagen fibre types form *planar* networks on the surface of the muscle fibres/fascicles. This is supported by corresponding studies on the endomysial layer by Trotter & Purslow [486] and Purslow & Trotter [391], and on the perimysial layer by Purslow [387, 388]. Next, we say that the fibre network on

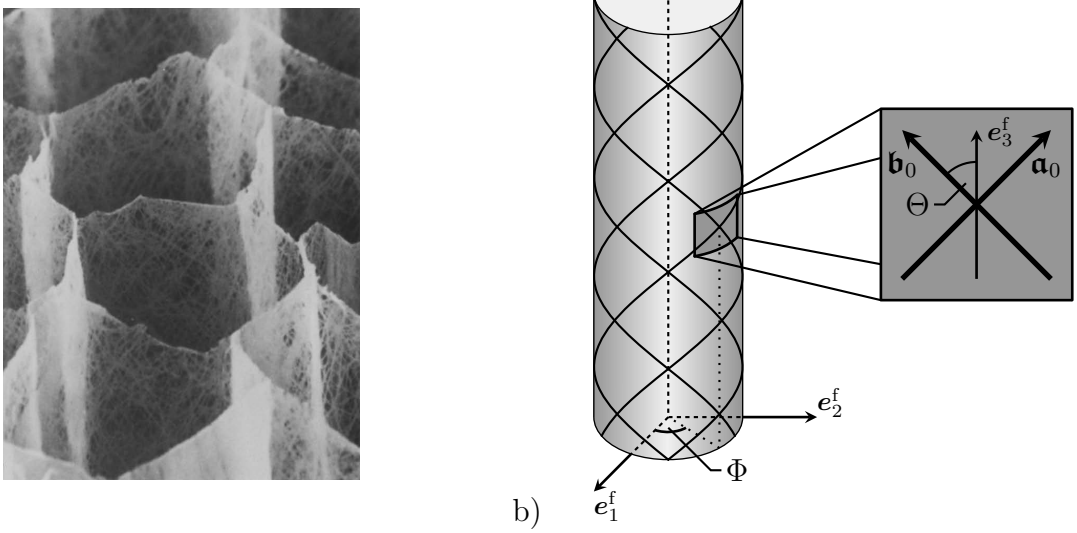

Figure 7.2: a) High resolution image of the endomysial layer and the collagen fibres contained therein. The muscle fibre has been extracted. Figure from Purslow & Trotter [391] with permission. b) An average (idealised) muscle fibre based on the shape tensor $\boldsymbol{Z}_\mathrm{i}$ with helically wrapped collagen fibres and the respective (tangential) unit vectors $\mathfrak{a}_0$ and $\mathfrak{b}_0$ on an infinitesimal surface element. The polar angle Θ defines the angle between the fibre unit vectors and the longitudinal axis of the muscle fibre, $\mathbf{e}_3^\mathrm{f}$.

the surface element of the idealised fibre/fascicle may contain two (mechanically equivalent) fibre families (clock- and counter-clockwise), which are parametrised by the two unit vectors

$$\begin{aligned}\mathfrak{a}_0(\Theta,\Phi) &= -\sin[\Theta]\sin[\Phi]\boldsymbol{e}_1^\mathrm{f} + \sin[\Theta]\cos[\Phi]\boldsymbol{e}_2^\mathrm{f} + \cos[\Theta]\boldsymbol{e}_3^\mathrm{f}\,,\\ \mathfrak{b}_0(\Theta,\Phi) &= +\sin[\Theta]\sin[\Phi]\boldsymbol{e}_1^\mathrm{f} - \sin[\Theta]\cos[\Phi]\boldsymbol{e}_2^\mathrm{f} + \cos[\Theta]\boldsymbol{e}_3^\mathrm{f}\end{aligned} \tag{7.11}$$

by means of a polar angle $\Theta \in [0,\pi)$ and an azimuthal angle $\Phi \in [0,2\pi)$, see Figure 7.2b. To account for the statistical orientation and dispersion of the individual collagen fibre types in the ECM, we assume the existence of an individual orientation density function (ODF) for each of them and that they read

$$\mathfrak{p}^\zeta(\mathfrak{a}_0) = \mathfrak{p}^\zeta(\mathfrak{b}_0) = \mathfrak{p}_\Theta^\zeta(\Theta)\,\mathfrak{p}_\Phi^\zeta(\Phi)\,. \tag{7.12}$$

Therein, the superscript ζ indicates the collagen fibre type and we implied that both fibre families of the same fibre type have an identical ODF. Further, we assume that the ODF can be split into a polar part $\mathfrak{p}_\Theta^\zeta(\Theta)$ and an azimuthal part $\mathfrak{p}_\Phi^\zeta(\Phi)$. It is reasonable to postulate for the azimuthal distribution a homogeneous relation, $\mathfrak{p}_\Phi^\zeta = \mathfrak{p}_\Phi = 1/(2\pi)$, since the planar fibre network should be uniform around the surface of the muscle fibres, see also Horowitz et al. [231]. The possibility to include two fibre families of the same fibre type is particularly useful for the description of the helical arrangement of type I fibres. In contrast, for the description of fibre types with random distribution it is sufficient to consider one fibre family. At this point it should be mentioned that the formulations presented here for the planar fibre network on the surface of the idealised muscle fibre are in line with the seminal studies on planar, two-dimensional collagen fibre networks by Lanir [275] and Lokshin & Lanir [294]. Furthermore, it is obvious that the two unit

vectors, $\mathfrak{a}_0$ and $\mathfrak{b}_0$, exhibit a clear similarity with the unit vector $\mathfrak{r}_0$ that was introduced in the context of the microsphere model in Chapter 6. This was already indicated by the choice of the angles Θ and Φ in the parametrisation of the vectors $\mathfrak{a}_0$ and $\mathfrak{b}_0$, which correspond to the polar and the azimuthal angle in the spherical $\boldsymbol{e}_i^{\mathrm{s}}$-coordinate system, respectively, see Figure 6.1b. These similarities allow us to consider the two vectors, $\mathfrak{a}_0$ and $\mathfrak{b}_0$, in the $\boldsymbol{e}_i^{\mathrm{s}}$- instead of the $\boldsymbol{e}_i^{\mathrm{f}}$-coordinate system and thus in the idealised model of the microsphere. Accordingly, all of the concepts introduced in Chapter 6 can be applied directly to the collagen fibre networks examined here. It is thus consequent to describe the elastic energy of a collagen fibre that is idealised by a unit vector $\mathfrak{a}_0$ or $\mathfrak{b}_0$ by means of individual hyperelastic potentials $\mathscr{W}_{\mathfrak{cf}}^{\zeta}$ for each collagen fibre type. Further, the kinematics of the two fibre families are defined by the maps

$$\boldsymbol{F}_{\mathfrak{a}}^{\zeta}(\Theta,\Phi):\ \mathfrak{a}_0 \mapsto \mathfrak{a}^{\zeta} = \boldsymbol{F}_{\mathfrak{a}}^{\zeta}\,\mathfrak{a}_0 \quad \text{and} \quad \boldsymbol{F}_{\mathfrak{b}}^{\zeta}(\Theta,\Phi):\ \mathfrak{b}_0 \mapsto \mathfrak{b}^{\zeta} = \boldsymbol{F}_{\mathfrak{b}}^{\zeta}\,\mathfrak{b}_0\,, \tag{7.13}$$

which transport the referential vectors $\mathfrak{a}_0$ and $\mathfrak{b}_0$ to their counterparts $\mathfrak{a}^{\zeta}$ and $\mathfrak{b}^{\zeta}$ in the actual configuration, respectively. With this, deformation measures like the ones defined in Eq. (6.3) can be defined accordingly. For instance, the actual stretches read

$$\lambda_{\mathfrak{a}}^{\zeta}(\Theta,\Phi) = |\mathfrak{a}^{\zeta}| = \sqrt{\mathfrak{a}^{\zeta}\cdot\mathfrak{a}^{\zeta}} \quad \text{and} \quad \lambda_{\mathfrak{b}}^{\zeta}(\Theta,\Phi) = |\mathfrak{b}^{\zeta}| = \sqrt{\mathfrak{b}^{\zeta}\cdot\mathfrak{b}^{\zeta}}\,. \tag{7.14}$$

To quantify the reorientation of individual vectors (and thus collagen fibres) it is useful to refer to some fixed coordinate axis. For instance, the reorientation of $\boldsymbol{a}_0$ and $\boldsymbol{b}_0$ with respect to the longitudinal axis of the muscle fibre, $\boldsymbol{e}_3^{\mathrm{f}} = \boldsymbol{e}_3^{\mathrm{s}}$, is measured by the difference of the referential polar angle Θ and the actual polar angles $\theta_{\mathfrak{a}}^{\zeta}$ and $\theta_{\mathfrak{b}}^{\zeta}$, which are computed from the relations

$$\cos[\theta_{\mathfrak{a}}^{\zeta}] = (\lambda_{\mathfrak{a}}^{\zeta})^{-1}\mathfrak{a}^{\zeta}\cdot\boldsymbol{e}_3^{\mathrm{s}} = (\lambda_{\mathfrak{a}}^{\zeta})^{-1}\mathfrak{a}_3^{\zeta} \quad \text{and} \quad \cos[\theta_{\mathfrak{b}}^{\zeta}] = (\lambda_{\mathfrak{b}}^{\zeta})^{-1}\mathfrak{b}^{\zeta}\cdot\boldsymbol{e}_3^{\mathrm{s}} = (\lambda_{\mathfrak{b}}^{\zeta})^{-1}\mathfrak{b}_3^{\zeta}\,, \tag{7.15}$$

compare Eq. (2.18). The distinct second-order tensors $\boldsymbol{F}_{\mathfrak{a}}^{\zeta}$ and $\boldsymbol{F}_{\mathfrak{b}}^{\zeta}$ in Eq. (7.13) allow for individual, non-affine deformations for each collagen fibre type. In general, those deformations have to be computed from the energy minimisation principle defined in Eq. (6.7). It should be noted in this connection that what was referred to in Chapter 6 as the macroscale of the fibre network here represents the *microscale* of the muscle. This means that the macroscopic deformation of the collagen fibre network is not the deformation gradient $\bar{\boldsymbol{F}}$ at the macroscopic position $\bar{\boldsymbol{X}}$, but the deformation gradient $\boldsymbol{F}_{\mathfrak{M}}$ at a *microscopic* local position $\boldsymbol{X} \in \mathcal{B}_0^{\mathfrak{M}}$. One could therefore say that the individual collagen fibres are defined on a further length scale below the microscale, which can be denoted as *nanoscale*[5]. In this work, however, we assume instead of individual non-affine kinematics for each collagen fibre type affine deformations within the collagen fibre network. This leads to formulations as provided in Section 6.2. Hence, the mapping tensors $\boldsymbol{F}_{\mathfrak{a}}^{\zeta}$ and $\boldsymbol{F}_{\mathfrak{b}}^{\zeta}$ coincide with the deformation gradient, $\boldsymbol{F}_{\mathfrak{M}}$, of the surrounding ECM tissue at the *microscopic* local position $\boldsymbol{X} \in \mathcal{B}_0^{\mathfrak{M}}$, such that

$$\boldsymbol{F}_{\mathfrak{a}}^{\zeta} = \boldsymbol{F}_{\mathfrak{b}}^{\zeta} = \boldsymbol{F}_{\mathfrak{M}}\,. \tag{7.16}$$

[5]We recall from Section 4.1 that the prefixes of the three length scales—micro, meso, and macro—do not refer to absolute sizes, but put the scales in relation to each other. Therefore, the nanoscale does not necessarily refer to the nanometre range (although this fits well in the present case), but is generally introduced as a length scale below the microscale. Based on the meaning of the Greek word *nános*, the nanoscale is accordingly a dwarf-scale.

This implies that associated deformation measures become independent of the collagen fibre types, such that $\mathfrak{a}^\zeta = \mathfrak{a}$, $\mathfrak{b}^\zeta = \mathfrak{b}$, $\lambda^\zeta_\mathfrak{a} = \lambda_\mathfrak{a}$, $\lambda^\zeta_\mathfrak{b} = \lambda_\mathfrak{b}$, $\theta^\zeta_\mathfrak{a} = \theta_\mathfrak{a}$, and $\theta^\zeta_\mathfrak{b} = \theta_\mathfrak{b}$. It was noted in Section 6.2 as well as in Section 4.3.5 that the assumption of uniform deformations can serve as a good prediction if justified by experimental evidence. In this connection, Chandran & Barocas [75], Jayyosi et al. [248], and Krasny et al. [260] carried out detailed studies and compared results based on the affinity assumption with real deformations in collagen fibre networks observed from high resolution images. They observed that collagen fibre networks generally show non-affine deformations, but that the deviations resulting from the affinity assumption are often in an acceptable range. In addition, pronounced non-affine effects often come into play during deformations which are far from the physiologically sensible range for muscles.

As a last remark in relation to the kinematics of the fibre network, we note that the interaction of the two fibre families can be accounted for by means of appropriate strain measures, such as the one which is usually referred to as J_8-invariant. It is obtained by formulating structural tensors $\boldsymbol{M}_\mathfrak{a} = \mathfrak{a}_0 \otimes \mathfrak{a}_0$ and $\boldsymbol{M}_\mathfrak{b} = \mathfrak{b}_0 \otimes \mathfrak{b}_0$ for the two fibre families and introducing the scalar measure $\mathrm{tr}[\boldsymbol{M}_\mathfrak{a}\boldsymbol{M}_\mathfrak{b}\boldsymbol{C}_\mathfrak{M}] = (\mathfrak{a} \otimes \mathfrak{a}_0) \cdot (\mathfrak{b} \otimes \mathfrak{b}_0) = \cos[2\Theta]\mathfrak{a} \cdot \mathfrak{b}$, where $\boldsymbol{C}_\mathfrak{M} = \boldsymbol{F}^T_\mathfrak{M}\boldsymbol{F}_\mathfrak{M}$ and $\mathfrak{a}_0 \cdot \mathfrak{b}_0 = \cos[2\Theta]$, see Spencer [457]. This strain measure can be used as an argument for a correspondingly introduced interaction energy, as it was done, for example, in the works of Holzapfel & Ogden [223] and Nerurkar et al. [353], see also Chagnon et al. [74]. However, we do not use such formulations in this work.

To obtain the effective response of the collageneous network, averaging operators are introduced for each fibre type via

$$\big\langle(\cdot)\big\rangle^\zeta_\Omega := \frac{1}{2\pi}\int_\Omega \mathfrak{p}^\zeta_\Theta(\Theta)\,(\cdot)\,\mathrm{d}\Omega\,, \tag{7.17}$$

where we recall from Eq. (6.5) that $\mathrm{d}\Omega = \sin[\Theta]\,\mathrm{d}\Theta\,\mathrm{d}\Phi \in \Omega$ describes an infinitesimal area element on the microsphere surface Ω. Further, we obtain formulations reminiscent of the ones in Section 6.3, since we assumed a uniform fibre distribution in the azimuthal orientation space. Accordingly, the normalisation condition for the remaining polar parts of the ODF reads

$$\int_0^\pi \mathfrak{p}_\Theta(\Theta)\sin[\Theta]\,\mathrm{d}\Theta = 1\,. \tag{7.18}$$

It was further noted in Section 6.3 that the polar ODF must be a univariate, π-periodic function. A suitable formulation for the description of collagen networks is the von-Mises distribution function, which is also presented in Appendix B.2. It reads

$$\tilde{\mathfrak{p}}^\zeta_\Theta(\Theta) = \frac{\exp\big[b^\zeta\,\cos[2\,(\Theta - \Theta^\zeta_\mathrm{m})]\big]}{2\,\pi\,I_0(b^\zeta)}\,, \tag{7.19}$$

where Θ^ζ_m is the mean of the distribution of a specific collagen fibre type, b^ζ is a parameter for the spreading around the mean, and I_0 is the modified Bessel function of first kind of order zero, given in Eq. (B.32). After a consistent normalisation due to Eq. (7.18), the resulting polar ODF is given by $\mathfrak{p}^\zeta_\Theta(\Theta) = \tilde{\mathfrak{p}}^\zeta_\Theta(\Theta)/I^\zeta$, where $I^\zeta = \int_0^\pi \tilde{\mathfrak{p}}^\zeta_\Theta(\Theta)\,\sin[\Theta]\,\mathrm{d}\Theta$.

Finally, the resulting energy $\mathscr{W}^\mathfrak{M}_\mathrm{c}$ for the collageneous part of the extracellular matrix phase is obtained by the sum of the effective network responses of all accounted collagen fibre types. The contribution of each collagen fibre type will be taken into consideration

by introducing volume fractions n^ζ for the individual collagen fibre types, along with the saturation condition $\sum_\zeta n^\zeta = 1$. With that, we obtain the *transversely isotropic* energy

$$\mathscr{W}_{\mathrm{c}}^{\mathfrak{M}}(\boldsymbol{F}_{\mathfrak{M}}) = \sum_{\zeta} n^\zeta \left\langle \mathscr{W}_{\mathfrak{cf}}^{\zeta}(\lambda_{\mathfrak{a}}) + \mathscr{W}_{\mathfrak{cf}}^{\zeta}(\lambda_{\mathfrak{b}}) \right\rangle_{\Omega}^{\zeta}. \tag{7.20}$$

For collagen fibre types that only consist of one fibre family, the second summand is omitted. Further, by exploiting the structure of the vectors $\mathfrak{a}_0$ and $\mathfrak{b}_0$, it becomes clear that they equally contribute to the average network quantities and that any difference in orientation of the two fibre families will be averaged out. Hence, it suffices for fibre types that consist of two fibre families to account for the contribution of one fibre family twice.

The predominant collagen fibres in the extracellular matrix of skeletal muscles are of type I and III. These two types add up to a volume fraction of about 95% of the total collagen amount in the endomysium, reported by Duance et al. [102], Light & Champion [288], and Listrat et al. [291]. As it is known that especially collagen of type I plays a key role for the mechanical behaviour of biological tissues, see Gelse et al. [156], we restrict ourselves to the consideration of type-I fibres, resulting in $\zeta = \{\mathrm{I}\}$. We therefore also omit the contribution of type-III fibres, which are much more compliant than fibres of type I, see Asgari et al. [14], and form a more loose, non-aligned mesh of fibres, see Kovanen [259]. Combining all arguments and definitions from above finally leads for the anisotropic network energy to the compact form

$$\mathscr{W}_{\mathrm{c}}^{\mathfrak{M}}(\boldsymbol{F}_{\mathfrak{M}}) = 2\, n^{\mathrm{I}} \left\langle \mathscr{W}_{\mathfrak{cf}}(\lambda_{\mathfrak{a}}) \right\rangle_{\Omega}, \tag{7.21}$$

where n^{I} is the volume fraction of type-I collagen in the ECM. For the sake of a compact notation, we omit from Eq. (7.21) onwards the superscript I for the strain energy $\mathscr{W}_{\mathfrak{cf}}^{\mathrm{I}}$, for the ODF $\mathfrak{p}_{\Theta}^{\mathrm{I}}$ and, accordingly, for the ODF parameters $\Theta_{\mathrm{m}}^{\mathrm{I}}$ and b^{I}, as well as the average operator $\langle(\cdot)\rangle_{\Omega}^{\mathrm{I}}$. Further, it has been tacitly assumed in the course of these explanations that the fibre energy $\mathscr{W}_{\mathfrak{cf}}$ depends on the stretch $\lambda_{\mathfrak{a}}$. Such a formulation is employed in the following, but can be generalised in a straightforward manner to include additional deformations measures, such as the ones defined in Eq. (6.3), see also Section 6.2.2. Consequently, a stretch-based formulation for the fibre energy entails for the first Piola–Kirchhoff stress of the collagen reinforcement

$$\boldsymbol{P}_{\mathrm{c}}^{\mathfrak{M}}(\boldsymbol{F}_{\mathfrak{M}}) = \partial_{\boldsymbol{F}_{\mathfrak{M}}} \mathscr{W}_{\mathrm{c}}^{\mathfrak{M}} = 2\, n^{\mathrm{I}} \left\langle \frac{P_{\mathfrak{cf}}(\lambda_{\mathfrak{a}})}{\lambda_{\mathfrak{a}}}\, \mathfrak{a} \otimes \mathfrak{a}_0 \right\rangle_{\Omega}, \tag{7.22}$$

where $P_{\mathfrak{cf}} = \partial_{\lambda_{\mathfrak{a}}} \mathscr{W}_{\mathfrak{cf}}$ is the scalar fibre stress, compare Eq. (6.18). The stiffness tensor $\mathbb{L}_{\mathrm{c}}^{\mathfrak{M}}$ is accordingly obtained from Eq. (6.21). In order to complete the modelling part on the ECM, we remain with the specification of the fibre energy $\mathscr{W}_{\mathfrak{cf}}$ of a single collagen type-I fibre. That is the focus in the next section.

7.2.3 Modelling of collagen fibres

It has already been pointed out before that collageneous structures are important components in biological tissues and that collagen fibres of type I play a decisive role in the mechanical behaviour of the ECM. In turn, the mechanical properties of collagen fibres, here expressed in form of the hyperelastic potential $\mathscr{W}_{\mathfrak{cf}}$, are determined by their hierarchical microstructure and the shape of the fibres themselves. We mention here again that

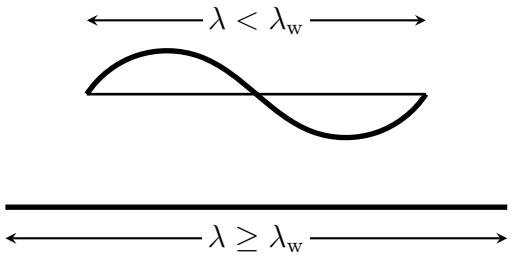

Figure 7.3: Crimped and uncrimped state of a collagen fibre with initial waviness λ_w.

only a brief overview on the physiological characteristics is given and we refer to the standard textbook of Fratzl [134] and the references contained therein for a deeper insight into the topic. Starting on the smallest (considered) length scale, collagen fibres consist of triple helical tropocollagen molecules with a diameter of about 1.5 nm (10^{-9} m) and a length of about 300 nm. Multiple molecules are arranged in staggered arrays and form collagen fibrils with diameters of about 50–250 nm. The molecules interact on the fibril-level through intermolecular covalent cross-links (between two molecules) and so-called weak bonds. Finally, bundles of densely packed fibrils form the collagen fibre. However, it should be noted that the distinction between fibril and fibre is sometimes a little vague. Collagen fibres usually appear in a crimped (curled, wavy, crinkled) form in the unloaded reference configuration. The same applies to many of the substructures of collagen fibres, such as the intermolecular cross-links. These properties have a major influence on the shape of the stretch-stress curve that arises when the collagen fibre is subjected to a tensile force in its longitudinal axis. Namely, this entails a classical J-shaped stretch-stress curve which consists of a flat toe region at lower stretches, an intermediate heel region and a quasi-linear region at higher stretches. In the toe region, the collagen fibre is crimped and the resistance against tensile load is mainly due to a straightening of the collagen fibre itself as well as to according straightening and alignment of underlying microstructures like the collagen molecules. A large proportion of the elastic energy in this stretch range is entropic in nature and stems from the removal of disorder in the molecular microstructure, see Misof et al. [336] and Buehler & Wong [64]. As the stretch increases, one can identify a threshold stretch λ_w at which the collagen fibre itself becomes fully straightened, as depicted in Figure 7.3. Beyond this point, the elastic energy is mainly energetic in nature and stems from the elongation of the collagen molecules and intermolecular sliding. This means that the strain energy of a collagen fibre results from the stretch-induced changes of the entropy $\eta_{\mathfrak{cf}}$ and the internal energy $\varepsilon_{\mathfrak{cf}}$ and is given by $\mathscr{W}_{\mathfrak{cf}} = \rho_{\mathfrak{cf}0}(\varepsilon_{\mathfrak{cf}} - \theta\eta_{\mathfrak{cf}})$, compare Eq. (6.23). Comprehensive multiscale models which take into account entropic and energetic mechanisms during collagen stretching were proposed by, for example, Buehler [63], Tang et al. [474], Maceri et al. [306, 307], and Marino & Vairo [313]. These models are based on a detailed description of the underlying microstructure and subsequent upscaling and homogenisation steps. They rely on microstructural parameters, such as the cross-link stiffness, and can be particularly helpful when modelling pathological cases which go along changes of associated structures. Since these multiscale approaches are often associated with considerable additional computational effort, Marino et al. [311] investigated how the microstructurally-based parameters correlate with the parameters of generic strain-energy functions such as the exponential-based model from Eq. (3.175). However, instead of employing multiscale models, one may proceed with a rather con-

stitutive, structural-based approach by postulating that the energy of a fibre can be split via

$$\mathscr{W}_{\mathfrak{cf}}(\lambda) = \mathscr{W}_{\mathfrak{cf}}^{\mathrm{b}}(\lambda) + \mathscr{W}_{\mathfrak{cf}}^{\mathrm{s}}(\lambda)\,. \tag{7.23}$$

Therein, the contribution $\mathscr{W}_{\mathfrak{cf}}^{\mathrm{b}}$ accounts for the bending stiffness of the crimped collagen fibre (and associated entropic effects in its microstructure) whereas $\mathscr{W}_{\mathfrak{cf}}^{\mathrm{s}}$ accounts for the stretch-based elasticity of the uncrimped fibre. The first contribution may be obtained by assuming specific geometrical forms for the fibre and formulating according structural models. By doing so, a helical spring model was formulated by Freed & Doehring [136] and Grytz & Meschke [172], an elastica-based model by Garikipati et al. [150], and a crimped beam model by Marino & Wriggers [314]. Ultimately, the energy contribution $\mathscr{W}_{\mathfrak{cf}}^{\mathrm{b}}$, associated with the toe region, is very small compared to the stretch-based contribution $\mathscr{W}_{\mathfrak{cf}}^{\mathrm{s}}$ and a reasonable assumption is to omit the first term in Eq. (7.23). Hence, by setting $\mathscr{W}_{\mathfrak{cf}}^{\mathrm{b}} = 0$, the energy is fully specified by the stretch-based term, such that $\mathscr{W}_{\mathfrak{cf}} = \mathscr{W}_{\mathfrak{cf}}^{\mathrm{s}}$. Subsequently, a simple but very useful prescription for the energy reads

$$\mathscr{W}_{\mathfrak{cf}}(\lambda) = \begin{cases} \frac{1}{2}\mu_{\mathfrak{cf}}\,(\lambda - \lambda_{\mathrm{w}})^2 & \text{if } \lambda \geq \lambda_{\mathrm{w}} \\ 0 & \text{else}\,, \end{cases} \tag{7.24}$$

which has been proposed in the classical works of Lake & Armeniades [273], Lanir [275] and Decraemer et al. [93]. This formulation is similar to the quadratic potential in Eq. (3.174), but it was added a case distinction[6] to exclude fibres which are not stretched beyond the *initial waviness* λ_{w}. Hence, we postulate that collagen fibres only store energy when they are fully uncrimped and that they have *no compressive stiffness*. The derivation of Eq. (7.24) with respect to the stretch yields the scalar stress

$$P_{\mathfrak{cf}}(\lambda) = \partial_\lambda \mathscr{W}_{\mathfrak{cf}}(\lambda) = \begin{cases} \mu_{\mathfrak{cf}}\,(\lambda - \lambda_{\mathrm{w}}) & \text{if } \lambda \geq \lambda_{\mathrm{w}} \\ 0 & \text{else}\,, \end{cases} \tag{7.25}$$

which is required to compute the stress $\boldsymbol{P}_{\mathrm{c}}^{\mathfrak{M}}$ in Eq. (7.22). We clearly see that $P_{\mathfrak{cf}}$ describes a linear stretch-stress relationship for stretches beyond the initial waviness λ_{w}. This is an advantage of this model, since strain-energy functions like the exponential one in Eq. (3.175) tend to overestimate stresses at higher stretches due to their highly nonlinear nature. The same applies to the frequently used worm-like chain model. It was previously noted that this model describes entropic elasticity, which, when used for collagen fibres, leads to an unphysical inextensibility at high stretches, see Maceri et al. [306, 307]. Here, we can proceed with a further derivation of the stress $P_{\mathfrak{cf}}$ which yields the scalar stiffness

$$L_{\mathfrak{cf}}(\lambda) = \partial_{\lambda^2}^2 \mathscr{W}_{\mathfrak{cf}}(\lambda) = \begin{cases} \mu_{\mathfrak{cf}} & \text{if } \lambda \geq \lambda_{\mathrm{w}} \\ 0 & \text{else}\,. \end{cases} \tag{7.26}$$

Hence, the scalar stiffness represents a piecewise constant step function, where the step is at λ_{w} and has the value of the fibre stiffness $\mu_{\mathfrak{cf}}$.

It is remarked that strain-energy functions of the form given in Eq. (7.24) are often accompanied with a distribution function for the initial waviness λ_{w}, denoted by $\mathfrak{p}_{\lambda_{\mathrm{w}}}$. This

[6] Such a case distinction can also be formulated by means of *Macaulay brackets* (also known as *Föppl symbol*) $\langle(\cdot)\rangle = [(\cdot) + |(\cdot)|]/2$, such that $\mathscr{W}_{\mathfrak{cf}}(\lambda) = \mu_{\mathfrak{cf}}\langle\lambda - \lambda_{\mathrm{w}}\rangle^2/2$. However, this entails a risk of confusion with the averaging operators that are also defined via angle brackets and is therefore not used here.

is based on the assumption that a vector (a space orientation) describes not only one single fibre, but an entire population of fibres with different degrees of crimp. This generally leads to an integral formulation for the strain-energy function of one space orientation. We provide some further details and remarks on this aspect in Appendix B.3. Moreover, we formulate closed-form solutions for the case that $\mathfrak{p}_{\lambda_w}$ take the form of Beta and triangular distributions. In the following, however, we proceed with formulation (7.24), which is equivalent to choosing a Dirac delta function for $\mathfrak{p}_{\lambda_w}$.

Finally, it is interesting to compare the material model for the ECM formulated in Sections 7.2.2 and 7.2.3 with the modelling assumptions for fibrous tissues that were formulated in the seminal work of Lanir [276]:

(L1) *Each fiber is thin and perfectly flexible. It has no compressive strength and if contracted will buckle under zero load.*
(L2) *The effect of the matrix flow during deformation is that of a hydrostatic pressure. The flow stops at the point when the forces binding the matrix to the fibers counteract the effect of the pressure.*
(L3) *Each fiber is subjected to a uniaxial strain which is the tensorial transformation of the overall strain in the fiber's direction (affine deformation).*
(L4) *The kinematics of the fiber vector [...], correspond to that of a straight fiber and are subject to the assumptions [...][(L1)-(L3)]. Thus a stretched fiber coincides with its vector.*
(L5) *The unfolding of the fiber during deformation squeezes the fluid matrix. The matrix's reaction is through hydrostatic pressure.*

We may refer to them as *Lanir's assumptions for fibrous tissues*. Accordance with these assumptions is not really a must, but they provide a good overview of the most important phenomena in fibrous tissues that should be taken into account and are therefore good indicators for the suitability of the model. In our case, (L1) is taken into account by the energy function selected in Eq. (7.24) for individual collagen fibres and (L3) is covered by the affine deformation prescription in Eq. (7.16). (L2) agrees with the here made assumption that the contribution of the ground substance of the ECM is mostly through hydrostatic pressure in order to maintain the incompressibility of the tissue. (L4) and (L5) were added by Lanir for tissues with crimped collagen fibres. (L4) is fully in line with the basic principle of the microsphere model which states that fibres are idealised by a straight vector that connects the end points of the fibre, see Section 6.1. Finally, concerning (L5), the model does not directly include the effect of the matrix squeezing during fibre uncrimping (unfolding), but accounts for the hydrostatic pressure of the matrix upon deformation in a general sense.

7.3 The effective behaviour on the macroscale

In this section we formulate the effective strain energy at the macroscopic point $\bar{\mathscr{P}}$ which occurs due to a macroscopic deformation $\bar{\boldsymbol{F}}$. Two approaches for this will be presented in the following. The first one formulates an estimate for the macroscopic energy by means of the tangent second-order homogenisation method presented in Chapter 5. The second approach is based on the Voigt assumption and therefore postulates that the deformations in the microstructure are uniform. In both cases, the model assumptions made up to

this point and the constitutive modelling of the two phases on the microscale lead to an *incompressible*, *transversely isotropic* material behaviour on the macroscale. In turn, this entails that the macroscopic material response becomes a function of an appropriate transversely isotropic set of macroscopic strain invariants, which serves as integrity basis for the macroscopic Cauchy–Green strain $\bar{\boldsymbol{C}}$ and the structural tensor $\bar{\boldsymbol{M}}$, where the latter indicates the direction of the muscle fibres. The transverse isotropy results from the statistical considerations in Section 7.1.3, in particular the definition of the shape tensor $\boldsymbol{Z}_{\mathrm{d}}^{\mathfrak{F}\mathfrak{M}}$, and from the description of the two phases. In turn, the transverse isotropy of the energy $\mathscr{W}_{\mathrm{c}}^{\mathfrak{M}}$ is a direct consequence of the shape tensor $\boldsymbol{Z}_{\mathrm{i}}$, which describes the average shape of the muscle fibres in the $\mathscr{RVE}$. This means that the material symmetry on the macroscale follows directly from the composition of the microstructure and the arrangement of the two phases. Changes in these statistical descriptions would directly result in corresponding material symmetries on the macroscale.

7.3.1 The effective behaviour based on variational homogenisation

Appropriate *estimates* for the effective macroscopic strain energy of the multiscale muscle model can be generated by means of the TSO homogenisation method from Chapter 5. It takes into account the microstructural composition (described by the characteristic functions $\mathscr{X}^{\alpha}$) by means of one- and two-point probabilities through the volume fractions and the microstructural $\mathbb{P}$-tensor, which in turn depends on the shape tensors $\boldsymbol{Z}_{\mathrm{d}}^{\mathfrak{F}\mathfrak{M}}$ *and* $\boldsymbol{Z}_{\mathrm{i}}$. This means that the TSO estimate accounts for the shape and the orientation of the fibres (the inclusion) and their distribution. The TSO estimate for the effective macroscopic strain-energy function of a two-phase composite with fibrous microstructure and incompressible, transversely isotropic phases is given in Eq. (5.64) and reads

$$\widetilde{\mathscr{W}}(\bar{\boldsymbol{F}}) = n^{\mathfrak{F}}\left[\mathscr{W}_{\mu}^{\mathfrak{F}}(\bar{\boldsymbol{F}}_{\mathfrak{F}}) + \tfrac{1}{2}(\bar{\boldsymbol{F}}-\bar{\boldsymbol{F}}_{\mathfrak{F}})\cdot\boldsymbol{P}_{\mu\wp}^{\mathfrak{F}}(\bar{\boldsymbol{F}}_{\mathfrak{F}},\wp^{\mathfrak{F}})\right] + n^{\mathfrak{M}}\left[\mathscr{W}_{\mu}^{\mathfrak{M}}(\bar{\boldsymbol{F}}_{\mathfrak{M}}) + \tfrac{1}{2}(\bar{\boldsymbol{F}}-\bar{\boldsymbol{F}}_{\mathfrak{M}})\cdot\boldsymbol{P}_{\mu}^{\mathfrak{M}}(\bar{\boldsymbol{F}}_{\mathfrak{M}})\right], \tag{7.27}$$

where $\boldsymbol{P}_{\mu\wp}^{\mathfrak{F}} = \boldsymbol{P}_{\mu}^{\mathfrak{F}} + \wp^{\mathfrak{F}}\bar{\boldsymbol{F}}_{\mathfrak{F}}^{-T}$. The macroscopic deformation gradient $\bar{\boldsymbol{F}}$ in expression (7.27) is formulated in the generic form (5.83), along with (5.84), whereas the fibre deformation $\bar{\boldsymbol{F}}_{\mathfrak{F}}$ is given by Eqs (5.85) and (5.87). The matrix deformation $\bar{\boldsymbol{F}}_{\mathfrak{M}}$ is expressed in terms of $\bar{\boldsymbol{F}}_{\mathfrak{F}}$ by utilising the overall average condition (5.18). Consequently, the computation of the energy $\widetilde{\mathscr{W}}$ demands to solve for *four scalar unknowns*. These are the three unknown coefficients of the average fibre deformation $\bar{\boldsymbol{F}}_{\mathfrak{F}}$, hence, the longitudinal shear $\bar{\gamma}_{\mathfrak{F}\ell}$, the transverse shear $\bar{\gamma}_{\mathfrak{F}\mathrm{t}}$ and the coupling measure $\bar{\phi}_{\mathfrak{F}\gamma}$, and the constraint pressure $\wp^{\mathfrak{F}}$. The required four scalar equations are the (1,1)-, (2,2)-, (3,1)-, and (3,2)-components of the tensorial equation (5.79). Further, the macroscopic first Piola–Kirchhoff stress tensor $\widetilde{\boldsymbol{P}} = \partial_{\bar{\boldsymbol{F}}}\widetilde{\mathscr{W}}$ can be computed from Eq. (C.7), along with the associated remarks.

7.3.2 The effective behaviour based on the Voigt assumption

We have to assume that a heterogeneous deformation field on the microscale based on a variational energy minimisation is the most accurate solution we can obtain. However, it has already been mentioned a few times in this work that the assumption of homogeneous microscopic deformations may be a suitable approach if it can be justified by further considerations. For the specific case of skeletal muscle tissue, Fung [145] provides arguments

motivated through its underlying physiology why the relative motion of the two phases might be of minor importance. He states that

> *"[...]the muscle cells and the surrounding tissues are so well integrated that their relative motion has probably little significance."*

Thus, FUNG does not deny heterogeneous deformations per se, but he considers their influence on the mechanical behaviour of the overall muscle to be negligible. The reason for this is a somewhat broader interpretation of the importance of the protein structures, such as dystrophin, that has already been mentioned in Section 7.1.2. Instead of only assuming perfect bonding at the interface between muscle fibre and ECM, FUNG's postulate goes a step further and states a more general, very close interconnection of the two phases. Based on these explanations, it seems sensible to suggest an alternative uniform prescription

$$\boldsymbol{F}(\boldsymbol{X}) = \bar{\boldsymbol{F}} \tag{7.28}$$

for the microscopic deformations. This entails the *Voigt estimate*

$$\bar{\mathscr{W}}_{\mathrm{V}}(\bar{\boldsymbol{F}}) = n^{\mathfrak{F}}\, \mathscr{W}_{\mu}^{\mathfrak{F}}(\bar{\boldsymbol{F}}) + n^{\mathfrak{M}}\, \mathscr{W}_{\mu}^{\mathfrak{M}}(\bar{\boldsymbol{F}}) \tag{7.29}$$

for the macroscopic strain-energy function. It was noted in Section 7.1.2 that pathological changes in muscle tissue can weaken the internal structure and question the assumption of perfect bonding at the interface of the two phases. Of course, this applies all the more to the affinity assumption made here for the entire microscopic deformation. This means that the use of the Voigt estimate (7.29) should be restricted especially to the modelling and simulation of healthy muscle tissue. Further, it was noted in Section 4.3.5 that the Voigt estimate generally takes into account the microstructure only by means of the volume fractions, which describe the one-point probabilities of the characteristic functions $\mathscr{X}^{\alpha}$. However, in addition to this explicit consideration of the microstructural statistics, it is very interesting to note that the energy in Eq. (7.29) also contains an implicit dependence on the shape tensor $\boldsymbol{Z}_{\mathrm{i}}$ through the strain-energy function $\mathscr{W}_{\mathrm{c}}^{\mathfrak{M}}$. This means that the Voigt estimate takes into account the shape and the orientation of the muscle fibres. Finally, the macroscopic first Piola–Kirchhoff stress tensor based on the Voigt estimate reads

$$\bar{\boldsymbol{P}}_{\mathrm{V}}(\bar{\boldsymbol{F}}) = \partial_{\bar{\boldsymbol{F}}} \bar{\mathscr{W}}_{\mathrm{V}} - \bar{\wp}\, \bar{J}\, \bar{\boldsymbol{F}}^{-T} = n^{\mathfrak{F}}\, \boldsymbol{P}_{\mu}^{\mathfrak{F}}(\bar{\boldsymbol{F}}) + n^{\mathfrak{M}}\, \boldsymbol{P}_{\mu}^{\mathfrak{M}}(\bar{\boldsymbol{F}}) - \bar{\wp}\, \bar{J}\, \bar{\boldsymbol{F}}^{-T}\,. \tag{7.30}$$

Therein, $\partial_{\bar{\boldsymbol{F}}} \bar{\mathscr{W}}_{\mathrm{V}}$ constitutes the macroscopic extra stress and $\bar{\wp}$ is a macroscopic Lagrange multiplier which comes into play because of the macroscopic incompressibility constraint (7.5), compare Eq. (3.27).

8 Parameters, Results and Discussion of the Multiscale Muscle Model

8.1 Model Parameters

The constitutive modelling of the two phases in Section 7.2 results in an overall model for skeletal muscle tissue with *eight model parameters*. Table 8.1 summarises these parameters, classifies them as material or structural parameters, and describes the microstructural meaning. The three material parameters $\mu^{\mathfrak{F}}$, $\mu^{\mathfrak{M}}$, $\mu_{\mathfrak{cf}}$ are directly connected to stiffnesses of the microstructural components, whereas the two volume fractions $n^{\mathfrak{M}}$, n^{I} refer to the microstructural composition of the material and the three remaining parameters λ_{w}, Θ_{m}, b characterise the structure of the collagen type-I fibre network. It becomes obvious that especially the collagen network plays a key role within this new modelling approach. The choice of specific model parameters is a crucial step towards a meaningful material model, thus, we aim to give a broad overview over literature data and variations of the three material and the five structural parameters in this section.

8.1.1 Material parameters

As shown in Table 8.1, the proposed model contains three material parameters related to the stiffness of microstructural components. One of the parameters describes the stiffness of the muscle fibres while the other two describe stiffnesses inside the extracellular matrix structure.

Muscle fibre The choice of a Neo-Hookean energy for the description of the muscle fibres was motivated in Section 7.2.1 by the nearly-linear stretch-stress relationships observed by Meyer & Lieber [324] and Smith et al. [452]. Consequently, the data of Smith et al. [452] are used for the estimation of the material parameter $\mu^{\mathfrak{F}}$. Therein, the relevant experiments are performed on isolated muscle fibres of human gracilis and semitendinosus muscles. Taking the reported averaged sarcomere slack length of $2.31\,\mu$m, see Smith et al. [452], as the stress-free reference configuration, a standard least-squares fitting routine yields the parameter $\mu^{\mathfrak{F}}_{\mathrm{grac}} = 12.452\,\mathrm{kN/m^2}$ for the gracilis muscle data and $\mu^{\mathfrak{F}}_{\mathrm{semi}} =$

parameter	classification	meaning
$n^{\mathfrak{M}}$	structural	volume fraction of the ECM
n^{I}	structural	volume fraction of type-I collagen fibres inside the ECM
$\mu^{\mathfrak{F}}$	material	(passive) stiffness of the muscle fibre
$\mu^{\mathfrak{M}}$	material	stiffness of the isotropic groundmatrix of the ECM
$\mu_{\mathfrak{cf}}$	material	stiffness of type-I collagen fibres/fibrils
λ_{w}	structural	waviness of the type-I collagen fibres
Θ_{m}	structural	mean preferred orientation of the type-I collagen fibres
b	structural	spreading/dispersion of the type-I collagen fibres

Table 8.1: Summary, classification and meaning of the eight model parameters for the presented skeletal muscle model, which result from the constitutive modelling of the two phases in Section 7.2.

study	ECM groundmatrix stiffness [kN/m^2] (± SD)	specimen	
[226]	61.046	abdominal aorta	rat
	9.5852	tail artery	
[222]	0.3	adventitia layer	rabbit carotid artery
	3	media layer	
[225]	15.12 ± 9.32	adventitia layer	human coronary artery
	2.54 ± 1.26	media layer	
	55.8 ± 21.18	intima layer	
[109]	0.5	nucleus pulposus	human intervertebral disc
	950	annulus fibrosus	

Table 8.2: Collection of stiffness values for the Neo-Hookean material parameter describing the groundmatrix part of the extracellular matrix in different biological tissues. The data from Holzapfel & Weizsäcker [226] and Holzapfel et al. [225] result from own experiments, whereas the model of Holzapfel et al. [222] was fitted to experimental data by Chuong & Fung [77] and the model of Ehlers et al. [109] was fitted to experimental data by Iatridis et al. [238]. (SD=standard deviation)

$14.440\,\mathrm{kN/m^2}$ for the semitendinosus muscle data. Utilising both muscle data in a single optimisation step, an averaged parameter for the muscle fibre of $\mu^{\mathfrak{F}} = 13.446\,\mathrm{kN/m^2}$ is obtained. This is equivalent to the mean between $\mu^{\mathfrak{F}}_{\mathrm{grac}}$ and $\mu^{\mathfrak{F}}_{\mathrm{semi}}$. Recalling that the muscle fibre stiffness is of less influence on the overall muscle stiffness and the fact that $\mu^{\mathfrak{F}}_{\mathrm{grac}}$ and $\mu^{\mathfrak{F}}_{\mathrm{semi}}$ differ only moderately, we proceed with $\mu^{\mathfrak{F}} = 13.446\,\mathrm{kN/m^2}$ to describe the mechanical behaviour of the skeletal muscle fibre.

Extracellular matrix The constitutive description of the ECM in terms of the energy $\mathscr{W}^{\mathfrak{M}}$ contains the two material parameters $\mu^{\mathfrak{M}}$ and $\mu_{\mathfrak{cf}}$, which account for the stiffness of the ECM groundmatrix and the collagen type-I fibres, respectively.

As explained in Section 7.2.2, the groundmatrix energy part $\mathscr{W}^{\mathfrak{M}}_{\mathrm{g}}$ and its material parameter $\mu^{\mathfrak{M}}$ account for the non-collageneous parts of the extracellular matrix, which are, for instance, the elastin fibres and proteoglycans. A collection of reported values for the Neo-Hookean stiffness parameter $\mu^{\mathfrak{M}}$ is given in Table 8.2. Obviously, the summarised stiffness values show a very broad variation not only between the different types of specimen but also between different subjects of the same tissue type, observable from the standard deviations in the experiments of Holzapfel et al. [225]. In general, these variations make it very difficult to find an appropriate and reliable parameter for the ECM groundmatrix, especially for materials where the ECM occupies large portions of the tissue, like in the specimen used in the reported experiments. In muscle tissue, however, the groundmatrix of extracellular matrix content is small. Further, the elastin fibres in the groundmatrix have an about 1000 times smaller stiffness than collagen fibres, see Gosline et al. [167], which means that the contribution of the collagen fibres clearly dominates the passive mechanical behaviour of the tissue. Given the range of reported numbers, for example by Holzapfel et al. [225], the groundmatrix stiffness parameter is chosen herein as $\mu^{\mathfrak{M}} = 40\,\mathrm{kN/m^2}$, which is a reasonable choice given the overall range of reported parameters.

The second material parameter related to the ECM is the stiffness $\mu_{\mathfrak{cf}}$ of a collagen type-I fibre. Due to its importance for the mechanical behaviour of many different biological

tissues, there exist a comprehensive body of literature about the properties of type-I collagen fibres. The general stretch-stress relation of collagen fibres can be described by a flat toe region at the beginning that eventually evolves to a nearly-linear stretch-stress curve after the initially crimped fibres have been uncrimped at higher stretches. Thus, most studies report on the constant stiffness of the linear stretch-strain region in the form of a scalar modulus, which is sometimes also referred to as Young's modulus. However, Young's modulus is no suitable term for a stiffness quantity in the finite deformation regime and the scalar modulus (or an incremental Young's modulus) has to be properly defined. For instance, a scalar nominal tangent moduli can be formulated as $E_{\mathrm{P}} = \partial_\lambda P = \partial^2_{\lambda^2}\mathscr{W}$ and, analogously, a scalar Cauchy tangent moduli might be introduced as $E_\sigma = \partial_{\ln[\lambda]}\sigma$, see Mihai & Goriely [333]. From the previous consideration, we are already familiar with the nominal description and we identify $P = \partial_\lambda \mathscr{W}$ as the scalar nominal stress, whereas $\sigma = \lambda\,\partial_\lambda \mathscr{W}$ is a scalar Cauchy stress (λ is of course the stretch parameter). With these considerations and the definition given in Eq. (7.24), the parameter $\mu_{\mathfrak{cf}}$ is identified as a constant nominal tangent modulus. From experimental studies, however, the nature of the moduli provided in these studies is not always clear and care needs to be taken. Moreover, experiments based on methods like indentation do not necessarily provide information on the required tensile stiffness due to the anisotropy of the collagen fibres, see Wenger et al. [513]. Further, the experimentally observed collagen stiffness seems to be dependent on the surrounding conditions (for example, ambient or in solution), see van der Rijt et al. [401]. *Nominal* moduli for the tensile stiffness of collagen type-I fibrils/fibres were reported by, for example, Sasaki & Odajima [418] and Gentleman et al. [159]. Sasaki & Odajima [418] reports a value of $43\,\mathrm{GN/m^2}$ and Gentleman et al. [159] fibre-diameter-dependent values ranging between $26.97\,\mathrm{GN/m^2}$ and $48.47\,\mathrm{GN/m^2}$. In both of these studies, the collagen was extracted from the bovine achilles tendon. Shen et al. [436] measured moduli in a range of $860 \pm 450\,\mathrm{MN/m^2}$ for collagen extracted from the sea cucumber dermis. These magnitudes were also reported in the studies of van der Rijt et al. [401], which were used by Gindre et al. [163] in their simulations.

8.1.2 Structural parameters

In addition to the material parameters, the proposed model also requires the specification of the five structural parameters associated with its microstructure, which are the two volume fractions $n^{\mathfrak{M}}$ and n^{I}, and the three parameters λ_{w}, Θ_{m} and b describing the collageneous network, see Table 8.1. Assuming experimental muscle tissue specimen sizes in the millimetre or centimetre range, the specimen contain representative amounts of muscle fibres and muscle fibre bundles. Thus, to compare model predictions with experimental results, structural parameters for endo- and perimysium need to be taken into account by appropriate adding or averaging, see also Gindre et al. [163].

The volume fractions $n^{\mathfrak{F}}$ and $n^{\mathfrak{M}}$ The volume fraction $n^{\mathfrak{M}}$ accounts for the amount of connective tissue and is obtained by the sum of the perimysial content $n^{\mathfrak{M}}_{\mathrm{peri}}$ and the endomysial content $n^{\mathfrak{M}}_{\mathrm{endo}}$, hence:

$$n^{\mathfrak{M}} = n^{\mathfrak{M}}_{\mathrm{peri}} + n^{\mathfrak{M}}_{\mathrm{endo}}\,. \tag{8.1}$$

For bovine muscles, Purslow [389] reported values in the range of $0.43\% - 4.6\%$ for $n^{\mathfrak{M}}_{\mathrm{peri}}$ and $0.47\% - 1.2\%$ for $n^{\mathfrak{M}}_{\mathrm{endo}}$. In general, they observed higher variations for the perimysium

	amount of dry connective tissue w.r.t. to total dry muscle		**amount of collagen type I w.r.t. to the sum of types I and III**	
muscle	perimysium $n^{\mathfrak{M}}_{\text{peri}}$ [%]	endomysium $n^{\mathfrak{M}}_{\text{endo}}$ [%]	perimysium $n^{\text{I}}_{\text{peri}}$ [%]	endomysium $n^{\text{I}}_{\text{endo}}$ [%]
a)	1.4	0.5	56.8	44.8
b)	1.7	0.3	75.5	46.7
c)	4.7	0.3	59.3	41.5
d)	6.4	0.1	58.3	43.6
e)	7.0	n.d.	63.5	41.4
f)	3.3	0.5	59.5	41.9

Table 8.3: Experimental data on the microstructural composition of the perimysial- and endomysial layers for six bovine muscles extracted from data published in LIGHT ET AL. [289]. a) Psoas major, b) Longissimus dorsi, c) Pectoralis profundis, d) Semitendinosus, e) Gastrocnemius, f) Sternomandibularis. (w.r.t.= with respect to, n.d.=not determined)

than for the endomysium. LIGHT ET AL. [289] presented an extensive study on six different types of bovine muscles and reported $1.4\% - 7.0\%$ for $n^{\mathfrak{M}}_{\text{peri}}$ and $0.1\% - 0.5\%$ for $n^{\mathfrak{M}}_{\text{endo}}$. The experimental results of LIGHT ET AL. [289] are summarised in Table 8.3. For the volume fraction $n^{\mathfrak{M}}$ (without distinguishing between peri- and endomysial contribution), LIEBER ET AL. [287] found a value of 5%.

The volume fraction n^{I} The volume fraction n^{I} can be calculated by a weighted mean between the peri- and the endomysial tissues via

$$n^{\text{I}} = \frac{n^{\mathfrak{M}}_{\text{peri}}\, n^{\text{coll}}_{\text{peri}}\, n^{\text{I\&III}}_{\text{peri}}\, n^{\text{I}}_{\text{peri}} + n^{\mathfrak{M}}_{\text{endo}}\, n^{\text{coll}}_{\text{endo}}\, n^{\text{I\&III}}_{\text{endo}}\, n^{\text{I}}_{\text{endo}}}{n^{\mathfrak{M}}_{\text{peri}} + n^{\mathfrak{M}}_{\text{endo}}} \,. \tag{8.2}$$

Therein, $n^{\text{coll}}_{\text{peri}}$ and $n^{\text{coll}}_{\text{endo}}$ account for the amount of collageneous tissue inside the respective connective tissues, while $n^{\text{I\&III}}_{\text{peri}}$ and $n^{\text{I\&III}}_{\text{endo}}$ describe the amount of collagen type-I & -III fibres inside the respective collageneous tissues. Based on the works of LIGHT & CHAMPION [288] and LIGHT ET AL. [289], $n^{\text{coll}}_{\text{peri}}$ is 95.3%, $n^{\text{coll}}_{\text{endo}}$ is 42.4%, and $n^{\text{I\&III}}_{\text{peri}}$ is equal to $n^{\text{I\&III}}_{\text{endo}}$ and 95%. Table 8.3 lists $n^{\text{I}}_{\text{peri}}$ and $n^{\text{I}}_{\text{endo}}$ for six bovine muscles. For the semitendinosus muscle, for example, n^{I} is 0.52 and for psoas major, n^{I} is 0.43. This coincides with the range of values reported in LISTRAT ET AL. [291].

The waviness parameter λ_{w} For the waviness parameter λ_{w}, we refer to a recent study of MOHAMMADKHAH ET AL. [339]. They comprehensively investigated the waviness of collagen fibres in chicken and porcine skeletal muscle tissue for the undeformed and for various deformed states. MOHAMMADKHAH ET AL. [339] experimentally determined for the reference configuration a λ_{w} between 1.12 and 1.17. For completeness, we also refer to the images in the works of ROWE [410] and TROTTER & PURSLOW [486], where the crimped state of the fibres is depicted very nicely and which can serve as a basis for an image-based estimation of the waviness parameter.

The mean orientation Θ_{m} The mean orientation Θ_{m} of the collagen fibre type I fibres in the perimysial layer is frequently reported to be around 55 degree, see, for example, ROWE [410] and PURSLOW [387, 389]. In the endomysial layer, Θ_{m} is found to be around 59 degree, as reported by, for example, PURSLOW & TROTTER [391].

The collagen dispersion b Further, the parameter b describes the spreading/dispersion of the collagen type-I fibres around the mean orientation Θ_{m}. Figure B.6b shows the π-periodic von Mises probability density function $\mathfrak{p}_\Theta$ for some exemplary values of b. Comparing these probabilities to experimentally measured distributions for the endomysial layer by Purslow & Trotter [391], it can be concluded that in endomysium b ranges around 1 and thus shows a rather wide distribution over the polar orientation space. Yet, the study of Purslow & Trotter [391] refined the understanding of the collagen distribution in the endomysial layer, which before was commonly assumed to be completely randomly oriented, such as in Trotter & Purslow [486]. In contrast, the collagen fibres in the perimysial layer are much more aligned around the mean orientation Θ_{m} and form well-ordered sheets of criss-crossed arrangement, see, for instance, Rowe [411] or Purslow [387]. Unfortunately, there are no experimental studies reporting on the collagen orientation in the perimysium in the form of detailed distribution diagrams. However, from Figure B.6b it can be concluded that a value for the parameter b around 10 might well describe the aligned characteristic of the perimysial collageneous tissue. A reasonable range for the spreading parameter b describing endo- and perimysium in an averaged sense might thus be given between around 1 and 10.

For completeness, we remark that if distinct values are given for the peri- and the endomysium, the network quantities $\lambda_{\mathrm{w}}, \Theta_{\mathrm{m}}, b$ are derived by the weighted averaging

$$\Gamma = \frac{n^{\mathfrak{M}}_{\mathrm{peri}}\,\Gamma_{\mathrm{peri}} + n^{\mathfrak{M}}_{\mathrm{endo}}\,\Gamma_{\mathrm{endo}}}{n^{\mathfrak{M}}_{\mathrm{peri}} + n^{\mathfrak{M}}_{\mathrm{endo}}} \tag{8.3}$$

between the peri- and endomysial quantities, Γ_{peri} and Γ_{endo}, for $\Gamma = \{\lambda_{\mathrm{w}}, \Theta_{\mathrm{m}}, b\}$.

8.2 Results and Discussion

In this section, results for the previously introduced muscle model are presented and discussed. We focus on the microstructure-originated characteristics of the presented constitutive description rather than on an extensive calibration of the model parameters to macroscopic experiments. Further, the following examples shall depict the capabilities of the new model to predict macroscopic properties without explicitly assuming them in the form of macroscopic constitutive assumptions. In this sense, it suffices in the following to consider the Voigt estimate $\bar{\mathscr{W}}_{\mathrm{V}}$ as the macroscopic strain energy of the muscle tissue. We first present in Section 8.2.1 results for the collagen fibre stretch in order to demonstrate that the microstructure exhibits distinct reactions if subjected to different macroscopic deformations. Moreover, we will show that a few microscopic model parameters are sufficient to capture with the new model the experimentally-observed anisotropic mechanical behaviour of skeletal passive muscle tissue, in particular if the tissue is subjected to uniaxial tension experiments in muscle fibre direction (Section 8.2.2) and transverse to the muscle fibre direction (Section 8.2.3). The dependence of the new model on the full set of transversely isotropic invariants will be highlighted in Sections 8.2.4 and 8.2.5, where it is shown that the $\bar{I}_2$- and $\bar{J}_5$-dependencies are direct consequences of the presented multiscale modelling framework without the need of calibrating any according macroscopic material parameter. Remark that the simulations in Sections 8.2.2 to 8.2.5 are performed using a self-written Matlab code, which allows to compute the integrals involved in the averaging operation $\langle(\cdot)\rangle_\Omega$ for the energy $\mathscr{W}_{\mathrm{c}}^{\mathfrak{M}}$ and the stress $\boldsymbol{P}_{\mathrm{c}}^{\mathfrak{M}}$ of the collageneous tissue by

means of the build-in adaptive quadrature function *integral2*, see SHAMPINE [431, 432]. The accuracy of the integration is ensured by setting the tolerances of *integral2* to 10^{-6}. However, such adaptive quadrature schemes are not optimal with respect to computational efficiency and appropriate quadrature schemes with a fix number of suitable chosen discrete points as introduced in Section 6.4 should be considered for scenarios where the simulation time becomes a critical factor.

8.2.1 Macroscopically-driven collagen fibre stretch

First, we investigate the potential of choosing a comprehensive description for the collagen fibre kinematics as introduced within this model. The deformation of the collagen fibres on the microscale is driven by the macroscopic deformation, $\bar{\boldsymbol{F}}$, and comprises a length change and a reorientation of the collagen fibre end-to-end axis. Thereby, the collagen kinematics follow in the presented model from the detailed description of the microstructure and are not artificially introduced as a macroscopic constitutive assumption. This clearly distinguishes the proposed model from other microstructurally-based muscle models like the ones by GINDRE ET AL. [163] and SPYROU ET AL. [459, 460]. For a fibre which is parametrised by vector $\mathfrak{a}_0$, see Eq. (7.11), length changes due to a general macroscopic deformation, described by the generic tensor $\bar{\boldsymbol{F}}^{\iota}$, are given by

$$\lambda_{\mathfrak{a}}(\bar{\lambda}_{\mathrm{l}}, \bar{\gamma}_{\mathrm{l}}, \bar{\gamma}_{\mathrm{t}}, \bar{\psi}_{\gamma}; \Theta, \Phi) = \big\{ \bar{\lambda}_{\mathrm{l}}^{-1} \sin^2[\Theta] \sin^2[\Phi] + (\bar{\lambda}_{\mathrm{l}}^{-1/2} \sin[\Theta] \cos[\Phi] - \bar{\gamma}_{\mathrm{t}} \sin[\Theta] \sin[\Phi])^2 + (\bar{\lambda}_{\mathrm{l}} \cos[\Theta] - \bar{\gamma}_{\mathrm{l}} \sin[\Theta] \sin[\Phi - \bar{\psi}_{\gamma}])^2 \big\}^{1/2} . \tag{8.4}$$

Therein, we made use of the incompressible formulation (3.103) for $\bar{\boldsymbol{F}}^{\iota}$, such that $\lambda_{\mathfrak{a}}$ becomes a direct function of the four macroscopic strain invariants $\{\bar{\lambda}_{\mathrm{l}}, \bar{\gamma}_{\mathrm{l}}, \bar{\gamma}_{\mathrm{t}}, \bar{\psi}_{\gamma}\}$. Now, we investigate the microscopic collagen fibre stretch as a consequence of applying certain specific macroscopic loading conditions. This is achieved by subsequently simplifying Eq. (8.4) for the cases of pure uniaxial stretch ($\bar{\gamma}_{\ell} = \bar{\gamma}_{\mathrm{t}} = 0$), longitudinal shear ($\bar{\lambda}_{\ell} = 1$, $\bar{\gamma}_{\mathrm{t}} = 0$), and transverse shear ($\bar{\lambda}_{\ell} = 1$, $\bar{\gamma}_{\ell} = 0$). To illustrate the fibre stretch $\lambda_{\mathfrak{a}}$ over the range of Θ and Φ, we make use of an azimuthal equidistant projection plot. In such plots, the upper half of a three-dimensional unit sphere is projected onto a two-dimensional plane, see Figure 8.1. The restriction to the upper half sphere ($\Theta \in [0, \pi/2]$) is justified by symmetry and entails a clearer visualisation of the results. Further, since the investigations in this section are purely kinematical, no model parameters have to be specified.

For uniaxial stretch in the preferred direction ($\bar{\gamma}_{\ell} = \bar{\gamma}_{\mathrm{t}} = 0$), relation (8.4) for the collagen stretch can be simplified to

$$\lambda_{\mathfrak{a}}\big|_{\bar{\gamma}_{\ell} = \bar{\gamma}_{\mathrm{t}} = 0} = \sqrt{(\bar{\lambda}_{\ell}^3 \cos^2[\Theta] + \sin^2[\Theta])/\bar{\lambda}_{\ell}} , \tag{8.5}$$

and the stretch becomes independent of the azimuthal angle Φ and the coupling invariant $\bar{\psi}_{\gamma}$. A collagen-stretch model of form (8.5) was also proposed by PURSLOW [387] and serves as full kinematical description for the collagen fibres in, for example, GINDRE ET AL. [163] and SPYROU ET AL. [459, 460]. However, in those works, relation (8.5) is constitutively obtained by considering the change in length of the diagonal of a rectangle, where the latter depicts the unwrapped surface of an incompressible cylinder subject to a stretch $\bar{\lambda}_{\ell}$. In contrast, in the proposed model Eq. (8.5) is directly obtained from the microscopic descriptions of the collageneous structure. This rigorous microstructural approach will

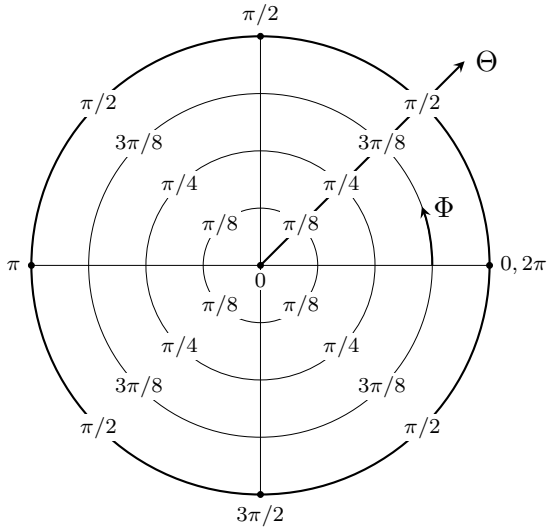

Figure 8.1: Illustration of the azimuthal equidistant projection over the upper half of the unit sphere. The azimuthal angle of the three-dimensional space, ψ, is depicted in the two-dimensional projection as angular/azimuthal angle, while the polar angle Θ is depicted in radial direction and ranges from 0 to $\pi/2$.

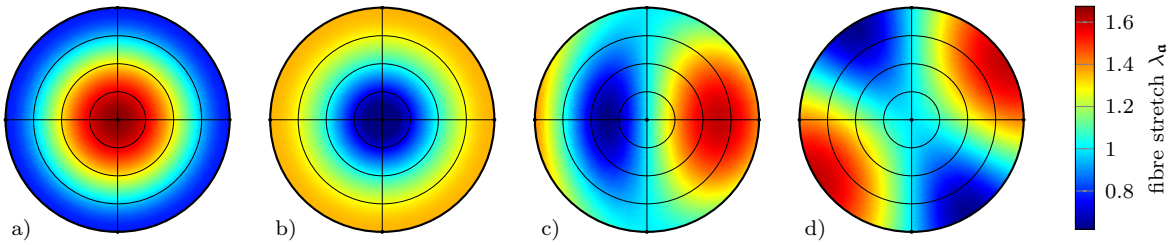

Figure 8.2: Projection plot of the collagen fibre stretch $\lambda_{\mathfrak{a}}$ due to a) a uniaxial tensile stretch $\bar{\lambda}_\ell = 1.675$ in preferred direction $\bar{\boldsymbol{a}}$, b) a uniaxial compressive stretch $\bar{\lambda}_\ell = 0.539$, c) a longitudinal shear deformation $\bar{\gamma}_\ell = 1.0$ with $\bar{\psi}_\gamma = 0$ and d) a transverse shear deformation $\bar{\gamma}_\mathrm{t} = 1.0$. The range of values is $\lambda_{\mathfrak{a}} \in \{0.773, 1.675\}$ for a), $\lambda_{\mathfrak{a}} \in \{0.539, 1.362\}$ for b), and $\lambda_{\mathfrak{a}} \in \{0.618, 1.618\}$ for c) and d).

especially prove to be beneficial when the collagen fibres are subjected to general and more complex macroscopic deformations.

Figure 8.2a depicts the resulting projection plot for the collagen stretch $\lambda_{\mathfrak{a}}$ for a macroscopic stretch of $\bar{\lambda}_\ell = 1.675$. The plot exhibits radial symmetry due to the Φ-independence of relation (8.5). Moreover, the maximum value for the collagen stretch occurs at $\Theta = 0$ and is equal to the applied macroscopic stretch $\bar{\lambda}_\ell$, whereas the minimum value at $\Theta = \pi/2$ is exactly the transverse stretch $1/\sqrt{\bar{\lambda}_\ell}$. The stretch $\bar{\lambda}_\ell = 1.675$ is chosen such that the axisymmetric shear $\bar{\gamma}_\mathrm{a}$ is 1.0.

Figure 8.2b shows the distribution of the collagen fibre stretch for a macroscopic compressive stretch of $\bar{\lambda}_\ell = 0.539$, which corresponds to $\bar{\gamma}_\mathrm{a} = -1$. The plot is radial symmetric like Figure 8.2a. However, the minimum value of the collagen stretch now occurs at $\Theta = 0$ and equals the applied macroscopic stretch $\bar{\lambda}_\ell$, while the maximum value is observed at $\Theta = \pi/2$.

For a longitudinal shear deformation ($\bar{\lambda}_\ell = 1, \bar{\gamma}_\mathrm{t} = 0$), Eq. (8.4) simplifies to

$$\lambda_{\mathfrak{a}}\big|_{\bar{\lambda}_\ell=1,\bar{\gamma}_\mathrm{t}=0} = \sqrt{\sin^2[\Theta] - (\bar{\gamma}_\ell \sin[\Theta] \sin[\Phi - \bar{\psi}_\gamma] - \cos[\Theta])^2}\,. \tag{8.6}$$

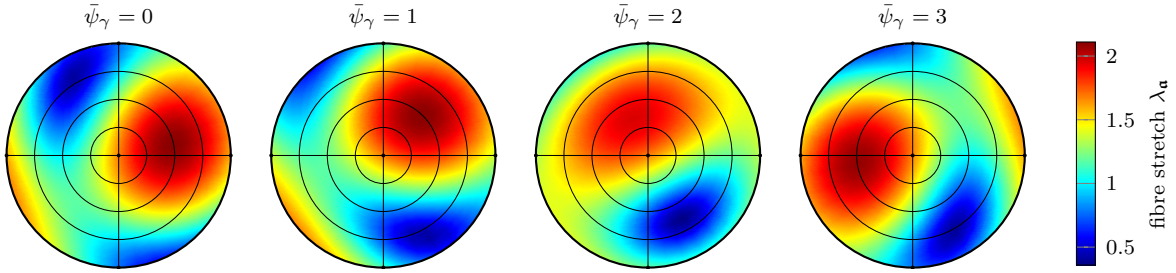

Figure 8.3: Projection plot of the collagen fibre stretch $\lambda_{\mathfrak{a}}$ due to a combined stretch and shear loading with $\bar{\lambda}_\ell = 1.675$, $\bar{\gamma}_\ell = \bar{\gamma}_\mathrm{t} = 1.0$, and four different values $\{0, 1, 2, 3\}$ of the coupling invariant $\bar{\psi}_\gamma$. The range of values over all four cases is $\lambda_{\mathfrak{a}} \in \{0.359, 2.110\}$.

In contrast to Eq. (8.5) of the previously investigated uniaxial loading case, the collagen fibre stretch is now dependent on the azimuthal angle Φ and the macroscopic coupling invariant $\bar{\psi}_\gamma$. However, the dependence on $\bar{\psi}_\gamma$ only phase shifts the collagen stretch with respect to the azimuthal orientation and does not alter the averaged results after the integration over the range $\Phi \in [0, 2\pi)$ within the operator $\langle(\cdot)\rangle_\Omega$. Hence, the network energy $\mathscr{W}_\mathrm{c}^{\mathfrak{M}}$ is for the longitudinal shear independent on the choice of $\bar{\psi}_\gamma$. This confirms the statement that $\bar{\psi}_\gamma$ can be chosen arbitrarily whenever $\bar{\gamma}_\ell\,\bar{\gamma}_\mathrm{t} = 0$, see Section 3.5.4. The collagen stretches resulting from $\bar{\gamma}_\ell = 1.0$ and $\bar{\psi}_\gamma = 0$ in Eq. (8.6) are plotted in Figure 8.2c.

For transverse shear, the collagen stretch is given by

$$\lambda_{\mathfrak{a}}\big|_{\bar{\lambda}_\ell=1,\bar{\gamma}_\ell=0} = \sqrt{\cos^2[\Theta] + \sin^2[\Theta]\left(\sin^2[\Phi] + (\cos[\Phi] - \bar{\gamma}_\mathrm{t}\sin[\Phi])^2\right)}\,. \tag{8.7}$$

This relation is independent of the coupling invariant $\bar{\psi}_\gamma$ as expected. The result for a transverse shear $\bar{\gamma}_\mathrm{t} = 1.0$ is shown in Figure 8.2d. As for the longitudinal shear, the dependence on the azimuthal angle Φ indicates that this projection plot does not obey radial symmetry.

In order to highlight the generality of Eq. (8.4), we also want to investigate the scenario of combined axisymmetric, longitudinal and transverse shear deformation with $\bar{\lambda}_\ell = 1.675$ (corresponding to $\bar{\gamma}_\mathrm{a} = 1.0$) and $\bar{\gamma}_\ell = \bar{\gamma}_\mathrm{t} = 1.0$. Under these conditions, the collagen stretch $\lambda_{\mathfrak{a}}$ additionally depends on the coupling invariant $\bar{\psi}_\gamma$. Figure 8.3 exemplary shows the collagen stretch for four different values $\bar{\psi}_\gamma = \{0, 1, 2, 3\}$. From Figure 8.3, one clearly observes that the four different loadings not only cause a phase shift but also affect the results of the integration when evaluating the averaging operation $\langle(\cdot)\rangle_\Omega$ and, hence, the network energy $\mathscr{W}_\mathrm{c}^{\mathfrak{M}}$.

Concluding this section, we want to emphasise that the comprehensive description for the collagen fibre kinematics within the presented model results in distinct fibre-stretch distributions for different macroscopic deformations. By recalling the case distinction in the collagen fibre energy as defined in Eq. (7.24), it becomes clear that the detailed knowledge about the stretch distribution is essential for the exclusion of fibres which are not stretched beyond the waviness threshold, hence for fibres with $\lambda_{\mathfrak{a}} < \lambda_\mathrm{w}$, which should not contribute to the network energy. This switch is very important in collageneous tissue, as discussed, for example, by Holzapfel & Ogden [224]. The present model includes the switch for general macroscopic loadings in a natural way without the need of computing critical angles or any other additional procedure.

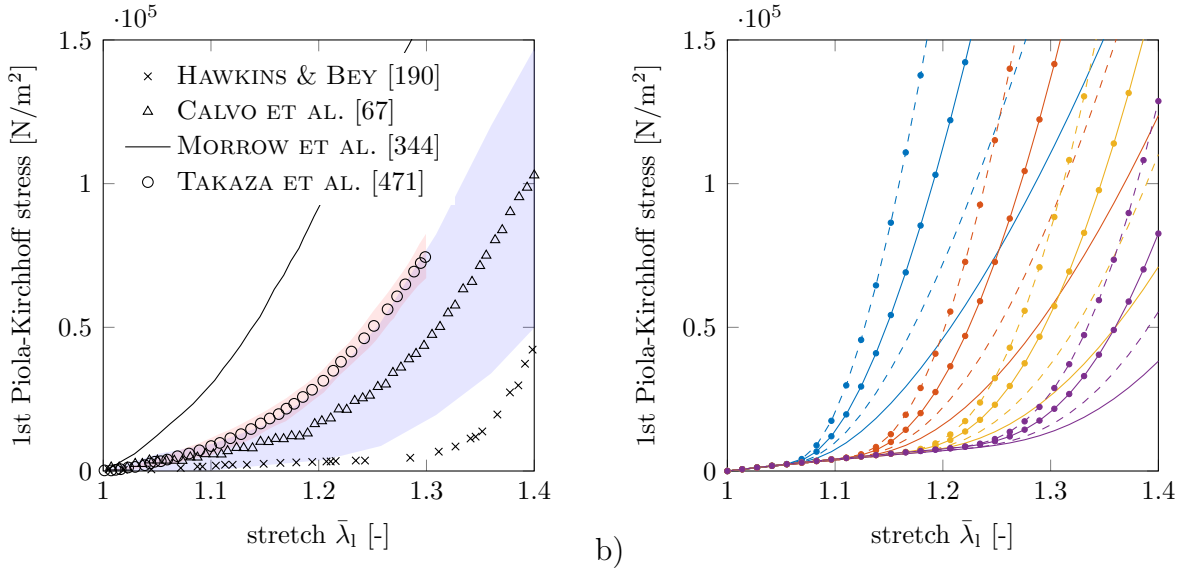

Figure 8.4: a) Collection of tensile experiments on skeletal muscle tissue. The blue and red shaded areas depict the standard deviations of the results of Calvo et al. [67] and Takaza et al. [471], respectively. The experiments of Hawkins & Bey [190] and Calvo et al. [67] were performed on rat tibialis anterior muscles, whereas Morrow et al. [344] used rabbit digitorum longus muscles and Takaza et al. [471] used pig longissimus dorsi muscles. b) Collection of simulation results for uniaxial tension and different combinations of model parameters. Lines without and with markers depict volume fractions according to longissimus dorsi and semitendinosus, respectively. Solid and dashed lines define the different collagen stiffnesses $\mu_{\mathfrak{cf}} = \{300, 500\}$ MN/m^2, and the line colours {blue, red, yellow, purple} stand for the different wavinesses $\lambda_{\mathrm{w}} = \{1.05, 1.1, 1.15, 1.2\}$.

8.2.2 Uniaxial tension in muscle fibre direction

Most mechanical tests on skeletal muscle tissue are tension tests in the direction of the muscle fibre orientation, for example, in Hawkins & Bey [190], Calvo et al. [67], Morrow et al. [344], and Takaza et al. [471]. Figure 8.4a shows the results of these experimental studies in one graph. This figure impressively demonstrates the large inter-tissue variations, since Hawkins & Bey [190] and Calvo et al. [67] performed experiments on the rat tibialis anterior, Morrow et al. [344] on the rabbit digitorum longus muscle, and Takaza et al. [471] on the pig longissimus dorsi muscle. Noticeable are the different shapes of the stress-strain relations, which strongly indicates microstructural alterations in the specimen. In addition, Figure 8.4a shows the large intra-tissue variations, visible through the large standard deviation in the experiments of Calvo et al. [67]. This suggests that microstructural variations are also present among specimen of the same muscle type.

In what follows, we demonstrate the ability of the proposed model to capture such variations by varying the model parameters for ranges reported in literature and summarised in Section 8.1. Note, it is not the aim to calibrate the model to macroscopic experimental data. The macroscopic behaviour should be a consequence of microstructurally changes and not the microstructural material parameters a consequence of macroscopic behaviour. A description based on macroscopic calibration does not make sense within the context of this work, as we aim to clearly follow a bottom-up approach and to investigate how changes in the microstructural components effect the macroscopic behaviour.

To demonstrate the model's ability to capture microstructural variations on the mac-

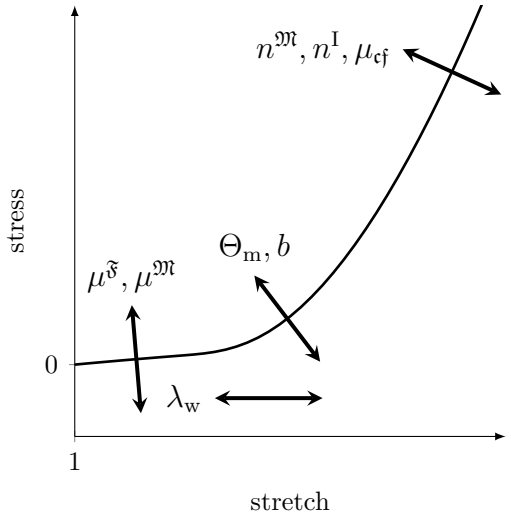

Figure 8.5: Schematic diagram of the main influence regions of the model parameters on the strain-stress-curve of skeletal muscle tissue subject to uniaxial tension in muscle fibre direction.

roscopic scale, we assume $n^{\mathfrak{M}} \in \{0.02, 0.065\}$ and $n^{\mathrm{I}} \in \{0.63, 0.52\}$ (hence, the values for the longissimus dorsi and semitendinosus given in Table 8.3). The values for the collagen stiffness are $\mu_{\mathfrak{cf}} = \{300, 500\}$ MN/m^2 and four distinct waviness parameters, $\lambda_{\mathrm{w}} \in \{1.05, 1.1, 1.15, 1.2\}$. The remaining parameters are $\mu^{\mathfrak{F}} = 13.446\,\mathrm{kN/m^2}$, $\mu^{\mathfrak{M}} = 40\,\mathrm{kN/m^2}$, $\Theta_{\mathrm{m}} = 55°$, and $b = 5$. The amount of parameter combinations was chosen such that individual stretch-stress curves can still be distinguished and linked to the according parameters. Further, the deformation gradient is given by $\bar{\boldsymbol{F}} = \bar{\lambda}_\ell^{-1/2}(\boldsymbol{e}_1 \otimes \boldsymbol{e}_1 + \boldsymbol{e}_2 \otimes \boldsymbol{e}_2) + \bar{\lambda}_\ell\, \boldsymbol{e}_3 \otimes \boldsymbol{e}_3$ and $\bar{\boldsymbol{a}} = \boldsymbol{e}_3$. We want to remark that for these uniaxial (axisymmetric) deformations, the deformation field in the microstructure is indeed uniform and the Voigt assumption in Eq. (7.28) depicts an exact result for the considered classes of materials. This means that the energy $\bar{\mathscr{W}}_{\mathrm{V}}$ is identical to the TSO-based energy $\widetilde{\mathscr{W}}$ from Eq. (7.27). Moreover, the collagen fibre kinematics under this loading condition are according to Eq. (8.5). The stress responses for $\bar{\lambda}_\ell \in [1.0, 1.4]$ are shown in Figure 8.4a. By comparing those results with the experiments in Figure 8.4a, one observes that the range of simulation results qualitatively matches the experimentally measured stress curves. Individual characteristics and shapes of the experimental curves, for example shorter or longer toe region, can be represented by the model by altering the respective microstructural parameters, for example the waviness λ_{w}. The exact correlation of the model parameters on specific regions of the stretch-stress-curve would require an appropriate sensitivity analysis on the parameters, which is not the scope of this paper. However, a schematic diagram for the main influence regions of the model parameters during uniaxial stretch can be provided in form of Figure 8.5, where it is especially highlighted that the amount and the stiffness of collagen type-I fibres influence the slope of the curve at higher stretches.

A quantitative comparison between experimental results and our proposed approach does not make sense, since none of the existing experimental studies report on the required microstructural components that are needed for our proposed approach. Moreover, the workflow from cutting, freezing, thawing to testing of tissue specimen encompasses many challenges and even small changes within the prepared tissue may alter the experimental results. Hence only a qualitative comparison is possible. On the other hand, one

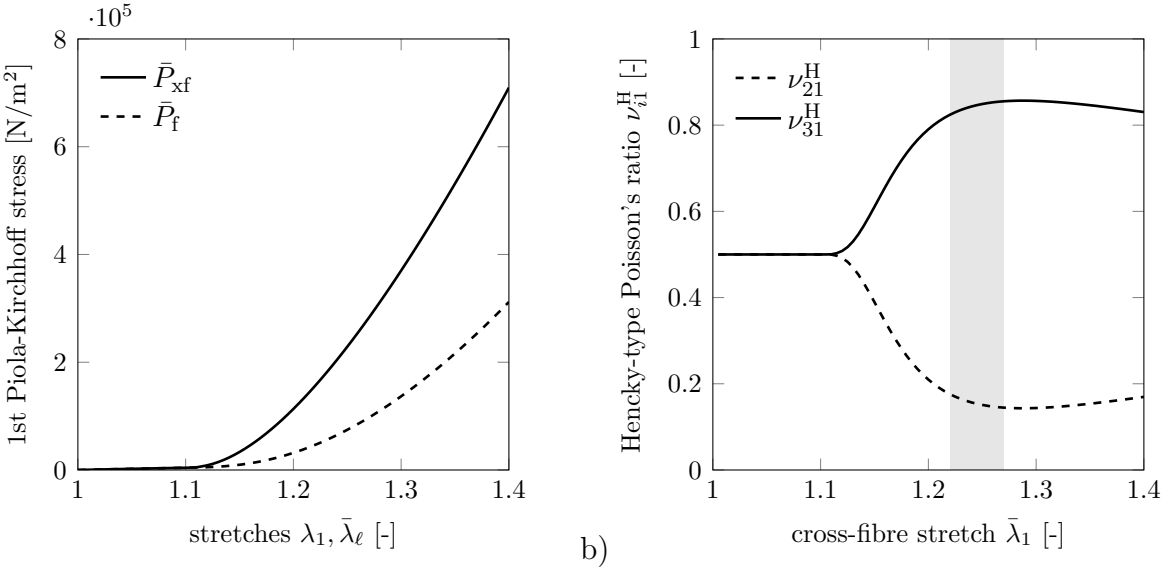

Figure 8.6: a) Stress responses $\bar{P}_{\mathrm{xf}}$ and $\bar{P}_{\mathrm{f}}$ due to a uniaxial stretch λ_1 transverse to the muscle fibre direction or a uniaxial stretch $\bar{\lambda}_\ell$ in muscle fibre direction, respectively. b) Hencky-type Poisson's ratios ν_{21}^{H} and ν_{31}^{H} due to the stretch λ_1 transverse to the muscle fibre direction. The shaded area indicates the stretch range in which Takaza et al. [471] measured nearly constant values for ν_{21}^{H} and ν_{31}^{H}.

can alter material parameters and hence systematically investigate how the variation of individual components alter the macroscopic behaviour using well-defined in-silico experiments. Furthermore, we have already pointed out that a common issue in modelling soft biological tissue is the identification of the stress-free reference configuration. This is a particular challenge for materials with a prominent toe region at low stretches, as it is the case for skeletal muscle tissue. This uncertainty in defining the stress-free reference configuration can cause large shifts in the stretch-strain curves and differences between simulations and experiments.

8.2.3 Uniaxial tension transverse to the muscle fibre direction

Next, we consider uniaxial tensile deformation transverse to the muscle fibre direction. To do so, we assume that $\bar{\boldsymbol{a}}_0 = \boldsymbol{e}_3$ and that a stretch λ_1 is applied in $\boldsymbol{e}_1$-direction. Then, with the deformation gradient $\bar{\boldsymbol{F}} = \lambda_1\, \boldsymbol{e}_1 \otimes \boldsymbol{e}_1 + \lambda_2\, \boldsymbol{e}_2 \otimes \boldsymbol{e}_2 + \lambda_3\, \boldsymbol{e}_3 \otimes \boldsymbol{e}_3$, the incompressibility constraint (7.5) resulting in $\lambda_2 = (\lambda_1 \lambda_3)^{-1}$, and the boundary conditions $\bar{P}_{22} = \bar{P}_{33} = 0$ for the stress tensor coefficients of the unloaded directions, one can compute the remaining unknown stretch λ_3, see Merodio & Ogden [323]. Moreover, we choose from the previous section a fixed subset of parameters, which will be used here and in the following examples: $n^{\mathfrak{M}} = 0.065$, $n^{\mathrm{I}} = 0.52$, $\mu_{\mathfrak{cf}} = 300 \cdot 10^6\ \mathrm{N/m^2}$, $\lambda_{\mathrm{w}} = 1.1$ and $\mu^{\mathfrak{F}} = 13446\,\mathrm{N/m^2}$, $\mu^{\mathfrak{M}} = 40 \cdot 10^3\,\mathrm{N/m^2}$, $\Theta_{\mathrm{m}} = 55°$, and $b = 5$. Figure 8.6a depicts the stress response $\bar{P}_{\mathrm{xf}}$ in $\boldsymbol{e}_1$-direction due to the stretch λ_1. For comparison, the plot also contains the stress response $\bar{P}_{\mathrm{f}}$ if a uniaxial extension $\bar{\lambda}_\ell$ is applied in muscle fibre direction. The results reveal that the tissue is much stiffer in its transverse direction than in fibre direction. This effect was also experimentally observed by, for instance, Nie et al. [354], Takaza et al. [471], Mohammadkhah et al. [338], and Wheatley et al. [515]. These matching findings in simulation and experiments also strongly suggest that muscle tissue should not be modelled as a fibre-reinforced material on the macroscopic scale, since the muscle fibres

do not necessarily reinforce the material but just lead to an overall transversely isotropic structure.

Further, the differences between the stretches λ_2 and λ_3 in the unloaded directions can be described in terms of Hencky-type Poisson's ratios $\nu_{i1}^{\mathrm{H}} = -\ln[\lambda_i]/\ln[\lambda_1]$ for $i = 2, 3$. Therein, ν_{i1}^{H} depict the extensions of the classical linear Poisson's ratio to the finite-deformation regime, as explained by Mihai & Goriely [333]. They are based on the logarithmic Hencky strain, introduced in Section 2.1.5, which for the given diagonal form of the deformation gradient simply reads $\bar{\boldsymbol{E}}_0 = \ln[\lambda_1]\,\boldsymbol{e}_1 \otimes \boldsymbol{e}_1 + \ln[\lambda_2]\,\boldsymbol{e}_2 \otimes \boldsymbol{e}_2 + \ln[\lambda_3]\,\boldsymbol{e}_3 \otimes \boldsymbol{e}_3$. The results for ν_{21}^{H} and ν_{31}^{H} are shown in Figure 8.6b. While the mechanical behaviour exhibits isotropic behaviour for low stretches, hence, $\nu_{21}^{\mathrm{H}} = \nu_{31}^{\mathrm{H}} = 0.5$ for small λ_1-stretches, an anisotropic material behaviour can be observed at higher stretches. In this case, the ratio ν_{31}^{H}, which is related to the muscle fibre direction, significantly increases if compared to ν_{21}^{H}, which is related to the plane that is transverse to the muscle fibre direction. Note, due to the tissue incompressibility, $\nu_{21}^{\mathrm{H}} + \nu_{31}^{\mathrm{H}} = 1$. For the considered deformation scenario, Takaza et al. [471] experimentally measured $\nu_{21}^{\mathrm{H}} = 0.28$ and $\nu_{31}^{\mathrm{H}} = 0.74$. Mohammadkhah et al. [338] reported $\nu_{21}^{\mathrm{H}} = 0.17$ and $\nu_{31}^{\mathrm{H}} = 0.83$. In order to compare these constant values with the results obtained from our approach, we first need to specify the stretch range in which the experimental values were observed. Takaza et al. [471] as well as Mohammadkhah et al. [338] preloaded the tissue specimen before testing. Taking into account the preloading, Takaza et al. [471] observed a nearly constant Poisson's ratio for $1.22 \leq \lambda_1 \leq 1.27$. This range is shaded grey in Figure 8.6b. One can observe from Figure 8.6b that the simulation predicts in this range quite constant Poisson ratios with $\nu_{21}^{\mathrm{H}} \in [0.14, 0.18]$ and $\nu_{31}^{\mathrm{H}} \in [0.82, 0.86]$. Further, the simulation results for this stretch range also agree very well with the experimental results of Mohammadkhah et al. [338].

8.2.4 Simple shear deformation

For a transversely isotropic material with preferred direction $\bar{\boldsymbol{a}} = \boldsymbol{e}_3$, we know that one has to distinguish between a longitudinal (out-of-plane) simple shear $\bar{\boldsymbol{F}} = \boldsymbol{I} + \bar{\gamma}_\ell\,\boldsymbol{e}_3 \otimes \boldsymbol{e}_1$ and a transverse (in-plane) simple shear $\bar{\boldsymbol{F}} = \boldsymbol{I} + \bar{\gamma}_{\mathrm{t}}\,\boldsymbol{e}_2 \otimes \boldsymbol{e}_1$. Further, one can further consider an axisymmetric shear deformation, achieved by applying the uniaxial tension $\bar{\boldsymbol{F}} = \bar{\lambda}_\ell^{-1/2}(\boldsymbol{e}_1 \otimes \boldsymbol{e}_1 + \boldsymbol{e}_2 \otimes \boldsymbol{e}_2) + \bar{\lambda}_\ell\,\boldsymbol{e}_3 \otimes \boldsymbol{e}_3$, in which the stretch $\bar{\lambda}_\ell$ is defined in terms of the axisymmetric shear value $\bar{\gamma}_{\mathrm{a}}$. The model parameters are chosen as previously (see Section 8.2.3).

Figure 8.7a shows the results for three shear modes, hence, axisymmetric, longitudinal and transverse shear deformations $\gamma_j \in [0, 1]$ with $j = \{\mathrm{a}, \mathrm{l}, \mathrm{t}\}$. Therein, the results are presented in terms of the nominal stress quantities $\bar{P}_j = \partial_{\gamma_j} \bar{\mathscr{W}}_j$ for $j = \{\mathrm{a}, \mathrm{l}, \mathrm{t}\}$. The stiffest response is observed for the longitudinal shear, while the axisymmetric shear shows the lowest stress response. The greater stiffness of longitudinal shear modes compared to transverse ones has also been observed in experimental studies by means of shear wave elastography by Papazoglou et al. [368] (see also, for example, Gennisson et al. [157] and Sinkus et al. [443] for anisotropy measurements of muscles and soft tissues via elastography). Note, the collagen fibre stretches, which are due to the three shear modes and which are described by Eqs (8.5), (8.6), (8.7), are visualised in Figures 8.2a, 8.2c, 8.2d, respectively. It has to be pointed out that the distinct stress responses of the three different shear modes are direct consequences of the detailed kinematical description of the collagen

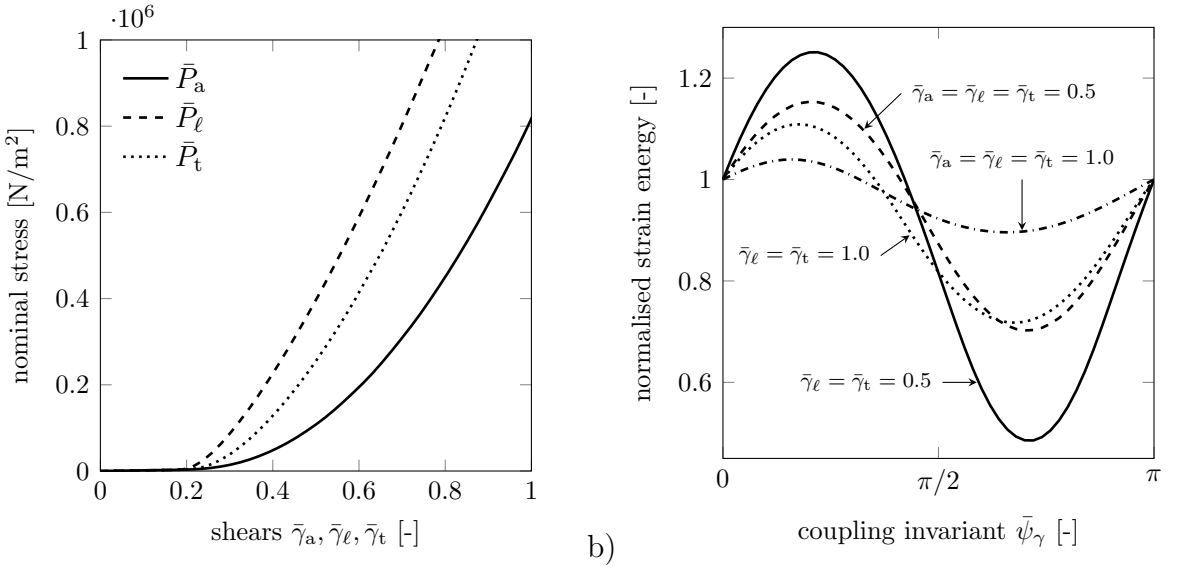

Figure 8.7: a) Comparison of the stresses $\bar{P}_a$, $\bar{P}_\ell$, and $\bar{P}_t$ resulting from axisymmetric, longitudinal and transverse shear deformations, respectively. b) Normalised strain energies $\bar{\mathscr{W}}/\bar{\mathscr{W}}|_{\bar{\psi}_\gamma=0}$ for four different combinations of coupled shear deformations.

fibres described in Eq. (8.4). In contrast, a model that models collagen solely based on the muscle fibre stretch, $\bar{\lambda}_\ell$, as, for example, used by Gindre et al. [163] or Spyrou et al. [459], neglects any collagen contribution during longitudinal and/or transverse shear (due to $\bar{\lambda}_\ell = 1$). Moreover, being able to capture different mechanical responses for longitudinal ($\bar{\gamma}_\ell$) and transverse shear ($\bar{\gamma}_t$), together with the previous reported link between invariant sets $\mathscr{I}^I_{ti}$ and $\mathscr{I}^i_{ti}$, see Eqs (3.93) and (3.96), allows one to conclude a clear dependency of the new model on the macroscopic $\bar{J}_5$-invariant. As a consequence, the proposed macroscopic model naturally depends on invariants $\bar{J}_4$ and $\bar{J}_5$ and not, like for most macroscopically-based muscle models, only on the $\bar{J}_4$-invariant. It is also worth mentioning that the advantage of the presented model is not only that it includes a $\bar{J}_5$-dependence, but that the multiscale framework and the microstructural parameters completely define how this dependency appears on the macroscale. In contrast, Blemker et al. [47] considered a $\bar{J}_5$-dependence and thus different longitudinal and transverse shear stiffnesses in their phenomenological model, but set them equal at last because of the lack of macroscopic experimental data to which the model should have been calibrated.

8.2.5 Coupled shear deformation

Similarly to the investigation of the $\bar{J}_5$-dependence in the previous section, we now investigate the influence of the $\bar{I}_2$-invariant on the overall energy of the new model. With Eqs $(3.97)_5$ and $(3.98)_2$ in mind, this dependency is examined by considering coupled shear deformations and varying the coupling invariant $\bar{\psi}_\gamma$. The influence of $\bar{\psi}_\gamma$ on the collagen fibre stretch $\lambda_{\mathfrak{a}}$ has been shown in Section 8.2.1 and Figure 8.3. Now, to investigate the influence of the coupling invariant $\bar{\psi}_\gamma$ on the overall energy $\bar{\mathscr{W}}$, the following four different deformations will be considered herein: Coupled longitudinal and transverse shear with (i) $\bar{\gamma}_\ell = \bar{\gamma}_t = 0.5$ and (ii) $\bar{\gamma}_\ell = \bar{\gamma}_t = 1.0$, as well as the coupling of all three shear modes with (iii) $\bar{\gamma}_a = \bar{\gamma}_\ell = \bar{\gamma}_t = 0.5$ and (iv) $\bar{\gamma}_a = \bar{\gamma}_\ell = \bar{\gamma}_t = 1.0$. Model parameters are chosen

as previously (see Section 8.2.3). The results for the macroscopic strain energy $\bar{\mathscr{W}}(\bar{\psi}_\gamma)$ normalised to $\bar{\mathscr{W}}|_{\bar{\psi}_\gamma=0}$ are shown in Figure 8.7b. The results reveal a pronounced dependency on the coupling invariant $\bar{\psi}_\gamma$, however, the magnitude shows to be dependent on the applied deformation. From the strong $\bar{\psi}_\gamma$-dependency, it follows that the new model exhibits strong emphasis on the macroscopic $\bar{I}_2$-invariant. We want to stress again that this dependency is also a direct consequence of the microstructural settings and the choice of the microstructurally-based model parameters and does not require any calibration on the macroscale.

8.2.6 Future investigations

The focus in this chapter was to show whether the new multiscale muscle model is able to qualitatively represent typical characteristics of skeletal muscle tissue and its anisotropic properties. Further possible investigations should primarily focus on examining further direction-dependent properties of the material model and comparing them to experimental data. In particular, the model should be investigated for compressive loading scenarios and the associated direction-dependent stress states. Very interesting experimental studies on such scenarios were carried out by Pietsch et al. [371] and Böl et al. [53]. The simulation of compressive loadings is also of interest when examining a characteristic to which Mohammadkhah et al. [338] referred to as tension-compression-asymmetry. They mean by this that they observed that the tensile stress of muscle tissue is about two orders of magnitude higher than the stress under compressive deformations. However, it is very difficult to produce reliable experimental results for this setup, especially because a preload/prestretch is often applied to tissue samples before the tensile test, which complicates the subsequent comparability with the compression tests (which are usually not preloaded). The preloading step before the testing heavily influences the stretch-stress curve because of the flat toe region at lower stretches. Finally, it would be interesting to consider simple shear deformations with regard to the Poynting effect, see Poynting [385]. In this context, Destrade et al. [96] observed that, depending on the orientation of the tissue sample, simple shear deformations of biological materials can be associated by a negative or a positive Poynting effects. Appropriate investigations would give further insights into the anisotropic characteristics of muscle tissue and could represent a further validation of the here presented muscle model.

9 Conclusion & Outlook

Es soll sich regen, schaffend handeln,
Erst sich gestalten, dann verwandeln;
Nur scheinbar steht's Momente still.
Das Ewige regt sich fort in allen;
Denn alles muß in Nichts zerfallen,
Wenn es im Sein beharren will.

Johann Wolfgang von Goethe

This work dealt with continuum-mechanical methods for the multiscale modelling of materials and the subsequent formulation of a novel microstructurally-based multiscale material model for skeletal muscle tissue. After a detailed discussion of the principles of continuum mechanics and constitutive material theory, the work provided a comprehensive introduction of the basic concepts of scale transition and homogenisation concepts. These approaches are particularly necessary when classical single-scale modelling approaches are not applicable, either because there is insufficient large-scale data available or more insights into small-scale effects of the material are desired. This is especially the case when considering (soft) biological tissues and in particular for skeletal muscle tissue.

The concluding remarks in this chapter primarily focus on the two most important results of the present work. This is firstly the formulation of novel analytical estimates for the effective strain energy of two-phase materials and secondly the introduction of a multiscale approach for the modelling of skeletal muscle tissue.

An analytical estimate for hyperelastic two-phase composites In Chapter 5 of this thesis, a novel *estimate for the effective stored energy of a two-phase composite with aligned fibrous microstructure and hyperelastic, incompressible, anisotropic phases* was derived. The estimate is based on the tangent second-order homogenisation method proposed by Ponte Castañeda & Tiberio [382]. The method is consistently adapted for scenarios that are particularly important for the modelling of biological soft tissue, which in particular includes the case that the phases are anisotropic and incompressible. To take into account the incompressibility of the fibre phase, we performed an asymptotic analysis of the deformation field in the fibre phase, which resulted in a consistent constraint equation for the phase average of the fibre and an additional constraint pressure term. By doing so, the constraint pressure induces in the fibre phase an additional hydrostatic stress component and provides a replacement for the volumetric terms, which would become indeterminate in the incompressible fibre limit. Further, we performed an asymptotic analysis to get regular expressions of the underlying equations in the incompressible matrix limit. To obtain the resulting estimate for incompressible and generally anisotropic phases requires one to solve for *six scalar unknowns*, which are the five unknown coefficients of the average fibre deformation gradient $\bar{\boldsymbol{F}}_{\mathrm{F}}$ and the constraint pressure $\wp$. This can easily be done numerically. If the two phases exhibit transversely isotropic behaviour and the preferred directions are collinear to the alignment of the fibrous inclu-

sions, then the number of unknown coefficients of $\bar{\boldsymbol{F}}_{\mathrm{F}}$ reduces from six to four. Further, if the phases are described as augmented isotropic materials with anisotropic J_4-dependent contributions, then one can additively split the overall effective energy and homogenise the J_4-dependent anisotropic phase energies with a simple Voigt-type averaging. This result is quite remarkable and useful for most fibre-embedded materials that are typically modelled by superimposing a mildly nonlinear isotropic part with a highly nonlinear J_4-dependent anisotropic contribution. For such materials, the homogenised nonlinear term can be efficiently obtained by employing an easy-to-handle Voigt-type averaging. Besides exhibiting a high degree of accuracy for most of the relevant scenarios, the biggest advantage of the proposed TSO method is probably its relatively simple and handleable structure and its applicability to very general phase properties. This generality is very important, in particular, for applications to biological tissues.

A multiscale framework for the modelling of skeletal muscle tissue One main goal of this thesis was the detailed introduction and discussion of a *multiscale continuum-mechanical modelling framework* for the description of skeletal muscle tissue. The key feature of this model is that the macroscopic material response is entirely based on the mechanical description of the material characteristics and composition on smaller scales. In detail, a *two-phase model* was proposed and the two phases were identified as the muscle fibres and the extracellular matrix (the collageneous tissues). Differentiating between muscle fibre and extracellular matrix has the advantage that the mechanical (or other) properties of the two phases can be described individually, as opposed to a macroscopic single-scale modelling approach. This is beneficial as there often exist more comprehensive and *higher quality experimental data for microscopic constituents* than on the macroscale. The descriptions of the phases and the application of analytical homogenisation schemes entailed a constitutive muscle model for the macroscopic behaviour of skeletal muscle tissue with eight model parameters. The key advantage of this approach is that the parameters have *direct microstructural meanings*. Moreover, this novel modelling approach does not require any calibration on the macroscale, on which data obtained from experiments are rather uncertain, limited, simplified, and error-prone. This clearly differentiates the proposed model from single-scale material models, in which the material parameters are obtained (and limited) through extensive macroscopic calibration to experimental data. Five of the eight model parameters are structural parameters and can ideally be determined by utilising image-based methods, which means that no material tests are necessary. The remaining three material parameters in the new model are directly related to the stiffness of microstructural components, for which extensive and reliable data is available in the literature. Further, as a consequence of the multiscale approach, macroscopic material characteristics like incompressibility and transverse isotropy follow *directly from the microscopic considerations* and are not added as constitutive assumptions on the macroscale. In this sense, the presented results focused on emphasising the model capability of predicting macroscopic characteristics directly from the microstructural settings. For instance, it was shown that the transversely isotropic framework relies on all five strain invariants, while for macroscopic single-scale muscle models the dependencies have to be included in a constitutive fashion. The results presented in this thesis are based on a Voigt assumption, which means that the deformation in the microstructure is assumed to be uniform. This is an appropriate assumption for healthy muscle tissue and sufficient to demonstrate the qualitative capabilities of the model. However, the microstructure and the composition of

living tissues can undergo severe changes and the assignment of modelling assumptions is a highly dynamic process. For example, the consideration of diseased tissue, in which the strong integration of the microstructural components is no longer given, requires that the microscopic deformation is calculated on the basis of a *variational minimisation principle*. Such an approach was introduced in this work by means of an estimate based on the also presented TSO homogenisation method.

The new modelling framework offers great potential for a variety of applications, in particular for scenarios where the microstructure of the muscle tissue undergoes *morphological changes*. Such structural changes are often associated with diseases and pathological conditions and can be directly included in the model through the adaption of the respective microstructurally-based model parameters. The advantage in connection with the multiscale model is that there is rich literature and a large number of studies that deal in detail with the accompanying changes in the microstructure and provide much data that can be used for the model. Diseases and phenomena that were considered in such a way are for example immobilisation by Hibino et al. [204] and Jalal et al. [246], cerebral palsy by Smith et al. [452], abberant repair and development of fibrosis by Mann et al. [309], botulinum neurotoxin therapies in patients with spasticity by Thacker et al. [476], and stroke by Jalal et al. [246]. The model can also be combined with studies on remodelling processes in the collageneous structures, such as those of Kuhl et al. [267] and Menzel & Waffenschmidt [321]. The same applies for problems such as failure and rupture of single collagen fibres, see Cacho et al. [66] or Veres & Lee [492]. A very promising extension would also be the combination with agent-based models, such as the ones by Martin et al. [317] or Lee et al. [282], to be able to simulate growth and atrophy processes in the tissue or phenomena like wound healing. Some of the mentioned applications may require appropriate extensions of the presented model and it has to be investigated whether this only affects the energy formulations of the two phases or even requires the addition of a third phase. For instance, pathological cases which are accompanied by high volume fractions of intramuscular fat might require the formulation of three-phase models and the consideration of appropriate constitutive models for fat tissue, see Mihai et al. [332].

An indispensable part of future studies is the further investigation of the mechanical structure of the muscle fibre and respective extensions of the multiscale muscle model. The here considered experimental data set a solid foundation for assuming a nearly-linear behaviour of the muscle fibre in this work. Yet, possible anisotropy and more distinct nonlinearity of the muscle fibre, as observed by, for example, Linke et al. [290], should be investigated. Without a doubt, however, the incorporation of active contractile effects is the most important upcoming extension of the model. Ideally, this is done by directly describing the elastic energy in the sarcomeres, especially in the actin, myosin and titin proteins. This way, the active behaviour can be directly integrated into the multiscale model by describing the increased elastic potential of the activated muscle fibre.

Finally, it should be noted that an extended multiscale model may lead to considerable additional computational effort and can only be used to a limited extent for some applications, such as for the implementation in finite-element software. In such cases, it could be helpful to utilise surrogate models, as proposed by Wirtz et al. [520], or to correlate the microstructurally-based model parameters with those of generic and easy-to-handle strain-energy functions, such as shown by Marino et al. [311].

Epilogue

Some comments on the concept of phenomenology

If one deals with multiscale modelling and the corresponding literature, one inevitably comes across the concept of *phenomenology*. Unfortunately, however, the term is often given a negative connotation when used in the context of continuum mechanics. In many cases it is employed to describe models that are not based on multiscale approaches, often with the addition "only". Such comparisons are intended to show the superiority of any kinds of special models over such which are "only phenomenological". The author does not know when this became common in the continuum-mechanical community (maybe it is also elsewhere), but it must be said that I unfortunately also used such terms myself. That was before I was made aware[1] that phenomenology is not just a loose term but a philosophical school that is concerned with the structures of experience and consciousness. It is particularly connected to the Austrian-German philosopher and mathematician Edmund Gustav Albrecht Husserl (1859-1938). On the contrary, I am (clearly) not a philosopher, but I believe that I have understood the basic ideas of phenomenology to such an extent that I can say that the use of the term in continuum mechanics should be enjoyed with more caution. To explain this briefly, we have to note that the concept of observable *phenomena* is (obviously) the central construct of phenomenology. This can be, for example, an experimentally measured stress-strain curve (hence, an observed material behaviour). The observation of such phenomena is thereby regarded as a decisive step for gaining knowledge[2]. Applied to the basic problem of continuum mechanics, which is finding appropriate constitutive formulations, this means that the description of the phenomenon "stress-strain curve" by means of suitable mathematical tools is a proper phenomenological approach. If this is done correctly, this approach *cannot* be wrong or insufficient. A phenomenological approach guarantees an unbiased and objective view on the things as they are and it does not require any further subjective opinion of the observer. However, problems may arise if the procedure is not based on the description of observed phenomena. An example for this comes from skeletal muscle modelling: For a long time, experiments on muscle tissue were mainly (if not even exclusively) performed in a uniaxial manner along the muscle fibre. This would be sufficient for the description of the material behaviour exactly for this deformation state. Yet, in a three-dimensional setting, one needs to describe the material behaviour also for other loadings and, for instance, requires the stiffness of the material across the muscle fibre, too. The existence of fibres in the material has led some researchers to assume that muscle is a fibre-*reinforced* material and that the stiffness of the material in the transverse plane would be lower. However, a number of recent experiments[3] led to the generally accepted assumption that the transverse direction is even stiffer. A critical statement now would be that the incorrect modelling was due to the "inadequate phenomenological models" and that better models were needed. This is of course wrong. The falsity of the assumption that muscle is a fibre-reinforced material is

[1] One of the reasons was reading the novel *Schlafende Sonne* by Thomas Lehr.

[2] A beautiful German word for this is *Erkenntnisgewinn* and describes what should always be the uppermost maxim in (not only, but most of all) scientific research.

[3] See the references in the main text.

because of a lack of proper phenomenology in the modelling process. In order to describe the material behaviour transverse to the muscle fibre, one should observe the corresponding phenomenon first, namely a proper experimental stress-strain curve for this type of loading. The observation that muscle tissue contains fibres a priori has nothing to do with the objective assessment of the transverse mechanical behaviour. However, of course, it can help to deduce the material symmetry properties of the material and to perform the necessary material testing.

Now, to jump forward a little bit, I want to comment on the fact that multiscale modelling approaches are often considered as a superior alternative to phenomenological approaches. I do not agree with that. Using multiscale modelling approaches does not (must not!) prevent from following the ideas of phenomenology. It is in fact ridiculous to think that a multiscale approach would be non-phenomenological. Even if a model includes smaller scales, like a continuum-mechanical microscale (for instance in the range of micrometres), it is in a physical sense still "macroscopic" and relies on phenomenological concepts like pressure, volume, temperature, heat, and work (or even mass). Further, the constitutive modelling is in multiscale approaches just shifted from larger to smaller scales, but is of course still necessary. In turn, this modelling step still demands for a proper description of the experimentally derived stress-strain curves (phenomena!) of the phases on smaller scales.

This short excursion may provide some clarifications for the classification[4] of different methods and models in continuum mechanics. The author thinks that an attempt should be made to avoid incorrect use and the associated discrediting of an entire philosophical study. For a lot of applications in continuum mechanics, for instance, the pairing "multiscale models and single-scale models" seems to be a better distinguishing feature than the misleading pairing "multiscale and phenomenological".

To conclude the present thoughts and to emphasise the importance of the term phenomenon once more, we quote Clifford Truesdell [490]:

> *"The task of the theorist is to bring order into the chaos of the phenomena of nature, to invent a language by which a class of these phenomena can be described efficiently and simply."*

A comment on the law of parsimony in multiscale modelling

The modelling of materials by means of a multiscale approach may possibly result in a large set of model parameters. This is because the properties of a variety of small-scale structures and their interactions have to be included and accounted for. In this work, for instance, the multiscale muscle model contains eight model parameters, see Table 8.1. I

[4] In biomechanics, one also finds the pairing "phenomenological versus biophysical". This is also not fully appropriate. In addition to the fact that a model cannot be non-phenomenological, a model which aims on describing a biological material (or system) that is not biophysical would be very poor. To see this, we have to consult the definition of biophysics that is provided by the *Biophysical Society*: "Biophysics is the field that applies the theories and methods of physics to understand how biological systems work." (https://www.biophysics.org/what-is-biophysics). Any kind of model should be based on physics (for example the physical balance relations) and the term "biophysical" is not completely suitable to distinguish it from other methods. For example, also a simple Neo-Hookean material model can be named biophysical if it properly describes the behaviour of a biological material.

made the experience that this number of parameters makes some people think that the modelling would conflict with the *law of parsimony* and ideas like Occam's razor. However, this objection is inappropriate. The set of model parameters that results from a modelling ansatz across several scales usually does not have the meaning of "fitting parameters", whose only task is to ensure that an existing stress-strain curve is exactly reproduced. The multiscale approach is therefore not in competition with a simpler (single-scale) constitutive material description, since it does not have the task of being calibratable to the macroscopic behaviour, but rather provides further insights and relationships between small-scale structures. Lokshin & Lanir [294] formulated a very descriptive explanation and clarification in the context of their model:

> *"A common objection is that under high number of parameters, a model can fit to a wide spectrum of behaviors merely by virtue of the high number of adjustable parameters. While this is a valid objection, especially in phenomenological models, the present case of structure-based formulation is different, and for several reasons: first, the parameters represent entities having well defined structural or mechanical significance which are key determinants of the tissue's response. Hence the parameters are not mere mathematical factors, as is the case in phenomenological models."*

Appendix

A Tensor calculus

This appendix provides some basics and explanations on tensor calculus. The notation used in this work mainly follows the book of DE BOER [51] and the thereon based lecture notes of EHLERS [107]. Important parts of DE BOER's book [51], originally in German, can also be found as English translation in the appendix of DE BOER [52]. We refer the reader to these very comprehensive works for a more general introduction to the field of vectors and tensors and the very basics of tensor calculus, like distributive or commutative properties of tensor multiplications, fundamentals of vector and tensor analysis as well as integral theorems and further topics. Further extensive explanations can also be found in the book of ITSKOV [243], wherein however the notation might differ to the herein employed. In this appendix, we will give a rather pragmatic overview specialised to the needs of this work. Calculation rules may be introduced without a proof and we refer to the mentioned literature for further details.

A.1 Basics

With few exceptions, we denote scalars (zeroth-order tensors) by light small letters $\{a, b, c, \dots\} \in \mathcal{R}$ or Greek letters $\{\alpha, \beta, \gamma, \dots\} \in \mathcal{R}$. Yet, especially Greek letters might have fixed meanings for specific quantities. Vectors (first-order tensors) are usually denoted by small boldface letters $\{\boldsymbol{a}, \boldsymbol{b}, \boldsymbol{c}, \dots\} \in \mathcal{R}^n$, where n stands for the dimensionality of the vector, which is a three-dimensional Euclicdian space in this work. Their index notation is given by $\boldsymbol{a} = a_i\, \boldsymbol{e}_i$, where a_i is a vector of coefficients, $\boldsymbol{e}_i$ is the Cartesian basis, and i ranges from 1 to n such that $i = 1, 2, 3$ for $n = 3$. With some abuse of the convention, some vectors are indicated by capital letters to highlight their referential representation in contrast to their actual one. Second-order tensors are mostly denoted by boldface capital letters $\{\boldsymbol{A}, \boldsymbol{B}, \boldsymbol{C}, \dots, \boldsymbol{\mathscr{A}}, \boldsymbol{\mathscr{B}}, \boldsymbol{\mathscr{C}}, \dots\} \in \mathcal{R}^{n\otimes n}$. Their index notation reads $\boldsymbol{A} = A_{ij}\, \boldsymbol{e}_i \otimes \boldsymbol{e}_j$, where (mostly) $i, j = 1, 2, 3$. The dyadic product "$\otimes$" defines an outer product, such that, for instance, two vectors result in a second-order tensor $\boldsymbol{a} \otimes \boldsymbol{b} = a_i b_j\, \boldsymbol{e}_i \otimes \boldsymbol{e}_j$. Two vectors can as well be connected by a dot product "$\cdot$", such that $\boldsymbol{a} \cdot \boldsymbol{b} = a_i b_i$. Therein and elsewhere, the occurrence of double indices demands the usage of the *Einstein summation convention*, which means that, for instance, $a_i b_i$ serves as a shorthand notation of the sum $\sum_{i=1}^{n} a_i b_i$. In this work, the dot product always defines an inner product with a scalar as result, hence, $\boldsymbol{a} \cdot \boldsymbol{b} = \langle \boldsymbol{a}, \boldsymbol{b} \rangle$. When applied to higher than first-order tensors, this means that the single dot does not indicate a simple contraction. Multiplications between second-order tensors can be a scalar dot product $\boldsymbol{A} \cdot \boldsymbol{B} = \langle \boldsymbol{A}, \boldsymbol{B} \rangle = A_{ij} B_{ij}$, cross and double cross products as defined in Section A.2, a tensor product (simple contraction) $\boldsymbol{AB} = A_{ik} B_{kj}\, \boldsymbol{e}_i \otimes \boldsymbol{e}_j$, or a dyadic (outer) tensor product $\boldsymbol{A} \otimes \boldsymbol{B} = A_{ij} B_{jk}\, \boldsymbol{e}_i \otimes \boldsymbol{e}_j \otimes \boldsymbol{e}_k \otimes \boldsymbol{e}_l$. Therein, the simple contraction as well as contractions in general are carried out by utilising the *Kronecker delta* symbol, as defined in Eq. (A.1). Hence, $\boldsymbol{AB} = (A_{ij}\, \boldsymbol{e}_i \otimes \boldsymbol{e}_j)\, (B_{kl}\, \boldsymbol{e}_k \otimes \boldsymbol{e}_l) = A_{ij} B_{kl} \delta_{jk}\, \boldsymbol{e}_i \otimes \boldsymbol{e}_l = A_{ij} B_{jl}\, \boldsymbol{e}_i \otimes \boldsymbol{e}_l$. Moreover, fourth-order tensor are usually denoted by blackboard bold capital letters $\{\mathbb{A}, \mathbb{B}, \mathbb{C}\} \in \mathcal{R}^{n\otimes n\otimes n\otimes n}$. Their index notation is given by $\mathbb{A} = \mathrm{A}_{ijkl}\, \boldsymbol{e}_i \otimes \boldsymbol{e}_j \otimes \boldsymbol{e}_k \otimes \boldsymbol{e}_l$, where the four-dimensional coefficient matrix is designated by an upright capital letter (in contrast to italic capital letters for second-order tensors). Furthermore, the rather rarely

used third-order tensors are written as $\underline{\boldsymbol{A}^3} = A^3_{ijk}\, \boldsymbol{e}_i \otimes \boldsymbol{e}_j \otimes \boldsymbol{e}_k$, whereas sixth-order tensors read $\underline{\mathbb{A}^6} = \mathrm{A}^{\underline{6}}_{ijklst}\, \boldsymbol{e}_i \otimes \boldsymbol{e}_j \otimes \boldsymbol{e}_k \otimes \boldsymbol{e}_l \otimes \boldsymbol{e}_s \otimes \boldsymbol{e}_t$. Products of tensors of equal order result in tensors of the same order. This settles the required number of contractions, hence, $\boldsymbol{A}\boldsymbol{B} = \boldsymbol{C}$ (simple contraction) and $\mathbb{A}\mathbb{B} = \mathbb{C}$ (double contraction). If a tensor is applied on a tensor of lower order, the order difference of these two defines the order of the resulting tensor and the required number of contractions, hence, $\boldsymbol{A}\boldsymbol{a} = \boldsymbol{b}$ (simple contraction) and $\mathbb{A}\boldsymbol{A} = \boldsymbol{B}$ (double contraction). Finally, the transposition of second-order tensors gives $\boldsymbol{A}^T = A_{ji}\, \boldsymbol{e}_i \otimes \boldsymbol{e}_j = A_{ij}\, \boldsymbol{e}_j \otimes \boldsymbol{e}_i$. Any second-order tensor $\boldsymbol{A}$ can be decomposed into a symmetric part $\mathrm{sym}[\boldsymbol{A}] = (\boldsymbol{A} + \boldsymbol{A}^T)/2 = \mathrm{sym}[\boldsymbol{A}]^T$ and a skew-symmetric part $\mathrm{skw}[\boldsymbol{A}] = (\boldsymbol{A} - \boldsymbol{A}^T)/2 = -\mathrm{skw}[\boldsymbol{A}]^T$, such that $\boldsymbol{A} = \mathrm{sym}[\boldsymbol{A}] + \mathrm{skw}[\boldsymbol{A}]$. In turn, a tensor $\boldsymbol{A}$ is symmetric if $\mathrm{skw}[\boldsymbol{A}] = \boldsymbol{0}$. Transpositions of third and higher-order tensors require an indication such as $\mathbb{A}^{T_{ij}}$, where the transposition consequently denotes an interchanging of the i-th and j-th basis. Remarks on the different symmetry properties of fourth-order tensors are provided in Section A.7.2.

A.2 Fundamental tensors

The introduction of an important set of fundamental (identity) tensors relies on the definition of the *Kronecker delta*:

$$\delta_{ij} = \begin{cases} 1 & \text{if } i = j \\ 0 & \text{if } i \neq j\,. \end{cases} \tag{A.1}$$

This means that in a three-dimensional space, where $i, j = 1, 2, 3$, the only non-zero combinations are $\delta_{11} = \delta_{22} = \delta_{33} = 1$. Based on the Kronecker delta, the following quantities are introduced:

- The second-order fundamental (identity) tensor:

$$\boldsymbol{I} = \delta_{ij}\, \boldsymbol{e}_i \otimes \boldsymbol{e}_j : \quad \begin{cases} \boldsymbol{I}\boldsymbol{u} = \boldsymbol{u} \\ \boldsymbol{I}\boldsymbol{A} = \boldsymbol{A} \end{cases} \quad : \text{identical map} \tag{A.2}$$

- The fourth-order fundamental tensors:

$$\begin{aligned} \mathbb{I} = (\boldsymbol{I} \otimes \boldsymbol{I})^{T_{23}} : &\quad \begin{cases} \mathbb{I}\,\boldsymbol{A} = \boldsymbol{A} \\ \mathbb{I}\,\mathbb{A} = \mathbb{A} \end{cases} && : \text{identical map} \\ \mathbb{I}_T = (\boldsymbol{I} \otimes \boldsymbol{I})^{T_{24}} : &\quad \mathbb{I}_T\,\boldsymbol{A} = \boldsymbol{A}^T && : \text{transposing map}^1 \\ \mathbb{I}_{\mathrm{tr}} = \boldsymbol{I} \otimes \boldsymbol{I} \quad : &\quad \mathbb{I}_{\mathrm{tr}}\,\boldsymbol{A} = \mathrm{tr}[\boldsymbol{A}]\boldsymbol{I} && : \text{tracing map} \\ \mathbb{I}_{\mathrm{sym}} = \tfrac{1}{2}(\mathbb{I} + \mathbb{I}_T) \ : &\quad \mathbb{I}_{\mathrm{sym}}\,\boldsymbol{A} = \mathrm{sym}[\boldsymbol{A}] && : \text{symmetrising map}^1 \end{aligned} \tag{A.3}$$

- The sixth-order fundamental tensor

$$\underline{\mathbb{I}^6} = ((\boldsymbol{I} \otimes \boldsymbol{I} \otimes \boldsymbol{I})^{T_{35}})^{T_{24}} : \qquad \underline{\mathbb{I}^6}\,\underline{\boldsymbol{B}^3} = \underline{\boldsymbol{B}^3} \quad : \text{identical map} \tag{A.4}$$

[1] Note that the transposing and the symmetrising maps become identical maps in the space of symmetric second-order tensors, meaning that $\mathbb{I}_T\,\boldsymbol{A} = \mathbb{I}_{\mathrm{sym}}\,\boldsymbol{A} = \mathbb{I}\,\boldsymbol{A} = \boldsymbol{A}$ if $\boldsymbol{A} \in \mathcal{SYM}(3)$.

Another class of fundamental tensors relies on the introduction of the *Levi-Civita symbol*

$$\epsilon_{ijk} = \begin{cases} 1 & \text{even permutation} \\ 0 & \text{double indexing} \\ -1 & \text{odd permutation.} \end{cases} \tag{A.5}$$

This means that the only non-zero combinations are $\epsilon_{123} = \epsilon_{231} = \epsilon_{312} = 1$ and $\epsilon_{321} = \epsilon_{213} = \epsilon_{132} = -1$. Based on the Levi-Civita symbol, we obtain the following quantities:

- The third-order fundamental (permutation) tensor

$$\boldsymbol{\mathcal{E}} = \epsilon_{ijk}\, \boldsymbol{e}_i \otimes \boldsymbol{e}_j \otimes \boldsymbol{e}_k : \quad \begin{cases} \boldsymbol{u} \times \boldsymbol{v} = \boldsymbol{\mathcal{E}}(\boldsymbol{u} \otimes \boldsymbol{v}) & : \text{vector cross product} \\ \boldsymbol{A} \times \boldsymbol{B} = \boldsymbol{\mathcal{E}}(\boldsymbol{A}\boldsymbol{B}^T) & : \text{tensor cross product} \end{cases} \tag{A.6}$$

- The sixth-order permutation tensor:

$$\underline{\boldsymbol{\mathcal{E}}}^6 = (((\boldsymbol{\mathcal{E}} \otimes \boldsymbol{\mathcal{E}})^{T_{45}})^{T_{35}})^{T_{23}}: \qquad \boldsymbol{A} \gg \boldsymbol{B} = \underline{\boldsymbol{\mathcal{E}}}^6(\boldsymbol{A} \otimes \boldsymbol{B}) \quad : \text{tensor double cross product} \tag{A.7}$$

A.3 Selected rules of tensor calculus

Selected rules for the trace, transpose, inverse, determinant and cofactor:

$$\operatorname{tr}[\boldsymbol{A}] = \boldsymbol{A} \cdot \boldsymbol{I} \tag{A.8}$$
$$\operatorname{tr}[\boldsymbol{A}\boldsymbol{B}] = \boldsymbol{A}\boldsymbol{B} \cdot \boldsymbol{I} = \boldsymbol{A}^T \cdot \boldsymbol{B} = \boldsymbol{A} \cdot \boldsymbol{B}^T \tag{A.9}$$
$$(\boldsymbol{A}\boldsymbol{B})^T = \boldsymbol{B}^T\boldsymbol{A}^T \tag{A.10}$$
$$(\boldsymbol{A}\boldsymbol{B})^{-1} = \boldsymbol{B}^{-1}\boldsymbol{A}^{-1} \tag{A.11}$$
$$\operatorname{tr}[\boldsymbol{A}\boldsymbol{B}] = \boldsymbol{A}\boldsymbol{B} \cdot \boldsymbol{I} = \boldsymbol{A}^T \cdot \boldsymbol{B} = \boldsymbol{A} \cdot \boldsymbol{B}^T \tag{A.12}$$
$$\det[\boldsymbol{A}^T] = \det[\boldsymbol{A}] \tag{A.13}$$
$$\det[\alpha\boldsymbol{A}] = \alpha^3 \det[\boldsymbol{A}] \tag{A.14}$$
$$\det[\boldsymbol{A}\boldsymbol{B}] = \det[\boldsymbol{A}] \det[\boldsymbol{B}] \tag{A.15}$$
$$\det[\boldsymbol{A} + \boldsymbol{B}] = \det[\boldsymbol{A}] + \operatorname{cof}[\boldsymbol{A}] \cdot \boldsymbol{B} + \boldsymbol{A} \cdot \operatorname{cof}[\boldsymbol{B}] + \det[\boldsymbol{B}] \tag{A.16}$$
$$\operatorname{cof}[\boldsymbol{A}\boldsymbol{B}] = \operatorname{cof}[\boldsymbol{A}] \operatorname{cof}[\boldsymbol{B}] \tag{A.17}$$
$$\operatorname{cof}[\boldsymbol{A}^T] = (\operatorname{cof}[\boldsymbol{A}])^T = \operatorname{cof}[\boldsymbol{A}]^T \tag{A.18}$$
$$\operatorname{cof}[\alpha\boldsymbol{A}] = \alpha^2 \operatorname{cof}[\boldsymbol{A}] \tag{A.19}$$

Selected rules for the divergence operator:

$$\left.\begin{aligned} \operatorname{Div}[\boldsymbol{A}\boldsymbol{u}] &= \boldsymbol{A}^T \cdot \operatorname{Grad}[\boldsymbol{u}] + \operatorname{Div}[\boldsymbol{A}^T] \cdot \boldsymbol{u} \\ \operatorname{Div}[A_{ij} u_j\, \boldsymbol{e}_i] &= A_{ij} u_{j,i} + A_{ij,i} u_j \end{aligned}\right\} \tag{A.20}$$

$$\left.\begin{aligned} \operatorname{Div}[\boldsymbol{u} \otimes \boldsymbol{A}] &= \boldsymbol{u} \otimes \operatorname{Div}[\boldsymbol{A}] + \operatorname{Grad}[\boldsymbol{u}]\boldsymbol{A}^T \\ \operatorname{Div}[u_i A_{jk}\, \boldsymbol{e}_i \otimes \boldsymbol{e}_j \otimes \boldsymbol{e}_k] &= (u_i A_{jk,k} + u_{i,k} A_{jk})\, \boldsymbol{e}_i \otimes \boldsymbol{e}_j \end{aligned}\right\} \tag{A.21}$$

$$\left.\begin{aligned} \mathrm{Div}[\boldsymbol{A}\otimes\boldsymbol{u}] &= \boldsymbol{A}\otimes\mathrm{Div}[\boldsymbol{u}] + \mathrm{Grad}[\boldsymbol{A}]\boldsymbol{u} \\ \mathrm{Div}[A_{ij}u_k\,\boldsymbol{e}_i\otimes\boldsymbol{e}_j\otimes\boldsymbol{e}_k] &= (A_{ij}u_{k,k} + A_{ij,k}u_k)\,\boldsymbol{e}_i\otimes\boldsymbol{e}_j \end{aligned}\right\} \tag{A.22}$$

$$\left.\begin{aligned} \mathrm{Div}[(\boldsymbol{A}\otimes\boldsymbol{u})^{T_{23}}] &= \boldsymbol{A}\otimes\mathrm{Grad}^T[\boldsymbol{u}] + \mathrm{Div}[\boldsymbol{A}]\otimes\boldsymbol{u} \\ \mathrm{Div}[A_{ik}u_j\,\boldsymbol{e}_i\otimes\boldsymbol{e}_j\otimes\boldsymbol{e}_k] &= (A_{ik}u_{j,k} + A_{ik,k}u_j)\,\boldsymbol{e}_i\otimes\boldsymbol{e}_j \end{aligned}\right\} \tag{A.23}$$

Selected integral theorems:

$$\int_{\mathcal{V}}\mathrm{Grad}[\boldsymbol{u}]\,\mathrm{d}V = \int_{\partial\mathcal{V}}\boldsymbol{u}\otimes\boldsymbol{N}\mathrm{d}A \tag{A.24}$$

$$\int_{\mathcal{V}}\mathrm{Div}[\boldsymbol{u}]\,\mathrm{d}V = \int_{\partial\mathcal{V}}\boldsymbol{u}\cdot\boldsymbol{N}\mathrm{d}A \tag{A.25}$$

$$\int_{\mathcal{V}}\mathrm{Div}[\boldsymbol{A}]\,\mathrm{d}V = \int_{\partial\mathcal{V}}\boldsymbol{A}\boldsymbol{N}\mathrm{d}A \tag{A.26}$$

$$\int_{\mathcal{V}}\mathrm{Div}[\boldsymbol{A}^{\underline{3}}]\,\mathrm{d}V = \int_{\partial\mathcal{V}}\boldsymbol{A}^{\underline{3}}\boldsymbol{N}\mathrm{d}A \tag{A.27}$$

A.4 The (outer) tensor double cross product

The (outer) tensor double cross product between two second-order tensors $\boldsymbol{A}\in\mathcal{R}^{3\otimes3}$ and $\boldsymbol{B}\in\mathcal{R}^{3\otimes3}$ is introduced in terms of the sixth-order permutation tensor $\boldsymbol{\mathcal{E}}^{\underline{6}}$ in Eq. (A.7). The double cross product preserves the order of the two input tensors and results in a second-order tensor as well. In index notation, it reads

$$\boldsymbol{A}\gg\!\ll\boldsymbol{B} \;=\; A_{kl}\,B_{st}\,\epsilon_{ksi}\,\epsilon_{ltj}\,\boldsymbol{e}_i\otimes\boldsymbol{e}_j\,, \tag{A.28}$$

where ϵ is the Levi-Civita symbol that has been defined in Eq. (A.5). The double cross product is related to the vector cross product via

$$(\boldsymbol{A}\gg\!\ll\boldsymbol{B})(\boldsymbol{u}\times\boldsymbol{v}) \;=\; \boldsymbol{A}\boldsymbol{u}\times\boldsymbol{B}\boldsymbol{v} \;-\; \boldsymbol{A}\boldsymbol{v}\times\boldsymbol{B}\boldsymbol{u}\,, \tag{A.29}$$

where $\boldsymbol{u}\in\mathcal{R}^3$ and $\boldsymbol{v}\in\mathcal{R}^3$ are two arbitrary vectors. Some basic calculation rules of the double cross product are

$$\boldsymbol{A}\gg\!\ll\boldsymbol{B} = \boldsymbol{B}\gg\!\ll\boldsymbol{A}\,, \tag{A.30}$$

$$(\boldsymbol{A}\gg\!\ll\boldsymbol{B})^T = \boldsymbol{A}^T\gg\!\ll\boldsymbol{B}^T\,, \tag{A.31}$$

$$(\boldsymbol{A}\gg\!\ll\boldsymbol{B})\cdot\boldsymbol{C} = (\boldsymbol{B}\gg\!\ll\boldsymbol{C})\cdot\boldsymbol{A} = (\boldsymbol{C}\gg\!\ll\boldsymbol{A})\cdot\boldsymbol{B}\,. \tag{A.32}$$

Some useful identities in terms of the trace operator are given by

$$\boldsymbol{A}\gg\!\ll\boldsymbol{B} = (\mathrm{tr}[\boldsymbol{A}]\,\mathrm{tr}[\boldsymbol{B}] - \mathrm{tr}[\boldsymbol{A}\boldsymbol{B}])\boldsymbol{I} - \mathrm{tr}[\boldsymbol{A}]\boldsymbol{B}^T - \mathrm{tr}[\boldsymbol{B}]\boldsymbol{A}^T + \boldsymbol{A}^T\boldsymbol{B}^T + \boldsymbol{B}^T\boldsymbol{A}^T\,, \tag{A.33}$$

$$\boldsymbol{A}\gg\!\ll\boldsymbol{A} = (\mathrm{tr}[\boldsymbol{A}]^2 - \mathrm{tr}[\boldsymbol{A}^2])\boldsymbol{I} + 2(\boldsymbol{A}^T - \mathrm{tr}[\boldsymbol{A}]\boldsymbol{I})\boldsymbol{A}^T\,, \tag{A.34}$$

$$\boldsymbol{A}\gg\!\ll\boldsymbol{I} = \mathrm{tr}[\boldsymbol{A}]\boldsymbol{I} - \boldsymbol{A}^T\,. \tag{A.35}$$

The double cross product offers a very pleasant notation for operations like the cofactor, the determinant, and the inverse of a tensor and allows to write them in a compact and closed-form way. Doing so, for an arbitrary second-order tensor $\boldsymbol{A}$ these quantities read

$$\mathrm{cof}[\boldsymbol{A}] = \tfrac{1}{2}(\boldsymbol{A}\gg\!\ll\boldsymbol{A})\,,\quad \det[\boldsymbol{A}] \;=\; \tfrac{1}{6}(\boldsymbol{A}\gg\!\ll\boldsymbol{A})\cdot\boldsymbol{A}\,,\quad \text{and}\quad \boldsymbol{A}^{-1} = \frac{3\,\boldsymbol{A}^T\gg\!\ll\boldsymbol{A}^T}{(\boldsymbol{A}\gg\!\ll\boldsymbol{A})\cdot\boldsymbol{A}}\,, \tag{A.36}$$

respectively. In (A.36), we used the relation $\boldsymbol{A}^{-1} = \det^{-1}[\boldsymbol{A}]\,\mathrm{cof}[\boldsymbol{A}^T]$ in order to obtain the expression for the inverse. Furthermore, the principal invariants of a tensor $\boldsymbol{A}$ are given by

$$I_1^{\boldsymbol{A}} = \mathrm{tr}[\boldsymbol{A}]\,, \quad I_2^{\boldsymbol{A}} = \mathrm{tr}\big[\mathrm{cof}[\boldsymbol{A}]\big]\,, \quad I_3^{\boldsymbol{A}} = \det[\boldsymbol{A}]\,, \tag{A.37}$$

see also Eq. (3.73). The relations $(\mathrm{A}.36)_1$ and $(\mathrm{A}.36)_2$ allow to express these principal invariants as

$$I_1^{\boldsymbol{A}} = \tfrac{1}{2}(\boldsymbol{A} \gg\!\ll \boldsymbol{I}) \cdot \boldsymbol{I}\,, \qquad I_2^{\boldsymbol{A}} = \tfrac{1}{2}(\boldsymbol{A} \gg\!\ll \boldsymbol{A}) \cdot \boldsymbol{I}\,, \qquad I_3^{\boldsymbol{A}} = \tfrac{1}{6}(\boldsymbol{A} \gg\!\ll \boldsymbol{A}) \cdot \boldsymbol{A}\,. \tag{A.38}$$

Using Eq. (A.34), we find the alternative identities

$$I_2^{\boldsymbol{A}} = \tfrac{1}{2}(\mathrm{tr}[\boldsymbol{A}]^2 - \mathrm{tr}[\boldsymbol{A}^2])\,, \qquad I_3^{\boldsymbol{A}} = \tfrac{1}{6}(\mathrm{tr}[\boldsymbol{A}]^3 - 3\,\mathrm{tr}[\boldsymbol{A}]\,\mathrm{tr}[\boldsymbol{A}^2] + 2\,\mathrm{tr}[\boldsymbol{A}^3]) \tag{A.39}$$

for the second and third invariant, respectively. Further explanations on the beneficial implications of the double cross product notation in continuum mechanics can be found in de Boer [51] and Bonet et al. [55].

A.5 The eigenvalue problem and the null space of tensors

The eigenvalue problem of an arbitrary second-order tensor $\boldsymbol{A} \in \mathcal{R}^{3\otimes 3}$ is given by

$$\boldsymbol{A}\boldsymbol{b} = \lambda_{\boldsymbol{A}}\boldsymbol{b} \quad \Leftrightarrow \quad (\boldsymbol{A} - \lambda_{\boldsymbol{A}}\boldsymbol{I})\boldsymbol{b} = \boldsymbol{0}\,, \tag{A.40}$$

where $\lambda_{\boldsymbol{A}}$ denotes an eigenvalue and $\boldsymbol{b} \in \mathcal{R}^3$ the associated eigenvector of $\boldsymbol{A}$. For non-trivial solutions $\boldsymbol{b} \neq \boldsymbol{0}$, it is demanded that the *characteristic polynomial*, defined as $p_{\boldsymbol{A}} = \det[\boldsymbol{A} - \lambda_{\boldsymbol{A}}\boldsymbol{I}]$, is equal to zero. With Eqs (A.16) and (A.37), the evaluation of the characteristic polynomial delivers

$$\begin{aligned} p_{\boldsymbol{A}} &= \det[\boldsymbol{A} - \lambda_{\boldsymbol{A}}\boldsymbol{I}] \\ &= \det[\boldsymbol{A}] - \mathrm{cof}[\boldsymbol{A}] \cdot \lambda_{\boldsymbol{A}}\boldsymbol{I} + \boldsymbol{A} \cdot \mathrm{cof}[-\lambda_{\boldsymbol{A}}\boldsymbol{I}] + \det[-\lambda_{\boldsymbol{A}}\boldsymbol{I}] \\ &= \det[\boldsymbol{A}] - \lambda_{\boldsymbol{A}}\,\mathrm{cof}[\boldsymbol{A}] \cdot \boldsymbol{I} + \lambda_{\boldsymbol{A}}^2\boldsymbol{A} \cdot \boldsymbol{I} - \lambda_{\boldsymbol{A}}^3 \\ &= I_3^{\boldsymbol{A}} - \lambda_{\boldsymbol{A}} I_2^{\boldsymbol{A}} + \lambda_{\boldsymbol{A}}^2 I_1^{\boldsymbol{A}} - \lambda_{\boldsymbol{A}}^3\,. \end{aligned} \tag{A.41}$$

Hence, $p_{\boldsymbol{A}} = 0$ represents a cubic function for the three eigenvalues $\lambda_{\boldsymbol{A}}$. It can easily be shown that the characteristic polynomial and, consequently, the eigenvalues are invariant with respect to a rotated tensor $\boldsymbol{A}^+ = \boldsymbol{Q}\boldsymbol{A}\boldsymbol{Q}^T$ where $\boldsymbol{Q} \in \mathcal{SO}(3)$. This follows from

$$\begin{aligned} p_{\boldsymbol{A}}^+ &= \det[\boldsymbol{A}^+ - \lambda_{\boldsymbol{A}}^+\boldsymbol{I}] \\ &= \det[\boldsymbol{Q}\boldsymbol{A}\boldsymbol{Q}^T - \lambda_{\boldsymbol{A}}^+\boldsymbol{I}] \\ &= \det[\boldsymbol{Q}\boldsymbol{A}\boldsymbol{Q}^T] - \lambda_{\boldsymbol{A}}^+\,\mathrm{cof}[\boldsymbol{Q}\boldsymbol{A}\boldsymbol{Q}^T] \cdot \boldsymbol{I} + (\lambda_{\boldsymbol{A}}^+)^2\boldsymbol{Q}\boldsymbol{A}\boldsymbol{Q}^T \cdot \boldsymbol{I} - (\lambda_{\boldsymbol{A}}^+)^3 \end{aligned} \tag{A.42}$$

and an investigation of the determinant

$$\det[\boldsymbol{Q}\boldsymbol{A}\boldsymbol{Q}^T] = \det[\boldsymbol{Q}]\det[\boldsymbol{A}]\det[\boldsymbol{Q}^T] = \det[\boldsymbol{A}]\,, \tag{A.43}$$

the cofactor

$$\begin{aligned} \mathrm{cof}[\boldsymbol{Q}\boldsymbol{A}\boldsymbol{Q}^T] \cdot \boldsymbol{I} &= \mathrm{cof}[\boldsymbol{Q}]\,\mathrm{cof}[\boldsymbol{A}]\,\mathrm{cof}[\boldsymbol{Q}^T] \cdot \boldsymbol{I} = \boldsymbol{Q}\,\mathrm{cof}[\boldsymbol{A}]\boldsymbol{Q}^T \cdot \boldsymbol{I} \\ &= \mathrm{cof}[\boldsymbol{A}]\boldsymbol{Q}^T\boldsymbol{Q} \cdot \boldsymbol{I} = \mathrm{cof}[\boldsymbol{A}] \cdot \boldsymbol{I}\,, \end{aligned} \tag{A.44}$$

as well as

$$\boldsymbol{Q}\boldsymbol{A}\boldsymbol{Q}^T \cdot \boldsymbol{I} = \boldsymbol{A}\boldsymbol{Q}^T\boldsymbol{Q} \cdot \boldsymbol{I} = \boldsymbol{A} \cdot \boldsymbol{I}\,. \tag{A.45}$$

It directly follows from these considerations that

$$p_{\boldsymbol{A}}^{+} = p_{\boldsymbol{A}} \quad \Rightarrow \quad \lambda_{\boldsymbol{A}}^{+} = \lambda_{\boldsymbol{A}}\,. \tag{A.46}$$

It is remarked that the identities in Eqs (A.43), (A.44), and (A.45) are no surprise, since these three expressions are nothing else than the principal invariants of $\boldsymbol{A}$, which are of course invariant with respect to transformations $\boldsymbol{Q}\boldsymbol{A}\boldsymbol{Q}^T$.

Moreover, the tensor $\boldsymbol{A} \in \mathcal{R}^{3\otimes 3}$ has *full rank*, denoted by $\mathrm{rank}[\boldsymbol{A}] = 3$, if none of the eigenvalues $\lambda_{\boldsymbol{A}}$ is zero or, equivalently, if $\det[\boldsymbol{A}] \neq 0$. However, if these conditions are not satisfied, then $\mathrm{rank}[\boldsymbol{A}] < 3$ and there is a *null space* or *kernel*

$$\ker[\boldsymbol{A}] = \{\mathbf{n} \in \mathcal{R}^3 \,|\, \boldsymbol{A}\,\mathbf{n} = \mathbf{0}\}\,. \tag{A.47}$$

Therein, $\mathbf{n}$ is (are) the eigenvector(s) associated to the zero eigenvalue(s). The dimension of the null space $\ker[\boldsymbol{A}]$ is defined as the *nullity*, denoted by $\mathrm{nullity}[\boldsymbol{A}]$. For instance, $\mathrm{nullity}[\boldsymbol{A}] = 1$ if exactly one eigenvalue is zero. Further, the nullity and the rank of a tensor are related through

$$\mathrm{rank}[\boldsymbol{A}] + \mathrm{nullity}[\boldsymbol{A}] = \dim[\boldsymbol{A}]\,, \tag{A.48}$$

where $\dim[\boldsymbol{A}] = 3$ for $\boldsymbol{A} \in \mathcal{R}^{3\otimes 3}$.

Now, we apply the previously outlined principles to the eigenvalue problem of a fourth-order tensor $\mathbb{A} \in \mathcal{R}^{3\otimes 3\otimes 3\otimes 3}$ and formulate

$$\mathbb{A}\,\boldsymbol{B} = \lambda_{\mathbb{A}}\boldsymbol{B} \quad \Leftrightarrow \quad (\mathbb{A} - \lambda_{\mathbb{A}}\,\mathbb{I})\boldsymbol{B} = \mathbf{0}\,. \tag{A.49}$$

Therein, $\lambda_{\mathbb{A}}$ is an eigenvalue of $\mathbb{A}$ and $\boldsymbol{B} \in \mathcal{R}^{3\otimes 3}$ denotes the associated second-order *eigentensor*. In analogy to the eigenvalue problem for second-order tensors, one has to proceed with the formulation of a characteristic polynomial

$$p_{\mathbb{A}} = \det[\mathbb{A} - \lambda_{\mathbb{A}}\,\mathbb{I}] = 0\,. \tag{A.50}$$

This expression demands for the calculation of a determinant of a fourth-order tensor, which is not as straightforward as for second-order tensors. Valuable investigations on the treatment of this problem and some solutions can be found in the fundamental works of Betten [33, 34] and Betten & Helisch [35]. They outlined the idea of introducing two-dimensional matrix representations of the coefficients of fourth-order tensors. This concept is also followed and explained by Itskov [241]. Here, we introduce suitable matrix representations for fourth-order tensors and the associated vector representation of second-order tensors in Section A.7.2. Doing so, the $3^4 = 81$ coefficients of a fourth-order tensor are arranged as $\mathcal{R}^{9\times 9}$-matrix. This allows for a straightforward computation of the determinant and, consequently, of the eigenvalues $\lambda_{\mathbb{A}}$. The $\mathcal{R}^{9\times 9}$-matrix form suggests that a fourth-order tensor generally has nine eigenvalues. Hence, a full-ranked fourth-order tensor $\mathbb{A}$ has $\mathrm{rank}[\mathbb{A}] = 9$. In analogy to the previous considerations, the respective

eigentensor that is associated with a zero eigenvalue depicts a null space of the fourth-order tensor and we can write

$$\ker[\mathbb{A}] = \{\mathfrak{N} \in \mathcal{R}^{3\otimes 3} \,|\, \mathbb{A}\,\mathfrak{N} = \mathbf{0}\}\,. \tag{A.51}$$

Subsequently, a similar relation to Eq. (A.48) is formulated as

$$\operatorname{rank}[\mathbb{A}] + \operatorname{nullity}[\mathbb{A}] = \dim[\mathbb{A}]\,, \tag{A.52}$$

where $\dim[\mathbb{A}] = 9$ for $\mathbb{A} \in \mathcal{R}^{3\otimes 3\otimes 3\otimes 3}$.

A.6 Tensor analysis

Some selected derivatives in the field of tensor analysis are given in this section. Further basic relations can be found in Ehlers [107], whereas the focus here is on providing derivatives that involve fourth-order tensors.

The derivatives of the principal invariants read

$$\frac{\partial I_1^{\boldsymbol{A}}}{\partial \boldsymbol{A}} = \frac{\operatorname{tr}[\boldsymbol{A}]}{\partial \boldsymbol{A}} = \boldsymbol{I} \tag{A.53}$$

$$\frac{\partial I_2^{\boldsymbol{A}}}{\partial \boldsymbol{A}} = \boldsymbol{A} \barwedge \boldsymbol{I} = \operatorname{tr}[\boldsymbol{A}]\boldsymbol{I} - \boldsymbol{A}^T \tag{A.54}$$

$$\frac{\partial I_3^{\boldsymbol{A}}}{\partial \boldsymbol{A}} = \frac{\det[\boldsymbol{A}]}{\partial \boldsymbol{A}} = \tfrac{1}{2}\boldsymbol{A} \barwedge \boldsymbol{A} = \operatorname{cof}[\boldsymbol{A}] \tag{A.55}$$

Selected product rules for time derivatives of vectors:

$$(\boldsymbol{a} \cdot \boldsymbol{b})^{\bullet} = \dot{\boldsymbol{a}} \cdot \boldsymbol{b} + \boldsymbol{a} \cdot \dot{\boldsymbol{b}} \tag{A.56}$$

$$(\boldsymbol{a} \times \boldsymbol{b})^{\bullet} = \dot{\boldsymbol{a}} \times \boldsymbol{b} + \boldsymbol{a} \times \dot{\boldsymbol{b}} \tag{A.57}$$

Some selected derivation rules:

$$\frac{\partial \boldsymbol{A}}{\partial \boldsymbol{A}} = \mathbb{I} \tag{A.58}$$

$$\frac{\partial \boldsymbol{A}}{\partial \boldsymbol{A}} = \mathbb{I}_{\text{sym}} \quad \text{if}^{\,2}\, \boldsymbol{A} \in \mathcal{SYM} \tag{A.59}$$

$$\frac{\partial \boldsymbol{A}^{-1}}{\partial \boldsymbol{A}} = -(\boldsymbol{A}^{-1} \otimes \boldsymbol{A}^{-T})^{T_{23}} \tag{A.60}$$

$$\frac{\partial \boldsymbol{A}^{-T}}{\partial \boldsymbol{A}} = -(\boldsymbol{A}^{-T} \otimes \boldsymbol{A}^{-T})^{T_{24}} \tag{A.61}$$

$$\frac{\partial \operatorname{cof}[\boldsymbol{A}]}{\partial \boldsymbol{A}} = \det[\boldsymbol{A}]\big((\boldsymbol{A}^{-T} \otimes \boldsymbol{A}^{-T}) - (\boldsymbol{A}^{-T} \otimes \boldsymbol{A}^{-T})^{T_{24}}\big) \tag{A.62}$$

$$\frac{\partial(\alpha \boldsymbol{A})}{\partial \boldsymbol{C}} = \boldsymbol{A} \otimes \frac{\partial \alpha}{\partial \boldsymbol{C}} + \alpha \frac{\partial \boldsymbol{A}}{\partial \boldsymbol{C}} \tag{A.63}$$

$$\frac{\partial(\boldsymbol{A} \cdot \boldsymbol{B})}{\partial \boldsymbol{C}} = \Big(\frac{\partial \boldsymbol{A}}{\partial \boldsymbol{C}}\Big)^T \boldsymbol{B} + \Big(\frac{\partial \boldsymbol{B}}{\partial \boldsymbol{C}}\Big)^T \boldsymbol{A} \tag{A.64}$$

[2] If $\boldsymbol{A} \in \mathcal{SYM}$ belongs to the group of symmetric tensors, the derivative $\frac{\partial \boldsymbol{A}}{\partial \boldsymbol{A}} = \frac{\partial A_{ij}}{\partial A_{kl}}\, \boldsymbol{e}_i \otimes \boldsymbol{e}_j \otimes \boldsymbol{e}_k \otimes \boldsymbol{e}_l$ has to be minor symmetric, such that $\frac{\partial A_{ij}}{\partial A_{kl}} = \frac{\partial A_{ji}}{\partial A_{kl}} = \frac{\partial A_{ij}}{\partial A_{lk}}$ (see Section A.7.2 and Table A.2 for more details on the symmetries of fourth-order tensors). It is easy to see that $\mathbb{I}$ is not minor symmetric, since $\mathbb{I}^{T_{12}} = \mathbb{I}^{T_{34}} = \mathbb{I}_T \neq \mathbb{I}$. In contrast, $\mathbb{I}_{\text{sym}}^{T_{12}} = \mathbb{I}_{\text{sym}}^{T_{34}} = \mathbb{I}_{\text{sym}}$.

$$\frac{\partial \boldsymbol{A}^{-1}}{\partial \boldsymbol{B}} = -\Big(\Big[\Big(\Big(\Big[\Big(\frac{\partial \boldsymbol{A}}{\partial \boldsymbol{B}}\Big)^{T_{24}} \boldsymbol{A}^{-1}\Big]^{\underline{4}}\Big)^{T_{24}}\Big)^{T_{14}} \boldsymbol{A}^{-T}\Big]^{\underline{4}}\Big)^{T_{14}} = -(A^{-1})_{is}\,\frac{\partial A_{st}}{\partial B_{kl}}\,(A^{-1})_{tj}\,\boldsymbol{e}_i \otimes \boldsymbol{e}_j \otimes \boldsymbol{e}_k \otimes \boldsymbol{e}_l \tag{A.65}$$

$$\frac{\partial(\alpha\mathbb{A})}{\partial \boldsymbol{C}} = \mathbb{A} \otimes \frac{\partial \alpha}{\partial \boldsymbol{C}} + \alpha\,\frac{\partial \mathbb{A}}{\partial \boldsymbol{C}} = \Big(\mathrm{A}_{ijkl}\,\frac{\partial \alpha}{\partial C_{mn}} + \alpha\,\frac{\partial \mathrm{A}_{ijkl}}{\partial C_{mn}}\Big)\,\boldsymbol{e}_i \otimes \boldsymbol{e}_j \otimes \boldsymbol{e}_k \otimes \boldsymbol{e}_l \otimes \boldsymbol{e}_m \otimes \boldsymbol{e}_n \tag{A.66}$$

$$\frac{\partial(\mathbb{A}\boldsymbol{u})}{\partial \boldsymbol{C}} = \Big(\Big(\frac{\partial \mathbb{A}}{\partial \boldsymbol{C}}\Big)^{T_{46}}\Big)^{T_{56}} \boldsymbol{u} + \mathbb{A}\,\frac{\partial \boldsymbol{u}}{\partial \boldsymbol{C}} = \Big(\frac{\partial \mathrm{A}_{ijkl}}{\partial C_{mn}}\,u_l + \mathrm{A}_{ijkl}\,\frac{\partial u_l}{\partial C_{mn}}\Big)\,\boldsymbol{e}_i \otimes \boldsymbol{e}_j \otimes \boldsymbol{e}_k \otimes \boldsymbol{e}_m \otimes \boldsymbol{e}_n \tag{A.67}$$

$$\frac{\partial(\mathbb{A}\boldsymbol{B})}{\partial \boldsymbol{C}} = \Big(\Big(\frac{\partial \mathbb{A}}{\partial \boldsymbol{C}}\Big)^{T_{35}}\Big)^{T_{46}} \boldsymbol{B} + \mathbb{A}\,\frac{\partial \boldsymbol{B}}{\partial \boldsymbol{C}} = \Big(\frac{\partial \mathrm{A}_{ijkl}}{\partial C_{mn}}\,B_{kl} + \mathrm{A}_{ijkl}\,\frac{\partial B_{kl}}{\partial C_{mn}}\Big)\,\boldsymbol{e}_i \otimes \boldsymbol{e}_j \otimes \boldsymbol{e}_m \otimes \boldsymbol{e}_n \tag{A.68}$$

$$\frac{\partial(\mathbb{A}\mathbb{B})}{\partial \boldsymbol{C}} = \Big(\Big(\Big[\Big(\Big(\frac{\partial \mathbb{A}}{\partial \boldsymbol{C}}\Big)^{T_{35}}\Big)^{T_{46}}\Big]^{\underline{6}}\mathbb{B}\Big)^{T_{35}}\Big)^{T_{46}} + \Big[\mathbb{A}\,\frac{\partial \mathbb{B}}{\partial \boldsymbol{C}}\Big]^{\underline{6}} = \Big(\frac{\partial \mathrm{A}_{ijst}}{\partial C_{mn}}\,\mathrm{B}_{stkl} + \mathrm{A}_{ijst}\,\frac{\partial \mathrm{B}_{stkl}}{\partial C_{mn}}\Big)\,\boldsymbol{e}_i \otimes \boldsymbol{e}_j \otimes \boldsymbol{e}_k \otimes \boldsymbol{e}_l \otimes \boldsymbol{e}_m \otimes \boldsymbol{e}_n \tag{A.69}$$

$$\frac{\partial(\boldsymbol{u} \otimes \boldsymbol{v})}{\partial \boldsymbol{C}} = \Big(\Big(\frac{\partial \boldsymbol{u}}{\partial \boldsymbol{C}} \otimes \boldsymbol{v}\Big)^{T_{24}}\Big)^{T_{34}} + \boldsymbol{u} \otimes \frac{\partial \boldsymbol{v}}{\partial \boldsymbol{C}} = \Big(\frac{\partial u_i}{\partial C_{kl}}\,v_j + u_i\,\frac{\partial v_j}{\partial C_{kl}}\Big)\,\boldsymbol{e}_i \otimes \boldsymbol{e}_j \otimes \boldsymbol{e}_k \otimes \boldsymbol{e}_l \tag{A.70}$$

$$\frac{\partial(\boldsymbol{A} \otimes \boldsymbol{B})}{\partial \boldsymbol{C}} = \Big(\Big(\frac{\partial \boldsymbol{A}}{\partial \boldsymbol{C}} \otimes \boldsymbol{B}\Big)^{T_{35}}\Big)^{T_{46}} + \boldsymbol{A} \otimes \frac{\partial \boldsymbol{B}}{\partial \boldsymbol{C}} = \Big(\frac{\partial A_{ij}}{\partial C_{mn}}\,B_{kl} + A_{ij}\,\frac{\partial B_{kl}}{\partial C_{mn}}\Big)\,\boldsymbol{e}_i \otimes \boldsymbol{e}_j \otimes \boldsymbol{e}_k \otimes \boldsymbol{e}_l \otimes \boldsymbol{e}_m \otimes \boldsymbol{e}_n \tag{A.71}$$

$$\frac{\partial(\boldsymbol{A} \otimes \boldsymbol{B})^{T_{23}}}{\partial \boldsymbol{C}} = \Big(\Big(\Big(\frac{\partial \boldsymbol{A}}{\partial \boldsymbol{C}} \otimes \boldsymbol{B}\Big)^{T_{23}}\Big)^{T_{46}}\Big)^{T_{25}} + \Big(\boldsymbol{A} \otimes \frac{\partial \boldsymbol{B}}{\partial \boldsymbol{C}}\Big)^{T_{23}} = \Big(\frac{\partial A_{ik}}{\partial C_{mn}}\,B_{jl} + A_{ik}\,\frac{\partial B_{jl}}{\partial C_{mn}}\Big)\,\boldsymbol{e}_i \otimes \boldsymbol{e}_j \otimes \boldsymbol{e}_k \otimes \boldsymbol{e}_l \otimes \boldsymbol{e}_m \otimes \boldsymbol{e}_n \tag{A.72}$$

$$\frac{\partial(\boldsymbol{A} \otimes \boldsymbol{B})^{T_{24}}}{\partial \boldsymbol{C}} = \Big(\Big(\Big(\frac{\partial \boldsymbol{A}}{\partial \boldsymbol{C}} \otimes \boldsymbol{B}\Big)^{T_{24}}\Big)^{T_{26}}\Big)^{T_{35}} + \Big(\boldsymbol{A} \otimes \frac{\partial \boldsymbol{B}}{\partial \boldsymbol{C}}\Big)^{T_{24}} = \Big(\frac{\partial A_{il}}{\partial C_{mn}}\,B_{kj} + A_{il}\,\frac{\partial B_{kj}}{\partial C_{mn}}\Big)\,\boldsymbol{e}_i \otimes \boldsymbol{e}_j \otimes \boldsymbol{e}_k \otimes \boldsymbol{e}_l \otimes \boldsymbol{e}_m \otimes \boldsymbol{e}_n \tag{A.73}$$

$$\frac{\partial(\boldsymbol{A} \otimes \boldsymbol{u} \otimes \boldsymbol{v})}{\partial \boldsymbol{C}} = \Big(\Big(\frac{\partial \boldsymbol{A}}{\partial \boldsymbol{C}} \otimes \boldsymbol{u} \otimes \boldsymbol{v}\Big)^{T_{35}}\Big)^{T_{46}} + \Big(\Big(\boldsymbol{A} \otimes \frac{\partial \boldsymbol{u}}{\partial \boldsymbol{C}} \otimes \boldsymbol{v}\Big)^{T_{46}}\Big)^{T_{56}} + \boldsymbol{A} \otimes \boldsymbol{u} \otimes \frac{\partial \boldsymbol{v}}{\partial \boldsymbol{C}} \tag{A.74}$$

Table A.1: Some selected tensor derivation rules. Therein, $(\cdot)^{\underline{i}}$ represents an incomplete mapping and i indicates the order of the resulting tensor. The incomplete mapping requires to carry out a sufficient number of inner contractions, see Ehlers [107].

A.7 On fourth-order tensors

A.7.1 Derivation of the nominal stress and elasticity tensors

For the derivation of nominal stresses and elasticity tensors of an invariant-based strain-energy function of a transversely isotropic material, it is essential to formulate the derivatives of the invariants with respect to the deformation gradient $\boldsymbol{F}$. Those quantites are called tensor generators. For the set $\mathscr{I}^{\imath}_{\mathrm{ti}}$, they read

$$\begin{aligned} &\partial_{\boldsymbol{F}} I_1 = 2\,\boldsymbol{F}\,, \quad \partial_{\boldsymbol{F}} I_2 = 2\,\boldsymbol{F}(I_1\boldsymbol{I} - \boldsymbol{C})\,, \quad \partial_{\boldsymbol{F}} J = J\,\boldsymbol{F}^{-T}\,, \\ &\partial_{\boldsymbol{F}} J_4 = 2\,\boldsymbol{F}\boldsymbol{M}\,, \quad \partial_{\boldsymbol{F}} J_5 = 2\,(\boldsymbol{F}\boldsymbol{C}\boldsymbol{M} + \boldsymbol{F}\boldsymbol{M}\boldsymbol{C})\,. \end{aligned} \tag{A.75}$$

Accordingly, the first Piola-Kirchhoff (nominal) stress tensor associated with a strain-energy function

$$\mathscr{W} = \mathscr{W}(\mathscr{I}^{\imath}_{\mathrm{ti}}) = \mathscr{W}(I_1, I_2, J, J_4, J_5) \tag{A.76}$$

is given by

$$\begin{aligned} \boldsymbol{P} = \partial_{\boldsymbol{F}}\mathscr{W} &= 2\,\partial_{I_1}\mathscr{W}\,\boldsymbol{F} + 2\,\partial_{I_2}\mathscr{W}\,\boldsymbol{F}(I_1\boldsymbol{I} - \boldsymbol{C}) + J\partial_J\mathscr{W}\,\boldsymbol{F}^{-T} \\ &\quad + 2\,\partial_{J_4}\mathscr{W}\,\boldsymbol{F}\boldsymbol{M} + 2\,\partial_{J_5}\mathscr{W}\,(\boldsymbol{F}\boldsymbol{C}\boldsymbol{M} + \boldsymbol{F}\boldsymbol{M}\boldsymbol{C})\,. \end{aligned} \tag{A.77}$$

The second derivative of $\mathscr{W}$ with respect to $\boldsymbol{F}$ requires repeated use of the chain rule and leads to some lengthy expressions for the stiffness tensor $\mathbb{L}$. For the sake of brevity, we therefore restrict attention to a strain-energy function $\mathscr{W}(I_1, J, J_4, J_5)$ which results in the stiffness tensor

$$\begin{aligned} \mathbb{L} = \partial_{\boldsymbol{F}}\boldsymbol{P} &= \partial^2_{\boldsymbol{F}\boldsymbol{F}}\mathscr{W} \\ &= 2\,\partial_{I_1}\mathscr{W}\,\mathbb{I} + 4\,\partial^2_{I_1^2}\mathscr{W}\,\boldsymbol{F}\otimes\boldsymbol{F} + J\,\partial_J\mathscr{W}\left(\boldsymbol{F}^{-T}\otimes\boldsymbol{F}^{-T} - (\boldsymbol{F}^{-T}\otimes\boldsymbol{F}^{-T})^{T_{24}}\right) \\ &\quad + J^2\,\partial^2_{J^2}\mathscr{W}\,\boldsymbol{F}^{-T}\otimes\boldsymbol{F}^{-T} + 2\,\partial_{J_4}\mathscr{W}\,(\boldsymbol{I}\otimes\boldsymbol{M})^{T_{23}} + 4\,\partial^2_{J_4^2}\mathscr{W}\,\boldsymbol{F}\boldsymbol{M}\otimes\boldsymbol{F}\boldsymbol{M} \\ &\quad + 2\,\partial_{J_5}\mathscr{W}\left((\boldsymbol{I}\otimes\boldsymbol{C}\boldsymbol{M})^{T_{23}} + (\boldsymbol{I}\otimes\boldsymbol{M}\boldsymbol{C})^{T_{23}} + (\boldsymbol{F}\boldsymbol{F}^T\otimes\boldsymbol{M})^{T_{23}} + (\boldsymbol{F}\boldsymbol{M}\boldsymbol{F}^T\otimes\boldsymbol{I})^{T_{23}}\right. \\ &\quad \left. + (\boldsymbol{F}\otimes\boldsymbol{F}\boldsymbol{M})^{T_{24}} + (\boldsymbol{F}\boldsymbol{M}\otimes\boldsymbol{F})^{T_{24}}\right) + 4\,\partial^2_{J_5^2}\mathscr{W}\,\tilde{\boldsymbol{M}}\otimes\tilde{\boldsymbol{M}} \\ &\quad + 2\,J\partial^2_{I_1 J}\mathscr{W}\,(\boldsymbol{F}\otimes\boldsymbol{F}^{-T} + \boldsymbol{F}^{-T}\otimes\boldsymbol{F}) + 4\,\partial^2_{I_1 J_4}\mathscr{W}\,(\boldsymbol{F}\otimes\boldsymbol{F}\boldsymbol{M} + \boldsymbol{F}\boldsymbol{M}\otimes\boldsymbol{F}) \\ &\quad + 4\,\partial^2_{I_1 J_5}\mathscr{W}\,(\boldsymbol{F}\otimes\tilde{\boldsymbol{M}} + \tilde{\boldsymbol{M}}\otimes\boldsymbol{F}) + 2\,J\,\partial^2_{J J_4}\mathscr{W}\,(\boldsymbol{F}^{-T}\otimes\boldsymbol{F}\boldsymbol{M} + \boldsymbol{F}\boldsymbol{M}\otimes\boldsymbol{F}^{-T}) \\ &\quad + 2\,J\,\partial^2_{J J_5}\mathscr{W}\,(\boldsymbol{F}^{-T}\otimes\tilde{\boldsymbol{M}} + \tilde{\boldsymbol{M}}\otimes\boldsymbol{F}^{-T}) + 4\,\partial^2_{J_4 J_5}\mathscr{W}\,(\boldsymbol{F}\boldsymbol{M}\otimes\tilde{\boldsymbol{M}} + \tilde{\boldsymbol{M}}\otimes\boldsymbol{F}\boldsymbol{M})\,, \end{aligned} \tag{A.78}$$

with the abbreviation $\tilde{\boldsymbol{M}} = \boldsymbol{F}\boldsymbol{M}\boldsymbol{C} + \boldsymbol{F}\boldsymbol{C}\boldsymbol{M}$. If one considers isotropic, generalised Neo-Hookean materials $\mathscr{W}(I_1, J)$, the stress and the stiffness tensor reduce to

$$\boldsymbol{P} = 2\,\partial_{I_1}\mathscr{W}\,\boldsymbol{F} + J\,\partial_J\mathscr{W}\,\boldsymbol{F}^{-T} \tag{A.79}$$

and

$$\begin{aligned} \mathbb{L} = 2\,\partial_{I_1}\mathscr{W}\,\mathbb{I} + 4\,\partial^2_{I_1^2}\mathscr{W}\,\boldsymbol{F}\otimes\boldsymbol{F} + 2\,J\,\partial^2_{I_1 J}\mathscr{W}\,(\boldsymbol{F}\otimes\boldsymbol{F}^{-T} + \boldsymbol{F}^{-T}\otimes\boldsymbol{F}) \\ + (J\,\partial_J\mathscr{W} + J^2\,\partial^2_{J^2}\mathscr{W})\,\boldsymbol{F}^{-T}\otimes\boldsymbol{F}^{-T} - J\,\partial_J\mathscr{W}\,(\boldsymbol{F}^{-T}\otimes\boldsymbol{F}^{-T})^{T_{24}}\,, \end{aligned} \tag{A.80}$$

respectively. If one further neglects coupling between I_1 and J one obtains the stiffness tensor

$$\begin{aligned} \mathbb{L} = 2\,\partial_{I_1}\mathscr{W}\,\mathbb{I} + 4\,\partial^2_{I_1^2}\mathscr{W}\,\boldsymbol{F}\otimes\boldsymbol{F} + (J\partial_J\mathscr{W} + J^2\partial^2_{J^2}\mathscr{W})\,\boldsymbol{F}^{-T}\otimes\boldsymbol{F}^{-T} \\ - J\partial_J\mathscr{W}\,(\boldsymbol{F}^{-T}\otimes\boldsymbol{F}^{-T})^{T_{24}}\,. \end{aligned} \tag{A.81}$$

A.7.2 Matrix representations of fourth-order tensors

Fourth-order tensors frequently arise in the field of continuum mechanics and a lot of situations require the computation of the inverse or the determinant of these tensors. In theory, such operations are well defined and straightforward extensions of the theory of second-order tensors. However, fourth-order tensors have a four-dimensional coefficient matrices, which is a little bit cumbersome in practical use. For example, dealing with fourth-order tensors in numerical codes (for example in commercial software like MATLAB) has the drawback that a lot of standard operations and functions available for two-dimensional matrices cannot be directly used for fourth-order tensors and their four-dimensional coefficient matrices. Thus, it proves useful for a variety of applications to introduce a specific two-dimensional matrix representation, denoted by A, for the 81 coefficients A_{ijkl} of a fourth-order tensor $\mathbb{A} = \mathrm{A}_{ijkl}\,\boldsymbol{e}_i \otimes \boldsymbol{e}_j \otimes \boldsymbol{e}_k \otimes \boldsymbol{e}_l$ $(i,j,k,l = 1,2,3)$ and, accordingly, a vector representation, denoted by B, for the 9 coefficients B_{ij} of a second-order tensor $\boldsymbol{B} = B_{ij}\,\boldsymbol{e}_i \otimes \boldsymbol{e}_j$. Such formulations were for example proposed by ITSKOV [241] and BALZANI [24]. Here, we suggest a representation where coefficient pairs ij and kl are transformed according to

$$\begin{aligned}[11]\to[1],\quad [12]\to[2],\quad [13]\to[3],\quad [21]\to[4],\quad [22]\to[5],\\ [23]\to[6],\quad [31]\to[7],\quad [32]\to[8],\quad [33]\to[9]\,,\end{aligned} \tag{A.82}$$

which results in the two-dimensional matrix forms

$$\mathrm{A} = \begin{bmatrix} \mathrm{A}_{1111} & \mathrm{A}_{1112} & \mathrm{A}_{1113} & \mathrm{A}_{1121} & \mathrm{A}_{1122} & \mathrm{A}_{1123} & \mathrm{A}_{1131} & \mathrm{A}_{1132} & \mathrm{A}_{1133} \\ \mathrm{A}_{1211} & \mathrm{A}_{1212} & \mathrm{A}_{1213} & \mathrm{A}_{1221} & \mathrm{A}_{1222} & \mathrm{A}_{1223} & \mathrm{A}_{1231} & \mathrm{A}_{1232} & \mathrm{A}_{1233} \\ \mathrm{A}_{1311} & \mathrm{A}_{1312} & \mathrm{A}_{1313} & \mathrm{A}_{1321} & \mathrm{A}_{1322} & \mathrm{A}_{1323} & \mathrm{A}_{1331} & \mathrm{A}_{1332} & \mathrm{A}_{1333} \\ \mathrm{A}_{2111} & \mathrm{A}_{2112} & \mathrm{A}_{2113} & \mathrm{A}_{2121} & \mathrm{A}_{2122} & \mathrm{A}_{2123} & \mathrm{A}_{2131} & \mathrm{A}_{2132} & \mathrm{A}_{2133} \\ \mathrm{A}_{2211} & \mathrm{A}_{2212} & \mathrm{A}_{2213} & \mathrm{A}_{2221} & \mathrm{A}_{2222} & \mathrm{A}_{2223} & \mathrm{A}_{2231} & \mathrm{A}_{2232} & \mathrm{A}_{2233} \\ \mathrm{A}_{2311} & \mathrm{A}_{2312} & \mathrm{A}_{2313} & \mathrm{A}_{2321} & \mathrm{A}_{2322} & \mathrm{A}_{2323} & \mathrm{A}_{2331} & \mathrm{A}_{2332} & \mathrm{A}_{2333} \\ \mathrm{A}_{3111} & \mathrm{A}_{3112} & \mathrm{A}_{3113} & \mathrm{A}_{3121} & \mathrm{A}_{3122} & \mathrm{A}_{3123} & \mathrm{A}_{3131} & \mathrm{A}_{3132} & \mathrm{A}_{3133} \\ \mathrm{A}_{3211} & \mathrm{A}_{3212} & \mathrm{A}_{3213} & \mathrm{A}_{3221} & \mathrm{A}_{3222} & \mathrm{A}_{3223} & \mathrm{A}_{3231} & \mathrm{A}_{3232} & \mathrm{A}_{3233} \\ \mathrm{A}_{3311} & \mathrm{A}_{3312} & \mathrm{A}_{3313} & \mathrm{A}_{3321} & \mathrm{A}_{3322} & \mathrm{A}_{3323} & \mathrm{A}_{3331} & \mathrm{A}_{3332} & \mathrm{A}_{3333} \end{bmatrix}, \quad B = \begin{bmatrix} B_{11} \\ B_{12} \\ B_{13} \\ B_{21} \\ B_{22} \\ B_{23} \\ B_{31} \\ B_{32} \\ B_{33} \end{bmatrix}. \tag{A.83}$$

Thus, A is represented as a $\mathcal{R}^{9\times9}$-matrix, whereas B becomes a $\mathcal{R}^{9\times1}$-matrix (vector). With these representations at hand, the coefficients of the tensor product $\mathbb{A}\boldsymbol{B}$ can be simply calculated by the standard matrix-vector multiplication $\mathrm{A}B$. Consequently, the main advantage of the representations (A.83) is that they easily allow to calculate, for example, the rank, determinant, or null space of a fourth-order tensor by using numerical codes and functions written for two-dimensional matrices. Furthermore, the coefficients of the fourth-order inverse $\mathbb{A}^{-1}$ are obtained by calculating the two-dimensional inverse A^{-1}, since the matrix multiplication $\mathrm{A}^{-1}\mathrm{A}$ equals the 9×9-identity matrix. Also note that $(\mathrm{A}.83)_1$ makes clear that a fourth-order tensor in the three-dimensional space has $\dim[\mathbb{A}] = 9$ and that, in turn, $\mathrm{rank}[\mathbb{A}] = 9$ holds for a full-ranked fourth-order tensor $\mathbb{A}$. A major symmetry of the tensor $\mathbb{A}$, described by $\mathbb{A} = \mathbb{A}^T = (\mathbb{A}^{T_{13}})^{T_{24}}$, shows up through the symmetry of the matrix representation A. Hence, this leads to the common procedure of dropping out the lower diagonal of the matrix as independent coefficients and there remain 45 independent coefficients. If a fourth-order tensor $\mathbb{A}$ exhibits minor symmetry, accompanied with $\mathbb{A} = \mathbb{A}^{T_{12}} = \mathbb{A}^{T_{34}}$, alternative matrix representations prove useful, such

symmetry	**rule**	**independent coefficients**
none	$\mathbb{A}$	$3^4 = 81$
major	$\mathbb{A} = \mathbb{A}^T$	$\left(\!\binom{9}{2}\!\right) = 45$
minor	$\mathbb{A} = \mathbb{A}^{T_{12}} = \mathbb{A}^{T_{34}}$	$6^2 = 36$
major and minor (super)	$\mathbb{A} = \mathbb{A}^T = \mathbb{A}^{T_{12}} = \mathbb{A}^{T_{34}}$	$\left(\!\binom{6}{2}\!\right) = 21$
total (complete)	$\mathbb{A} = \mathbb{A}^T = \mathbb{A}^{T_{12}} = \mathbb{A}^{T_{34}} = \mathbb{A}^{T_{23}}$	$\left(\!\binom{3}{4}\!\right) = \binom{6}{4} = 15$

Table A.2: Overview on the different symmetry rules of fourth-order tensors and the associated number of independent coefficients. Therein, $\binom{n}{k} = \frac{n!}{k!(n-k)!}$ is the *binomial coefficient* and $\left(\!\binom{n}{k}\!\right) = \binom{n+k-1}{k}$ is the so-called *multiset coefficient*, which are valuable tools from the field of combinatorics and allow for a straightforward derivation of the number of independent coefficients.

as the prominent *Voigt notation*, see Voigt [496]. Since a minor symmetric fourth-order tensor only has 36 independent coefficients, this representation is given by a $\mathcal{R}^{6\times6}$-matrix and reads

$$[\mathrm{A}_{ijkl}]^{\mathrm{V}} = \begin{bmatrix} \mathrm{A}_{1111} & \mathrm{A}_{1122} & \mathrm{A}_{1133} & \mathrm{A}_{1123} & \mathrm{A}_{1113} & \mathrm{A}_{1112} \\ \mathrm{A}_{2211} & \mathrm{A}_{2222} & \mathrm{A}_{2233} & \mathrm{A}_{2223} & \mathrm{A}_{2213} & \mathrm{A}_{2212} \\ \mathrm{A}_{3311} & \mathrm{A}_{3322} & \mathrm{A}_{3333} & \mathrm{A}_{3323} & \mathrm{A}_{3313} & \mathrm{A}_{3312} \\ \mathrm{A}_{2311} & \mathrm{A}_{2322} & \mathrm{A}_{2333} & \mathrm{A}_{2323} & \mathrm{A}_{2313} & \mathrm{A}_{2312} \\ \mathrm{A}_{1311} & \mathrm{A}_{1322} & \mathrm{A}_{1333} & \mathrm{A}_{1323} & \mathrm{A}_{1313} & \mathrm{A}_{1312} \\ \mathrm{A}_{1211} & \mathrm{A}_{1222} & \mathrm{A}_{1233} & \mathrm{A}_{1223} & \mathrm{A}_{1213} & \mathrm{A}_{1212} \end{bmatrix} . \tag{A.84}$$

Minor and major symmetry of a fourth-order tensor is expressed by the symmetry of the matrix representation $[\mathrm{A}_{ijkl}]^{\mathrm{V}}$ and the number of independent coefficients consequently reduces to 21. This is also referred to as super symmetry. A fourth-order tensor which in addition to the super symmetry also holds the condition $\mathbb{A} = \mathbb{A}^{T_{23}}$ is totally symmetric. This is also called complete symmetry, because a fourth-order tensor is then completely symmetric in all indices. In the theory of continuum mechanics, the various symmetry conditions arise, for instance, in the different formulations of the fourth-order elasticity tensors. Major symmetry immediately follows from the occurrence of a hyperelastic potential and holds for all of the discussed elasticity tensors in this work. In addition, minor symmetry is given when the associated second-order stress tensor is symmetric. Hence, the large-strain material formulation $\mathbb{C}$ as well as the small-strain version $\mathbb{L}_{\mathrm{lin}}$ are super (major and minor) symmetric, as a result of the associated symmetry of the stress tensors $\boldsymbol{S}$ and $\boldsymbol{\sigma}_{\mathrm{lin}}$, respectively. In the theory of linear, small-strain elasticity, one can observe total symmetry of the elasticity tensor in the so-called *rari-constant theory*, while the far more frequently employed super symmetry of the elasticity tensor is associated with the *multi-constant theory*, see, for example, Love [300] or Campanella & Tonon [68]. In this context, the additional symmetry condition $\mathbb{A} = \mathbb{A}^{T_{23}}$ is referred to as *Cauchy relation*. Furthermore, total symmetry arises when a fourth-order tensor is composed of the dyadic product of four equal vectors. This is the case, for example, for the dyadic product $\boldsymbol{M} \otimes \boldsymbol{M} = \boldsymbol{a}_0 \otimes \boldsymbol{a}_0 \otimes \boldsymbol{a}_0 \otimes \boldsymbol{a}_0$ of the structural tensor $\boldsymbol{M}$.

An overview on the different symmetry conditions and the resulting number of independent coefficients of a fourth-order tensor in the three-dimensional space is given in Table A.2.

For completeness, we provide the matrix representations of the subspace tensors $\{\mathbb{A}\}^\flat$ and $\{\boldsymbol{B}\}^\flat$, which are employed in Chapter 5. In this subspace, fourth- and second-order

tensors are defined by $\{\mathbb{A} = \mathrm{A}_{ijkl}\, \boldsymbol{e}_i \otimes \boldsymbol{e}_j \otimes \boldsymbol{e}_k \otimes \boldsymbol{e}_l\}^\flat$ and $\{\boldsymbol{B} = B_{ij}\, \boldsymbol{e}_i \otimes \boldsymbol{e}_j\}^\flat$, respectively, with $i, k = 1, 2, 3$ and $j, l = 1, 2$. The associated matrix representations are given by

$$\big\{\mathrm{A}\big\}^\flat = \begin{bmatrix} \mathrm{A}_{1111} & \mathrm{A}_{1112} & \mathrm{A}_{1121} & \mathrm{A}_{1122} & \mathrm{A}_{1131} & \mathrm{A}_{1132} \\ \mathrm{A}_{1211} & \mathrm{A}_{1212} & \mathrm{A}_{1221} & \mathrm{A}_{1222} & \mathrm{A}_{1231} & \mathrm{A}_{1232} \\ \mathrm{A}_{2111} & \mathrm{A}_{2112} & \mathrm{A}_{2121} & \mathrm{A}_{2122} & \mathrm{A}_{2131} & \mathrm{A}_{2132} \\ \mathrm{A}_{2211} & \mathrm{A}_{2212} & \mathrm{A}_{2221} & \mathrm{A}_{2222} & \mathrm{A}_{2231} & \mathrm{A}_{2232} \\ \mathrm{A}_{3111} & \mathrm{A}_{3112} & \mathrm{A}_{3121} & \mathrm{A}_{3122} & \mathrm{A}_{3131} & \mathrm{A}_{3132} \\ \mathrm{A}_{3211} & \mathrm{A}_{3212} & \mathrm{A}_{3221} & \mathrm{A}_{3222} & \mathrm{A}_{3231} & \mathrm{A}_{3232} \end{bmatrix}, \quad \big\{B\big\}^\flat = \begin{bmatrix} B_{11} \\ B_{12} \\ B_{21} \\ B_{22} \\ B_{31} \\ B_{32} \end{bmatrix}, \tag{A.85}$$

which means that $\{\mathrm{A}\}^\flat$ becomes a $\mathcal{R}^{6\times6}$-matrix. However, this matrix form must not be confused with the Voigt notation which results in a $\mathcal{R}^{6\times6}$-matrix as well.

A.7.3 On the representation of transversely isotropic elasticity tensors

The elasticity tensor of transversely isotropic, linear-elastic materials can be represented as a linear combination of six elementary fourth-order tensors $\mathbb{E}^{[\alpha]} = \mathrm{E}^{[\alpha]}_{ijkl}\, \boldsymbol{e}_i \otimes \boldsymbol{e}_j \otimes \boldsymbol{e}_k \otimes \boldsymbol{e}_l$, $\alpha = 1, 2, 3, 4, 5, 6$, which were proposed by Walpole [499, 500]. Further details are also provided by Ponte Castañeda [378]. The six elementary tensors are strongly related to the two structural tensors $\boldsymbol{M}$ and $\boldsymbol{D} = \boldsymbol{I} - \boldsymbol{M}$, which were introduced in Eqs (3.82) and (3.88), respectively. A linear combination $a\boldsymbol{M} + b\boldsymbol{D}$, with arbitrary $a, b \in \mathcal{R}$, of these two tensors gives a formulation of a general transversely-isotropic, second-order tensor. Consequently, the definition of the six elementary fourth-order tensors is based on the various possible dyadic (outer) products between $\boldsymbol{M}$ and $\boldsymbol{D}$ and the originally provided index notations read

$$\begin{aligned} \mathrm{E}^{[1]}_{ijkl} &= \tfrac{1}{2}\, D_{ij} D_{kl}\,, \\ \mathrm{E}^{[2]}_{ijkl} &= M_{ij} M_{kl}\,, \\ \mathrm{E}^{[3]}_{ijkl} &= \tfrac{1}{2}\left(D_{ik} D_{jl} + D_{il} D_{jk} - D_{ij} D_{kl}\right), \\ \mathrm{E}^{[4]}_{ijkl} &= \tfrac{1}{2}\left(M_{il} D_{jk} + D_{il} M_{jk} + M_{ik} D_{jl} + D_{ik} M_{jl}\right), \\ \mathrm{E}^{[5]}_{ijkl} &= M_{ij} D_{kl}\,, \\ \mathrm{E}^{[6]}_{ijkl} &= D_{ij} M_{kl}\,. \end{aligned} \tag{A.86}$$

A reformulation in absolute tensor notation gives the expressions

$$\begin{aligned} \mathbb{E}^{[1]} &= \tfrac{1}{2}\,(\boldsymbol{D} \otimes \boldsymbol{D})\,, \\ \mathbb{E}^{[2]} &= \boldsymbol{M} \otimes \boldsymbol{M}\,, \\ \mathbb{E}^{[3]} &= \tfrac{1}{2}\left((\boldsymbol{D} \otimes \boldsymbol{D})^{T_{23}} + (\boldsymbol{D} \otimes \boldsymbol{D})^{T_{24}} - \boldsymbol{D} \otimes \boldsymbol{D}\right), \\ \mathbb{E}^{[4]} &= \tfrac{1}{2}\left((\boldsymbol{M} \otimes \boldsymbol{D} + \boldsymbol{D} \otimes \boldsymbol{M})^{T_{23}} + (\boldsymbol{M} \otimes \boldsymbol{D} + \boldsymbol{D} \otimes \boldsymbol{M})^{T_{24}}\right), \\ \mathbb{E}^{[5]} &= \boldsymbol{M} \otimes \boldsymbol{D}\,, \\ \mathbb{E}^{[6]} &= \boldsymbol{D} \otimes \boldsymbol{M}\,. \end{aligned} \tag{A.87}$$

As the structural tensor $\boldsymbol{D}$ is a combination of the identity tensor $\boldsymbol{I}$ and the structural tensor $\boldsymbol{M}$, we can also formulate the six elementary tensors as combinations solely of $\boldsymbol{I}$

and $\boldsymbol{M}$:

$$\begin{aligned}
\mathbb{E}^{[1]} &= \tfrac{1}{2}\left(\boldsymbol{I}\otimes\boldsymbol{I} - \boldsymbol{I}\otimes\boldsymbol{M} - \boldsymbol{M}\otimes\boldsymbol{I} + \boldsymbol{M}\otimes\boldsymbol{M}\right), \\
\mathbb{E}^{[2]} &= \boldsymbol{M}\otimes\boldsymbol{M}, \\
\mathbb{E}^{[3]} &= \tfrac{1}{2}\big(-\boldsymbol{I}\otimes\boldsymbol{I} + \boldsymbol{I}\otimes\boldsymbol{M} + \boldsymbol{M}\otimes\boldsymbol{I} + \boldsymbol{M}\otimes\boldsymbol{M} + \\
&\quad + (\boldsymbol{I}\otimes\boldsymbol{I} - \boldsymbol{I}\otimes\boldsymbol{M} - \boldsymbol{M}\otimes\boldsymbol{I})^{T_{23}} + (\boldsymbol{I}\otimes\boldsymbol{I} - \boldsymbol{I}\otimes\boldsymbol{M} - \boldsymbol{M}\otimes\boldsymbol{I})^{T_{24}}\big), \\
\mathbb{E}^{[4]} &= \tfrac{1}{2}\big((\boldsymbol{I}\otimes\boldsymbol{M} + \boldsymbol{M}\otimes\boldsymbol{I})^{T_{23}} + (\boldsymbol{I}\otimes\boldsymbol{M} + \boldsymbol{M}\otimes\boldsymbol{I})^{T_{24}}\big) - 2\,\boldsymbol{M}\otimes\boldsymbol{M}, \\
\mathbb{E}^{[5]} &= \boldsymbol{M}\otimes\boldsymbol{I} - \boldsymbol{M}\otimes\boldsymbol{M}, \\
\mathbb{E}^{[6]} &= \boldsymbol{I}\otimes\boldsymbol{M} - \boldsymbol{M}\otimes\boldsymbol{M}.
\end{aligned} \tag{A.88}$$

The first four tensors are idempotent projection tensors and fulfil the relations $\mathbb{E}^{[\alpha]}\mathbb{E}^{[\alpha]} = \mathbb{E}^{[\alpha]}$ and $\mathbb{E}^{[\alpha]}\mathbb{E}^{[\beta]} = \mathbb{O}$ for $\alpha, \beta = 1, 2, 3, 4$ and $\alpha \neq \beta$. They are in fact an additive decomposition of the symmetrising map, which is easy to deduce from Eqs (A.88), hence,

$$\mathbb{E}^{[1]} + \mathbb{E}^{[2]} + \mathbb{E}^{[3]} + \mathbb{E}^{[4]} = \tfrac{1}{2}\left((\boldsymbol{I}\otimes\boldsymbol{I})^{T_{23}} + (\boldsymbol{I}\otimes\boldsymbol{I})^{T_{24}}\right) = \mathbb{I}_{\mathrm{sym}}. \tag{A.89}$$

In contrast, the two tensors $\mathbb{E}^{[5]}$ and $\mathbb{E}^{[6]}$ are nilpotent, hence, $\mathbb{E}^{[5]}\mathbb{E}^{[5]} = \mathbb{E}^{[6]}\mathbb{E}^{[6]} = \mathbb{O}$. They are involved in a sum which yields the tracing map:

$$2\mathbb{E}^{[1]} + \mathbb{E}^{[2]} + \mathbb{E}^{[5]} + \mathbb{E}^{[6]} = \boldsymbol{I}\otimes\boldsymbol{I} = \mathbb{I}_{\mathrm{tr}}. \tag{A.90}$$

Further projection tensors appear by certain combinations of the six elementary tensors. For instance, an axisymmetric projection tensor can be formulated as

$$\mathbb{E}^{[\mathrm{a}]} = \tfrac{1}{3}\left(\mathbb{E}^{[1]} + 2\mathbb{E}^{[2]} - \mathbb{E}^{[5]} - \mathbb{E}^{[6]}\right). \tag{A.91}$$

It is idempotent, $\mathbb{E}^{[\mathrm{a}]}\mathbb{E}^{[\mathrm{a}]} = \mathbb{E}^{[\mathrm{a}]}$, and obeys "orthogonality" with the projection tensors $\mathbb{E}^{[3]}$ and $\mathbb{E}^{[4]}$, such that $\mathbb{E}^{[\mathrm{a}]}\mathbb{E}^{[3]} = \mathbb{E}^{[3]}\mathbb{E}^{[\mathrm{a}]} = \mathbb{O}$ and $\mathbb{E}^{[\mathrm{a}]}\mathbb{E}^{[4]} = \mathbb{E}^{[4]}\mathbb{E}^{[\mathrm{a}]} = \mathbb{O}$. Two further projection tensors are

$$\mathbb{J} = \tfrac{1}{3}\left(2\mathbb{E}^{[1]} + \mathbb{E}^{[2]} + \mathbb{E}^{[5]} + \mathbb{E}^{[6]}\right) = \tfrac{1}{3}\mathbb{I}_{\mathrm{tr}} \quad \text{and} \quad \mathbb{K} = \mathbb{E}^{[\mathrm{a}]} + \mathbb{E}^{[3]} + \mathbb{E}^{[4]}, \tag{A.92}$$

which satisfy the relations $\mathbb{J} + \mathbb{K} = \mathbb{I}_{\mathrm{sym}}$, $\mathbb{J}\mathbb{J} = \mathbb{J}$, $\mathbb{K}\mathbb{K} = \mathbb{K}$, and $\mathbb{J}\mathbb{K} = \mathbb{K}\mathbb{J} = \mathbb{O}$.

Note, for completeness, that a slightly different set of elementary tensors was given by Walpole [501]. However, it can be shown that the tensors therein are just rearranged forms of the ones presented here.

B Further mathematical explanations and details

B.1 The Legendre transform

Basics Consider a scalar- and finite-valued, differentiable function $f(\mathcal{X})$. The generalised argument $\mathcal{X}$ may be a scalar $\mathcal{X} \in \mathcal{R}$ ($f : \mathcal{R} \to \mathcal{R}$), vector $\mathcal{X} \in \mathcal{R}^3$ ($f : \mathcal{R}^3 \to \mathcal{R}$), second-order tensor $\mathcal{X} \in \mathcal{R}^{3\otimes 3}$ ($f : \mathcal{R}^{3\otimes 3} \to \mathcal{R}$), or higher-order tensor. The function f is assumed to be convex in $\mathcal{X}$, see, for example Eqs (3.112) for corresponding convexity conditions if $\mathcal{X} \in \mathcal{R}^{3\otimes 3}$. We say that the derivative of f with respect to its argument $\mathcal{X}$ is given by $\mathcal{Y} = \partial_{\mathcal{X}} f$. Obviously, the dimension of $\mathcal{Y}$ is equal to the dimension of the argument $\mathcal{X}$. For scalar-valued $\mathcal{X}$, the derivative $\mathcal{Y}$ is nothing more than the slope of the curve f. Now, the *Legendre transform* of f is defined as

$$f^\star(\mathcal{Y}) = \langle \mathcal{X}, \mathcal{Y} \rangle - f(\mathcal{X}) \tag{B.1}$$

where the original argument $\mathcal{X}$ has to be replaced by solving $\mathcal{Y} = \partial_{\mathcal{X}} f$ for $\mathcal{X}$ and substituting it into $f^\star(\mathcal{Y})$. The expression $\langle \mathcal{X}, \mathcal{Y} \rangle$ stands for the inner product of $\mathcal{X}$ and $\mathcal{Y}$, which is a simple multiplication of $\mathcal{X}$ and $\mathcal{Y}$ for a scalar $\mathcal{X}$ and an appropriate scalar dot product for vector- and tensor-valued $\mathcal{X}$. The function $f^\star$ is called *dual* to the original function f and it is dependent on $\mathcal{Y}$. The interesting feature of the Legendre transform is that the derivative of the dual function with respect to the new argument $\mathcal{Y}$ is now given by $\partial_{\mathcal{Y}} f^\star = \mathcal{X}$. This connection motivates the designation of $\{\mathcal{X}, \mathcal{Y}\}$ as a so-called *conjugate pair*. The concept of the Legendre transformation can be generalised to non-convex functions $f(\mathcal{X})$, if we replace the definition of $f^\star$ in Eq. (B.1) by

$$f^\star(\mathcal{Y}) := \sup_{\mathcal{X}} \{ \langle \mathcal{X}, \mathcal{Y} \rangle - f(\mathcal{X}) \} , \tag{B.2}$$

which is referred to as the *Legendre-Fenchel transformation* or *convex conjugate*. In Eq. (B.2), sup is the supremum. The Legendre-Fenchel transform is not only a generalisation of the Legendre transform to non-convex functions f, but it can even be used for non-smooth f which are not continuously differentiable. In that case, one may have several subgradients $\mathcal{Y} \in \partial_{\mathcal{X}} f$ as elements of the subdifferential $\partial_{\mathcal{X}} f$ instead of a derivative $\mathcal{Y} = \partial_{\mathcal{X}} f$. However, independent of the convexity and smoothness properties of the function f, its dual function $f^\star$ is always convex. Furthermore, the two functions f and $f^\star$ are related through the *Fenchel inequality*

$$\langle \mathcal{X}, \mathcal{Y} \rangle \leq f(\mathcal{X}) + f^\star(\mathcal{Y}) \quad \forall \mathcal{X}, \mathcal{Y} . \tag{B.3}$$

With the knowledge that the dual function $f^\star$ is always convex, it becomes clear that the Legendre-Fenchel transform $(f^\star)^\star := f^{\star\star}$ of the dual function is convex as well. Thus, the double transform $f^{\star\star}$ cannot be the involution of f if it is a non-convex function. In this case, $f^{\star\star}$ rather has the remarkable property that it depicts the *convex envelope* $\mathcal{C}f(\mathcal{X})$ of the function f. This is also referred to as convexification. If f is convex, however, the double transform $f^{\star\star}$ it the involution of f, which leads us to

$$f^{\star\star}(\mathcal{X}) = \sup_{\mathcal{Y}} \{ \langle \mathcal{X}, \mathcal{Y} \rangle - f^\star(\mathcal{Y}) \} = \begin{cases} f(\mathcal{X}) & \text{if } f(\mathcal{X}) \text{ is convex} \\ \mathcal{C}f(\mathcal{X}) & \text{if } f(\mathcal{X}) \text{ is non-convex.} \end{cases} \tag{B.4}$$

In any case, we have the inequality

$$f^{\star\star}(\mathcal{X}) \leq f(\mathcal{X})\,. \tag{B.5}$$

Now, we want to introduce a generalisation of the classical Legendre transformation, which proves very useful in this work. This generalised transformation is defined by

$$f^*(\mathcal{Y}) := \operatorname*{stat}_{\mathcal{X}}\{\langle \mathcal{X}, \mathcal{Y}\rangle - f(\mathcal{X})\} \tag{B.6}$$

and the difference to the previously introduced transforms is indicated by writing f^* instead of $f^\star$. The generalised Legendre transform f^* is defined in Eq. (B.6) by means of a stationarity operation. It is performed by formulating the stationarity condition

$$\partial_{\mathcal{X}}\{\langle \mathcal{X}, \mathcal{Y}\rangle - f(\mathcal{X})\} = \mathcal{Y} - \partial_{\mathcal{X}} f(\mathcal{X}) \quad \Rightarrow \quad \mathcal{Y} = \partial_{\mathcal{X}} f(\mathcal{X})\,, \tag{B.7}$$

solving it for $\mathcal{X}$ and inserting the result back into Eq. (B.6) to get the transform $f^*(\mathcal{Y})$. This is essentially the approach of the original Legendre transformation, as defined in Eq. (B.1). However, the applicability of the generalised Legendre transform is extended to non-convex and non-smooth functions. This makes it similar to the Legendre-Fenchel transformation, however, there are important differences. The Legendre-Fenchel transform $f^\star$, defined by Eq. (B.2), seeks for a supremum. That means that if there are multiple solutions of the stationary condition $\mathcal{Y} = \partial_{\mathcal{X}} f(\mathcal{X})$, one proceeds with the solution which maximises the transform $f^\star$. This optimisation step is the reason for the convexity of $f^\star$. In turn, the generalised Legendre transformation does not perform such an optimisation and, based on that observation, we note that the transform f^* is not necessarily convex. This means that the generalised Legendre transform f^* can be *multi-valued*, whereas the Legendre-Fenchel transform $f^\star$ is single-valued. In short, we can conclude that f^* contains more information than the supremisation-based $f^\star$. This has implications on the double transform $(f^*)^* := f^{**}$, which is found to always give the original function f, regardless of the convexity properties of f. Hence, we can write

$$f^{**}(\mathcal{X}) = \operatorname*{stat}_{\mathcal{Y}}\{\langle \mathcal{X}, \mathcal{Y}\rangle - f^*(\mathcal{Y})\} = f(\mathcal{X})\,. \tag{B.8}$$

Example The concept of the Legendre- and the Legendre-Fenchel transformation shall be briefly shown here based on a one-dimensional function $f : \mathcal{R} \to \mathcal{R}$, defined by

$$f(x) = x^2 - |x|\,. \tag{B.9}$$

Hence, the general argument $\mathcal{X}$ simply becomes a scalar variable $x \in \mathcal{R}$. A visualisation of the function $f(x)$ over x is provided in Figure B.1a. With this, we directly see that f is non-convex and that it is not differentiable at $x = 0$, which is caused by the absolute value function $|x|$. However, as we noted above, we can formulate a subdifferential $\partial_x f$ at $x = 0$. This subdifferential contains all possible subgradients, which essentially means that it depicts a range of values determined by the limit values of the derivative from the left and from the right. For the given function f, it is easy to compute the limit values $\lim_{x\to 0^-} \partial_x f = 1$ and $\lim_{x\to 0^+} \partial_x f = -1$. The subdifferential at $x = 0$ is thus given by $\partial_x f = [-1, 1]$. Together with the derivatives at $x \neq 0$, we have

$$\partial_x f(x) = \begin{cases} 2x + 1 & \text{if } x < 0 \\ [-1, 1] & \text{if } x = 0 \\ 2x - 1 & \text{if } x > 0\,, \end{cases} \tag{B.10}$$

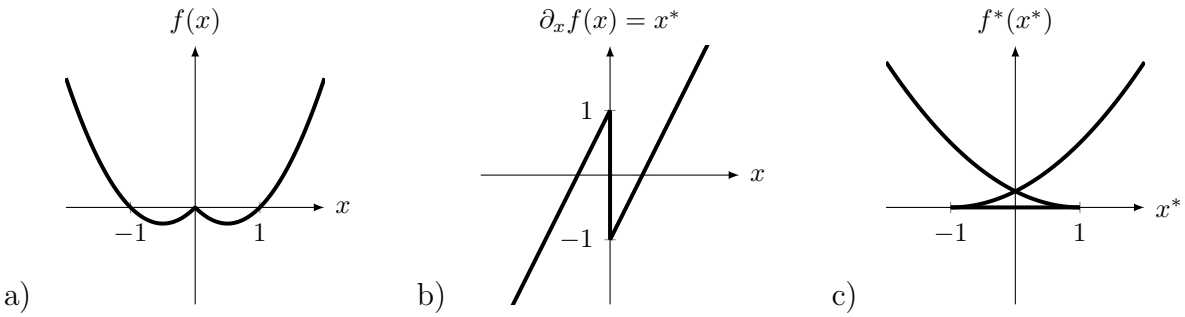

Figure B.1: Visualisation of the generalised Legendre transformation. a) The original function $f(x) = x^2 - |x|$, b) the derivative $\partial_x f(x)$ of f for $x \neq 0$ and the subdifferential of f at $x = 0$, c) the swallowtail-shaped generalised Legendre transform $f^*(x^*)$.

see Figure B.1b. Now, Eq. (B.6) for the generalised Legendre transform and the associated stationary condition read

$$f^*(x^*) = \operatorname*{stat}_x \{x x^* - f(x)\} \quad \text{and} \quad x^* = \partial_x f(x)\,, \tag{B.11}$$

respectively. Hence, the dual variable $\mathcal{Y}$ is now denoted by x^*. Subsequently, the stationarity condition $(\text{B.11})_2$ is solved for x by making use of Eq. (B.10), yielding

$$x = \begin{cases} \frac{1}{2}(x^* - 1) & \text{if } x^* < 1 \\ 0 & \text{if } x^* \in [-1, 1] \\ \frac{1}{2}(x^* + 1) & \text{if } x^* > -1\,. \end{cases} \tag{B.12}$$

Obviously, there are multiple values for x in the range $x^* \in [-1, 1]$ due to the non-convexity of f. However, we keep all these solutions and substitute them into Eq. $(\text{B.11})_2$ to get the generalised Legendre transform

$$f^*(x^*) = \begin{cases} \frac{1}{4}(x^* - 1)^2 & \text{if } x^* < 1 \\ 0 & \text{if } x^* \in [-1, 1] \\ \frac{1}{4}(x^* + 1)^2 & \text{if } x^* > -1\,. \end{cases} \tag{B.13}$$

By looking at the visualisation of f^* in Figure B.1c, we directly see that the generalised Legendre dual of the non-convex function f is non-convex and multi-valued and that the curve of f^* has a so-called swallowtail shape. For instance, the curve of f^* intersects the axis at $x^* = 0$ three times. Recalling that x^* is the derivative (or subdifferential) $\partial_x f$, this tells us that the curve of f has three extrema, which are of course the two global minima at $x = \pm 1/2$ and the local maximum at $x = 0$. Subsequently, we can apply the generalised Legendre transformation on $f^*(x^*)$, giving

$$f^{**}(x) = \operatorname*{stat}_{x^*} \{x x^* - f^*(x^*)\} = x^2 - |x| = f(x)\,. \tag{B.14}$$

Therein, we note that the stationarity condition reads $x = \partial_{x^*} f^*$, which highlights the duality of the conjugate pair $\{x, x^*\}$ once more. We note that the double transform f^{**} is identical to the original function f, as expected.

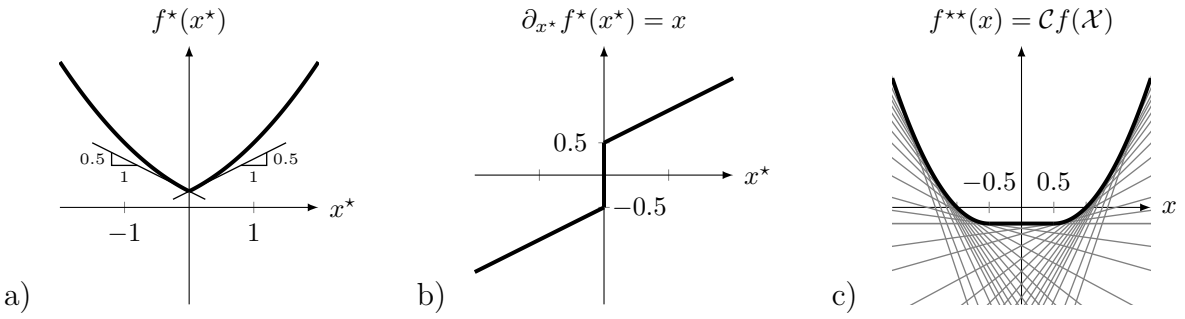

Figure B.2: Visualisation of the Legendre-Fenchel transformation. a) The dual function $f^\star(x^\star)$ of f, b) the derivative $\partial_{x^\star} f^\star$ of $f^\star$ for $x^\star \neq 0$ and the subdifferential of $f^\star$ at $x^\star = 0$, c) the double Legendre-Fenchel transform $f^{\star\star}(x)$ and (in grey) tangents on $f^{\star\star}$. The convexity of $f^{\star\star}$ is elucidated since none of the tangents is above the curve $f^{\star\star}$, which is essentially the second convexity statement $(3.112)_2$.

Now, we compute the Legendre-Fenchel transform $f^\star$ of f to show the difference to the generalised Legendre transform f^*. From Eq. (B.2), we know that

$$f^\star(x^\star) = \sup_x \{x x^\star - f(x)\} \quad \text{and} \quad x^\star = \partial_x f(x)\,, \tag{B.15}$$

where the latter equation is the stationary condition and we denote the conjugate variable with $x^\star$. The stationarity condition is the same as for the Legendre transformation and results in expression (B.12) for the variable x by replacing x^* with $x^\star$. However, instead of keeping all solutions for x, we only proceed with those ones which maximise the expression $x x^\star - f(x)$ for a given $x^\star$. This is the essence of the supremum. The Legendre-Fenchel transform is then obtained as

$$f^\star(x^\star) = \begin{cases} \frac{1}{4}(x^\star - 1)^2 & \text{if } x^\star < 0 \\ \frac{1}{4}(x^\star + 1)^2 & \text{if } x^\star \geq 0\,, \end{cases} \tag{B.16}$$

see Figure B.2a. We observe that the graph of $f^\star$ is identical to f^* above the point where f^* intersects itself. However, $f^\star$ misses the part below this point and therefore represents a convex and single-valued function. At $x^\star = 0$, the curve of the dual function $f^\star$ is non-differentiable, but we can find the subdifferential $\partial_{x^\star} f^\star \in [-1/2, 1/2]$. This is plotted in Figure B.2b, together with the derivatives at $x^\star \neq 0$. Recalling the fundamental duality relation between x and $x^\star$, we know that $x = \partial_{x^\star} f^\star$ and observe from Figure B.2b that there is a one-to-one relation between $x^\star$ and its conjugate argument x. Thus, we lost the information about the non-convex part of the original function f. Computing now the double Legendre-Fenchel transform gives the convex envelope of f:

$$f^{\star\star}(x) = \sup_{x^\star} \{x x^\star - f^\star(x^\star)\} = \left\{ \begin{cases} x^2 + x & \text{if } x < -\frac{1}{2} \\ -\frac{1}{4} & \text{if } x \in [-\frac{1}{2}, \frac{1}{2}] \\ x^2 - x & \text{if } x > \frac{1}{2} \end{cases} \right\} = \mathcal{C}f(\mathcal{X})\,. \tag{B.17}$$

Hence, the non-convex part of f between $x = -1/2$ and $x = 1/2$ is replaced in $f^{\star\star}$ by a straight line with slope $\partial_x f^{\star\star} = x^\star = 0$.

B.2 Fundamentals on probability theory

Probability density functions are a fundamental mathematical tool for the statistical description of continuously distributed variables. In the continuum-mechanical context, those variables may represent any kind of field, such as deformation or stress fields. However, particularly useful are probability density functions for the description of structural characteristics of a material, especially in multiscale studies, as explained in Section 4.2. In this section, basics and examples are presented for the description of a scalar variable $\mathfrak{X} \in \mathcal{R}$. Yet, most of the concepts can be generalised to higher dimensions in a straightforward manner.

Basics The probability $\mathfrak{Pr}$ that a continuously distributed variable $\mathfrak{X}$ ranges in the interval $[a, b]$, with $\{a, b \in \mathcal{R}; a < b\}$, is described by means of a *univariate probability density function* (PDF) $\mathfrak{p}_\mathfrak{X}$ in terms of the relation

$$\mathfrak{Pr}(\mathfrak{X} \in [a, b]) = \int_a^b \mathfrak{p}_\mathfrak{X}(\mathfrak{x}) \, \mathrm{d}\mathfrak{x} \,. \tag{B.18}$$

The support of the PDF is given by $\mathfrak{R}_\mathfrak{X} = \{\mathfrak{x} \in \mathcal{R} : \mathfrak{p}_\mathfrak{X}(\mathfrak{x}) > 0\}$. Hence, the PDF has an infinite support $\mathfrak{R}_\mathfrak{X} = \mathcal{R} = (-\infty, \infty)$ if the variable $\mathfrak{X}$ is distributed over the whole range of $\mathcal{R}$, whereas the PDF has a finite support $\mathfrak{R}_\mathfrak{X} = [\mathfrak{x}^\flat, \mathfrak{x}^\sharp]$ if the variable $\mathfrak{X}$ is distributed in a closed interval $[\mathfrak{x}^\flat, \mathfrak{x}^\sharp]$. The PDF is zero outside of $\mathfrak{R}_\mathfrak{X}$. Further, it is straightforward to formulate the *cumulative distribution function* (CDF)

$$\mathfrak{F}_\mathfrak{X}(\mathfrak{x}) = \mathfrak{Pr}(\mathfrak{X} \leq \mathfrak{x}) = \int_{-\infty}^{\mathfrak{x}} \mathfrak{p}_\mathfrak{X}(u) \, \mathrm{d}u \,, \tag{B.19}$$

where the lower bound can be replaced by $\mathfrak{r}^\flat$ for PDF with finite support. Since it is reasonable that the overall probability $\mathfrak{Pr}(\mathfrak{X} \in \mathfrak{R}_\mathfrak{X})$ is one, we have the limit value $\lim_{\mathfrak{r}\to\infty} \mathfrak{F}_\mathfrak{X} = 1$ for infinite supports and $\mathfrak{F}_\mathfrak{X}|_{\mathfrak{x}=\mathfrak{x}^\sharp} = 1$ for finite supports. Next, it is useful to consider the moments of a PDF in order to describe the distributions in a statistical sense. The first (raw) moment defines the *mean* value $\bar{\mathfrak{x}}$, which represents the expectation value of the distribution. It reads

$$\bar{\mathfrak{x}} := \mathrm{E}[\mathfrak{X}] = \int_{\mathfrak{R}_\mathfrak{X}} \mathfrak{x} \, \mathfrak{p}_\mathfrak{X}(\mathfrak{x}) \, \mathrm{d}\mathfrak{x} \,. \tag{B.20}$$

With this, it is possible to distinguish between raw moments with respect to zero and the central moments with respect to the mean. The n-th central moment is defined as

$$\mathrm{E}\big[(\mathfrak{X} - \mathrm{E}[\mathfrak{X}])^n\big] = \int_{\mathfrak{R}_\mathfrak{X}} (\mathfrak{x} - \bar{\mathfrak{x}})^n \, \mathfrak{p}_\mathfrak{X} \, \mathrm{d}\mathfrak{x} \,. \tag{B.21}$$

It is easy to see that $\mathrm{E}\big[(\mathfrak{X} - \mathrm{E}[\mathfrak{X}])^0\big] = 1$ and $\mathrm{E}\big[(\mathfrak{X} - \mathrm{E}[\mathfrak{X}])^1\big] = 0$. The second central moment is defined as the *variance*

$$\sigma_\mathfrak{x}^2 := \mathrm{E}\big[(\mathfrak{X} - \mathrm{E}[\mathfrak{X}])^2\big] \tag{B.22}$$

and its square root denotes the *standard deviation* $\sigma_\mathfrak{x}$. In addition to the moments, it is also possible to further characterise the distribution in terms of other measures. For

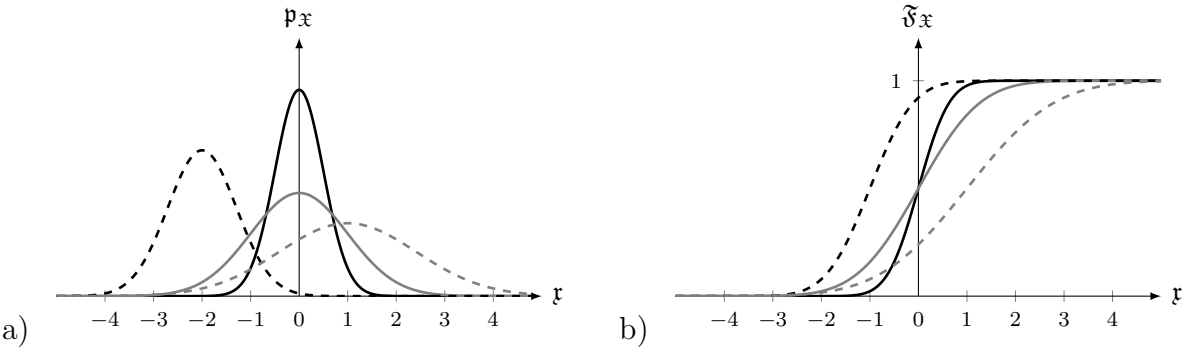

Figure B.3: Visualisation of the normal (Gaussian) distribution. a) The probability density function $\mathfrak{p}_\mathfrak{X}$. b) The cumulative distribution function $\mathfrak{F}_\mathfrak{X}$. $\mathcal{N}(0, 0.25)$ solid black, $\mathcal{N}(0, 1)$ solid gray, $\mathcal{N}(-1, 0.5)$ dashed black, $\mathcal{N}(1, 2)$ dashed gray.

instance, the *mode* $\mathfrak{x}^\mathrm{m}$ is the most likely value of the distribution. Hence, it depicts the argument of the maximum (peak) of the PDF, such that

$$\mathfrak{x}^\mathrm{m} = \arg\max_{\mathfrak{x}\in\mathfrak{R}_\mathfrak{X}} \mathfrak{p}_\mathfrak{X}(\mathfrak{x})\,. \tag{B.23}$$

This means that the CDF has an inflection point at $\mathfrak{x}^\mathrm{m}$. We recall that if the structure of a material shall be described, one usually has to proceed from such statistical measures and does not have the full knowledge on the continuous distribution of a variable $\mathfrak{X}$. In turn, one has to choose a suitable PDF which can be constructed on the basis of values such as the mean or the variance. Four examples of such functions are discussed in the following.

Examples

- Normal (Gaussian) distribution

$$\mathfrak{X} \sim \mathcal{N}(\bar{\mathfrak{x}}, \sigma_\mathfrak{x}^2)\,, \quad \mathfrak{p}_\mathfrak{X}(\mathfrak{x}) = \frac{1}{\sqrt{2\pi\sigma_\mathfrak{x}^2}} \exp\Big[-\frac{(\mathfrak{x}-\bar{\mathfrak{x}})^2}{2\sigma_\mathfrak{x}^2}\Big]\,, \quad \mathfrak{F}_\mathfrak{X}(\mathfrak{x}) = \frac{1}{2}\Big(1+\mathrm{erf}\Big[\frac{\mathfrak{x}-\bar{\mathfrak{x}}}{\sqrt{2\sigma_\mathfrak{x}^2}}\Big]\Big) \tag{B.24}$$

Therein, $\mathfrak{X} \sim \mathcal{N}(\bar{\mathfrak{x}}, \sigma_\mathfrak{x}^2)$ means that the variable $\mathfrak{X}$ has the probability distribution of $\mathcal{N}(\bar{\mathfrak{x}}, \sigma_\mathfrak{x}^2)$. The normal distribution is dependent on two parameters, which are the mean and the variance. It is symmetric with respect to the mean and has infinite support. The support, mean, mode and the variance of the normal distribution as well as the following distributions are summarised in Table B.1. Further, the CDF contains the *error function*

$$\mathrm{erf}[x] = \frac{1}{\sqrt{\pi}} \int_{-x}^{x} \exp[-t^2]\,\mathrm{d}t\,, \tag{B.25}$$

which entails the typical sigmoidal shape for this function. The Gaussian distribution is visualised in Figure (B.3) for four different parameter combinations.

- Beta distribution

$$\mathfrak{X} \sim \mathrm{Beta}(\beta_1, \beta_2)\,, \quad \mathfrak{p}_\mathfrak{X}(\mathfrak{x}) = \frac{\mathfrak{x}^{\beta_1-1}\,(1-\mathfrak{x})^{\beta_2-1}}{\mathcal{B}[\beta_1, \beta_2]}\,, \quad \mathfrak{F}_\mathfrak{X}(\mathfrak{x}) = \mathcal{I}_\mathfrak{x}[\beta_1, \beta_2] \tag{B.26}$$

distribution	**support** $\mathfrak{R}_\mathfrak{x}$	**mean** $\bar{\mathfrak{x}}$	**mode** $\mathfrak{x}^\mathrm{m}$	**variance** $\sigma_\mathfrak{x}^2$
$\mathcal{N}(\bar{\mathfrak{x}}, \sigma_\mathfrak{x}^2)$	$(-\infty, \infty)$	$\bar{\mathfrak{x}}$	$\bar{\mathfrak{x}}$	$\sigma_\mathfrak{x}^2$
$\mathrm{Beta}(\beta_1, \beta_2)$	$(0, 1)$	$\frac{\beta_1}{\beta_1+\beta_2}$	$\frac{\beta_1-1}{\beta_1+\beta_2-2}$	$\frac{\beta_1\beta_2}{(\beta_1+\beta_2)^2\,(\beta_1+\beta_2+1)}$
$\mathrm{Beta}(\beta_1, \beta_2, \mathfrak{x}^\flat, \mathfrak{x}^\sharp)$	$(\mathfrak{x}^\flat, \mathfrak{x}^\sharp)$	$\frac{\beta_1\mathfrak{x}^\sharp+\beta_2\mathfrak{x}^\flat}{\beta_1+\beta_2}$	$\frac{(\beta_1-1)\mathfrak{x}^\sharp+(\beta_2-1)\mathfrak{x}^\flat}{\beta_1+\beta_2-2}$	$\frac{\beta_1\beta_2\,(\mathfrak{x}^\sharp-\mathfrak{x}^\flat)^2}{(\beta_1+\beta_2)^2\,(\beta_1+\beta_2+1)}$
$\mathrm{Tri}(\mathfrak{x}^\flat, \mathfrak{x}^\mathrm{m}, \mathfrak{x}^\sharp)$	$(\mathfrak{x}^\flat, \mathfrak{x}^\sharp)$	$\frac{\mathfrak{x}^\flat+\mathfrak{x}^\mathrm{m}+\mathfrak{x}^\sharp}{3}$	$\mathfrak{x}^\mathrm{m}$	$\frac{(\mathfrak{x}^\sharp-\mathfrak{x}^\flat)^2+(\mathfrak{x}^\sharp-\mathfrak{x}^\mathrm{m})^2+(\mathfrak{x}^\mathrm{m}-\mathfrak{x}^\flat)^2}{36}$

Table B.1: Selected properties of the normal, Beta, four-parameter Beta and the triangular distribution. For the Beta distributions it is assumed that $\beta_1 > 1/2$ and $\beta_2 > 1/2$.

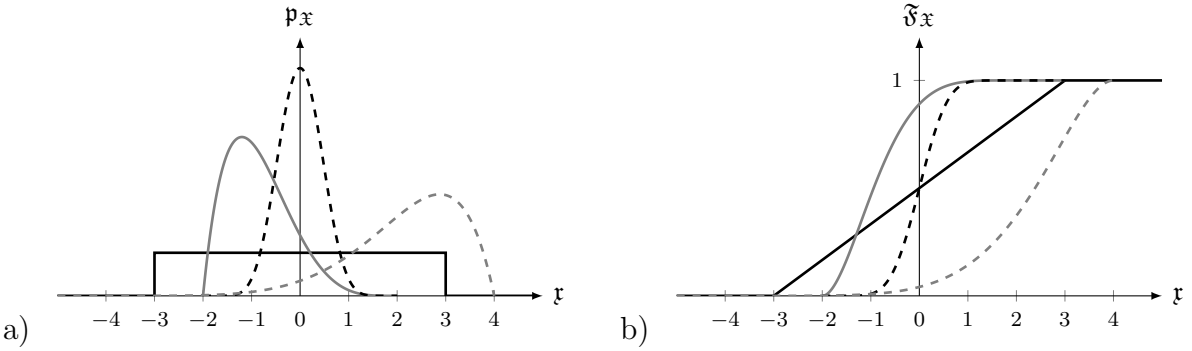

Figure B.4: Visualisation of the (four-parameter) Beta distribution. a) The probability density function $\mathfrak{p}_\mathfrak{X}$. b) The cumulative distribution function $\mathfrak{F}_\mathfrak{X}$. $\mathrm{Beta}(-3, 3, 1, 1)$ solid black, $\mathrm{Beta}(-2, 2, 1, 5)$ solid gray, $\mathrm{Beta}(-2, 2, 10, 10)$ dashed black, $\mathrm{Beta}(-5, 4, 8, 2)$ dashed gray.

Therein, the Beta function $\mathcal{B}[\beta_1, \beta_2]$ and the incomplete Beta function $\mathcal{B}_x[\beta_1, \beta_2]$ are given by

$$\mathcal{B}[\beta_1, \beta_2] = \int_0^1 t^{\beta_1-1}\,(1-t)^{\beta_2-1}\,\mathrm{d}t \quad \text{and} \quad \mathcal{B}_x[\beta_1, \beta_2] = \int_0^x t^{\beta_1-1}\,(1-t)^{\beta_2-1}\,\mathrm{d}t\,. \tag{B.27}$$

Further, $\mathcal{I}_x = \mathcal{B}_x[\beta_1, \beta_2]/\mathcal{B}[\beta_1, \beta_2]$ is the incomplete regularised Beta function and entails the sigmoidal shape of the CDF. The Beta distribution has finite support $\mathfrak{R}_\mathfrak{x} = [0, 1]$ and relies on two parameters, β_1 and β_2. Further characteristics of the Beta distribution are discussed in the context of the four-parameter Beta function in the following.

- Four-parameter (scaled and shifted) Beta distribution

$$\mathfrak{X} \sim \mathrm{Beta}(\beta_1, \beta_2, \mathfrak{x}^\flat, \mathfrak{x}^\sharp)\,, \quad \mathfrak{p}_\mathfrak{X}(\mathfrak{x}) = \frac{(\mathfrak{x}-\mathfrak{x}^\flat)^{\beta_1-1}\,(\mathfrak{x}^\sharp-\mathfrak{x})^{\beta_2-1}}{(\mathfrak{x}^\sharp-\mathfrak{x}^\flat)^{\beta_1+\beta_2-1}\,\mathcal{B}[\beta_1, \beta_2]}\,, \quad \mathfrak{F}_\mathfrak{X}(\mathfrak{x}) = \mathcal{I}_{\tau_\mathfrak{x}}[\beta_1, \beta_2] \tag{B.28}$$

where $\tau_\mathfrak{x} = (\mathfrak{x}-\mathfrak{x}^\flat)/(\mathfrak{x}^\sharp-\mathfrak{x}^\flat)$. The four-parameter Beta distribution scales the support from the interval $[0, 1]$ to the interval $[\mathfrak{x}^\flat, \mathfrak{x}^\sharp]$, which is very practical in many applications. The scaled Beta distribution is visualised in Figure (B.4) for four different parameter combinations. From there, we see that it allows to describe very different distributions. For instance, $\beta_1 = \beta_2 = 1$ results in a uniform distribution of the values between $\mathfrak{x}^\flat$ and $\mathfrak{x}^\sharp$. Another special case (not shown here) is given when $\beta_1 = \beta_2 = 1/2$, resulting in an Arcsine distribution that has *two* modes at the boundaries of the support. In general, the

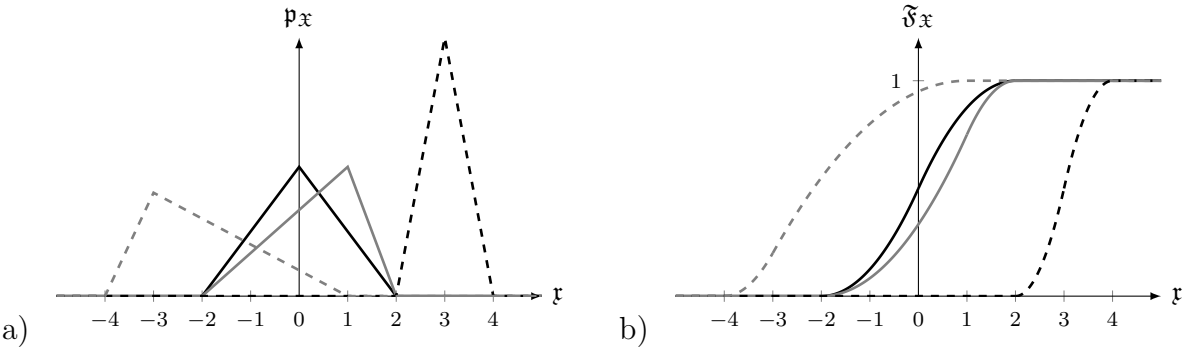

Figure B.5: Visualisation of the triangular distribution. a) The probability density function $\mathfrak{p}_\mathfrak{X}$. b) The cumulative distribution function $\mathfrak{F}_\mathfrak{X}$. Tri$(-2, 0, 2)$ solid black, Tri$(-2, 1, 2)$ solid gray, Tri$(2, 3, 4)$ dashed black, Tri$(-4, -3, 1)$ dashed gray.

Beta distribution is symmetric with respect to the mean (which is provided in Table B.1) whenever $\beta_1 = \beta_2$. Yet, distinct choices for the two parameters allow to describe very general asymmetric distributions.

- Triangular distribution

$$\mathfrak{X} \sim \mathrm{Tri}(\mathfrak{x}^\flat, \mathfrak{x}^\mathrm{m}, \mathfrak{x}^\sharp)\,, \quad \mathfrak{p}_\mathfrak{X}(\mathfrak{x}) = \begin{cases} \dfrac{2\,(\mathfrak{x} - \mathfrak{x}^\flat)}{(\mathfrak{x}^\sharp - \mathfrak{x}^\flat)(\mathfrak{x}^\mathrm{m} - \mathfrak{x}^\flat)} & \text{if } \mathfrak{x} \in [\mathfrak{x}^\flat, \mathfrak{x}^\mathrm{m}]\,, \\ \dfrac{2\,(\mathfrak{x}^\sharp - \mathfrak{x})}{(\mathfrak{x}^\sharp - \mathfrak{x}^\flat)(\mathfrak{x}^\sharp - \mathfrak{x}^\mathrm{m})} & \text{if } \mathfrak{x} \in (\mathfrak{x}^\mathrm{m}, \mathfrak{x}^\sharp]\,, \end{cases} . \tag{B.29}$$

The triangular distribution provides an easy and very good way if only very few statistical measures are given and a more detailed description by means of a Beta distribution may not be sensible. It is defined in terms of three parameters and has the finite support $[\mathfrak{x}^\flat, \mathfrak{x}^\sharp]$. Despite its simple structure, the triangular distribution is very flexible, as highlighted in Figure B.5. It allows to describe symmetric as well as asymmetric distributions around the mean. Further, the expressions for the ODF and the CDF (not displayed here) only contain simple polynomials, which are easy to implement and to evaluate. This can be an advantage in comparison to the Beta distribution, which demands the evaluation of different forms of Beta functions.

Directional statistics The probabilistic description of a variable $\mathfrak{X}_\theta$ on a repeating periodic interval (such as a variable on a circle) requires the consideration of directional statistics, which is also referred to as circular or spherical statistics. A comprehensive overview on this field is given in the textbook of Mardia & Jupp [310]. The key difference to the standard treatment discussed so far is that the ODF now has to account for the periodicity of the probability with which events may occur. For instance, if the variable $\mathfrak{X}_\theta$ is defined on the circle, which means on the interval between 0 and 2π, any probability $\mathfrak{p}(\mathfrak{X}_\theta + 2n\pi)$, $n \in \mathcal{N}$, should be identical to $\mathfrak{p}(\mathfrak{X}_\theta)$. However, it is easy to formulate suitable 2π-periodic *wrapped orientation density functions* via

$$\mathfrak{p}_\mathrm{w}(\mathfrak{X}_\theta) = \sum_{k=-\infty}^{\infty} \mathfrak{p}(\mathfrak{X}_\theta + 2\pi k)\,, \tag{B.30}$$

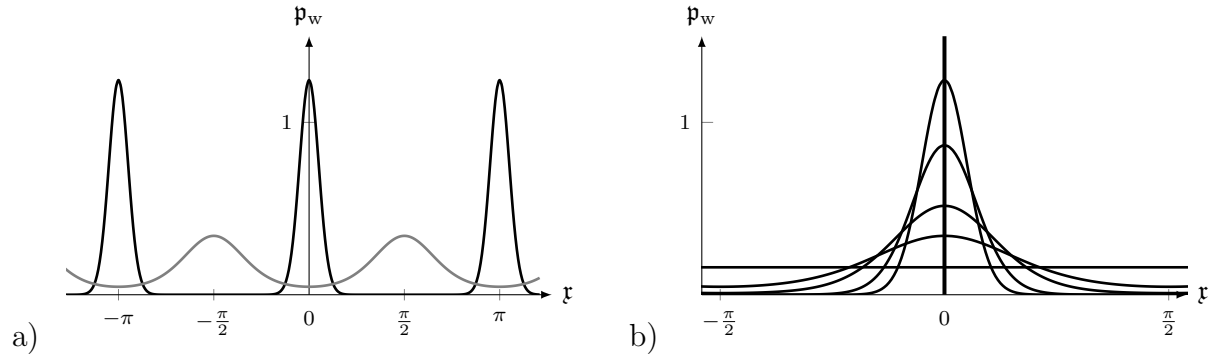

Figure B.6: The π-periodic von Mises orientation distribution function. a) π-Mises$(0, 10)$ black, π-Mises$(\pi/2, 1)$ gray. b) $\bar{\mathfrak{x}}_\theta = 0$ and $b = \{0, 1, 2, 5, 10\}$.

where one can apply any standard ODF $\mathfrak{p}$. Thus, we can formulate, for example, wrapped versions of the normal or the Beta distribution. Yet, this might result in tedious expressions because of the sum from minus to plus infinity. As an alternative to a wrapped version of the normal distribution, one can use the 2π-periodic *von Mises distribution*, defined as

$$\mathfrak{X}_\theta \sim \mathrm{Mises}(\bar{\mathfrak{x}}_\theta, b)\,, \quad \mathfrak{p}_{\mathfrak{X}_\theta}(\mathfrak{x}) = \frac{\exp\big[b\cos[\mathfrak{x} - \bar{\mathfrak{x}}_\theta]\big]}{2\pi I_0(b)} \tag{B.31}$$

where

$$I_0(x) = \frac{1}{\pi}\int_0^\pi \exp\big[x\cos[t]\big]\,\mathrm{d}t \tag{B.32}$$

is the modified Bessel function of first kind of order zero. The von Mises ODF contains two parameters. These are the mean $\bar{\mathfrak{x}}_\theta$ and a parameter b that describes the dispersion of the probability around the mean value. Moreover, if a variable $\mathfrak{X}_\theta$ is rather described on an interval $[0, \pi]$, Eq. (B.30) can accordingly be defined as

$$\mathfrak{p}_\mathrm{w}(\mathfrak{X}_\theta) = \sum_{k=-\infty}^{\infty} \mathfrak{p}(\mathfrak{X}_\theta + \pi k)\,. \tag{B.33}$$

The π-periodic version of the von Mises ODF reads

$$\mathfrak{X}_\theta \sim \pi\text{-Mises}(\bar{\mathfrak{x}}_\theta, b)\,, \quad \mathfrak{p}_{\mathfrak{X}_\theta}(\mathfrak{x}) = \frac{\exp\big[b\cos[2(\mathfrak{x} - \bar{\mathfrak{x}}_\theta)]\big]}{\pi I_0(b)}\,. \tag{B.34}$$

The periodicity of this function becomes clear from looking at Figure B.6a. Further, the influence of parameter b is shown in Figure B.6b. If $b \to \infty$, the von Mises distribution becomes a Dirac delta function at $\bar{\mathfrak{x}}_\theta$.

B.3 Population-based modelling of space orientations

The network models from Chapter 6 rely on the definition of a strain-energy function $\mathscr{W}_\mathfrak{r}$ for each space orientation, which in turn was described by a vector $\mathfrak{r}_0$. This analogously holds for the network model for the collageneous network in Section 7.2.2, where a space orientation was described by a vector $\mathfrak{a}_0$ or $\mathfrak{b}_0$. If the energy of one space orientation,

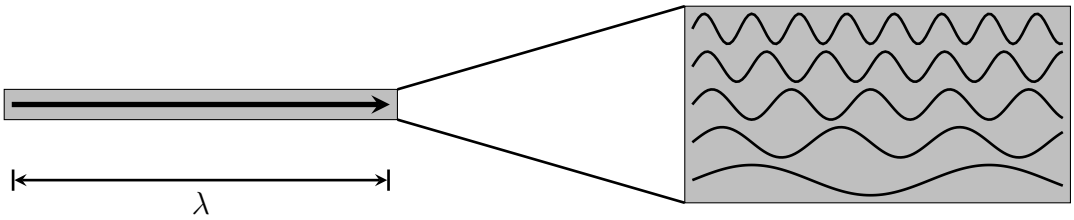

Figure B.7: A space orientation which represents a population of fibres with different degrees of crimp.

say $\mathfrak{r}_0$, is described by a strain-energy function of the form introduced in Eq. (7.24), one might conclude that the vector $\mathfrak{r}_0$ either describes exactly one single fibre with specific waviness λ_w or that the vector $\mathfrak{r}_0$ describes a whole population of fibres which all have the same waviness. In relation to the latter, however, it seems reasonable to assume that the fibres have different degrees of crimp, as shown in Figure B.7, and to accompany the energy formulation with stochastical descriptions for the distribution of the waviness λ_w in terms of a *undulation distribution function*. The distribution function shall be denoted by $\mathfrak{p}_{\lambda_\mathrm{w}}$. Alternative terms in the literature are waviness or crimping distribution function. Fan & Sacks [124] referred to it as *fractional ensemble fiber recruitment*, whereas the early work of Soong & Huang [454] called it a *collagen arrival density*. Regardless of how the distribution is named, the resulting strain-energy function for a space orientation is given by the integral formulation

$$\mathscr{W}_\mathfrak{r}(\lambda) = \int_{\lambda_\mathrm{w}^\flat}^{\lambda} \mathscr{W}_\mathfrak{cf}(\lambda, \lambda_\mathrm{w})\, \mathfrak{p}_{\lambda_\mathrm{w}}(\lambda_\mathrm{w})\, \mathrm{d}\lambda_\mathrm{w} \tag{B.35}$$

where $\lambda_\mathrm{w}^\flat$ is the lower bound of the distribution. A physically meaningful requirement for the lower bound is $\lambda_\mathrm{w}^\flat > 0$, since stretches are always non-negative (see Section 2.1.3). Interestingly, this constraint allows the occurrence of fibres that are uncrimped and store elastic energy in the reference configuration. Of course, this contradicts the assumption of an energy- and stress-free reference configuration and rather leads to a residually stressed material. In turn, requiring an energy- and stress-free reference state of $\mathscr{W}_\mathfrak{r}$ leads to $\lambda_\mathrm{w}^\flat \geq 1$. There is no similar constraint for the upper bound $\lambda_\mathrm{w}^\sharp$, but it makes sense to postulate that the waviness of the curliest fibre is still finite. Hence, the function $\mathfrak{p}_{\lambda_\mathrm{w}}$ should be chosen from the set of continuous, univariate probability distributions with support on a bounded interval $[\lambda_\mathrm{w}^\flat, \lambda_\mathrm{w}^\sharp]$. One such function is the four-parameter Beta distribution, which was introduced in the previous section. A distribution $\lambda_\mathrm{w} \sim \mathrm{Beta}(\beta_1, \beta_2, \lambda_\mathrm{w}^\flat, \lambda_\mathrm{w}^\sharp)$ for the waviness of the fibres has been used in the studies of, for example, Sverdlik & Lanir [467], Lokshin & Lanir [294], Chen et al. [76], Fan & Sacks [124], Fata et al. [125], Weisbecker et al. [510], and Avazmohammadi et al. [18]. However, also probability distributions with support on a semi-infinite interval $[\lambda_\mathrm{w}^\flat, \infty]$ have been used in the literature, such as the Gamma distribution by Sacks [413] and Bischoff [36] and the Weibull distribution by Hurschler et al. [234]. The early works of Lake & Armeniades [273], Decraemer et al. [93], and Lanir [276] considered a classical Gaussian normal distribution, which however may include unphysical non-zero probabilities for negative threshold stretches λ_w due to its unbounded support and should thus be avoided.

By looking at Eq. (B.35), we see that the incorporation of such probability functions naturally leads to an integral formulation for the energy of one space orientation. This

eventually leads to some cumbersome expressions in combination with network models, since this leads to triple integrals for the resulting network quantities. It would therefore be very practical if the integral in Eq. (B.35) could be solved analytically. This is done in the following for a Beta-distributed waviness as well as a triangularly distributed waviness by utilising the computer algebra software MATHEMATICA. Before presenting these results, however, it must be noted that the direct calculation of analytical solutions for the integral in Eq. (B.35) is not possible. Instead, the expression has to be reformulated into the convolution

$$\mathscr{W}_{\mathfrak{r}}(\lambda) = \mathscr{W}_{\mathfrak{cf}}(\lambda) * \mathfrak{p}_{\lambda_{\mathrm{w}}}(\lambda)\,. \tag{B.36}$$

Strictly speaking, this convolution is equivalent to the integral in Eq. (B.35) with integration boundaries from $-\infty$ to λ, but since the value of the integral from $-\infty$ to $\lambda_{\mathrm{w}}^{\flat}$ is zero, the results are completely equivalent. With this convolution-based expression, it is possible to find closed-form expressions for the energy $\mathscr{W}_{\mathfrak{r}}$. For a Beta-distributed fibre waviness, meaning that $\lambda_{\mathrm{w}} \sim \mathrm{Beta}(\beta_1, \beta_2, \lambda_{\mathrm{w}}^{\flat}, \lambda_{\mathrm{w}}^{\sharp})$, we obtain

$$\mathscr{W}_{\mathfrak{r}}(\lambda) = \begin{cases} 0 & \text{if } \lambda \leq \lambda_{\mathrm{w}}^{\flat}\,, \\ \mu_{\mathfrak{cf}}\, \frac{(\lambda_{\mathrm{w}}^{\sharp}-\lambda_{\mathrm{w}}^{\flat})^{-\beta_1}(\lambda-\lambda_{\mathrm{w}}^{\flat})^{2+\beta_1}\,\Gamma[\beta_1]\,{}_2\tilde{\mathcal{F}}_1[\beta_1,1-\beta_2,3+\beta_1,\tau_1]}{\mathcal{B}[\beta_1,\beta_2]} & \text{if } \lambda \in (\lambda_{\mathrm{w}}^{\flat}, \lambda_{\mathrm{w}}^{\sharp}]\,, \\ \mu_{\mathfrak{cf}}\, \frac{(\beta_1^2+\beta_1)(\lambda-\lambda_{\mathrm{w}}^{\sharp})^2+2\,\beta_1\beta_2(\lambda-\lambda_{\mathrm{w}}^{\sharp})(\lambda-\lambda_{\mathrm{w}}^{\flat})+(\beta_2^2+\beta_2)(\lambda-\lambda_{\mathrm{w}}^{\flat})^2}{2\,(\beta_1+\beta_2)(1+\beta_1+\beta_2)} & \text{if } \lambda \in (\lambda_{\mathrm{w}}^{\flat}, \lambda_{\mathrm{w}}^{\sharp}]\,, \end{cases} \tag{B.37}$$

where

$$\tau_1 = \frac{\lambda - \lambda_{\mathrm{w}}^{\flat}}{\lambda_{\mathrm{w}}^{\sharp} - \lambda_{\mathrm{w}}^{\flat}} \quad \text{and} \quad {}_2\tilde{\mathcal{F}}_1[a,b,c,d] = \frac{{}_2\mathcal{F}_1[a,b,c,d]}{\Gamma[c]} \tag{B.38}$$

Therein, ${}_2\mathcal{F}_1$ is the Gaussian hypergeometric function and $\Gamma[c] = (c-1)!$ is the Gamma function. Further details on such (a little bit exotic) mathematical functions can be found in the mathematical handbook of BRONSHTEIN ET AL. [60] and the comprehensive overview by OLVER ET AL. [366] on all kinds of mathematical functions. Subsequently, the scalar stress $P_{\mathfrak{r}}$ and the scalar stiffness $L_{\mathfrak{r}}$ can be obtained by means of a simple derivation of Eq. (B.37) with respect to stretch λ. Yet, instead of directly deriving the quite lengthy expression (B.37), it is useful to compute $P_{\mathfrak{r}}$ and $L_{\mathfrak{r}}$ by means of the relations

$$P_{\mathfrak{r}}(\lambda) = \partial_\lambda \mathscr{W}_{\mathfrak{r}}(\lambda) = \partial_\lambda \mathscr{W}_{\mathfrak{cf}}(\lambda) * \mathfrak{p}_{\lambda_{\mathrm{w}}}(\lambda) = P_{\mathfrak{cf}}(\lambda) * \mathfrak{p}_{\lambda_{\mathrm{w}}}(\lambda) \tag{B.39}$$

and

$$L_{\mathfrak{r}}(\lambda) = \partial_\lambda P_{\mathfrak{r}}(\lambda) = \partial_\lambda P_{\mathfrak{cf}}(\lambda) * \mathfrak{p}_{\lambda_{\mathrm{w}}}(\lambda) = L_{\mathfrak{cf}}(\lambda) * \mathfrak{p}_{\lambda_{\mathrm{w}}}(\lambda)\,. \tag{B.40}$$

This is because $P_{\mathfrak{cf}}$ and $L_{\mathfrak{cf}}$ become gradually simpler expressions, see Eqs (7.25) and (7.26), and the calculation from Eqs (B.39) and (B.40) usually leads to a more compact appearance of the results. In any case, the stress $P_{\mathfrak{r}}$ is given as

$$P_{\mathfrak{r}}(\lambda) = \begin{cases} 0 & \text{if } \lambda \leq \lambda_{\mathrm{w}}^{\flat}\,, \\ \mu_{\mathfrak{cf}} \left(\tau_2\, \mathcal{I}_{\tau_1}[\beta_1,\beta_2] + \frac{(\lambda_{\mathrm{w}}^{\sharp}-\lambda_{\mathrm{w}}^{\flat})\,\tau_1^{\beta_1}(1-\tau_1)^{\beta_2}}{(\beta_1+\beta_2)\,\mathcal{B}[\beta_1,\beta_2]} \right) & \text{if } \lambda \in (\lambda_{\mathrm{w}}^{\flat}, \lambda_{\mathrm{w}}^{\sharp}]\,, \\ \mu_{\mathfrak{cf}}\,\tau_2 & \text{if } \lambda > \lambda_{\mathrm{w}}^{\sharp}\,, \end{cases} \tag{B.41}$$

where

$$\tau_2 = \frac{\beta_1\,(\lambda - \lambda_{\mathrm{w}}^{\sharp}) + \beta_2\,(\lambda - \lambda_{\mathrm{w}}^{\flat})}{\beta_1 + \beta_2}\,. \tag{B.42}$$

The stiffness is given by the compact expression

$$L_{\mathfrak{r}}(\lambda) = \begin{cases} 0 & \text{if } \lambda \leq \lambda_{\mathrm{w}}^{\flat}\,, \\ \mu_{\mathfrak{cf}}\,\mathcal{I}_{\tau_1}[\beta_1, \beta_2] & \text{if } \lambda \in (\lambda_{\mathrm{w}}^{\flat}, \lambda_{\mathrm{w}}^{\sharp}]\,, \\ \mu_{\mathfrak{cf}} & \text{if } \lambda > \lambda_{\mathrm{w}}^{\sharp}\,. \end{cases} \tag{B.43}$$

In Eqs (B.41) and (B.43), $\mathcal{I}_{\tau_1}[\beta_1, \beta_2]$ is the incomplete regularised Beta function which was introduced in the context of Eq. (B.26). We directly see that the stiffness $L_{\mathfrak{r}}$ is nothing else than the CDF of the Beta distribution scaled by the collagen fibre stiffness $\mu_{\mathfrak{cf}}$. Hence, the step function that describes $L_{\mathfrak{cf}}$ is transformed to a sigmoidal curve for $L_{\mathfrak{r}}$.

The strain-energy function $\mathscr{W}_{\mathfrak{r}}$ for triangularly distributed initial wavinesses $\lambda_{\mathrm{w}} \sim \mathrm{Tri}(\lambda_{\mathrm{w}}^{\flat}, \lambda_{\mathrm{w}}^{\mathrm{m}}, \lambda_{\mathrm{w}}^{\sharp})$ can be formulated by an analog evaluation of the convolution-based expressions and reads

$$\mathscr{W}_{\mathfrak{r}}(\lambda) = \begin{cases} 0 & \text{if } \lambda \leq \lambda_{\mathrm{w}}^{\flat}\,, \\ \mu_{\mathfrak{cf}}\,\frac{(\lambda-\lambda_{\mathrm{w}}^{\flat})^4}{12\,(\lambda_{\mathrm{w}}^{\sharp}-\lambda_{\mathrm{w}}^{\flat})(\lambda_{\mathrm{w}}^{\mathrm{m}}-\lambda_{\mathrm{w}}^{\flat})} & \text{if } \lambda \in (\lambda_{\mathrm{w}}^{\flat}, \lambda_{\mathrm{w}}^{\mathrm{m}}]\,, \\ \mu_{\mathfrak{cf}}\,\left(-\frac{(\lambda_{\mathrm{w}}^{\sharp}-\lambda)^4}{12\,(\lambda_{\mathrm{w}}^{\sharp}-\lambda_{\mathrm{w}}^{\mathrm{m}})(\lambda_{\mathrm{w}}^{\sharp}-\lambda_{\mathrm{w}}^{\flat})} + \frac{(\lambda-\bar{\lambda}_{\mathrm{w}})^2+\sigma_{\lambda_{\mathrm{w}}}^2}{2}\right) & \text{if } \lambda \in (\lambda_{\mathrm{w}}^{\mathrm{m}}, \lambda_{\mathrm{w}}^{\sharp}]\,, \\ \mu_{\mathfrak{cf}}\,\frac{(\lambda-\bar{\lambda}_{\mathrm{w}})^2+\sigma_{\lambda_{\mathrm{w}}}^2}{2} & \text{if } \lambda > \lambda_{\mathrm{w}}^{\sharp}\,, \end{cases} \tag{B.44}$$

where $\bar{\lambda}_{\mathrm{w}} = (\lambda_{\mathrm{w}}^{\flat} + \lambda_{\mathrm{w}}^{\mathrm{m}} + \lambda_{\mathrm{w}}^{\sharp})/3$ is the mean, $\lambda_{\mathrm{w}}^{\mathrm{m}}$ is the mode, $\sigma_{\lambda_{\mathrm{w}}}^2$ is the variance, see Table B.1. The nice feature of the triangular distribution is that the resulting expressions only contain simple polynomials, which allows a very simple implementation. To complete these investigations, the scalar stress is given by

$$P_{\mathfrak{r}}(\lambda) = \begin{cases} 0 & \text{if } \lambda \leq \lambda_{\mathrm{w}}^{\flat}\,, \\ \mu_{\mathfrak{cf}}\,\frac{(\lambda-\lambda_{\mathrm{w}}^{\flat})^3}{3\,(\lambda_{\mathrm{w}}^{\sharp}-\lambda_{\mathrm{w}}^{\flat})(\lambda_{\mathrm{w}}^{\mathrm{m}}-\lambda_{\mathrm{w}}^{\flat})} & \text{if } \lambda \in (\lambda_{\mathrm{w}}^{\flat}, \lambda_{\mathrm{w}}^{\mathrm{m}}]\,, \\ \mu_{\mathfrak{cf}}\,\left(\frac{(\lambda_{\mathrm{w}}^{\sharp}-\lambda)^3}{3\,(\lambda_{\mathrm{w}}^{\sharp}-\lambda_{\mathrm{w}}^{\mathrm{m}})(\lambda_{\mathrm{w}}^{\sharp}-\lambda_{\mathrm{w}}^{\flat})} + \lambda - \bar{\lambda}_{\mathrm{w}}\right) & \text{if } \lambda \in (\lambda_{\mathrm{w}}^{\mathrm{m}}, \lambda_{\mathrm{w}}^{\sharp}]\,, \\ \mu_{\mathfrak{cf}}\,(\lambda - \bar{\lambda}_{\mathrm{w}}) & \text{if } \lambda > \lambda_{\mathrm{w}}^{\sharp}\,, \end{cases} \tag{B.45}$$

and the scalar stiffness reads

$$L_{\mathfrak{r}}(\lambda) = \begin{cases} 0 & \text{if } \lambda \leq \lambda_{\mathrm{w}}^{\flat}\,, \\ \mu_{\mathfrak{cf}}\,\frac{(\lambda-\lambda_{\mathrm{w}}^{\flat})^2}{(\lambda_{\mathrm{w}}^{\sharp}-\lambda_{\mathrm{w}}^{\flat})(\lambda_{\mathrm{w}}^{\mathrm{m}}-\lambda_{\mathrm{w}}^{\flat})} & \text{if } \lambda \in (\lambda_{\mathrm{w}}^{\flat}, \lambda_{\mathrm{w}}^{\mathrm{m}}]\,, \\ \mu_{\mathfrak{cf}}\,\left(1 - \frac{(\lambda_{\mathrm{w}}^{\sharp}-\lambda)^2}{(\lambda_{\mathrm{w}}^{\sharp}-\lambda_{\mathrm{w}}^{\mathrm{m}})(\lambda_{\mathrm{w}}^{\sharp}-\lambda_{\mathrm{w}}^{\flat})}\right) & \text{if } \lambda \in (\lambda_{\mathrm{w}}^{\mathrm{m}}, \lambda_{\mathrm{w}}^{\sharp}]\,, \\ \mu_{\mathfrak{cf}} & \text{if } \lambda > \lambda_{\mathrm{w}}^{\sharp}\,. \end{cases} \tag{B.46}$$

C Further remarks and results of the TSO estimates from Chapter 5

C.1 Macroscopic stress tensor

The first Piola-Kirchhoff stress tensor is derived from the macroscopic potential $\bar{\mathscr{W}}$ by a derivation with respect to the macroscopic deformation gradient $\bar{\boldsymbol{F}}$, see Eq. (4.5). Accordingly, the effective stress tensor associated with the TSO estimate $\widetilde{\mathscr{W}}$ defined in Eq. (5.15) is derived as

$$\begin{aligned}\widetilde{\boldsymbol{P}} = \partial_{\bar{\boldsymbol{F}}}\widetilde{\mathscr{W}} &= \partial_{\bar{\boldsymbol{F}}}\Big\{ \sum_{\alpha} n^{\alpha}\big[\mathscr{W}^{\alpha}(\bar{\boldsymbol{F}}_{\alpha}) + \tfrac{1}{2}(\bar{\boldsymbol{F}}-\bar{\boldsymbol{F}}_{\alpha})\cdot\boldsymbol{P}^{\alpha}(\bar{\boldsymbol{F}}_{\alpha})\big]\Big\} \\ &= \sum_{\alpha} n^{\alpha}\Big[\mathbb{F}_{\alpha}^{T}\boldsymbol{P}^{\alpha}(\bar{\boldsymbol{F}}_{\alpha}) + \tfrac{1}{2}\big[(\mathbb{I}-\mathbb{F}_{\alpha}^{T})\boldsymbol{P}^{\alpha}(\bar{\boldsymbol{F}}_{\alpha}) + \mathbb{F}_{\alpha}^{T}\mathbb{L}^{\alpha}(\bar{\boldsymbol{F}}_{\alpha})(\bar{\boldsymbol{F}}-\bar{\boldsymbol{F}}_{\alpha})\big]\Big] \\ &= \sum_{\alpha} \tfrac{1}{2} n^{\alpha}\big[(\mathbb{I}+\mathbb{F}_{\alpha}^{T})\boldsymbol{P}^{\alpha}(\bar{\boldsymbol{F}}_{\alpha}) + \mathbb{F}_{\alpha}^{T}\mathbb{L}^{\alpha}(\bar{\boldsymbol{F}}_{\alpha})(\bar{\boldsymbol{F}}-\bar{\boldsymbol{F}}_{\alpha})\big]\,.\end{aligned} \tag{C.1}$$

In this process, one has to utilise the tensor derivation rule (A.64). The stress tensor $\widetilde{\boldsymbol{P}}$ contains not only the phase averages $\bar{\boldsymbol{F}}_{\alpha}$, but also their derivatives with respect to the macroscopic deformation gradient, defined by the fourth-order tensors

$$\mathbb{F}_{\alpha} := \partial_{\bar{\boldsymbol{F}}}\bar{\boldsymbol{F}}_{\alpha}\,. \tag{C.2}$$

Hence, in order to calculate the macroscopic stress tensor $\widetilde{\boldsymbol{P}}$ for a two-phase composite, one has to solve for the $2\times 81 = 162$ unknown coefficients of $\mathbb{F}_{\mathrm{F}}$ and $\mathbb{F}_{\mathrm{M}}$. To do so, we first note that 81 scalar equations can be obtained from a derivation of the overall average condition (5.18) with respect to $\bar{\boldsymbol{F}}$, giving

$$\partial_{\bar{\boldsymbol{F}}}\Big\{\bar{\boldsymbol{F}} = n^{\mathrm{F}}\,\bar{\boldsymbol{F}}_{\mathrm{F}} + n^{\mathrm{M}}\,\bar{\boldsymbol{F}}_{\mathrm{M}}\Big\} \quad\Rightarrow\quad \mathbb{I} = n^{\mathrm{F}}\,\mathbb{F}_{\mathrm{F}} + n^{\mathrm{M}}\,\mathbb{F}_{\mathrm{M}}\,. \tag{C.3}$$

With this, the 81 coefficients of $\mathbb{F}_{\mathrm{M}}$ can be expressed in terms of $\mathbb{F}_{\mathrm{F}}$. In turn, the remaining 81 coefficients of $\mathbb{F}_{\mathrm{F}}$ are obtained by accordingly deriving the tensorial equation (5.26) with respect to $\bar{\boldsymbol{F}}$, hence

$$\partial_{\bar{\boldsymbol{F}}}\Big\{\bar{\boldsymbol{F}} - \bar{\boldsymbol{F}}_{\mathrm{F}} = \mathbb{P}\,[\mathbb{L}^{\mathrm{M}}(\bar{\boldsymbol{F}}-\bar{\boldsymbol{F}}_{\mathrm{F}}) - n^{\mathrm{M}}\,\Delta\boldsymbol{P}]\Big\}\,. \tag{C.4}$$

To exploit this expression, one has to utilise the derivation rules provided in Appendix (A.6), in particular the ones associated with fourth-order tensors, such as Eqs (A.68) and (A.69). Further, one has to be careful with the elasticity tensor $\mathbb{L}^{\mathrm{M}}$ of the matrix, since calculating the derivatives in Eq. (C.4) will result in terms $\mathbb{L}^{\mathrm{M}}(\bar{\boldsymbol{F}})$, evaluated at the overall deformation gradient, and terms $\mathbb{L}^{\mathrm{M}}(\bar{\boldsymbol{F}}_{\mathrm{M}})$, evaluated at the phase average $\bar{\boldsymbol{F}}_{\mathrm{M}}$, which arise from the derivative $\partial_{\boldsymbol{F}}\boldsymbol{P}^{\mathrm{M}}(\bar{\boldsymbol{F}}_{\mathrm{M}})$.

Two-phase fibre composites In Section 5.1.2, we put the focus on two-phase composites with fibrous microstructure, which entailed that the $(i,3)$-coefficients $(i=1,2,3)$ of the phase averages $\bar{\boldsymbol{F}}_{\mathrm{F}}$ and $\bar{\boldsymbol{F}}_{\mathrm{M}}$ are uniform and equal to the respective coefficients $\bar{F}_{i3}$ of

the macroscopic deformation gradient, see Eq. (5.31). The remaining unknown coefficients are computed by means of the subspace equation (5.32). Accordingly, the computation of $\mathbb{F}_{\mathrm{F}}$ has to separated. The derivative of Eq. (5.31) with respect to $\bar{\boldsymbol{F}}$ directly provides 27 scalar equations:

$$\partial_{\bar{\boldsymbol{F}}}\Big\{(\bar{\boldsymbol{F}}_{\mathrm{F}})_{i3} = \bar{F}_{i3}\Big\} \quad \rightarrow \quad (\mathbb{F}_{\mathrm{F}})_{i3st} = \mathrm{I}_{i3st} = \delta_{is}\delta_{3l}\,. \tag{C.5}$$

The remaining 54 scalar equations have to be derived from Eq. (5.32) via

$$\partial_{\bar{\boldsymbol{F}}}\Big\{\big\{[\mathbb{P}^{-1} - \mathbb{L}^{\mathrm{M}}](\bar{\boldsymbol{F}} - \bar{\boldsymbol{F}}_{\mathrm{F}}) + n^{\mathrm{M}}\,\Delta\boldsymbol{P} = \boldsymbol{0}\big\}^{\flat}\Big\}\,, \tag{C.6}$$

which has to be solved for the 54 unknown coefficients $(\mathbb{F}_{\mathrm{F}})_{ijst} = \partial_{F_{st}}(F_{\mathrm{F}})_{ij}$ for $i,s,t = 1,2,3$ and $j = 1,2$.

Incompressible two-phase fibre composites For fibre composite with incompressible phases, an estimate for the macroscopic energy $\widetilde{\mathscr{W}}$ was derived in Section 5.2.3 in terms of Eq. (5.64). The associated first Piola-Kirchhoff stress tensor is given by

$$\begin{aligned}
\widetilde{\boldsymbol{P}} = \partial_{\bar{\boldsymbol{F}}}\widetilde{\mathscr{W}_{\mu}} &= \partial_{\bar{\boldsymbol{F}}}\Big\{\sum_{\alpha} n^{\alpha}\big[\mathscr{W}_{\mu}^{\alpha}(\bar{\boldsymbol{F}}_{\alpha}) + \tfrac{1}{2}(\bar{\boldsymbol{F}} - \bar{\boldsymbol{F}}_{\alpha})\cdot\boldsymbol{P}_{\mu}^{\alpha}(\bar{\boldsymbol{F}}_{\alpha})\big] + \tfrac{1}{2}n^{\mathrm{F}}(\bar{\boldsymbol{F}} - \bar{\boldsymbol{F}}_{\mathrm{F}})\cdot\wp^{\mathrm{F}}\bar{\boldsymbol{F}}_{\mathrm{F}}^{-T}\Big\} \\
&= \sum_{\alpha}\tfrac{1}{2}n^{\alpha}\big[(\mathbb{I} + \mathbb{F}_{\alpha}^{T})\boldsymbol{P}_{\mu}^{\alpha}(\bar{\boldsymbol{F}}_{\alpha}) + \mathbb{F}_{\alpha}^{T}\mathbb{L}_{\mu}^{\alpha}(\bar{\boldsymbol{F}}_{\alpha})(\bar{\boldsymbol{F}} - \bar{\boldsymbol{F}}_{\alpha})\big] \\
&+ \tfrac{1}{2}n^{\mathrm{F}}\big[(\mathbb{I} - \mathbb{F}_{\mathrm{F}}^{T})\wp^{\mathrm{F}}\boldsymbol{F}_{\mathrm{F}}^{-T} + \big(\boldsymbol{F}_{\mathrm{F}}^{-T}\otimes\partial_{\bar{\boldsymbol{F}}}\wp^{\mathrm{F}} - \wp^{\mathrm{F}}\mathbb{F}_{\mathrm{F}}^{T}(\boldsymbol{F}_{\mathrm{F}}^{-T}\otimes\boldsymbol{F}_{\mathrm{F}}^{-T})^{T_{24}}\big)^{T}(\bar{\boldsymbol{F}} - \boldsymbol{F}_{\mathrm{F}}^{-T})\big]\,.
\end{aligned} \tag{C.7}$$

Of course, we know from Section (3.3.2) that $\widetilde{\boldsymbol{P}}$ constitutes in the context of macroscopic incompressibility the extra stress which has to be supplemented by a term $\bar{\wp}\bar{\boldsymbol{F}}^{-T}$ that includes the Lagrange multiplier $\bar{\wp}$ in order to satisfy the macroscopic incompressibility constraint (5.61). The term $\bar{\wp}\bar{\boldsymbol{F}}^{-T}$ thereby replaces the stress contribution $\widetilde{\boldsymbol{P}}_{\Lambda}(\bar{\boldsymbol{F}}) = \partial_{\bar{\boldsymbol{F}}}\widetilde{\mathscr{W}_{\Lambda}}(\bar{\boldsymbol{F}}) = \tilde{\Lambda}_{\infty}\bar{J}(\bar{J}-1)\bar{\boldsymbol{F}}^{-T}$ from the overall energy split (5.59), which in the macroscopic incompressible limit contains an indeterminate form "$\infty\times 0$" because the macroscopic Lamé constant $\tilde{\Lambda}_{\infty}$ tends to infinity and $(\bar{J}-1)$ tends to zero. Moreover, the stress tensor $\widetilde{\boldsymbol{P}}$ in (C.7) contains in addition to the two fourth-order tensors $\mathbb{F}_{\mathrm{F}}$ and $\mathbb{F}_{\mathrm{M}}$ also the second-order tensor $\partial_{\bar{\boldsymbol{F}}}\wp^{\mathrm{F}}$, which denotes the derivative of the constraint pressure (Lagrange multiplier) $\wp^{\mathrm{F}}$ with respect to $\bar{\boldsymbol{F}}$. Hence, $81 + 81 + 9$ scalar unknowns have to be solved to determine the stress tensor $\widetilde{\boldsymbol{P}}$. As before, we still have 81 scalar equations from Eq. (C.3) and 27 scalar equations from Eq. (C.5). Further, 54 equations are obtained from

$$\lim_{\Lambda^{\mathrm{M}}\rightarrow\infty}\partial_{\bar{\boldsymbol{F}}}\Big\{\big\{[\mathbb{P}^{-1} - \mathbb{L}^{\mathrm{M}}](\bar{\boldsymbol{F}} - \bar{\boldsymbol{F}}_{\mathrm{F}}) + n^{\mathrm{M}}\,\Delta\boldsymbol{P}_{\mu\wp} = \boldsymbol{0}\big\}^{\flat}\Big\}\,. \tag{C.8}$$

This means that it proves useful to first calculate the derivative of Eq. (5.63) and subsequently the limit as $\Lambda^{\mathrm{M}}\rightarrow\infty$. This is simpler than directly calculating the derivative of Eq. (5.79). Finally, the remaining 9 equations have to be constructed from appropriately addressing the incompressibility constraint (5.45) in the fibre phase and the resulting constraint upon the tensor $\mathbb{F}_{\mathrm{F}}$.

C.2 Implications of augmented isotropic phases with J_4-based anisotropic parts

For the considered fibre composites with collinear orientation of the cylindrical inclusions and the phase's preferred direction, together with phase energies of the form as given in (5.93), it can be shown that the J_4-dependent anisotropic phase energy terms do not alter the microscopic deformation tensors $\bar{\boldsymbol{F}}_\alpha$. As stated in Section 5.3.4, this is because the solution of Eq. (5.79) becomes independent of the J_4-based energy terms. This fact is explained in the following in more detail.

We first note that the matrix energy enters Eq. (5.79) by means of the elasticity tensor $\mathbb{L}^{\mathrm{M}}_\mu$ and the microstructural tensor $\{\mathbb{X}_0\}^\flat$. Further, both phases contribute to Eq. (5.79) through the stress tensors $\boldsymbol{P}^\alpha_\mu$. Hence, we have to show that each of these quantities does not alter the solution of Eq. (5.79). For matrix energies as given in (5.93), the associated dilatational part of the elasticity tensor is

$$\mathbb{L}^{\mathrm{M}}_\mu(\boldsymbol{C},\boldsymbol{M}) = \mathbb{L}^{\mathrm{M}}_{\mathrm{iso}}(I_1,I_2) + \mathbb{L}^{\mathrm{M}}_{\mathrm{aniso}}(J_4) + \mathbb{L}^{\mathrm{M}J}_\mu(J)\,, \tag{C.9}$$

where the anisotropic, J_4-dependent term is given by

$$\mathbb{L}^{\mathrm{M}}_{\mathrm{aniso}} = \partial^2_{\boldsymbol{F}\boldsymbol{F}}\mathscr{W}^{\mathrm{M}}_{\mathrm{aniso}} = 2\,\partial_{J_4}\mathscr{W}^{\mathrm{M}}_{\mathrm{aniso}}\,(\boldsymbol{I}\otimes\boldsymbol{M})^{T_{23}} + 4\,\partial^2_{J_4^2}\mathscr{W}^{\mathrm{M}}_{\mathrm{aniso}}\,\boldsymbol{F}\boldsymbol{M}\otimes\boldsymbol{F}\boldsymbol{M}\,. \tag{C.10}$$

Making use of the expanded form (C.9), $\mathscr{A}_\mu$ in $(5.67)_2$ can subsequently be formulated as

$$\mathscr{A}_\mu = \big((\mathbb{L}^{\mathrm{M}}_{\mathrm{iso}})^{T_{23}}\boldsymbol{\xi}\big)\boldsymbol{\xi} + \big((\mathbb{L}^{\mathrm{M}}_{\mathrm{aniso}})^{T_{23}}\boldsymbol{\xi}\big)\boldsymbol{\xi} + \big((\mathbb{L}^{\mathrm{M}J}_\mu)^{T_{23}}\boldsymbol{\xi}\big)\boldsymbol{\xi}\,. \tag{C.11}$$

Now, inserting (C.10) in (C.11) and recalling the collinearity of the axis of transverse isotropy of the matrix phase and the cylindrical inclusions, one can observe that the J_4-dependent tensor bases of $\mathbb{L}^{\mathrm{M}}_{\mathrm{aniso}}$ are

$$\begin{aligned}\Big(\big((\boldsymbol{I}\otimes\boldsymbol{M})^{T_{23}}\big)^{T_{23}}\boldsymbol{\xi}\Big)\boldsymbol{\xi} &= \delta_{ij}\,M_{kl}\,\xi_k\,\xi_l\,\boldsymbol{e}_i\otimes\boldsymbol{e}_j = \boldsymbol{0} \quad \text{and}\\ \big((\boldsymbol{F}\boldsymbol{M}\otimes\boldsymbol{F}\boldsymbol{M})^{T_{23}}\boldsymbol{\xi}\big)\boldsymbol{\xi} &= F_{im}\,M_{mk}\,F_{jn}\,M_{nl}\,\xi_k\,\xi_l\,\boldsymbol{e}_i\otimes\boldsymbol{e}_j = \boldsymbol{0}\,.\end{aligned} \tag{C.12}$$

This holds since $\boldsymbol{M} = \boldsymbol{e}_3\otimes\boldsymbol{e}_3$ and $\xi_3 = 0$. Hence, it can easily be shown that the dilatational part $\mathscr{A}_\mu$ of the acoustic tensor does not contain any J_4-dependent terms. From this, one can conclude that $\mathbb{P}_0$, $\mathbb{P}_1$, $\mathbb{P}_2$ as well as $\{\mathbb{X}_0\}^\flat$ are also independent of any J_4-dependent part of $\mathscr{W}^{\mathrm{M}}_\mu$.

Next, we investigate how the anisotropic elasticity tensor $\mathbb{L}^{\mathrm{M}}_{\mathrm{aniso}}$, given by (C.10), and the anisotropic stress tensors $\boldsymbol{P}^\alpha_{\mathrm{aniso}} = \partial_{\boldsymbol{F}}\mathscr{W}^\alpha_{\mathrm{aniso}} = 2\,\partial_{J_4}\mathscr{W}^\alpha_{\mathrm{aniso}}\,\boldsymbol{F}\boldsymbol{M}$ enter Eq. (5.79). Therefore we note that the dilatational elasticity tensor $\mathbb{L}^{\mathrm{M}}_\mu$ and the stress tensors $\boldsymbol{P}^\alpha_\mu$ in Eq. (5.79) only occur in the subspace form. Subsequently, we can observe that for the J_4-dependent tensor bases of the elasticity tensor,

$$\begin{aligned}\big\{(\boldsymbol{I}\otimes\boldsymbol{M})^{T_{23}} = \delta_{ik}\,M_{jl}\,\boldsymbol{e}_i\otimes\boldsymbol{e}_j\otimes\boldsymbol{e}_k\otimes\boldsymbol{e}_l = \mathbb{O}\big\}^\flat \quad &\text{and}\\ \big\{\boldsymbol{F}\boldsymbol{M}\otimes\boldsymbol{F}\boldsymbol{M} = F_{im}\,M_{mj}\,F_{kn}\,M_{nl}\,\boldsymbol{e}_i\otimes\boldsymbol{e}_j\otimes\boldsymbol{e}_k\otimes\boldsymbol{e}_l = \mathbb{O}\big\}^\flat\,,&\end{aligned} \tag{C.13}$$

and for the J_4-dependent tensor base of the stress tensor,

$$\big\{\boldsymbol{F}\boldsymbol{M} = F_{im}\,M_{mj}\,\boldsymbol{e}_i\otimes\boldsymbol{e}_j = \boldsymbol{0}\big\}^\flat \tag{C.14}$$

holds since $\{\boldsymbol{M}=\boldsymbol{0}\}^\flat$. Hence, for the considered class of composites with phase energies as defined in (5.93), the solution of Eq. (5.79) is independent of any anisotropic parts of the two phases.

C.3 Estimates for composites with a matrix phase described by an isotropic Neo-Hookean part augmented by a J_4-dependent anisotropic energy term

In Chapter 5, general TSO results were provided for composites with incompressible and transversely isotropic phases. In this connection, estimates for the effective strain energy are obtained by solving Eq. (5.79), subject to condition (5.45), and substituting the results into expression (5.64). Further, setting up Eq. (5.79) requires the computation of the integrals in $(5.72)_2$. Therein, the integrands are dependent on the elasticity tensors $\mathbb{L}^{\mathrm{M}}_{\mu}$ and $\mathbb{L}^{\mathrm{M}}_{\Lambda}$ of the matrix phase through Eqs (5.67)-(5.71). Typically no closed-form solutions can be found for the integrals $(5.72)_2$ and, in turn, there exist no closed-form expression for the effective energy $\widetilde{\mathscr{W}}$ for general loading conditions and general nonlinear matrix behaviour. However, it is possible to simplify the results and to obtain closed-form relations if the strain-energy of the matrix phase is described by an isotropic Neo-Hookean part augmented by a J_4-dependent anisotropic energy term. This is the focus of this section, which subsequently proceeds from matrix energies of the form

$$\mathscr{W}^{\mathrm{M}}_{\mu}(I_1, J, J_4) = \tfrac{1}{2}\mu^{\mathrm{M}}\,(I_1 - 3) + \mathscr{W}^{\mathrm{M}}_{\mathrm{aniso}}(J_4) + \tfrac{1}{2}\mu^{\mathrm{M}}\,(J-1)(J-3)\,. \tag{C.15}$$

Note that this formulation is still anisotropic and the transversely isotropic term $\mathscr{W}^{\mathrm{M}}_{\mathrm{aniso}}$ can be a highly nonlinear, J_4-dependent strain-energy function.

C.3.1 Explicit representation of the microstructural tensor $\{\mathbb{X}_0\}^{\flat}$

First note that, for the class of matrix energies defined by (C.15), the second derivative $\partial^2_{I_1^2}\mathscr{W}^{\mathrm{M}}_{\mu}$ equals zero. This substantially simplifies the expression for the elasticity tensor $\mathbb{L}^{\mathrm{M}}_{\mu}$ and, subsequently, the tensors $\boldsymbol{\mathscr{B}}_0$, $\boldsymbol{\mathscr{B}}_1$ and $\boldsymbol{\mathscr{B}}_2$, which are needed for the computation of $\{\mathbb{X}_0\}^{\flat}$, see 5.2.3. Moreover, as stated in Section 5.3.1 and shown in C.2, the tensors $\boldsymbol{\mathscr{B}}_0$, $\boldsymbol{\mathscr{B}}_1$ and $\boldsymbol{\mathscr{B}}_2$ are independent of any transversely isotropic (potentially highly nonlinear) J_4-based contribution $\mathscr{W}^{\mathrm{M}}_{\mathrm{aniso}}$ of the matrix energy. Thus, by further making use of an overall deformation gradient tensor $\bar{\boldsymbol{F}}$ of the form (5.83), it is possible to calculate the integrals in $(5.72)_2$ *analytically* and to obtain explicit expressions for the microstructural tensors $\mathbb{P}_0$, $\mathbb{P}_1$, $\mathbb{P}_2$. These explicit expressions enable us to find an analytical solution for the pseudoinverse $\mathbf{G} = \mathbf{P}^{\dagger}$ and to identify the resulting ten non-zero coefficients of the tensor $\{\mathbb{X}_0\}^{\flat}$, namely,

$$\begin{gathered}
(\mathbb{X}_0)_{1111} = (1 + \bar{\lambda}_\ell + 2\,\bar{\lambda}_1^2\,\bar{\lambda}_\ell)\,\mu^{\mathrm{M}}/(\bar{\lambda}_1^2\,\bar{\lambda}_\ell)\,, \quad (\mathbb{X}_0)_{2222} = (2 + \bar{\lambda}_1^2\,\bar{\lambda}_\ell\,(1 + \bar{\lambda}_\ell))\,\mu^{\mathrm{M}}\,, \\
(\mathbb{X}_0)_{1122} = (\mathbb{X}_0)_{2211} = (\bar{\lambda}_\ell - 1)\,\mu^{\mathrm{M}}\,, \quad (\mathbb{X}_0)_{1221} = (\mathbb{X}_0)_{2112} = \mu^{\mathrm{M}}\,, \\
(\mathbb{X}_0)_{1212} = (2 + \bar{\lambda}_2/\bar{\lambda}_1)\,\mu^{\mathrm{M}}\,, \quad (\mathbb{X}_0)_{2121} = (2 + \bar{\lambda}_1/\bar{\lambda}_2)\,\mu^{\mathrm{M}}\,, \\
(\mathbb{X}_0)_{3131} = (\mathbb{X}_0)_{3232} = 2\,\mu^{\mathrm{M}}\,,
\end{gathered} \tag{C.16}$$

where $\bar{\lambda}_1$ and $\bar{\lambda}_2$ are determined by Eqs (5.84). The compact forms of $\mathbb{L}^{\mathrm{M}}_{\mu}$ and $\{\mathbb{X}_0\}^{\flat}$ result in a significant simplification of Eq. (5.79). In particular, the (2,2)-component of Eq. (5.79) can now be used to obtain an analytical expression for the constraint pressure $\wp^{\mathrm{F}}$. In turn, this expression can then be substituted into the (1,1)-component and $\wp^{\mathrm{F}}$ drops from the set of unknowns. Moreover, it can be shown that the dependence of the

overall energy on the overall coupling invariant $\bar{\phi}_\gamma$ completely vanishes. Subsequently, the fibre phase invariant $\bar{\phi}_{\alpha\gamma}$ can be identically set to $\bar{\phi}_\gamma$, that is, $\bar{\phi}_\gamma = \bar{\phi}_{\alpha\gamma} = 0$. This means that the (3,2)-component of Eq. (5.79) is of no further use. As a consequence, the (3,1)- and the (1,1)-components of Eq. (5.79) represent the two scalar equations for the two unknown shear measures $\bar{\gamma}_{\mathrm{F}\ell}$ and $\bar{\gamma}_{\mathrm{Ft}}$, respectively. They remain coupled only through the first invariant $\bar{I}_1^{\mathrm{F}} = \bar{\lambda}_\ell^2 + 2\,\bar{\lambda}_\ell^{-1} + \bar{\gamma}_{\mathrm{F}\ell}^2 + \bar{\gamma}_{\mathrm{Ft}}^2$, which may occur in the first derivatives $\partial_{I_1}\mathscr{W}_\mu^{\mathrm{F}}$ and $\partial_{J_5}\mathscr{W}_\mu^{\mathrm{F}}$ in the term $\Delta\boldsymbol{P}_{\mu\wp}$. Whenever the overall longitudinal or the transverse shear is zero, the two equations for the unknowns $\bar{\gamma}_{\mathrm{F}\ell}$ and $\bar{\gamma}_{\mathrm{Ft}}$ become fully *uncoupled*, leading to $\bar{\gamma}_{\mathrm{F}\ell} = 0$ for $\bar{\gamma}_\ell = 0$ and $\bar{\gamma}_{\mathrm{Ft}} = 0$ for $\bar{\gamma}_{\mathrm{t}} = 0$. Concluding, a matrix energy of the form (C.15) reduces the homogenisation to determining the *two unknown* shear measures $\{\bar{\gamma}_{\mathrm{F}\ell}, \bar{\gamma}_{\mathrm{Ft}}\}$, or, equivalently, $\{\bar{\gamma}_{\mathrm{F}\ell}, \bar{\lambda}_{\mathrm{F}1}\}$. Further, the effective energy becomes a function of only three macroscopic invariants, that is,

$$\widetilde{\mathscr{W}} = \widetilde{\mathscr{W}}(\bar{\lambda}_\ell, \bar{\gamma}_\ell, \bar{\gamma}_{\mathrm{t}}) = \widetilde{\mathscr{W}}(\bar{I}_1, \bar{J}_4, \bar{J}_5)\,. \tag{C.17}$$

where the $\bar{I}_2$-independence directly follows from Eq. (3.97). In order to provide some specific results but at the same time avoiding lengthy expressions, we show in the following explicit results for two specific loading scenarios for composites with I_2-independent fibres. Subsequently, we present estimates for general loading conditions for composites where the isotropic part of the both phases is described by a Neo-Hookean energy.

C.3.2 Estimates for combined axisymmetric and longitudinal shear

Based on the previous findings, we first investigate the case of combined axisymmetric and longitudinal shear loading, i. e. $\bar{\gamma}_{\mathrm{t}} = 0$. The average longitudinal shear $\bar{\gamma}_{\mathrm{F}\ell}$ of the fibre can then be directly calculated from the relation

$$\bar{\gamma}_{\mathrm{F}\ell} - \frac{2\,\bar{\gamma}_\ell\,\mu^{\mathrm{M}}}{2\,n^{\mathrm{M}}\left(\partial_{I_1}\mathscr{W}_\mu^{\mathrm{F}}(\bar{I}_1^{\mathrm{F}}, \bar{J}_4, \bar{J}_5^{\mathrm{F}}) + \bar{\lambda}_\ell^2\,\partial_{J_5}\mathscr{W}_\mu^{\mathrm{F}}(\bar{I}_1^{\mathrm{F}}, \bar{J}_4, \bar{J}_5^{\mathrm{F}})\right) + (1 + n^{\mathrm{F}})\,\mu^{\mathrm{M}}} = 0\,, \tag{C.18}$$

where $\bar{I}_1^{\mathrm{F}} = \bar{\lambda}_\ell^2 + 2\,\bar{\lambda}_\ell^{-1} + \bar{\gamma}_{\mathrm{F}\ell}^2$, $\bar{J}_4 = \bar{\lambda}_\ell^2$, and $\bar{J}_5^{\mathrm{F}} = \bar{\lambda}_\ell^2(\bar{\lambda}_\ell^2 + \bar{\gamma}_{\mathrm{F}\ell}^2)$. It is clear that the derivatives $\partial_{I_1}\mathscr{W}_\mu^{\mathrm{F}}$ and $\partial_{J_5}\mathscr{W}_\mu^{\mathrm{F}}$ may, because of $\bar{I}_1^{\mathrm{F}}$ and $\bar{J}_5^{\mathrm{F}}$, still be a function of $\bar{\gamma}_{\mathrm{F}\ell}$. Hence, the possibility of finding closed-form solutions for $\bar{\gamma}_{\mathrm{F}\ell}$ from Eq. (C.18) generally depends on the chosen strain-energy functions $\mathscr{W}_{\mathrm{iso}}^{\mathrm{F}}$, $\mathscr{W}_{\mathrm{aniso}}^{\mathrm{F}}$, and $\mathscr{W}_{\mathrm{coupl}}^{\mathrm{F}}$. Explicit results for the case that the isotropic part $\mathscr{W}_{\mathrm{iso}}^{\mathrm{F}}$ of the fibres exhibits Neo-Hookean behaviour will be presented in Section C.3.4. The effective energy for combined axisymmetric and longitudinal shear is given by

$$\begin{aligned}
&\widetilde{\mathscr{W}}(\bar{\lambda}_\ell, \bar{\gamma}_\ell) \\
&= n^{\mathrm{F}}\left[\mathscr{W}_\mu^{\mathrm{F}}(\bar{I}_1^{\mathrm{F}}, \bar{J}_4, \bar{J}_5^{\mathrm{F}}) + (\bar{\gamma}_\ell - \bar{\gamma}_{\mathrm{F}\ell})\,\bar{\gamma}_{\mathrm{F}\ell}\left(\partial_{I_1}\mathscr{W}_\mu^{\mathrm{F}}(\bar{I}_1^{\mathrm{F}}, \bar{J}_4, \bar{J}_5^{\mathrm{F}}) + \bar{\lambda}_\ell^2\,\partial_{J_5}\mathscr{W}_\mu^{\mathrm{F}}(\bar{I}_1^{\mathrm{F}}, \bar{J}_4, \bar{J}_5^{\mathrm{F}})\right)\right] \\
&+ n^{\mathrm{M}}\left[\tfrac{1}{2}\,\mu^{\mathrm{M}}(\bar{\lambda}_\ell^2 + 2\,\bar{\lambda}_\ell^{-1} + \bar{\gamma}_{\mathrm{M}\ell}^2 - 3) + \mathscr{W}_{\mathrm{aniso}}^{\mathrm{M}}(\bar{J}_4) + \tfrac{1}{2}\,(\bar{\gamma}_\ell - \bar{\gamma}_{\mathrm{M}\ell})\,\bar{\gamma}_{\mathrm{M}\ell}\,\mu^{\mathrm{M}}\right],
\end{aligned} \tag{C.19}$$

where $\bar{\gamma}_{\mathrm{M}\ell} = (\bar{\gamma}_\ell - n^{\mathrm{F}}\bar{\gamma}_{\mathrm{F}\ell})/n^{\mathrm{M}}$. Note that for this loading scenario it holds that $\det[\bar{\boldsymbol{F}}_{\mathrm{M}}] = 1$, entailing that the J-dependent part $\mathscr{W}_\mu^{\mathrm{M}J}$ of $\mathscr{W}_\mu^{\mathrm{M}}$ vanishes.

C.3.3 Estimates for combined axisymmetric and transverse shear

For a combined axisymmetric and transverse shear deformation, i. e. $\bar{\gamma}_\ell = 0$, the homogenisation reduces to determining the unknown stretch $\bar{\lambda}_{\mathrm{F}1}$ by solving the following equation

$$\begin{aligned}
&\frac{1}{(n^{\mathrm{M}})^2\,\bar{\lambda}_1^2\,\bar{\lambda}_{\mathrm{F}1}^3\,\bar{\lambda}_\ell^2}\Big[2\,(n^{\mathrm{M}})^3\,\partial_{I_1}\mathscr{W}_\mu^{\mathrm{F}}(\bar{I}_1^{\mathrm{F}},\bar{J}_4,\bar{J}_5)\,\bar{\lambda}_1^2\,(1-\bar{\lambda}_{\mathrm{F}1}^4\,\bar{\lambda}_\ell^2)\\
&\quad+\mu^{\mathrm{M}}\Big(n^{\mathrm{F}}\,(\bar{\lambda}_1-\bar{\lambda}_{\mathrm{F}1})^3\,\bar{\lambda}_\ell^2\,(\bar{\lambda}_1+\bar{\lambda}_{\mathrm{F}1})+(n^{\mathrm{M}})^3\,\bar{\lambda}_1^2\,(\bar{\lambda}_{\mathrm{F}1}^4\,\bar{\lambda}_\ell^2-1)\\
&+(n^{\mathrm{M}})^2\,(\bar{\lambda}_1-\bar{\lambda}_{\mathrm{F}1})\left[\bar{\lambda}_\ell\,(\bar{\lambda}_1^3+\bar{\lambda}_{\mathrm{F}1}^3)+\bar{\lambda}_1\,(2+\bar{\lambda}_{\mathrm{F}1}^2\,\bar{\lambda}_\ell)+\bar{\lambda}_1^2\,\bar{\lambda}_{\mathrm{F}1}\,\bar{\lambda}_\ell\left(1+2\,\bar{\lambda}_{\mathrm{F}1}^2\,\bar{\lambda}_\ell\right)\right]\Big)\Big]=\;0\,.
\end{aligned}\tag{C.20}$$

Recalling that the relation between the stretch $\bar{\lambda}_{\mathrm{F}1}$ and the shear parameter $\bar{\gamma}_{\mathrm{F}t}$ is given by Eq. $(5.87)_1$, the equation above can also be formulated in terms of $\bar{\gamma}_{\mathrm{F}t}$. However, using $\bar{\lambda}_{\mathrm{F}1}$ leads to more compact expressions. The effective energy for combined axisymmetric and transverse shear deformation is obtained by

$$\begin{aligned}
&\widetilde{\mathscr{W}}(\bar{\lambda}_\ell,\bar{\gamma}_{\mathrm{t}})\\
&=n^{\mathrm{F}}\,\mathscr{W}_\mu^{\mathrm{F}}(\bar{I}_1^{\mathrm{F}},\bar{J}_4,\bar{J}_5)+n^{\mathrm{M}}\left[\frac{\mu^{\mathrm{M}}}{2}\left(\Big(\frac{\bar{\lambda}_1-n^{\mathrm{F}}\bar{\lambda}_{\mathrm{F}1}}{n^{\mathrm{M}}}\Big)^2+\Big(\frac{\bar{\lambda}_{\mathrm{F}1}-n^{\mathrm{F}}\bar{\lambda}_1}{n^{\mathrm{M}}\bar{\lambda}_1\bar{\lambda}_\ell\bar{\lambda}_{\mathrm{F}1}}\Big)^2+\bar{\lambda}_\ell^2-3\right.\right.\\
&\left.\left.+\,n^{\mathrm{F}}\,(\bar{\lambda}_1-\bar{\lambda}_{\mathrm{F}1})^2\,\frac{n^{\mathrm{F}}\,(\bar{\lambda}_1^2+\bar{\lambda}_{\mathrm{F}1}^2)+2\,(1-3n^{\mathrm{F}}+(n^{\mathrm{F}})^2)\,\bar{\lambda}_1\bar{\lambda}_{\mathrm{F}1}}{((n^{\mathrm{M}})^2\bar{\lambda}_1\bar{\lambda}_{\mathrm{F}1})^2}\right)+\mathscr{W}_{\mathrm{aniso}}^{\mathrm{M}}(\bar{J}_4)\right]\\
&+\frac{n^{\mathrm{F}}\,(\bar{\lambda}_1-\bar{\lambda}_{\mathrm{F}1})}{2\,(n^{\mathrm{M}})^3\,\bar{\lambda}_1^2\bar{\lambda}_{\mathrm{F}1}^3\bar{\lambda}_\ell^2}\Big[2\,\partial_{I_1}\mathscr{W}_\mu^{\mathrm{F}}(\bar{I}_1^{\mathrm{F}},\bar{J}_4,\bar{J}_5)\,(n^{\mathrm{M}})^3\,\bar{\lambda}_1^2\,(\bar{\lambda}_\ell^2\,\bar{\lambda}_{\mathrm{F}1}^4-1)\\
&+\mu^{\mathrm{M}}\Big(-n^{\mathrm{F}}\bar{\lambda}_\ell^2\,(\bar{\lambda}_1-\bar{\lambda}_{\mathrm{F}1})^3\,(\bar{\lambda}_1+\bar{\lambda}_{\mathrm{F}1})+(n^{\mathrm{M}})^3\bar{\lambda}_1^2\,(1-\bar{\lambda}_\ell^2\bar{\lambda}_{\mathrm{F}1}^4)\\
&+(n^{\mathrm{M}})^2\,(\bar{\lambda}_1-\bar{\lambda}_{\mathrm{F}1})\left[\bar{\lambda}_{\mathrm{F}1}-\bar{\lambda}_1^3\bar{\lambda}_\ell-\bar{\lambda}_1^2\bar{\lambda}_{\mathrm{F}1}^3\bar{\lambda}_\ell^2-\bar{\lambda}_1\left(2-\bar{\lambda}_{\mathrm{F}1}^2\bar{\lambda}_\ell+2\,\bar{\lambda}_{\mathrm{F}1}^2\bar{\lambda}_\ell^2\right)\right]\Big)\Big]\,.
\end{aligned}\tag{C.21}$$

In Eqs (C.20) and (C.21), the arguments of the fibre energy $\mathscr{W}_\mu^{\mathrm{F}}$ and its first derivative $\partial_{I_1}\mathscr{W}_\mu^{\mathrm{F}}$ are given by $\bar{I}_1^{\mathrm{F}}=\bar{\lambda}_\ell^2+2\,\bar{\lambda}_\ell^{-1}+\bar{\gamma}_{\mathrm{F}t}^2=\bar{\lambda}_\ell^2+\bar{\lambda}_{\mathrm{F}1}^2+(\bar{\lambda}_\ell\bar{\lambda}_{\mathrm{F}1})^{-2}$, $\bar{J}_4=\bar{\lambda}_\ell^2$, and $\bar{J}_5=\bar{\lambda}_\ell^4$.

C.3.4 Estimates for general loading conditions and composites with a fibre phase exhibiting neo-Hookean behaviour for the isotropic part of the energy

Now, we consider composites that exhibit for the isotropic part of the matrix phase as well as for the fibre phase Neo-Hookean behaviour. The energy of the fibre is then given by

$$\mathscr{W}_\mu^{\mathrm{F}}(I_1,J_4,J_5)=\tfrac{1}{2}\mu^{\mathrm{F}}\,(I_1-3)+\tfrac{1}{2}\mu^{\mathrm{F}}\,(J-1)(J-3)+\mathscr{W}_{\mathrm{aniso}}^{\mathrm{F}}(J_4,J_5)\,.\tag{C.22}$$

Of course, the J-dependent term $\mathscr{W}_\mu^{\mathrm{F}J}$ does not contribute to the energy due to the incompressibility condition (5.45). However, it has to be kept in expression (C.22) to be consistent in the derivation of the stress tensor $\boldsymbol{P}^{\mathrm{F}}$. The longitudinal and transverse shear modes become *fully uncoupled* for composites with phase energies described by (C.15) and (C.22). In this case, the shear values $\bar{\gamma}_{\mathrm{F}\ell}$ and $\bar{\gamma}_{\mathrm{F}t}$ (or, equivalently, the stretch $\bar{\lambda}_{\mathrm{F}1}$) can be determined independently from each other. This is true for general loading conditions.

The average longitudinal shear $\bar{\gamma}_{\mathrm{F}\ell}$ in the fibre phase is now calculated from

$$\bar{\gamma}_{\mathrm{F}\ell} - \frac{2\,\bar{\gamma}_\ell\,\mu^{\mathrm{M}}}{n^{\mathrm{M}}\,(\mu^{\mathrm{F}} + 2\,\bar{\lambda}_\ell^2\,\partial_{J_5}\mathscr{W}^{\mathrm{F}}_{\mathrm{aniso}}(\bar{J}_4, \bar{J}_5^{\mathrm{F}})) + (1+n^{\mathrm{F}})\,\mu^{\mathrm{M}}} = 0\,. \tag{C.23}$$

This equation is obtained by making use of $\partial_{I_1}\mathscr{W}^{\mathrm{F}}_{\mu} = \mu^{\mathrm{F}}/2$ in Eq. (C.18). For a general nonlinear behaviour of the anisotropic energy part $\mathscr{W}^{\mathrm{F}}_{\mathrm{aniso}}$, Eq. (C.23) depends on $\bar{\gamma}_{\mathrm{F}\ell}$ explicitly as well as implicitly through $\bar{J}_5^{\mathrm{F}} = \bar{\lambda}_\ell^2(\bar{\lambda}_\ell^2 + \bar{\gamma}_{\mathrm{F}\ell}^2)$. However, by dropping the J_5-dependence and assuming a J_4-dependent anisotropic behaviour of the fibre phase ($\partial_{J_5}\mathscr{W}^{\mathrm{F}}_{\mathrm{aniso}} = 0$), Eq. (C.23) reduces to the explicit relation

$$\bar{\gamma}_{\mathrm{F}\ell} = \frac{2\,\bar{\gamma}_\ell\,\mu^{\mathrm{M}}}{n^{\mathrm{M}}\,\mu^{\mathrm{F}} + (1+n^{\mathrm{F}})\,\mu^{\mathrm{M}}}\,. \tag{C.24}$$

Hence, for a composite where both phases are described by Neo-Hookean isotropic energies augmented by anisotropic, J_4-dependent contributions, the effective strain energy is given by

$$\begin{aligned}
\widetilde{\mathscr{W}}(\bar{\lambda}_\ell, \bar{\gamma}_\ell, \bar{\gamma}_{\mathrm{t}}) &= n^{\mathrm{F}}\left[\frac{\mu^{\mathrm{F}}}{2}\left(\bar{\lambda}_\ell^2 + \bar{\lambda}_{\mathrm{F1}}^2 + \left(\frac{1}{\bar{\lambda}_\ell\bar{\lambda}_{\mathrm{F1}}}\right)^2 - 3\right)\right] \\
&\quad + n^{\mathrm{M}}\left[\frac{\mu^{\mathrm{M}}}{2}\left(\left(\frac{\bar{\lambda}_1 - n^{\mathrm{F}}\bar{\lambda}_{\mathrm{F1}}}{n^{\mathrm{M}}}\right)^2 + \left(\frac{\bar{\lambda}_{\mathrm{F1}} - n^{\mathrm{F}}\bar{\lambda}_1}{n^{\mathrm{M}}\bar{\lambda}_1\bar{\lambda}_\ell\bar{\lambda}_{\mathrm{F1}}}\right)^2 + \bar{\lambda}_\ell^2 - 3\right.\right. \\
&\quad \left.\left. + n^{\mathrm{F}}\,(\bar{\lambda}_1 - \bar{\lambda}_{\mathrm{F1}})^2\,\frac{n^{\mathrm{F}}\,(\bar{\lambda}_1^2 + \bar{\lambda}_{\mathrm{F1}}^2) + 2\,(1 - 3n^{\mathrm{F}} + (n^{\mathrm{F}})^2)\,\bar{\lambda}_1\bar{\lambda}_{\mathrm{F1}}}{((n^{\mathrm{M}})^2\bar{\lambda}_1\bar{\lambda}_{\mathrm{F1}})^2}\right)\right] \\
&\quad + \frac{n^{\mathrm{F}}\,(\bar{\lambda}_1 - \bar{\lambda}_{\mathrm{F1}})}{2\,(n^{\mathrm{M}})^3\,\bar{\lambda}_1^2\bar{\lambda}_{\mathrm{F1}}^3\bar{\lambda}_\ell^2}\Big[\mu^{\mathrm{F}}\,(n^{\mathrm{M}})^3\,\bar{\lambda}_1^2\,(\bar{\lambda}_\ell^2\,\bar{\lambda}_{\mathrm{F1}}^4 - 1) \\
&\quad + \mu^{\mathrm{M}}\Big(-n^{\mathrm{F}}\bar{\lambda}_\ell^2\,(\bar{\lambda}_1 - \bar{\lambda}_{\mathrm{F1}})^3\,(\bar{\lambda}_1 + \bar{\lambda}_{\mathrm{F1}}) + (n^{\mathrm{M}})^3\bar{\lambda}_1^2\,(1 - \bar{\lambda}_\ell^2\bar{\lambda}_{\mathrm{F1}}^4) \\
&\quad + (n^{\mathrm{M}})^2\,(\bar{\lambda}_1 - \bar{\lambda}_{\mathrm{F1}})\left(\bar{\lambda}_{\mathrm{F1}} - \bar{\lambda}_1^3\bar{\lambda}_\ell - \bar{\lambda}_1^2\bar{\lambda}_{\mathrm{F1}}^3\bar{\lambda}_\ell^2 - \bar{\lambda}_1\left(2 - \bar{\lambda}_{\mathrm{F1}}^2\bar{\lambda}_\ell + 2\,\bar{\lambda}_{\mathrm{F1}}^2\bar{\lambda}_\ell^2\right)\right)\Big)\Big] \\
&\quad + \frac{\tilde{\mu}}{2}\,\bar{\gamma}_\ell^2 + \sum_\alpha n^\alpha\,\mathscr{W}^\alpha_{\mathrm{aniso}}(\bar{J}_4)\,,
\end{aligned} \tag{C.25}$$

where $\bar{J}_4 = \bar{\lambda}_\ell^2$ and $\bar{\lambda}_{\mathrm{F1}}$ has to be calculated from Eq. (C.20) with $\partial_{I_1}\mathscr{W}^{\mathrm{F}}_{\mu} = \mu^{\mathrm{F}}/2$. Further, the effective longitudinal shear modulus, $\tilde{\mu}$, is provided by Eq. $(5.98)_2$.

In conclusion, Eq. (C.25) provides an expression of the effective energy for general combined deformations. It is explicit except for one scalar unknown, the transverse fibre shear $\bar{\gamma}_{\mathrm{Ft}}$ (or $\bar{\lambda}_{\mathrm{F1}}$), which in a numerical setting can easily be calculated from the algebraic equation (C.20). Moreover, the anisotropic energy terms, $\mathscr{W}^\alpha_{\mathrm{aniso}}(\bar{J}_4)$, are added up by a Voigt-type averaging and are unaffected by macroscopic longitudinal or transverse shear deformation. This is in agreement with the observations in Section 5.3.4. Furthermore, if we use Eq. (C.25) and restrict ourselves to an isotropic matrix phase ($\mathscr{W}^{\mathrm{M}}_{\mathrm{aniso}} = 0$) and combined axisymmetric and longitudinal shear deformation ($\bar{\gamma}_{\mathrm{t}} = 0$), we observe that the new estimate $\widetilde{\mathscr{W}}$ is identical to the LI estimate $\widetilde{\mathscr{W}}_{\mathrm{LI}}$ by Lopez-Pamies & Idiart [297]. If we further restrict attention to isotropic Neo-Hookean phases (i. e. $\mathscr{W}^{\mathrm{F}}_{\mathrm{aniso}} = \mathscr{W}^{\mathrm{M}}_{\mathrm{aniso}} = 0$), the new estimate becomes identical to the BHS estimate $\widetilde{\mathscr{W}}_{\mathrm{BHS}}$ by deBotton et al. [92].

Bibliography

[1] Aaron, B. B. & Gosline, J. M.: *Elastin as a Random-Network Elastomer: A Mechanical and Optical Analysis of Single Elastin Fibers.* Biopolymers **20** (1981), 1247–1260.

[2] Abeyaratne, R. & Knowles, J. K.: *On the driving traction acting on a surface of strain discontinuity in a continuum.* Journal of the Mechanics and Physics of Solids **38** (1990), 345–360.

[3] Advani, S. G. & Tucker III, C. L.: *The Use of Tensors to Describe and Predict Fiber Orientation in Short Fiber Composites.* Journal of Rheology **31** (1987), 751–784.

[4] Agoras, M.; Lopez-Pamies, O. & Ponte Castañeda, P.: *A general hyperelastic model for incompressible fiber-reinforced elastomers.* Journal of the Mechanics and Physics of Solids **57** (2009), 268–286.

[5] Agoras, M.; Lopez-Pamies, O. & Ponte Castañeda, P.: *Onset of macroscopic instabilities in fiber-reinforced elastomers at finite strain.* Journal of the Mechanics and Physics of Solids **57** (2009), 1828–1850.

[6] Ahamed, T.; Dorfmann, L. & Ogden, R. W.: *Modelling of residually stressed materials with application to AAA.* Journal of the Mechanical Behavior of Biomedical Materials **61** (2016), 221–234.

[7] Alastrué, V.; Martínez, M. A.; Doblaré, M. & Menzel, A.: *Anisotropic micro-sphere-based finite elasticity applied to blood vessel modelling.* Journal of the Mechanics and Physics of Solids **57** (2009), 178–203.

[8] Alastrué, V.; Peña, E.; Martínez, M. A. & Doblaré, M.: *Experimental study and constitutive modelling of the passive mechanical properties of the ovine infrarenal vena cava tissue.* Journal of Biomechanics **41** (2008), 3038–3045.

[9] Alhasadi, M. F. & Federico, S.: *Relation between Eshelby stress and Eshelby fourth-order tensor within an ellipsoidal inclusion.* Acta Mechanica **228** (2017), 1045–1069.

[10] Allaire, G.: *Mathematical Approaches and Methods.* In Hornung, U. (Editor): *Homogenization and Porous Media.* Springer Science+Business Media, New York 1997, pp. 225–250.

[11] Antman, S. S. & Marlow, R. S.: *Material Constraints, Lagrange Multipliers, and Compatibility. Applications to Rod and Shell Theories.* Archive for Rational Mechanics and Analysis **116** (1991), 257–299.

[12] Apel, N.: *Approaches to the Description of Anisotropic Material Behaviour at Finite Elastic and Plastic Deformations - Theory and Numerics.* Dissertation, Bericht Nr. I-12 aus dem Institut für Mechanik, Universität Stuttgart (2004).

[13] Arruda, E. M. & Boyce, M. C.: *A three-dimensional constitutive model for the large stretch behavior of rubber elastic materials.* Journal of the Mechanics and Physics of Solids **41** (1993), 389–412.

[14] Asgari, M.; Latifi, N.; Heris, H. K.; Vali, H. & Mongeau, L.: In vitro *fibrillogenesis of tropocollagen type III in collagen type I affects its relative fibrillar topology and mechanics*. Scientific Reports **7** (2017), 1–10.

[15] Ateshian, G. A.; Rajan, V.; Chahine, N. O.; Canal, C. E. & Hung, C. T.: *Modeling the Matrix of Articular Cartilage Using a Continuous Fiber Angular Distribution Predicts Many Observed Phenomena*. Journal of Biomechanical Engineering **131** (2009), 061003–061003–10.

[16] Atkin, R. J. & Craine, R. E.: *Continuum theories of mixtures: Basic theory and historical developement*. The Quarterly Journal of Mechanics and Applied Mathematics **29** (1976), 209–244.

[17] Aurenhammer, F.: *Voronoi Diagrams – A Survey of a Fundamental Geometric Data Structure*. ACM Computing Surveys **23** (1991), 345–405.

[18] Avazmohammadi, R.; Hill, M. R.; Simon, M. A.; Zhang, W. & Sacks, M. S.: *A novel constitutive model for passive right ventricular myocardium: evidence for myofiber-collagen fiber mechanical coupling*. Biomechanics and Modeling in Mechanobiology **16** (2017), 561–581.

[19] Avazmohammadi, R. & Ponte Castañeda, P.: *Tangent Second-Order Estimates for the Large-Strain, Macroscopic Response of Particle-Reinforced Elastomers*. Journal of Elasticity **112** (2013), 139–183.

[20] Avazmohammadi, R. & Ponte Castañeda, P.: *On the macroscopic response, microstructure evolution, and macroscopic stability of short-fibre-reinforced elastomers at finite strains: I - Analytical results*. Philosophical Magazine **94** (2014), 1031–1067.

[21] Avazmohammadi, R. & Ponte Castañeda, P.: *Macroscopic constitutive relations for elastomers reinforced with short aligned fibers: Instabilities and post-bifurcation response*. Journal of the Mechanics and Physics of Solids **97** (2016), 37–67.

[22] Avrachenkov, K. E.; Haviv, M. & Howlett, P. G.: *Inversion of analytic matrix functions that are singular at the origin*. SIAM Journal on Matrix Analysis and Applications **22** (2001), 1175–1189.

[23] Ball, J. M.: *Convexity Conditions and Existence Theorems in Nonlinear Elasticity*. Archive for Rational Mechanics and Analysis **63** (1976), 337–403.

[24] Balzani, D.: *Polyconvex Anisotropic Energies and Modeling of Damage Applied to Arterial Walls*. Dissertation, Universität Darmstadt (2006).

[25] Bažant, Z. P. & Oh, B. H.: *Microplane Model for Progressive Fracture of Concrete and Rock*. Journal of Engineering Mechanics **111** (1985).

[26] Bažant, Z. P. & Oh, B. H.: *Efficient Numerical Integration on the Surface of a Sphere*. Zeitschrift für Angewandte Mathematik und Mechanik **66** (1986), 37–49.

[27] Beatty, M. F.: *Topics in finite elasticity: Hyperelasticity of rubber, elastomers, and biological tissues—with examples*. Applied Mechanics Reviews **40** (1987), 1699–1734.

[28] Beatty, M. F.: *An Average-Stretch Full-Network Model for Rubber Elasticity*. Journal of Elasticity **70** (2003), 65–86.

[29] Ben-Israel, A. & Greville, T. N. E.: *Generalized Inverses*. Springer, New York 2003.

[30] Bensoussan, A.; Lions, J.-L. & Papanicolaou, G.: *Asymptotic analysis for periodic structures*. North-Holland, Amsterdam 1978.

[31] Benveniste, Y.: *A new approach to the application of Mori-Tanaka's theory in composite materials*. Mechanics of Materials **6** (1987), 147–157.

[32] Beran, M. J.: *Statistical continuum theories*. Interscience Publishers, New York 1968.

[33] Betten, J.: *Integrity basis for a second-order and a fourth-order tensor*. International Journal of Mathematics and Mathematical Sciences **5** (1982), 87–96.

[34] Betten, J.: *Invariants of fourth-order tensors*. In Boehler, J.-P. (Editor): *Applications of Tensor Functions in Solid Mechanics*. Springer-Verlag, Wien 1987, CISM Courses and Lectures No. 292, pp. 203–226.

[35] Betten, J. & Helisch, W.: *Irreduzible Invarianten eines Tensors vierter Stufe*. Zeitschrift für Angewandte Mathematik und Mechanik **72** (1992), 45–57.

[36] Bischoff, J. E.: *Continuous versus discrete (invariant) representations of fibrous structure for modeling non-linear anisotropic soft tissue behavior*. International Journal of Non-Linear Mechanics **41** (2006), 167–179.

[37] Bischoff, J. E.; Arruda, E. A. & Grosh, K.: *A Microstructurally Based Orthotropic Hyperelastic Constitutive Law*. Transactions of the ASME **69** (2002), 570–579.

[38] Bischoff, J. E.; Arruda, E. M. & Grosh, K.: *A new constitutive model for the compressibility of elastomers at finite deformations*. Rubber Chemistry and Technology **74** (2001), 541–559.

[39] Bischoff-Beiermann, B. & Bruhns, O. T.: *A physically motivated set of invariants and tensor generators in the case of transverse isotropy*. Internation Journal of Engineering Science **32** (1994), 1531–1552.

[40] Bleiler, C.; Ponte Castañeda, P. & Röhrle, O.: *Towards effective mechanical properties of skeletal muscle tissue via homogenisation*. Proceedings in Applied Mathematics and Mechanics **15** (2015), 83–84.

[41] Bleiler, C.; Ponte Castañeda, P. & Röhrle, O.: *Multiscale modelling of skeletal muscle tissue by incorporating microstructural effects*. Proceedings in Applied Mathematics and Mechanics **16** (2016), 75–76.

[42] Bleiler, C.; Ponte Castañeda, P. & Röhrle, O.: *A homogenisation method for the multiscale modelling of transversely isotropic skeletal muscle tissue*. Proceedings in Applied Mathematics and Mechanics **17** (2017), 183–184.

[43] Bleiler, C.; Ponte Castañeda, P. & Röhrle, O.: *A novel microstructurally-based material model to describe passive skeletal muscle tissue.* In Floryan, J. M. (Editor): *Contributions to the Foundations of Multidisciplinary Research in Mechanics*, IUTAM 2017, vol. 3, ISBN 978-0-660-05459-9, pp. 1921–1922.

[44] Bleiler, C.; Ponte Castañeda, P. & Röhrle, O.: *A microstructurally-based, multi-scale, continuum-mechanical model for the passive behaviour of skeletal muscle tissue.* Journal of the Mechanical Behavior of Biomedical Materials **97** (2019), 171–186.

[45] Bleiler, C.; Ponte Castañeda, P. & Röhrle, O.: *Tangent second-order homogenisation estimates for incompressible hyperelastic composites with fibrous microstructures and anisotropic phases.* Journal of the Mechanics and Physics of Solids **147** (2021).

[46] Bleiler, C.; Wagner, A.; Stadelmann, V. A.; Windolf, M.; Köstler, H.; Boger, A.; Gueorguiev-Rüegg, B.; Ehlers, W. & Röhrle, O.: *Multiphasic modelling of bone-cement injection into vertebral cancellous bone.* International Journal for Numerical Methods in Biomedical Engineering **31** (2015), 37–57, ISSN 2040-7947.

[47] Blemker, S. S.; Pinsky, P. M. & Delp, S. L.: *A 3D model of muscle reveals the causes of nonuniform strains in the biceps brachii.* Journal of Biomechanics **38** (2005), 657–665.

[48] Bobeth, M. & Diener, G.: *Static elastic and thermoelastic field fluctuations in multiphase composites.* Journal of the Mechanics and Physics of Solids **35** (1987), 137–149.

[49] Bock, M.; Kumar Tyagi, A.; Kreft, J.-U. & Alt, W.: *Generalized Voronoi Tessellation as a Model of Two-dimensional Cell Tissue Dynamics.* Bulletin of Mathematical Biology **72** (2010), 1696–1731.

[50] Boehler, J. P.: *On Irreducible Representation for Isotropic Scalar Functions.* Zeitschrift für Angewandte Mathematik und Mechanik **57** (1977), 323–327.

[51] de Boer, R.: *Vektor- und Tensorrechnung für Ingenieure.* Springer-Verlag, Berlin 1982.

[52] de Boer, R.: *Theory of Porous Media - Highlights in Historical Development and Current State.* Springer-Verlag, Berlin 2000.

[53] Böl, M.; Ehret, A. E.; Leichsenring, K.; Weichert, C. & Kruse, R.: *On the anisotropy of skeletal muscle tissue under compression.* Acta Biomaterialia **10** (2014), 3225–3234.

[54] Böl, M.; Stark, H. & Schilling, N.: *On a phenomenological model for fatigue effects in skeletal muscles.* Journal of Theoretical Biology **281** (2011), 122–132.

[55] Bonet, J.; Gil, A. J. & Ortigosa, R.: *On a tensor cross product based formulation of large strain solid mechanics.* International Journal of Solids and Structures **84** (2016), 49–63.

[56] Bornert, M. & Ponte Castañeda, P.: *Second-order estimates of the self-consistent type for viscoplastic polycrystals*. Proceedings of the Royal Society A **454** (1998), 3035–3045.

[57] Bowen, R. M.: *Theory of mixtures*. In Eringen, A. C. (Editor): *Continuum Physics, Vol. III*. Academic Press, New York 1976, pp. 1–127.

[58] Boyce, M. C. & Arruda, E. M.: *Constitutive Models of Rubber Elasticity: A Review*. Rubber Chemistry and Technology **73** (2000), 504–523.

[59] Braides, A. & Defranceschi, A.: *Homogenization of Multiple Integrals*. Oxford Lecture Series in Mathematics and its Applications 12, Clarendon Press, Oxford 1998.

[60] Bronshtein, I. N.; Semendyayev, K. A.; Musiol, G. & Muehlig, H.: *Handbook of Mathematics*. Springer, Berlin 2007, 5 edn.

[61] Brun, M.; Lopez-Pamies, O. & Ponte Castañeda, P.: *Homogenization estimates for fiber-reinforced elastomers with periodic microstructures*. International Journal of Solids and Structures **44** (2007), 5953–5979.

[62] Budiansky, B.: *On the elastic moduli of some heterogeneous materials*. Journal of the Mechanics and Physics of Solids **13** (1965), 223–227.

[63] Buehler, M. J.: *Nanomechanics of collagen fibrils under varying cross-link densities: Atomistic and continuum studies*. Journal of the Mechanical Behavior of Biomedical Materials **1** (2008), 59–67.

[64] Buehler, M. J. & Wong, S. Y.: *Entropic Elasticity Controls Nanomechanics of Single Tropocollagen Molecules*. Biophysical Journal **93** (2007), 37–43.

[65] Buryachenko, V.: *Micromechanics of Heterogeneous Materials*. Springer, New York 2007.

[66] Cacho, F.; Elbischger, P. J.; Rodríguez, J. F.; Doblaré, M. & Holzapfel, G. A.: *A constitutive model for fibrous tissues considering collagen fiber crimp*. International Journal of Non-Linear Mechanics **42** (2007), 391–402.

[67] Calvo, B.; Ramírez, A.; Alonso, A.; Grasa, J.; Soteras, F.; Osta, R. & Muñoz, M. J.: *Passive nonlinear elastic behaviour of skeletal muscle: Experimental results and model formulation*. Journal of Biomechanics **43** (2010), 318–325.

[68] Campanella, A. & Tonon, M. L.: *A Note on the Cauchy Relations*. Meccanica **29** (1994), 105–108.

[69] Caner, F. C. & Carol, I.: *Microplane Constitutive Model and Computational Framework for Blood Vessel Tissue*. Journal of Biomechanical Engineering **128** (2006), 419–427.

[70] Caner, F. C.; Guo, Z.; Moran, B.; Bažant, Z. P. & Carol, I.: *Hyperelastic Anisotropic Microplane Constitutive Model for Annulus Fibrosus*. Transactions of the ASME **129** (2007), 632–641.

[71] Carew, T. E.; Vaishnav, R. N. & Patel, D. J.: *Compressibility of the Arterial Wall*. Circulation Research **23** (1968), 61–68.

[72] Carlson, D. E. & Tortorelli, D. A.: *On Hyperelasticity with Internal Constraints*. Journal of Elasticity **42** (1996), 91–98.

[73] Carol, I.; Jirásek, M. & Bažant, Z. P.: *A framework for microplane models at large strain, with application to hyperelasticity*. International Journal of Solids and Structures **41** (2004), 511–557.

[74] Chagnon, G.; Rebouah, M. & Favier, D.: *Hyperelastic Energy Densities for Soft Biological Tissues: A Review*. Journal of Elasticity **120** (2015), 129–160.

[75] Chandran, P. L. & Barocas, V. H.: *Affine Versus Non-Affine Fibril Kinematics in Collagen Networks: Theoretical Studies of Network Behavior*. Journal of Biomechanical Engineering **128** (2006), 259–270.

[76] Chen, H.; Liu, Y.; Zhao, X.; Lanir, Y. & Kassab, G. S.: *A micromechanics finite-strain constitutive model of fibrous tissue*. Journal of the Mechanics and Physics of Solids **59** (2011), 1823–1837.

[77] Chuong, C. J. & Fung, Y. C.: *Three-Dimensional Stress Distribution in Arteries*. Journal of Biomechanical Engineering **105** (1983), 268–274.

[78] Chuong, C. J. & Fung, Y. C.: *Compressibility and constitutive equation of arterial wall in radial compression experiments*. Journal of Biomechanics **17** (1984), 35–40.

[79] Chuong, C. J. & Fung, Y. C.: *On Residual Stresses in Arteries*. Journal of Biomedical Engineering **108** (1986), 189–192.

[80] Ciarlet, P. G.: *Mathematical Elasticity - Volume I: Three-Dimensional Elasticity*. Elsevier Science Publishers B.V., North-Holland 1988.

[81] Coleman, B. D. & Gurtin, M. E.: *Thermodynamics with Internal State Variables*. Journal of Chemical Physics **47** (1967), 597–613.

[82] Coleman, B. D. & Noll, W.: *On the Thermostatics of Continuous Media*. Archive for Rational Mechanics and Analysis **4** (1959), 97–128.

[83] Coleman, B. D. & Noll, W.: *The Thermodynamics of Elastic Materials with Heat Conduction and Viscosity*. Archive for Rational Mechanics and Analysis **13** (1963), 167–178.

[84] Criscione, J. C.; Douglas, A. S. & Hunter, W. C.: *Physically based strain invariant set for materials exhibiting transversely isotropic behavior*. Journal of the Mechanics and Physics of Solids **49** (2001), 871–897.

[85] Curnier, A.: *Computational Methods in Solid Mechanics*. Springer Science+Business Media, Dordrecht 1994.

[86] Dacorogna, B.: *Remarques sur les notions de polyconvexité, quasi-convexité et convexité de rang 1*. Journal de Mathématiques Pures et Appliquées **64** (1985), 403–438.

[87] Dacorogna, B.: *Direct Methods in the Calculus of Variations*. Springer Science+Business Media, New York 2008, 2 edn.

[88] Dal Maso, G.: *An Introduction to Γ-Convergence*. Springer Science+Business Media, New York 1993.

[89] De Giorgi, E.: *Sulla convergenza di alcune successioni di integrali del tipo dell'area*. Rendiconti di Matematica **8** (1975), 277–294.

[90] Deam, R. T. & Edwards, S. F.: *The theory of rubber elasticity*. Philosophical Transactions of the Royal Society A **280** (1976), 317–353.

[91] deBotton, G.: *Transversely isotropic sequentially laminated composites in finite elasticity*. Journal of the Mechanics and Physics of Solids **53** (2005), 1334–1361.

[92] deBotton, G.; Hariton, I. & Socolsky, E. A.: *Neo-Hookean fibre-reinforced composites in finite elasticity*. Journal of the Mechanics and Physics of Solids **54** (2006), 533–559.

[93] Decraemer, W. F.; Maes, M. A. & Vanhuyse, V. J.: *An elastic stress-strain relation for soft biological tissues based on a structural model*. Journal of Biomechanics **13** (1980), 463–468.

[94] Delfino, A.; Stergiopulos, N.; Moore, J. E. & Meister, J.-J.: *Residual strain effects on the stress field in a thick wall finite element model of the human carotid bifurcation*. Journal of Biomechanics **30** (1997), 777–786.

[95] Demiray, H.: *A note on the elasticity of soft biological tissues*. Journal of Biomechanics **5** (1972), 309–311.

[96] Destrade, M.; Horgan, C. O. & Murphy, J. G.: *Dominant negative Poynting effect in simple shearing of soft tissues*. Journal of Engineering Mathematics **95** (2015), 87–98.

[97] Dirichlet, G. L.: *Über die Reduction der positiven quadratischen Formen mit drei unbestimmten ganzen Zahlen*. Journal für die reine und angewandte Mathematik **40** (1850), 209–227.

[98] Dorrington, K. L. & McCrum, N. G.: *Elastin as a Rubber*. Biopolymers **16** (1977), 1201–1222.

[99] Drugan, W. J. & Willis, J. R.: *A micromechanics-based nonlocal constitutive equation and estimates of representative volume element size for elastic composites*. Journal of the Mechanics and Physics of Solids **44** (1996), 497–524.

[100] Du, Q.; Faber, V. & Gunzburger, M.: *Centroidal Voronoi Tessellations: Applications and Algorithms*. SIAM Review **41** (1999), 637–676.

[101] Du, Q. & Wang, D.: *Anisotropic Centroidal Voronoi Tessellations and Their Applications*. SIAM Journal on Scientific Computing **26** (2005), 737–761.

[102] Duance, V. C.; Restall, D. J.; Beard, H.; Bourne, F. J. & Bailey, A. J.: *The location of three collagen types in skeletal muscle*. FEBS Letters **79** (1977), 248–252.

[103] Dvorak, G. J.: *On Uniform Fields in Heterogeneous Media*. Proceedings of the Royal Society of London. Series A, Mathematical and Physical Sciences **431** (1990), 89–110.

[104] Eckart, C.: *The Thermodynamics of Irreversible Processes - I. The Simple Fluid.* Physical Review **58** (1940), 267–269.

[105] Edwards, S. F. & Vilgis, T. A.: *The tube model theory of rubber elasticity.* Reports on Progress in Physics **51** (1988), 243–297.

[106] Ehlers, W.: *Foundations of multiphasic and porous materials.* In Ehlers, W. & Bluhm, J. (Editors): *Porous Media: Theory, Experiments and Numerical Applications.* Springer-Verlag, Berlin 2002, pp. 3–86.

[107] Ehlers, W.: *Vector and Tensor Calculus - An Introduction.* Lecture notes, Institute of Applied Mechanics (Chair of Continuum Mechanics), University of Stuttgart (2018).

[108] Ehlers, W. & Eipper, G.: *The simple tension problem at large volumetric strains computed from finite hyperelastic material laws.* Acta Mechanica **130** (1998), 17–27.

[109] Ehlers, W.; Karajan, N. & Markert, B.: *An extended biphasic model for charged hydrated tissues with application to the intervertebral disc.* Biomechanics and Modeling in Mechanobiology **8** (2009), 233–251.

[110] Ehlers, W. & Wagner, A.: *Multi-component modelling of human brain tissue: a contribution to the constitutive and computational description of deformation, flow and diffusion processes with application to the invasive drug-delivery problem.* Computer Methods in Biomechanics and Biomedical Engineering **18** (2015), 861–879.

[111] Ehret, A. E.: *On a molecular statistical basis for Ogden's model of rubber elasticity.* Journal of the Mechanics and Physics of Solids **78** (2015), 249–268.

[112] Ehret, A. E.; Böl, M. & Itskov, M.: *A continuum constitutive model for the active behaviour of skeletal muscle.* Journal of the Mechanics and Physics of Solids **59** (2011), 625–636.

[113] Ehret, A. E.; Itskov, M. & Schmid, H.: *Numerical integration on the sphere and its effect on the material symmetry of constitutive equations–A comparative study.* International Journal for Numerical Methods in Engineering **81** (2010), 189–206.

[114] Einstein, A.: *Eine neue Bestimmung der Moleküldimensionen.* Annalen der Physik **324** (1906), 289–306.

[115] Elliott, G. F.; Lowy, J. & Worthington, C. R.: *An X-ray and light-diffraction study of the filament lattice of striated muscle in the living state and in rigor.* Journal of Molecular Biology **6** (1963), 31–36.

[116] Elliott, G. F. & Millman, B. M.: *Low-angle X-ray diffraction studies of living striated muscle during contraction.* Journal of Molecular Biology **25** (1967), 31–36.

[117] Ericksen, J. L.: *On the Propagation of Waves in Isotropic Incompressible Perfectly Elastic Materials.* Journal of Rational Mechanics and Analysis **2** (1953), 329–337.

[118] Ericksen, J. L. & Rivlin, R. S.: *Large Elastic Deformations of Homogeneous Anisotropic Materials.* Journal of Rational Mechanics and Analysis **3** (1954), 281–301.

[119] Eringen, A. C.: *Nonlocal Continuum Field Theories*. Springer-Verlag, New York 2002.

[120] Eringen, A. C. & Maugin, G. A.: *Electrodynamics of Continua I - Foundations and Solid Media*. Springer-Verlag, New York 1990.

[121] Eshelby, J. D.: *The force on an elastic singularity*. Philosophical Transactions of the Royal Society. Series A **244** (1951), 87–112.

[122] Eshelby, J. D.: *The determination of the elastic field of an ellipsoidal inclusion, and related problems*. Proceedings of the Royal Society of London A: Mathematical, Physical and Engineering Sciences **241** (1957), 376–396.

[123] Eshelby, J. D.: *The elastic energy-momentum tensor*. Journal of Elasticity **5** (1975), 321–335.

[124] Fan, R. & Sacks, M. S.: *Simulation of planar soft tissues using a structural constitutive model: Finite element implementation and validation*. Journal of Biomechanics **47** (2014), 2043–2054.

[125] Fata, B.; Zhang, W.; Amini, R. & Sacks, M. S.: *Insights Into Regional Adaptations in the Growing Pulmonary Artery Using a Meso-Scale Structural Model: Effects of Ascending Aorta Impingement*. Journal of Biomechanical Engineering **136** (2014), 1–13.

[126] Federico, S.; Grillo, A. & Imatani, S.: *The linear elasticity tensor of incompressible materials*. Mathematics and Mechanics of Solids **20** (2015), 643–662.

[127] Federico, S. & Herzog, W.: *Towards an analytical model of soft biological tissues*. Journal of Biomechanics **41** (2008), 3309–3313.

[128] Fenn, W. O.: *Electrolytes in muscle*. Physiological Reviews **16** (1936), 450–487.

[129] Flory, P. J.: *Thermodynamic relations for high elastic materials*. Transactions of the Faraday Society **57** (1961), 829–838.

[130] Flory, P. J.: *Statistical thermodynamics of random networks*. Proceedings of the Royal Society A **351** (1976), 351–380.

[131] Flory, P. J. & Rehner, J.: *Statistical Mechanics of Cross-Linked Polymer Networks*. The Journal of Chemical Physics **11** (1943), 512–520.

[132] Francfort, G. A. & Murat, F.: *Homogenization and Optimal Bounds in Linear Elasticity*. Archive for Rational Mechanics and Analysis **94** (1986), 307–334.

[133] Franchi, M. & Paruolo, P.: *Inverting a matrix function around a singularity via local rank factorization*. SIAM Journal on Matrix Analysis and Applications **37** (2016), 774–797.

[134] Fratzl, P.: *Collagen: Structure and Mechanics*. Springer Science+Business Media, New York 2008.

[135] Fratzl, P. & Weinkamer, R.: *Nature's hierarchical materials*. Progress in Materials Science **52** (2007), 1263–1334.

[136] Freed, A. D. & Doehring, T. C.: *Elastic Model for Crimped Collagen Fibrils*. Journal of Biomechanical Engineering **127** (2005), 587–593.

[137] Freed, A. D.; Einstein, D. R. & Vesely, I.: *Invariant formulation for dispersed transverse isotropy in aortic heart valves.* Biomechanics and Modeling in Mechanobiology **4** (2005), 100–117.

[138] Freed, A. D. & Srinivasa, A. R.: *Logarithmic strain and its material derivative for a QR decomposition of the deformation gradient.* Acta Mechanica **226** (2015), 2645–2670.

[139] Frewer, M.: *More clarity on the concept of material frame-indifference in classical continuum mechanics.* Acta Mechanica **202** (2009), 213–246.

[140] Fried, E.: *An elementary molecular-statistical basis for the Mooney and Rivlin–Saunders theories of rubber elasticity.* Journal of the Mechanics and Physics of Solids **50** (2002), 571–582.

[141] Fung, Y. C.: *Inversion of a Class of Nonlinear Stress-Strain Relationships of Biological Soft Tissues.* Journal of Biomechanical Engineering **101** (1979), 23–27.

[142] Fung, Y. C.: *On the foundations of biomechanics.* Journal of Applied Mechanics **50** (1983), 1003–1009.

[143] Fung, Y. C.: *Biomechanics: Motion, Flow, Stress, and Growth.* Springer-Verlag, New York 1990.

[144] Fung, Y. C.: *What Are the Residual Stresses Doing in Our Blood Vessels?* Annals of Biomedical Engineering **19** (1991), 237–249.

[145] Fung, Y. C.: *Biomechanics: Mechanical Properties of Living Tissues.* Springer-Verlag, New York 2010, 2 edn.

[146] Fung, Y. C. B.: *Elasticity of soft tissues in simple elongation.* American Journal of Physiology **213** (1967), 1532–1544.

[147] Furer, J. & Ponte Castañeda, P.: *A symmetric fully optimized second-order method for nonlinear homogenization.* Zeitschrift für Angewandte Mathematik und Mechanik **98** (2018), 222–254.

[148] Furer, J. & Ponte Castañeda, P.: *Reinforced elastomers: Homogenization, macroscopic stability and relaxation.* Journal of the Mechanics and Physics of Solids **136** (2020), 103689.

[149] Garikipati, K.; Arruda, E. M.; Grosh, K.; Narayanan, H. & Calve, S.: *A continuum treatment of growth in biological tissue: the coupling of mass transport and mechanics.* Journal of the Mechanics and Physics of Solids **52** (2004), 1595–1625.

[150] Garikipati, K.; Göktepe, S. & Miehe, C.: *Elastica-based strain energy functions for soft biological tissue.* Journal of the Mechanics and Physics of Solids **56** (2008), 1693–1713.

[151] Gasser, T. C.; Ogden, R. W. & Holzapfel, G. A.: *Hyperelastic modelling of arterial layers with distributed collagen fibre orientations.* Journal of the Royal Society Interface **3** (2006), 15–35.

[152] Gautieri, A.; Vesentini, S.; Redaelli, A. & Buehler, M. J.: *Hierarchical Structure and Nanomechanics of Collagen Microfibrils from the Atomistic Scale Up.* Nano Letters **11** (2011), 757–766.

[153] Gee, M. W.; Förster, C. & Wall, W. A.: *A computational strategy for prestressing patient-specific biomechanical problems under finite deformation*. International Journal for Numerical Methods in Biomedical Engineering **26** (2010), 52–72.

[154] Geers, M. G. D.; Kouznetsova, V. G. & Brekelmans, W. A. M.: *Multi-scale computational homogenization: Trends and challenges*. Journal of Computational and Applied Mathematics **234** (2010), 2175–2182.

[155] Geers, M. G. D.; Kouznetsova, V. G.; Matouš, K. & Yvonnet, J.: *Homogenization Methods and Multiscale Modeling: Nonlinear Problems*. In Stein, E.; de Borst, R. & Hughes, T. J. R. (Editors): *Encyclopedia of Computational Mechanics Second Edition*. 2017.

[156] Gelse, K.; Pöschl, E. & Aigner, T.: *Collagens—structure, function, and biosynthesis*. Advanced Drug Delivery Reviews **55** (2003), 1531–1546.

[157] Gennisson, J.-L.; Catheline, S.; Chaffaï, S. & Fink, M.: *Transient elastography in anisotropic medium: Application to the measurement of slow and fast shear wave speeds in muscles*. The Journal of the Acoustical Society of America **114** (2003), 536–541.

[158] Gent, A. N.: *A New Constitutive Relation for Rubber*. Rubber Chemistry and Technology **69** (1996), 59–61.

[159] Gentleman, E.; Lay, A. N.; Dickerson, D. A.; Nauman, E. A.; Livesay, G. A. & Dee, K. C.: *Mechanical characterization of collagen fibers and scaffolds for tissue engineering*. Biomaterials **24** (2003), 3805–3813.

[160] Geymonat, G.; Müller, S. & Triantafyllidis, N.: *Homogenization of Nonlinearly Elastic Materials, Microscopic Bifurcation and Macroscopic Loss of Rank-One Convexity*. Archive for Rational Mechanics and Analysis **122** (1993), 231–290.

[161] Ghosh, S.; Lee, K. & Moorthy, S.: *Multiple scale analysis of heterogeneous elastic structures using homogenization theory and voronoi cell finite element method*. International Journal of Solids and Structures **32** (1995), 27–62.

[162] Gillies, A. R. & Lieber, R. L.: *Structure and function of the skeletal muscle extracellular matrix*. Muscle & Nerve **44** (2011), 318–331.

[163] Gindre, J.; Takaza, M.; Moerman, K. M. & Simms, C. K.: *A structural model of passive skeletal muscle shows two reinforcement processes in resisting deformation*. Journal of the Mechanical Behavior of Biomedical Materials **22** (2013), 84–94.

[164] Göktepe, S.; Menzel, A. & Kuhl, E.: *The generalized Hill model: A kinematic approach towards active muscle contraction*. Journal of the Mechanics and Physics of Solids **72** (2014), 20–39.

[165] Goldstein, M. A.; Michael, L. H.; Schroeter, J. P. & Sass, R. L.: *Structural States in the Z Band of Skeletal Muscle Correlate with States of Active and Passive Tension*. Journal of General Physiology **92** (1988), 113–119.

[166] Gollapudi, S. K. & Lin, D. C.: *Experimental determination of sarcomere force-length relationship in type-I human skeletal muscle fibers*. Journal of Biomechanics **42** (2009), 2011–2016.

[167] Gosline, J.; Lillie, M.; Carrington, E.; Guerette, P.; Ortlepp, C. & Savage, K.: *Elastic proteins: biological roles and mechanical properties.* Philosophical Transactions of the Royal Society B **357** (2002), 121–132.

[168] Gosline, J. M.: *Hydrophobic Interaction and a Model for Elasticity of Elastin.* Biopolymers **17** (1978), 677–695.

[169] Gou, P.-F.: *Strain energy function for biological tissues.* Journal of Biomechanics **3** (1970), 547–550.

[170] Govindjee, S.; Zoller, M. J. & Hackl, K.: *A fully-relaxed variationally-consistent framework for inelastic micro-sphere models: Finite viscoelasticity.* Journal of the Mechanics and Physics of Solids **127** (2019), 1–19.

[171] Gray, W. G. & Hassanizadeh, M.: *Macroscale continuum mechanics for multiphase porous-media flow including phases, interfaces, common lines and common points.* Advances in Water Resources **21** (1998), 261–281.

[172] Grytz, R. & Meschke, G.: *Constitutive modeling of crimped collagen fibrils in soft tissues.* Journal of the Mechanical Behavior of Biomedical Materials **2** (2009), 522–533.

[173] Guo, Z.; Peng, X. & Moran, B.: *Large deformation response of a hyperelastic fibre reinforced composite: Theoretical model and numerical validation.* Composites: Part A **38** (2007), 1842–1851.

[174] Gurtin, M. E.: *Configurational Forces as Basic Concepts of Continuum Physics*, vol. 137 of *Applied Mathematical Sciences*. Springer-Verlag, New York 2000.

[175] Gurtin, M. E. & Murdoch, A. I.: *A continuum theory of elastic material surfaces.* Archive for Rational Mechanics and Analysis **57** (1975), 291–323.

[176] Gurtin, M. E. & Podio-Guidugli, P.: *The Thermodynamics of Constrained Materials.* Archive for Rational Mechanics and Analysis **51** (1973), 192–208.

[177] Gurtin, M. E.; Weissmüller, J. & Larché, F.: *A general theory of curved deformable interfaces in solids at equilibrium.* Philosophical Magazine A **78** (1998), 1093–1109.

[178] Gurtin, M. E. & Williams, W. O.: *On the Inclusion of the Complete Symmetry Group in the Unimodular Group.* Archive for Rational Mechanics and Analysis **23** (1966), 163–172.

[179] Hargens, A. R.; Tipton, C. M.; Gollnick, P. D.; Mubarak, S. J.; Tucker, B. J. & Akeson, W. H.: *Fluid shifts and muscle function in humans during acute simulated weightlessness.* Journal of Applied Physiology **54** (1983), 1003–1009.

[180] Hartmann, S. & Neff, P.: *Polyconvexity of generalized polynomial-type hyperelastic strain energy functions for near-incompressibility.* International Journal of Solids and Structures **40** (2003), 2767–2791.

[181] Hashin, Z.: *The Elastic Moduli of Heterogeneous Materials.* Journal of Applied Mechanics **29** (1962), 143–150.

[182] Hashin, Z.: *Analysis of Properties of Fiber Composites With Anisotropic Constituents.* Journal of Applied Mechanics **46** (1979), 543–550.

[183] Hashin, Z.: *Analysis of Composite Materials – A Survey*. Journal of Applied Mechanics **50** (1983), 481–505.

[184] Hashin, Z. & Rosen, B. W.: *The Elastic Moduli of Fiber-Reinforced Materials*. Journal of Applied Mechanics **31** (1964), 223–232.

[185] Hashin, Z. & Shtrikman, S.: *On some variational principles in anisotropic and nonhomogeneous elasticity*. Journal of the Mechanics and Physics of Solids **10** (1962), 335–342.

[186] Hashin, Z. & Shtrikman, S.: *A variational approach to the theory of the elastic behaviour of polycrystals*. Journal of the Mechanics and Physics of Solids **10** (1962), 343–352.

[187] Hashin, Z. & Shtrikman, S.: *A variational approach to the theory of the elastic behaviour of multiphase materials*. Journal of the Mechanics and Physics of Solids **11** (1963), 127–140.

[188] Hassanizadeh, M. & Gray, W. G.: *General conservation equations for mulitphase systems: 1. Averaging procedure*. Advances in Water Resources **2** (1979), 131–144.

[189] Haupt, P.: *Continuum Mechanics and Theory of Materials*. Springer-Verlag, Berlin 2002, 2 edn.

[190] Hawkins, D. & Bey, M.: *A Comprehensive Approach for Studying Muscle-Tendon Mechanics*. Journal of Biomechanical Engineering **116** (1994), 51–55.

[191] He, Q.-C.; Quang, H. L. & Feng, Z.-Q.: *Exact Results for the Homogenization of Elastic Fiber-Reinforced Solids at Finite Strain*. Journal of Elasticity **83** (2006), 153–177.

[192] Heidlauf, T.; Klotz, T.; Rode, C.; Altan, E.; Bleiler, C.; Siebert, T. & Röhrle, O.: *A multi-scale continuum model of skeletal muscle mechanics predicting force enhancement based on actin-titin interaction*. Biomechanics and Modeling in Mechanobiology **15** (2016), 1423–1437.

[193] Heidlauf, T. & Röhrle, O.: *Modeling the Chemoelectromechanical Behavior of Skeletal Muscle Using the Parallel Open-Source Software Library OpenCMISS*. Computational and Mathematical Methods in Medicine **2013** (2013), 14 pages.

[194] Heinrich, G. & Kaliske, M.: *Theoretical and numerical formulation of a molecular based constitutive tube-model of rubber elasticity*. Computational and Theoretical Polymer Science **7** (1997), 227–241.

[195] Heinrich, G. & Straube, E.: *On the strength and deformation dependence of the tube-like topological constraints of polymer networks, melts and concentrated solutions - I. The polymer network case*. Acta Polymerica **34** (1983).

[196] Heinrich, G.; Straube, E. & Helmis, G.: *Rubber Elasticity of Polymer Networks: Theories*. In *Polymer Physics. Advances in Polymer Science*. Springer 1988, vol. 85, pp. 33–87.

[197] Helfenstein, J.; Jabareen, M.; Mazza, E. & Govindjee, S.: *On non-physical response in models for fiber-reinforced hyperelastic materials.* International Journal of Solids and Structures **47** (2010), 2056–2061.

[198] Hellam, D. C. & Podolsky, R. J.: *Force measurements in skinned muscle fibres.* Journal of Physiology **200** (1969), 807–819.

[199] Hellmich, C.; Barthélémy, J.-F. & Dormieux, L.: *Mineral-collagen interactions in elasticity of bone ultrastructure - a continuum micromechanics approach.* European Journal of Mechanics A/Solids **23** (2004), 783–810.

[200] Heo, S. & Xu, Y.: *Constructing fully symmetric cubature formulae for the sphere.* Mathematics of Computation **70** (2001), 269–279.

[201] Hernández-Gascón, B.; Grasa, J.; Calvo, B. & Rodríguez, J. F.: *A 3D electro-mechanical continuum model for simulating skeletal muscle contraction.* Journal of Theoretical Biology **335** (2013), 108–118.

[202] Hershey, A. V.: *The elasticity of an isotropic aggregate of anisotropic cubic crystals.* ASME Journal of Applied Mechanics **21** (1954), 236–240.

[203] Herzog, W.: *The multiple roles of titin in muscle contraction and force production.* Biophysical Reviews **10** (2018), 1187–1199.

[204] Hibino, I.; Okita, M.; Inoue, T.; Banno, Y. & Hoso, M.: *Effect of Immobilization on Insoluble Collagen Concentration and Type I and Type III Collagen Isoforms of Rat Soleus Muscle.* Journal of the Japanese Physical Therapy Association **11** (2008), 1–6.

[205] Hilbert, D.: *Ueber die Theorie der algebraischen Formen.* Mathematische Annalen **36** (1890), 473–534.

[206] Hill, A. V.: *The State of Water in Muscle and Blood and the Osmotic Behaviour of Muscle.* Proceedings of the Royal Society B **106** (1930), 477–505.

[207] Hill, A. V.: *The heat of shortening and the dynamic constants of muscle.* Proceedings of the Royal Society of London **126** (1938), 136–195.

[208] Hill, A. V. & Kupalov, P. S.: *The Vapour Pressure of Muscle.* Proceedings of the Royal Society B **106** (1930), 445–477.

[209] Hill, R.: *On uniqueness and stability in the theory of finite elastic strain.* Journal of the Mechanics and Physics of Solids **5** (1957), 229–241.

[210] Hill, R.: *Elastic properties of reinforced solids: Some theoretical principles.* Journal of the Mechanics and Physics of Solids **11** (1963), 357–372.

[211] Hill, R.: *Continuum micro-mechanics of elastoplastic polycrystals.* Journal of the Mechanics and Physics of Solids **13** (1965), 89–101.

[212] Hill, R.: *A self-consistent mechanics of composite materials.* Journal of the Mechanics and Physics of Solids **13** (1965), 213–222.

[213] Hill, R.: *On constitutive inequalities for simple materials – I.* Journal of the Mechanics and Physics of Solids **16** (1968), 229–242.

[214] Hill, R.: *On constitutive macro-variables for heterogeneous solids at finite strain*. Proceedings of the Royal Society of London. Series A, Mathematical and Physical Sciences **326** (1972), 131–147.

[215] Hill, R.: *On macroscopic effects of heterogeneity in elastoplastic media at finite strain*. Mathematical Proceedings of the Cambridge Philosophical Society **95** (1984), 481–494.

[216] Hodgkin, A. L. & Huxley, A. F.: *A quantitative description of membrane current and its application to conduction and excitation in nerve*. The Journal of Physiology **117** (1952), 500–544.

[217] Hoeve, C. A. J. & Flory, P. J.: *The Elastic Properties of Elastin*. Journal of the American Chemical Society **80** (1958), 6523–6526.

[218] Hoeve, C. A. J. & Flory, P. J.: *The Elastic Properties of Elastin*. Biopolymers **13** (1974), 677–686.

[219] Hoger, A.: *On the Residual Stress Possible in an Elastic Body with Material Symmetry*. Archive for Rational Mechanics and Analysis **88** (1985), 271–289.

[220] Hoger, A.: *On the determination of residual stress in an elastic body*. Journal of Elasticity **16** (1986), 303–324.

[221] Holzapfel, G. A.: *Nonlinear Solid Mechanics*. John Wiley & Sons LTD, Chichester, West Sussex, England 2000.

[222] Holzapfel, G. A.; Gasser, T. C. & Ogden, R. W.: *A New Constitutive Framework for Arterial Wall Mechanics and a Comparative Study of Material Models*. Journal of Elasticity **61** (2000), 1–48.

[223] Holzapfel, G. A. & Ogden, R. W.: *Constitutive modelling of passive myocardium: a structurally based framework for material characterization*. Philosophical Transactions of the Royal Society A **367** (2009), 3445–3475.

[224] Holzapfel, G. A. & Ogden, R. W.: *On the tension-compression switch in soft fibrous solids*. European Journal of Mechanics A/Solids **49** (2015), 561–569.

[225] Holzapfel, G. A.; Sommer, G.; Gasser, C. T. & Regitnig, P.: *Determination of layer-specific mechanical properties of human coronary arteries with nonatherosclerotic intimal thickening and related constitutive modeling*. American Journal of Physiology - Heart and Circulatory Physiology **289** (2005), H2048–H2058.

[226] Holzapfel, G. A. & Weizsäcker, H. W.: *Biomechanical behavior of the arterial wall and its numerical characterization*. Computers in Biology and Medicine **28** (1998), 377–392.

[227] Honda, H.: *Description of Cellular Patterns by Dirichlet Domains: The Two-Dimensional Case*. Journal of Theoretical Biology **72** (1978), 523–530.

[228] Honda, H.: *Geometrical Models for Cells in Tissues*. International Review of Cytology **81** (1983), 191–248.

[229] Horgan, C. O. & Saccomandi, G.: *A Molecular-Statistical Basis for the Gent Constitutive Model of Rubber Elasticity*. Journal of Elasticity **68** (2002), 167–176.

[230] Horgan, C. O. & Saccomandi, G.: *Superposition of Generalized Plane Strain on Anti-Plane Shear Deformations in Isotropic Incompressible Hyperelastic Materials*. Journal of Elasticity **73** (2003), 221–235.

[231] Horowitz, A.; Lanir, Y.; Yin, F. C. P.; Perl, M.; Sheinman, I. & Strumpf, R. K.: *Structural Three-Dimensional Constitutive Law for the Passive Myocardium*. Journal of Biomechanical Engineering **110** (1988), 200–207.

[232] Humphrey, J.: *Continuum biomechanics of soft biological tissues*. Proceedings of the Royal Society A **459** (2003), 3–46.

[233] Humphrey, J. D.; Strumpf, R. K. & Yin, F. C. P.: *Determination of a Constitutive Relation for Passive Myocardium: I. A New Functional Form*. Journal of Biomechanical Engineering **112** (1990), 333–339.

[234] Hurschler, C.; Loitz-Ramage, B. & Vanderby, R.: *A Structurally Based Stress-Stretch Relationship for Tendon and Ligament*. Transactions of the ASME **119** (1997), 392–399.

[235] Huxley, A. F.: *Muscle structure and theories of contraction*. Progress in Biophysics and Biophysical Chemistry **7** (1957), 255–318.

[236] Huxley, A. F. & Simmons, R. M.: *Proposed Mechanism of Force Generation on Striated Muscle*. Nature **233** (1971), 533–538.

[237] Huxley, H. E.: *X-ray analysis and the problem of muscle*. Proceedings of the Royal Society B **141** (1953), 59–62.

[238] Iatridis, J. C.; Setton, L. A.; Weidenbaum, M. & Mow, V. C.: *The viscoelastic behavior of the non-degenerate human lumbar nucleus pulposus in shear*. Journal of Biomechanics **30** (1997), 1005–1013.

[239] Idiart, M. I. & Ponte Castañeda, P.: *Field statistics in nonlinear composites. I. Theory*. Proceedings of the Royal Society A **463** (2007), 183–202.

[240] Iseri, L. T.; Alexander, L. C.; McCaughey, R. S.; Boyle, A. J. & Myers, G. B.: *Water and electrolyte content of cardiac and skeletal muscle in heart failure and myocardial infarction*. American Heart Journal **43** (1952), 215–227.

[241] Itskov, M.: *On the theory of fourth-order tensors and their applications in computational mechanics*. Computational Methods in Applied Mechanics and Engineering **189** (2000), 419–438.

[242] Itskov, M.: *On the accuracy of numerical integration over the unit sphere applied to full network models*. Computational Mechanics **57** (2016), 859–865.

[243] Itskov, M.: *Tensor Algebra and Tensor Analysis for Engineers*. Springer Nature Switzerland, Cham 2019, 5 edn.

[244] Itskov, M. & Aksel, N.: *A class of orthotropic and transversely isotropic hyperelastic constitutive models based on a polyconvex strain energy function*. International Journal of Solids and Structures **41** (2004), 3833–3848.

[245] Itskov, M.; Ehret, A. E. & Dargazany, R.: *A Full-Network Rubber Elastictiy Model based on Analytical Integration*. Mathematics and Mechanics of Solids **15** (2010), 655–671.

[246] Jalal, N.; Gracies, J.-M. & Zidi, M.: *Mechanical and microstructural changes of skeletal muscle following immobilization and/or stroke*. Biomechanics and Modeling in Mechanobiology **19** (2020), 61–80.

[247] James, H. M. & Guth, E.: *Theory of the Elastic Properties of Rubber*. The Journal of Chemical Physics **11** (1943), 455–481.

[248] Jayyosi, C.; Affagard, J.-S.; Ducourthial, G.; Bonod-Bidaud, C.; Lynch, B.; Bancelin, S.; Ruggiero, F.; Schanne-Klein, M.-C.; Allain, J.-M.; Bruyère-Garnier, K. & Coret, M.: *Affine kinematics in planar fibrous connective tissues: an experimental investigation*. Biomechanics and Modeling in Mechanobiology **16** (2017), 1459–1473.

[249] Johansson, T.; Meier, P. & Blickhan, R.: *A Finite-Element Model for the Mechanical Analysis of Skeletal Muscles*. Journal of Theoretical Biology **206** (2000), 131–149.

[250] Kanit, T.; Forest, S.; Galliet, I.; Mounoury, V. & Jeulin, D.: *Determination of the size of the representative volume element for random composites: statistical and numerical approach*. International Journal of Solids and Structures **40** (2003), 3647–3679.

[251] Kearsley, E. A.: *Note: Strain Invariants Expressed as Average Stretches*. Journal of Rheology **33** (1989), 757–760.

[252] Kjær, M.: *Role of Extracellular Matrix in Adaptation of Tendon and Skeletal Muscle to Mechanical Loading*. Physiological Reviews **84** (2004), 649–698.

[253] Knowles, J. K. & Sternberg, E.: *On the Failure of Ellipticity of the Equations for Finite Elastostatic Plane Strain*. Archive for Rational Mechanics and Analysis **63** (1976), 321–336.

[254] Knowles, J. K. & Sternberg, E.: *On the failure of ellipticity and the emergence of discontinuous deformation gradients in plane finite elastostatics*. Journal of Elasticity **8** (1978), 329–379.

[255] Kohn, R. V. & Strang, G.: *Optimal Design and Relaxation of Variational Problems, II*. Communications on Pure and Applied Mathematics **39** (1986), 139–182.

[256] Kolmogorov, A. N.: *Foundations of the Theory of Probability*. Chelsea Publishing Company, New York 1950.

[257] Kondaurov, V. I. & Nikitin, L. V.: *Finite strains of viscoelastic muscle tissue*. Journal of Applied Mathematics and Mechanics **51** (1987), 346–353.

[258] Kouznetsova, V.; Geers, M. G. D. & Brekelmans, W. A. M.: *Multi-scale constitutive modelling of heterogeneous materials with a gradient-enhanced computational homogenization scheme*. International Journal for Numerical Methods in Engineering **54** (2002), 1235–1260.

[259] Kovanen, V.: *Intramuscular Extracellular Matrix: Complex Environment of Muscle Cells*. Exercise and Sport Sciences Reviews **30** (2002), 20–25.

[260] Krasny, W.; Morin, C.; Magoariec, H. & Avril, S.: *A comprehensive study of layer-specific morphological changes in the microstructure of carotid arteries under uniaxial load*. Acta Biomaterialia **57** (2017), 342–351.

[261] Kratky, O. & Porod, G.: *Röntgenuntersuchung gelöster Fadenmoleküle*. Recueil des Travaux Chimiques des Pays-Bas **68** (1949), 1106–1122.

[262] Krawietz, A.: *Materialtheorie - Mathematische Beschreibung des phänomenologischen thermomechanischen Verhaltens*. Springer-Verlag, Berlin 1986.

[263] Kreher, W.: *Residual stresses and stored elastic energy of composites and polycrystalls*. Journal of the Mechanics and Physics of Solids **38** (1990), 115–128.

[264] Kröner, E.: *Berechnung der elastischen Konstanten des Vielkristalls aus den Konstanten des Einkristalls*. Zeitschrift für Physik **151** (1958), 504–518.

[265] Kröner, E.: *Statistical Continuum Mechanics*. CISM Courses and Lectures No. 92, Springer-Verlag, Wien 1971.

[266] Kroon, M.: *An 8-chain Model for Rubber-like Materials Accounting for Non-affine Chain Deformations and Topological Constraints*. Journal of Elasticity **102** (2011), 99–116.

[267] Kuhl, E.; Garikipati, K.; Arruda, E. M. & Grosh, K.: *Remodeling of biological tissue: Mechanically induced reorientation of a transversely isotropic chain network*. Journal of the Mechanics and Physics of Solids **53** (2005), 1552–1573.

[268] Kuhn, W.: *Über die Gestalt fadenförmiger Moleküle in Lösungen*. Kolloid-Zeitschrift **68** (1934), 2–15.

[269] Kuhn, W.: *Beziehungen zwischen Molekülgröße, statistischer Molekülgestalt und elastischen Eigenschaften hochpolymerer Stoffe*. Kolloid-Zeitschrift **73** (1936), 258–271.

[270] Kuhn, W. & Grün, F.: *Beziehungen zwischen elastischen Konstanten und Dehnungsdoppelbrechung hochelastischer Stoffe*. Kolloid-Zeitschrift **101** (1942), 248–271.

[271] Labelle, F. & Shewchuk, J. R.: *Anisotropic Voronoi Diagrams and Guaranteed-Quality Anisotropic Mesh Generation*. Proceedings of the Nineteenth Annual Symposium on Computational Geometry (2003), 191–200.

[272] Lahellec, N.; Mazerolle, F. & Michel, J. C.: *Second-order estimate of the macroscopic behavior of periodic hyperelastic composites: theory and experimental validation*. Journal of the Mechanics and Physics of Solids **52** (2004), 27–49.

[273] Lake, L. W. & Armeniades, C. D.: *Structure-property relations of aortic tissue*. Transactions - American Society for Artificial Internal Organs **18** (1972), 202–208.

[274] Lanczos, C.: *The variational principles of mechanics*. Dover Publications, New York 1986 [1970], republication of 4th edn.

[275] Lanir, Y.: *A structural theory for the homogeneous biaxial stress-strain relationships in flat collageneous tissues*. Journal of Biomechanics **12** (1979), 423–436.

[276] Lanir, Y.: *Constitutive equations for fibrous connective tissues.* Journal of Biomechanics **16** (1983), 1–12.

[277] Lanir, Y.: *Mechanisms of Residual Stress in Soft Tissues.* Journal of Biomechanical Engineering **131** (2009), 1–5.

[278] Laws, N.: *On the thermostatics of composite materials.* Journal of the Mechanics and Physics of Solids **21** (1973), 9–17.

[279] Lebedev, V. I.: *Quadratures on a sphere.* USSR Computational Mathematics and Mathematical Physics **16** (1976), 10–24.

[280] Lebedev, V. I. & Laikov, D. N.: *A Quadrature Formula for the Sphere of the 131st Algebraic Order of Accuracy.* Doklady Mathematics **59** (1999), 477–481.

[281] Lee, E. H. & Liu, D. T.: *Finite-Strain Elastic-Plastic Theory with Application to Plane-Wave Analysis.* Journal of Applied Physics **38** (1967), 19–27.

[282] Lee, J.-J.; Talman, L.; Peirce, S. M. & Holmes, J. W.: *Spatial scaling in multiscale models: methods for coupling agent-based and finite-element models of wound healing.* Biomechanics and Modeling in Mechanobiology **18** (2019), 1297–1309.

[283] Levin, V. M.: *Thermal expansion coefficients of heterogeneous materials* (in Russian). Mekhanika Tverdogo Tela **1** (1967), 88–94.

[284] Li, Y.; Lang, P. & Linke, W. A.: *Titin stiffness modifies the force-generating region of muscle sarcomeres.* Scientific Reports **6** (2016), 1–9.

[285] Lieber, R. L.: *Skeletal Muscle. Structure, Function and Plasticity.* Lippincott Williams & Wilkins 2010, 3 edn.

[286] Lieber, R. L. & Baskin, R. J.: *Intersarcomere Dynamics of Single Muscle Fibers During Fixed-End Tetani.* The Journal of General Physiology **82** (1983), 347–364.

[287] Lieber, R. L.; Runesson, E.; Einarsson, F. & Fridén, J.: *Inferior mechanical properties of spastic muscle bundles due to hypertrophic but compromised extracellular matrix material.* Muscle & Nerve **28** (2003), 464–471.

[288] Light, N. & Champion, A. E.: *Characterization of muscle epimysium, perimysium and endomysium collagens.* Biochemical Journal **219** (1984), 1017–1026.

[289] Light, N.; Champion, A. E.; Voyle, C. & Bailey, A. J.: *The Role of Epimysial, Perimysial and Endomysial Collagen in Determining Texture in Six Bovine Muscles.* Meat Science **13** (1985), 137–149.

[290] Linke, W. A.; Ivemeyer, M.; Mundel, P.; Stockmeier, M. R. & Kolmerer, B.: *Nature of PEVK-titin elasticity in skeletal muscle.* Proceedings of the National Academy of Sciences **95** (1998), 8052– 8057.

[291] Listrat, A.; Picard, B. & Geay, Y.: *Age-related changes and location of type I, III, IV, V and VI collagens during development of four foetal skeletal muscles of double-muscled and normal bovine animals.* Tissue & Cell **31** (1999), 17–27.

[292] Liu, I.-S. & Sampaio, R.: *Remarks on material frame-indifference controversy.* Acta Mechanica **225** (2014), 331–348.

[293] Lloyd, S. P.: *Least Squares Quantization in PCM.* IEEE Transactions on Information Theory **28** (1982), 129–137.

[294] Lokshin, O. & Lanir, Y.: *Micro and macro rheology of planar tissues.* Biomaterials **30** (2009), 3118–3127.

[295] Lopez-Pamies, O.: *On the Effective Behavior, Microstructure Evolution, and Macroscopic Stability of Elastomeric Composites.* Dissertation, University of Pennsylvania (2006).

[296] Lopez-Pamies, O.: *A new I_1-based hyperelastic model for rubber elastic materials.* Comptes Rendus Mecanique **338** (2010), 3–11.

[297] Lopez-Pamies, O. & Idiart, M. I.: *Fiber-reinforced hyperelastic solids: a realizable homogenization constitutive theory.* Journal of Engineering Mathematics **68** (2010), 57–83.

[298] Lopez-Pamies, O. & Ponte Castañeda, P.: *Second-Order Homogenization Estimates Incorporating Field Fluctuations in Finite Elasticity.* Mathematics and Mechanics of Solids **9** (2004), 243–270.

[299] Lopez-Pamies, O. & Ponte Castañeda, P.: *On the overall behavior, microstructure evolution, and macroscopic stability in reinforced rubbers at large deformations: I–Theory.* Journal of the Mechanics and Physics of Solids **54** (2006), 807–830.

[300] Love, A. E. H.: *A treatise on the mathematical theory of elasticity.* Cambridge University Press, Cambridge 1892.

[301] Lu, B. & Torquato, S.: *Lineal-path function for random heterogeneous materials.* Physical Review A **45** (1992), 922–929.

[302] Lu, J. & Zhang, L.: *Physically motivated invariant formulation for transversely isotropic hyperelasticity.* International Journal of Solids and Structures **42** (2005), 6015–6031.

[303] Lu, Y.; Parker, K. H. & Wang, W.: *Effects of osmotic pressure in the extracellular matrix on tissue deformation.* Philosophical Transactions of the Royal Society A **364** (2006), 1407–1422.

[304] Luther, P. K.: *The vertebrate muscle Z-disc: sarcomere anchor for structure and signalling.* Journal of Muscle Research & Cell Motility **30** (2009), 171–185.

[305] Mabuma, J.; Schwarze, M.; Hurschler, C.; Markert, B. & Ehlers, W.: *Effects of osteoarthritis and pathological walking on contact stresses in femoral cartilage.* Biomechanics and Modeling in Mechanobiology **14** (2015), 1167–1180.

[306] Maceri, F.; Marino, M. & Vairo, G.: *A unified multiscale mechanical model for soft collagenous tissues with regular fiber arrangement.* Journal of Biomechanics **43** (2010), 355–363.

[307] Maceri, F.; Marino, M. & Vairo, G.: *Age-Dependent Arterial Mechanics via a Multiscale Elastic Approach.* International Journal for Computational Methods in Engineering Science and Mechanics **14** (2013), 141–151.

[308] MacIntosh, B. R.; Gardiner, P. F. & McComas, A. J.: *Skeletal Muscle. Form and Function.* Human Kinetics 2006, 2 edn.

[309] Mann, C. J.; Perdiguero, E.; Kharraz, Y.; Aguilar, S.; Pessina, P.; Serrano, A. L. & Muñoz-Cánoves, P.: *Aberrant repair and fibrosis development in skeletal muscle*. Skeletal Muscle **1** (2011), 1–20.

[310] Mardia, K. V. & Jupp, P. E.: *Directional Statistics*. Wiley Series in Probability and Statistics, John Wiley & Sons Ltd, Chichester 2000.

[311] Marino, M.; von Hoegen, M.; Schröder, J. & Wriggers, P.: *Direct and inverse identification of constitutive parameters from the structure of soft tissues. Part 1: micro- and nanostructure of collagen fibers*. Biomechanics and Modeling in Mechanobiology **17** (2018), 1011–1036.

[312] Marino, M. & Vairo, G.: *Multiscale Elastic Models of Collagen Bio-structures: From Cross-Linked Molecules to Soft Tissues*. In Gefen, A. (Editor): *Multiscale Computer Modeling in Biomechanics and Biomedical Engineering*. Springer-Verlag, Berlin 2013, Studies in Mechanobiology, Tissue Engineering and Biomaterials, vol 14, pp. 73–102.

[313] Marino, M. & Vairo, G.: *Influence of inter-molecular interactions on the elasto-damage mechanics of collagen fibrils: A bottom-up approach towards macroscopic tissue modeling*. Journal of the Mechanics and Physics of Solids **73** (2014), 38–54.

[314] Marino, M. & Wriggers, P.: *Finite strain response of crimped fibers under uniaxial traction: An analytical approach applied to collagen*. Journal of the Mechanics and Physics of Solids **98** (2017), 429–453.

[315] Marko, J. F. & Siggia, E. D.: *Stretching DNA*. Macromolecules **28** (1995), 8759–8770.

[316] Marsden, J. E. & Hughes, T. J. R.: *Mathematical foundations of elasticity*. Dover Publications, New York 1994.

[317] Martin, K. S.; Blemker, S. S. & Peirce, S. M.: *Agent-based computational model investigates muscle-specific responses to disuse-induced atrophy*. Journal of Applied Physiology **118** (2015), 1299–1309.

[318] Martins, J. A. C.; Pato, M. P. M. & Pires, E. B.: *A finite element model of skeletal muscles*. Virtual and Physical Prototyping **1** (2006), 159–170.

[319] Martins, J. A. C.; Pires, E. B.; Salvado, R. & Dinis, P. B.: *A numerical model of passive and active behavior of skeletal muscles*. Computational Methods in Applied Mechanics and Engineering **151** (1998), 419–433.

[320] Mayne, R. & Sanderson, R. D.: *The Extracellular Matrix of Skeletal Muscle*. Collagen and Related Research **5** (1985), 449–468.

[321] Menzel, A. & Waffenschmidt, T.: *A microsphere-based remodelling formulationfor anisotropic biological tissues*. Philosophical Transactions of the Royal Society A **367** (2009), 3499–3523.

[322] Merodio, J. & Ogden, R. W.: *Instabilities and loss of ellipticity in fiber-reinforced compressible non-linearly elastic solids under plane deformation*. International Journal of Solids and Structures **40** (2003), 4707–4727.

[323] Merodio, J. & Ogden, R. W.: *Mechanical response of fiber-reinforced incompressible non-linearly elastic solids*. International Journal of Non-Linear Mechanics **40** (2005), 213–227.

[324] Meyer, G. A. & Lieber, R. L.: *Elucidation of extracellular matrix mechanics from muscle fibers and fiber bundles*. Journal of Biomechanics **44** (2011), 771–773.

[325] Michel, J.-C.; Lopez-Pamies, O.; Ponte Castañeda, P. & Triantafyllidis, N.: *Microscopic and macroscopic instabilities in finitely strained porous elastomers*. Journal of the Mechanics and Physics of Solids **55** (2007), 900–938.

[326] Michel, J. C.; Lopez-Pamies, O.; Ponte Castañeda, P. & Triantafyllidis, N.: *Microscopic and macroscopic instabilities in finitely strained fiber-reinforced elastomers*. Journal of the Mechanics and Physics of Solids **58** (2010), 1776–1803.

[327] Michel, J. C.; Moulinec, H. & Suquet, P.: *Effective properties of composite materials with periodic microstructure: a computational approach*. Computer Methods in Applied Mechanics and Engineering **172** (1999), 109–143.

[328] Miehe, C.: *Aspects of the fomulation and finite element implementation of large strain isotropic elasticity*. International Journal for Numerical Methods in Engineering **37** (1994), 1981–2004.

[329] Miehe, C.; Göktepe, S. & Lulei, F.: *A micro-macro approach to rubber-like materials–Part I: the non-affine micro-sphere model of rubber elasticity*. Journal of the Mechanics and Physics of Solids **52** (2004), 2617–2660.

[330] Miehe, C.; Schotte, J. & Schröder, J.: *Computational micro-macro transitions and overall moduli in the analysis of polycrystals at large strains*. Computational Materials Science **16** (1999), 372–382.

[331] Miehe, C.; Schröder, J. & Becker, M.: *Computational homogenization analysis in finite elasticity: material and structural instabilities on the micro- and macro-scales of periodic composites and their interaction*. Computational Methods in Applied Mechanics and Engineering **191** (2002), 4971–5005.

[332] Mihai, L. A.; Chin, L.; Janmey, P. A. & Goriely, A.: *A comparison of hyperelastic constitutive models applicable to brain and fat tissues*. Journal of the Royal Society Interface **12** (2015), 1–12.

[333] Mihai, L. A. & Goriely, A.: *How to characterize a nonlinear elastic material? A review on nonlinear constitutive parameters in isotropic finite elasticity*. Proceedings of the Royal Society A **473** (2017), 1–33.

[334] Millman, B. M.; Racey, T. J. & Matsubara, I.: *Effects of hyperosmotic solutions on the filament lattice of intact frog skeletal muscle*. Biophysical Journal **33** (1981), 189–202.

[335] Milton, G. W.: *The Theory of Composites*. Cambridge University Press, Cambridge 2002.

[336] Misof, K.; Rapp, G. & Fratzl, P.: *A New Molecular Model for Collagen Elasticity Based on Synchrotron X-Ray Scattering Evidence*. Biophysical Journal **72** (1997), 1376–1381.

[337] Mistry, S. J. & Govindjee, S.: *A micro-mechanically based continuum model for strain-induced crystallization in natural rubber*. International Journal of Solids and Structures **51** (2014), 530–539.

[338] Mohammadkhah, M.; Murphy, P. & Simms, C. K.: *The in vitro passive elastic response of chicken pectoralis muscle to applied tensile and compressive deformation*. Journal of the Mechanical Behavior of Biomedical Materials **62** (2016), 468–480.

[339] Mohammadkhah, M.; Murphy, P. & Simms, C. K.: *Collagen fibril organization in chicken and porcine skeletal muscle perimysium under applied tension and compression*. Journal of the Mechanical Behavior of Biomedical Materials **77** (2018), 734–744.

[340] Mooney, M.: *A Theory of Large Elastic Deformation*. Journal of Applied Physics **11** (1940), 582–592.

[341] Moraleda, J.; Segurado, J. & Llorca, J.: *Finite deformation of incompressible fiber-reinforced elastomers: A computational micromechanics approach*. Journal of the Mechanics and Physics of Solids **57** (2009), 1596–1613.

[342] Mori, T. & Tanaka, K.: *Average stress in matrix and average elastic energy of materials with misfitting inclusions*. Acta Metallurgica **21** (1973), 571–574.

[343] Morrey, C. B.: *Quasi-convexity and the lower semicontinuity of multiple integrals*. Pacific Journal of Mathematics **2** (1951), 25–53.

[344] Morrow, D. A.; Haut Donahue, T. L.; Odegard, G. M. & Kaufman, K. R.: *Transversely isotropic tensile material properties of skeletal muscle tissue*. Journal of the Mechanical Behavior of Biomedical Materials **3** (2010), 124–129.

[345] Moulinec, H. & Suquet, P.: *A numerical method for computing the overall response of nonlinear composites with complex microstructure*. Computer Methods in Applied Mechanics and Engineering **157** (1998), 69–94.

[346] Müller, I.: *On the Entropy Inequality*. Archive for Rational Mechanics and Analysis **26** (1967), 118–141.

[347] Müller, I. & Weiss, W.: *Entropy and Energy - A Universal Competition*. Springer-Verlag, Berlin 2005.

[348] Müller, S.: *Homogenization of Nonconvex Integral Functionals and Cellular Elastic Materials*. Archive for Rational Mechanics and Analysis **99** (1987).

[349] Nardinocchi, P. & Teresi, L.: *On the Active Response of Soft Living Tissues*. Journal of Elasticity **88** (2007), 27–39.

[350] Neff, P.; Eidel, B. & Martin, R. J.: *Geometry of Logarithmic Strain Measures in Solid Mechanics*. Archive for Rational Mechanics and Analysis **222** (2016), 507–572.

[351] Nemat-Nasser, S.: *Averaging theorems in finite deformation plasticity*. Mechanics of Materials **31** (1999), 493–523.

[352] Nemat-Nasser, S. & Hori, M.: *Micromechanics: overall properties of heterogeneous materials*. Elsevier, Amsterdam 1999, 2 edn.

[353] Nerurkar, N. L.; Mauck, R. L. & Elliott, D. M.: *Modeling interlamellar interactions in angle-ply biologic laminates for annulus fibrosus tissue engineering.* Biomechanics and Modeling in Mechanobiology **10** (2011), 973–984.

[354] Nie, X.; Cheng, J.-I.; Chen, W. W. & Weerasooriya, T.: *Dynamic Tensile Response of Porcine Muscle.* Journal of Applied Mechanics **78** (2011), 1–5.

[355] Noll, W.: *On the Continuity of the Solid and Fluid States.* Journal of Rational Mechanics and Analysis **4** (1955), 3–81.

[356] Noll, W.: *A mathematical theory of the mechanical behavior of continuous media.* Archive for Rational Mechanics and Analysis **2** (1958), 197–226.

[357] Noll, W.: *A Frame-Free Formulation of Elasticity.* Journal of Elasticity **83** (2006), 291–307.

[358] Oden, J. T. & Reddy, J. N.: *Variational Methods in Theoretical Mechanics.* Springer-Verlag, Berlin 1976.

[359] Ogden, R.: *Nearly isochoric elastic deformations: Application to rubberlike solids.* Journal of the Mechanics and Physics of Solids **26** (1978), 37–57.

[360] Ogden, R. W.: *Extremum principles in non-linear elasticity and their application to composites - I. Theory.* International Journal of Solids and Structures **14** (1978), 265–282.

[361] Ogden, R. W.: *Elastic Deformations of Rubberlike Solids.* Mechanics Of Solids (1982), 499–537.

[362] Ogden, R. W.: *Non-Linear Elastic Deformations.* Dover Publications, Mineola, NY 1997.

[363] Ogden, R. W.: *Nonlinear Elasticity, Anisotropy, Material Stability and Residual Stresses in Soft Tissue.* In Holzapfel, G. A. & Ogden, R. W. (Editors): *Biomechanics of Soft Tissue in Cardiovascular Systems.* Springer 2003, CISM Courses and Lectures No. 441, pp. 65–108.

[364] Ogneva, I. V.; Lebedev, D. V. & Shenkman, B. S.: *Transversal Stiffness and Young's Modulus of Single Fibers from Rat Soleus Muscle Probed by Atomic Force Microscopy.* Biophysical Journal **98** (2010), 418–424.

[365] Olson, T.: *Improvements on Taylor's upper bound for rigid-plastic composites.* Materials Science and Engineering: A **175** (1994), 15–20.

[366] Olver, F. W. J.; Lozier, D. W.; Boisvert, R. F. & Clark, C. W. (Editors): *NIST Handbook of Mathematical Functions.* Cambridge University Press, Cambridge 2010.

[367] Oomens, C. W. J.; Maenhout, M.; van Oijen, C. H.; Drost, M. R. & Baaijens, F. P.: *Finite element modelling of contracting skeletal muscle.* Philosophical Transactions of the Royal Society B **358** (2003), 1453–1460.

[368] Papazoglou, S.; Rump, J.; Braun, J. & Sack, I.: *Shear Wave Group Velocity Inversion in MR Elastography of Human Skeletal Muscle.* Magnetic Resonance in Medicine **56** (2006), 489–497.

[369] Penn, R. W.: *Volume Changes Accompanying the Extension of Rubber*. Transactions of the Society of Rheology **14** (1970), 509–517.

[370] Pezzuto, S.; Ambrosi, D. & Quarteroni, A.: *An orthotropic active-strain model for the myocardium mechanics and its numerical approximation*. European Journal of Mechanics A/Solids **48** (2014), 83–96.

[371] Pietsch, R.; Wheatley, B. B.; Haut Donahue, T. L.; Gilbrecht, R.; Prabhu, R.; Liao, J. & Williams, L. N.: *Anisotropic Compressive Properties of Passive Porcine Muscle Tissue*. Journal of Biomechanical Engineering **136** (2014), 1–7.

[372] Podio-Guidugli, P.: *On the Mechanical Modeling of Matter, Molecular and Continuum*. Journal of Elasticity **135** (2019), 435–456.

[373] Ponte Castañeda, P.: *The overall constitutive behaviour of nonlinearly elastic composites*. Proceedings of the Royal Society A **422** (1989), 147–171.

[374] Ponte Castañeda, P.: *The effective mechanical properties of nonlinear isotropic composites*. Journal of the Mechanics and Physics of Solids **39** (1991), 45–71.

[375] Ponte Castañeda, P.: *New variational principles in plasticity and their application to composite materials*. Journal of the Mechanics and Physics of Solids **40** (1992), 1757–1788.

[376] Ponte Castañeda, P.: *Exact Second-Order Estimates for the Effective Mechanical Properties of Nonlinear Composite Materials*. Journal of the Mechanics and Physics of Solids **44** (1996), 827–862.

[377] Ponte Castañeda, P.: *Second-order homogenization estimates for nonlinear composites incorporating field fluctuations: I–theory*. Journal of the Mechanics and Physics of Solids **50** (2002), 737–757.

[378] Ponte Castañeda, P.: *Heterogeneous Materials*. Lecture notes, École Polytechnique, Department of Mechanics (2005).

[379] Ponte Castañeda, P.: *Fully optimized second-order variational estimates for the macroscopic response and field statistics in viscoplastic crystalline composites*. Proceedings of the Royal Society A **471** (2015).

[380] Ponte Castañeda, P.: *Stationary variational estimates for the effective response and field fluctuations in nonlinear composites*. Journal of the Mechanics and Physics of Solids **96** (2016), 660–682.

[381] Ponte Castañeda, P. & Suquet, P.: *Nonlinear Composites*. Advances in Applied Mechanics **34** (1998), 171–302.

[382] Ponte Castañeda, P. & Tiberio, E.: *A second-order homogenization method in finite elasticity and applications to black-filled elastomers*. Journal of the Mechanics and Physics of Solids **48** (2000), 1389–1411.

[383] Ponte Castañeda, P. & Willis, J. R.: *The effect of spatial distribution on the effective behaviour of composite materials and cracked media*. Journal of the Mechanics and Physics of Solids **43** (1995), 1919–1951.

[384] Ponte Castañeda, P. & Willis, J. R.: *Variational second-order estimates for nonlinear composites*. Proceedings of the Royal Society of London A: Mathematical, Physical and Engineering Sciences **455** (1999), 1799–1811.

[385] Poynting, J. H.: *On Pressure Perpendicular to the Shear Planes in Finite Pure Shears, and on the Lengthening of Loaded Wires when Twisted*. Proceedings of the Royal Society A **82** (1909), 546–559.

[386] Prado, L. G.; Makarenko, I.; Andresen, C.; Krüger, M.; Opitz, C. A. & Linke, W. A.: *Isoform Diversity of Giant Proteins in Relation to Passive and Active Contractile Properties of Rabbit Skeletal Muscles*. The Journal of General Physiology **126** (2005), 461–480.

[387] Purslow, P. P.: *Strain-induced reorientation of an intramuscular connective tissue network: implications for passive muscle elasticity*. Journal of Biomechanics **22** (1989), 21–31.

[388] Purslow, P. P.: *The Extracellular Matrix of Skeletal and Cardiac Muscle*. In Fratzl, P. (Editor): *Collagen: Structure and Mechanics*. Springer Science+Business Media, New York 2008, pp. 325–357.

[389] Purslow, P. P.: *Muscle fascia and force transmission*. Journal of Bodywork & Movement Therapies **14** (2010), 411–417.

[390] Purslow, P. P. & Duance, V. C.: *Structure and Function of Intramuscular Connective Tissue*. In Hukins, D. W. L. (Editor): *Connective Tissue Matrix. Topics in Molecular and Structural Biology*. Palgrave, London 1990.

[391] Purslow, P. P. & Trotter, J. A.: *The morphology and mechanical properties of endomysium in series-fibred muscles: variations with muscle length*. Journal of Muscle Research & Cell Motility **15** (1994), 299–308.

[392] Qiu, G. Y. & Pence, T. J.: *Loss of Ellipticity in Plane Deformation of a Simple Directionally Reinforced Incompressible Nonlinearly Elastic Solid*. Journal of Elasticity **49** (1997), 31–63.

[393] Qiu, G. Y. & Pence, T. J.: *Remarks on the Behavior of Simple Directionally Reinforced Incompressible Nonlinearly Elastic Solids*. Journal of Elasticity **49** (1997), 1–30.

[394] Rajagopal, K. R. & Srinivasa, A. R.: *A Gibbs-potential-based formulation for obtaining the response functions for a class of viscoelastic materials*. Proceedings of the Royal Society A **467** (2011), 37–58.

[395] Rajagopal, K. R. & Srinivasa, A. R.: *An implicit thermomechanical theory based on a Gibbs potential formulation for describing the response of thermoviscoelastic solids*. International Journal of Engineering Science **70** (2013), 15–28.

[396] Rehorn, M. R.; Schroer, A. K. & Blemker, S. S.: *The passive properties of muscle fibers are velocity dependent*. Journal of Biomechanics **47** (2014), 687–693.

[397] Reisinger, A. G.; Pahr, D. H. & Zysset, P. K.: *Sensitivity analysis and parametric study of elastic properties of an unidirectional mineralized bone fibril-array using mean field methods*. Biomechanics and Modeling in Mechanobiology **9** (2010), 499–510.

[398] Reuss, A.: *Berechnung der Fließgrenze von Mischkristallen auf Grund der Plastizitätsbedingung für Einkristalle*. Zeitschrift für Angewandte Mathematik und Mechanik **9** (1929), 49–58.

[399] Richter, H.: *Das isotrope Elastizitätsgesetz*. Zeitschrift für Angewandte Mathematik und Mechanik **28** (1948), 205–209.

[400] Ricken, T.; Dahmen, U. & Dirsch, O.: *A biphasic model for sinusoidal liver perfusion remodeling after outflow obstruction*. Biomechanics and Modeling in Mechanobiology **9** (2010), 435–450.

[401] van der Rijt, J. A. J.; van der Werf, K. O.; Bennink, M. L.; Dijkstra, P. J. & Feijen, J.: *Micromechanical Testing of Individual Collagen Fibrils*. Macromolecular Bioscience **6** (2006), 697–702.

[402] Rivlin, R. S.: *Large Elastic Deformations of Isotropic Materials. I. Fundamental Concepts*. Philosophical Transactions of the Royal Society of London. Series A, Mathematical and Physical Sciences **240** (1948), 459–490.

[403] Rivlin, R. S. & Ericksen, J. L.: *Stress-Deformation Relations for Isotropic Materials*. Journal of Rational Mechanics and Analysis **4** (1955).

[404] Rivlin, R. S. & Saunders, D. W.: *Large Elastic Deformations of Isotropic Materials. VII. Experiments on the Deformation of Rubber*. Philosophical Transactions of the Royal Society of London. Series A, Mathematical and Physical Sciences **243** (1952), 251–288.

[405] Rockafellar, R. T.: *Convex Analysis*. Princeton University Press, Princeton 1970.

[406] Rodriguez, E. K.; Hoger, A. & McCulloch, A. D.: *Stress-dependent finite growth in soft elastic tissues*. Journal of Biomechanics **27** (1994), 455–467.

[407] Röhrle, O.; Davidson, J. B. & Pullan, A. J.: *Bridging scales: A three-dimensional electromechanical finite element model of skeletal muscle*. SIAM Journal on Scientific Computing **30** (2008), 2882–2904.

[408] Röhrle, O. & Pullan, A. J.: *Three-dimensional finite element modelling of muscle forces during mastication*. Journal of Biomechanics **40** (2007), 3363–3372.

[409] Röhrle, O.; Yavuz, U. Ş.; Klotz, T.; Negro, F. & Heidlauf, T.: *Multiscale modeling of the neuromuscular system: Coupling neurophysiology and skeletal muscle mechanics*. WIREs Systems Biology and Medicine **11** (2019), 1–43.

[410] Rowe, R. W. D.: *Collagen fibre arrangement in intramuscular connective tissue. Changes associated with muscle shortening and their possible relevance to raw meat toughness measurements*. Internation Journal for Food Science and Technology **9** (1974), 501–508.

[411] Rowe, R. W. D.: *Morphology of perimysial and endomysial connective tissue in skeletal muscle*. Tissue & Cell **13** (1981), 681–690.

[412] Sachs, G.: *Zur Ableitung einer Fließbedingung*. In *Mitteilungen der deutschen Materialprüfungsanstalten*. Springer, Berlin 1929, pp. 94–97.

[413] Sacks, M. S.: *Incorporation of Experimentally-Derived Fiber Orientation into a Structural Constitutive Model for Planar Collagenous Tissues*. Journal of Biomechanical Engineering **125** (2003), 280–287.

[414] Sain, M. K. & Massey, J. L.: *Invertibility of Linear Time-Invariant Dynamical Systems*. IEEE Transactions on Automatic Control **AC-14** (1969), 141–149.

[415] Sánchez-Gutiérrez, D.; Sáez, A.; Gómez-Gálvez, P.; Paradas, C. & Escudero, L. M.: *Rules of tissue packing involving different cell types: human muscle organization*. Scientific Reports **7** (2017), 1–14.

[416] Sánchez-Gutiérrez, D.; Tozluoglu, M.; Barry, J. D.; Pascual, A.; Mao, Y. & Escudero, L. M.: *Fundamental physical cellular constraints drive self-organization of tissues*. The EMBO Journal **35** (2016), 77–88.

[417] Sansour, C.: *On the physical assumptions underlying the volumetric-isochoric split and the case of anisotropy*. European Journal of Mechanics A/Solids **27** (2008), 28–39.

[418] Sasaki, N. & Odajima, S.: *Elongation mechanism of collagen fibrils and force-strain relations of tendon at each level of structural hierarchy*. Journal of Biomechanics **29** (1996), 1131–1136.

[419] Schmalbruch, H.: *Skeletal Muscle*. Springer-Verlag, Berlin 1985.

[420] Schröder, J.: *Theoretische und algorithmische Konzepte zur phänomenologischen Beschreibung anisotropen Materialverhaltens*. Dissertation, Bericht Nr. F 97/3 aus dem Institut für Baumechanik und Numerische Mechanik, Universität Hannover (1996).

[421] Schröder, J.: *Homogenisierungsverfahren der nichtlinearen Kontinuumsmechanik unter Beachtung von Stabilitätsproblemen*. Habilitation, Bericht Nr. I-7 aus dem Institut für Mechanik (Bauwesen), Universität Stuttgart (2000).

[422] Schröder, J.: *A numerical two-scale homogenization scheme: the FE^2-method*. In Schröder, J. & Hackl, K. (Editors): *Plasticity and Beyond*. Springer 2014, vol. 550 of *CISM International Centre for Mechanical Sciences*, pp. 1–64.

[423] Schröder, J.; Balzani, D. & Brands, D.: *Approximation of random microstructures by periodic statistically similar representative volume elements based on lineal-path functions*. Archive of Applied Mechanics **81** (2011), 975–997.

[424] Schröder, J.; von Hoegen, M. & Neff, P.: *The exponentiated Hencky energy: anisotropic extension and case studies*. Computational Mechanics **61** (2018), 657–685.

[425] Schröder, J. & Neff, P.: *Invariant formulation of hyperelastic transverse isotropy based on polyconvex free energy functions*. International Journal of Solids and Structures **40** (2003), 401–445.

[426] Schröder, J.; Neff, P. & Balzani, D.: *A variational approach for materially stable anisotropic hyperelasticity*. International Journal of Solids and Structures **42** (2005), 4352–4371.

[427] Schur, I.: *Vorlesungen über Invariantentheorie*. Springer-Verlag, Berlin 1968.

[428] Scott, N. H. & Hayes, M.: *A note on wave propagation in internally constrained hyperelastic materials*. Wave Motion **7** (1985), 601–605.

[429] Seth, B. R.: *Generalized Strain Measure with Application to Physical Problems*. In Reiner, M. & Abir, D. (Editors): *Second-Order Effects in Elasticity, Plasticity and Fluid Dynamics*. Jerusalem Academic Press 1964, pp. 162–172.

[430] Sewell, M. J.: *Maximum and minimum principles*. Cambridge University Press, Cambridge 1987.

[431] Shampine, L. F.: MATLAB *program for quadrature in 2D*. Applied Mathematics and Computation **202** (2008), 266–274.

[432] Shampine, L. F.: *Vectorized adaptive quadrature in* MATLAB. Journal of Computational and Applied Mathematics **211** (2008), 131–140.

[433] Shams, M.; Destrade, M. & Ogden, R. W.: *Initial stresses in elastic solids: Constitutive laws and acoustoelasticity*. Wave Motion **48** (2011), 552–567.

[434] Sharafi, B. & Blemker, S. S.: *A micromechanical model of skeletal muscle to explore the effects of fiber and fascicle geometry*. Journal of Biomechanics **43** (2010), 3207–3213.

[435] Sharifimajd, B. & Stålhand, J.: *A continuum model for skeletal muscle contraction at homogeneous finite deformations*. Biomechanics and Modeling in Mechanobiology **12** (2013), 965–973.

[436] Shen, Z. L.; Dodge, M. R.; Kahn, H.; Ballarini, R. & Eppel, S. J.: *Stress-Strain Experiments on Individual Collagen Fibrils*. Biophysical Journal **95** (2008), 3956–3963.

[437] Shinozaki, N.; Sibuya, M. & Tanabe, K.: *Numerical algorithms for the Moore-Penrose inverse of a matrix: Direct methods*. Annals of the Institute of Statistical Mathematics **24** (1972), 193–203.

[438] Šilhavý, M.: *The Mechanics and Thermodynamics of Continuous Media*. Springer-Verlag, Berlin 1997.

[439] Silling, S. A.: *Reformulation of elasticity theory for discontinuities and long-range forces*. Journal of the Mechanics and Physics of Solids **48** (2000), 175–209.

[440] Simo, J. C. & Marsden, J. E.: *On the Rotated Stress Tensor and the Material Version of the Doyle-Ericksen Formula*. Archive for Rational Mechanics and Analysis **86** (1984), 213–231.

[441] Simo, J. C. & Pister, K. S.: *Remarks on rate constitutive equations for finite deformation*. Computer Methods in Applied Mechanics and Engineering **46** (1984), 201–215.

[442] Simo, J. C.; Taylor, R. L. & Pister, K. S.: *Variational and projection methods for the volume constraint in finite deformation elasto-plasticity*. Computer Methods in Applied Mechanics and Engineering **51** (1985), 177–208.

[443] Sinkus, R.; Tanter, M.; Catheline, S.; Lorenzen, J.; Kuhl, C.; Sondermann, E. & Fink, M.: *Imaging Anisotropic and Viscous Properties of Breast Tissue by Magnetic Resonance-Elastography.* Magnetic Resonance in Medicine **53** (2005), 372–387.

[444] Sjøgaard, G. & Saltin, B.: *Extra- and intracellular water spaces in muscles of man at rest and with dynamic exercise.* American Journal of Physiology – Regulatory, Integrative and Comparative Physiology **243** (1982), R271–R280.

[445] Slesarenko, V. & Rudykh, S.: *Microscopic and macroscopic instabilities in hyperelastic fiber composites.* Journal of the Mechanics and Physics of Solids **99** (2017), 471–482.

[446] Sloan, I. H. & Womersley, R. S.: *Extremal systems of points and numerical integration on the sphere.* Advances in Computational Mathematics **21** (2004), 107–125.

[447] Smit, R. J. M.; Brekelmans, W. A. M. & Meijer, H. E. H.: *Prediction of the mechanical behavior of nonlinear heterogeneous systems by multi-level finite element modeling.* Computer Methods in Applied Mechanics and Engineering **155** (1998), 181–192.

[448] Smith, D. R.: *An Introduction to Continuum Mechanics.* Springer Science+ Business Media, Dordrecht 1993.

[449] Smith, G. F.: *On a Fundamental Error in Two Papers of C.-C. Wang "On Representations for Isotropic Functions, Parts I and II".* Archive for Rational Mechanics and Analysis **36** (1970), 161–165.

[450] Smith, G. F.: *On isotropic functions of symmetric tensors, skew-symmetric tensors and vectors.* International Journal of Engineering Science **9** (1971), 899–916.

[451] Smith, L. R.; Gerace-Fowler, L. & Lieber, R. L.: *Muscle extracellular matrix applies a transverse stress on fibers with axial strain.* Journal of Biomechanics **44** (2011), 1618–1620.

[452] Smith, L. R.; Lee, K. S.; Ward, S. R.; Chambers, H. G. & Lieber, R. L.: *Hamstring contractures in children with spastic cerebral palsy result from a stiffer extracellular matrix and increased* in vivo *sarcomere length.* Journal of Physiology **589** (2011), 2625–2639.

[453] Smith, L. R.; Meyer, G. & Lieber, R. L.: *Systems analysis of biological networks in skeletal muscle function.* WIREs Systems Biology and Medicine **5** (2013), 55–71.

[454] Soong, T. T. & Huang, W. N.: *A stochastic model for biological tissue elasticity in simple elongation.* Journal of Biomechanics **6** (1973), 451–458.

[455] Spencer, A. J. M.: *Theory of Invariants.* In Eringen, A. C. (Editor): *Continuum Physics, Volume 1.* Academic Press, New York 1971, pp. 239–353.

[456] Spencer, A. J. M.: *Deformations of Fibre-reinforced Materials.* Clarendon Press, Oxford 1972.

[457] Spencer, A. J. M.: *Constitutive theory for strongly anisotropic solids*. In Spencer, A. J. M. (Editor): *Continuum theory of the mechanics of fibre-reinforced composites*. Springer-Verlag 1984, CISM Courses and Lectures No. 282, pp. 1–32.

[458] Spencer, A. J. M.: *Isotropic Polynomial Invariants and Tensor Functions*. In Boehler, J.-P. (Editor): *Applications of Tensor Functions in Solid Mechanics*. Springer-Verlag, Wien 1987, CISM Courses and Lecture No. 292.

[459] Spyrou, L. A.; Agoras, M. & Danas, K.: *A homogenization model of the Voigt type for skeletal muscle*. Journal of Theoretical Biology **414** (2017), 50–61.

[460] Spyrou, L. A.; Brisard, S. & Danas, K.: *Multiscale modeling of skeletal muscle tissues based on analytical and numerical homogenization*. Journal of the Mechanical Behavior of Biomedical Materials **92** (2019), 97–117.

[461] Srinivasa, A. R.: *On the use of the upper triangular (or QR) decomposition for developing constitutive equations for Green-elastic materials*. International Journal of Engineering Science **60** (2012), 1–12.

[462] Stålhand, J.; Klarbring, A. & Holzapfel, G. A.: *Smooth muscle contraction: Mechanochemical formulation for homogeneous finite strains*. Progress in Biophysics and Molecular Biology **96** (2008), 465–481.

[463] Steigmann, D. J.: *Frame-invariant Polyconvex Strain-energy Functions for Some Anisotropic Solids*. Mathematics and Mechanics of Solids **8** (2003), 497–506.

[464] Suquet, P. (Editor): *Continuum Micromechanics*. Springer Verlag, Wien 1997.

[465] Suquet, P. M.: *Overall potentials and extremal surfaces of power law or ideally plastic composites*. Journal of the Mechanics and Physics of Solids **41** (1993), 981–1002.

[466] Svendsen, B. & Bertram, A.: *On frame-indifference and form-invariance in constitutive theory*. Acta Mechanica **132** (1999), 195–207.

[467] Sverdlik, A. & Lanir, Y.: *Time-Dependent Mechanical Behavior of Sheep Digital Tendons, Including the Effects of Preconditioning*. Transactions of the ASME **124** (2002), 78–84.

[468] Tadmor, E. B. & Miller, R. E.: *Modeling Materials: Continuum, Atomistic and Multiscale Techniques*. Cambridge University Press, Cambridge 2011.

[469] Tadmor, E. B.; Phillips, R. & Ortiz, M.: *Mixed Atomistic and Continuum Models of Deformation in Solids*. Mangmuir **12** (1996), 4529–4534.

[470] Takaza, M.; Cooney, G. M.; McManus, G.; Stafford, P. & Simms, C. K.: *Assessing the microstructural response to applied deformation in porcine passive skeletal muscle*. Journal of the Mechanical Behavior of Biomedical Materials **40** (2014), 115–126.

[471] Takaza, M.; Moerman, K. M.; Gindre, J.; Lyons, G. & Simms, C. K.: *The anisotropic mechanical behaviour of passive skeletal muscle tissue subjected to large tensile strain*. Journal of the Mechanical Behavior of Biomedical Materials **17** (2013), 209–220.

[472] Talbot, D. R. S. & Willis, J. R.: *Variational Principles for Inhomogeneous Non-linear Media*. IMA Journal of Applied Mathematics **35** (1985), 39–54.

[473] Talbot, D. R. S. & Willis, J. R.: *Some simple explicit bounds for the overall behaviour of nonlinear composites*. International Journal of Solids and Structures **29** (1992), 1981–1987.

[474] Tang, H.; Buehler, M. J. & Moran, B.: *A Constitutive Model of Soft Tissue: From Nanoscale Collagen to Tissue Continuum*. Annals of Biomedical Engineering **37** (2009), 1117–1130.

[475] Taylor, G. I.: *Plastic strain in metals*. Journal of the Institute of Metals **62** (1938), 307–324.

[476] Thacker, B. E.; Tomiya, A.; Hulst, J. B.; Suzuki, K. P.; Bremner, S. N.; Gastwirt, R. F.; Greaser, M. L.; Lieber, R. L. & Ward, S. R.: *Passive Mechanical Properties and Related Proteins Change with Botulinum Neurotoxin A Injection of Normal Skeletal Muscle*. Journal of Orthopaedic Research **30** (2012), 497–502.

[477] Tkachuk, M. & Linder, C.: *The maximal advance path constraint for the homogenization of materials with random network microstructure*. Philosophical Magazine **92** (2012), 2779–2808.

[478] Torquato, S.: *Random Heterogeneous Materials - Microstructure and Macroscopic Properties*. Springer-Verlag, New York 2002.

[479] Treloar, L. R. G.: *The elasticity of a network of long-chain molecules — II*. Transactions of the Faraday Society **39** (1943), 241–246.

[480] Treloar, L. R. G.: *The elasticity of a network of long-chain molecules — III*. Transactions of the Faraday Society **42** (1946), 83–94.

[481] Treloar, L. R. G.: *The photoelastic properties of short-chain molecular networks*. Transactions of the Faraday Society **50** (1954), 881–896.

[482] Treloar, L. R. G.: *The physics of rubber elasticity*. Clarendon Press, Oxford 1975, 3 edn.

[483] Treloar, L. R. G. & Riding, G.: *A non-Gaussian theory for rubber in biaxial strain. I. Mechanical properties*. Proceedings of the Royal Society A **369** (1979), 261–280.

[484] Triantafyllidis, N. & Abeyaratne, R.: *Instabilities of a Finitely Deformed Fiber-Reinforced Elastic Material*. Journal of Applied Mechanics **50** (1983), 149–156.

[485] Triantafyllidis, N. & Maker, B. N.: *On the Comparison Between Microscopic and Macroscopic Instability Mechanisms in a Class of Fiber-Reinforced Composites*. Journal of Applied Mechanics **52** (1985), 794–800.

[486] Trotter, J. A. & Purslow, P. P.: *Functional Morphology of the Endomysium in Series Fibered Muscles*. Journal of Morphology **212** (1992), 109–122.

[487] Truesdell, C.: *A New Definition of a Fluid, II. The Maxwellian Fluid*. Journal de Mathématiques Pures et Appliquées **30** (1951), 111–155.

[488] Truesdell, C.: *The Elements of Continuum Mechanics*. Springer-Verlag, New York 1966.

[489] Truesdell, C.: *Rational Thermodynamics*. Springer-Verlag, New York 1984, 2 edn.

[490] Truesdell, C. & Noll, W.: *The Non-Linear Field Theories of Mechanics*. Springer-Verlag, Berlin Heidelberg 2004, 3 edn.

[491] Valanis, K. C. & Landel, R. F.: *The Strain-Energy Function of a Hyperelastic Material in Terms of the Extension Ratios*. Journal of Applied Physics **38** (1967), 2997–3002.

[492] Veres, S. P. & Lee, J. M.: *Designed to Fail: A Novel Mode of Collagen Fibril Disruption and its Relevance to Tissue Toughness*. Biophysical Journal **102** (2012), 2876–2884.

[493] Verron, E.: *Questioning numerical integration methods for microsphere (and microplane) constitutive equations*. Mechanics of Materials **89** (2015), 216–228.

[494] Virgilio, K. M.; Martin, K. S.; Peirce, S. M. & Blemker, S. S.: *Multiscale models of skeletal muscle reveal the complex effects of muscular dystrophy on tissue mechanics and damage susceptibility*. Interface Focus **5** (2015), 20140080.

[495] Voigt, W.: *Ueber die Beziehung zwischen den beiden Elasticitätsconstanten isotroper Körper*. Annalen der Physik **274** (1889), 573–587.

[496] Voigt, W.: *Lehrbuch der Kristallphysik*. Springer Fachmedien, Wiesbaden 1966 [1928].

[497] Voronoi, G.: *Nouvelles applications des paramètres continus à la théorie des formes quadratiques. Premier mémoire. Sur quelques propriétés des formes quadratiques positives parfaites.* and *Premiére partie. Théorie générale des formes quadratiques positives parfaites et des domaines qui leur eorrespondent.* Journal für die reine und angewandte Mathematik **133** (1908), 97–178.

[498] Wall, F. T. & Flory, P. J.: *Statistical Thermodynamics of Rubber Elasticity*. The Journal of Chemical Physics **19** (1951), 1435–1439.

[499] Walpole, L. J.: *On the overall elastic moduli of composite materials*. Journal of the Mechanics and Physics of Solids **17** (1969), 235–251.

[500] Walpole, L. J.: *Elastic Behavior of Composite Materials: Theoretical Foundations*. Advances in Applied Mechanics **21** (1981), 169–242.

[501] Walpole, L. J.: *Fourth-rank tensors of the thirty-two crystal classes: multiplication tables*. Proceedings of the Royal Society A **391** (1984), 149–179.

[502] Wang, C.-C.: *On Representations for Isotropic Functions - Part I. Isotropic Functions of Symmetric Tensors and Vectors*. Archive for Rational Mechanics and Analysis **33** (1969), 249–267.

[503] Wang, C.-C.: *On Representations for Isotropic Functions - Part II. Isotropic Functions of Skew-Symmetric Tensors, Symmetric Tensors, and Vectors*. Archive for Rational Mechanics and Analysis **33** (1969), 268–287.

[504] Wang, C.-C.: *A New Representation Theorem for Isotropic Functions: An Answer to Professor G. F. Smith's Criticism of my Papers on Representations for Isotropic Functions Part 1. Scalar-Valued Isotropic Functions*. Archive for Rational Mechanics and Analysis **36** (1970), 166–197.

[505] Wang, M. C. & Guth, E.: *Statistical Theory of Networks of Non-Gaussian Flexible Chains*. The Journal of Chemical Physics **20** (1952), 1144–1157.

[506] Ward, S. R. & Lieber, R. L.: *Density and hydration of fresh and fixed human skeletal muscle*. Journal of Biomechanics **38** (2005), 2317–2320.

[507] Watton, P. N.; Ventikos, Y. & Holzapfel, G. A.: *Modelling the mechanical response of elastin for arterial tissue*. Journal of Biomechanics **42** (2009), 1320–1325.

[508] Weber, H. H. & Portzehl, H.: *Muscle Contraction and Fibrous Muscle Proteins*. Advances in Protein Chemistry **7** (1952), 161–252.

[509] Weis-Fogh, T. & Andersen, S. O.: *New Molecular Model for the Long-range Elasticity of Elastin*. Nature **227** (1970), 718–721.

[510] Weisbecker, H.; Unterberger, M. J. & Holzapfel, G. A.: *Constitutive modelling of arteries considering fibre recruitment and three-dimensional fibre distribution*. Journal of the Royal Society Interface **12** (2015), 20150111.

[511] Weiss, J. A.; Maker, B. N. & Govindjee, S.: *Finite element implementation of incompressible, transversely isotropic hyperelasticity*. Computer Methods in Applied Mechanics and Engineering **135** (1996), 107–128.

[512] Weizsäcker, H. W.; Holzapfel, G. A.; Desch, G. W. & Pascale, K.: *Strain Energy Density Function for Arteries from Different Topographical Sites*. Biomedical Engineering / Biomedizinische Technik **40** (1995), 139–141.

[513] Wenger, M. P. E.; Bozec, L.; Horton, M. A. & Mesquida, P.: *Mechanical properties of collagen fibrils*. Biophysical Journal **93** (2007), 1255–1263.

[514] Weyl, H.: *The Classical Groups : Their Invariants and Representations*. Princeton University Press, Princeton 1946.

[515] Wheatley, B. B.; Odegard, G. M.; Kaufman, K. R. & Haut Donahue, T. L.: *How does tissue preparation affect skeletal muscle transverse isotropy?* Journal of Biomechanics **49** (2016), 3056–3060.

[516] Willis, J. R.: *Bounds and self-consistent estimates for the overall properties of anisotropic composites*. Journal of the Mechanics and Physics of Solids **25** (1977), 185–202.

[517] Willis, J. R.: *Variational and Related Methods for the Overall Properties of Composites*. Advances in Applied Mechanics **21** (1981), 1–78.

[518] Willis, J. R.: *The Overall Elastic Response of Composite Materials*. Journal of Applied Mechanics **50** (1983), 1202–1209.

[519] Willis, J. R.: *Variational Estimates for the Overall Response of an Inhomogeneous Nonlinear Dielectric.* In Ericksen, J. L.; Kinderlehrer, D.; Kohn, R. & Lions, J. L. (Editors): *Homogenization and Effective Moduli of Materials and Media.* Springer, New York 1986, The IMA Volumes in Mathematics and its Applications, vol 1.

[520] Wirtz, D.; Karajan, N. & Haasdonk, B.: *Surrogate modeling of multiscale models using kernel methods.* International Journal for Numerical Methods in Engineering **101** (2014), 1–28.

[521] Womersley, R. S. & Sloan, I. H.: *How good can polynomial interpolation on the sphere be?* Advances in Computational Mathematics **14** (2001), 195–226.

[522] Wu, P. D. & van der Giessen, E.: *On improved network models for rubber elasticity and their applications to orientation hardening in glassy polymers.* Journal of the Mechanics and Physics of Solids **41** (1993), 427–456.

[523] Zajac, F. E.: *Muscle and tendon: properties, models, scaling, and application to biomechanics and motor control.* Critical reviews in biomedical engineering **17** (1989), 359–411.

[524] Zaoui, A.: *Continuum Micromechanics: Survey.* Journal of Engineering Mechanics **128** (2002), 808–816.

[525] Zee, L. & Sternberg, E.: *Ordinary and Strong Ellipticity in the Equilibrium Theory of Incompressible Hyperelastic Solids.* Archive for Rational Mechanics and Analysis **83** (1983), 53–90.

[526] Zheng, Q.-S.: *Theory of representations for tensor functions - a unified invariant approach to constitutive equations.* Applied Mechanics Reviews **47** (1994).

[527] Zheng, Q.-S. & Spencer, A. J. M.: *Tensors which characterize anisotropies.* International Journal of Engineering Science **31** (1993), 679–693.

[528] Zohdi, T. I. & Wriggers, P.: *An Introduction to Computational Micromechanics.* Springer-Verlag, Berlin 2008, 2 edn.

Released Report Series

CBM-01 Thomas Heidlauf: *Chemo-Electro-Mechanical Modelling of the Neuromuscular System*, September 2015

CBM-02 Michael Sprenger: *A 3D Continuum-Mechanical Model for Forward-Dynamics Simulations of the Upper Limb*, October 2015

CBM-03 Ellankavi Ramasamy: *A Modelling-Simulation-Analysis Workflow for Investigating Socket-Stump Interaction*, April 2019

CBM-04 Andreas Hessenthaler: *Multilevel Convergence Analysis: Parallel-in-Time Integration for Fluid-Structure Interaction Problems with Applications in Cardiac Flow Modeling*, February 2020

CBM-05 Mylena Mordhorst: *Towards a Stable and Fast Dynamic Skeletal Muscle Model*, April 2020

CBM-06 Pouyan Asgharzadeh: *Image-based Analysis of Biological Network Structures using Machine Learning and Continuum Mechanics*, May 2020